



School of chemistry

Cardiff University, Cardiff Catalysis Institute (CCI)

---

# Direct synthesis of $H_2O_2$ at ambient conditions and its applicability for water treatment with Fenton's catalysts

---

Thesis submitted in accordance with the requirements of  
Cardiff University for the degree of doctor of philosophy by:

**Alba Santos-Hernandez**

2022

## Table of contents

<b>Overview</b> .....	VI
<b>Acknowledgements</b> .....	IX
<b>Chapter 1: Introduction to Fenton's oxidation with in-situ H<sub>2</sub>O<sub>2</sub> for water treatment.</b>	
<b>1.1 Introduction to catalysis</b> .....	1
1.1.1 Introduction to heterogeneous catalysis. ....	3
1.1.2 Basics about kinetics and reaction mechanisms for a heterogeneous catalysed reaction.....	7
<b>1.2 Hydrogen peroxide (H<sub>2</sub>O<sub>2</sub>)</b> .....	10
1.2.1 General introduction to H <sub>2</sub> O <sub>2</sub> . ....	10
1.2.2 Industrial manufacturing routes for H <sub>2</sub> O <sub>2</sub> . ....	11
1.2.3 Introduction to the direct synthesis of H <sub>2</sub> O <sub>2</sub> from H <sub>2</sub> and O <sub>2</sub> gas. ....	15
1.2.3.1 Supported palladium (Pd) catalysts for the direct synthesis of H <sub>2</sub> O <sub>2</sub> . ....	16
1.2.3.2 Supported gold-palladium (AuPd) catalysts for the direct synthesis of H <sub>2</sub> O <sub>2</sub> . ..	22
1.2.3.3 Other metallic promoters of Pd catalysts for the direct synthesis of H <sub>2</sub> O <sub>2</sub> . ....	29
1.2.3.4 Mechanism of H <sub>2</sub> O <sub>2</sub> and H <sub>2</sub> O formation over Pd and AuPd supported catalysts. ....	34
<b>1.3 Water treatment</b> . ....	37
1.3.1 Oxidation reactions for water treatment.....	37
1.3.2 Fenton's oxidations: activation of H <sub>2</sub> O <sub>2</sub> with Fe salts. ....	39
1.3.3 Heterogeneous Fenton's oxidations. ....	40
1.3.3.1 Phenol oxidation with heterogeneous Fenton catalysts and commercial H <sub>2</sub> O <sub>2</sub> . ....	41
1.3.3.2 Phenol oxidation with heterogeneous Fenton catalyst and <i>in-situ</i> H <sub>2</sub> O <sub>2</sub> . ....	48
<b>1.4 Research objectives</b> . ....	50
<b>1.5 References</b> . ....	53
<b>Chapter 2: Experimental procedure and theory.</b>	
<b>2.1 Reagents</b> . ....	64
<b>2.2 Catalysts synthesis</b> . ....	65
2.2.1 Modified impregnation.....	65
2.2.2 Hydrothermal synthesis.....	66

2.2.2.1 Direct synthesis of HZSM-5 (SiO <sub>2</sub> :Al <sub>2</sub> O <sub>3</sub> ) (28:1) containing Fe. ....	66
2.2.3 General background about atomic spectroscopy.....	67
2.2.3.1 Determination of the metal loading by means of MP-AES.....	70
<b>2.3 Catalysts testing.</b> .....	<b>70</b>
2.3.1 Description of the reaction conditions for the evaluation of mono and bi-metallic 1 wt.% AuPd/TiO <sub>2</sub> catalysts towards the direct synthesis and degradation of H <sub>2</sub> O <sub>2</sub> .....	70
2.3.1.1 Reaction set-up procedure towards the direct synthesis and degradation of H <sub>2</sub> O <sub>2</sub> using an Autoclave (Parr Instrument).....	72
2.3.2 Reaction set-up procedure to test the catalyst's activity towards the degradation of phenol, post-reaction analysis and subsequent calculations. ....	77
2.3.2.1 Identification and quantification of the phenol conversion and its products by means of HPLC. ....	78
2.3.2.2 Gas replacements experiments for the degradation of phenol using mono and bi-metallic 1 wt.% FePd/TiO <sub>2</sub> and 0.50 wt.% Pd/ X wt.% Fe-HZSM-5 (X: 3.0-0.06) catalysts. ....	80
2.3.2.3 Re-usability of the bi-metallic 1 wt.% FePd/TiO <sub>2</sub> and 0.50 wt.% Pd/ X wt.% Fe-HZSM-5 (X: 3.0-0.06) catalysts towards the degradation of phenol. ....	80
2.3.3 Reproducibility of the catalytic activity.....	80
<b>2.4 Introduction to molecular spectroscopy.</b> .....	<b>81</b>
2.4.1 Introduction to molecular spectroscopy.....	81
2.4.2 Basics about ultraviolet-visible spectroscopy (UV-Vis).....	84
2.4.3 Basics about diffuse reflectance ultraviolet-visible spectroscopy (DR UV-Vis) .....	86
2.4.3.1 Determination of the Fe species for the mono and bi-metallic 0.50 wt.% Pd/ X wt.% Fe-HZSM-5 (X:3.0-0.06) catalysts by means of DR UV-Vis.....	86
2.4.4 Basics about fourier transform infrared (FT-IR) and raman spectroscopy.....	86
2.4.4.1 Determination of the Fe species of the mono and bi-metallic 0.50 wt.% Pd/ X wt.% Fe-HZSM-5 (X:3.0-0.06) catalyst by means of FT-IR and UV-Raman. ....	90
2.4.5 Basics about CO-diffuse reflectance infrared fourier transform spectroscopy (CO-DRIFTS). ....	91
2.4.5.1 Analysis of mono and bi-metallic 1 wt.% FePd/TiO <sub>2</sub> and 0.5 wt.% Pd/ X wt.% Fe-HZSM-5 (X: 3.0-0.06) catalysts by means of CO-DRIFTS. ....	92
2.4.6 Basics about x-ray photoelectron spectroscopy (XPS).....	92

2.4.6.1 Analysis of the mono and bi-metallic 1 wt.% AuPd/TiO <sub>2</sub> , 1 wt.% FePd/TiO <sub>2</sub> and 0.5 wt.% Pd/ X wt.% Fe-HZSM-5 (X: 3.0-0.06) catalysts by XPS. ....	95
2.4.7 Basics about x-ray diffraction (XRD) spectroscopy.....	95
2.4.7.1 Analysis of the mono and bi-metallic 1 wt.% AuPd/TiO <sub>2</sub> , 1 wt.% FePd/TiO <sub>2</sub> and 0.5 wt.% Pd/ X wt.% Fe-HZSM-5 (X: 3.0-0.0) catalysts by XRD.....	97
<b>2.5 Basics about microscopy techniques. ....</b>	<b>97</b>
2.5.1 Transmission electron microscopy (TEM). ....	98
2.5.1.1 Determination of the nanoparticle size and distribution for 1 wt.% AuPd/TiO <sub>2</sub> , 1 wt.% FePd/TiO <sub>2</sub> and 0.5 wt.% Pd/ X wt.% Fe-HZSM-5 (X: 3.0-0.06) catalysts by TEM. ....	100
<b>2.6 Physisorption.....</b>	<b>100</b>
2.6.1 Brunauer-Emmett-Teller isotherm. ....	100
2.6.1.1 Physical characterisation of mono and bi-metallic 0.5 wt.% Pd/ X wt.% Fe-HZSM-5 (X: 3.0-0.06) catalysts by physisorption analysis.....	100
<b>2.7 References. ....</b>	<b>102</b>
<b>Chapter 3: Direct synthesis of H<sub>2</sub>O<sub>2</sub> with AuPd on TiO<sub>2</sub> catalysts at ambient temperature.</b>	
<b>3.1 Introduction.....</b>	<b>105</b>
<b>3.2 Results and discussion.....</b>	<b>107</b>
3.2.1 Activity of the mono and bi-metallic 1.0 wt.% AuPd/TiO <sub>2</sub> catalysts at (2°C,CH <sub>3</sub> OH-H <sub>2</sub> O,CO <sub>2</sub> ) conditions towards the direct synthesis and degradation of H <sub>2</sub> O <sub>2</sub> . ....	107
3.2.2 Activity of mono and bi-metallic 1.0 wt.% AuPd/TiO <sub>2</sub> catalysts at (25 °C,CH <sub>3</sub> OH-H <sub>2</sub> O,CO <sub>2</sub> ) conditions towards the direct synthesis and degradation of H <sub>2</sub> O <sub>2</sub> . ....	109
3.2.3 Activity of the mono and bi-metallic 1.0 wt.% AuPd/TiO <sub>2</sub> catalysts towards the direct synthesis and degradation of H <sub>2</sub> O <sub>2</sub> at (25 °C,H <sub>2</sub> O,CO <sub>2</sub> ) and (25 °C, H <sub>2</sub> O,N <sub>2</sub> ).....	110
3.2.4 Comparison of the H <sub>2</sub> conversion and H <sub>2</sub> O <sub>2</sub> selectivity for the bi-metallic 0.5 wt.% Au-0.5 wt.% Pd/TiO <sub>2</sub> catalyst during the direct synthesis of H <sub>2</sub> O <sub>2</sub> .....	115
3.2.5 Effect of the H <sub>2</sub> solubility towards the formation of H <sub>2</sub> O <sub>2</sub> .....	116
3.2.6 Time on-line activity towards the formation of H <sub>2</sub> O <sub>2</sub> at (2°C,CH <sub>3</sub> OH-H <sub>2</sub> O,CO <sub>2</sub> ) and (25°C,H <sub>2</sub> O,N <sub>2</sub> ) conditions.....	117
<b>3.3 Characterisation of the mono and bi-metallic 1 wt.% AuPd/TiO<sub>2</sub> catalysts. ....</b>	<b>118</b>
<b>3.4 Conclusions. ....</b>	<b>123</b>

<b>3.5 References.</b> .....	124
<b>3.6 Supplementary information.</b> .....	127
<b>Chapter 4: Oxidation of phenol with FePd impregnated catalysts on TiO<sub>2</sub>.</b>	
<b>4.1 Introduction.</b> .....	134
<b>4.2 Results and discussion.</b> .....	137
4.2.1 Oxidation of phenol with pre-formed H <sub>2</sub> O <sub>2</sub> .....	137
4.2.2 Oxidation of phenol using Fenton metals and pre-formed H <sub>2</sub> O <sub>2</sub> . .....	137
4.2.3 Characterisation and activity of Pd-Fenton metals based catalysts towards the degradation of phenol, direct synthesis and degradation of H <sub>2</sub> O <sub>2</sub> .....	138
4.2.4 Characterisation of the mono and bi-metallic 1 wt.% FePd/TiO <sub>2</sub> catalysts.....	144
4.2.4.1 Activity of the mono and bi-metallic 1 wt.% FePd/TiO <sub>2</sub> catalysts towards the direct synthesis and degradation of H <sub>2</sub> O <sub>2</sub> .....	149
4.2.4.2 Activity of the mono and bi-metallic 1 wt.% FePd/TiO <sub>2</sub> catalysts towards the degradation of phenol. ....	153
4.2.5 Re-usability of the bi-metallic 0.5 wt.% Fe-0.5 wt.% Pd/TiO <sub>2</sub> catalyst towards the degradation of phenol. ....	160
<b>4.3 Conclusions.</b> .....	162
<b>4.4 References.</b> .....	163
<b>4.5 Supplementary information.</b> .....	168
<b>Chapter 5: Oxidation of phenol with Pd impregnated on HZSM-5 containing Fe.</b>	
<b>5.1 Introduction.</b> .....	182
<b>5.2 Results and discussion.</b> .....	184
5.2.1 Characterisation of the mono and bi-metallic 0.5 wt.% Pd/ X wt.% Fe-HZSM-5 (X: 3.0-0) catalysts. ....	184
5.2.2 Activity of the bi-metallic 0.5 wt. % Pd/ X wt.% Fe-HZSM-5 (X: 3.0-0) catalysts towards the direct synthesis and degradation of H <sub>2</sub> O <sub>2</sub> .....	191
5.2.3 Speciation of the Fe in the bi-metallic 0.5 wt. % Pd/ X wt.% Fe-HZSM-5 (X: 3.0-0) catalysts and their activity towards the degradation of phenol.....	196
5.2.4 Characterisation and re-usability of the bi-metallic 0.5 wt.% Pd/ 0.5 wt.% Fe-HZSM-5 catalyst towards the degradation of phenol. ....	206
<b>5.3 Conclusions.</b> .....	208

<b>5.4 References.</b> .....	210
<b>5.5 Supplementary information.</b> .....	214
<b>Chapter 6: Conclusions and future work.</b>	
<b>6.1 Brief thesis introduction.</b> .....	233
6.1.1 Thesis objectives and summary. ....	234
<b>6.2 Conclusions and final remarks.</b> .....	235
<b>6.3 Alternative lines of research for future work.</b> .....	245
<b>6.4 References.</b> .....	249

## Overview

Hydrogen peroxide ( $\text{H}_2\text{O}_2$ ) is a colourless liquid oxidant widely applied in several industrial activities such as bleaching, chemical synthesis, mining and disinfection. Currently, over 4 million tons of  $\text{H}_2\text{O}_2$  were reported in 2021 to be annually produced to meet the demands of the general public. In 1832 a variant of Thenard's process became the first manufacturing route for the production of  $\text{H}_2\text{O}_2$ . Nowadays, there are known three industrial routes to obtain  $\text{H}_2\text{O}_2$ ; *i*) the oxidation of primary and secondary alcohols, *ii*) the electrochemical synthesis *iii*) anthraquinone autoxidation process. The latter is the main industrial route accounting for the 95 % of the annual  $\text{H}_2\text{O}_2$  production. This is a multistep process that involve the hydrogenation of the anthraquinone to 2-alkylanthrahydroquinone and its subsequent oxidation to re-generate the anthraquinone and give  $\text{H}_2\text{O}_2$ . However, the  $\text{H}_2\text{O}_2$  generated needs to be separated from the organic solvents that were employed as the working carrier for the anthraquinone molecule, and subsequently, the solution containing the  $\text{H}_2\text{O}_2$  needs to be purified to remove any impurities generated as a result of undesired side reactions and residues of organic solvents that remain after the separation. These two steps, separation and purification, lead to an aqueous solution of 70 wt.% of  $\text{H}_2\text{O}_2$ . However, there are many drawbacks associated with this industrial route. In addition to the high energy consumption associated with the separation and purification of the  $\text{H}_2\text{O}_2$ , the limited stability of the  $\text{H}_2\text{O}_2$  in the aqueous solution (70 wt.%) requires the inclusion of stabilisers to prohibit its degradation that lead to form  $\text{H}_2\text{O}$ . Also, this highly concentrated solution of  $\text{H}_2\text{O}_2$  (70 wt.%) needs to be diluted to concentrations more suitable for a safety transportation (2-8 wt.%), requiring further water consumption that leads to an increase of the overall cost of the process. However, many applications require the use of relatively low concentrations  $\text{H}_2\text{O}_2$  including bleaching, chemical synthesis and cosmetics (< 9 wt.%) and < 0.1 wt.% for water treatment, therefore the high energy demand of the separation and purification steps of the initial phases of  $\text{H}_2\text{O}_2$  production are effectively wasted. Hence, there is an interest in developing technologies to decentralise the production of  $\text{H}_2\text{O}_2$  to reduce the cost and make the process more environmentally friendly as well as reduce the risk in transportation.

The direct synthesis of  $\text{H}_2\text{O}_2$  from  $\text{H}_2$  and  $\text{O}_2$  would be a more atomically and straight forward route for small scale and on-site production. The direct synthesis of  $\text{H}_2\text{O}_2$  is commonly undertaken at sub-ambient temperatures (2 °C) and usually employs a mixture of organic solvents such as methanol and water. These conditions are chosen to avoid the degradation of  $\text{H}_2\text{O}_2$  which leads to the formation of  $\text{H}_2\text{O}$ , reducing the overall selectivity of the process. However, these conditions, are not considered environmentally friendly or industrially applicable due to the high energy demand associated with the process of cooling. In addition, for some applications where  $\text{H}_2\text{O}_2$  is generated and consumed *in-situ*, the presence of organic solvents can be an inconvenience. For instance, for water treatment

purposes, the organic solvent must be removed during the treatment process to make the treated water suitable for consumption or suitable to pour into the water effluents. Bi-metallic AuPd supported catalysts have been widely reported in the literature to be more selective than mono-metallic Pd systems towards the direct synthesis of H<sub>2</sub>O<sub>2</sub>. It has been documented that Au can control the dispersion of Pd, modifying by this way its nanoparticle size, shape and surface configuration so as to make it more selective towards the direct synthesis of H<sub>2</sub>O<sub>2</sub>. With these prior studies and the need to reduce the cost of the process associated with H<sub>2</sub>O<sub>2</sub> production in mind, the aim of Chapter 3 was to study the activity towards the direct synthesis and degradation of H<sub>2</sub>O<sub>2</sub> with different AuPd bi-metallic supported catalysts (1 wt.% AuPd/TiO<sub>2</sub>), made by modified impregnation, at conditions more suitable for industrial processes (ambient temperature (25 °C) and water-only in the reaction medium). The results showed that the catalyst's activity and selectivity towards the direct synthesis of H<sub>2</sub>O<sub>2</sub> was driven by the reaction conditions used. However, the addition of Au to the mono-metallic Pd system was seen to be key to improve the activity and selectivity towards the direct synthesis of H<sub>2</sub>O<sub>2</sub> –in comparison to the mono-metallic Pd and Au analogue- under conditions considered to be more favourable on industrial scale (25 °C and H<sub>2</sub>O-only as solvent). Thus, this led to the conclusion that Au is key in controlling the selectivity of Pd catalysts towards the direct synthesis of H<sub>2</sub>O<sub>2</sub>, although the utilisation of other secondary metals in recent years has also shown promise in controlling its selectivity.

Water remediation employing green oxidants such as H<sub>2</sub>O<sub>2</sub> would be highly convenient since H<sub>2</sub>O<sub>2</sub> produces only H<sub>2</sub>O as a result of the oxidation reactions. Another positive aspect of employing H<sub>2</sub>O<sub>2</sub> as water remediation, is that H<sub>2</sub>O<sub>2</sub> does not produce disinfection by-products (DBPs) which are detrimental to human health. These DBPs are formed due to the reaction of dissolved organic matter (DOM) with some oxidants such as chlorine (Cl<sub>2</sub>) that is still applied for water remediation. The main drawback is that H<sub>2</sub>O<sub>2</sub> is not effective to oxidise aromatics, which may be present in polluted waters such as antibiotics. However, reactive oxygen species (ROS), that refers to any specie with one or more unpaired electrons (superoxide (O<sub>2</sub><sup>•-</sup>), hydroxyl (HO<sup>•</sup>), peroxy (RO<sub>2</sub><sup>•</sup>) and hydroperoxy (HOO<sup>•</sup>) radicals), can be generated through the cleavage of H<sub>2</sub>O<sub>2</sub>, offering greater oxidation potential than the H<sub>2</sub>O<sub>2</sub> itself. Thus, catalyst that could synthesise *in-situ* H<sub>2</sub>O<sub>2</sub> and its subsequent conversion to ROS at ambient temperature and water-only in the reaction medium would be highly desirable for water treatment process. Chapter 4 aimed to identify key bi-metallic and tri-metallic combinations of supported metals which are active for both H<sub>2</sub>O<sub>2</sub> synthesis and its conversion to ROS (1 wt.% XPd/TiO<sub>2</sub>; X: Fe, Cu, Co, Au). These catalysts prepared by modified impregnation were investigated towards the direct synthesis and degradation of H<sub>2</sub>O<sub>2</sub> and towards the degradation of phenol, which was used as a model pollutant commonly found in industrial waste waters. Among the four bi-metallic

combinations tested (1 wt.% XPd/TiO<sub>2</sub>, X: Fe, Cu, Co, Au), the bi-metallic 1 wt.% AuPd/TiO<sub>2</sub> showed the lower activity towards the degradation of phenol, revealing the inefficient activity of H<sub>2</sub>O<sub>2</sub> in oxidising aromatics. On the other hand, the bi-metallic 1 wt.% FePd /TiO<sub>2</sub> supported catalyst showed better performance towards the degradation of phenol in comparison to the other two bi-metallic CoPd/TiO<sub>2</sub> and CuPd/TiO<sub>2</sub> catalysts. It was suspected that the low activity towards the degradation of phenol that the bi-metallic 1 wt.% CoPd/TiO<sub>2</sub> and 1 wt.% CuPd/TiO<sub>2</sub> catalysts presented could have been related to the Co and Cu poisoning the Pd active sites, avoiding the *in-situ* formation of H<sub>2</sub>O<sub>2</sub> and enhancing its degradation. The impregnation of the Fe on the surface of the support, alongside Pd, led to the generation of Fe<sub>x</sub>O<sub>y</sub> species which were easily leached by the generation of the di-acids which were synthesised as a result of the oxidation of phenol. As such, despite 1 wt.% FePd/TiO<sub>2</sub> showed promising activity, they are not suitable for application in *in-situ* oxidative treatment of waste streams. Subsequently, further synthetic routes were investigated in order to stabilise Fe during the oxidation of phenol, which was the scope of Chapter 5. In this chapter, Pd impregnated on HZSM-5 support containing Fe immobilised in the zeolitic channels (0.5 wt.% Pd/ X wt.% Fe-HZSM-5, X: 3-0.06), were studied for phenol degradation. It was hypothesised that through the attachment of Fe species within the HZSM-5 channels, the stability of Fe against leaching would be improved. While the leaching of Fe was significantly reduced, and the resulting catalyst were found to be more active and stable than those developed in Chapter 4 (1 wt.% FePd/TiO<sub>2</sub>), the loading of Fe had to be significantly increased to see relevant activity. The crystallinity of the HZSM-5 got compromised when the amount of Fe increased, which led to produce instable Fe species as those found for the bi-metallic 1 wt.% FePd/TiO<sub>2</sub> catalysts. In addition to this, Pd was found to leach during the direct synthesis of H<sub>2</sub>O<sub>2</sub> and during the degradation of phenol, which it was not the case for the bi-metallic 1 wt.% FePd/TiO<sub>2</sub> catalysts. Therefore, it was concluded that further investigation about how to improve the activity and stability of the bi-metallic 0.5 wt.% Pd/ X wt.% Fe-HZSM-5 (X: 3-0.06) catalysts needed to be developed to make them suitable for commercialization.

## **Acknowledgements**

I would like to give my gratitude to a number of people who have been there for me during the course of my studies. Firstly, to Graham for giving me the opportunity to study within the CCI and secondly to Richard who has been my main support and confidence. Thank you Rich for always having a smile on your face whatever my problem was. Also, I would like to give a special thank you to Sankar for letting me collaborate with his group.

I will always remember a number of post-docs and technicians who were always there with a smile in their faces; Mark, Sam, Greg and Chris thank you for helping me with the analysis and equipment setups for my experiments. Thank you as well to Dave Morgan, the expert in XPS who carried out the analysis of my samples and to Tom Davies who have analysed my samples for TEM.

I wish all the best to all my office mates and work mates. I really hope to be able to meet again sometime in the future. All the best to Tom Richards, Alex Barnes & Matt, Anna – the Greek one-, Naomi, Rhodri, Tanja & Stephan, Justyna, Heba, Laura, Susana, Charlie, Keiko & Guillermo, Leticia and Felipe. I became a better chemist and a better person since I started in the CCI. Also, I would like to mention other people I have met in Cardiff; Martha & Max, Celia, Veronica & Phoebe, Vanessa, Alba, Macarena, Amir, Aguste, Tatiana – Pura vida mae-, Judith & Ivan. Thank you for all the moments and happy times you guys have shared with me.

# Chapter 1: Introduction to Fenton's oxidation with *in-situ* H<sub>2</sub>O<sub>2</sub> for water treatment.

## 1.1 Introduction to catalysis.

The term catalysis was first introduced in 1836 by J.J. Berzelius who came to define it as a compound that increases the chemical reaction but it is not consumed.<sup>1</sup> However, catalysis had been applied much earlier than that, for instance in the production of wine and beer. Among the first industrial catalytic processes, there are a few inorganic chemicals such as the production sulphuric acid (H<sub>2</sub>SO<sub>4</sub>) in the mid-18<sup>th</sup> century from the oxidation of sulfur dioxide (SO<sub>2</sub>) into sulfur trioxide (SO<sub>3</sub>) using nitric oxide (NO) as catalyst. One of the most renowned catalytic process was the synthesis of ammonia (NH<sub>3</sub>) from nitrogen (N<sub>2</sub>) and hydrogen (H<sub>2</sub>) with an osmium (Os) catalyst, which was discovered in 1908 by Fritz Haber. This process can be considered a major breakthrough in the field of catalysis, providing large amounts of affordable fertilizer and greatly improving crop yields.<sup>2</sup> After further study, iron supported catalysts were found to be highly active and far more affordable than the Os-based materials, allowing for the commercialisation of what is known now as the Haber-Bosch Process.<sup>2</sup>

Nowadays, catalysts are widely used and they play a fundamental role in the manufacture of the vast majority of chemicals used in society. Table 1.1 shows some industrial heterogeneous catalysed reactions currently in use.<sup>3</sup> As the table shows, catalysts are also key in achieving a cleaner environment, both by the destruction of pollutants in the air – such as the catalyst in the car exhaust- and through the development of industrial process with less energy requirements and fewer unwanted by-products.<sup>4</sup> Thus, catalysis is part of the twelve principles of green chemistry that were introduced in 1998 by Paul Anastas and John Warner.<sup>5</sup> These principles are a set of guidelines to design new chemical processes that are more environmentally friendly and efficient, for instance by avoiding organic solvents if possible and by maximizing atom efficiency.<sup>5</sup> The conversion of the reactants, selectivity towards the desired product (mols of desired product by mols of reactant consumed) and yield (conversion times selectivity) are often reported for a specific synthetic reaction in order to determine its efficiency. However, these metrics only account for the consumption of the reagents and the formation of products, whereas they do not take into account the waste generated during the process (water, metal oxides, gasses...). Thus, there are a few means that have been introduced in order to analyse quantitatively the efficiency and the environmentally friendliness of an industrialised process. The E-factor is

a term introduced by Roger Sheldon in 1994 that measures the kg waste/kg desired product. Petrochemicals (E-factor of <0.1) and bulk chemicals (E-factor of 1-5) are the least polluting in comparison to pharmaceuticals (E-factor of 5-50) or fine chemicals companies (E-factor of 20-100), as these last two usually work with stoichiometric reagents and multistep synthesis procedures. To give an example, take the oxidation of diphenylmethanol to benzophenone that also produces chromium sulphate ( $\text{Cr}_2(\text{SO}_4)_3$ ) and water. Even if this reaction was 100 % selective with 100 % yield of benzophenone,  $\text{Cr}_2(\text{SO}_4)_3$  and water would be still produced at the end of the reaction. Therefore, the E-factor exist to take into consideration this fact. The atom economy is another term that was introduced by Barry Trost in 1991 and it is also similar to the E-factor. The atom economy evaluates which atoms of the reactants are incorporated into the desired product. With the atom economy and E-factor is feasible to evaluate chemical reactions employing a quantitative result for a better comparison between industrial processes.<sup>2</sup> However, the type of waste generated has also been taken into account, since as the previous example with the oxidation of diphenylmethanol,  $\text{Cr}_2(\text{SO}_4)_3$  is considered a hazard waste whereas water would be considered an environmental friendly waste. Thus, Sheldon introduced the environmental quotient (EQ) which is the E-factor times by an unfriendliness quotient, Q. This Q has a number assigned depending on how hazardous the waste is. For instance, water has Q equal to 0, a benign salt like NaCl has Q equal to 1 and toxic waste have Q values between 100-1000. Thus, catalytic routes that can avoid the formation of waste are highly desirable besides on being more economic.<sup>6</sup>

**Table 1.1:** Production of common chemicals via industrialised heterogeneous catalysed reactions.<sup>2,6</sup>

<b>Process</b>	<b>Catalyst</b>	<b>End-use</b>
<b>Haber-Bosch</b>	Magnetite (Fe)	Fertilizer and explosives
<b>Methanol synthesis</b>	Cu/ZnO/Al <sub>2</sub> O <sub>3</sub>	Bulk chemicals, fuel
<b>Fischer-Tropsch</b>	Co,Fe	Automotive fuel
<b>Cracking</b>	Clays	Fuel, detergents
<b>Alkylation</b>	Zeolites, clays, silicates	High-octane fuel
<b>Dehydrogenation/reforming</b>	Pt/Al <sub>2</sub> O <sub>3</sub>	Polymers, bulk chemicals
<b>Hydrodesulfurization</b>	Co/Mo sulfides	Automotive fuel
<b>Hydrocracking</b>	Pt on zeolites or aluminosilicates	Automotive, aviation fuel
<b>Isomerization</b>	HZSM-5	Polymers, bulk chemicals
<b>Polymerization</b>	Ti, Ziegler-Natta	Polymers, bulk chemicals
<b>Oxidation</b>	Vanadium oxide	Polymers
<b>Ammonia oxidation</b>	Pt-Rh	Nitric acid
<b>Sulphuric acid</b>	Vanadium oxide	Sulphuric acid
<b>Vinyl chloride</b>	Cu	Polyvinyl chloride (PVC), fabrics
<b>Propylene ammoxidation</b>	Bi-Mo, Fe-Sb oxides	Acrylonitrile
<b>Methanation from CO<sub>2</sub></b>	Ni	Methane (CH <sub>4</sub> )
<b>Water-gas shift reaction</b>	Fe oxide, Cu-ZnO	
<b>Oxidation of CO and hydrocarbons (car exhaust)</b>	Pt, Pd	CO <sub>2</sub> , N <sub>2</sub> and H <sub>2</sub> O <sub>2</sub>
<b>Reduction of NO<sub>x</sub> (in exhaust)</b>	Rh, vanadium oxide	N <sub>2</sub>
<b>Hydrogenation of vegetable oils</b>	Ni	Biofuels and fine chemicals
<b>Polymerization of ethylene, Ethylene</b>	Cr, TiCl <sub>x</sub> /MgCl <sub>2</sub> Ag	Adhesives, elastomers Ethylene oxide to make ethylene glycol, polyester, surfactants and detergents.

### 1.1.1 Introduction to heterogeneous catalysis.

The international union of pure and applied chemistry (IUPAC) gives the following definition:

***“A catalyst is a substance that increases the rate of the reaction without modifying the overall standard Gibbs energy change in the reaction; the process is called catalysis. This definition is equivalent to the statement that the catalyst does not enter into the overall reaction; it is both a reactant and a product of the reaction.”<sup>17</sup>***

Energy profiles are schematic representations of the mechanism for a given reaction. Figure 1.1 depicts two energy profiles for a catalysed and un-catalysed reaction. The scheme shows that the overall Gibbs energy is the same for both energy profiles. This means that thermodynamically unfavourable reactions ( $\Delta G > 0$ ) cannot be made favourable ( $\Delta G < 0$ ) by the catalyst. The catalyst introduces a new path that changes the mechanism of the reaction, giving rise to new transition states ( $\Delta^\ddagger G$ ) with lower activation energy ( $E_a$ ). One key requirement for the catalytic reaction to release the desired product, is that any of the intermediates formed should be more thermodynamically stable than the product desired to be obtained.<sup>4</sup>

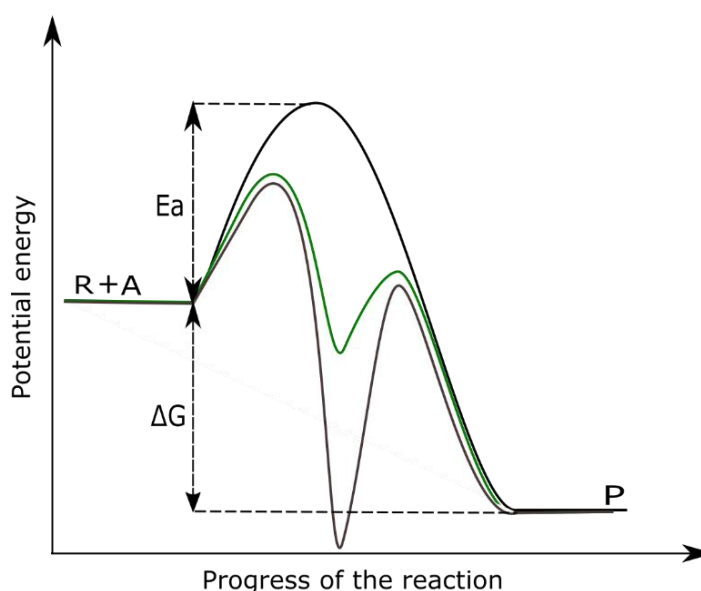


**Figure 1.1:** Schematic representation of the energy profile for given reaction represented as  $R + A \rightarrow P$ . The un-catalysed reaction (black) with higher  $E_a$  compared to the catalysed one (green). The catalysed path (grey) presents a stable intermediate.

Catalysis can be sub-divided depending on the physical state of the catalyst used. Homogeneous catalysts refer to those processes where the catalyst is found in the same phase as the reactants. To give an example, the hydrogenation of alkenes and alkynes with hydrogen ( $H_2$ ) is feasible with the addition of a complex of rhodium (I), ( $Rh^{+1}$ ),  $[RhCl(PPh_3)_3]$  known as Wilkinson's catalyst.<sup>4</sup> In this example, the catalyst consists in an organometallic compound, where the  $Rh^{+1}$  is the Lewis acid and the chloride ( $Cl^-$ ) and phosphines ( $PPh_3$ ) are the ligands.<sup>8</sup> The major disadvantage of homogeneous catalysis is the separation of the catalyst from the reactants and the products generated, since they all are in the same

phase. On the other hand, the separation of heterogeneous catalysts from the reaction mixture is theoretically facile, making the process more efficient and environmentally friendly. Besides, heterogeneous catalysts are typically robust at high temperatures and therefore tolerate a wide range of operating conditions.<sup>4</sup> Heterogeneous catalysts are materials that exist in a different phase to that of the reagents, typically solid-liquid, solid-gaseous or solid-liquid-gaseous systems. For example, finely divided platinum-rhodium alloy particles supported on  $\gamma$ -alumina ( $\text{PtRh}/\gamma\text{-Al}_2\text{O}_3$ ) are used as catalytic converters of vehicles to oxidise carbon monoxide (CO) to carbon dioxide ( $\text{CO}_2$ ) and reduce the NOx (NO and  $\text{N}_2\text{O}_3$ ) to nitrogen ( $\text{N}_2$ ).<sup>4</sup> Enzymes are another type of catalysts, made of proteins or nucleic acids that contain an active site which is very specific for a certain substrate to bind.<sup>8</sup> Among the three types of catalysts, this thesis will only develop and look in detail into the activity and characteristics of heterogeneous catalysts.<sup>2</sup>

As previously mentioned, in a heterogeneous catalytic reaction, the catalyst is in a solid state whereas the reactants are in liquid or gas phase. Thus, the reaction rate is principally relied on the mass transfer or diffusion between these three phases.<sup>2,9</sup> A heterogeneous catalytic reaction can be divided into seven steps, which are depicted in Figure 1.2. First, there is the diffusion of the reactants from the bulk phase (solution) to the external surface of the catalyst (film diffusion or interphase diffusion). Subsequently, the reactants need to diffuse through the internal pores or channels to reach the active sites (pore diffusion or intraparticle diffusion). The reactants are then adsorbed on the active sites (the reactant A adsorbed in the active site is referred in Figure 1.2 as  $A^*$ ) which consequently permits the chemical reaction to occur. The products formed after the reaction need to be desorbed from the active sites ( $B^* \rightarrow B$ ), diffuse back through the internal pores of the catalyst to the surface and finally diffuse back to the bulk of the solution.<sup>9</sup>

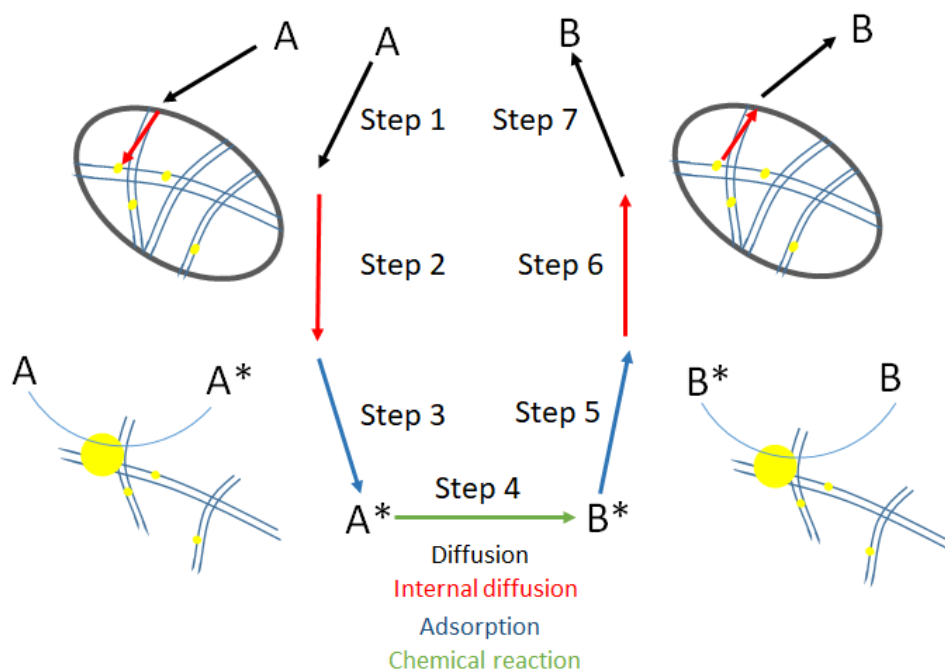


**Figure 1.2:** Steps undertaken during a heterogeneous catalytic reaction for a given reaction represented as  $A \rightarrow B$ .

The adsorption of reagents, chemical reaction and desorption of products are sequential steps. If the diffusion in steps 1,2,6 and 7 is very fast, assuming there is not any obstacle for the reactants to reach to the active site within the pores, then, the concentration of the reactants in the bulk are the same as in the pores. In this scenario there is no resistance of the mass transfer to the rate of the reaction. If the diffusion from the bulk to the catalyst surface is slow, then the external mass transfer becomes an important parameter to the overall reaction rate.<sup>9</sup> To give an example of a heterogeneous catalysed reaction, the direct synthesis of  $H_2O_2$  is a three-phase reaction, involving gasses ( $O_2$  and  $H_2$ ), liquid (reaction medium) and a solid (the catalyst where the active sites are). In this scenario, the sequence to obtain  $H_2O_2$  would involve; *i*) saturation of  $H_2$  and  $O_2$  gas in the reaction medium, *ii*) interphase diffusion of the  $H_2$  and  $O_2$  dissolved in the reaction medium to the surface of the catalyst where the entrance to the pores are, *iii*) pore diffusion of the  $H_2$  and  $O_2$  though the channels so as to reach the active sites, *iv*) adsorption of the  $H_2$  and  $O_2$  on the active site (assuming that  $H_2$  is the only one who dissociate ( $2H^*$  and  $O_2^*$ )), *v*) chemical reaction ((assuming this is the only reaction occurring)  $H_2 + O_2 \rightarrow H_2O_2$ ), *vi*) desorption of the  $H_2O_2$  from the active sites, *vii*) pore diffusion of the  $H_2O_2$  through the channels to the exit or pore mouth, *viii*) interphase diffusion of the  $H_2O_2$  from the surface of the catalyst to the solution where it remains.

### 1.1.2 Basics about kinetics and reaction mechanisms for a heterogeneous catalysed reaction.

Kinetics are a series of mathematical equations that describe the rate at which a chemical reaction happens. These mathematical rate expressions are indispensable in catalysis for the design of chemical reactors and their process control, because kinetics allow to adjust the amount/type of catalyst, temperature, pressure and concentration of the reactants in order to obtain the most optimum operational conditions for the manufacture of the desired product.<sup>6</sup>

For a given reaction ( $2R + A \rightarrow B$ ), the consumption of the reactants and the formation of the products along the course of the reaction can be described as in Equation 1 (Eq. 1). This equation describes mathematically the disappearance of the reactants, R and A that would lead to the formation of the product B for a given time. Thus, the rate of reaction,  $v$ , can be described as shown in Eq. 2, where  $k$ , is known to be the rate constant that depends on the temperature. Each specie has assigned an order of reaction described as  $r$  for [R],  $a$  for [A] and  $b$  for [B], which are meant to relate how the concentration of that particular reactant is being consumed or formed with time. In order to work out the order of a reaction for one particular specie *i.e* [R], the isolation method is commonly applied, where the concentration of the other reactant, in this case [A] is by far much larger than [R] ( $[A] \gg [R]$ ), thus [A] is considered to be constant as an approximation to simplify the calculations. Table 1.2 presents the integration of the differential equations according to the order (0, 1, 2 or 3) of reactant [R]. The kinetic studies are carried out at very short reaction times in order to work away from the equilibrium of the reaction.<sup>6</sup>

**Eq. 1**

$$-\frac{1}{2} \frac{d[R]}{dt} = -\frac{d[A]}{dt} = +\frac{d[B]}{dt}$$

**Eq. 2**

$$v = k([R]^r, [A]^a, [B]^b)$$

**Table 1.2:** Resolution of differential rate equations for a given reaction ( $2R + A \rightarrow B$ ).<sup>6</sup>

Order of the reaction	Differential equation	Solution	Units of k
0	$-\frac{1}{2} \frac{d[R]}{dt} = k[R]^0$	$[R]_f = [R]_i - 2kt$	mol/L s
1	$-\frac{1}{2} \frac{d[R]}{dt} = k[R]^1$	$\ln[R]_f = \ln[R]_i - 2kt$	1/s
2	$-\frac{1}{2} \frac{d[R]}{dt} = k[R]^2$	$\ln \frac{1}{[R]_f} = \frac{1}{[R]_i} + 2kt$	mol/L s
3	$-\frac{1}{2} \frac{d[R]}{dt} = k[R]^3$	$\frac{1}{2[R]_f^2} = \frac{1}{2[R]_i^2} + 2kt$	mol/L s

**Nomenclature:**  $[R]_f$  (concentration of  $[R]$  at a time= $f$  in mol/L),  $[R]_i$  (concentration of  $[R]$  at a time= $i=0$  in mol/L),  $t$  (time in seconds (s)).

The arrhenius equation (Eq. 3) is employed to determine the activation energy ( $E_a$ ) for a given reaction by plotting the  $\ln K$  (where,  $k$  is the constant rate) versus  $1/T$  (where,  $T$  is the temperature). What this equation indicates is that the higher  $E_a$  is, the higher the temperature will needed to be in order to increase the rate of the reaction.<sup>6</sup>

### Eq. 3

$$\ln k = \ln A - \frac{E_a}{RT}$$

Where,

$A$ = frequency factor (1/s).

$E_a$ = activation energy (kJ/mol).

$T$ = temperature (K).

$R$ = constant (J/mol K).

For a heterogeneous catalysed reaction, the adsorption of the reactants on the active sites of the catalyst are required before the chemical reaction can take place. The distribution of an adsorbate on a surface depends on the pressure of the gas (if the reagent is present in the gaseous phase), the temperature, the nature and area of the catalyst and the nature of the adsorbate. There are known two types of adsorption: chemisorption and physisorption. The difference lies in the strength the adsorbate bonds to the surface of the catalyst, chemisorption occurs when the adsorbate is bonded covalently to the surface of the catalyst, on the contrary during the physisorption the adsorbate is bonded with Van der Waals interactions. Also, the adsorbate chemisorbed loses its free translation movement on the surface due to the covalent bonds, therefore having a negative entropy. The enthalpy for both types of adsorptions is also one of the main difference, where physisorption can reach enthalpies much lower (*i.e c.a* -200 kJ/mol) than chemisorption (*i.e c.a* -20 kJ/mol).<sup>6</sup> The coating degree,  $\theta$ , defines the total number of adsorbate adsorbed on the surface of an adsorbant versus the total possible position given by one gram of it (Eq. 4).<sup>6</sup>

**Eq. 4**

$$\theta = \frac{\text{number of occupied positions}}{\text{total number of available positions}}$$

The first chemisorbed adsorption isotherm was developed by Irving Langmuir, who studied the deterioration of tungsten (W) filaments in electric bulbs. His theory assumes that all adsorption sites are equivalent (each adsorption site is referred as \*) and that the adsorbed molecules do not interact. If the adsorbed molecule is in equilibrium with the bulk phase (Eq. 5), the following steps can be written (Eq. 5.1-5.2). The linearization of Eq. 5.2 rises Eq. 5.3, where the volume of the monolayer,  $V_m$ , can be determined by plotting  $1/v$  vs  $1/P$  and finding the intercept.<sup>6</sup>

**Eq. 5****Eq. 5.1**

$$K_R P_R (N(1-\theta)) = K_{-R} N \theta$$

**Eq. 5.2**

$$\theta = \frac{K_R P}{K_R P + K_{-R}} \times \frac{1/K_{-R}}{1/K_{-R}} = \frac{KP}{1+KP}$$

**Eq. 5.3**

$$\frac{1}{v} = \frac{1}{V_m} + \frac{1}{V_m KP}$$

Where;

$V_m$  = volume of a monolayer.

$v$  = volume of gas adsorbed.

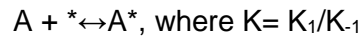
$P$  = pressure of the gas adsorbed.

$K$  = temperature of the experiment.

Langmuir-Hinshelwood and Eley-Rideal form an important class of heterogeneous catalytic reactions. These are two types of reaction mechanisms that involve the adsorption of the reactants to the surface of the catalyst, the chemical reaction and the desorption of the products from the surface of the catalyst to the bulk. The Langmuir-Hinshelwood mechanism state that the chemical reaction takes place when both of the reactants are absorbed on the surface, on the other hand, for the Eley-Rideal mechanism, the chemical reaction happens when one of the reactants is absorbed on the surface of the catalyst and react with the other reactant yet in the bulk phase.<sup>6</sup>

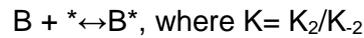
An example of a reaction mechanism that proceeds though the Langmuir-Hinshelwood could involve the following steps for an arbitrary given reaction ( $A + B \rightarrow AB$ ) (Eq. 6 to Eq. 9). Each one of this steps have its corresponding rate,  $r$ .<sup>6</sup>

**Eq. 6**



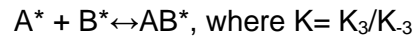
$$\text{Rate: } r_1 = K_1 P_A \theta^* - K_{-1} \theta_A$$

**Eq. 7**



$$\text{Rate: } r_2 = K_2 P_B \theta^* - K_{-2} \theta_B$$

**Eq. 8**



$$\text{Rate: } r_3 = K_3 \theta_B \theta_A - K_{-3} \theta_{AB} \theta^*$$

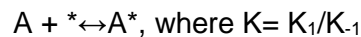
**Eq. 9**



$$\text{Rate: } r_4 = K_4 \theta_{AB} - K_{-4} P_{AB} \theta^*$$

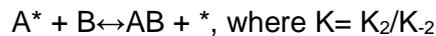
An example of Eley-Rideal mechanism can proceed as stated in Eq.10 and Eq 11 for an arbitrary given reaction of  $(A + B \rightarrow AB)$ .<sup>6</sup>

**Eq. 10**



$$\text{Rate: } r_1 = K_1 P_A \theta^* - K_{-1} \theta_A$$

**Eq. 11**



$$\text{Rate: } r_2 = K_2 \theta_A P_B - K_{-2} P_{AB} \theta^*$$

One way to determine if the reaction proceeds through a Langmuir-Hinshelwood or Eley-Rideal is by monitoring the coverage of A to the surface of the catalyst ( $A^*$ ). If the rate of the reaction increases along with increasing the adsorbed  $A^*$ , then the mechanism goes by Eley-Rideal. Otherwise, Langmuir-Hinshelwood mechanism needs both reactants to be adsorbed on the surface ( $A^*$  and  $B^*$ ) in order for the reaction to happen. If the surface is all covered with  $A^*$ , there will not be enough sites for B to get adsorbed ( $B^*$ ), which will make decrease the rate of the reaction.<sup>6</sup> To give an example, the oxidation of CO to  $CO_2$  with Pt catalyst ( $2CO + O_2 \rightarrow 2CO_2$ ) follow a Langmuir-Hinshelwood mechanism. In this scenario, the rate of adsorption of CO to the surface is greater than the  $O_2$ . If the pressure of CO increases, the rate of the reaction would decrease, since it would not be enough active sites for  $O_2$  to bind.<sup>6</sup>

## 1.2 Hydrogen peroxide ( $H_2O_2$ ).

### 1.2.1 General introduction to $H_2O_2$ .

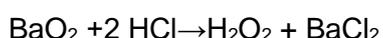
$H_2O_2$  is a colourless liquid, highly soluble in water and a versatile oxidant that is effective over the whole pH range giving water as the only co-product.<sup>10</sup> It has been reported in 2021

that the global annual demand of H<sub>2</sub>O<sub>2</sub> is over 4 million tones.<sup>11</sup> Belgium's Solvay, Germany's Evonik and France's Arkema dominate more than 50 % of the H<sub>2</sub>O<sub>2</sub> production.<sup>12</sup> Applications of H<sub>2</sub>O<sub>2</sub> ranges from bleaching of textiles and paper, food and agriculture industry such as aseptic packaging and antiparasitic in salmon farming, mining and water treatment via advanced oxidation processes (AOPs).<sup>12</sup> Catalytic oxidation of organic compounds using commercial H<sub>2</sub>O<sub>2</sub> also play an essential role in the formation of important industrial chemicals.<sup>13,14</sup> In 2008, Evonik (Degusa) and SKC first industrialised the commercialisation for the oxidation of propylene to propylene oxide (PO) with H<sub>2</sub>O<sub>2</sub> and TS-1 as catalyst. This process can be considered environmentally friendly using H<sub>2</sub>O<sub>2</sub> since only H<sub>2</sub>O is generated as a co-product.<sup>15</sup> However, the main disadvantages of using commercial H<sub>2</sub>O<sub>2</sub> is its costs and safety issues associated with its transportation to its point of use, besides the need to dilute it down to more suitable concentrations (2-8 wt.%).<sup>16,17</sup>

### 1.2.2 Industrial manufacturing routes for H<sub>2</sub>O<sub>2</sub>.

H<sub>2</sub>O<sub>2</sub> was discovered in 1818 by Louis-Jacques Thenard.<sup>18</sup> The process consisted in dissolving barium peroxide (BaO<sub>2</sub>) in hydrochloric acid (HCl) to form H<sub>2</sub>O<sub>2</sub> (Eq. 12).<sup>18</sup> It was not until 1832 where a variant of Thenard's process, that used flourosilic acid instead of HCl, became the first mass produced route to obtain H<sub>2</sub>O<sub>2</sub>.<sup>18</sup>

#### Eq. 12



Several manufacture routes have been developed over the years since the Thenard's variant was first implemented. Sieber and co-workers<sup>19</sup> and Fierro and co-workers<sup>10</sup> categorised and explained respectively in detailed the three routes that have been used for the manufacture of this renowned chemical; *i*) the oxidation of primary and secondary alcohols, *ii*) the electrochemical synthesis and *iii*) the anthraquinone autoxidation process.<sup>19,10</sup> The oxidation of primary and secondary alcohols involved the oxidation of 1-propanol with O<sub>2</sub>, which was used by Shell from the 1957 to 1980's to give the 2-propanone and H<sub>2</sub>O<sub>2</sub>. However, separating the H<sub>2</sub>O<sub>2</sub> from the 2-propanol and 2-propanone was a difficult task leading to low yields of aqueous solution of H<sub>2</sub>O<sub>2</sub>.<sup>10</sup> Arco chemical and Repsol Quimica also manufacture H<sub>2</sub>O<sub>2</sub> via methylbenzylalcohol oxidation, where the methylbenzylalcohol is oxidised with O<sub>2</sub> to give acetophenone and H<sub>2</sub>O<sub>2</sub>. In this scenario, the H<sub>2</sub>O<sub>2</sub> is separated from the acetophenone to obtain an aqueous solution of H<sub>2</sub>O<sub>2</sub> and recover the acetophenone to be reduced back to the original methylbenzylalcohol.<sup>10</sup> The manufacture of H<sub>2</sub>O<sub>2</sub> through the electrochemical process was developed by Dow company and involved a solution containing sodium hydroxide (NaOH). In this case, the O<sub>2</sub>, obtained from the oxidation of the hydroxyl (-OH) is reduced to hydrogen dioxide (HO<sub>2</sub><sup>-</sup>) to give NaHO<sub>2</sub> (alkaline peroxide). This route is best for applications where there is no requirement to

separate the NaOH from the H<sub>2</sub>O<sub>2</sub> such as in pulp bleaching.<sup>10</sup> Finally, the anthraquinone autoxidation process, which was introduced in Germany in the 1940's, is currently the main manufacture route for H<sub>2</sub>O<sub>2</sub> since it accounts for the 95 % of the annual H<sub>2</sub>O<sub>2</sub> production.<sup>20,11</sup> The anthraquinone (AQ), dissolved in suitable organic solvents, is hydrogenated to form 2-alkylanthrahydroquinone (AHQ). This process needs to be carefully controlled to avoid the over-hydrogenation of the un-substituted AQ rings, leading to the un-desired generation of 5,6,7,8- tetrahydroanthraquinone (THAHQ).<sup>10</sup> The AHQ solution is subsequently filtered to remove the catalyst and exposed to oxygen (O<sub>2</sub>) to form the original AQ- to be recycled- and H<sub>2</sub>O<sub>2</sub> (Figure 1.3).<sup>10</sup> In order to separate the H<sub>2</sub>O<sub>2</sub> from the organic matrix solution, demineralised water is added to the top of a high liquid-liquid extraction column. The water flows down the column over perforated trays while the organic solvents are pumped up the column. The water reaches the bottom of the extraction column containing 25-35 wt.% of aqueous H<sub>2</sub>O<sub>2</sub>, while the organic solvents at the top are pumped back to be recycled. The aqueous H<sub>2</sub>O<sub>2</sub> solution needs to be purified and vacuum distilled until obtaining a 70 wt.% H<sub>2</sub>O<sub>2</sub> solution. This concentrated solution needs to be stabilised by the addition of acids and stored in tanks for final use. The transportation of the aqueous H<sub>2</sub>O<sub>2</sub> is a major concern due to the risk of explosion H<sub>2</sub>O<sub>2</sub> has, in fact, there has been several reports where lorries caught fire, for instance in England in 2005.<sup>21,22</sup> Thus, the on-site production of appropriate concentrations of aqueous H<sub>2</sub>O<sub>2</sub> would alleviate many of the safety concerns associated with commercial H<sub>2</sub>O<sub>2</sub>.<sup>16,17</sup>

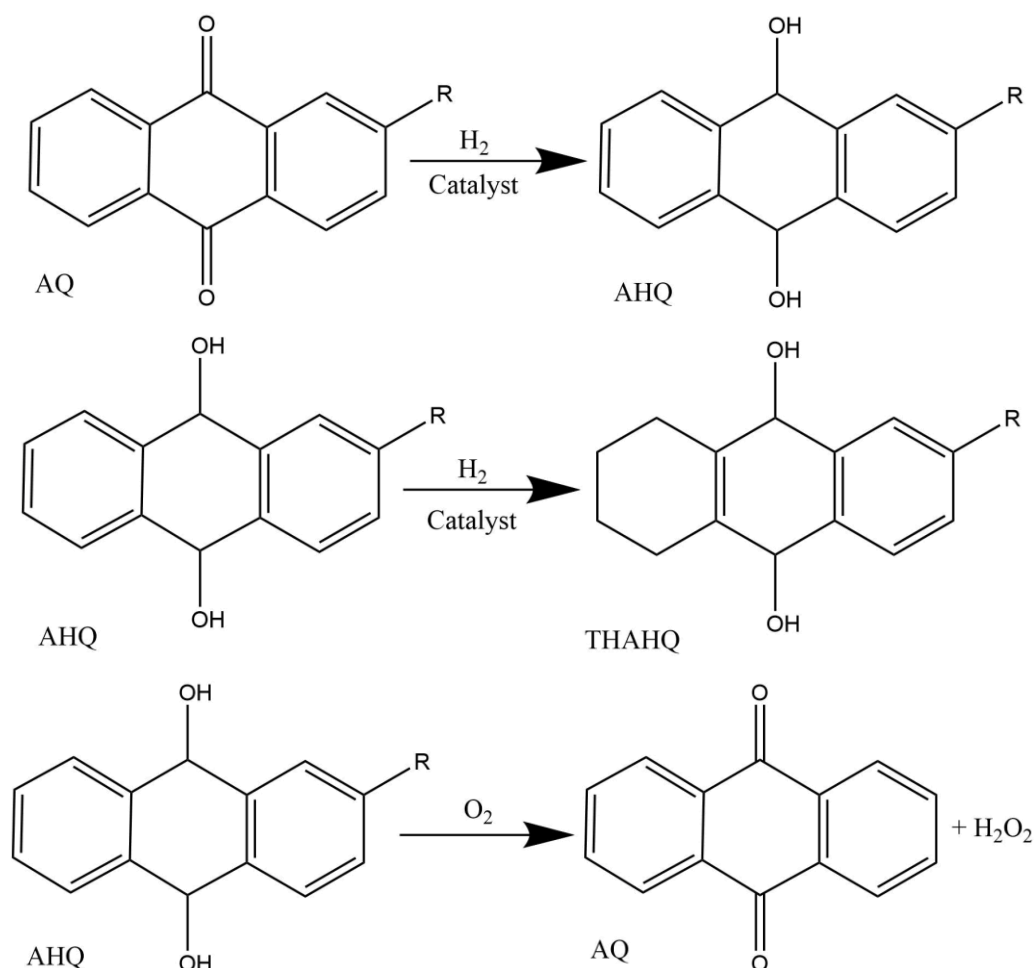


**Figure 1.3:** Production of  $H_2O_2$  by the anthraquinone autoxidation process. **Nomenclature:** Anthraquinone (AQ), 2-alkylanthrahydroquinone (AHQ) and 5,6,7,8 tetrahydroanthraquinone (THAHQ).

The key benefits of the anthraquinone autoxidation process is that it uses mild temperatures and avoid the direct contact of  $O_2$  and  $H_2$  gases, allowing for the formation of relatively high concentrations of  $H_2O_2$  to be produced in the initial phases of the process. On the other hand, there are major concerns about this route:

- The ratio between  $H_2/AQ$  and the AQ exposure time during the hydrogenation is difficult to control, which leads to the undesired formation of THAHQ that has to be continually removed. Also, the solvent is also hydrogenated and oxidised during the AQ cycle, which needs to be also removed. In fact, Beckman *et.al.*, reported in 2003 that approximately 24 million pounds of solvent must be synthesised annually to make up for the loss of the organic solvents during the  $H_2O_2$  synthetic process. The report concluded that the cost associated to the loss of AQ and  $H_2$  due to the generation of undesired products such as the THAHQ and the waste of organic solvents increased the overall cost of  $H_2O_2$  over 12 % at that time.<sup>23</sup>
- The aqueous  $H_2O_2$  solution (25-35 wt.%) after the extraction from the organic matrix solvents needs to be purified and vacuum distilled in order to remove residues of

organic solvents that are still present, generating aqueous H<sub>2</sub>O<sub>2</sub> solution of 70 wt.%. These two steps of purification and distillation involve more energy consumption to the overall process. Beckman *et al.*, reported that the production of H<sub>2</sub>O<sub>2</sub> was 2 million tons per year (in 2003), which required nearly 10 trillion BTU's (British Thermal Units) (corresponding to c.a 293 million kw h<sup>-1</sup>) to be consumed annually to remove the impurities of the organic solvents that were remained in solution after the extraction of the aqueous H<sub>2</sub>O<sub>2</sub>.<sup>23</sup> However, accounting that the current annual H<sub>2</sub>O<sub>2</sub> production is over 4 million tonnes per year,<sup>11</sup> the energy consumption would double the energy Beckman *et al.*, reported in 2003.

- The dilution of the concentrated aqueous H<sub>2</sub>O<sub>2</sub> solution from 70 % to 2-8 wt.% is required for a safe transportation, which generates an increase to the cost of the production.<sup>20</sup>
- The formation of other residues such as; exhaust gas (mesitylene isomers), waste water (containing aromatics, 2-ethyl-anthraquinone, tri-octyl phosphate, tert-butyl urea and K<sub>2</sub>CO<sub>3</sub> (lye) and solid waste (activated Al<sub>2</sub>O<sub>3</sub>) are also formed.<sup>20</sup>

Thus, there is an interest in developing new technologies to decentralise the production of H<sub>2</sub>O<sub>2</sub> and reduce the environmental and financial cost associated with the anthraquinone autoxidation process. Many applications require less < 9 wt.% of H<sub>2</sub>O<sub>2</sub> (pulp and bleaching, chemical synthesis, medical and cosmetic uses) and less than < 0.1 wt.% of H<sub>2</sub>O<sub>2</sub> is required for water treatment purposes.<sup>22</sup> Therefore, the production of H<sub>2</sub>O<sub>2</sub> on-site that could generate concentrations c.a 10 wt.% would be highly desirable in order to avoid the drawbacks stated above in relation with the anthraquinone autoxidation process.<sup>10,20,24,19</sup>

There are several technologies that are currently being investigated for on-site production of H<sub>2</sub>O<sub>2</sub>. For instance, Huang and co-workers<sup>25</sup> have published in 2021 the activity of nanocrystals of Pd doped with sulphur supported on TiO<sub>2</sub> and C for the direct synthesis of H<sub>2</sub>O<sub>2</sub> through electrochemical synthesis (from the reduction of O<sub>2</sub>, reporting 12 mmol L<sup>-1</sup> of H<sub>2</sub>O<sub>2</sub> with 90.8 % selectivity) and photocatalytic synthesis obtaining 35 micromol h<sup>-1</sup> of H<sub>2</sub>O<sub>2</sub>.<sup>25</sup> An alternative approach was reported in 2021 by Cullen and co-workers<sup>11</sup> who obtained a rate of formation of 76.5 mg h<sup>-1</sup> of H<sub>2</sub>O<sub>2</sub> employing only water and an argon plasma whose energy was sourced from solar panels.<sup>11</sup> Another common methodology is the direct synthesis of H<sub>2</sub>O<sub>2</sub> from H<sub>2</sub> and O<sub>2</sub> gas using CO<sub>2</sub>, N<sub>2</sub> or Ar as gaseous diluents to work below the explosive limits. For instance, Yu and co-workers reported in 2021 a bi-metallic Pd@Pt nanocrystal catalysts (Pt/Pd molar ratio of 0.04) with an activity of 2000 mmol<sub>H<sub>2</sub>O<sub>2</sub></sub> g<sup>-1</sup><sub>cat</sub> h<sup>-1</sup> with approximately 20 % H<sub>2</sub> conversion and 60 % H<sub>2</sub>O<sub>2</sub> selectivity.<sup>26</sup> Other sources of H<sub>2</sub> have also been considered to avoid the direct contact of H<sub>2</sub> and O<sub>2</sub> gas during the direct synthesis of H<sub>2</sub>O<sub>2</sub>. For instance, Li and co-workers<sup>27</sup> reported in 2021 the formation of 50 wt.% of H<sub>2</sub>O<sub>2</sub> (99.3 % H<sub>2</sub>O<sub>2</sub> selectivity) by using hydroxylamine

hydrochloride ( $\text{NH}_2\text{OH}\cdot\text{HCl}$ ) as  $\text{H}_2$  source in contact with  $\text{O}_2$  gas and metal-free activated carbon fibres doped with  $\text{N}_2$  groups using pyridine  $\text{N}_2$  as a source. This approach reports promising concentrations of  $\text{H}_2\text{O}_2$  at ambient temperature ( $25\text{ }^\circ\text{C}$ ), however, the reaction required the pH to be regulated at 8.6.<sup>27</sup> Besides, it would be highly advisable to achieve a full conversion of  $\text{NH}_2\text{OH}$  or find means of purification to remove the  $\text{NH}_2\text{OH}$  before the treated water is consumed or pour into the water effluents since  $\text{NH}_2\text{OH}$  is known to be irritant, corrosive, toxic and harmful for the environment.<sup>28</sup>

From this point forward this thesis will focus on the study of the direct synthesis of  $\text{H}_2\text{O}_2$  using diluted gas mixtures of  $\text{H}_2$  and  $\text{O}_2$  gas (*i.e.*  $\text{H}_2$ ,  $\text{O}_2/\text{CO}_2$  or  $\text{H}_2$ ,  $\text{O}_2/\text{N}_2$ ) with supported metallic catalysts. The following part of the introduction offers an overview of the types of supported metallic catalysts that have been investigated (*i.e.* Pd, Au-Pd, Ag-Pd among others combinations) as well as the strategies taken during the synthesis of these supported catalysts to improve the selectivity of these metals towards the formation of  $\text{H}_2\text{O}_2$ .

### **1.2.3 Introduction to the direct synthesis of $\text{H}_2\text{O}_2$ from $\text{H}_2$ and $\text{O}_2$ gas.**

The first patent detailing a direct synthesis route dates from 1914 for Henkel and Weber.<sup>17</sup> There are two reason why the direct synthesis has not been commercialised yet. The first one concerns the combustion of  $\text{H}_2$  and  $\text{O}_2$  gas mixtures, which can occur in a wide range of concentrations ranging between 94-4 mol %  $\text{H}_2$ . The second reason is referred to the competing side reactions (hydrogenation and decomposition) that are commonly taken place during the direct synthesis of  $\text{H}_2\text{O}_2$ , undesirably leading to form  $\text{H}_2\text{O}$ . These competing side reactions (combustion, hydrogenation and decomposition) are thermodynamically more spontaneous than the direct formation of  $\text{H}_2\text{O}_2$  (Figure 1.4).<sup>29</sup> Thus, research has focused on generating supported metallic catalysts with greater selectivity and activity towards  $\text{H}_2\text{O}_2$  production, trying to avoid the formation of  $\text{H}_2\text{O}$ .<sup>17</sup> The combustion reaction has been reported to contribute to the degradation of  $\text{H}_2\text{O}_2$  in greater extent at high temperatures (*c.a*  $17\text{ }^\circ\text{C}$ ). However, working with dilutions of less than  $< 4$  mol % of  $\text{H}_2$  aids to control and minimise it.<sup>30</sup> Thus, the main undesired side reactions are the hydrogenation and decomposition of  $\text{H}_2\text{O}_2$ , which are often measured and reported together, namely  $\text{H}_2\text{O}_2$  degradation.<sup>17,20</sup>

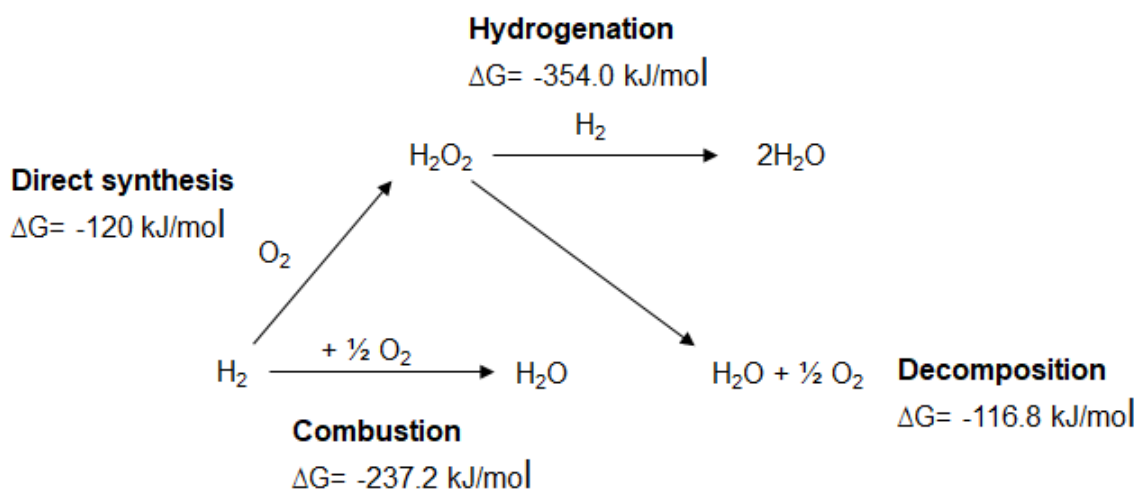


**Figure 1.4:** Schematic representation of *in-situ*  $\text{H}_2\text{O}_2$  and  $\text{H}_2\text{O}$  formation during the direct synthesis from  $\text{H}_2$  and  $\text{O}_2$  gas.

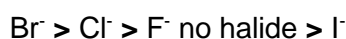
### 1.2.3.1 Supported palladium (Pd) catalysts for the direct synthesis of $\text{H}_2\text{O}_2$ .

Pd is among the noble metals more active towards the direct synthesis of  $\text{H}_2\text{O}_2$ .<sup>29</sup> However, Pd also presents activity for the hydrogenation and decomposition, decreasing the final concentration of  $\text{H}_2\text{O}_2$ .<sup>29</sup> Increasing the selectivity of mono-metallic Pd supported catalysts towards the formation of  $\text{H}_2\text{O}_2$  have been one of the main objectives that have led to investigate different synthetic strategies such as the addition of acids and/or halides to the reaction medium (*i.e.*  $\text{H}_2\text{SO}_4$ , KBr) among others approaches. The characterisation of the Pd nanoparticles by means of spectroscopic and microscopic techniques have also aided to identify the key characteristics of the Pd nanoparticles that drive its selectivity and activity towards the direct formation of  $\text{H}_2\text{O}_2$ . This section aims to overview the activity and characteristics of some reported mono-metallic Pd supported catalysts during the direct synthesis of  $\text{H}_2\text{O}_2$  and discuss some of the common strategies used to enhance its selectivity towards  $\text{H}_2\text{O}_2$ . Table 1.3 lists the activity and selectivity towards the formation of  $\text{H}_2\text{O}_2$  and  $\text{H}_2$  conversion for the mono-metallic Pd supported catalysts discussed in this section for an easier comparison between catalysts. The  $\text{H}_2$  conversion value indicates how active the metal is in dissociating the  $\text{H}_2$  molecule, however, if the moles of  $\text{H}_2$  converted cannot all be accounted for the formation of  $\text{H}_2\text{O}_2$  (according to the reaction  $\text{H}_2 + \text{O}_2 \rightarrow \text{H}_2\text{O}_2$ ), this would indicate that part of the  $\text{H}_2$  moles were used to degrade  $\text{H}_2\text{O}_2$  and form  $\text{H}_2\text{O}$ , therefore, leading to low selectivity's of  $\text{H}_2\text{O}_2$ .

This overview starts by showing how the activity of supported Pd catalysts towards the formation of  $\text{H}_2\text{O}_2$  can vary depending on its oxidation state. For instance, Sansare and co-workers,<sup>31</sup> Choudhary T.V. and co-workers<sup>32</sup> and Choudhary V.T and co-workers<sup>33</sup> demonstrate that the oxidation state of Pd highly influences the catalytic activity towards the direct synthesis of  $\text{H}_2\text{O}_2$ . Metallic palladium ( $\text{Pd}^0$ ) catalysts proved to be active in dissociating  $\text{H}_2$ , but since they did not produce  $\text{H}_2\text{O}_2$ , let the authors to conclude that the

Pd<sup>0</sup> presented selectivity towards the formation of H<sub>2</sub>O by hydrogenating and decomposing the H<sub>2</sub>O<sub>2</sub>. Relatively recently, in 2018, Wang and co-workers<sup>34</sup> concluded, based on computational studies, that the oxidation state of the Pd is one of the most important parameters that needed to be tuned to control the selectivity of Pd.<sup>34</sup> They concluded that what determines the formation of H<sub>2</sub>O or H<sub>2</sub>O<sub>2</sub> are; *i*) the adsorption of the O<sub>2</sub> and H<sub>2</sub> on the surface of the metal or active site, *ii*) the cleavage propensity of the O-O bond of the O<sub>2</sub>, OOH and H<sub>2</sub>O<sub>2</sub> (leading to form H<sub>2</sub>O) and *iii*) O<sub>2</sub>, OOH and H<sub>2</sub>O<sub>2</sub> binding strength to the metal. They evidenced that PdO is less active in dissociating H<sub>2</sub> but since it has less facility to break the O-O bond, it is more selective towards the formation of H<sub>2</sub>O<sub>2</sub> than the analogue Pd<sup>0</sup>.<sup>34</sup>

The addition of mineral acids and halide promoters is a known strategy to improve the selectivity towards H<sub>2</sub>O<sub>2</sub> of mono-metallic supported Pd catalysts by suppressing decomposition and hydrogenation pathways.<sup>17</sup> For instance, Samanta and co-workers<sup>35</sup> studied the addition of halides (KCl, KBr, KI and KF) in acidified solvents with phosphoric acid (H<sub>3</sub>PO<sub>4</sub>) as a source of Brønsted acids (H<sup>+</sup>) using reduced 5 wt.% Pd/C supported catalyst. The use of mineral acids (0.03 M H<sub>3</sub>PO<sub>4</sub>, 1.5 % H<sub>2</sub>O<sub>2</sub> selectivity) or halides (2.7 mM KBr, 0 % H<sub>2</sub>O<sub>2</sub> selectivity) individually with 5 wt.% Pd<sup>0</sup>/C catalyst showed minimal activity towards the formation of H<sub>2</sub>O<sub>2</sub>. Contrarily, this 5 wt.% Pd<sup>0</sup>/C catalyst showed high activity towards the hydrogenation and decomposition of H<sub>2</sub>O<sub>2</sub> (0.03 M H<sub>3</sub>PO<sub>4</sub>, 57.2 % H<sub>2</sub>O selectivity, 61.4 % decomposition) and (2.7mM KBr, 38.5 % H<sub>2</sub>O selectivity, 18 % decomposition).<sup>35</sup> Samanta and co-workers<sup>35</sup> determined that the addition of both, H<sup>+</sup> and halides together was essential to enhance H<sub>2</sub>O<sub>2</sub> selectivity up to 11.5 % using the 5 wt.% Pd<sup>0</sup>/C catalyst. However, the same group have shown that if the Pd is completely oxidised to PdO, the addition of mineral acids (without halides) was enough to enhance the selectivity towards the formation of H<sub>2</sub>O<sub>2</sub> using 2.5 wt.% PdO/H-β catalyst and 0.016 M HCl.<sup>36</sup> Despite this, the amount of mineral acids needs to be carefully measured, since high concentrations promoted Pd leaching.<sup>35</sup> The halides can be sequenced in order of promoting H<sub>2</sub>O<sub>2</sub> selectivity with mono-metallic supported Pd catalysts as follows:



The role of the Cl<sup>-</sup> and Br<sup>-</sup> is considered to be associated with the inhibition of the O-O bond cleavage, whereas the H<sup>+</sup> facilitate the adsorption of halide anion on the Pd clusters, modifying its electronic properties.<sup>37</sup> However, the addition of acids is undesirable for industrial purposes because their use can lead to reactor corrosion in addition to an increase in the cost due to subsequent separation from the product stream.<sup>38</sup> To avoid this, the halides have been incorporated on the catalyst before or after the impregnation of the active

metal. For instance, Choudhary and co-workers<sup>33</sup> studied the incorporation of halides (NH<sub>4</sub>Cl, NH<sub>4</sub>Br, NH<sub>4</sub>F, NH<sub>4</sub>I) over mono-metallic Pd supported on Al<sub>2</sub>O<sub>3</sub>. They concluded that the addition of halides before or after the incorporation of the metal was not relevant in terms of activity. Among all the halides, Br<sup>-</sup> had the ability to promote the activity for H<sub>2</sub>O<sub>2</sub> irrespective of the oxidation state of the Pd (5 wt.% PdO/Al<sub>2</sub>O<sub>3</sub> (32.8 % H<sub>2</sub> conversion, 53.8 % selectivity of H<sub>2</sub>O<sub>2</sub>) and 5 wt.% Pd<sup>0</sup>/Al<sub>2</sub>O<sub>3</sub> (45.8 % H<sub>2</sub> conversion, 52.2 % selectivity of H<sub>2</sub>O<sub>2</sub>)).<sup>33</sup> However, the amount of Br<sup>-</sup> needed to be controlled as high concentrations could poison the active sites decreasing the overall activity.<sup>33</sup> Salmi and co-workers<sup>39</sup> have also studied how the activity and selectivity changes with the presence of Br<sup>-</sup> using 1 wt.% Pd/C catalyst. They soaked a certain amount of solid catalyst (1 wt.% Pd/C) with solutions containing different concentration of Br<sup>-</sup> to determine the effect this halide had on catalytic activity and selectivity. They evidenced that the addition of Br<sup>-</sup> produced modifications on the Pd nanoparticles in terms of specific surface area, oxidation state of the Pd and nanoparticle size. These modifications let the authors to report the best catalytic system to be 1 wt.% Pd/C with a 140 Br<sup>-</sup>/Pd molar ratio (30 % selectivity of H<sub>2</sub>O<sub>2</sub> with c.a 90 % H<sub>2</sub> conversion) with higher selectivity than the unmodified analogue material (10 % selectivity of H<sub>2</sub>O<sub>2</sub> with c.a 90 % H<sub>2</sub> conversion).<sup>39</sup> The addition of acids can be also avoided by using acidic supports, which could serve as an alternative acidic source for the direct synthesis of H<sub>2</sub>O<sub>2</sub>.<sup>40</sup> Song and co-workers<sup>41,40,42</sup> have extensively studied the acidification of supports to improve the selectivity of mono-metallic Pd supported catalysts. For instance, on SBA-15 functionalised with SO<sub>3</sub>H with acidity of 0.79 mmolH<sup>+</sup>/g (0.5 wt.% Pd/SBA-15-SO<sub>3</sub>H), enhanced H<sub>2</sub>O<sub>2</sub> selectivity by 30 %, compared to the Pd supported on bare SBA-15 with <5 % selectivity.<sup>41</sup> The same group also reported Pd supported on two types of functionalised supports; TiO<sub>2</sub> and SiO<sub>2</sub> doped with ZrO (Pd/TiO<sub>2</sub>-ZrO), where the addition of ZrO to TiO<sub>2</sub> enhanced H<sub>2</sub>O<sub>2</sub> selectivity (0.5 wt.% Pd/TiO<sub>2</sub>-ZrO (75 % mol ZrO), 85 % H<sub>2</sub> conversion, 10 % H<sub>2</sub>O<sub>2</sub> selectivity) due to presenting a higher level of acidity compared to the unmodified TiO<sub>2</sub> supported material (0.5 wt.% Pd/TiO<sub>2</sub>, 60 % H<sub>2</sub> conversion, <5 % H<sub>2</sub>O<sub>2</sub> selectivity).<sup>40</sup> The 0.5 wt.% Pd/SiO<sub>2</sub>-SO<sub>3</sub>H catalyst also presented higher selectivity (25 % H<sub>2</sub> conversion, 25 % H<sub>2</sub>O<sub>2</sub> selectivity) than the non-functionalised support (0.5 wt.% Pd/SiO<sub>2</sub>, 70 % H<sub>2</sub> conversion, <5 % H<sub>2</sub>O<sub>2</sub> selectivity).<sup>42</sup> Strukul and co-workers<sup>43</sup> also investigated mono-metallic 2.5 wt.% PdO supported catalysts with ZrO doped with SO<sub>4</sub><sup>2-</sup>, Cl<sup>-</sup>, F<sup>-</sup>, Br<sup>-</sup> in water, CH<sub>3</sub>CH<sub>2</sub>OH and CH<sub>3</sub>OH solvents. They found out that the activity towards the production of H<sub>2</sub>O<sub>2</sub> was shown to vary depending on the solvent and the catalyst used. The highest activity in water was given by 2.5 wt.% PdO/ZrO-F (66 mol<sub>H<sub>2</sub>O<sub>2</sub></sub> kg<sub>cat</sub><sup>-1</sup> h<sup>-1</sup>), in CH<sub>3</sub>CH<sub>2</sub>OH by 2.5 wt.% PdO/ZrO-SO<sub>4</sub><sup>2-</sup> (173 mol<sub>H<sub>2</sub>O<sub>2</sub></sub> kg<sub>cat</sub><sup>-1</sup> h<sup>-1</sup>) and in CH<sub>3</sub>OH by 2.5 wt.% PdO/ZrO-F, 2.5 wt.% PdO/ZrO-SO<sub>4</sub><sup>2-</sup> and 2.5 wt.% PdO/ZrO (all three presented the same activity (520 mol<sub>H<sub>2</sub>O<sub>2</sub></sub> kg<sub>cat</sub><sup>-1</sup> h<sup>-1</sup>)).<sup>43</sup> As the results showed, there was not any significant difference in the activity of the catalysts when using a doped or non-doped support when CH<sub>3</sub>OH was used

as a solvent.<sup>43</sup> Also, they investigated the activity as a function of the oxidation state of Pd with 2.5 wt.% PdO/ZrO-SO<sub>4</sub><sup>2-</sup>, 2.5 wt.% Pd<sup>0</sup>/ZrO-SO<sub>4</sub><sup>2-</sup> and 2.5 wt.% Pd<sup>0</sup>PdO/ZrO-SO<sub>4</sub><sup>2-</sup> in CH<sub>3</sub>CH<sub>2</sub>OH as a solvent.<sup>43</sup> They concluded that the 2.5 wt.% Pd<sup>0</sup>/ZrO-SO<sub>4</sub><sup>2-</sup> catalyst offered higher productivity than the 2.5 wt.% PdO/ZrO-SO<sub>4</sub><sup>2-</sup> analogue but the selectivity of 2.5 wt.% Pd<sup>0</sup>/ZrO-SO<sub>4</sub><sup>2-</sup> rapidly decreased. On the other hand, partially reducing the Pd in 2.5 wt.% Pd<sup>0</sup>PdO/ZrO-SO<sub>4</sub><sup>2-</sup> catalyst showed the best activity with a 800 mol<sub>H<sub>2</sub>O<sub>2</sub></sub> kg<sub>cat</sub><sup>-1</sup> h<sup>-1</sup>.<sup>43</sup> This results indicated that there is an optimum ratio between Pd<sup>0</sup>/PdO in order to balance the high activity of Pd<sup>0</sup> to dissociate H<sub>2</sub> and the high selectivity of PdO in making H<sub>2</sub>O<sub>2</sub> by avoiding the O-O bond cleavage.

The type of the support used to deposit the metal nanoparticles have shown to have an effect on the activity of the Pd nanoparticles. For instance, Hutchings and co-workers<sup>44</sup> studied the activity of the 5 wt.% Pd supported on Al<sub>2</sub>O<sub>3</sub> (9 mol<sub>H<sub>2</sub>O<sub>2</sub></sub> kg<sub>cat</sub><sup>-1</sup> h<sup>-1</sup>), TiO<sub>2</sub> (30 mol<sub>H<sub>2</sub>O<sub>2</sub></sub> kg<sub>cat</sub><sup>-1</sup> h<sup>-1</sup>), C (55 mol<sub>H<sub>2</sub>O<sub>2</sub></sub> kg<sub>cat</sub><sup>-1</sup> h<sup>-1</sup>), MgO (29 mol<sub>H<sub>2</sub>O<sub>2</sub></sub> kg<sub>cat</sub><sup>-1</sup> h<sup>-1</sup>). They determined that C was the most promising among all the supports tested. What it was clear from their results was that the support can drive the type of Pd nanoparticles generated.<sup>44</sup> The same conclusions were drawn by Miquel and co-workers<sup>45</sup> when they tested 2.5 wt.% Pd catalysts on C (1.7 wt.% H<sub>2</sub>O<sub>2</sub>, 23 % H<sub>2</sub> conversion), SiO<sub>2</sub> (0.47 wt.% H<sub>2</sub>O<sub>2</sub>, 21 % H<sub>2</sub> conversion), Al<sub>2</sub>O<sub>3</sub> (0.58 wt.% H<sub>2</sub>O<sub>2</sub>, 27 % H<sub>2</sub> conversion), TiO<sub>2</sub> (0.56 wt.% H<sub>2</sub>O<sub>2</sub>, 31 % H<sub>2</sub> conversion), ZrO<sub>2</sub> (0.67 wt.% H<sub>2</sub>O<sub>2</sub>, 38 % H<sub>2</sub> conversion), CeO<sub>2</sub> (0.39 wt.% H<sub>2</sub>O<sub>2</sub>, 19 % H<sub>2</sub> conversion) and SBA-15 (0.39 wt.% H<sub>2</sub>O<sub>2</sub>, 17 H<sub>2</sub> conversion).<sup>45</sup> In all these catalysts, the Pd mean particle size ranged between 5-4.3 nm except for the SiO<sub>2</sub> (8.5 nm) and the dispersion of the Pd ranged between 0.28-0.24 nm except for the SiO<sub>2</sub> with a 0.16 nm.<sup>45</sup> Miquel and co-workers<sup>45</sup> followed the study of a 2.5 wt.% Pd supported on a wide range of different types of C. They concluded that the surface functionality of the support can massively influence the selectivity of the mono-metallic Pd catalysts towards the direct synthesis of H<sub>2</sub>O<sub>2</sub> and that the 2.5 wt.% Pd supported on black carbon such as XC-72, with relatively ordered graphitic structure and low concentration of carboxylic groups favoured the H<sub>2</sub>O<sub>2</sub> formation (2.5 wt.% Pd/ XC-72, 1.67 wt.% H<sub>2</sub>O<sub>2</sub>, 23 % H<sub>2</sub> conversion). They also concluded that the physicochemical properties of the carbon, chemical state and particle size of the Pd were also relevant characteristics that need to be taken into account when generating mono-metallic Pd supported catalysts.<sup>45</sup> Similar conclusions were stated by Boccuzzi and co-workers<sup>46</sup> who determined that the type of carbon has a major influence and those that present less distorted areas have better activity towards H<sub>2</sub>O<sub>2</sub> production.<sup>46</sup> They correlated the activity of a 1.5 wt.% Pd catalyst supported on SiO<sub>2</sub>, ZrO, ZrO-SO<sub>4</sub><sup>2-</sup>, CeO<sub>2</sub>-SO<sub>4</sub><sup>2-</sup>, CeO<sub>2</sub> with the dispersion and active sites of Pd on the surface.<sup>46</sup> They evidenced that the activity and H<sub>2</sub>O<sub>2</sub> selectivity increased with the acidity of the support (SiO<sub>2</sub>> ZrO-SO<sub>4</sub><sup>2-</sup> > ZrO> CeO<sub>2</sub>-SO<sub>4</sub><sup>2-</sup>>CeO<sub>2</sub>) with the exception of SiO<sub>2</sub>.<sup>46</sup> They proposed

that this trend could be explain in terms of the Pd particle size; since  $\text{SiO}_2 > \text{ZrO-SO}_4^{2-}$  presented an average particle size of 4 nm, whereas  $\text{ZrO} > \text{CeO}_2\text{-SO}_4^{2-} > \text{CeO}_2$  had 1 nm average.<sup>46</sup> The chemisorption of  $\text{O}_2$  on non-defective Pd sites (less energetic) proceeds without dissociation, which leads to the desired  $\text{H}_2\text{O}_2$ . On the contrary, defective sites on Pd nanoparticles such as edges and corners, will dissociate chemisorbed  $\text{O}_2$  leading to the formation of  $\text{H}_2\text{O}$ . They concluded that 1.5 wt.% Pd/ $\text{SiO}_2$  (100mM of  $\text{H}_2\text{O}_2$ , 60 % selectivity of  $\text{H}_2\text{O}_2$ ) had the best activity, because this catalyst had the optimal dispersion to provide Pd nanoparticles between 2-3 nm with less energetic sites.<sup>46</sup> Han and co-workers<sup>47</sup> also investigated the correlation between the nanoparticle size of the Pd and its selectivity towards the direct synthesis of  $\text{H}_2\text{O}_2$ . They evidenced that increasing the loading of Pd led to bigger nanoparticles which were becoming less selective towards the formation of  $\text{H}_2\text{O}_2$ . Their final conclusion stated that the most optimum nanoparticle size to make the formation of  $\text{H}_2\text{O}_2$  prevailing over  $\text{H}_2\text{O}$  was between 1.4-2.5 nm.<sup>47</sup> These studies suggest that each particle size might have a particular nanoparticle Pd shape, whose crystallinity might be influencing the activity. In fact, the selectivity and activity of a catalyst is known to be influenced by the facets enclosed in a particular crystal lattice exposed to the surface,<sup>48</sup> for instance, cubic Pd ( $\{100\}$  facet) nanoparticles are more active than octahedral Pd nanoparticles ( $\{111\}$  facet) in electro catalytic oxygen-reduction reactions.<sup>49</sup> From a synthetic point of view, multi-facet nanoparticles are thermodynamically favoured than single faced nanoparticles, thus, synthetic routes that favoured single-facet are desirable.<sup>50,48</sup> The facets of Pd nanocrystals ( $\{100\}$ ,  $\{110\}$ ,  $\{111\}$ ), which are believed to present different activity according to DFT calculations, where each facet can weaker the O-O bond differently provoking its cleavage. For instance,  $\{111\}$  seems to stretch O-O bond to 0.137 nm whereas  $\{110\}$  and  $\{100\}$  stretch the bond to 0.413 and 0.124 nm respectively promoting its dissociation.<sup>51,52,53</sup> However, this topic is still controversial since other authors claim that the  $\{100\}$  is the most active towards the direct synthesis of  $\text{H}_2\text{O}_2$ .<sup>54</sup>

**Table 1.3:** Comparison between the catalysts activity towards the formation and selectivity of H<sub>2</sub>O<sub>2</sub> and H<sub>2</sub> conversion data for the mono-metallic Pd supported catalysts discussed in the literature above.

Catalysts	H <sub>2</sub> O <sub>2</sub> activity	H <sub>2</sub> O <sub>2</sub> selectivity	H <sub>2</sub> conversion
2.5 wt.% Pd <sup>0</sup> /Ga <sub>2</sub> O <sub>3</sub> <sup>31</sup>	0 wt. %	n.d	20.3 %
2.5 wt.% PdO/Ga <sub>2</sub> O <sub>3</sub> <sup>31</sup>	17.95 wt. %	n.d	21.1 %
2.5 wt.% Pd <sup>0</sup> /Hβ <sup>32</sup>	0 wt. %	0 %	65 %
2.5 wt.% PdO/Hβ <sup>32</sup>	10 wt. %	c.a 20 %	c.a 32.5 %
2.5 wt.% Pd <sup>0</sup> /SiO <sub>2</sub> <sup>33</sup>	0 wt. %	0	50.3 %
2.5 wt.% PdO/SiO <sub>2</sub> <sup>33</sup>	8.3 wt. %	21.3 %	38.9 %
5 wt.% Pd <sup>0</sup> /C <sup>35</sup>	n.d	11.5 %	36.2 %
2.5 wt.% PdO/H-β <sup>36</sup>	n.d	70 %	20 %
5 wt.% Pd <sup>0</sup> /Al <sub>2</sub> O <sub>3</sub> <sup>55</sup>	23.9 wt. %	52.2 %	45.8 %
5 wt.% PdO/Al <sub>2</sub> O <sub>3</sub> <sup>55</sup>	18.6 wt. %	53.8 %	32.8 %
0.5 wt.% Pd/SBA-15-SO <sub>3</sub> H <sup>41</sup>	10 wt. %	30 %	c.a 40 %
0.5 wt.% Pd/TiO <sub>2</sub> -ZrO <sup>40</sup>	10 wt. %	10 %	85 %
0.5 wt.% Pd/SiO <sub>2</sub> -SO <sub>3</sub> H <sup>42</sup>	c.a 6 wt. %	25 %	25 %
2.5 wt.% Pd <sup>0</sup> PdO/ZrO-SO <sub>4</sub> <sup>2-43</sup>	0.2 wt. %	28	70 %
5 wt.% Pd/C <sup>44</sup>	55 mol <sub>H<sub>2</sub>O<sub>2</sub></sub> kg <sub>cat</sub> <sup>-1</sup> h <sup>-1</sup>	n.d	n.d
2.5 wt.% Pd/XC-72 <sup>45</sup>	1.67 wt. %	74 %	23 %
1.5 wt.% Pd/SiO <sub>2</sub> <sup>46</sup>	100 mM	60 %	n.d
1 wt.% Pd/C (140 molar ratio Br/Pd) <sup>39</sup>	n.d	30 %	c.a 90 %

**n.d:** not determined. **Reaction conditions:** **Reference 31:** 150 mL aqueous solution (0.02 M H<sub>2</sub>SO<sub>4</sub>), catalyst (0.5 g), 2.8 mol % H<sub>2</sub> with O<sub>2</sub> (flow rate: 11.5 cm<sup>3</sup>/min), atmospheric pressure, 25 °C, 3 h. **Reference 32:** 150 mL aqueous solution (0.03 M H<sub>3</sub>PO<sub>4</sub>), catalyst (0.5 g), 4.6 mol % H<sub>2</sub> with O<sub>2</sub> (flow rate: 0.7 mL/min), atmospheric pressure, 25 °C, 3 h. **Reference 33:** 150 mL aqueous solution (0.03 M H<sub>3</sub>PO<sub>4</sub>), catalyst (0.5 g), 4.6 mol % H<sub>2</sub> with O<sub>2</sub> (flow rate: 15.5 mL/min), atmospheric pressure, 27 °C, 3 h. **Reference 35:** 150 mL aqueous solution (0.03 M H<sub>3</sub>PO<sub>4</sub>, 2.7 mmol/L KBr), catalyst (0.5 g), 4.6 mol % H<sub>2</sub> with O<sub>2</sub> (flow rate: 15.5 mL/min), atmospheric pressure, 27 °C, 3 h. **Reference 36:** 150 mL aqueous solution (0.016 M HCl), catalyst (0.5 g), 1.7 mol % H<sub>2</sub> with O<sub>2</sub> (flow rate: 15.5 mL/min), atmospheric pressure, 22 °C, 3 h. **Reference 55:** 150 mL aqueous solution (0.03 M H<sub>3</sub>PO<sub>4</sub>, 5 wt.% NH<sub>4</sub>Br), catalyst (0.5 g), 4.6 mol % H<sub>2</sub> with O<sub>2</sub> (flow rate: 15.5 mL/min), atmospheric pressure, 27 °C, 3 h. **Reference 41:** 80 mL CH<sub>3</sub>OH, catalyst (1.0 g), H<sub>2</sub>/N<sub>2</sub> (25 mol % H<sub>2</sub>) and O<sub>2</sub>/N<sub>2</sub> (50 mol % O<sub>2</sub>) (flow rate: 44 cm<sup>3</sup>/min), 1000 rpm, 28 °C, 6 h. **Reference 40:** 80 mL CH<sub>3</sub>OH, catalyst (1.0 g), H<sub>2</sub>/N<sub>2</sub> (25 mol % H<sub>2</sub>) and O<sub>2</sub>/N<sub>2</sub> (50 mol % O<sub>2</sub>) (flow rate: 44 cm<sup>3</sup>/min), 1000 rpm, 28 °C, 6 h. **Reference 42:** 80 mL CH<sub>3</sub>OH, catalyst (1.0 g), H<sub>2</sub>/N<sub>2</sub> (25 mol % H<sub>2</sub>) and O<sub>2</sub>/N<sub>2</sub> (50 mol % O<sub>2</sub>) (flow rate: 44 cm<sup>3</sup>/min), 1000 rpm, 28 °C, 6 h. **Reference 43:** 100 mL CH<sub>3</sub>CH<sub>2</sub>OH (0.03 M H<sub>2</sub>SO<sub>4</sub>), catalyst (0.135 g), H<sub>2</sub>, O<sub>2</sub>/N<sub>2</sub> (H<sub>2</sub>:O<sub>2</sub>:N<sub>2</sub>, 10:10:80, flow rate: 50 cm<sup>3</sup>/min), 20 °C, 2 h. **Reference 44:** 8.5 g (5.6 g CH<sub>3</sub>OH, 2.9 g H<sub>2</sub>O), catalyst (0.05 g), 420 psi of 5 % H<sub>2</sub> /CO<sub>2</sub>, 160 psi of 25 % O<sub>2</sub>/CO<sub>2</sub>, 1200 rpm, 2 °C, 0.5 h. **Reference 45:** 60 mL (50 mL CH<sub>3</sub>CH<sub>2</sub>OH, 10 mL water, 28 mM HCl), catalyst (0.05 g), H<sub>2</sub>, O<sub>2</sub>/N<sub>2</sub> (H<sub>2</sub>:O<sub>2</sub>:N<sub>2</sub>, 1:4:1, 60 cm<sup>3</sup>/min), 10 °C, 4 h. **Reference 46:** 100 mL CH<sub>3</sub>OH (0.03M H<sub>2</sub>SO<sub>4</sub>), catalyst (0.05 g), H<sub>2</sub>, O<sub>2</sub>/CO<sub>2</sub> (H<sub>2</sub>:O<sub>2</sub>:CO<sub>2</sub>: 3.6: 7.2: 89.2, 10 atm), 1200 rpm, 20 °C, 5 h. **Reference 39:** 420 mL CH<sub>3</sub>OH, catalyst (0.15 g), flowing H<sub>2</sub>, 6 bar O<sub>2</sub>, 20.2 bar CO<sub>2</sub> (3.5 % H<sub>2</sub>: 21.5 % O<sub>2</sub>: 75 % CO<sub>2</sub>), 1000 rpm, 3 °C, 3 h.

### 1.2.3.2 Supported gold-palladium (AuPd) catalysts for the direct synthesis of H<sub>2</sub>O<sub>2</sub>.

For many years Au has been used for fine jewellery and art work, therefore Au as material has had little interest in chemistry.<sup>56</sup> However, in 1987 Haruta and co-workers<sup>57</sup> reported that supported nanoparticles of Au were active towards the oxidation of CO at ambient temperature.<sup>57</sup> This led to lots of studies using supported Au nanoparticles for the synthesis of vinyl chloride, selective hydrogenations, besides CO oxidations.<sup>56</sup> Hutchings and co-workers<sup>58</sup> reported in 2002 that mono-metallic Au supported on Al<sub>2</sub>O<sub>3</sub> (5 wt.% Au/Al<sub>2</sub>O<sub>3</sub>) also had activity towards the direct synthesis of H<sub>2</sub>O<sub>2</sub> and when alloyed with Pd (2.5 wt.% Au-2.5 wt.% Pd/Al<sub>2</sub>O<sub>3</sub>), the activity was greatly enhanced compared to mono-metallic 5 wt.% Pd/Al<sub>2</sub>O<sub>3</sub> supported catalyst.<sup>58</sup> Their results showed that the 2.5 wt.% Au-2.5 wt.% Pd/Al<sub>2</sub>O<sub>3</sub> catalyst presented the highest productivity (4460 mol<sub>H<sub>2</sub>O<sub>2</sub></sub> kg<sub>cat</sub><sup>-1</sup> h<sup>-1</sup>) followed by the 5 wt.% Au/Al<sub>2</sub>O<sub>3</sub> (1530 mol<sub>H<sub>2</sub>O<sub>2</sub></sub> kg<sub>cat</sub><sup>-1</sup> h<sup>-1</sup>) and 5 wt.% Pd/Al<sub>2</sub>O<sub>3</sub> (370 mol<sub>H<sub>2</sub>O<sub>2</sub></sub> kg<sub>cat</sub><sup>-1</sup> h<sup>-1</sup>).<sup>58</sup> They concluded that there was a synergic effect between the two metals, with Pd acting as a promoter of the Au.<sup>58</sup> Many authors have been investigating over the years what are the parameters and the characteristics that AuPd nanoparticles need to have to achieve outstanding performance towards the direct synthesis of H<sub>2</sub>O<sub>2</sub>. Table 1.4 lists the activity and selectivity towards the formation of H<sub>2</sub>O<sub>2</sub> as well as H<sub>2</sub> conversion for some AuPd bi-metallic supported catalysts discussed in this section for the sake of comparison.

The inhibition of O-O bond cleavage has been reported as a key factor in promoting catalytic selectivity towards the direct synthesis of H<sub>2</sub>O<sub>2</sub>. In fact, the addition of Au to Pd has shown to greatly suppress the cleavage of O-O bond that leads to the formation of H<sub>2</sub>O. For instance, Han and co-workers<sup>59</sup> synthesised a series of bi-metallic AuPd supported catalysts varying the Pd: Au ratio but keeping a fixed loading (3 wt.% AuPd/TiO<sub>2</sub>). They evidenced that the best Pd: Au ratio was the bi-metallic 2.0 wt.% Pd- 1.0 wt.% Au/TiO<sub>2</sub> catalyst with a H<sub>2</sub>O<sub>2</sub> synthesis rate of 2330 mol<sub>H<sub>2</sub>O<sub>2</sub></sub> kg<sub>cat</sub><sup>-1</sup> h<sup>-1</sup>.<sup>59</sup> They determined that the hydrogenation rate increased rapidly with increasing the Pd: Au ratio. The analysis and experimental data obtained from the CO-diffuse reflectance infrared fourier transform spectroscopy (CO-DRIFTS) revealed that increasing the Pd: Au ratio enhanced the formation of contiguous Pd ensembles responsible for the hydrogenation of H<sub>2</sub>O<sub>2</sub>.<sup>59</sup> They evidenced that the Au had a dilution effect, segregating the Pd ensembles and forming individual Pd atoms. According to their conclusions, mono dispersed Pd atoms surrounded by Au were the ones capable to enhance the selectivity towards the H<sub>2</sub>O<sub>2</sub> and minimise its hydrogenation.<sup>59</sup> In addition to this, Zecca and co-workers have also evidenced that the addition of Au as a secondary metal to Pd aided to limit the combustion of H<sub>2</sub>.<sup>60</sup>

Some authors have also reported that the dispersion of Pd nanoparticles is one of the key parameters when it comes to synthesise supported metal catalysts for the direct synthesis

for H<sub>2</sub>O<sub>2</sub>. For instance, Strukul and co-workers<sup>61</sup> evidenced the effect that Au had on Pd when the metals were deposited on sulphated ZrO and CeO<sub>2</sub>.<sup>61</sup> They concluded that the bi-metallic PdAu/ZrO-SO<sub>4</sub><sup>2-</sup> (1270 mol<sub>H<sub>2</sub>O<sub>2</sub></sub> kg<sub>cat</sub><sup>-1</sup> h<sup>-1</sup>) and PdAu/CeO<sub>2</sub>-SO<sub>4</sub><sup>2-</sup> catalysts (720 mol<sub>H<sub>2</sub>O<sub>2</sub></sub> kg<sub>cat</sub><sup>-1</sup> h<sup>-1</sup>) were more active than the mono-metallic Pd/ ZrO-SO<sub>4</sub><sup>2-</sup> (1070 mol<sub>H<sub>2</sub>O<sub>2</sub></sub> kg<sub>cat</sub><sup>-1</sup> h<sup>-1</sup>) and Pd/ CeO<sub>2</sub>-SO<sub>4</sub><sup>2-</sup> (370 mol<sub>H<sub>2</sub>O<sub>2</sub></sub> kg<sub>cat</sub><sup>-1</sup> h<sup>-1</sup>) ones due to the Au enhancing the dispersion of Pd.<sup>61</sup> In addition, they found that Au promoted the formation of less defective sites (faces {111} of Pd) as well as donating electron density to Pd.<sup>61</sup> Mikkola and co-workers<sup>62</sup> also evidenced this electronic effect of Au on Pd by x-ray photoelectron spectroscopy (XPS) and justified it by the Pd being more electronegative than Au, reporting that a bi-metallic AuPd system supported on titania-nanowires (1.0 wt.% Au-1.0 wt.% Pd/NWs-TiO<sub>2</sub>) offered greater selectivity towards the H<sub>2</sub>O<sub>2</sub> (25 %) in comparison to the mono-metallic Pd (1.0 wt.% Pd/NWs-TiO<sub>2</sub>) catalyst with a selectivity *c.a* 5 %.<sup>62</sup> Other authors have also reported better performance of bi-metallic AuPd supported catalysts in comparison to the mono-metallic analogues, such as Matsumoto and co-workers<sup>63</sup> who investigated the activity of different ratios of bi-metallic AuPd colloidal suspension towards the direct synthesis of H<sub>2</sub>O<sub>2</sub>. They determined that the most optimum colloidal suspension was 75 mol % Au-25 mol % Pd which presented a rate of H<sub>2</sub>O<sub>2</sub> formation of 60 mM h<sup>-1</sup> and 100 % H<sub>2</sub>O<sub>2</sub> selectivity. On the other hand, 100 mol % Pd suspension presented *c.a* 70 mM h<sup>-1</sup> formation and 50 % selectivity of H<sub>2</sub>O<sub>2</sub>.<sup>63</sup> According to their conclusions the bi-metallic 75 mol % Au-25 mol % Pd was the ratio that gave the lowest rate of H<sub>2</sub>O<sub>2</sub> decomposition because it had the highest percentage of Au on the surface. Thus, they concluded that Au was actually enhancing the selectivity of Pd towards the H<sub>2</sub>O<sub>2</sub>.<sup>63</sup>

There are several reports in the literature working with different supports as a means of enhancing the selectivity of the AuPd nanoparticles towards the direct synthesis of H<sub>2</sub>O<sub>2</sub>. For instance, Hutchings and co-workers<sup>44</sup> synthesised bi-metallic 2.5 wt.% Au- 2.5 wt.% Pd nanoparticles supported on a wide range of supports such as C, TiO<sub>2</sub>, Al<sub>2</sub>O<sub>3</sub> and MgO. The bi-metallic 2.5 wt.% Au- 2.5 wt.% Pd /C, (110 mol<sub>H<sub>2</sub>O<sub>2</sub></sub> kg<sub>cat</sub><sup>-1</sup> h<sup>-1</sup>, 80 % selectivity H<sub>2</sub>O<sub>2</sub>) and 2.5 wt.% Au- 2.5 wt.% Pd /TiO<sub>2</sub> (64 mol<sub>H<sub>2</sub>O<sub>2</sub></sub> kg<sub>cat</sub><sup>-1</sup> h<sup>-1</sup>, 70 % selectivity H<sub>2</sub>O<sub>2</sub>) catalysts have shown the most promising results towards the direct synthesis of H<sub>2</sub>O<sub>2</sub>. They evidenced that there was a correlation between the acidity of the supports and the rate of H<sub>2</sub>O<sub>2</sub>. Bi-metallic AuPd supported catalysts on C and TiO<sub>2</sub> had the highest productivity of H<sub>2</sub>O<sub>2</sub> with the lowest rate of hydrogenation. The authors concluded that supports with low isoelectronic points such as C were the most promising because the isoelectric point controls the surface charge, and basic supports enhance the selectivity of the metals towards the formation of H<sub>2</sub>O. This is another evidence showing how avoiding the O-O bond cleavage is the main objective towards obtaining the best performance.<sup>44</sup> Other authors have employed and investigated other types of carbons that could also lead to size-controlled AuPd

nanoparticles formation, which is believed to have an effect in the selectivity of the AuPd catalysts as it happened to the mono-metallic Pd systems. For instance, Choi and co-workers<sup>64</sup> reported a series of bi-metallic AuPd catalysts on a wide range of carbons (activated carbon (AC), multiwalled carbon nanotubes (MWNTs), carbon black (CB), ordered mesoporous carbon (CMK-3G)). The supports were pre-treated with 0.23 M of HNO<sub>3</sub> before the incorporation of the Au and Pd to generate oxygen functional groups on the surface. They showed that the dispersion of the nanoparticles had a correlation with the density of oxygen functional groups on the surface of the carbon. In fact, the bi-metallic AuPd catalysts supported on AC, CMK-3 and CMK-3G had greater dispersion of metal particles than the bi-metallic AuPd catalysts supported on carbon with low oxygen content (CB and MWNT). The shift in the binding energy of metallic gold (Au<sup>0</sup>) and Pd<sup>2+</sup> (shift of -0.3 eV for Au<sup>0</sup> and 0.2 eV shift for Pd<sup>2+</sup>) seen for the bi-metallic AuPd supported on AC, CMK-3 and CMK-3G led the authors conclude that these catalysts presented AuPd alloyed nanoparticles. On the other hand, bi-metallic AuPd supported on CB and MWNT did not show any shift in the XPS binding energy. Besides, x-ray diffraction (XRD) spectroscopy showed reflections for large Au particles of these two last catalysts. The authors conclude that the oxygen functional group content on the surface of the carbon affected the dispersion and subsequently the formation of AuPd alloyed nanoparticles.<sup>64</sup> The bi-metallic 2.5 wt.% Au-2.5 wt.% Pd/CB (100 % H<sub>2</sub> conversion, c.a 15 % H<sub>2</sub>O<sub>2</sub> selectivity) and 2.5 wt.% Au-2.5 wt.% Pd/MWNTs (100 % H<sub>2</sub> conversion, c.a 5 % H<sub>2</sub>O<sub>2</sub> selectivity) catalysts had the fastest consumption of H<sub>2</sub> but poorer H<sub>2</sub>O<sub>2</sub> selectivity due to the unsuccessful formation AuPd alloys.<sup>64</sup> In addition to this, they evidence that 2.5 wt.% Au-2.5 wt.% Pd/CB and 2.5 wt.% Au-2.5 wt.% Pd/MWNTs presented a greater activity towards the hydrogenation and decomposition which they related to the presence of segregated Pd-only nanoparticles within these two catalysts.<sup>64</sup> They also evidenced that the selectivity towards the H<sub>2</sub>O<sub>2</sub> could be related to the pore volume of the support, where the 2.5 wt.% Au-2.5 wt.% Pd/CMK-3G catalyst (60 % H<sub>2</sub> conversion, 60 % selectivity of H<sub>2</sub>O<sub>2</sub>) presented higher selectivity than the 2.5 wt.% Au-2.5 wt.% Pd/AC analogue (40 % H<sub>2</sub> conversion, 40 % H<sub>2</sub>O<sub>2</sub> selectivity).<sup>64</sup> Zecca and co-workers<sup>65</sup> also supported the evidence of the Au benefiting and promoting the activity and selectivity of Pd. They reported that bi-metallic AuPd supported catalysts (2 wt.% Au-2 wt.% Pd/ MD10-4) gave better activity towards the direct synthesis of H<sub>2</sub>O<sub>2</sub> (109 mmolH<sub>2</sub>O<sub>2</sub>/molH<sub>2</sub>) compared to the mono-metallic Pd one (3 wt.% Pd/ MD10-4, 64. mmolH<sub>2</sub>O<sub>2</sub>/molH<sub>2</sub>).<sup>65</sup> They concluded that the reason for the bi-metallic AuPd catalyst to have better activity than the mono-metallic Pd one was attributed to the formation of AuPd alloys. They claimed that the 99 % of the nanoparticles of the 2 wt.% Au-2 wt.% Pd/ MD10-4 catalyst were AuPd alloys.<sup>65</sup>

The literature discussed in this section so far let to conclude that Au is able to modify structurally the Pd nanoparticles. For instance, as Strukul and co-workers<sup>61</sup> reported previously, Au is able to promote the formation of Pd nanoparticles with less defective sites (faces {111} of Pd) or as Han and co-workers<sup>59</sup> claiming that Au has a diluent effect on Pd nanoparticles. However, what Choi and co-workers<sup>64</sup> as well as Zecca and co-workers<sup>65</sup> stated clear is that the formation of AuPd alloys is essential for Au to be able to modify structurally the Pd nanoparticles and subsequently enhance its selectivity towards the direct synthesis of H<sub>2</sub>O<sub>2</sub>.

Besides the formation of AuPd alloys to be a key factor to enhance the selectivity towards the direct synthesis of H<sub>2</sub>O<sub>2</sub>, the size of the AuPd alloyed nanoparticles are also a key parameter as Neira D'Angelo and co-workers<sup>66</sup> have also evidenced. They investigated how to control the size of mono and bi-metallic AuPd nanoparticles and avoid the aggregation of Pd by using silica capillaries coated with polyelectrolyte multilayers (PEMs).<sup>66</sup> These PEMs, which contain highly distributed charged surfaces for binding metal ions, aid to inhibit the formation of Pd ensembles that are commonly reported to be selective towards the degradation of H<sub>2</sub>O<sub>2</sub>.<sup>66</sup> They reported the activity towards the direct synthesis of H<sub>2</sub>O<sub>2</sub> of the mono and bi-metallic AuPd catalysts supported on silica capillaries with two coatings of 2PEMs; 1.56 wt.% Pd/2PEMs (80 mol<sub>H<sub>2</sub>O<sub>2</sub></sub> kg<sub>cat</sub><sup>-1</sup> h<sup>-1</sup> of H<sub>2</sub>O<sub>2</sub>, 40 % H<sub>2</sub> conversion, c.a 40 % H<sub>2</sub>O<sub>2</sub> selectivity), 0.96 wt.% Au/2PEMs (100 mol<sub>H<sub>2</sub>O<sub>2</sub></sub> kg<sub>cat</sub><sup>-1</sup> h<sup>-1</sup> of H<sub>2</sub>O<sub>2</sub>, 25 % H<sub>2</sub> conversion, 70 % H<sub>2</sub>O<sub>2</sub> selectivity) and 0.73 wt.% Au-1.01 wt.% Pd/2PEMs (200 mol<sub>H<sub>2</sub>O<sub>2</sub></sub> kg<sub>cat</sub><sup>-1</sup> h<sup>-1</sup>, 40 % H<sub>2</sub> conversion, 70 % H<sub>2</sub>O<sub>2</sub> selectivity).<sup>66</sup> The results after the testing evidenced that bi-metallic over-performed the mono-metallic analogues, not only in terms of H<sub>2</sub>O<sub>2</sub> production, but in terms of stability since the 1.56 wt.% Pd/2PEMs leached during the course of the reaction. The high activity shown for the mono-metallic 0.96 wt.% Au/2PEMs (0.6 ± 0.2 nm) catalyst in comparison to the 1.56 wt.% Pd/2PEMs (1 ± 0.3 nm) catalyst was justified by the small Au nanoparticles this PEMs allowed to achieve. They concluded that using a support that allows the formation of AuPd nanoparticles whose size can be controlled leads to catalysts (e.g. 0.73 wt.% Au-1.01 wt.% Pd/2PEMs, 0.8 ± 0.2 nm) with high activity for the direct synthesis of H<sub>2</sub>O<sub>2</sub>.<sup>66</sup>

As mentioned with the mono-metallic Pd catalysts, pre-treatment of the support has also been investigated in order to suppress the side reaction with acids (2% HNO<sub>3</sub>); Gudarzi *et al.*, with 2.5 wt.% Pd- 2.5 wt.% Au/C<sup>67</sup>, Edwards *et al.* with 2.5 wt.% Au-2.5 wt.% Pd supported on C,<sup>68</sup> Al<sub>2</sub>O<sub>3</sub><sup>68</sup> and SiO<sub>2</sub><sup>68</sup> and TiO<sub>2</sub><sup>69,68</sup> and Ntainjua *et al.* with 2.5 wt.% Pd-2.5 wt.% Au /CeO<sub>2</sub><sup>70</sup> have been investigated. All these instances show an enhancement in the activity towards H<sub>2</sub>O<sub>2</sub> formation compared to the AuPd analogue on bare support without pre-treatment with HNO<sub>3</sub>. Edwards *et al.*, stated that the best performance was achieved

when the support was pre-treated before the incorporation of the metals.<sup>68</sup> The bi-metallic 2.5 wt.% Au-2.5 wt.%Pd/C catalyst pre-treated with 2 wt.% acetic acid ( $\text{CH}_3\text{COOH}$ ) presented the best activity, followed by the supports pre-treated with 2 wt.%  $\text{HNO}_3$ , 2 wt.% hydrochloric acid (HCl) and 2 wt.%  $\text{H}_3\text{PO}_4$ .<sup>68</sup> Edwards *et al.*, concluded that the acidity aids to narrow the particle size distribution, enhancing the dispersion of Au, generating smaller AuPd nanoparticles with the same morphology.<sup>68</sup> The results reported from Edwards *et al.*, allow to state that developing a synthetic catalytic methodology to successfully form bi-metallic AuPd alloy size-controlled nanoparticles are key to obtain promising activity towards the direct synthesis of  $\text{H}_2\text{O}_2$ . Sankar *et al.*, developed a synthetic methodology namely, modified impregnation, where the impregnation of the support with palladium chloride ( $\text{PdCl}_2$ ) -acidified with HCl (0.58M)- and chloroauric acid ( $\text{HAuCl}_4$ ), followed by a reduction treatment, generates highly active AuPd supported alloyed nanoparticles. It has been reported that the addition of  $\text{Cl}^-$  promotes the formation of  $\text{AuCl}_4^-$  and  $\text{PdCl}_4^-$ , which helps to homogenise both metals in solution in order to enhance the dispersion during the impregnation.<sup>71</sup> The reduction step after the impregnation was found to be critical in order to achieve the best catalytic stability, at expenses of the activity, which decreases with increasing the reduction temperature.<sup>71</sup> The non-reduced 0.5 wt.% Au-0.5 wt.% Pd/ $\text{TiO}_2$  catalyst lost its activity from 99 to 40 mol  $\text{H}_2\text{O}_2$   $\text{kg}_{\text{cat}}^{-1}$   $\text{h}^{-1}$  upon re-use, however, after the reduction (5%  $\text{H}_2/\text{Ar}$ , 400 °C, 4h), the catalyst was able to keep the activity after four consecutive reactions.<sup>71</sup> Scanning transmission electron microscope (STEM) studies of fresh and reduced samples at different temperatures determined that the reduction step helped the formation of homogeneous AuPd alloys with narrow particle size distribution (2-5 nm).<sup>71</sup> Boccuzzi and co-workers<sup>46</sup> also evidenced how the stability and re-usability of the bi-metallic AuPd supported catalyst was found to be influenced by the calcination temperature and treatment atmosphere. Boccuzzi and co-workers found that despite the un-calcined 1.5 wt.% AuPd/ $\text{SiO}_2$  catalyst presented the highest activity, it deactivated over time due to Pd leaching, whereas the calcined at 500 °C was stable upon-reuse.<sup>46</sup> Thus, the calcination treatment seemed to be a requisite to generate stable AuPd supported nanoparticles as Boccuzzi and co-workers stated. The same tendency was reported for bi-metallic 2.5 wt.5 Au-2.5 wt.% Pd/ $\text{TiO}_2$  catalysts studied by Hutchings co-workers.<sup>72</sup> The XPS studies over a range of bi-metallic 2.5 wt.5 Au-2.5 wt.% Pd/ $\text{TiO}_2$  catalysts, fresh and calcined at different temperatures, evidenced the formation of core Au/Pd shell whose stability was greater than the un-calcined catalyst.<sup>72</sup> Kiely and co-workers<sup>73</sup> also reported the formation of core Au/Pd shell nanoparticles studied by scanning transmission electron microscopy x-ray energy dispersive spectroscopy (STEM-XEDS) over a rage of fresh and calcined 2.5 wt.% Au-2.5 wt.% Pd/ $\text{Al}_2\text{O}_3$  samples. The Au core/Pd shell morphology is formed during the calcination treatment and the degree of segregation and extend of the shell thickness increases with temperature (Figure 1.5).<sup>73</sup>

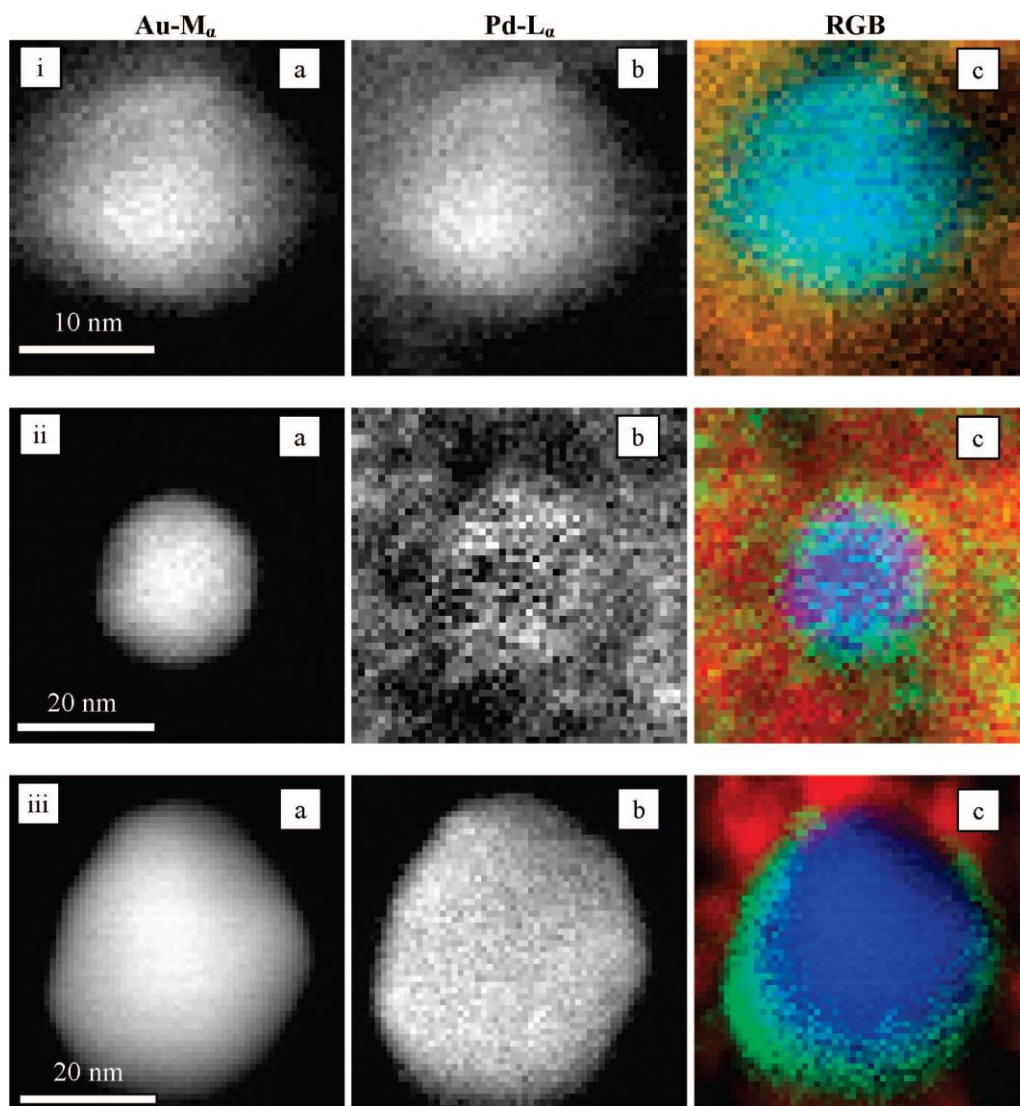


**Figure 1.5:** Montage of STEM-XEDS data of the bi-metallic 2.5 wt.% Au-2.5 wt.% Pd/Al<sub>2</sub>O<sub>3</sub> catalysts at various heat treatments. **Nomenclature:** **(i)** Uncalcined, **(ii)** calcined at 200 °C, and **(iii)** calcined at 400 °C. **a)** Au-M<sub>R</sub>, **b)** Pd-L<sub>R</sub> and **c)** RGB reconstruction where **red)** Al, **green)** Pd and **blue)** Au.<sup>73</sup>

**Table 1.4:** Comparison between the catalyst's activity towards the formation and selectivity of H<sub>2</sub>O<sub>2</sub> and H<sub>2</sub> conversion for the bi-metallic AuPd supported catalysts discussed in the literature above.

Catalysts	H <sub>2</sub> O <sub>2</sub> activity	H <sub>2</sub> O <sub>2</sub> selectivity	H <sub>2</sub> conversion
2.5 wt.% Au-2.5 wt.% Pd/Al <sub>2</sub> O <sub>3</sub> <sup>58</sup>	4460 mol <sub>H<sub>2</sub>O<sub>2</sub></sub> kg <sub>cat</sub> <sup>-1</sup> h <sup>-1</sup>	n.d	n.d
2.0 wt.% Pd-1.0 wt.% Au/TiO <sub>2</sub> <sup>59</sup>	2330 mol <sub>H<sub>2</sub>O<sub>2</sub></sub> kg <sub>cat</sub> <sup>-1</sup> h <sup>-1</sup>	48.1 %	29.7 %
1.25 wt.% Pd-1.25 wt.% Au/ZrO-SO <sub>4</sub> <sup>2-61</sup>	1270 mol <sub>H<sub>2</sub>O<sub>2</sub></sub> kg <sub>cat</sub> <sup>-1</sup> h <sup>-1</sup>	61 %	n.d
1.25 wt.% Pd-1.25 wt.% Au/CeO <sub>2</sub> -SO <sub>4</sub> <sup>2-61</sup>	720 mol <sub>H<sub>2</sub>O<sub>2</sub></sub> kg <sub>cat</sub> <sup>-1</sup> h <sup>-1</sup>	50 %	n.d
1.0 wt.% Au-1.0 wt.% Pd/NWs-TiO <sub>2</sub> <sup>62</sup>	n.d	25 %	n.d
2.0 wt.% Au-2.0 wt.% Pd/MD10-4 <sup>65</sup>	109 mmol <sub>H<sub>2</sub>O<sub>2</sub></sub> /mol H <sub>2</sub>	n.d	n.d
2.5 wt.% Au-2.5 wt.% Pd/C <sup>44</sup>	110 mol <sub>H<sub>2</sub>O<sub>2</sub></sub> kg <sub>cat</sub> <sup>-1</sup> h <sup>-1</sup>	80 %	n.d
2.5 wt.% Au- 2.5 wt.% Pd /TiO <sub>2</sub> <sup>44</sup>	64 mol <sub>H<sub>2</sub>O<sub>2</sub></sub> kg <sub>cat</sub> <sup>-1</sup> h <sup>-1</sup>	70 %	n.d
2.5 wt.% Au-2.5 wt.% Pd/CMK-3G <sup>64</sup>	0.5 wt.%	60 %	60 %
0.73 wt.% Au-1.01 wt.% Pd/2PEMs <sup>66</sup>	200 mol <sub>H<sub>2</sub>O<sub>2</sub></sub> kg <sub>cat</sub> <sup>-1</sup> h <sup>-1</sup>	70 %	40 %
2.5 wt.% Pd- 2.5 wt.% Au/C <sup>67</sup>	791 mol <sub>H<sub>2</sub>O<sub>2</sub></sub> kg <sub>cat</sub> <sup>-1</sup> h <sup>-1</sup>	56 %	58 %
2.5 wt.% Au-2.5 wt.% Pd/C <sup>68</sup>	160 mol <sub>H<sub>2</sub>O<sub>2</sub></sub> kg <sub>cat</sub> <sup>-1</sup> h <sup>-1</sup>	> 98 %	n.d
2.5 wt.% Pd-2.5 wt.% Au /CeO <sub>2</sub> <sup>70</sup>	85 mol <sub>H<sub>2</sub>O<sub>2</sub></sub> kg <sub>cat</sub> <sup>-1</sup> h <sup>-1</sup>	38 %	31 %
0.75 mol % Pd-0.25 mol % Au <sup>63</sup>	60 mM h <sup>-1</sup>	c.a 100 %	n.d

**n.d:** no determined. **Reaction conditions:** **Reference 58:** 8.5 g (5.6 g CH<sub>3</sub>OH, 2.9 g H<sub>2</sub>O), catalyst (0.05 g), 420 psi of 5 % H<sub>2</sub>/CO<sub>2</sub>, 160 psi of 25 % O<sub>2</sub>/CO<sub>2</sub>, 1200 rpm, 2 °C, 0.5 h. **Reference 59:** 60 mL of CH<sub>3</sub>CH<sub>2</sub>OH (0.38 mL H<sub>2</sub>SO<sub>4</sub> (95 %)), catalyst (0.05 g), H<sub>2</sub> (9 cm<sup>3</sup>/min) (H<sub>2</sub>, O<sub>2</sub>/N<sub>2</sub>, flow rate: 60 cm<sup>3</sup>/min), atmospheric pressure, 10 °C, 0.5 h. **Reference 61:** 100 mL of CH<sub>3</sub>OH (0.03 M H<sub>2</sub>SO<sub>4</sub>), catalyst (0.135 g), H<sub>2</sub> (9 cm<sup>3</sup>/min) (H<sub>2</sub>, O<sub>2</sub>/N<sub>2</sub>, flow rate: 60 cm<sup>3</sup>/min), atmospheric pressure, 1000 rpm, 20 °C, 3 h. **Reference 62:** 200 mL of CH<sub>3</sub>OH (0.03 M H<sub>2</sub>SO<sub>4</sub>), catalyst (0.06 g), H<sub>2</sub> (3.5 mol %) (H<sub>2</sub>, O<sub>2</sub>/N<sub>2</sub>, flow rate: 300 cm<sup>3</sup>/min), 20 bar, 1000 rpm, 10 °C, 0.5 h. **Reference 44:** 8.5 g (5.6 g CH<sub>3</sub>OH, 2.9 g H<sub>2</sub>O), catalyst (0.05 g), 420 psi of 5 % H<sub>2</sub> /CO<sub>2</sub>, 160 psi of 25 % O<sub>2</sub>/CO<sub>2</sub>, 1200 rpm, 2 °C, 0.5 h. **Reference 65:** 5 g (2.6 g H<sub>2</sub>O, 2.4 g CH<sub>3</sub>OH), catalyst (0.05g), 5 bar of 5 % H<sub>2</sub>/CO<sub>2</sub>, 15 bar of 25 % O<sub>2</sub>/CO<sub>2</sub>, -10 °C, 1.5 h. **Reference 64:** 16.65 g (11.1 g CH<sub>3</sub>OH, 5.55 g H<sub>2</sub>O), catalyst

(0.02 g), (H<sub>2</sub>:O<sub>2</sub>:N<sub>2</sub>, molar ratio: 1:10:9, 3.0 MPa), 900 rpm, 5 °C, 8 h. **Reference 66:** H<sub>2</sub>O (0.05 M H<sub>2</sub>SO<sub>4</sub>, 9 ppm NaBr, 20 % CH<sub>3</sub>CN), H<sub>2</sub>, O<sub>2</sub>/N<sub>2</sub> (H<sub>2</sub>:O<sub>2</sub>/N<sub>2</sub>, 20 bar, flow rate 0.1 cm<sup>3</sup>/min), 42 °C, 2 h. **Reference 67:** 176 g CH<sub>3</sub>OH, catalyst (0.06 g), 3.2 bar H<sub>2</sub> and 5 bar O<sub>2</sub> (38.4 bar of total pressure with H<sub>2</sub>, O<sub>2</sub>/CO<sub>2</sub>), 1250 rpm, -1 °C, 3 h. **Reference 68:** 8.5 g (5.6 g CH<sub>3</sub>OH, 2.9 g H<sub>2</sub>O), catalyst (0.01 g), 420 psi of 5 % H<sub>2</sub>/CO<sub>2</sub>, 160 psi of 25 % O<sub>2</sub>/CO<sub>2</sub>, 1200 rpm, 2 °C, 0.5 h. **Reference 70:** 8.5 g (5.6 g CH<sub>3</sub>OH, 2.9 g H<sub>2</sub>O), catalyst (0.01 g), 420 psi of 5 % H<sub>2</sub>/CO<sub>2</sub>, 160 psi of 25 % O<sub>2</sub>/CO<sub>2</sub>, 1200 rpm, 2 °C, 0.5 h. **Reference 63:** (1.85 mM metallic colloid, 84 mM NaCl, 0.365 M H<sub>2</sub>SO<sub>4</sub>), (H<sub>2</sub>:O<sub>2</sub> 1:1, flow rate: 100 mL/min), 10 °C, 2 h.

### 1.2.3.3 Other metallic promoters of Pd catalysts for the direct synthesis of H<sub>2</sub>O<sub>2</sub>.

A diverse combinations of bi-metallic supported Pd catalyst such as Pt-Pd<sup>74,75,76</sup>, Pd-Sn<sup>77,78</sup>, Au-Pd<sup>76,79</sup>, Ga-Pd<sup>80</sup>, Ir-Pd<sup>80</sup>, Rh-Pd<sup>32</sup>, Ru-Pd<sup>32,81</sup>, Cu-Pd<sup>82</sup>, Ni-Pd<sup>83</sup>, Na-Pd<sup>84</sup> and tri-metallic such as Pt-Au-Pd<sup>85</sup>, X-Au-Pd (X: Pt, Zn, Ga, Ni, Sn, Co, Cu, In)<sup>86</sup> and RuAuPd<sup>81</sup> have been investigated in order to increase the selectivity of the Pd towards the formation of H<sub>2</sub>O<sub>2</sub>. Table 1.5 presents the activity towards the formation of H<sub>2</sub>O<sub>2</sub> and its selectivity as well as the H<sub>2</sub> conversion for the bi-metallic XPd and tri-metallic XAuPd supported catalysts discussed in this section for a better comparison between them. In all these instances, the addition of a second or third metal to Pd or to AuPd enhance the activity and selectivity to H<sub>2</sub>O<sub>2</sub> synthesis. However, there are discrepancy between authors when using Cu and Ag with Pd and AuPd supported catalysts. For instance, Hutchings and co-workers reported that Cu (0.5 wt.% Pd/ Cs<sub>2.5</sub>H<sub>0.5</sub>PW<sub>12</sub>O<sub>40</sub>, 85 mol<sub>H<sub>2</sub>O<sub>2</sub></sub> kg<sub>cat</sub><sup>-1</sup> h<sup>-1</sup> of H<sub>2</sub>O<sub>2</sub>) could poison the Pd active sites required to activate H<sub>2</sub> to form H<sub>2</sub>O<sub>2</sub> (0.5 wt.% Pd-0.5 wt.% Cu/ Cs<sub>2.5</sub>H<sub>0.5</sub>PW<sub>12</sub>O<sub>40</sub> 4 mol<sub>H<sub>2</sub>O<sub>2</sub></sub> kg<sub>cat</sub><sup>-1</sup> h<sup>-1</sup> of H<sub>2</sub>O<sub>2</sub>), since the bi-metallic CuPd presented less activity than the mono-metallic Pd analogue.<sup>82</sup> However, Barnes *et.al.*, reported excellent activity with the addition of low dopants to the bi-metallic AuPd catalysts (0.975 wt.% AuPd- 0.025 wt.% X/TiO<sub>2</sub>) (X: Pt, Zn, Ga, Ni, Sn, Co, Cu).<sup>86</sup> Among all the tri-metallic combinations tested, Cu, Ni and Zn (0.975 wt.% AuPd- 0.025 wt.% X/TiO<sub>2</sub>) (X: Zn, Ni, Cu) presented the most promising activity (100 mol<sub>H<sub>2</sub>O<sub>2</sub></sub> kg<sub>cat</sub><sup>-1</sup> h<sup>-1</sup>, 107 mol<sub>H<sub>2</sub>O<sub>2</sub></sub> kg<sub>cat</sub><sup>-1</sup> h<sup>-1</sup> and 94 mol<sub>H<sub>2</sub>O<sub>2</sub></sub> kg<sub>cat</sub><sup>-1</sup> h<sup>-1</sup> respectively) in comparison to the bi-metallic 1 wt.% AuPd/TiO<sub>2</sub> that gave 61 mol<sub>H<sub>2</sub>O<sub>2</sub></sub> kg<sub>cat</sub><sup>-1</sup> h<sup>-1</sup>.<sup>86</sup> The enhancement in activity towards the direct synthesis of H<sub>2</sub>O<sub>2</sub> in comparison to the bi-metallic analogue was attributed to have formed Pd<sup>0</sup>-Pd<sup>2+</sup> domains that enhanced the H<sub>2</sub> conversion.<sup>86</sup> Some authors have also shown opposite conclusions about the benefits that Ag has on Pd supported catalysts. Edwards and co-workers<sup>79</sup> reported a bi-metallic 2.5 wt.% Pd-2.5 wt. % Ag/TiO<sub>2</sub> catalysts with a 3 mol<sub>H<sub>2</sub>O<sub>2</sub></sub> kg<sub>cat</sub><sup>-1</sup> h<sup>-1</sup>, which offered lower activity towards the direct synthesis of H<sub>2</sub>O<sub>2</sub> in comparison to the mono-metallic 5 wt.% Pd/TiO<sub>2</sub> analogue (106 mol<sub>H<sub>2</sub>O<sub>2</sub></sub> kg<sub>cat</sub><sup>-1</sup> h<sup>-1</sup>).<sup>79</sup> In this scenario, the increasing loading of Ag, decreased the activity towards the direct synthesis of H<sub>2</sub>O<sub>2</sub>. In fact, as the Ag content increased so it did the decomposition of H<sub>2</sub>O<sub>2</sub>, leading to a decrease in the productivity.<sup>79</sup> They concluded that the formation of palladium beta hydride (Pd H-β), which is the key feature for the dissociation of H<sub>2</sub>, was being suppressed by the presence of Ag, according to hydrogen temperature programmed reduction experiments (H<sub>2</sub>-TPR) and XPS. The same conclusions

were drawn from Strukul and co-workers<sup>76</sup> when studying bi-metallic AgPd supported catalysts, stating that the increasing presence of Ag, made decrease the presence of Pd H- $\beta$ . However, Strukul and co-workers<sup>76</sup> reported a better performance of bi-metallic X wt.% Pd-X wt.% Ag (Pd:Ag: 10 molar ratio) supported on alfa-Al<sub>2</sub>O<sub>3</sub> asymmetric membrane (AAM) (X wt.% Pd-X wt.% Ag (Pd:Ag: 10 molar ratio)/AAM, c.a. 300 ppm H<sub>2</sub>O<sub>2</sub>) than the Pd analogue (X wt.% Pd/AAM, c.a. 100 ppm H<sub>2</sub>O<sub>2</sub>). They claimed that the addition of Ag on X wt.% Pd-X wt.% Ag (Pd:Ag: 10 molar ratio)/AAM made morphological changes on the particles (100-500 nm) leading to chemisorbed O<sub>2</sub> sites with less defects and thus minimising the formation of H<sub>2</sub>O.<sup>76</sup>

On the other hand, Pt seemed to enhance the selectivity of the Pd towards the direct synthesis of H<sub>2</sub>O<sub>2</sub> in small amounts as it has been reported for some authors. For instance, Lunsford and co-workers<sup>75</sup> found that the incorporation of small amounts of Pt at ratios as small as 0.01 (Pt/Pt+Pd) enhanced the rate of H<sub>2</sub>O<sub>2</sub> formation which remained constant up to a ratio of 0.5 (Pt/Pt+Pd)/SiO<sub>2</sub> (total loading of 0.54 wt.%). The maximum rate (56 mmolH<sub>2</sub>O<sub>2</sub> g<sub>Pd</sub><sup>-1</sup> min<sup>-1</sup>, 20-25 % H<sub>2</sub> conversion and 50-60 % H<sub>2</sub>O<sub>2</sub> selectivity) was observed for ratios between 0.025 and 0.1 with Cl<sup>-</sup> ions in solution at a concentration of 0.0004 M. The maximum rate of H<sub>2</sub>O<sub>2</sub> (56 mmolH<sub>2</sub>O<sub>2</sub> g<sub>Pd</sub><sup>-1</sup> min<sup>-1</sup>) was 5 times higher than the same catalyst reported with Pd-only.<sup>75</sup> The enhancement in activity for the bi-metallic PtPd supported catalysts in comparison to the mono-metallic one was attributed to two factors according to the authors, *i*) small amount of platinum tuned the electronic state of Pd, which resulted in the inhibition of O–O bond cleavage, *ii*) an enrichment of Pd expose to the surface of the catalysts that also helped to enhance the activity.<sup>75</sup> The same behaviour was seen by Hutchings and co-workers<sup>85</sup> with the addition of Pt to AuPd supported catalysts.<sup>85</sup> They identified three tri-metallic PdAuPt compositions that outperform the bi-metallic system 2.5 wt.% Au-2.5 wt.% Pd/ Ce<sub>2</sub>O<sub>3</sub> (68 mol<sub>H<sub>2</sub>O<sub>2</sub></sub> kg<sub>cat</sub><sup>-1</sup> h<sup>-1</sup>), these being: 0.625 wt.% Au-3.75 wt.% Pd-0.625 wt.% Pt/ Ce<sub>2</sub>O<sub>3</sub> (153 mol<sub>H<sub>2</sub>O<sub>2</sub></sub> kg<sub>cat</sub><sup>-1</sup> h<sup>-1</sup>), 2.4 wt.% Au-2.4 wt.% Pd-0.2 wt.% Pt/ Ce<sub>2</sub>O<sub>3</sub> (170 mol<sub>H<sub>2</sub>O<sub>2</sub></sub> kg<sub>cat</sub><sup>-1</sup> h<sup>-1</sup>) and 2.30 wt.% Au-2.50 wt.% Pd-0.2 wt.% Pt/ Ce<sub>2</sub>O<sub>3</sub> (155 mol<sub>H<sub>2</sub>O<sub>2</sub></sub> kg<sub>cat</sub><sup>-1</sup> h<sup>-1</sup>). They evidence that the improvement in the activity with the addition of Pt to a bi-metallic AuPd system, resulted from electronic effects that were achieved through the formation of core-shell structures.<sup>85</sup>

The addition of a second metal such as Ga and Ir to Pd was investigated by Behrens and co-workers.<sup>80</sup> Their results evidenced that the mono and bi-metallic (Pd, GaPd and IrPd) catalysts displayed similar activity towards H<sub>2</sub>O<sub>2</sub> production (Pd/TiO<sub>2</sub> 100 mol<sub>H<sub>2</sub>O<sub>2</sub></sub> kg<sub>cat</sub><sup>-1</sup> h<sup>-1</sup> production of H<sub>2</sub>O<sub>2</sub>, 1000 mol<sub>H<sub>2</sub>O<sub>2</sub></sub> kg<sub>cat</sub><sup>-1</sup> h<sup>-1</sup> degradation of H<sub>2</sub>O<sub>2</sub>), (PdIr (Pd:Ir: 2:1 molar ratio)/TiO<sub>2</sub> 100 mol<sub>H<sub>2</sub>O<sub>2</sub></sub> kg<sub>cat</sub><sup>-1</sup> h<sup>-1</sup> production of H<sub>2</sub>O<sub>2</sub>, 800 mol<sub>H<sub>2</sub>O<sub>2</sub></sub> kg<sub>cat</sub><sup>-1</sup> h<sup>-1</sup> degradation of H<sub>2</sub>O<sub>2</sub>) and (PdGa (Pd:Ga: 2:1 molar ratio)/TiO<sub>2</sub> 110 mol<sub>H<sub>2</sub>O<sub>2</sub></sub> kg<sub>cat</sub><sup>-1</sup> h<sup>-1</sup> production of H<sub>2</sub>O<sub>2</sub>,

600 mol<sub>H<sub>2</sub>O<sub>2</sub></sub> kg<sub>cat</sub><sup>-1</sup> h<sup>-1</sup> degradation of H<sub>2</sub>O<sub>2</sub>). However, the degradation activity of the PdGa catalyst was significantly reduced.<sup>80</sup> They concluded that the addition of Ga and Ir had partially oxidised Pd<sup>0</sup> to PdO, which is known to present lower degradation activity than the Pd<sup>0</sup>.

It is possible to conclude that the incorporation of secondary metals to Pd or a third metal to bi-metallic AuPd systems can change the selectivity and activity of the Pd or AuPd respectively by modifying the nanoparticle composition and the size of the nanoparticles. These two parameters can subsequently influence the dispersion, size and crystallinity of the metal nanoparticles. However, Gao and co-workers<sup>87</sup> have determined that the Pd-shell atoms are also a relevant factor that influence the activity and selectivity towards H<sub>2</sub>O<sub>2</sub>. Thus, they investigated the addition of a secondary metal (more electronegative than Pd) in order to tune the electron valance of the Pd and accelerate its activity and selectivity towards the direct synthesis of H<sub>2</sub>O<sub>2</sub>.<sup>87</sup> They investigated the activity towards the direct synthesis and degradation of H<sub>2</sub>O<sub>2</sub> and plotted against the average valence electrons of Pd ( $\theta$ ) for a series of bi-metallic and tri-metallic Pd supported systems (Pd-W, Pd-Pb, Au-Pd-W, Au-Pd-Pb, Au-Pd-Mo, Au-Pd-Ru, Au-Pd-Pt).<sup>87</sup> They found that the bi-metallic and tri-metallic systems which gave the best activity towards the direct synthesis of H<sub>2</sub>O<sub>2</sub> and low degradation fall between Pd average valance of  $\theta = 9.95-9.85$ .<sup>87</sup> According to their conclusions, any bi-metallic or tri-metallic system that induces an average Pd electronic valance between 9.95-9.85, would be a promising catalysts for the direct synthesis of H<sub>2</sub>O<sub>2</sub>.<sup>87</sup> Thus, they concluded that bi-metallic systems of WPd and PbPd could outperformed the bi-metallic AuPd catalysts and MoAuPd, WAuPd, IrAuPd, OsAuPd, RuAuPd and RhAuPd could outperform the tri-metallic PtAuPd ones.<sup>87</sup> Actually, Hutchings and co-workers<sup>81</sup> developed bi-metallic 0.5 wt.% Ru-4.5 wt.% Pd/TiO<sub>2</sub> (143 mol<sub>H<sub>2</sub>O<sub>2</sub></sub> kg<sub>cat</sub><sup>-1</sup> h<sup>-1</sup>) and tri-metallic 0.45 wt.% Ru-0.05 wt.% Au-4.5 wt.% Pd/TiO<sub>2</sub> (153 mol<sub>H<sub>2</sub>O<sub>2</sub></sub> kg<sub>cat</sub><sup>-1</sup> h<sup>-1</sup>) supported catalysts which showed promising activity towards the direct synthesis of H<sub>2</sub>O<sub>2</sub> in comparison to the mono-metallic analogue of 0.5 w.% Ru/TiO<sub>2</sub> (14 mol<sub>H<sub>2</sub>O<sub>2</sub></sub> kg<sub>cat</sub><sup>-1</sup> h<sup>-1</sup>), 0.5 wt.% Au/TiO<sub>2</sub> (4 mol<sub>H<sub>2</sub>O<sub>2</sub></sub> kg<sub>cat</sub><sup>-1</sup> h<sup>-1</sup>) and 0.5 wt.% Pd/TiO<sub>2</sub> (30 mol<sub>H<sub>2</sub>O<sub>2</sub></sub> kg<sub>cat</sub><sup>-1</sup> h<sup>-1</sup>) catalysts.<sup>81</sup> Choudhary and co-workers<sup>32</sup> have also reported bi-metallic X wt.% Ru-2.5 wt.% Pd/ZrO<sub>2</sub> (0.15 atom ratio Ru:Pd) supported catalysts with promising activity (10 wt.% H<sub>2</sub>O<sub>2</sub>, 40 % H<sub>2</sub> conversion).<sup>32</sup> Another promising combination was reported from Lewis and co-workers<sup>83</sup> with a bi-metallic 0.5 wt.% Pd-4.5 wt.% Ni/TiO<sub>2</sub> (300 ppm of H<sub>2</sub>O<sub>2</sub>, 20 % selectivity of H<sub>2</sub>O<sub>2</sub>) supported catalysts in water only solvents and without any halides or acids in the medium.<sup>83</sup>

Another interesting bi-metallic composition was reported by Lee and co-workers<sup>84</sup> with NaPd supported on TiO<sub>2</sub> catalyst (0.83 wt.% Pd-0.51 wt.% Na/TiO<sub>2</sub>) which achieved promising productivity of H<sub>2</sub>O<sub>2</sub> (600 mol<sub>H<sub>2</sub>O<sub>2</sub></sub> kg<sub>cat</sub><sup>-1</sup> h<sup>-1</sup>) in comparison to the mono-metallic

analogue 0.81 wt.% Pd/TiO<sub>2</sub> (315 mol<sub>H<sub>2</sub>O<sub>2</sub></sub> kg<sub>cat</sub><sup>-1</sup> h<sup>-1</sup>).<sup>84</sup> As it was concluded in the previous bi-metallic systems, nanoparticle dispersion played a crucial role according to the authors, since the bi-metallic NaPd catalyst presented smaller nanoparticles with higher dispersion than the mono-metallic Pd analogue.<sup>84</sup> They also pointed out that the bi-metallic NaPd system did not present Pd H-β in comparison to the mono-metallic Pd analogue, which according to the authors made decrease the hydrogenation of the H<sub>2</sub>O<sub>2</sub>, thus avoiding the formation of H<sub>2</sub>O.<sup>84</sup> It seems that the Pd H-β presence needs to be somehow controlled, since it can dissociate the H<sub>2</sub> as ideally should happen to make H<sub>2</sub>O<sub>2</sub> but it also can hydrogenate the H<sub>2</sub>O<sub>2</sub> to make H<sub>2</sub>O.

**Table 1.5:** Comparison between the catalysts activity towards the formation and selectivity of H<sub>2</sub>O<sub>2</sub> and H<sub>2</sub> conversion for the bi-metallic XPd and tri-metallic XAuPd supported catalysts discussed in the literature above.

Catalysts	H <sub>2</sub> O <sub>2</sub> activity	H <sub>2</sub> O <sub>2</sub> selectivity	H <sub>2</sub> conversion
<b>0.5 wt.% Pd-0.5 wt.% Cu/ Cs<sub>2.5</sub>H<sub>0.5</sub>PW<sub>12</sub>O<sub>40</sub><sup>82</sup></b>	4 mol <sub>H<sub>2</sub>O<sub>2</sub></sub> kg <sub>cat</sub> <sup>-1</sup> h <sup>-1</sup>	n.d	n.d
<b>0.54 wt.% PtPd/SiO<sub>2</sub> (Pt/Pt+Pd ratio from 0.025- 0.1)<sup>75</sup></b>	56 mmolH <sub>2</sub> O <sub>2</sub> g <sub>Pd</sub> <sup>-1</sup> 1 min <sup>-1</sup>	50-60 %	20-25 %
<b>4 wt.% Pd-1 wt.% Sn/TiO<sub>2</sub><sup>77</sup></b>	98.4 mol <sub>H<sub>2</sub>O<sub>2</sub></sub> kg <sub>cat</sub> <sup>-1</sup> h <sup>-1</sup>	n.d	n.d
<b>2 wt.% Pd-1 wt.% Sn/TiO<sub>2</sub><sup>78</sup></b>	80.7 mol <sub>H<sub>2</sub>O<sub>2</sub></sub> kg <sub>cat</sub> <sup>-1</sup> h <sup>-1</sup>	60.8 %	n.d
<b>2.5 wt.% Pd-2.5 wt.% Ag/TiO<sub>2</sub><sup>79</sup></b>	56 ppm	n.d	n.d
<b>X wt.% Pd-X wt.% Ag (Pd:Ag: 10 molar ratio)/AAM<sup>76</sup></b>	300 ppm	n.d	n.d
<b>2.4 wt.% Au-2.4 wt.% Pd-0.2 wt.% Pt/ Ce<sub>2</sub>O<sub>3</sub><sup>85</sup></b>	170 mol <sub>H<sub>2</sub>O<sub>2</sub></sub> kg <sub>cat</sub> <sup>-1</sup> h <sup>-1</sup>	n.d	n.d
<b>X wt.% Pd-X wt.% Ga (Pd:Ga: 2:1 molar ratio)/TiO<sub>2</sub><sup>80</sup></b>	110 mol <sub>H<sub>2</sub>O<sub>2</sub></sub> kg <sub>cat</sub> <sup>-1</sup> h <sup>-1</sup>	n.d	n.d
<b>X wt.% Pd-X wt.% Ir (Pd:Ir: 2:1 molar ratio)/TiO<sub>2</sub><sup>80</sup></b>	100 mol <sub>H<sub>2</sub>O<sub>2</sub></sub> kg <sub>cat</sub> <sup>-1</sup> h <sup>-1</sup>	n.d	n.d
<b>0.45 wt.% Ru-0.05 wt.% Au- 4.5 wt.% Pd/TiO<sub>2</sub><sup>81</sup></b>	153 mol <sub>H<sub>2</sub>O<sub>2</sub></sub> kg <sub>cat</sub> <sup>-1</sup> h <sup>-1</sup>	n.d	n.d
<b>X wt.% Ru-2.5 wt.% Pd (0.15 atom ratio Ru:Pd)/ZrO<sub>2</sub><sup>32</sup></b>	10 mol <sub>H<sub>2</sub>O<sub>2</sub></sub> kg <sub>cat</sub> <sup>-1</sup> h <sup>-1</sup>		40 %
<b>0.5 wt.% Pd-4.5 wt.% Ni/TiO<sub>2</sub><sup>83</sup></b>	300 ppm	20 %	n.d
<b>0.83 wt.% Pd-0.51 wt.% Na/TiO<sub>2</sub><sup>84</sup></b>	600 mol <sub>H<sub>2</sub>O<sub>2</sub></sub> kg <sub>cat</sub> <sup>-1</sup> h <sup>-1</sup>	70 %	20 %
<b>0.975 wt.% AuPd-0.025 wt.% Ni/TiO<sub>2</sub><sup>86</sup></b>	107 mol <sub>H<sub>2</sub>O<sub>2</sub></sub> kg <sub>cat</sub> <sup>-1</sup> h <sup>-1</sup>	41 %	32 %

**n.d:** no determined. **Reaction conditions:** **Reference 82:** 8.5 g (5.6 g CH<sub>3</sub>OH, 2.9 g H<sub>2</sub>O), catalyst (0.05 g), 420 psi of 5 % H<sub>2</sub>/CO<sub>2</sub>, 160 psi of 25 % O<sub>2</sub>/CO<sub>2</sub>, 1200 rpm, 2 °C, 0.5 h. **Reference 75:** 60 mL CH<sub>3</sub>CH<sub>2</sub>OH (0.12 M H<sub>2</sub>SO<sub>4</sub>, 0.0004 M HCl), catalyst (0.05 g), H<sub>2</sub>, O<sub>2</sub>/N<sub>2</sub> (H<sub>2</sub>:O<sub>2</sub>:N<sub>2</sub>, 0.5: 7.5:2, flow rate: 50 cm<sup>3</sup>/min), 10 °C, 4 h. **Reference 77:** 10 g (8 g CH<sub>3</sub>OH, 2 g H<sub>2</sub>O), catalyst (0.005 g), 3.6 MPa (5 % H<sub>2</sub>/N<sub>2</sub>) and 0.4 MPa (O<sub>2</sub>), 1000 rpm, 0 °C, 0.5 h. **Reference 78:** 10 g (7 g CH<sub>3</sub>OH, 3 g H<sub>2</sub>O), catalyst (0.01 g), 3.6 MPa (5 % H<sub>2</sub>/N<sub>2</sub>) and 0.4 MPa (O<sub>2</sub>), 1200 rpm, 0 °C, 0.5 h. **Reference 79:** 8.5 g (5.6 g CH<sub>3</sub>OH, 2.9 g H<sub>2</sub>O), catalyst (0.05 g), 420 psi of 5 % H<sub>2</sub>/CO<sub>2</sub>, 160 psi of 25 % O<sub>2</sub>/CO<sub>2</sub>, 1200 rpm, 2 °C, 0.5 h. **Reference 76:** 100 mL CH<sub>3</sub>OH (6 ppm Br<sup>-</sup>, 2.8 g/L H<sub>2</sub>SO<sub>4</sub>), 2 bar H<sub>2</sub>, O<sub>2</sub> fed at 25 mL/min, room temperature, 4.5 h. **Reference 85:** 8.5 g (5.6 g CH<sub>3</sub>OH, 2.9 g H<sub>2</sub>O), catalyst (0.05 g),

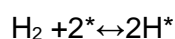
420 psi of 5 % H<sub>2</sub>/CO<sub>2</sub>, 160 psi of 25 % O<sub>2</sub>/CO<sub>2</sub>, 1200 rpm, 2 °C, 0.5 h. **Reference 80:** 8.5 g (5.6 g CH<sub>3</sub>OH, 2.9 g H<sub>2</sub>O), catalyst (0.05 g), 420 psi of 5 % H<sub>2</sub>/CO<sub>2</sub>, 160 psi of 25 % O<sub>2</sub>/CO<sub>2</sub>, 1200 rpm, 2°C, 0.5 h. **Reference 81:** 8.5 g (5.6 g CH<sub>3</sub>OH, 2.9 g H<sub>2</sub>O), catalyst (0.05 g), 420 psi of 5 % H<sub>2</sub>/CO<sub>2</sub>, 160 psi of 25 % O<sub>2</sub>/CO<sub>2</sub>, 1200 rpm, 2 °C, 0.5 h. **Reference 32:** 150 mL aqueous solution (0.03 M H<sub>2</sub>SO<sub>4</sub>), 4.6 mol % H<sub>2</sub>, O<sub>2</sub>, 25 °C, 3 h. **Reference 83:** 8.5 g H<sub>2</sub>O, catalyst (0.01 g), 420 psi of 5% H<sub>2</sub>/CO<sub>2</sub>, 160 psi of 25 % O<sub>2</sub>/CO<sub>2</sub>, 1200 rpm, 20 °C, 0.5 h. **Reference 84:** 150 mL (37.5 mL CH<sub>3</sub>CH<sub>2</sub>OH, 112.5 mL H<sub>2</sub>O, 0.15 mM KBr, 0.03 M H<sub>3</sub>PO<sub>4</sub>), catalyst (0.16 g), (H<sub>2</sub>:O<sub>2</sub>, 1:10, flow rate: 22 mL/min), 20 °C, 3 h. **Reference 86:** 8.5 g (5.6 g CH<sub>3</sub>OH, 2.9 g H<sub>2</sub>O), catalyst (0.05 g), 420 psi of 5 % H<sub>2</sub>/CO<sub>2</sub>, 160 psi of 25 % O<sub>2</sub>/CO<sub>2</sub>, 1200 rpm, 2 °C, 0.5 h.

#### 1.2.3.4 Mechanism of H<sub>2</sub>O<sub>2</sub> and H<sub>2</sub>O formation over Pd and AuPd supported catalysts.

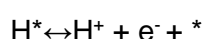
Determining the mechanism of H<sub>2</sub>O<sub>2</sub> and H<sub>2</sub>O formation is a complicated task since the mechanism changes dynamically during the course of the reaction as the oxidation state of catalyst may also change.<sup>88</sup> Also, the mechanism can vary with the reaction conditions, the catalyst and the H<sub>2</sub>:O<sub>2</sub> ratio employed.<sup>88</sup> The mechanism for the formation of H<sub>2</sub>O<sub>2</sub> (Eq. 13-18) and H<sub>2</sub>O (Eq. 19-24) involve the following steps according to Flaherty and co-workers<sup>89</sup> using mono-metallic Pd supported catalyst. The mechanism that they proposed involve the adsorption and dissociation of the H<sub>2</sub> molecule (Eq. 13) followed by the heterolytic H<sup>+</sup> oxidation (Eq. 14). However, the difference between producing H<sub>2</sub>O<sub>2</sub> or H<sub>2</sub>O lies in the cleavage of the O-O bond of the O<sub>2</sub><sup>\*</sup>, OOH<sup>\*\*</sup> and H<sub>2</sub>O<sub>2</sub><sup>\*\*</sup>. If the O-O bond in the O<sub>2</sub><sup>\*</sup> does not break, O<sub>2</sub><sup>\*</sup> undergoes two proton electron transfer to form hydroperoxy specie (OOH<sup>\*\*</sup>) (Eq. 16) and adsorbed H<sub>2</sub>O<sub>2</sub><sup>\*\*</sup> (Eq. 17). However, the cleavage of the O<sub>2</sub><sup>\*</sup>, OOH<sup>\*\*</sup> and H<sub>2</sub>O<sub>2</sub><sup>\*\*</sup> lead to the formation of H<sub>2</sub>O<sup>\*</sup> as Eq. 19, Eq. 20 and Eq. 24 show. However, the mechanism of formation of H<sub>2</sub>O<sub>2</sub> and H<sub>2</sub>O is still controversial, since other authors have reported a different mechanism, in where the adsorbed molecular O<sub>2</sub><sup>\*</sup> reacts with dissociative adsorbed H<sup>\*</sup>, suggesting that both reactants need to be adsorbed on the surface, before the O<sub>2</sub><sup>\*</sup> could undergo the proton electron transfer reaction.<sup>88,90</sup>

##### 1) H<sub>2</sub>O<sub>2</sub> formation

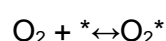
Eq. 13



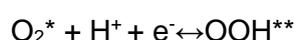
Eq. 14



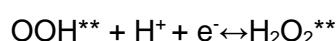
Eq. 15



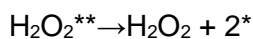
Eq. 16



Eq. 17

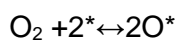


Eq. 18

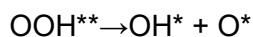


## 2) H<sub>2</sub>O formation

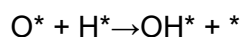
Eq. 19



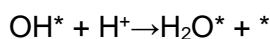
Eq. 20



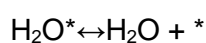
Eq. 21



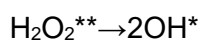
Eq. 22



Eq. 23



Eq. 24



Yoshizawa and co-workers<sup>91</sup> corroborated via computational studies that the mechanism of H<sub>2</sub>O<sub>2</sub> and H<sub>2</sub>O formation differs between mono-metallic Pd and bi-metallic AuPd catalysts. In fact, they showed how in the bi-metallic AuPd system, the O-O bond cleavage becomes inhibited. Figure 1.6 and Figure 1.7 clearly depicts very schematically the difference in H<sub>2</sub>O<sub>2</sub> and H<sub>2</sub>O formation for a mono-metallic Pd and bi-metallic AuPd supported catalysts respectively. According to Yoshizawa and co-workers, for a mono-metallic Pd supported catalyst, the formation of OOH\* has a lower  $\Delta^\ddagger G=21.2$  kcal/mol ( $\Delta G=3.8$  kcal/mol) than the dissociation of O<sub>2</sub>\*  $\Delta^\ddagger G=27.5$  kcal/mol ( $\Delta G=-42.2$  kcal/mol). According to the authors, the dissociation of O<sub>2</sub>\* has a higher energy barrier due to the Pd sites are already occupied by the H\*. This justifies the fact that the addition of halides, helps to increase the selectivity towards the direct synthesis of H<sub>2</sub>O<sub>2</sub>. The OOH\*\* intermediate can be subsequently desorbed ( $\Delta^\ddagger G=24.1$  Kcal/mol), hydrogenated ( $\Delta^\ddagger G=14.6$  Kcal/mol,  $\Delta G=1.7$  kcal/mol), or dissociated ( $\Delta^\ddagger G=8.1$  Kcal/mol,  $\Delta G=-31.7$  kcal/mol and  $\Delta^\ddagger G=6.3$  Kcal/mol,  $\Delta G=-44.2$  kcal/mol). The dissociation of the OOH\*\* is more favourable due to the formation of O-Pd bond which promotes the cleavage and enhances the formation of H<sub>2</sub>O.<sup>91</sup>

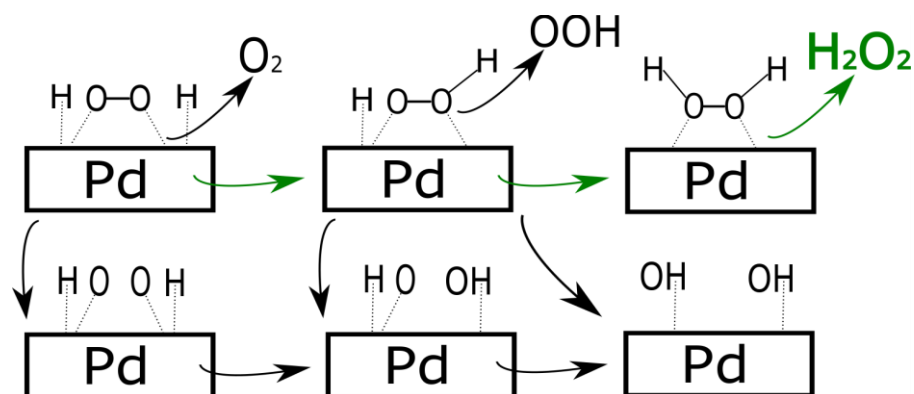


**Figure 1.6:** Schematic representation of H<sub>2</sub>O<sub>2</sub> and H<sub>2</sub>O formation over a mono-metallic Pd supported catalyst.

For a bi-metallic AuPd catalysts, the O<sub>2</sub> absorption will take place on the Au since all the Pd active sites are already occupied by H\* (Figure 1.7). In this scenario, after the formation of the OOH\*\* intermediate, its desorption is more facile ( $\Delta^\ddagger G=13.8$  Kcal/mol,  $\Delta G=2.7$  kcal/mol) than having its O-O bond broken ( $\Delta^\ddagger G=16.4$ ,  $\Delta G=-23.2$  kcal/mol) or hydrogenated leading to H<sub>2</sub>O ( $\Delta^\ddagger G=21.7$ ,  $\Delta G=-38.8$  kcal/mol). The  $\Delta^\ddagger G$  barrier for these two last side reactions have increased in comparison with those in the Pd, therefore the OOH\*\* will be desorbed. When the OOH is absorbed again, the un-hydrogenated O needs to be close to the Pd site where the H\* is in order for the OOH\*\* to be hydrogenated. In the second hydrogenation, the OOH\*\* can yield to H<sub>2</sub>O<sub>2</sub>\*\* ( $\Delta^\ddagger G=13.5$  kcal/mol,  $\Delta G=1.7$  kcal/mol) or it can be dissociated ( $\Delta^\ddagger G=16.0$  kcal/mol,  $\Delta G=-19.9$  kcal/mol) or forming two OH\* groups ( $\Delta^\ddagger G=22.2$  kcal/mol,  $\Delta G=-28.2$  kcal/mol). It is believed that the  $\Delta^\ddagger G$  for these side reactions are higher compared to the mono-metallic Pd because the Au-O bond is not strong enough to compensate for the O-O cleavage. Once the H<sub>2</sub>O<sub>2</sub>\*\* is formed, its desorption is more facile ( $\Delta^\ddagger G=2.5$  Kcal/mol,  $\Delta G=n/a$  kcal/mol) than having the O-O broken ( $\Delta^\ddagger G= 5.4$ Kcal/mol,  $\Delta G=-22.9$  kcal/mol).<sup>91</sup>

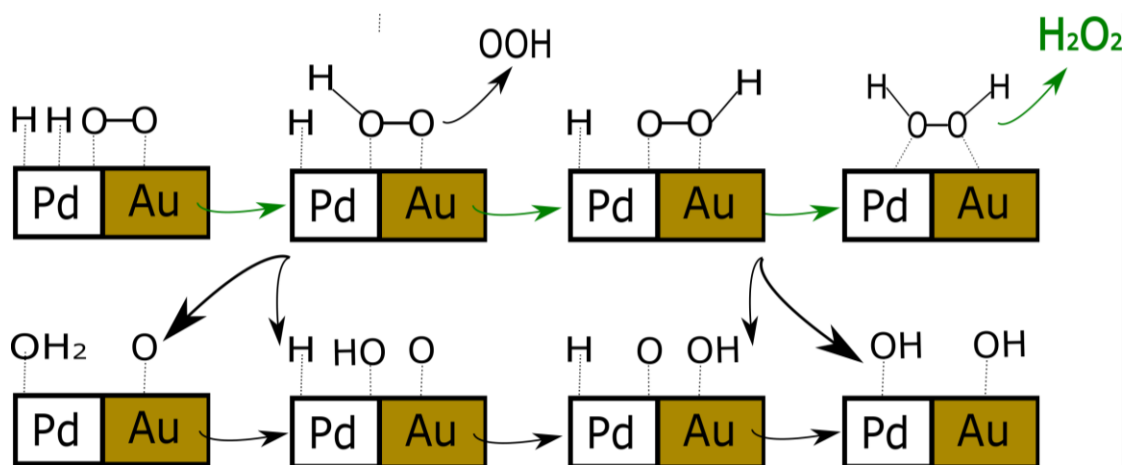


**Figure 1.7:** Schematic representation of H<sub>2</sub>O<sub>2</sub> and H<sub>2</sub>O formation over a bi-metallic AuPd supported catalyst.

### 1.3 Water treatment.

There has been an increasing demand of available water resources for consumption due to rapid industrialization and population growth. It is estimated that around 4 billion people have no or little access to cleaned and sanitized water supply.<sup>92</sup> This is expected to grow in short term due to discharge of micro pollutants and contaminants into the natural water cycle.<sup>92</sup> Water treatment is typically a process involving numerous steps and various technologies that are combined together to what is called primary, secondary and tertiary treatments. Primary treatments consist in the removal of solids such as paper, while secondary treatments aim to degrade certain soluble organic contaminants such as sugar, soap and detergents, food waste *etc.*<sup>93,94,95,96</sup> Tertiary treatments is the final stage in where the water is treated to be safe for consumption and/or to be discharge to the environment.<sup>94</sup> There are a wide variety of technologies that are selected according to the kind of pollutants left after primary and secondary treatments such as oxidations for persistence pharmaceutical pollutants like antibiotics.<sup>97</sup>

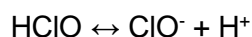
#### 1.3.1 Oxidation reactions for water treatment.

At the beginning of the 20<sup>th</sup> century, chlorine (Cl<sub>2</sub>) and ozone (O<sub>3</sub>) were introduced for the disinfection of water in industrialized countries and in combination with sand filtration, led to a decrease of waterborne disease.<sup>98</sup> Chlorination consist in employing Cl<sub>2</sub> gas or hypochlorite (HClO) as a means of water disinfection. Cl<sub>2</sub> hydrolyses in water to form HClO as shown in Eq. 25. HClO is a weak acid where decomposes according to Eq. 26.

##### Eq. 25



##### Eq. 26



Owing to its low cost, Cl<sub>2</sub> is globally the most widely used chemical oxidant for water disinfection.<sup>99</sup> It is usually used at one or two points during the water treatment process, for instance after post-treating water in order to maintain the disinfection levels down in the distribution system. Cl<sub>2</sub> can react with inorganic (Fe<sup>2+</sup>, As<sup>3+</sup>, NO<sub>2</sub>), organic (pesticides and pharmaceuticals) and micro pollutants. However, Cl<sub>2</sub> is not suitable for the oxidation of organic pollutants due to the formation of disinfection by-products (DBPs), which are formed due to the reaction of Cl<sub>2</sub> with dissolved organic matter (DOM). These DBPs were ascribed to cause cancer and miscarriages.<sup>99,98</sup> Therefore, despite Cl<sub>2</sub> is the most used chemical oxidant for drinking water due to its low cost, new advanced technologies are required in order to avoid the formation of DBPs.<sup>92,99,100</sup>

Numerous chemical oxidants have been used alone or in combination with adsorbents to optimize the process of micro pollutants elimination. Figure 1.8 presents the most common oxidative processes used in water treatment.

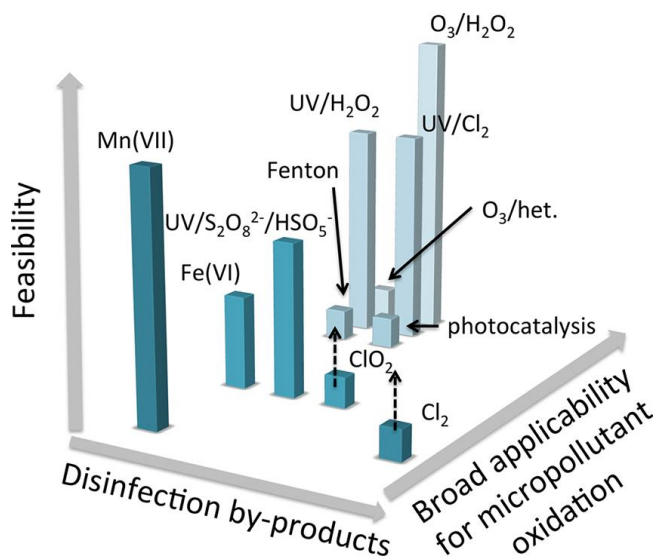


**Figure 1.8:** Comparison of various oxidative process for water treatment according to its feasibility, formation of DBPs and high broad applicability range of micro pollutants. The arrows for  $\text{Cl}_2$  and  $\text{ClO}_2$  shows that their feasibility is higher than the graph shows. **Example of how to read the graph:** Mn(VII) has low formation of DBPs, high feasibility (already widely applied) but it is very selective oxidant, so low range of micro pollutants oxidations.<sup>98</sup>

Advanced oxidation processes (AOPs) have already been applied for water treatment. They combine oxidants ( $\text{O}_3$  and/or hydrogen peroxide ( $\text{H}_2\text{O}_2$ )) with catalyst (iron sulphate ( $\text{FeSO}_4$ ), potassium permanganate ( $\text{KMnO}_4$ ), sodium persulfate ( $\text{Na}_2\text{S}_2\text{O}_8$ ), potassium peroxymonosulfate ( $\text{KHSO}_5$ )) and/or radiation (UV, sunlight or artificial light).<sup>101</sup> Under near ambient temperature and pressure, AOPs degrade organic pollutants based on the generation of reactive oxygen species (ROS) such as hydroxyl radical ( $\text{HO}^\bullet$ ) (Eq. 27-29), which is a stronger oxidant compared to other common oxidants used (Table 1.6).<sup>101</sup> The main drawback of AOPs is the high cost of reagents such as  $\text{O}_3$ ,  $\text{H}_2\text{O}_2$  and energy light sources. However, the use of renewable energy sources<sup>102</sup> as well as the generation of *in-situ*  $\text{H}_2\text{O}_2$  could reduce the cost.

**Eq. 27** Activation of  $\text{H}_2\text{O}_2$  with  $\text{O}_3$ <sup>103</sup>



**Eq. 28** Activation of  $\text{H}_2\text{O}_2$  with Fe salts<sup>103</sup>



**Eq. 29** Activation of  $\text{H}_2\text{O}_2$  with UV light<sup>103</sup>



**Table 1.6:** Potential oxidation of some common oxidants used.

Oxidant agent	Potential	Oxidant agent	Potential
$\cdot\text{OH}^{104}$	2.80 eV	$\text{HClO}_4^{104}$	1.49 eV
$\text{O}_2$ (atomic) <sup>104</sup>	2.42 eV	$\text{Cl}_2^{104}$	1.36 eV
$\text{O}_3^{104}$	2.08 eV	$\text{ClO}_2^{104}$	1.27 eV
$\text{Na}_2\text{SO}_4^{105}$	2.01 eV	$\text{O}_2$ (molecular) <sup>104</sup>	1.23 eV
$\text{H}_2\text{O}_2^{104}$	1.78 eV		

### 1.3.2 Fenton's oxidations: activation of $\text{H}_2\text{O}_2$ with Fe salts.

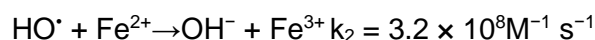
The activation of  $\text{H}_2\text{O}_2$  by  $\text{FeSO}_4$  were named after Henry J. Fenton, who reported that  $\text{H}_2\text{O}_2$  could be activated by Fe salts to oxidize tartaric acid in 1894.<sup>106</sup> Despite Fenton oxidations was not applied until 1960's, nowadays it is already applied for the treatment of highly polluted wastewater such as cosmetics, olive-mill, chemicals, pulp and paper, power plants or sawmills.<sup>106</sup>

Ferrous ion ( $\text{Fe}^{2+}$ ), added as a soluble  $\text{FeSO}_4$  salt, initiates and catalyses the decomposition of  $\text{H}_2\text{O}_2$ , resulting in the generation of  $\text{HO}\cdot$  (Eq. 30), which is a complex reaction sequence as shown below:<sup>103</sup> Eq. 30 is pH independent below pH ca. 3, however, the activity plateaus above pH c.a 4 due to the formation of iron hydroxide (II) ( $\text{Fe}(\text{OH})_2$ ) that is less reactive than  $\text{Fe}^{2+}$ .<sup>107</sup>

#### Eq. 30

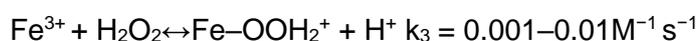


#### Eq. 31

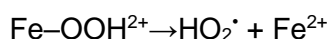


The reaction of  $\text{H}_2\text{O}_2$  with ferric ion ( $\text{Fe}^{3+}$ ) ions, referred as Fenton-like reactions, can regenerate the  $\text{Fe}^{2+}$  (Eq. 32-36).<sup>103</sup>

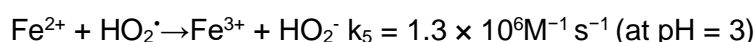
#### Eq. 32



#### Eq. 33



#### Eq. 34



#### Eq. 35

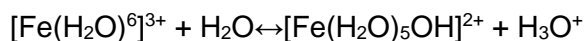


#### Eq. 36

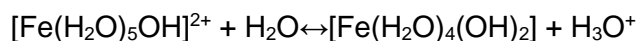


The main drawback of homogeneous Fenton oxidations is the formation of hydroxo complexes of Fe<sup>3+</sup> (Eq. 37-41). These reactions account for the coagulation capability of Fenton's reagent (sludge), which precipitate and reduce the amount of catalyst in the solution.<sup>103</sup>

**Eq. 37**

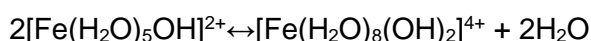


**Eq. 38**

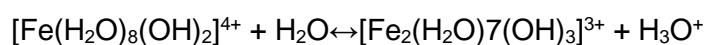


**Eq. 39**

Within pH 3 and 7, the above complexes become



**Eq. 40**



**Eq. 41**



The overall Fenton reaction can be written as follow (Eq. 42):<sup>103</sup>

**Eq. 42**



### 1.3.3 Heterogeneous Fenton's oxidations.

The main drawback of the homogeneous Fenton process is both; the loss of catalyst due to the formation of sludge and the pH adjustment (*ca.* 3) that would need to be neutralised at the end of the treatment process.<sup>108</sup> The use of catalytic wet peroxide oxidation (CWPO) or heterogeneous peroxide Fenton oxidation is a promising alternative. Using supported catalysts increases the surface area of the Fe species providing a matrix that enables the dispersion and chemical stability of the catalyst.<sup>106,109</sup> Besides, by a simple cost-effective procedures such as filtration, the catalyst would be removed from the solution. Supported Fe catalyst have shown great efficiency in the oxidation of a wide range of pollutants using commercial H<sub>2</sub>O<sub>2</sub>.<sup>109</sup> However, the activity and stability upon re-use of Fe supported catalyst has a great dependence on the synthetic route chosen and the Fe loading.<sup>110,109,111</sup> This is because the synthetic route, Fe loading as well as the post synthetic heat treatment (calcination, reduction, *etc.*) will dictate the types of Fe species generated, which each one may account for a certain activity and stability. For instance, the preferred synthetic route is to include the Fe during the synthesis of ZSM-5 zeolite (MFI, framework code of the international zeolite association (IZA)).<sup>112</sup> This way, Fe<sup>3+</sup> ions are atomically dispersed in the final crystalline lattice of the zeolite.<sup>112</sup> To make this ZSM-5 containing Fe<sup>3+</sup> catalytically active, part of the Fe is extracted from the lattice positions by post synthetic heat treatment

resulting in a wide variety of Fe species.<sup>112</sup> The Fe species may be roughly categorised in two types *i*) extra-framework Fe species (clusters and agglomerative Fe<sub>x</sub>O<sub>y</sub> particles) and *ii*) framework Fe species (Fe<sup>3+</sup> tetrahedrally coordinated in the ZSM-5 lattice, isolated Fe species and bi-nuclear Fe species immobilised in the framework channels). Their reactivity with H<sub>2</sub>O<sub>2</sub> may be group according to:

- i) The unavoidable leaching of extra-framework Fe from the catalysts giving rise to the undesired homogeneous Fenton reaction when reacting with H<sub>2</sub>O<sub>2</sub>.
- ii) The Fe “immobilised” within the zeolite structure giving heterogeneous Fenton reaction when reacting with the H<sub>2</sub>O<sub>2</sub>.

In most heterogeneous Fe catalysts, Fe mainly exist in as Fe<sup>3+</sup>, therefore the redox cycling of Fe<sup>3+</sup>/Fe<sup>2+</sup> is critical to keep the reaction going. However, compared to the reaction between Fe<sup>2+</sup> and H<sub>2</sub>O<sub>2</sub>, the reaction between Fe<sup>3+</sup> and H<sub>2</sub>O<sub>2</sub> is rate limiting with a rate between 0.01-0.001M<sup>-1</sup> s<sup>-1</sup>, which determines the overall efficiency. In addition, in these steps, H<sub>2</sub>O<sub>2</sub> is transformed to hydroperoxyl radical (HO<sub>2</sub>·), which is less reactive than the HO·.<sup>108</sup> There are several studies on how assist the heterogeneous Fenton reaction in order to increase its activity, such as UV-Vis assisted, electron or ultra-sonic assisted.<sup>113</sup>

#### **1.3.3.1 Phenol oxidation with heterogeneous Fenton catalysts and commercial H<sub>2</sub>O<sub>2</sub>.**

Phenol is a pollutant generated from industrial processes such as refineries, petrochemical plants and pharmaceuticals companies.<sup>114</sup> It can be found with a highest average concentration of 10 g/L along with other mono, di or tri-substituted-phenol derivatives, which are also considered hazardous.<sup>100</sup> Phenol is also a major concern for the environment, for instance, in Mediterranean countries, 30 million m<sup>3</sup> per year of olive oil containing high concentration of phenols are disposed.<sup>115</sup> The oxidation of phenol starts with the formation of phenol derivatives; catechol, 1,2-benzoquinone, hydroquinone, 1,4-benzoquinone and resorcinol. The ring opening rises the formation of carboxylic acids, which can be further oxidised until CO<sub>2</sub> and H<sub>2</sub>O (Figure 1.9).<sup>116</sup>

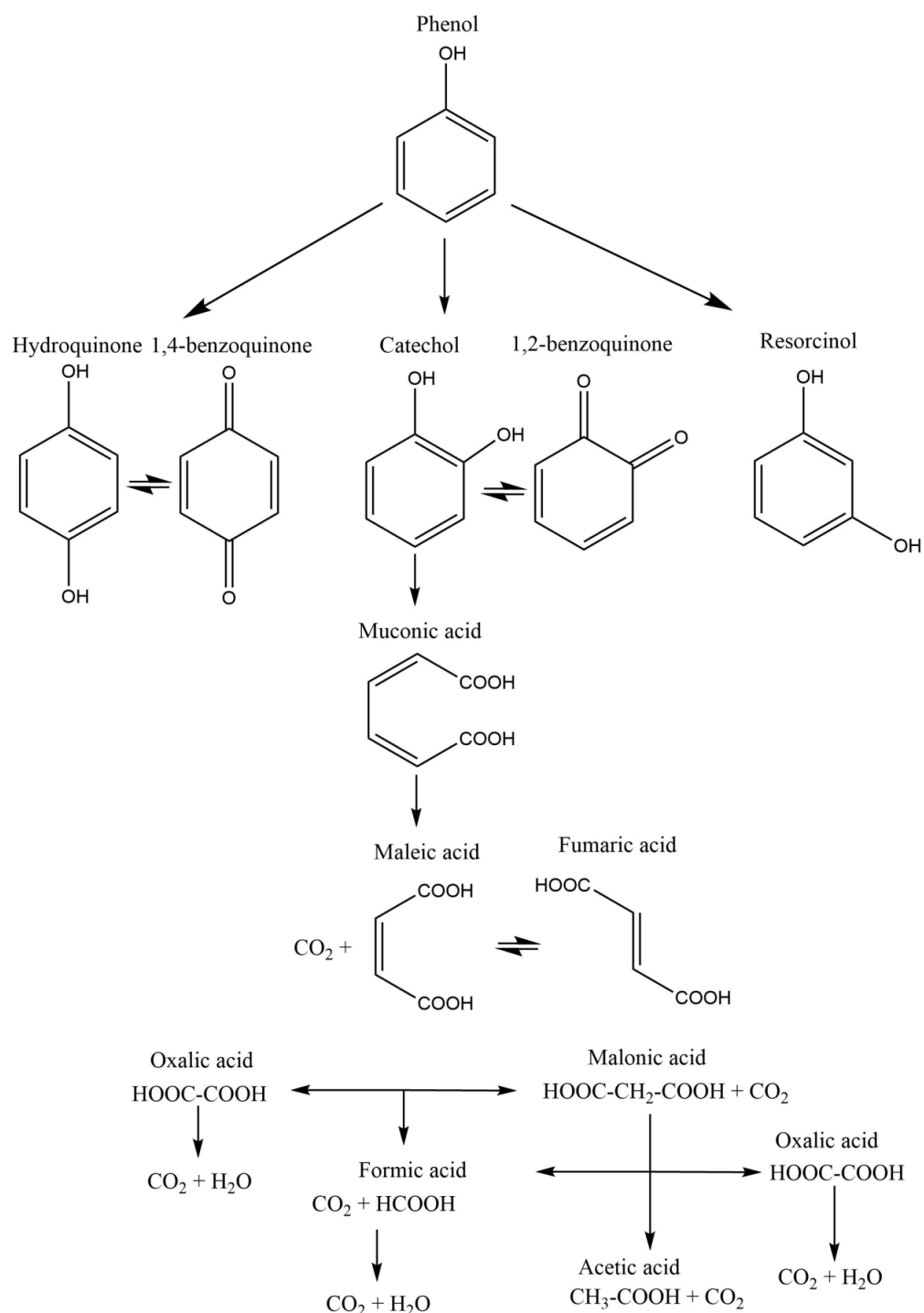


**Figure 1.9:** Schematic representation of the complete oxidation of phenol to CO<sub>2</sub> and H<sub>2</sub>O.<sup>116</sup>

The challenge in heterogeneous process is associated with the immobilisation of the Fe species over different supports in order to avoid Fe leaching and thus the deactivation of the catalyst upon reuse.<sup>117</sup> Various types of synthetic routes, supports and other monometallic metals alone or in combination with Fe have been investigated in order to address this. The activity towards the conversion of phenol, total organic carbon (TOC) removal, CO<sub>2</sub> selectivity and metal leaching for mono and bi-metallic FeCu with commercial H<sub>2</sub>O<sub>2</sub> are stated in Table 1.7 and Table 1.8 for the sake of comparison. TOC measures the

residual total carbon that remains in solution after the oxidation reaction has taken place. The CO<sub>2</sub> selectivity indicates the proportion of organic carbon that has been successfully removed from the solution and converted to CO<sub>2</sub>. For instance, TOC is usually measured before and after the reaction to determine the concentration of C in solution. To give an example, if 100 ppm and 50 ppm of C are measured before and after the reaction respectively, that would mean that 50 % of the C has been successfully removed from the solution as CO<sub>2</sub> gas. CO<sub>2</sub> measurements are usually employed to corroborate the TOC results. On the other hand, if 50 % of phenol has been successfully degraded, but TOC measurements indicate that there is still 100 ppm of C in the solution after the reaction, that would indicate that phenol has not been oxidised to CO<sub>2</sub> gas, instead it has been degraded to oxidative products such as phenol derivatives or di-acids as shown in Figure 1.9.

Soo Kim and co-workers<sup>117</sup> studied the crystallinity effect of the support towards the activity and stability of the Fe catalysts over ZSM-5, Zeolite-A, SiO<sub>2</sub> made by hydrothermal synthesis (Hsyn). The study concluded that 1.33 wt.% Fe/ZSM-5 presented the best activity and stability against leaching (90% phenol conversion, 6% Fe leaching) since the Fe was bonded in the framework and narrow channels. On the other hand, 1.02 wt.% Fe/Zeolite-A (40% conversion, 10% Fe leach) and 0.72 wt.% Fe/SiO<sub>2</sub> (30% conversion, 14% Fe leach) presented extra-framework Fe<sub>x</sub>O<sub>y</sub> species on the surfaces due to a poorer support crystallinity and thus, 1.02 wt.% Fe/Zeolite-A and 0.72 wt.% Fe/SiO<sub>2</sub> presented less stability.<sup>117</sup> Zhang and co-workers<sup>114</sup> prepared 1.5 wt.% Fe/ZSM-5 by Hsyn and 1.5 wt.% Fe<sub>2</sub>O<sub>3</sub>/ZSM-5 by incipient wetness impregnation (IWimp) and conclude that the framework (Fe) species and the extra-framework (Fe<sub>x</sub>O<sub>y</sub>) species have different activity.<sup>114</sup> Despite both had similar phenol conversion, 1.5 wt.% Fe/ZSM-5 (94.1 % conversion of phenol, 90.6 % CO<sub>2</sub> selectivity) and 1.5 wt.% Fe<sub>2</sub>O<sub>3</sub>/ZSM-5 (100 % conversion of phenol, 77.6 % CO<sub>2</sub> selectivity), the former was more active in completing the whole catalytic cycle from phenol to CO<sub>2</sub> and H<sub>2</sub>O, since the CO<sub>2</sub> selectivity is higher than for the mono-metallic 1.5 wt.% Fe<sub>2</sub>O<sub>3</sub>/ZSM-5 catalyst.<sup>114</sup> What this means is that the extra-framework (Fe<sub>x</sub>O<sub>y</sub>) species may be as active as the framework (Fe) ones to oxidise phenol, but not to oxidise the products generated as a result of the oxidation of phenol itself. Thus, the framework Fe species can complete the whole catalytic cycle, oxidising phenol, phenol derivatives and di-acids to CO<sub>2</sub> and H<sub>2</sub>O. This difference in the catalytic activity between the Fe species have also been drawn by Le Ha and co-workers.<sup>118</sup> In addition to this, Le Ha and co-workers studied the effect of Fe loading within the ZSM-5 structure (Fe/ZSM-5), varying the Si:Fe ratio from 203 to 43. The results showed that Fe/ZSM-5 (Si/Fe=203) catalyst presented 96 % of the Fe within the framework and 4 % as extra-framework, whereas, the Fe/ZSM-5 (Si/Fe=43) catalyst had 64 % Fe within the framework and 26 % as extra-framework. Thus, the lower the loading of Fe is, the greater proportion of framework Fe species are formed.<sup>118</sup> The

same conclusions were drawn by Gordo and co-workers<sup>110</sup> studying the Fe/TS-1 by Hsyn with different Fe loadings. They showed that the increasing loading of Fe/TS-1 from 0.64 wt.% to 4.43 wt.% made decreasing the crystallinity of the MFI structure as evidenced by XRD. The loss of crystallinity provoked the formation of extra-framework Fe species which they had leached at the end of the reaction.<sup>110</sup> The optimum heterogeneous Fenton catalyst should have no/little presence of extra-framework Fe species in order to avoid leaching as well as to be able to oxidise not only phenol but all the products formed as a result of its oxidation. Molina and co-workers<sup>111</sup> evidenced that the pore size of the support limits the diffusion of the products limiting their removal efficiency. They determined the TOC for both catalysts made by Hsyn (1.2 wt.% Fe/SiO<sub>2</sub>) and (1.2 wt.% Fe/SBA-15) made by co-condensation (Con). They concluded that, the poor catalytic activity of 1.2 wt.% Fe/SiO<sub>2</sub> by Hsyn towards the TOC removal (57.2 %) was due to its limited pore size (5.5 Å, 423 m<sup>2</sup>/g) compared to 1.2 wt.% Fe/SBA-15 by co-condensation (Con) with a TOC removal of 77.7 % (86 Å, 715 m<sup>2</sup>/g).<sup>111</sup>

**Table 1.7:** Activity towards the conversion of phenol, TOC removal, CO<sub>2</sub> selectivity and metal leaching (reported in ppm and % of metal leached respective the total loading of metal) with heterogeneous Fe catalysts and pre-formed H<sub>2</sub>O<sub>2</sub>. (Brackets indicate the catalytic synthetic route).

Catalysts	Phenol conversion	CO <sub>2</sub>	Metal leaching
	TOC removal	selectivity	Fe
<b>1.33 wt.% Fe/ZSM-5</b> <sup>117</sup> (Hsyn)	Phenol conv. (90 %)	n.d	6 %
<b>1.02 wt.% Fe/Zeolite-A</b> <sup>117</sup> (Hsyn)	Phenol conv. (40 %)	n.d	10 %
<b>0.72 wt.% Fe/SiO<sub>2</sub></b> <sup>117</sup> (Hsyn)	Phenol conv. (30 %)	n.d	14 %
<b>1.5 wt.% Fe/ZSM-5</b> <sup>114</sup> (Hsyn)	Phenol conv. (100 %)	77.6 %	4 ppm
<b>1.5 wt.% Fe<sub>2</sub>O<sub>3</sub>/ZSM-5</b> <sup>114</sup> IWimp	Phenol conv. (94.1 %)	90.6 %	6 ppm
<b>1.29 wt.% Fe/Na-Y</b> <sup>110</sup> Ion ex-change (IE)	Phenol conv. (n.d) TOC removal (78.5 %)	n.d	27.6 %
<b>1.08 wt.% Fe/USY</b> <sup>110</sup> (IE)	Phenol conv. (n.d) TOC removal (67.3%)	n.d	57.8 %
<b>0.33 wt.% Fe/ZSM-5</b> <sup>110</sup> (IE)	Phenol conv. (n.d) TOC removal (54.5 %)	n.d	73.9 %
<b>1.18 wt.% Fe/TS-1</b> <sup>110</sup> (Hsyn)	Phenol conv. (100 %) TOC removal (66.0 %)	n.d	18.3 %
<b>4 wt.% Fe<sub>2</sub>O<sub>3</sub>/Al<sub>2</sub>O<sub>3</sub></b> <sup>119</sup> Incipient wetness impregnation (IWimp)	Phenol conv. (100 %) TOC removal (60 %)	n.d	30 %
<b>1.2 wt% Fe/SBA-15</b> <sup>111</sup> (Con)	Phenol conv. (99.9 %) TOC removal (77.7 %)	n.d	75 %
<b>1.2 wt.% Fe/SiO<sub>2</sub></b> <sup>111</sup> (Hsyn)	Phenol conv. (99.3 %) TOC removal (57.2 %)	n.d	<10 %

**n.d:** no determined. **Reaction conditions: reference 117:** 250 mL phenol (10 ppm), catalyst (0.2 g/L), H<sub>2</sub>O<sub>2</sub> (2 %), H<sub>2</sub>SO<sub>4</sub> (pH=4), n.d rpm, 25 °C, 2 h. **Reference 114:** 200 mL phenol (2500 ppm), catalyst (0.5 g), H<sub>2</sub>O<sub>2</sub> (19,0000 ppm), pH=4, 400 rpm, 70 °C, 3 h. **Reference 110:** 140 mL phenol (1000 ppm), catalyst (0.084 g), H<sub>2</sub>O<sub>2</sub> (0.7 g), air (1MPa), 300 rpm, 100 °C, 2 h. **Reference 119:** 100 mL phenol (5000 ppm), H<sub>2</sub>O<sub>2</sub> (10 mL, 30 wt.%), 1000 rpm, 70 °C, 4 h. **Reference 111:** n.d g phenol (1000 ppm), catalyst (0.6 g/L), H<sub>2</sub>O<sub>2</sub> (5.1 g/L), 1MPa air, 350 rpm, 100 °C, 1.5 h.

Supported Cu heterogeneous catalyst have been studied and found to have high activity towards the oxidation of phenol (Table 1.8). Haure and co-workers<sup>120</sup> prepared a series of mono-metallic 30 wt.% CuO/ $\gamma$ -Al<sub>2</sub>O<sub>3</sub> catalyst by Molten method, that gave 100 % phenol conversion, 50 % TOC removal, with ca. 1.5 % Cu leaching at 50 °C. However, the conversion of phenol decreased to 40 % for the 4<sup>th</sup> run.<sup>120</sup> Zrncevic and co-workers<sup>121</sup> reported a more active supported 3.52 wt.% Cu/ZSM-5 and 3.54 wt.% Cu/Y catalysts made by IE. Their results concluded that the difference in activity from the Cu/ZSM-5 (95% conversion, 33.9 % TOC removal, 3.9% Cu leach) to Cu/Y-5 (100% conversion, 62.1 % TOC removal, 7.9 % Cu leach) was because the pore diameter of the H-ZSM-5 (0.54 x 0.56 nm) was very close to the size of the phenol (0.479 nm) and H<sub>2</sub>O<sub>2</sub> (0.248 nm).<sup>121</sup> In addition to this, Cu/Y presented more acid sites, which were believed to have aided to generating HO<sup>•</sup> radicals.<sup>121</sup> Both catalysts maintain their activity towards the conversion of phenol up to three re-uses.<sup>121</sup> The addition of the second metal such as Fe benefits the redox oxidation cycle, (Fe<sup>3+</sup>/Fe<sup>2+</sup> (standard reduction potential; 0.77 V) and Cu<sup>2+</sup>/Cu<sup>+</sup> (0.17 V)), because the reduction of Fe<sup>3+</sup> by Cu<sup>+</sup> is favourable in order to regenerate the Fe<sup>2+</sup> that is more active than the Fe<sup>3+</sup> analogue.<sup>122</sup> Guo and co-workers<sup>123</sup> studied the activity of mono and bi-metallic 10 wt.% FeCu(1:1)/ZSM-5 catalysts made by IWimp. They synthesised the ZSM-5 by Hsyn with two types of pore size, microporous (< 2nm) (MI) and mesoporous (<2-50> nm) (ME). They evidenced that the metal dispersion was enhanced when using ZSM-5 (ME) in comparison with ZSM-5 (MI). In terms of activity, 10 wt.% FeCu(1:1)/ZSM-5 (ME) (100 % phenol conversion, 10.7 % Cu and 8.1 % Fe leach) had greater activity compared to the bi-metallic 10 wt.% FeCu(1:1)/ZSM-5(MI) (60 % phenol conversion, 14.1 % Cu and 1.35 % Fe leach), which was concluded to be for the former having smaller particle size.<sup>123</sup> Despite of this, the metal leaching of Cu and Fe was still quite significant, which might be due to the methodology employed (IWimp) that has led to the formation of extra-framework Fe and Cu species (alfa-Fe<sub>2</sub>O<sub>3</sub> and CuO).

**Table 1.8:** Activity towards the conversion of phenol, TOC removal and metal leaching (reported in % of metal leached respective the total loading of metal) with mono and bi-metallic CuFe supported catalysts and pre-formed H<sub>2</sub>O<sub>2</sub>. (Brackets indicate the catalytic synthetic route).

<b>Catalysts</b>	<b>Phenol conversion</b>	<b>TOC</b>	<b>Metal leaching</b>
<b>30 wt.%CuO/y-Al<sub>2</sub>O<sub>3</sub></b> <sup>120</sup> (Molten)	100 %	50 %	1.5 %
<b>3.52 wt.% Cu/ZSM-5</b> <sup>121</sup> (IE)	95 %	33.9 %	3.9 %
<b>3.54 wt.% Cu/Y</b> <sup>121</sup> (IE)	100 %	62.1 %	7.9 %
<b>2.53 wt.% Cu/ZSM-5</b> <sup>124</sup> (Hsyn)	80 %	n.d	3.2 %
<b>2.53 wt.% Cu/ZSM-5</b> <sup>124</sup> (IE)	100 %	n.d	4.8 %
<b>10wt.%Cu/ZSM-5 (MI)</b> <sup>123</sup> (IWimp)	58 %	n.d	8.5 %
<b>10wt.%Cu/ZSM-5 (ME)</b> <sup>123</sup> (IWimp)	70 %	n.d	7.9 %
<b>10wt.%Fe/ZSM-5 (MI)</b> <sup>123</sup> (IWimp)	0	n.d	0.2 %
<b>10wt.%Fe/ZSM-5 (ME)</b> <sup>123</sup> (IWimp)	20 %	n.d	3.2 %
<b>10wt.%FeCu(1:1)/ZSM-5(MI)</b> <sup>123</sup>	60 %	n.d	14.1 % (Cu) 1.35 % (Fe)
<b>10wt.%FeCu(1:1)/ZSM-5(ME)</b> <sup>123</sup> (IWimp)	100 %	n.d	10.7 % (Cu) 8.1 % (Fe)
<b>1.2 wt.% Cu-2.3 wt.% Fe/C</b> <sup>122</sup> (Co-polymer self-assembly)	100 %	83.7 %	0.57 ppm Fe n.d (Cu)

**n.d:** no determined. **Reaction conditions: Reference 120:** 170 g phenol (1000 ppm), catalyst (1.75 g), H<sub>2</sub>O<sub>2</sub> (3.3 g), 800 rpm, 70 °C, 3 h. **Reference 121:** 200 g phenol (941 ppm), catalyst (0.02 g), H<sub>2</sub>O<sub>2</sub> (0.68 g), 200 rpm, 80 °C, 3 h. **Reference 124:** 200 mL phenol (941 ppm), catalyst (0.02 g), H<sub>2</sub>O<sub>2</sub> (0.1 M), 200 rpm, 80 °C, 3 h. **Reference 123:** 50 g phenol (1000 ppm), catalyst (0.02 g), H<sub>2</sub>O<sub>2</sub> (10.76 g), n.d rpm, 50 °C, 1.6 h. **Reference 122:** 100 mL (100 ppm), catalyst (0.03 g), H<sub>2</sub>O<sub>2</sub> (30 mM), H<sub>2</sub>SO<sub>4</sub> (pH=3), n.d rpm, 28 °C, 12 h.

The reaction conditions have shown to have great influence on the activity of supported Fenton catalysts. Rahman and co-workers<sup>125</sup> studied the effect of the temperature, mass of catalysts and molar ratio of reactants (phenol: H<sub>2</sub>O<sub>2</sub>) with a mono-metallic 10 wt.% Fe/SiO<sub>2</sub> catalyst made by sol extraction and sol-gel techniques.<sup>125</sup> An increase in temperature made enhancing the conversion of phenol from 43.3 % (30 °C) to 68.0 % (70 °C). However, higher temperature (80 °C) did not show any significant increase in phenol conversion (68.3 %) due to the decomposition of H<sub>2</sub>O<sub>2</sub>. The oxidation of phenol was also measured at different catalyst masses from 0.01 g to 0.07 g. The maximum efficiency was found at 0.03 g with a 68.0 % conversion, unfortunately, higher amounts decreased the conversion of phenol progressively down to 61.6 % with 0.07 g of catalyst. However, these differences in conversion due to the catalyst mass loading were not considered significant. On the other hand, the molar ratio of phenol: H<sub>2</sub>O<sub>2</sub> had a major influence in the conversion, the activity increased from 41.0 % with a 1:0.5 ratio to 95.2 % with a 1:2. Blank results proved that this high activity of 95.2 % was due to having Fe and H<sub>2</sub>O<sub>2</sub> in the same reaction mixture.<sup>125</sup>

### 1.3.3.2 Phenol oxidation with heterogeneous Fenton catalyst and *in-situ* H<sub>2</sub>O<sub>2</sub>.

The *in-situ* generation of H<sub>2</sub>O<sub>2</sub> could improve the efficiency in heterogeneous Fenton's oxidation reactions. First of all, generating H<sub>2</sub>O<sub>2</sub> on-site, would avoid problems associated with the transportation, storage and handling of high concentrated amounts of H<sub>2</sub>O<sub>2</sub>.<sup>126</sup> The main problem is the risk of explosion of H<sub>2</sub> and O<sub>2</sub> mixtures have. However, this have been overcome by different approaches and applied successfully to the oxidation of phenol; *i)* diluting the H<sub>2</sub> and O<sub>2</sub> gas feed with inert gas (CO<sub>2</sub>) below the explosive limit (< 4 mol % H<sub>2</sub>)<sup>24</sup> with FePd/TiO<sub>2</sub> catalysts<sup>127</sup> *ii)* using other sources of H<sub>2</sub>; hydrazine<sup>128,129</sup>, hydroxylamine<sup>130,129</sup>, formic acid<sup>126,131,132,133</sup> with O<sub>2</sub> with PdFe catalysts *iii)* reduction of molecular O<sub>2</sub> by electrochemistry with Fe catalysts<sup>134,135</sup> *iv)* reduction of molecular O<sub>2</sub> using enzymatic methodologies.<sup>136</sup> Table 1.9 compares the phenol conversion, TOC removal and metal leaching by using different H<sub>2</sub> source. Employing formic acid and hydroxylamine sulphate as a H<sub>2</sub> source seems to be the most promising approach since it does not require the addition of acids, contrarily to hydrazine hydrate, which inherent basic pH (*ca.* 9) promoted the decomposition of the *in-situ* H<sub>2</sub>O<sub>2</sub> and subsequently no degradation of phenol could be achieved.<sup>129</sup> However, ex-changing hydrazine hydrate for hydrazine sulphate would avoid the acidification of the solution.<sup>128</sup> The presence of Br<sup>-</sup> and the acidity brought from the

sulphate salt was found to be critical in order to have activity.<sup>128,132</sup> However, when the *in-situ* H<sub>2</sub>O<sub>2</sub> is used as a direct oxidant using formic acid, hydrazine hydrate and hydroxylamine sulphate as H<sub>2</sub> source, the addition of Br<sup>-</sup> was believed to poison FePd supported catalyst, since no degradation of phenol was achieved.<sup>129</sup> Little/no residual organic H<sub>2</sub> sources at the end of the reaction would be ideal, especially hydrazine hydrate and hydroxylamine sulphate since they are classified as carcinogenic.<sup>126</sup> Contrarily, using H<sub>2</sub> gas below the explosive limits, avoids the disadvantage of having remaining toxic reagents in the solution.

Great efficiency in phenol conversion, TOC removal and minimal leaching is achieved by reducing the O<sub>2</sub> electrochemically to produce *in-situ* H<sub>2</sub>O<sub>2</sub> (100 % phenol conversion, 99 % TOC removal).<sup>134</sup> In this instance, the *in-situ* H<sub>2</sub>O<sub>2</sub> was first generated employing an electrolysis cell, before being added to a batch reaction containing 50 ppm of phenol.<sup>134</sup> Finally, excellent phenol conversion and TOC removal was achieved by oxidation of phenol with enzymes as Table 1.9 shows. This was a one-pot tri-enzymatic cascade reaction where, the horseradish peroxidase (HRP) uses the *in-situ* H<sub>2</sub>O<sub>2</sub> (generated by a flavin protein, that uses NADH as a source of H<sup>+</sup>, to reduce molecular O<sub>2</sub>) to oxidise phenol. This approach is quite promising because apart from achieving high conversion of phenol, it does not generate further pollution caused by metal leaching.<sup>136</sup>

**Table 1.9:** Comparison of the activity for phenol oxidation, TOC removal and metal leaching for different H<sub>2</sub> sources. (Brackets indicate the catalytic synthetic route).

Catalysts	H <sub>2</sub> source	Phenol conversion	Metal leaching
2.5 wt.% Pd-2.5 wt.% Fe/TiO <sub>2</sub> <sup>127</sup> (Mimp)	5 % H <sub>2</sub> /CO <sub>2</sub>	78 %	(0 Pd, 38 % Fe)
5 wt.% Pd-1 wt.% Fe/ Al <sub>2</sub> O <sub>3</sub> <sup>129</sup> Conventional impregnation (Cimp)	Formic acid	ca. 90 % (78 % TOC removal)	(0 Pd, 0 Fe)
5 wt.% Pd-1 wt.% Fe/ Al <sub>2</sub> O <sub>3</sub> <sup>129</sup> (Cimp)	Hydrazine hydrate	70 % (40 % TOC removal)	(0 Pd, 20 % Fe)
5 wt.% Pd-1 wt.% Fe/ Al <sub>2</sub> O <sub>3</sub> <sup>129</sup> (Cimp)	Hydroxylamine sulphate	70 % (20% TOC removal)	(0 Pd, 8 % Fe)
9 wt.% Fe/C <sup>134</sup> (IWimp)	Electrochemic- al O <sub>2</sub> reduction	100 % (99 % TOC removal)	0.1 % Fe
Tri-enzymatic cascade reaction <sup>136</sup>	Enzymatic O <sub>2</sub> reduction	100 %	n/a

**n/a:** not applicable. **Reaction conditions: Reference 127:** 8.5 g phenol (1000 ppm), catalyst (0.01 g), 420 psi of 5 % H<sub>2</sub>/CO<sub>2</sub> and 160 psi 25 % O<sub>2</sub>/CO<sub>2</sub>, 1200 rpm, 30 °C, 2 h. **Reference 129: Formic acid:** 50 g phenol (100 ppm), catalyst (0.1 g), 40 mM formic acid and 20 mL/min flow of O<sub>2</sub>, n.d rpm, 25 °C, 6 h. **Reference 129: Hydrazine:** 50 g phenol (100 ppm), catalyst (0.1 g), 20 mM hydrazine hydrate (N<sub>2</sub>H<sub>4</sub>·H<sub>2</sub>O), pH ca. 3 (H<sub>2</sub>SO<sub>4</sub>) and 20 mL/min flow of O<sub>2</sub>, n.d rpm, 25 °C, 6 h. **Reference 129: Hydroxylamine:** 50 g phenol (100 ppm), catalyst (0.1 g), 40 mM hydroxylamine sulfate ((NH<sub>2</sub>OH)<sub>2</sub>·H<sub>2</sub>SO<sub>4</sub>) and 20 mL/min flow of O<sub>2</sub>, n.d rpm, 25 °C, 6 h. **Reference 134:** 40 mL phenol (50 ppm), 4.6 M ratio H<sub>2</sub>O<sub>2</sub>/phenol, 5.5 h. **Reference 136:** ultra centrifugal tube 1 mL phenol (1 mM), 0.1 M formic acid with nicotinamide and 0.1 M sodium phosphate with Flavin, 22 h.

#### 1.4 Research objectives.

This thesis will be focused on developing promising metal supported catalysts for water treatment remediation via reactive oxygen species (ROS) generation from *in-situ* H<sub>2</sub>O<sub>2</sub>. The activity of metal supported catalysts towards the direct synthesis of H<sub>2</sub>O<sub>2</sub> is commonly reported employing water with organic co-solvents and sub-ambient temperatures (< 10 °C) in order to stabilise the H<sub>2</sub>O<sub>2</sub> and minimise its degradation. These conditions are not suitable for water remediation, therefore the first chapter of results (Chapter 3) will study the capacity of a series of bi-metallic supported catalysts towards the direct synthesis and degradation of H<sub>2</sub>O<sub>2</sub> at conditions more suitable for water remediation (ambient temperatures (25 °C) and water-only as solvent). Bi-metallic AuPd supported catalysts have been discussed in this present chapter and they were shown to be the promising towards the direct synthesis

of  $\text{H}_2\text{O}_2$ . Several authors have shown that Au is able to drive the selectivity of the Pd towards the formation of  $\text{H}_2\text{O}_2$  via the generation of AuPd alloys nanoparticles with a size *c.a* 2.5 nm. Thus, to carry out this study, mono and bi-metallic AuPd supported catalysts on  $\text{TiO}_2$  will be prepared by modified impregnation. (1.0 wt.% Au/ $\text{TiO}_2$ , 0.75 wt.% Au-0.25 wt.% Pd/ $\text{TiO}_2$ , 0.50 wt.% Au-0.50 wt.% Pd/ $\text{TiO}_2$ , 0.25 wt.% Au-0.75 wt.% Pd/ $\text{TiO}_2$  and 1.0 wt.% Pd/ $\text{TiO}_2$ ). Their activity towards the direct synthesis and degradation of  $\text{H}_2\text{O}_2$  will be measured at different reaction conditions that will be changed stepwise, starting from mixtures of water and organic co-solvent (67 %  $\text{CH}_3\text{OH}$  in water) and sub-ambient temperatures (2 °C) to end up with water-only as solvent and ambient temperatures (25 °C). Therefore, it will be possible to determine how the catalytic activity and selectivity –for the whole set of catalysts- changes with the reaction conditions. In addition to this, this work is meant to determine if by increasing the Au:Pd ratio could enhance the activity and selectivity at conditions more suitable for water remediation, since Au has been acknowledged to be minimising the degradation of  $\text{H}_2\text{O}_2$ .

The activity towards the direct synthesis and degradation of  $\text{H}_2\text{O}_2$  for the mono and bi-metallic 1 wt.% AuPd/ $\text{TiO}_2$  catalysts will be performed using a Parr Instrument (Autoclave). The extent of  $\text{H}_2$  conversion and  $\text{H}_2\text{O}_2$  selectivity will be determined by analysis of the post-reaction gas phase by means of gas chromatography (GC). In addition, the analysis of the post-reaction solution after the direct synthesis of  $\text{H}_2\text{O}_2$  will be analysed by microwave plasma-atomic emission spectrometry (MP-AES) to quantify the stability of the Au and Pd against leaching. The set of catalysts will be characterised by means of spectroscopy and microscopy techniques to find a linkage between their nanoparticles mean size and metals oxidation with the catalytic activity. X-ray photoelectron spectroscopy (XPS) will be employed to determine the oxidation state of the Pd (Pd and  $\text{Pd}^{2+}$ ), which can influence the selectivity of the catalysts towards the direct synthesis of  $\text{H}_2\text{O}_2$ . X-ray diffraction (XRD) will be employed to determine the crystallinity structure of the  $\text{TiO}_2$  (P25) after the impregnation of the metals as well as to provide an approximate indication of metal nanoparticle size. The particle size and distribution are considered to be one of the key parameters responsible for dictating catalytic performance of AuPd bi-metallic catalysts for the direct synthesis of  $\text{H}_2\text{O}_2$ , therefore, transmission electron microscopy (TEM) will be employed for this used.

Chapter 4 will determine the efficiency in converting the *in-situ*  $\text{H}_2\text{O}_2$  into ROS to degrade a model polluted water containing 1000 ppm of phenol. Fenton-Pd based catalysts will be used to generate *in-situ*  $\text{H}_2\text{O}_2$ , which will be subsequently converted into ROS by the Fenton metal using only-water as solvent –with diluted phenol- at 30 °C. Bi-metallic combinations of 0.5 wt.% X-0.5 wt.% Pd/ $\text{TiO}_2$  (X: Cu, Fe, Co) catalysts will be synthesised by modified impregnation and tested towards the degradation of phenol in order to determine the most optimum Fenton metal (Cu, Fe and Co) to generate ROS from *in-situ*  $\text{H}_2\text{O}_2$ . Once the most

appropriate combination in terms of activity towards the degradation of phenol is determined, a series of mono and bi-metallic 1 wt.% XPd/TiO<sub>2</sub> catalyst with different X:Pd ratios (1.0 wt.% X/TiO<sub>2</sub>, 0.75 wt.% X-0.25 wt.% Pd/TiO<sub>2</sub>, 0.50 wt.% X-0.50 wt.% Pd/TiO<sub>2</sub>, 0.25 wt.% X-0.75 wt.% Pd/TiO<sub>2</sub> and 1.0 wt.% Pd/TiO<sub>2</sub>) will be made by modified impregnation to establish the most appropriate ratio between the Pd and the secondary metal to oxidise phenol. In addition, these set of mono and bi-metallic catalysts will be also tested towards the formation and degradation of H<sub>2</sub>O<sub>2</sub>, at the same reaction conditions as the degradation of phenol, in order to determine any correlation between the extent of phenol conversion and the formation/degradation of H<sub>2</sub>O<sub>2</sub>. The catalytic testing will be carried out using an autoclave (Parr Instruments) at 30 °C with no organic solvents present in the reaction medium. The conversion of phenol and the products generated as a result of the oxidation will be measured by means of high-pressure liquid chromatography (HPLC). The post-reaction solution after the direct synthesis of H<sub>2</sub>O<sub>2</sub> and degradation of phenol will be analysed by MP-AES in order to determine the stability of the Pd and the secondary metal during both sets of reactions. Finally, the extent of H<sub>2</sub> conversion and H<sub>2</sub>O<sub>2</sub> selectivity will be determined by GC analysis of the post-reaction gas phase.

In terms of characterisation, XPS analysis will be employed to determine the oxidation state of the secondary metal and Pd (Pd<sup>0</sup> and Pd<sup>2+</sup>). XRD will be employed to analyse the reflections arising from the support TiO<sub>2</sub> (P25) after the impregnation of the metals and to provide an indication of particle size. TEM will be used to calculate the mean particle size and distribution of the metal nanoparticles supported on the catalysts.

According to several authors in the reviewed literature of this present document, Fenton metals's stability and activity towards the degradation of phenol could be optimised by anchoring the metals in a framework structure such as a zeolite. Thus, Chapter 5 will find a synthetic route for the optimal catalyst formulations identified in Chapter 4, where HZSM-5 supports containing the optimal secondary Fenton metal will be introduced within the zeolitic framework by hydrothermal synthesis, followed by the addition of Pd by modified impregnation. The loading of Pd will be kept constant with a total loading of 0.5 wt.%, whereas secondary metal loading will be varied in order to find a correlation between the speciation of Fe (framework species, extra-framework clusters and agglomerates) and their respective stability and activity towards the degradation of phenol. These bi-metallic supported catalysts will be also investigated towards the direct synthesis and degradation of H<sub>2</sub>O<sub>2</sub> in order to determine any correlation between the conversion of phenol and the formation/degradation of H<sub>2</sub>O<sub>2</sub>. The conversion of phenol and the products generated as a result of the oxidation will be measured by means of HPLC, whereas the extent of H<sub>2</sub> conversion and H<sub>2</sub>O<sub>2</sub> selectivity will be determined by GC analysis of the post-reaction gas

phase. Finally, the post-reaction solution will be analysed by MP-AES to determine the extent of metal leaching during the degradation of phenol and direct synthesis of H<sub>2</sub>O<sub>2</sub>.

In terms of characterisation, XPS will be used for the determination of the oxidation state of each metal, XRD will be employed to determine the crystallinity of the bare synthesised zeolite and the zeolite containing active metals. Physisorption analysis will be used to determine the specific surface area and micropore volume of the bi-metallic formulations. Physisorption and XRD data are considered critical for these catalysts since they will determine if the introduction of the metals in the HZSM-5 has an effect in the crystallinity. TEM microscopy will be employed to obtain information about the mean particle size and distribution of the metal nanoparticles. Diffuse reflectance ultra-violet visible spectroscopy (DR UV-Vis) and Raman-UV will be employed to determine the speciation of the Fe in the catalysts since each different Fe specie can be accounted to a certain activity and stability.

The catalyst's synthetic methodologies used in this work, modified impregnation and hydrothermal synthesis as well as the catalyst's reactor settings for each reaction will be clearly defined stepwise in Chapter 2. Also, this chapter contains a general background about each spectroscopic and microscopic technique employed as a means of catalysts characterisation. Finally, Chapter 6 will draw the conclusions from each chapter of results and also outline other promising lines of investigation for future work.

## 1.5 References.

1. Stoltze, P. Introduction to heterogeneous catalysis (Wiley-VCH, 1998).
2. Rothenberg, G. Catalysis Concepts and green applications (Wiley-VCH, 2008).
3. Adams, C. Applied catalysis: A predictive socioeconomic history. *Top. Catal.* **52**, 924–934 (2009).
4. Atkins, P., Overton, T., Rourke, J., Weller, M., Armstrong, F. *Inorganic Chemistry*. (Shriver and Atkins, Oxford University Press, 2006).
5. Anastas, P., Eghbali, N. Green chemistry: Principles and practice. *Chem. Soc. Rev.* **39**, 301–312 (2010).
6. Chorkendorff, I., Niemantsverdriet, J.W. Concepts of modern catalysis and kinetics. (Wiley-VCH, 2003).
7. Svehla, G. Nomenclature of kinetic methods of analysis. *Pure Appl. Chem.* **65**, 2291–2298 (1993)
8. Atkins, Peter., de Paula, J. *Atkin's physical chemistry*. (Oxford University Press Inc., USA, 2008).
9. Klaewkla, R., Arend, M., Hoelderich, W. F. A Review of Mass Transfer Controlling the Reaction Rate in Heterogeneous Catalytic Systems. (InTech China, China, 2014).

10. Campos-Martin, J. M., Blanco-Brieva, G., Fierro, J. L. G. Hydrogen peroxide synthesis: An outlook beyond the anthraquinone process. *Angew. Chemie-Int. Ed.* **45**, 6962–6984 (2006).
11. Zhou, R., Zhang, T., Zhou, R., Wang, S., Mei, D., Mai-Prochnow, A., Weerasinghe, J., Fang, Z., Ostrikov, K., Cullen, P. Sustainable plasma-catalytic bubbles for hydrogen peroxide synthesis. *Green chem.* **23**, 2977–2985 (2021).
12. Ciriminna, R., Albanese, L., Meneguzzo, F., Pagliaro, M. Hydrogen Peroxide : A Key Chemical for Today's Sustainable Development. *Chemsuschem.* **9**, 3374–3381 (2016).
13. Nyamunda, B. C., Chigondo, F., Moyo, M., Guyo, U. Hydrogen peroxide as an oxidant for organic reactions. *J. Atoms and Molecules.* **3**, 22–44 (2013).
14. Noyori, R., Aoki, M., Sato, K., Noyori, R. Green oxidation with aqueous hydrogen peroxide. *ChemComm.* **34**, 1977–1986 (2003).
15. Russo, V., Tesser, R., Santacesaria, E. Serio, M. Di. Chemical and Technical Aspects of Propene Oxide Production via Hydrogen Peroxide ( HPPO Process ). *Ind. Eng. Chem. Res.* **52**, 1168-1178 (2013).
16. Khatib, S. J., Oyama, S. T. Direct Oxidation of Propylene to Propylene Oxide with Molecular Oxygen: A Review. *Catal. Rev-Sci. Eng.* **57**, 306–344 (2015).
17. Edwards, J. K., Freakley, S. J., Lewis, R. J., Pritchard, J. C., Hutchings, G. J. Advances in the direct synthesis of hydrogen peroxide from hydrogen and oxygen. *Catal. Today.* **248**, 3–9 (2015).
18. Wernimont, E., Ventura, M., Garboden, G., Mullens, P. Past and present uses of rocket grade hydrogen peroxide. *Gen. Kinet. LLC Aliso Viejo, CA.* 1–15 (1999).
19. Ranganathan, S., Sieber, V. Recent Advances in the Direct Synthesis of Hydrogen Peroxide Using Chemical Catalysis - A Review. *Catalysts.* **23**, 379–401 (2018).
20. Yi, Y., Wang, L., Li, G., Guo, H. A review on research progress in the direct synthesis of hydrogen peroxide from hydrogen and oxygen: Noble-metal catalytic method, fuel-cell method and plasma method. *Catal. Sci. Technol.* **6**, 1593–1610 (2016).
21. BBC News: [http://news.bbc.co.uk/2/hi/uk\\_news/england/london/4197500.stm](http://news.bbc.co.uk/2/hi/uk_news/england/london/4197500.stm)
22. Yang, S., Verdaguer-Casadevall, A., Arnarson, L., Silvioli, L., Čolić, V., Frydendal, R., Rossmeisl, J., Chorkendorff, Ib., Stephens, E.L. Toward the Decentralized Electrochemical Production of H<sub>2</sub>O<sub>2</sub> : A Focus on the Catalysis. *ACS Catal.* **8**, 4064–4081 (2018).
23. Beckman, E. J. Production of H<sub>2</sub>O<sub>2</sub> in CO<sub>2</sub> and its use in the direct synthesis of propylene oxide. *Green Context.* **5**, 332–336 (2003)
24. Samanta, C. Direct synthesis of hydrogen peroxide from hydrogen and oxygen: An overview of recent developments in the process. *Appl. Catal. A Gen.* **350**, 133–149 (2008).

25. Yang, T., Yang, C., Le, J., Yu, Z., Bu, L., Li, L., Bai, S., Shao, Q., Hu, Z., Pao, C-W., Cheng, J., Feng, Y., Huang, X. Atomically isolated Pd sites within Pd-S nanocrystals enable trifunctional catalysis for direct, electrocatalytic and photocatalytic syntheses of H<sub>2</sub> O<sub>2</sub>. *Nano research*. **15**, 1861–1867 (2022).
26. Kim, M.C., Han, G.H., Xiano, X., Song, J., Hong, E.J., Kim, H.K., Ahn, J.P., Han, S.S., Lee, K.Y., Yu, T. Applied Surface Science Anisotropic growth of Pt on Pd nanocube promotes direct synthesis of hydrogen peroxide. *Appl. Surf. Sci.* **562**, 150031-150040 (2021).
27. Song, W., Zhao, R., Yu, L., Xie, X., Sun, M., Li, Y. Enhanced Catalytic Hydrogen Peroxide Production from Hydroxylamine Oxidation on Modified Activated Carbon Fibers : The Role of Surface Chemistry. *Catalysts*. **11**, 1515-1533 (2021).
28. Hydroxylamine hydrochloride (Safety data sheet, Sigma aldrich 1–11 (2022)).
29. Lunsford, J. H. The direct formation of H<sub>2</sub>O<sub>2</sub> from H<sub>2</sub> and O<sub>2</sub> over palladium catalysts. *J. Catal.* **216**, 455–460 (2003).
30. Landon, P., Collier, P.J., Carley, A.F., Chadwick, D., Papworth, A.J., Burrows, A., Kiely, C.J., Hutchings, G.J. Direct synthesis of hydrogen peroxide from H<sub>2</sub> and O<sub>2</sub> using Pd and Au catalysts. *Phys. Chem. Chem. Phys.* **5**, 1917–1923 (2003).
31. Choudhary, V. R., Gaikwad, A. G., Sansare, S. D. Activation of supported Pd metal catalysts for selective oxidation of hydrogen to hydrogen peroxide. *Catal. Letters*. **83**, 235–239 (2002).
32. Choudhary, V. R., Samanta, C., Choudhary, T. V. Direct oxidation of H<sub>2</sub> to H<sub>2</sub>O<sub>2</sub> over Pd-based catalysts: Influence of oxidation state, support and metal additives. *Appl. Catal. A Gen.* **308**, 128–133 (2006).
33. Samanta, C., Choudhary, V. R. Direct formation of H<sub>2</sub>O<sub>2</sub> from H<sub>2</sub> and O<sub>2</sub> and decomposition/hydrogenation of H<sub>2</sub>O<sub>2</sub> in aqueous acidic reaction medium over halide-containing Pd/SiO<sub>2</sub> catalytic system. *Catal. Commun.* **8**, 2222–2228 (2007).
34. Wang, F., Xia, C., Visser, S. P. De., Wang, Y. How Does the Oxidation State of Palladium Surfaces Affect the Reactivity and Selectivity of Direct Synthesis of Hydrogen Peroxide from Hydrogen and Oxygen Gases ? A Density Functional Study. *J Am Chem Soc.* **141**, 901-910 (2019).
35. Choudhary, V. R., Samanta, C. Role of chloride or bromide anions and protons for promoting the selective oxidation of H<sub>2</sub> by O<sub>2</sub> to H<sub>2</sub>O<sub>2</sub> over supported Pd catalysts in an aqueous medium. *J. Catal.* **238**, 28–38 (2006).
36. Choudhary, V. R., Sansare, S. D., Gaikwad, A. G. Direct oxidation of H<sub>2</sub> to H<sub>2</sub>O<sub>2</sub> and decomposition of H<sub>2</sub>O<sub>2</sub> over oxidized and reduced Pd-containing zeolite catalysts in acidic medium. *Catalysis Letters*. **84**, 81–87 (2002).
37. Choudhary, V. R., Samanta, C., Jana, P. Hydrogenation of hydrogen peroxide over palladium/carbon in aqueous acidic medium containing different halide anions under

- static/flowing hydrogen. *Ind. Eng. Chem. Res.* **46**, 3237–3242 (2007).
38. Freakley, S. J. Freakley, S. J., Piccinini, M., Edwards, J. K., Ntainjua, E.N., Moulijn, J. A., Hutchings, G. J. Effect of reaction conditions on the direct synthesis of hydrogen peroxide with a AuPd/TiO<sub>2</sub> catalyst in a flow reactor. *ACS Catal.* **3**, 487–501 (2013).
  39. Biasi, P., Sterchele, S., Bizzotto, F., Maela, M., Lindholm, S., Ek, P., Bobacka, J., Mikkola, J-P., Salmi, T. Application of the catalyst wet pretreatment method (CWPM) for catalytic direct synthesis of H<sub>2</sub>O<sub>2</sub>. *A1 Journal.* **246**, 2007-2015 (2015).
  40. Park, S., Jeong G.S., Ji Chul J., Sung-Hyeon B., Tae J. K., Young-Min C., Seung-Hoon O., In Kyu S., Direct synthesis of hydrogen peroxide from hydrogen and oxygen over palladium catalysts supported on TiO<sub>2</sub>–ZrO<sub>2</sub> mixed metal oxides. *Catal. Commun.* **10**, 1762–1765 (2009).
  41. Park, S., Kim, T.J., Chung, K-Y., Oh, S-H., Song, I K. Direct Synthesis of Hydrogen Peroxide from Hydrogen and Oxygen over Palladium Catalyst Supported on SO<sub>3</sub>H-Functionalized SBA-15. *Catal Lett.* **130**, 296–300 (2009).
  42. Park, S., Baeck, S-H., Kim, T.J., Chung, Y-M., Oh, S-H., Song, I.K., Direct Synthesis of Hydrogen Peroxide from Hydrogen and Oxygen Over Palladium Catalysts Supported on SO<sub>3</sub> H-Functionalized SiO<sub>2</sub> and TiO<sub>2</sub>. *Catal Lett.* **130**, 604-607 (2009).
  43. Melada, S., Rioda, R., Menegazzo, F., Pinna, F., Strukul, G. Direct synthesis of hydrogen peroxide on zirconia-supported catalysts under mild conditions. *Journal of catalysis.* **239**, 422–430 (2006).
  44. Ntainjua, N.E., Edwards, J.K., Carley, A.F., Lopez-Sanchez, J.A., Moulijn, J.A., Herzing, A.A., Kiely, C.J., Hutchings, G.J. The role of the support in achieving high selectivity in the direct formation of hydrogen peroxide. *Green Chem.* **10**, 1162–1169 (2008).
  45. Hu, B., Weiping, D., Rongsheng, L., Qinghong, Z., Ye, W., Francine, D.J., Deschrijver, P., Frederique, D., Pierre, M., Carbon-supported palladium catalysts for the direct synthesis of hydrogen peroxide from hydrogen and oxygen. *J. Catal.* **319**, 15–26 (2014).
  46. Menegazzo, F., Signoretto, M., Frison, G., Pinna, F., Strukul, G., Manzoli, M., Boccuzzi, F., When high metal dispersion has a detrimental effect: Hydrogen peroxide direct synthesis under very mild and nonexplosive conditions catalyzed by Pd supported on silica. *J. Catal.* **290**, 143–150 (2012).
  47. Tian, P., Ouyang, L., Xu, X., Ao, C., Xu, X., Si, R., Shen., X., Lin, M., Xu, J., Han, Y.F. The origin of palladium particle size effects in the direct synthesis of H<sub>2</sub>O<sub>2</sub>: Is smaller better? *J. Catal.* **349**, 30–40 (2017).
  48. Lim, B. B., Majiong, J., Jing, T., Pedro, H.C., Camargo, Y.Z., Younan, X., Shape-Controlled Synthesis of Pd Nanocrystals in Aqueous Solutions. *Adv. Funct. Mater.*

- 19, 189–200 (2009).
49. Shao, M., Yu, T., Odell, J. H., Xia, Y., Structural dependence of oxygen reduction reaction on palladium nanocrystals. *ChemComm.* **47**, 6566–6568 (2011).
  50. Kim, S., Lee, D., Lee, K. Journal of Molecular Catalysis A : Chemical Direct synthesis of hydrogen peroxide from hydrogen and oxygen over single-crystal cubic palladium on silica catalysts. *Journal Mol. Catal. A, Chem.* **383–384**, 64–69 (2014).
  51. Ho, S., Kim, J., Soo, S., Kwan, H., Lee, Y. Direct Synthesis of Hydrogen Peroxide from Hydrogen and Oxygen Using Tailored Pd Nanocatalysts : A Review of Recent Findings. *Catal. Surv. from Asia.* **21**, 1–12 (2017).
  52. Pengfei, T., Like, O., Xinchao, X. U., Jing, X. U., Fan, H. A. N. Y. Density functional theory study of direct synthesis of H<sub>2</sub>O<sub>2</sub> from H<sub>2</sub> and O<sub>2</sub> on Pd ( 111 ), Pd ( 100 ), and Pd ( 110 ) surfaces. *Chinese J. Catal.* **34**, 1002–1012 (2013).
  53. Tian, P., Doudou, D., Yang, S., Fuzhen, X., Xingyan, X., Jing, X., Yi-Fan, H. Theoretical study of size effects on the direct synthesis of hydrogen peroxide over palladium catalysts. *J. Catal.* **369**, 95–104 (2019).
  54. Rossi, U., Zancanella, S., Artiglia, L., Granozzi, G., Canu, P. Direct synthesis of H<sub>2</sub>O<sub>2</sub> on model Pd surfaces. *Chem. Eng. J.* **207–208**, 845–850 (2012).
  55. Samanta, C., Choudhary, V. R. Direct synthesis of H<sub>2</sub>O<sub>2</sub> from H<sub>2</sub> and O<sub>2</sub> and decomposition/hydrogenation of H<sub>2</sub>O<sub>2</sub> in an aqueous acidic medium over halide-modified Pd/Al<sub>2</sub>O<sub>3</sub> catalysts. *Appl. Catal. A Gen.* **330**, 23–32 (2007).
  56. Dimitratos, N., Edwards, J. K., Kiely, C. J., Hutchings, G. J. Gold catalysis : helping create a sustainable future. *Appl. Petrochem. Res.* **2**, 7–14 (2012).
  57. Haruta, M. Novel catalysis of gold deposited on metal oxides. *Catal. Surv. from Japan* **1**, 61–73 (1997).
  58. Landon, P., Collier, P. J., Papworth, A. J., Kiely, J., Graham, J. Direct formation of hydrogen peroxide from H<sub>2</sub>/O<sub>2</sub> using a gold catalyst. *ChemComm.* **18**, 2058–2059 (2002).
  59. Ouyang, L., Guo-jin, D., Peng-fei, T., Tian-yuan, C., Guo-da, L., Jing, X., Yi-Fan, H. Insight into active sites of Pd–Au/TiO<sub>2</sub> catalysts in hydrogen peroxide synthesis directly from H<sub>2</sub> and O<sub>2</sub>. *Journal of Catalysis.* **311**, 129–136 (2014).
  60. Sterchele, S., Biasi, P., Centomo, P., Cantonc, P., Campestrini, S., Salmi, T., Zecca, M. Applied Catalysis A Pd-Au and Pd-Pt catalysts for the direct synthesis of hydrogen peroxide in absence of selectivity enhancers. *Applied Catal. A, Gen.* **468**, 160–174 (2013).
  61. Menegazzo, F., Burti, P., Signoreto, M., Manzoli, M., Vankovab, S., Boccuzzi, F., Pinna, F., Strukul, G. Effect of the addition of Au in zirconia and ceria supported Pd catalysts for the direct synthesis of hydrogen peroxide. *Journal of catalysis.* **257**, 369–381 (2008).

62. Gemo, N., Menegazzo, F., Biasi, P., Sarkar, A., Samikannu, A., Raut, D.G., Kord, K., Rautio, A.R., Mohl, M., Bostrom, D., Shchukarevc, A., Mikkola, J.P. TiO<sub>2</sub> nanoparticles: Vs. TiO<sub>2</sub> nanowires as support in hydrogen peroxide direct synthesis: The influence of N and Au doping. *RSC Adv.* **6**, 103311–103319 (2016).
63. Nomura, Y., Ishihara, T., Hata, Y., Kitawaki, K., Kaneko, K., Matsumoto, H. Nanocolloidal Pd-Au as Catalyst for the Direct Synthesis of Hydrogen Peroxide from H<sub>2</sub> and O<sub>2</sub>. *ChemSusChem.* **7**, 619–621 (2008).
64. Yook, S., Kwon, H. C., Kim, Y-G., Choi, W., Choi, M. Significant Roles of Carbon Pore and Surface Structure in AuPd/C Catalyst for Achieving High Chemoselectivity in Direct Hydrogen Peroxide Synthesis. *ACS Sustainable Chem. Eng.* **5**, 1208–1216 (2017).
65. Centomo, P., Canton, P., Burato, C., Meneghini, C., Zecca, M. Resonant-XRD Characterization of Nanoalloyed Au-Pd Catalysts for the Direct Synthesis of H<sub>2</sub>O<sub>2</sub>: Quantitative Analysis of Size Dependent Composition of the Nanoparticles. *Appl. Sci.* **9**, 2959-2973 (2019).
66. Kanungo, S., Paunovic, V., Schouten, J. C., D'angelo, F.N. Facile Synthesis of Catalytic AuPd Nanoparticles within Capillary Microreactors Using Polyelectrolyte Multilayers for the Direct Synthesis of H<sub>2</sub>O<sub>2</sub>. *Nano Lett.* **17**, 6481–6486 (2017).
67. Gudarzi, D., Ratchananusorn, W., Turunen, I., Heinonen, M. Promotional effects of Au in Pd–Au bimetallic catalysts supported on activated carbon cloth ( ACC ) for direct synthesis of H<sub>2</sub>O<sub>2</sub> from. *Catal. Today.* **248**, 58–68 (2015).
68. Edwards, J. K., Solsona, B., Ntainjua, E.N., Carley, A.F., Herzing, A.A., Kiely, C.J., Hutchings, G.J. Switching Off Hydrogen Peroxide Hydrogenation in the Direct Synthesis Process. *Science.* **323**, 1037–1041 (2009).
69. Edwards, J. K. *et al.* Direct synthesis of H<sub>2</sub>O<sub>2</sub> from H<sub>2</sub> and O<sub>2</sub> over gold, palladium, and gold-palladium catalysts supported on acid-pretreated TiO<sub>2</sub>. *Angew. Chemie - Int. Ed.* **48**, 8512–8515 (2009).
70. Ntainjua, E. N., Piccinini, M., Pritchard, J.C., Edwards, J.K., Carley, A.F., Kiely, C.J., Hutchings, G.J. Direct synthesis of hydrogen peroxide using ceria-supported gold and palladium catalysts. *Catal. Today.* **178**, 47–50 (2011).
71. Meenakshisundaram, S., He, Q., Moataz, M., Pritchard, J., Freakley, S.J., Edwards, J.K., Taylor, S.H., Morgan, D.J., Carley, A.F., Knight, D.W., Kiely, C.J., Hutchings, G.J. Synthesis of stable ligand-free gold-palladium nanoparticles using a simple excess anion method. *ACS Nano.* **6**, 6600–6613 (2012).
72. Edwards, J. K., Solsona, B.E., Landon, P., Carley, A.F., Herzing, A.A., Kiely, C.J., Hutchings, G.J. Direct synthesis of hydrogen peroxide from H<sub>2</sub> and O<sub>2</sub> using TiO<sub>2</sub>-supported Au-Pd catalysts. *J. Catal.* **236**, 69–79 (2005).
73. Herzing, A. A., Carley, A. F., Edwards, J. K., Hutchings, G. J., Kiely, C. J.

- Microstructural development and catalytic performance of Au-Pd nanoparticles on Al<sub>2</sub>O<sub>3</sub> supports: The effect of heat treatment temperature and atmosphere. *Chem. Mater.* **20**, 1492–1501 (2008).
74. Hasnat, M.A., Rahman, M.M., Borhanuddin, S.M., Siddiqua, A., Bahadur, N.M., Karim, M.R. Efficient hydrogen peroxide decomposition on bimetallic Pt–Pd surfaces. *Catalysis Communications.* **12**, 286–29 (2010).
  75. Liu, Q., Bauer, J. C., Schaak, R. E., Lunsford, J. H. Direct synthesis of H<sub>2</sub>O<sub>2</sub> from H<sub>2</sub> and O<sub>2</sub> over Pd-Pt/SiO<sub>2</sub> bimetallic catalysts in a H<sub>2</sub>SO<sub>4</sub>/ethanol system. *Appl. Catal. A Gen.* **339**, 130–136 (2008).
  76. Abate, S., Melada, S., Centi, G., Perathoner, S., Pinna, F., Strukul, G. Performances of Pd-Me (Me = Ag, Pt) catalysts in the direct synthesis of H<sub>2</sub>O<sub>2</sub> on catalytic membranes. *Catal. Today.* **117**, 193–198 (2006).
  77. Li, F., Shao, Q., Hu, M., Chen, Y., Huang, X. Hollow Pd-Sn Nanocrystals for Efficient Direct H<sub>2</sub>O<sub>2</sub> Synthesis: The Critical Role of Sn on Structure Evolution and Catalytic Performance. *ACS Catal.* **8**, 3418–3423 (2018).
  78. Zhang, J., Shao, Q., Zhang, Y., Bai, S., Feng, Y., Huang, X. Promoting the Direct H<sub>2</sub>O<sub>2</sub> Generation Catalysis by Using Hollow Pd–Sn Intermetallic Nanoparticles. *Small* **14**, 1–7 (2018).
  79. Khan, Z., Dummer, N. F., Edwards, J. K. Silver. Palladium catalysts for the direct synthesis of hydrogen peroxide. *Phil. Trans. R. Soc. A.* **376**, 1-12 (2017).
  80. Wang, S., Lewis, R.J., Doronkin, D.E., Morgan, D.J., Grunwaldt, J.D., Hutchings, G.J., Behrens, S. The direct synthesis of hydrogen peroxide from H<sub>2</sub> and O<sub>2</sub> using Pd–Ga and Pd–In catalysts. *Catal. Sci. Technol.* **10**, 1925–1932 (2020).
  81. Ntainjua, E. N., Freakley, S. J., Hutchings, G. J. Direct synthesis of hydrogen peroxide using ruthenium catalysts. *Top. Catal.* **55**, 718–722 (2012).
  82. Alotaibi, F., Al, S., Mohammad, M., Jennifer, A., Richard, K. E. Direct Synthesis of Hydrogen Peroxide Using Cs-Containing Heteropolyacid-Supported Palladium–Copper Catalysts. *Catal. Letters.* **149**, 998–1006 (2019).
  83. Crole, D.A., Underhill, R., Edwards, J.K., Shaw, G., Freakly, S.J., Hutchings, G.J., Lewis, R.J. The Direct Synthesis of Hydrogen Peroxide from H<sub>2</sub>. *Phil. Trans. R. Soc. A.* **378**, 1-11 (2020).
  84. Choa, Y-H., Hana, G-H., Hanb, S-S., Seo, M-g., Lee, K-Y. Effects of varying amounts of Na on Pd/TiO<sub>2</sub> for the direct synthesis of H<sub>2</sub>O<sub>2</sub>: Identification of the Pd dispersion and catalytic activity enhancement by changing the surface electronic states. *Mol. Catal.* **484**, 110732-110740 (2020).
  85. Edwards, J. K., Pritchard, P.J., Miedziak, P.J., Piccinini, M., Carley, A.F., He, Q., Kiely, C.J., Hutchings, G.J. The direct synthesis of hydrogen peroxide using platinum-promoted gold-palladium catalysts. *Angew. Chemie-Int. Ed.* **53**, 2381–2384 (2014).

86. Barnes, A., Lewis, R. J., Morgan, D. J., Davies, T. E., Hutchings, G. J. Enhancing catalytic performance of AuPd catalysts incorporation of base metals. *Catal. Sci. Technol.* **12**, 1986–1996 (2022).
87. Xu, H., Cheng, D., Gao, Y. Design of High-Performance Pd-Based Alloy Nanocatalysts for Direct Synthesis of H<sub>2</sub>O<sub>2</sub>. *ACS Catal.* **7**, 2164-2170 (2017).
88. Yao, Z., Zhao, J., Bunting, R.J., Zhao, C., Hu, P., Wang, J. Quantitative Insights into the Reaction Mechanism for the Direct Synthesis of H<sub>2</sub>O<sub>2</sub> over Transition Metals : Coverage-Dependent Microkinetic Modeling. *ACS Catalysis.* **11**, 1202–1221 (2021).
89. Wilson, N. M., Flaherty, D. W. Mechanism for the Direct Synthesis of H<sub>2</sub>O<sub>2</sub> on Pd Clusters : Heterolytic Reaction Pathways at the Liquid–Solid Interface. *JACS.* **138**, 574–586 (2016).
90. Song, X., Sun, K., Hao, X., Su, H-Y., Ma, X., Xu, Y. Facet-Dependent of Catalytic Selectivity : The Case of H<sub>2</sub>O<sub>2</sub> Direct Synthesis on Pd Surfaces. *J. Phys. Chem.* **43**, 26324–26337 (2019).
91. Li, J., Ishihara, T., Yoshizawa, K. Theoretical Revisit of the Direct Synthesis of H<sub>2</sub>O<sub>2</sub> on Pd and Au @ Pd Surfaces : A Comprehensive Mechanistic Study. *J. Phys. Chem. C.* **115**, 25359–25367 (2011).
92. Chong, M. N., Jin, B., Chow, C. W. K., Saint, C. Recent developments in photocatalytic water treatment technology: A review. *Water Res.* **44**, 2997–3027 (2010).
93. Bolisetty, S., Peydayesh, M., Mezzenga, R. Sustainable technologies for water purification from heavy metals: review and analysis. *Chem. Soc. Rev.* **48**, 463–487 (2019).
94. Gupta, V. K., Ali, I., Saleh, T. A., Nayak, A., Agarwal, S. Chemical treatment technologies for waste-water recycling-An overview. *RSC Adv.* **2**, 6380–6388 (2012).
95. Sonune, A.,Ghate, R. Developments in wastewater treatment methods. *Desalination* **167**, 55–63 (2004).
96. Pearce, C. I., Lloyd, J. R., Guthrie, J. T. The removal of colour from textile wastewater using whole bacterial cells : a review. *Dyes and pigments.* **58**, 179–196 (2003).
97. Adams, C., Wang, Y., Loftin, K., Meyer, M. Removal of antibiotics from surface and distilled water in conventional water treatment processes. *J. Environ. Eng.* **128**, 253–260 (2002).
98. Von Gunten, U. Oxidation Processes in Water Treatment: Are We on Track? *Environ. Sci. Technol.* **52**, 5062–5075 (2018).
99. Deborde, M., Von Gunten, U. Reactions of chlorine with inorganic and organic compounds during water treatment-Kinetics and mechanisms: A critical review. *Water Res.* **42**, 13–51 (2008).
100. Ge, F., Zhu, L., Chen, H. Effects of pH on the chlorination process of phenols in

- drinking water. *J. Hazard. Mater.* **133**, 99–105 (2006).
101. Sillanpää, M., Ncibi, M. C., Matilainen, A. Advanced oxidation processes for the removal of natural organic matter from drinking water sources: A comprehensive review. *J. Environ. Manage.* **208**, 56–76 (2018).
  102. Contreras, S., Pascual, E., Esplugas, S., Gim, J. Comparison of Different Advanced Oxidation Process for Phenol Degradation Comparison of different advanced oxidation processes for phenol degradation. *Water Res.* **1354**, 1034–1042 (2016).
  103. Neyens, E., Baeyens, J. A review of classic Fenton's peroxidation as an advanced oxidation technique. *J. Hazard. Mater.* **98**, 33–50 (2003).
  104. Sharma, S., Ruparelia, J. P., Patel, M. L. A general review on Advanced Oxidation Processes for waste water treatment. *International conference on current trends in technology.* 8–10 (2011).
  105. Waclawek, S., Lutze, H.V., Grübel, K., Padil, V.V.T., Cernik, M., Dionvsiou, D.D. Chemistry of persulfates in water and wastewater treatment: A review. *Chem. Eng. J.* **330**, 44–62 (2017).
  106. Munoz, M., de Pedro, Z. M., Casas, J. A., Rodriguez, J. J. Preparation of magnetite-based catalysts and their application in heterogeneous Fenton oxidation - A review. *Appl. Catal. B Environ.* **176–177**, 249–265 (2015).
  107. Pignatello, J. J., Oliveros, E., MacKay, A. Advanced oxidation processes for organic contaminant destruction based on the fenton reaction and related chemistry. *Crit. Rev. Environ. Sci. Technol.* **36**, 1–84 (2006).
  108. Zhu, Y., Zhu, R., Xi, Y., Zhu, J., Zhu, G., He, H. Strategies for enhancing the heterogeneous fenton catalytic reactivity: A review. *Appl. Catal. B Environ.* **255**, 117739-117750 (2019).
  109. Garrido-Ramírez, E. G., Theng, B. K. G., Mora, M. L. Clays and oxide minerals as catalysts and nanocatalysts in Fenton-like reactions-A review. *Appl. Clay Sci.* **47**, 182–192 (2010).
  110. Ovejero, G., Sotelo, J. L., Martínez, F., Melero, J. A., Gordo, L. Wet peroxide oxidation of phenolic solutions over different iron-containing zeolitic materials. *Ind. Eng. Chem. Res.* **40**, 3921–3928 (2001).
  111. Calleja, G., Melero, J. A., Martínez, F., Molina, R. Activity and resistance of iron-containing amorphous, zeolitic and mesostructured materials for wet peroxide oxidation of phenol. *Water Res.* **39**, 1741–1750 (2005).
  112. Li, G., Pidko, E. A., Van Santen, R. A., Li, C., Hensen, E. J. M. Stability of extraframework iron-containing complexes in ZSM-5 zeolite. *J. Phys. Chem. C* **117**, 413–426 (2013).
  113. He, J., Yang, X., Men, B., Wang, D. Interfacial mechanisms of heterogeneous Fenton reactions catalyzed by iron-based materials: A review. *J. Environ. Sci. (China)* **39**,

- 97–109 (2016).
114. Yan, Y., Jiang, S., Zhang, H. Catalytic wet oxidation of phenol with Fe-ZSM-5 catalysts. *RSC Adv.* **6**, 3850–3859 (2016).
  115. Herney-Ramirez, J., Vicente, M. A., Madeira, L. M. Heterogeneous photo-Fenton oxidation with pillared clay-based catalysts for wastewater treatment: A review. *Appl. Catal. B Environ.* **98**, 10–26 (2010).
  116. Zazo, J. A., Casas, J. A., Mohedano, A. F., Gilarranz, M. A., Rodríguez, J. J. Chemical pathway and kinetics of phenol oxidation by Fenton's reagent. *Environ. Sci. Technol.* **39**, 9295–9302 (2005).
  117. Ghaffari, Y., Gupta, N. K., Bae, J., Kim, K. S. Heterogeneous catalytic performance and stability of iron-loaded ZSM-5, zeolite-A, and silica for phenol degradation: A microscopic and spectroscopic approach. *Catalysts.* **9**, 1-17 (2019).
  118. Nguyen Huu Phu, Kim Hoa, T. T., Nguyen Van Tan, Hoang Vinh Thang , Pham Le Ha. Characterization and activity of Fe-ZSM-5 catalysts for the total oxidation of phenol in aqueous solutions. *Appl. Catal. B Environ.* **34**, 267–275 (2001).
  119. Luca, C., Ivorra, F., Massa, P., Fenoglio, R. Iron – alumina synergy in the heterogeneous Fenton-type peroxidation of phenol solutions. *Chem. Eng. J.* **268**, 280–289 (2015).
  120. Inchaurredo, N. S., Massa, P., Fenoglio, R., Font, J., Haure, P. Efficient catalytic wet peroxide oxidation of phenol at moderate temperature using a high-load supported copper catalyst. *Chem. Eng. J.* **198–199**, 426–434 (2012).
  121. Valkaj, K.M., Wittine, O., Margeta, K., Granato, T., Katoviæ, A., Zrnèevia, S. Phenol oxidation with hydrogen peroxide using Cu/ZSM5 and Cu/Y5 catalysts. *Polish J. Chem. Technol.* **13**, 28–36 (2011).
  122. Wang, Y., Zhao, H., Zhao, G. Applied Catalysis B: Environmental Iron-copper bimetallic nanoparticles embedded within ordered mesoporous carbon as effective and stable heterogeneous Fenton catalyst for the degradation of organic contaminants. *Applied Catal. B, Environ.* **164**, 396–406 (2015).
  123. Luo, L., Dai, C., Zhang, A., Wang, J., Liu, Min., Song, C., Guo, X. A facile strategy for enhancing FeCu bimetallic promotion for catalytic phenol oxidation. *Catal. Sci. Technol.* **5**, 3159–3165 (2015).
  124. Valkaj, K. M., Katovic, A., Zrnèevic, S. Investigation of the catalytic wet peroxide oxidation of phenol over different types of Cu/ZSM-5 catalyst. *J. Hazard. Mater.* **144**, 663–667 (2007).
  125. Adam, F., Andas, J., Rahman, I. A. A study on the oxidation of phenol by heterogeneous iron silica catalyst. *Chem. Eng. J.* **165**, 658–667 (2010).
  126. Contreras, S., Yalfani, M. S., Medina, F., Sueiras, J. E. Effect of support and second metal in catalytic in-situ generation of hydrogen peroxide by Pd-supported catalysts:

- Application in the removal of organic pollutants by means of the Fenton process. *Water Sci. Technol.* **63**, 2017–2024 (2011).
127. Underhill, R., Lewis, R.J., Freakly, S.J., Douthwaite, M., Miedziak, P.J., Akdim, O., Edwards, J.K., Hutchings, G.J. Oxidative Degradation of Phenol using in situ Generated Hydrogen Peroxide Combined with Fenton's Process. *Johnson Matthey Technol. Rev.* **62**, 417–425 (2018).
  128. Choudhary, V. R., Samanta, C., Jana, P. A novel route for in-situ H<sub>2</sub>O<sub>2</sub> generation from selective reduction of O<sub>2</sub> by hydrazine using heterogeneous Pd catalyst in an aqueous medium. *Chem. Commun.* **37(43)**, 5399–5401 (2005).
  129. Yalfani, M. S., Contreras, S., Medina, F., Sueiras, J. E. Hydrogen substitutes for the in situ generation of H<sub>2</sub>O<sub>2</sub>: An application in the Fenton reaction. *J. Hazard. Mater.* **192**, 340–346 (2011).
  130. Choudhary, V. R., Jana, P. In situ generation of hydrogen peroxide from reaction of O<sub>2</sub> with hydroxylamine from hydroxylammonium salt in neutral aqueous or non-aqueous medium using reusable Pd/Al<sub>2</sub>O<sub>3</sub> catalyst. *Catal. Commun.* **8**, 1578–1582 (2007).
  131. Hyde, J. R., Poliakoff, M. Supercritical hydrogenation and acid-catalysed reactions "without gases". *Chem. Commun.* **4**, 1482–1483 (2004).
  132. Yalfani, M. S., Contreras, S., Medina, F., Sueiras, J. Direct generation of hydrogen peroxide from formic acid and O<sub>2</sub> using heterogeneous Pd/γ-Al<sub>2</sub>O<sub>3</sub> catalysts. *Chem. Commun.* **33**, 3885–3887 (2008).
  133. Yalfani, M. S., Contreras, S., Medina, F., Sueiras, J. Phenol degradation by Fenton's process using catalytic in situ generated hydrogen peroxide. *Appl. Catal. B Environ.* **89**, 519–526 (2009).
  134. Zárate-Guzmán, A. I., González-Gutiérrez, L.V., Godínez, L.A., Medel-Reyes, A., Carrasco-Marin, F., Romero-Cano, L.A. Towards understanding of heterogeneous Fenton reaction using carbon-Fe catalysts coupled to in-situ H<sub>2</sub>O<sub>2</sub> electro-generation as clean technology for wastewater treatment. *Chemosphere* **224**, 698–706 (2019).
  135. Liu, W., Liu, H., Ai, Z. In-situ generated H<sub>2</sub>O<sub>2</sub> induced efficient visible light photo-electrochemical catalytic oxidation of PCP-Na with TiO<sub>2</sub>. *J. Hazard. Mater.* **288**, 97–103 (2015).
  136. Rocha-Martin, J., Velasco-Lozano, S., Guisán, J. M., López-Gallego, F. Oxidation of phenolic compounds catalyzed by immobilized multi-enzyme systems with integrated hydrogen peroxide production. *Green Chem.* **16**, 303–311 (2014).

# Chapter 2:

## Experimental procedure and theory.

### 2.1 Reagents.

#### Precursors

Palladium chloride, PdCl<sub>2</sub>, >99.9 %, Sigma Aldrich, CAS (7647-10-1).

Gold chloride trihydrate, HAuCl<sub>4</sub>\*3H<sub>2</sub>O, 99.9 %, Sigma Aldrich, CAS (16961-25-4).

Copper chloride, CuCl<sub>2</sub>, >99.995 %, Sigma Aldrich, CAS (7447-39-4).

Cobalt chloride, CoCl<sub>2</sub>, >97 %, Sigma Aldrich, CAS (7646-79-9).

Iron chloride, Fe<sub>3</sub>Cl, >97 %, Sigma Aldrich, CAS (7705-08-0).

Tetrapropylammonium hydroxide solution, C<sub>12</sub>H<sub>29</sub>NOTPAOH, 1 M in H<sub>2</sub>O, Sigma Aldrich, CAS (4499-86-9).

Tetraethyl orthosilicate, SiC<sub>8</sub>H<sub>20</sub>O<sub>4</sub>, TEOS, 98%, Sigma Aldrich, CAS (78-10-4).

Sodium aluminate, NaAlO<sub>2</sub>, 99 %, Alfa Aesar, CAS (1302-42-7).

Iron nitrate, Fe(NO<sub>3</sub>)<sub>3</sub>\*9H<sub>2</sub>O, 98 %, Sigma Aldrich, CAS (7782-61-8).

Ammonium nitrate, NH<sub>4</sub>NO<sub>3</sub>, 99 %, Merck, CAS (6484-52-2).

Ceria sulphate, Ce(SO<sub>4</sub>)<sub>2</sub>, Sigma Aldrich, CAS (13590-82-4).

#### Supports

Titanium dioxide, TiO<sub>2</sub>, P25, >99.5 %, Sigma Aldrich, CAS (13463-67-71).

Zeolite, NH<sub>3</sub>-ZSM-5 (SiO<sub>2</sub>:Al<sub>2</sub>O<sub>3</sub>) (23:1), Alfa Aesar, CAS (1318-02-1).

#### Indicators

Ferroun solution, C<sub>36</sub>H<sub>24</sub>FeN<sub>6</sub>, 0.1 wt.% in H<sub>2</sub>O, Sigma Aldrich, CAS (14634-91-4).

#### Solvents and solutions

Methanol, CH<sub>3</sub>OH, > 99 %, Fisher Scientific, CAS (67-56-1).

HPLC grade water, Fisher Scientific, CAS (7732-18-5).

Hydrogen peroxide, H<sub>2</sub>O<sub>2</sub>, 50 wt.%, Sigma Aldrich, CAS (7722-84-1).

Acetonitrile, C<sub>2</sub>H<sub>3</sub>N, 99.8 %, Sigma Aldrich, CAS (75-05-8).

Phosphoric acid, H<sub>3</sub>PO<sub>4</sub>, >85 %, Sigma Aldrich, CAS (7664-38-2).

Phenol, C<sub>6</sub>H<sub>6</sub>O, > 99 %, Sigma Aldrich, CAS (108-95-2).

#### Gases

25 % O<sub>2</sub>/CO<sub>2</sub>, BOC.

5 % H<sub>2</sub>/CO<sub>2</sub>, BOC.

25 % O<sub>2</sub>/CO<sub>2</sub>, BOC.

5 % H<sub>2</sub>/CO<sub>2</sub>, BOC.

Pure N<sub>2</sub>, BOC.

## 2.2 Catalysts synthesis.

### 2.2.1 Modified impregnation.

Modified impregnation methodology<sup>1</sup> was used to prepare mono and bi-metallic 1 wt.% AuPd/TiO<sub>2</sub> and 1 wt.% FePd/TiO<sub>2</sub> catalysts supported on TiO<sub>2</sub> (P25). Table 2.1 and Table 2.2 presents the precursor volumes required to prepare key catalytic materials that were studied in Chapter 3 and Chapter 4 respectively. The precursor solutions were prepared diluting the required amount of HAuCl<sub>4</sub>, PdCl<sub>2</sub> and FeCl<sub>3</sub> in distilled water to obtain a solution with a concentration of 12.25 mg/mL of Au, 6.01 mg/mL of Pd and 4.89 mg/mL of Fe respectively. The concentration of each metal in the precursor solution was determined by means of microwave plasma atomic emission spectroscopy (MP-AES) prior to its use to catalysts synthesis.

The experimental procedure to prepare 1 g of bi-metallic 0.5 wt.% Pd-0.5 wt.% Au/TiO<sub>2</sub> catalyst based on a modified impregnation methodology is specified below. The same methodology was used for the preparation of the other series of mono and bi-metallic 1 wt.% AuPd/TiO<sub>2</sub> and 1 wt.% FePd/TiO<sub>2</sub> catalysts, but employing the precursors and volumes required respectively for each one.<sup>1</sup> An aqueous acidified PdCl<sub>2</sub> solution (0.832 mL, 0.58 M HCl, [Pd]= 6.01 mg mL<sup>-1</sup>, Sigma Aldrich) and aqueous HAuCl<sub>4</sub>\*3H<sub>2</sub>O (0.408 mL, [Au]= 12.25 mg mL<sup>-1</sup>, Sigma Aldrich) were mixed in a 50 mL round bottom flask and heated to 60 °C (1000 rpm) in a thermostatically controlled oil bath, with the total volume fixed to 16 mL using distilled H<sub>2</sub>O. The Au and Pd during the synthesis were 0.312 mg/mL and 0.313 mg/mL respectively. Upon reaching 60 °C, the slurry was left stirring for an extra 15 min. Subsequently, the temperature was raised to 95 °C and left stirring overnight for 16 h to allow complete evaporation of the water. The resulting solid was grounded prior to heat treatment in reductive atmosphere (400 °C, 10 °C min<sup>-1</sup>, 5 % H<sub>2</sub>/Ar, 4 h).<sup>1</sup>

**Table 2.1:** Amount of HAuCl<sub>4</sub>\*3H<sub>2</sub>O and PdCl<sub>2</sub> (0.58M HCl) precursors for the preparation of mono and bi-metallic 1 wt.% AuPd/TiO<sub>2</sub> catalysts by modified impregnation.

Catalysts	HAuCl <sub>4</sub> *3H <sub>2</sub> O mL	PdCl <sub>2</sub> mL
1.0 wt.% Pd/TiO <sub>2</sub>	-	1.664
0.75 wt.% Pd -0.25 wt.% Au/TiO <sub>2</sub>	0.204	1.248
0.5 wt.% Pd-0.5 wt.% Au/TiO <sub>2</sub>	0.408	0.832
0.25 wt.% Pd-0.75 wt.% Au/TiO <sub>2</sub>	0.612	0.416

<b>1.0 wt.% Au/TiO<sub>2</sub></b>	0.816	-
------------------------------------	-------	---

**Metal concentration in the precursor solution:** Au= 12.25 mg/mL and Pd= 6.01 mg/mL.

**Table 2.2:** Amount of FeCl<sub>3</sub> and PdCl<sub>2</sub> (0.58M HCl) precursors for the preparation of mono and bi-metallic 1 wt.% FePd/TiO<sub>2</sub> catalysts by modified impregnation.

<b>Catalysts</b>	<b>FeCl<sub>3</sub></b> mL	<b>PdCl<sub>2</sub></b> mL
<b>1.0 wt.% Pd/TiO<sub>2</sub></b>	-	1.664
<b>0.75 wt.% Pd -0.25 wt.%Fe/TiO<sub>2</sub></b>	0.512	1.248
<b>0.5 wt.% Pd-0.5 wt.% Fe/TiO<sub>2</sub></b>	1.024	0.832
<b>0.25 wt.% Pd-0.75 wt.% Fe/TiO<sub>2</sub></b>	1.535	0.416
<b>1.0 wt.% Fe/TiO<sub>2</sub></b>	2.047	-

**Metal concentration in the precursor solution:** Fe= 4.885 mg/mL and Pd= 6.01 mg/mL.

To prepare 1g of bi-metallic 0.5 wt.% Cu-0.5 wt.% Pd/TiO<sub>2</sub> and 0.5 wt.% Co-0.5 wt.% Pd/TiO<sub>2</sub> catalysts, the same procedure was followed as for 0.5 wt.% Pd-0.5 wt.% Au/TiO<sub>2</sub> catalyst preparation but changing the Au precursor for 0.832 mL of CuCl<sub>2</sub> ([Cu]=6.01 mg/mL, Sigma Aldrich) and 0.769 mL of CoCl<sub>2</sub> ([Co]=6.5 mg/mL, Sigma Aldrich) respectively. The Cu and Co precursors were also prepared diluting the required amount of CuCl<sub>2</sub> and CoCl<sub>2</sub> to obtain a concentration of [Cu]=6.01 mg/mL and [Co]=6.50 mg/mL in solution. Both concentrations of Cu and Co in solution were determined by means of MP-AES.

The metal content in the synthesised catalysts was determined digesting a certain amount of solid in aqua regia and employing MP-AES as a means of analysis. Section 2.2.3 details the background theory of atomic spectroscopy and a sub-section with a detailed experimentally procedure of how the catalyst digestion and subsequent analysis by MP-AES was carried out.

## 2.2.2 Hydrothermal synthesis.

### 2.2.2.1 Direct synthesis of HZSM-5 (SiO<sub>2</sub>:Al<sub>2</sub>O<sub>3</sub>) (28:1) containing Fe.

A hydrothermal synthesis procedure was used to direct synthesise HZSM-5 (SiO<sub>2</sub>:Al<sub>2</sub>O<sub>3</sub>) (28:1) containing Fe. The direct synthesis of 1.0 wt.% Fe-HZSM-5 is described below as an example. Tetraethylorthosilicate (TEOS, 10.24 g, Alfa Aesar) was added dropwise to a solution of tetrapropylammonium hydroxide 1 M (TPAOH, 15 g, 1.0 M, Merck) and homogenised at 60 °C for 2 hours. Separately, NaAlO<sub>2</sub> (0.2901 g, Alfa Aesar) diluted in 5 mL of distilled water and Fe(NO<sub>3</sub>)<sub>3</sub>\*9H<sub>2</sub>O (0.232 g, Alfa Aesar) dissolved in 2.5 mL of distilled water were prepared and added dropwise to the TEOS–TPAOH mixture, separately, over

the course of 5 minutes. The gel was left stirring to have the mixture homogenised for 16 h at 60 °C, prior to crystallization in a 200 mL Teflon lined, Parr Instruments stainless-steel autoclave, equipped with pressure relief (72 h, 175 °C). After crystallisation, the resulting solid was filtered and washed with distilled water, until the filtrate reached a neutral pH. The resulting solid was dried (16 h, 70 °C), followed by calcination (flowing air, 550 °C, 3 h, 1 °C min<sup>-1</sup>) to remove the template (TPAOH). Subsequently, the sample was ion-exchanged with NH<sub>4</sub>NO<sub>3</sub> (Merck) (1.0 M, 30 mL g<sup>-1</sup> of zeolite) three times at 100 °C for 4 h, with the suspension filtered and the solid dried (16 h, 70 °C) between each reflux. The sample was activated at static air (550 °C, 3 h, 10 °C min<sup>-1</sup>). The same procedure was followed to prepare other mono-metallic HZSM-5 with different Fe content. Table 2.3 presents the amount Fe(NO<sub>3</sub>)<sub>3</sub>\*9H<sub>2</sub>O used during the synthesis of the rest of mono-metallic X wt.% Fe-HZSM-5 (X: 3.0–0.06) catalysts as well as the bare HZSM-5 with no Fe content (Bare HZSM-5).

**Table 2.3:** Amount of Fe(NO<sub>3</sub>)<sub>3</sub>\*9H<sub>2</sub>O for the preparation of mono-metallic X wt.% Fe-HZSM-5 (X: 3.0-0.06) and bare HZSM-5 catalysts by hydrothermal synthesis.

Catalysts	Fe(NO <sub>3</sub> ) <sub>3</sub> *9H <sub>2</sub> O g
<b>3.0 wt.% Fe-HZSM-5</b>	0.681
<b>2.0 wt.% Fe-HZSM-5</b>	0.454
<b>1.0 wt.% Fe-HZSM-5</b>	0.165
<b>0.5 wt.% Fe-HZSM-5</b>	0.113
<b>0.125 wt.% Fe-HZSM-5</b>	0.029
<b>0.06 wt.% Fe-HZSM-5</b>	0.013
<b>0 wt.% Fe (Bare HZSM-5)</b>	-

All the mono-metallic Fe catalysts shown in Table 2.3 had 0.5 wt.% of Pd added (0.718 mL, 0.58 M HCl, [Pd]= 6.97 mg mL<sup>-1</sup>, Sigma Aldrich) by modified impregnation procedure as shown in Section 2.2.1, to create bi-metallic 0.5 wt.% Pd/X wt.% Fe-ZSM-5 (X: 3.0-0) catalysts using X wt.% Fe-HZSM-5 as support.

### 2.2.3 General background about atomic spectroscopy.

Atomic spectroscopy includes a number of analytical techniques that are used to determine the elemental composition of a sample by examining its electromagnetic spectrum.<sup>2</sup> Atomic spectroscopy techniques include flame atomic absorption spectroscopy (FAAS), inductively coupled plasma optical emission spectroscopy (ICP-OES) and microwave plasma atomic emission spectroscopy (MP-AES). Those which identify an element by its mass spectrum

include inductively coupled plasma mass spectrometry (ICP-MS), and triple quadrupole inductively coupled plasma mass spectrometry (ICP-QQQ).<sup>2</sup>

MP-AES can be applied in several areas for the determination of a wide number of elements across the periodic table in concentrations from ng/mL.<sup>3</sup> The high sensitivity and its rapid multi-element analysis prompted its use in a wide range of areas such as in the analysis of greywaters, agriculture and in pharmaceuticals among others. In order to perform an analysis by MP-AES, the analyte needs to be in solution.<sup>3</sup> The liquid sample is injected directly into the instrument, which is subsequently converted into an aerosol, driven through the central channel of the plasma where it is atomized. The atoms continue to be excited and emit light at wavelengths characteristic for each element as the excited electron returns to lower energy states (Figure 2.1). The emitted wavelength is directed into a fast-scanning monochromator and towards a high efficient charged-coupled device (CCD) with a wavelength detection that ranges from 180 to 780 nm. Thus, the principle of this technique is that the computer records the emitted wavelength, whose intensity can be calibrated to subsequently determine the concentration of the analyte in solution. Table 2.4 presents the limit of detection of Au, Pd and Fe for a range of atomic spectroscopy techniques as well as the emitted wavelength at which these metals were analysed.<sup>3</sup>

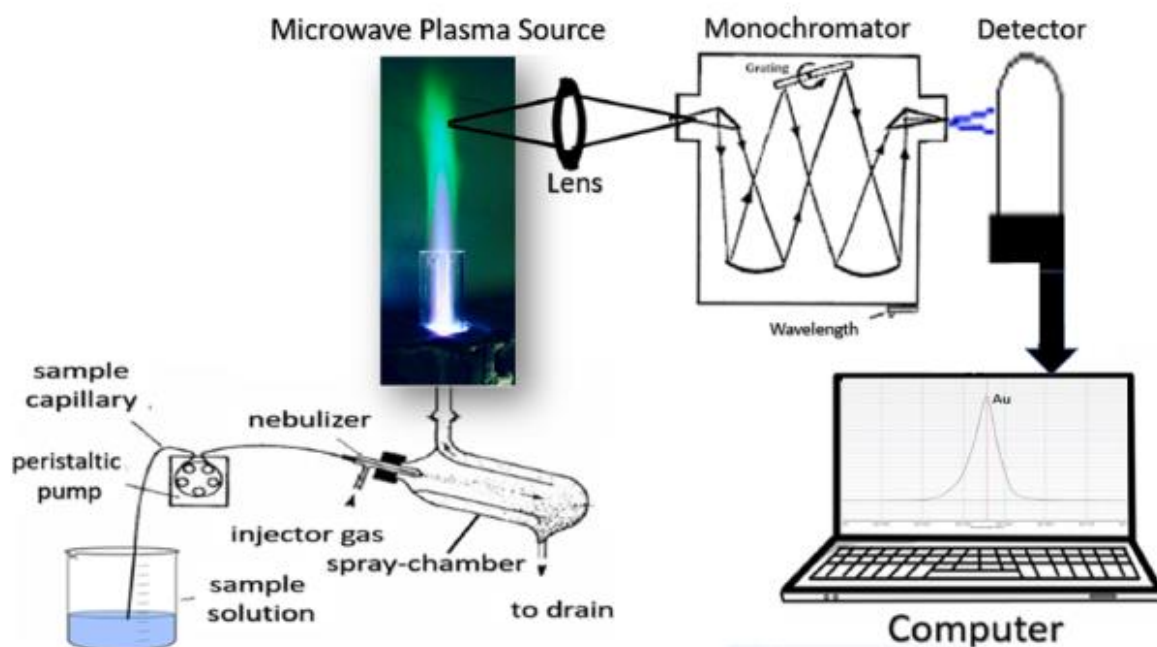


**Figure 2.1:** Schematic representation of a MP-AES instrument.<sup>3</sup>

**Table 2.4:** Emission wavelength and detection limits of atomic spectroscopy techniques for Au, Pd and Fe.<sup>3</sup>

<b>Element</b>	<b>Emission wavelength</b> nm	<b>F-AAS</b> ng/ml	<b>MP-AES</b> ng/ml	<b>ICP-AES</b> ng/ml	<b>ICP-MS</b> ng/ml
<b>Au</b>	264.148	6	1.8	20	0.003
<b>Pd</b>	405.781	-	3.8	-	0.005
<b>Fe</b>	324.754	5	1.6	2	0.570

As Table 2.4 shows, ICP-MS proves to give the lowest detection limit in comparison to the other techniques. However, this technique has spectroscopic interferences when two elements have the same mass isotopes such as Fe and Cr (c.a 54 amu), therefore, the MS detector will not be able to differentiate between these two elements. Also, ICP-MS require an internal standard or external drift corrector to overcome some of the limitations this technique has. For instance, suppression ion or enhancement effects arise from various causes such as changes in the sample transportation to the plasma, ionisation in the plasma or during the transmission to the ion beam, all of which directly affect the number of ions reaching the detector. The choice of an internal standard for multi-element analysis can be difficult because the element properties vary widely in this type of samples. Common choices are indium (In), rhodium (Rh) and gallium (Ga) because these elements are not usually present in samples in high concentrations.<sup>4</sup>

Two types of plasma can be used for AES, microwave plasma (MP-AES) or inductively coupled argon plasma (ICP-AES), both of which are excellent excitation sources for atomic emission spectroscopy.<sup>3</sup> Although each one presents its advantages and inconveniences in regard of the detection limits and analysis cost. For instance, MP-AES plasma runs by N<sub>2</sub> or air whereas ICP plasma runs by argon (Ar), thus, ICP analysis are higher in cost. ICP-AES presents higher detection limits than the MP-AES because the ICP-AES causes multiple ion emission lines that can produce spectral interferences. Since the MP-AES plasma runs at relatively lower temperature than the ICP-AES, most of the elements are in atomic state resulting in fewer emission lines, therefore allowing better reproducibility. In fact, more accurate determinations can be achieved with atomic emissions than ion emissions.<sup>3</sup> Despite of this, spectral interferences are also undesirably found during the analysis by MP-AES leading to systematic errors, which are those that can be related to the equipment and the laboratory environment, the operator and the methodology or procedure used. Continuing with the previous example, when two analytes in solution have similar emission wavelengths, this hinders their differentiation and subsequent errors in the analysis can occur. Another example of interference is known as matrix interference, which

involve the presence of acids such as  $\text{HClO}_4$  and  $\text{HCl}$ . These two show enhancement signal effects along with their increasing concentration, whereas the  $\text{HNO}_3$  gives the opposite tendency. Thus, the concentration of acids in solution are needed to be lower than  $< 10\%$  when using MP-AES. In addition to this, other ions such as  $\text{SO}_4^{2-}$  and  $\text{PO}_4^{3-}$  can react with the analyte producing species with low volatility in the plasma, and thus leading to errors during the analysis.<sup>3</sup>

#### **2.2.3.1 Determination of the metal loading by means of MP-AES.**

Here lies the procedure to determine the metal loading of the mono and bi-metallic 1.0 wt.% AuPd/TiO<sub>2</sub> and 1.0 wt.% FePd/TiO<sub>2</sub> catalysts employing an Agilent MP 4100 Expert software. 0.025 g of catalyst was digested for two days in 2.5 mL of aqua regia ( $\text{HCl}:\text{HNO}_3$  (3:1)) in a 25 mL volumetric flask. Safety precautions must be put in place before preparing aqua regia due to its high corrosiveness and irritability to the skin, eyes, and respiratory system. After the digestion, the solution was made up to 25 mL with distilled water to have less than 10 % acidic concentration of  $\text{HCl}$  and  $\text{HNO}_3$  before the analysis. Previously to the analysis, the instrument needed to be calibrated, selecting the appropriate wavelength (Table 2.4 for each metal (Au, Fe, Pd)) and the appropriate range of concentrations to ensure that the concentration of our analyte/s in solution fall within the calibration regime with a correlation of  $r^2 > 0.999$ .

The digestion of the mono and bi-metallic 0.5 wt.% Pd/X wt.% Fe-HZSM-5 catalysts could not be determined since the digestion of these type of materials require stronger oxidation reagents such as hydrofluoric acid (HF). The use of HF was not possible to be carried out in the laboratory due to the lack of safety measurements required to handle such an irritant and corrosive acid.

### **2.3 Catalysts testing.**

This section is divided in sub-sections according to the two different reactions investigated in this thesis, *i*) section 2.3.1 for the direct synthesis and degradation of  $\text{H}_2\text{O}_2$ , with a preliminary explanation of the different reaction conditions used in Chapter 3 and *ii*) section 2.3.2 for the degradation of phenol.

#### **2.3.1 Description of the reaction conditions for the evaluation of mono and bi-metallic 1 wt.% AuPd/TiO<sub>2</sub> catalysts towards the direct synthesis and degradation of H<sub>2</sub>O<sub>2</sub>.**

In Chapter 3, the activity of mono and bi-metallic 1 wt.% AuPd/TiO<sub>2</sub> catalysts, made by modified impregnation, were evaluated towards the direct synthesis and subsequent degradation of  $\text{H}_2\text{O}_2$  at four different reaction conditions, where the degradation activity accounted for both, the hydrogenation and decomposition activity, as shown in Figure 2.2.

These two reactions, direct synthesis and degradation, involve high pressures, toxic solvents and materials. Thus, especial precautions needed to be put in place before performing the testing.

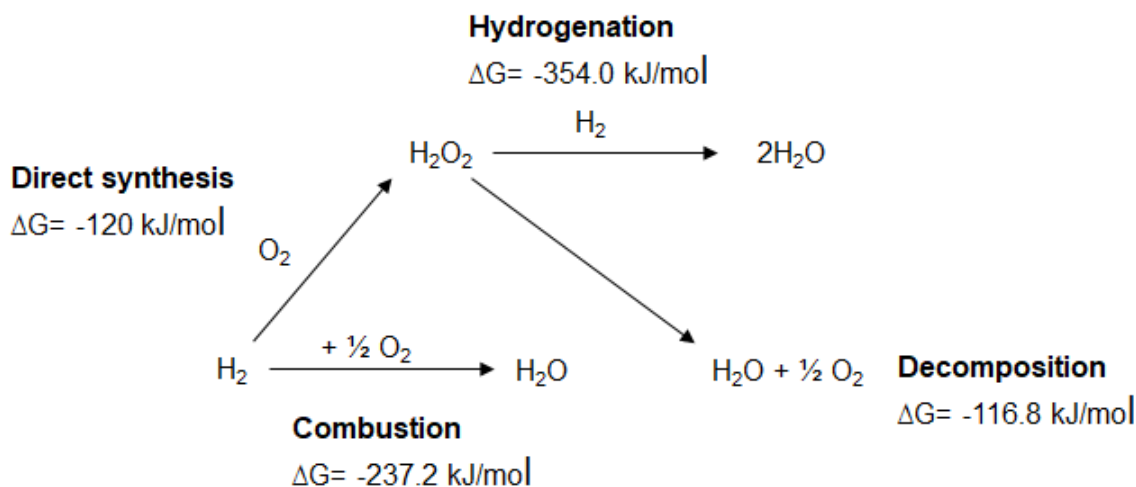


**Figure 2.2:** Schematic representation of *in-situ* H<sub>2</sub>O<sub>2</sub> and H<sub>2</sub>O formation during the direct synthesis from H<sub>2</sub> and O<sub>2</sub> gas.

Table 2.5 presents the difference between the four reaction conditions used to test the mono and bi-metallic 1 wt.% AuPd/TiO<sub>2</sub> catalysts in Chapter 3. These reaction conditions were labelled according to the temperature (2 °C or 25 °C), solvent composition (67 % methanol (CH<sub>3</sub>OH) in HPLC grade water or HPLC grade H<sub>2</sub>O-only) and the type of gas diluent (CO<sub>2</sub> or N<sub>2</sub>) employed. The catalyst amount (0.01 g), the speed of the reaction (1200 rpm), the gas composition and pressure (580 psi 5 % H<sub>2</sub>, 25 % O<sub>2</sub> diluted) and the time (0.5 h) remained un-changed.

**Table 2.5:** Reaction conditions for the direct synthesis of H<sub>2</sub>O<sub>2</sub> with mono and bi-metallic 1 wt.% AuPd/TiO<sub>2</sub> catalysts made by modified impregnation.

Name	Temperature	Reaction medium	Gas diluent
(2°C,CH <sub>3</sub> OH-H <sub>2</sub> O,CO <sub>2</sub> )	2 °C	67 % methanol (CH <sub>3</sub> OH) in HPLC grade water	CO <sub>2</sub>
(25°C,CH <sub>3</sub> OH-H <sub>2</sub> O,CO <sub>2</sub> )	25 °C	67 % methanol (CH <sub>3</sub> OH) in HPLC grade water	CO <sub>2</sub>
(25°C,H <sub>2</sub> O,CO <sub>2</sub> )	25 °C	HPLC grade water	CO <sub>2</sub>
(25°C,H <sub>2</sub> O,N <sub>2</sub> )	25 °C	HPLC grade water	N <sub>2</sub>

**Reaction conditions:** (2°C,CH<sub>3</sub>OH-H<sub>2</sub>O,CO<sub>2</sub>): 8.5 g (5.6 g CH<sub>3</sub>OH, 2.9 H<sub>2</sub>O), catalyst (0.01 g), 420 psi of 5 % H<sub>2</sub>/CO<sub>2</sub>, 160 psi of 25 % O<sub>2</sub>/CO<sub>2</sub>, 1200 rpm, 2 °C, 0.5 h. (25°C,CH<sub>3</sub>OH-H<sub>2</sub>O,CO<sub>2</sub>): 8.5 g (5.6 g CH<sub>3</sub>OH, 2.9 H<sub>2</sub>O), catalyst (0.01 g), 420 psi of 5 % H<sub>2</sub>/CO<sub>2</sub>, 160 psi of 25 % O<sub>2</sub>/CO<sub>2</sub>, 25 °C, 1200 rpm, 0.5 h. (25°C,H<sub>2</sub>O,CO<sub>2</sub>): 8.5 g H<sub>2</sub>O, catalyst (0.01 g), 420 psi of 5 % H<sub>2</sub>/CO<sub>2</sub>, 160 psi of 25 % O<sub>2</sub>/CO<sub>2</sub>, 1200 rpm, 25 °C, 0.5 h. (25°C,H<sub>2</sub>O,N<sub>2</sub>): 8.5 g H<sub>2</sub>O, catalyst (0.01 g), 420 psi of 5 % H<sub>2</sub>/N<sub>2</sub>, 160 psi of 25 % O<sub>2</sub>/N<sub>2</sub>, 1200 rpm, 25 °C, 0.5 h.

Table 2.6 presents the reaction conditions employed to evaluate catalytic activity towards H<sub>2</sub>O<sub>2</sub> degradation. As the table show, the reaction conditions were the same as for the direct synthesis of H<sub>2</sub>O<sub>2</sub> but adding 0.68 g of pre-formed H<sub>2</sub>O<sub>2</sub> (1.18 M of H<sub>2</sub>O<sub>2</sub>) in the reaction medium before the testing and using only hydrogen gas (420 psi 5 % H<sub>2</sub>/CO<sub>2</sub>). The 25 % O<sub>2</sub>/CO<sub>2</sub> needed to be removed, otherwise, *in-situ* H<sub>2</sub>O<sub>2</sub> would be generated.

**Table 2.6:** Reaction conditions for the degradation of H<sub>2</sub>O<sub>2</sub> with mono and bi-metallic 1 wt.% AuPd/TiO<sub>2</sub> catalysts made by modified impregnation.

Name	Temperature	Reaction medium	Gas diluent
(2°C,CH <sub>3</sub> OH-H <sub>2</sub> O,CO <sub>2</sub> )	2 °C	67 % methanol (CH <sub>3</sub> OH) in HPLC grade water and pre-formed H <sub>2</sub> O <sub>2</sub>	CO <sub>2</sub>
(25°C,CH <sub>3</sub> OH-H <sub>2</sub> O,CO <sub>2</sub> )	25 °C	67 % methanol (CH <sub>3</sub> OH) in HPLC grade water and pre-formed H <sub>2</sub> O <sub>2</sub>	CO <sub>2</sub>
(25°C,H <sub>2</sub> O,CO <sub>2</sub> )	25 °C	HPLC grade water and pre-formed H <sub>2</sub> O <sub>2</sub>	CO <sub>2</sub>
(25°C,H <sub>2</sub> O,N <sub>2</sub> )	25 °C	HPLC grade water and pre-formed H <sub>2</sub> O <sub>2</sub>	N <sub>2</sub>

**Reaction conditions:** (2°C,CH<sub>3</sub>OH-H<sub>2</sub>O,CO<sub>2</sub>): 8.5 g (5.6 g CH<sub>3</sub>OH, 0.68 g H<sub>2</sub>O<sub>2</sub>, 2.22 g H<sub>2</sub>O), catalyst (0.01 g), 420 psi of 5 % H<sub>2</sub>/CO<sub>2</sub>, 1200 rpm, 2°C, 0.5 h. (25°C,CH<sub>3</sub>OH-H<sub>2</sub>O,CO<sub>2</sub>): 8.5 g (5.6 g CH<sub>3</sub>OH, 0.68 g H<sub>2</sub>O<sub>2</sub>, 2.22 g H<sub>2</sub>O), catalyst (0.01 g), 420 psi of 5 % H<sub>2</sub>/CO<sub>2</sub>, 25 °C, 1200 rpm, 0.5 h. (25°C,H<sub>2</sub>O,CO<sub>2</sub>): 8.5 g (0.68 g H<sub>2</sub>O<sub>2</sub>, 7.92 g H<sub>2</sub>O), catalyst (0.01 g), 420 psi of 5 % H<sub>2</sub>/CO<sub>2</sub>, 1200 rpm, 25 °C, 0.5 h. (25°C,H<sub>2</sub>O,N<sub>2</sub>): 8.5 g (0.68 g H<sub>2</sub>O<sub>2</sub>, 7.92 g H<sub>2</sub>O), catalyst (0.01 g), 420 psi of 5 % H<sub>2</sub>/N<sub>2</sub>, 1200rpm, 25 °C, 0.5 h.

The activity of the mono and bi-metallic 1 wt.% AuPd/TiO<sub>2</sub> catalysts towards the direct synthesis and degradation of H<sub>2</sub>O<sub>2</sub> at the four different reaction conditions shown in Table 2.5 and 2.6 respectively were performed using an autoclave (Parr Instrument). Section 2.3.1.1 describes in detail how the reactor was used to conduct the experiments as well as the subsequent analysis and calculations to obtain the concentration of the synthesised H<sub>2</sub>O<sub>2</sub>, H<sub>2</sub> conversion and H<sub>2</sub>O<sub>2</sub> selectivity. The reaction medium was analysed by MP-AES to determine metal leaching (Au and Pd) for the two extreme opposite reaction conditions, (2°C,CH<sub>3</sub>OH-H<sub>2</sub>O,CO<sub>2</sub>) and (25°C,H<sub>2</sub>O,N<sub>2</sub>), during the direct synthesis of H<sub>2</sub>O<sub>2</sub>.

### 2.3.1.1 Reaction set-up procedure towards the direct synthesis and degradation of H<sub>2</sub>O<sub>2</sub> using an Autoclave (Parr Instrument).

Figure 2.3 shows a schematic representation of an autoclave reactor (Parr Instrument) used for the testing of the mono and bi-metallic 1 wt.% AuPd/TiO<sub>2</sub> catalysts at the four reaction conditions stated in Table 2.5 and Table 2.6 towards the direct synthesis and degradation of H<sub>2</sub>O<sub>2</sub> respectively.

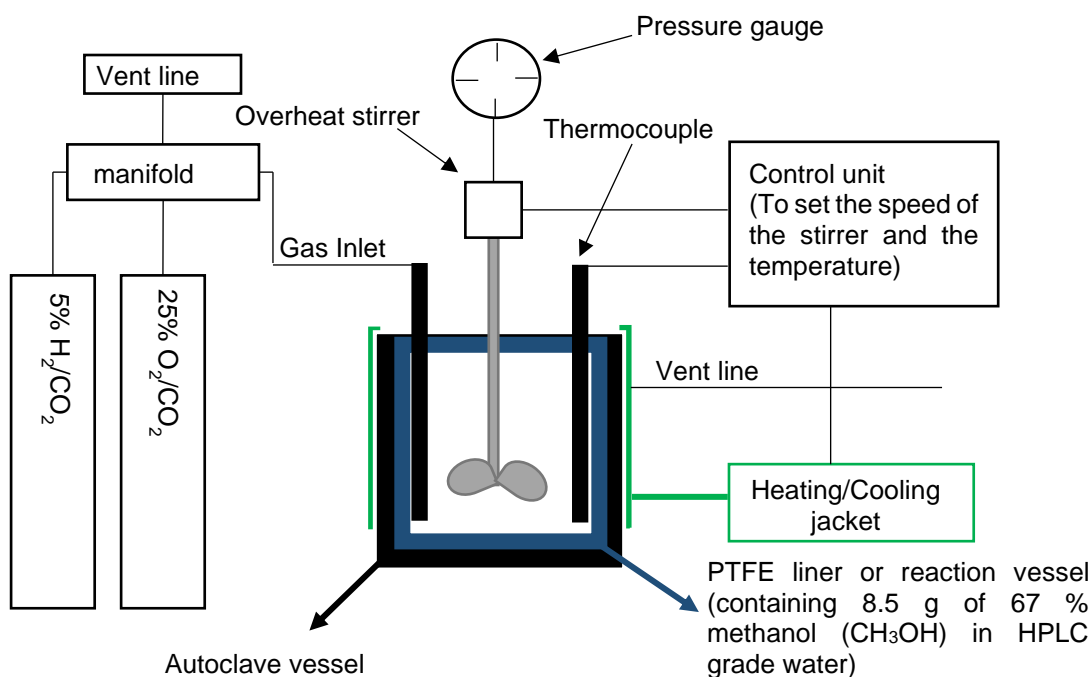


**Figure 2.3:** Schematic representation of an autoclave (Parr Instrument) reactor.

- **Reaction set-up procedure to test the catalyst's activity towards the direct synthesis of H<sub>2</sub>O<sub>2</sub> and its subsequent analysis and calculations.**

To give an example of how an autoclave functions, the following procedure gives an example for testing a bi-metallic 0.50 wt.% Au-0.50 wt.% Pd/TiO<sub>2</sub> catalysts at (2°C, CH<sub>3</sub>OH-H<sub>2</sub>O, CO<sub>2</sub>) conditions. The autoclave was a Parr Instrument stainless steel with nominal volume of 100 mL, equipped with a PTFE liner so that total volume is reduced to 66 mL and maximum working pressure of 2,030 psi. The PTFE liner was first charged with 0.50 wt.% Au-0.50 wt.% Pd/TiO<sub>2</sub> catalyst (0.01 g) and solvent (5.6 g of CH<sub>3</sub>OH, 2.9 g of H<sub>2</sub>O). The charged liner was then placed within the autoclave vessel (as shown in Figure 2.3) and screwed sealed. The sealed autoclave was then purged three times with 5 % H<sub>2</sub>/CO<sub>2</sub> (100 psi) before filling it with 420 psi of 5 % H<sub>2</sub>/CO<sub>2</sub>, followed by the addition of 160 psi of 25 % O<sub>2</sub>/CO<sub>2</sub>, reaching a total pressure of 580 psi, as seen displayed in the pressure gauge (Figure 2.3). Subsequently, the temperature was set to 2 °C in the control unit using a HAAKE K50 bath/circulator with an appropriate coolant to decrease and maintain the temperature constant during the reaction. Upon reaching 2 °C, the reaction was conducted for 0.5 h with a constant stirring (1200 rpm). The same procedure was followed to test the catalyst at (25°C, CH<sub>3</sub>OH-H<sub>2</sub>O, CO<sub>2</sub>), (25°C, H<sub>2</sub>O, CO<sub>2</sub>) and (25°C, H<sub>2</sub>O, N<sub>2</sub>) conditions, but applying the required solvent, temperature and gas diluent as stated in Table 2.5. The volume occupied by the 580 psi H<sub>2</sub>, O<sub>2</sub>/CO<sub>2</sub> gas within the autoclave was determined by water displacement to allow for accurate determination of H<sub>2</sub> conversion and H<sub>2</sub>O<sub>2</sub> selectivity.

Once the reaction has been completed, the gas was first recovered to determine the H<sub>2</sub> conversion by means of gas chromatography (GC). After the gas recovery, the autoclave was safe to be un-sealed and remove the liner containing the reaction medium (5.6 g of CH<sub>3</sub>OH, 2.9 g of H<sub>2</sub>O), the used catalyst and *in-situ* H<sub>2</sub>O<sub>2</sub>. The used catalyst was recovered and separated from the reaction medium employing a filter paper. Three aliquots of the reaction medium were weighed in a 30 mL disposable glass containers (c.a 0.5 g) and titrated with an acidified aqueous cerium sulphate (Ce(SO<sub>4</sub>)<sub>2</sub> solution in distilled H<sub>2</sub>O, ((0.14 M of H<sub>2</sub>SO<sub>4</sub>, [Ce]= 0.0085 M)) with ferroin as indicator, where the colour change from red to blue indicated the end of the titration. The reaction between the Ce(SO<sub>4</sub>)<sub>2</sub> and the H<sub>2</sub>O<sub>2</sub> proceeded according to the chemical reaction shown in Equation 1 (Eq. 1). The H<sub>2</sub>O<sub>2</sub> moles formed could be then calculated as Eq. 2 shows.

**Eq. 1**



**Eq. 2** Mols of *in-situ* H<sub>2</sub>O<sub>2</sub> formed.

$$\frac{\text{Volume of Ce}(\text{SO}_4)_2 \text{ consumed (L)} \times \text{Ce}(\text{SO}_4)_2 \text{ concentration (M)} \times \text{mass reaction medium (g)}}{2 \times \text{mass aliquote(g)}}$$

The activity of the catalyst towards the direct synthesis of H<sub>2</sub>O<sub>2</sub> was reported as productivity (mol<sub>H<sub>2</sub>O<sub>2</sub></sub> kg<sub>cat</sub><sup>-1</sup> h<sup>-1</sup>) or yield (wt.%) as Eq.3 and Eq 4 show respectively.

**Eq. 3** H<sub>2</sub>O<sub>2</sub> productivity.

$$\frac{\text{mols of } in\text{-situ H}_2\text{O}_2}{\text{catalyst weight (kg)} \times \text{reaction time (h)}}$$

**Eq. 4** H<sub>2</sub>O<sub>2</sub> yield.

$$\frac{\frac{\text{mols of } in\text{-situ H}_2\text{O}_2}{\text{H}_2\text{O}_2 \text{ molecular weight (g/mol)}}}{\text{mass reaction medium (g)}} \times 100$$

The H<sub>2</sub> conversion was determined by means of GC (Varian 3800 gas chromatogram, CP-wax 52 CB column, which was held at 30 °C for 15 min, equipped with a thermal conductivity detector (TCD) and using argon as a mobile phase). This technique separates volatile analytes according to their boiling point, except when there is a specific interaction with the stationary phase. The mobile phase consists on an inert gas to carry the analytes through the column towards the detector.<sup>5</sup> The separation of the H<sub>2</sub>, O<sub>2</sub>, CO<sub>2</sub> and N<sub>2</sub> was successfully accomplished and the retention time (t<sub>R</sub>) for each analyte is stated in Table 2.7. The t<sub>R</sub> refers to the time taken by a specific analyte to elute from the column and the difference in t<sub>R</sub> is what allows the separation and subsequent quantification.<sup>5</sup>

**Table 2.7:** Elution times for H<sub>2</sub>, O<sub>2</sub>, CO<sub>2</sub> and N<sub>2</sub> via GC analysis.

Analytes	t <sub>R</sub> min
H <sub>2</sub>	1.7
N <sub>2</sub>	2.0
O <sub>2</sub>	5.8
CO <sub>2</sub>	11.0

The counts of the H<sub>2</sub> and CO<sub>2</sub> were calculated from the integration of their peaks at t<sub>R</sub> 1.7 min and 11.0 min respectively. The CO<sub>2</sub> was employed as internal standard since it was in excess during the reaction towards the direct synthesis of H<sub>2</sub>O<sub>2</sub>. The ratio between the H<sub>2</sub> and CO<sub>2</sub> counts was subsequently calculated and compared to the ratio between the H<sub>2</sub> and CO<sub>2</sub> counts for a blank reaction (where no catalyst was employed). To give an example, a blank reaction at (2 °C, CH<sub>3</sub>OH-H<sub>2</sub>O, CO<sub>2</sub>) conditions would proceed by employing 8.5 g (5.6 g CH<sub>3</sub>OH, 2.9 H<sub>2</sub>O), 420 psi of 5 % H<sub>2</sub>/CO<sub>2</sub>, 160 psi of 25 % O<sub>2</sub>/CO<sub>2</sub>, 1200 rpm, 2°C, 0.5 h without a catalyst. By comparing the H<sub>2</sub>/CO<sub>2</sub> ratio in the presence and absence of the catalyst, H<sub>2</sub> conversion could be determined (Eq. 5). Given the range of reaction conditions used within this work, in concrete in Chapter 3, separate determinations of blank reactions had to be undertaken.

**Eq. 5** H<sub>2</sub> conversion calculation.

$$\frac{\text{Blank ratio} \left[ \frac{\text{H}_2}{\text{CO}_2 \text{ or N}_2} \right] - \text{Reaction ratio} \left[ \frac{\text{H}_2}{\text{CO}_2 \text{ or N}_2} \right]}{\text{Blank ratio} \left[ \frac{\text{H}_2}{\text{CO}_2 \text{ or N}_2} \right]} \times 100$$

The H<sub>2</sub>O<sub>2</sub> selectivity states how many mols of H<sub>2</sub> have been used to form *in-situ* H<sub>2</sub>O<sub>2</sub>. The calculation proceeded by establishing first the mols of H<sub>2</sub> introduced in the autoclave (580 psi H<sub>2</sub>, O<sub>2</sub>/CO<sub>2</sub> or N<sub>2</sub>) before the reaction started. This was calculated by applying the ideal gas law as Eq. 6 presents. Eq 7 allowed to calculate how many mols of H<sub>2</sub> were converted after the reaction, by timing the mols of H<sub>2</sub> found in Eq.6 with the H<sub>2</sub> conversion calculated in Eq.5. At this point, the ratio between the mols of *in-situ* H<sub>2</sub>O<sub>2</sub> (found in Eq. 2) and the mols of H<sub>2</sub> converted could be calculated in percentage, which allowed to obtain the selectivity of H<sub>2</sub>O<sub>2</sub> (Eq. 8).

**Eq. 6:** Mols of H<sub>2</sub> introduced.

$$n = \frac{PV}{RT}$$

where;

P = 21 psi of H<sub>2</sub> in 580 psi H<sub>2</sub>, O<sub>2</sub>/CO<sub>2</sub> or N<sub>2</sub>, which corresponds to c.a 1.43 atm.

T= 275.15 K.

V= 0.0575 L (the volume occupied by the gas (580 psi H<sub>2</sub>, O<sub>2</sub>/CO<sub>2</sub> or N<sub>2</sub>) during the reaction was determined via water displacement).

R= 0.08203 L atm K<sup>-1</sup> mol<sup>-1</sup>.

**Eq. 7:** Mols of H<sub>2</sub> converted.

$$\frac{\text{mols of H}_2 \times \text{H}_2 \text{ conversion}}{100}$$

**Eq. 8:** Selectivity of H<sub>2</sub>O<sub>2</sub>.

$$\frac{\text{mols of } in\text{-situ H}_2\text{O}_2}{\text{mols of H}_2 \text{ converted}} \times 100$$

- **Reaction set-up procedure to test the catalyst's activity towards the degradation of H<sub>2</sub>O<sub>2</sub> and its subsequent analysis and calculations.**

The catalysts activity towards the H<sub>2</sub>O<sub>2</sub> degradation was also carried out using the reactor shown in Figure 2.3. The procedure to test the degradation was the same as described for the direct synthesis of H<sub>2</sub>O<sub>2</sub> at (2°C, CH<sub>3</sub>OH-H<sub>2</sub>O, CO<sub>2</sub>) conditions but applying the modifications stated in Table 2.6. For instance, to test the degradation activity of a catalyst at (2°C, CH<sub>3</sub>OH-H<sub>2</sub>O, CO<sub>2</sub>) conditions, the liner was filled with 0,01 g of catalyst with a solvent composition made of CH<sub>3</sub>OH and H<sub>2</sub>O<sub>2</sub> with pre-formed H<sub>2</sub>O<sub>2</sub> (5.6 g CH<sub>3</sub>OH, 0.68 g H<sub>2</sub>O<sub>2</sub>, 2.22 g H<sub>2</sub>O). The temperature was let to cooled down to 2 °C and only 420 psi 5 % H<sub>2</sub>/CO<sub>2</sub> was used during the reaction. However, for this reaction, the exact concentration of H<sub>2</sub>O<sub>2</sub> (0.68 g) put in the liner initially needed to be determined by titrating three aliquots (c.a 0.03 g) with (Ce(SO<sub>4</sub>)<sub>2</sub>) acidified solution (0.14 M of H<sub>2</sub>SO<sub>4</sub>, [Ce]= 0.0085 M) with ferroin as indicator. After the reaction took place, the concentration of H<sub>2</sub>O<sub>2</sub> was also measured by titration and the two concentrations (before and after the reaction) were compared to determine the catalytic activity. The degradation activity was reported as productivity or percentage as Eq. 9 and Eq. 10 show respectively.

**Eq. 9** Degradation activity calculation with productivity units.

$$\text{H}_2\text{O}_2 (\text{molH}_2\text{O}_2 \text{ kg}_{\text{cat}}^{-1} \text{ h}^{-1})_{t=0} - \text{H}_2\text{O}_2 (\text{molH}_2\text{O}_2 \text{ kg}_{\text{cat}}^{-1} \text{ h}^{-1})_{t=0.5 \text{ h}}$$

**Eq.10** Degradation activity calculation with percentage

$$\frac{\text{H}_2\text{O}_2 (\text{molH}_2\text{O}_2 \text{ kg}_{\text{cat}}^{-1} \text{ h}^{-1})_{t=0} - \text{H}_2\text{O}_2 (\text{molH}_2\text{O}_2 \text{ kg}_{\text{cat}}^{-1} \text{ h}^{-1})_{t=0.5 \text{ h}}}{\text{H}_2\text{O}_2 (\text{molH}_2\text{O}_2 \text{ kg}_{\text{cat}}^{-1} \text{ h}^{-1})_{t=0}} \times 100$$

### 2.3.2 Reaction set-up procedure to test the catalyst's activity towards the degradation of phenol, post-reaction analysis and subsequent calculations.

The degradation of phenol was performed in an autoclave (Parr Instruments) as shown in Figure 2.3. Here lies a description of how to conduct the degradation of phenol using a 0.5 wt.% Fe-0.5 wt.% Pd/TiO<sub>2</sub> catalysts. The autoclave was a Parr Instrument stainless steel with nominal volume of 50 mL, equipped with a PTFE liner so that total volume is reduced to 33 mL and maximum working pressure of 2,030 psi. The PTFE liner was charged with the bi-metallic 0.5 wt.% Fe-0.5 wt.% Pd/TiO<sub>2</sub> (0.01 g) catalyst and 8.5 g of phenol (1000 ppm in distilled H<sub>2</sub>O). The PTFE liner was placed within the autoclave vessel and screwed sealed. The autoclave was purged three times with 5 % H<sub>2</sub>/CO<sub>2</sub> (100 psi) before filling it with 420 psi of 5 % H<sub>2</sub>/CO<sub>2</sub>, followed by the addition of 160 psi of 25 % O<sub>2</sub>/CO<sub>2</sub>, reaching a total pressure of 580 psi, as seen displayed in the pressure gauge (Figure 2.3). Subsequently, the temperature was set to increase up to 30 °C in the control unit. Once the temperature was reached, the reaction was conducted for 2 h at 1200 rpm. The volume occupied by the 580 psi H<sub>2</sub>,O<sub>2</sub>/CO<sub>2</sub> gas within the autoclave was determined by water displacement (0.043 L) to allow for accurate determination of H<sub>2</sub> conversion and H<sub>2</sub>O<sub>2</sub> selectivity

After the reaction had been completed, the gas was recovered to determine the H<sub>2</sub> conversion by means of GC (the gas chromatographer and the analysis of the gas phase was the same as explained for the direct synthesis of H<sub>2</sub>O<sub>2</sub>, see section 2.3.1.1). Once the gas had been collected, the remaining gas was vented and the autoclave un-sealed to recover the liner containing the used catalyst and the reaction medium. The used catalyst was recovered and separated from the reaction medium employing a filter (PTFE syringe of 0.45 micrometer). An aliquot of the filtered reaction medium was then placed in a glass vial to determine the conversion of phenol (%) and quantify the amount of phenol derivatives (catechol, hydroquinone, 1,4-benzoquinone and resorcinol) that were formed by means of high pressure liquid chromatography (HPLC). It was not possible to determine the residual *in-situ* H<sub>2</sub>O<sub>2</sub> that may have been remained at the of the reaction. This was because the reaction medium was coloured making not possible to visualise the colour-change when titrating it with Ce(SO<sub>4</sub>)<sub>2</sub>.

The direct synthesis and degradation activity of H<sub>2</sub>O<sub>2</sub> using mono and bi-metallic 1.0 wt.% FePd/TiO<sub>2</sub> and 0.5 wt.% Pd/X wt.% Fe-HZSM-5 (X: 3.0-0) catalysts were also determined at the same conditions as for the degradation of phenol (30 °C and 8.5 g of H<sub>2</sub>O). The catalysts activity determination towards the direct synthesis and degradation of H<sub>2</sub>O<sub>2</sub>, the H<sub>2</sub> conversion and H<sub>2</sub>O<sub>2</sub> selectivity were determined as described in section 2.3.1.1.

### 2.3.2.1 Identification and quantification of the phenol conversion and its products by means of HPLC.

Liquid chromatography (LC) is a well-known analysis technique used to separate a mixture of compounds that are present in the same liquid phase according to their physical and chemical properties. HPLC separates at high pressure mixtures of compounds according to the difference in the affinity towards the stationary phase (normal or reversed) and the mobile phase (polar or non-polar). In a reverse column, hydrocarbons (such as  $C_8H_{17}$  or  $C_3H_7$ ) are end-capped to the  $SiO_2$  coating inside the column to promote the affinity of non-polar analytes to it. Depending on the polarity of the analyte, it will have more affinity towards the stationary phase (non-polar) or towards the mobile phase (polar), which is what allows the separation. The detector must be selected according to the spectroscopic characteristics of the analytes. For instance, a diode-array detection (DAD) detector will be useful in order to detect analytes that absorb light in the UV-Vis region of the electromagnetic spectra (200-800 nm).<sup>5</sup> The rate of migration of an analyte through the stationary phase depends on the distribution ratio (D) (Eq. 11):<sup>5</sup>

#### Eq. 11

$$D = \frac{C_s}{C_m}$$

Where;

$C_s$  = total analyte concentration in the stationary phase.

$C_m$  = total analyte concentration in the mobile phase.

Large values of D indicate that the analyte elution through the column will be slow, whereas small values of D indicate that the solute will be eluted fast. Therefore, the higher the difference in D between two analytes in a sample, the easier will be to separate them since they will elute at different time ( $t_R$ ) (Eq. 12).<sup>5</sup>

#### Eq. 12

$$t_R = t_M (1+k)$$

Where;

$t_M$  or  $t_0$  = time taken for the mobile phase to go through the column (dead time).

$k$  = retention factor, directly proportional with D.

The analysis of the post-reaction medium after the degradation of phenol was carried out by HPLC, which allowed the determination of phenol conversion as well as the quantification of liquid products. The quantification of the residual phenol and the phenol derivatives (catechol, resorcinol, hydroquinone, 1,4-benzoquinone) could be carried out using an Agilent 1260 Infinity HPLC equipped with a reverse column (Agilent Poroshell 120 SB-C18, at 30 °C), flow gradient of mobile phase (HPLC grade water (0.2 wt. %  $H_3PO_4$ ) to acetonitrile ( $CN-CH_3$ )) ( $0.250 \text{ mL min}^{-1}$ ) and employing a DAD detector. Contrarily, the identification and subsequent quantification of the di-acids could not be determined, despite other analytical

strategies were tried, due to an excessive formation of other non-identified products. Thus, only phenol and phenol derivatives were successfully resolved and quantified applying the response factor (Rf) obtained from a calibration curve (Table 2.8). Eq. 13 shows how the concentration of the phenol and phenol derivatives were obtained by applying the Rf.

**Table 2.8:** Wavelength,  $t_R$  and Rf of phenol and phenol derivatives for HPLC analysis.

<b>Analytes</b>	<b><math>t_R</math></b> min	<b>Wavelength</b> nm	<b>Rf</b>
<b>Phenol</b>	11.264	278	6.930
<b>Catechol</b>	8.676	210	30.945
<b>Hydroquinone</b>	7.027	210	19.477
<b>1.4 benzoquinone</b>	9.555	254	75.404
<b>Resorcinol</b>	7.564	210	41.420

**Eq. 13**

$$\text{Area} = \text{Rf} \times [\text{analyte}]_{\text{ppm}}$$

Where;  
Area= area of the integrated peak.  
Rf= response factor.  
[analyte]= analyte concentration.

The conversion of phenol was determined by finding the residual concentration of phenol after the reaction and applying Eq. 14.

**Eq. 14**

$$\text{Phenol Conversion (\%)} = \frac{\text{Initial [Phenol]}_{\text{ppm}} - \text{After [phenol]}_{\text{ppm}}}{\text{Initial [phenol]}_{\text{ppm}}} \times 100$$

The selectivity towards the formation of phenol derivatives was calculated applying Eq. 15, where the total concentration of phenol derivatives was added together and divided by the concentration of phenol converted. Eq. 16 shows how the selectivity towards di-acids, CO<sub>2</sub> and H<sub>2</sub>O was estimated.

**Eq. 15**

$$\text{Selectivity of phenolic derivatives (\%)} = \frac{[\text{phenol derivatives}]_{\text{ppm}}}{[\text{phenol converted}]_{\text{ppm}}} \times 100$$

**Eq. 16**

$$\text{Selectivity of di-acids, CO}_2 \text{ and H}_2\text{O (\%)} = 100 - \text{selectivity of phenol derivatives}$$

### **2.3.2.2 Gas replacements experiments for the degradation of phenol using mono and bi-metallic 1 wt.% FePd/TiO<sub>2</sub> and 0.50 wt.% Pd/ X wt.% Fe-HZSM-5 (X: 3.0-0.06) catalysts.**

The gas replacement experiments were conducted for 2, 4, 6 and 8 hours. Here lies an example of how to conduct the data point of 4 h. An identical procedure to that outlined above for the degradation of phenol (section 2.3.2) was followed for a 2 h reaction time. After 2 h time, the stirring was stopped, and the reactant gas mixture (580 psi H<sub>2</sub>, O<sub>2</sub>/CO<sub>2</sub>) was vented prior to replacement with the standard pressures of 5 % H<sub>2</sub>/CO<sub>2</sub> (420 psi) and 25 % O<sub>2</sub>/CO<sub>2</sub> (160 psi). Once the gas phase was replaced, the reaction was stirred for an extra 2 h at 1200 rpm at 30 °C. After this time, the stirring was stopped, and the gas collected to determine the H<sub>2</sub> conversion by means of GC. An aliquot of the post-reaction mixture after filtration was placed in a glass vial to conduct the analysis by HPLC as explained in section 2.3.2.1. Therefore, to obtain the 6 h data point, two gas phase replacements were done, one at 2 h and one at 4 hours reaction time. Hence, the data points at 2, 4 and 6 h were carried out individually and that there was not on-line sampling between the 2, 4 and 6 hours' reaction times.

### **2.3.2.3 Re-usability of the bi-metallic 1 wt.% FePd/TiO<sub>2</sub> and 0.50 wt.% Pd/ X wt.% Fe-HZSM-5 (X: 3.0-0.06) catalysts towards the degradation of phenol.**

Approximately 50 mg of catalyst were tested for 2 hours towards the degradation of phenol. After this time, the reaction was stopped, and the catalyst filtered and dried overnight under vacuum for 16 h at 30 °C. The resulting solid, was labelled as used catalyst and re-tested towards the degradation of phenol.

### **2.3.3 Reproducibility of the catalytic activity.**

The catalyst's activity of the mono and bi-metallic 1 wt.% AuPd/TiO<sub>2</sub> catalysts in Chapter 3 were tested several times towards the direct synthesis and degradation at different reaction conditions. However, to determine the reproducibility, three different batches of each mono and bi-metallic 1 wt.% AuPd/TiO<sub>2</sub> catalysts were made and their activity tested three times towards the direct synthesis and degradation of H<sub>2</sub>O<sub>2</sub> for each reaction condition. The activity of the catalysts throughout this thesis is given by the mean value obtained from the catalytic results of the three different catalyst's batches. The mean value is given with the standard deviation subsequently calculated using the three results obtained for each different catalyst lot. If the standard deviation is not given when the catalytic activity is shown, this means that the catalyst was tested less than three times. The same reasoning was implemented to determine the reproducibility and subsequently the standard deviation for the catalyst activity in Chapter 4 and Chapter 5.

## 2.4 Introduction to molecular spectroscopy.

This section aims to introduce the spectroscopic and microscopic techniques that were employed to carry out the characterisation of the catalysts in each experimental chapter. Also, there is a sub-section that details the settings uploaded to each equipment to perform the catalyst's characterisation. However, before this, section 2.4.1 gathers the basics of molecular spectroscopy to explain what radiation is and how it can interact with matter.

### 2.4.1 Introduction to molecular spectroscopy.

Molecular spectroscopy is the study between the electromagnetic field and the matter. The electromagnetic radiation consists of an electric and magnetic field that oscillate at the same frequency,  $\nu$  ( $\text{s}^{-1}$  or Hz) and travels at vacuum at speed,  $c$ . The distance between adjacent crest at a given point in time is called wavelength,  $\lambda$  (Eq. 17).<sup>5</sup>

#### Eq. 17

$$\lambda = c / \nu$$

Where;

$c = 2.997925 \times 10^8 \text{ m s}^{-1}$

$\nu = \text{frequency s}^{-1}$  or Hz.

The frequency,  $\nu$  is often expressed as wavenumber  $\nu^{-}$ , which is usually used in infrared spectrometry (IR) Eq. 18.<sup>5</sup>

#### Eq. 18

$$\nu^{-} = 1 / \lambda$$

A molecule experiments alterations when interacts with the electromagnetic field such as experiment an electronic transition from the fundamental state to an excited state, it can have its bonds bended or stretched (vibrations), it can also rotate and translate from one position to another. Thus, the total energy of a molecule can be separated into a sum of individual contributions or parts (Eq. 19).<sup>5</sup> The electromagnetic field can be grouped according to the kind of alteration it produces to the matter (Table 2.9). Depending on the kind of disturbance produced, more energy will be required.<sup>5</sup>

#### Eq. 19

$$E = E_{\text{electronic}} + E_{\text{vibrations}} + E_{\text{rotation}} + E_{\text{translation}}$$

**Table 2.9:** Electromagnetic field and electromagnetic region.

<b>Wavelength range</b> cm <sup>-1</sup>	<b>Energy range</b> J/mol	<b>Spectroscopic technique</b>	<b>Processes occurring</b>
<b>50,000-11,000</b>	(1-6) x 10 <sup>5</sup>	UV-Vis	Electronic transitions
<b>5000-200</b>	(2-60) x 10 <sup>3</sup>	Infrared	Vibrations
<b>166-1.6</b>	20-2000	Microwave	Rotation
<b>1.1-0.3</b>	4-15	Electron spin resonance	Change in spin of unpaired electrons
<b>0.016-0.002</b>	(2-20) x 10 <sup>-2</sup>	Nuclear magnetic resonance	Change in spin
<b>0.002-0.0006</b>	(8-20) x 10 <sup>-3</sup>	Nuclear quadrupole resonance	Change in quadrupole orientation

It is also more convenient sometimes to refer to electromagnetic radiation as photons, which are understood as particles with a specific energy,  $E$  (Eq. 20). This is known as the wave-particle duality and it is very convenient in order to explain some physical phenomena such as the photoelectric effect, which is the basis for the x-ray photoelectron spectroscopy (XPS).<sup>5</sup> Thus, as the Eq. 20 presents, more  $\nu$  corresponds to high levels of  $E$  and shorter  $\lambda$ .

**Eq. 20**

$$E = h \nu$$

Where;

$h = 6.62608 \times 10^{-34} \text{ Js}^{-1}$  Planck's constant.

$\nu =$  frequency  $\text{s}^{-1}$  or Hz.

The interaction between the electromagnetic field and the matter occurs when the electric or magnetic part interact with a dipole moment that must be oscillating at the same frequency as the electromagnetic field. Thus, the matter only responds to a concrete discrete  $\nu$ , thus to a certain  $E$ . This suggests that the interaction between the photon and the matter are quantified. Therefore, the matter can only absorb a photon whose energy corresponds exactly to the difference between two energy levels of the atom or molecule (Eq. 21).<sup>5</sup>

**Eq. 21**

$$h \nu = E_2 - E_1$$

The intensity of the absorption band, will depend on three factors: the probability of transition (permitted or forbidden by selection rules), the initial distribution of Boltzmann and the concentration of the sample.<sup>5</sup>

### Probability of transition

The probability of the transition is given by the selection rules, which are established by resolving Schrodinger equation. The selection rules vary from technique to technique, and in general, an atom can experiment a transition when the vibrational quantum number is  $\Delta v = \pm 1$ . The transition from  $v=0$  to  $v=1$ , is referred as fundamental transition as it is usually the more intense. Despite the transition is sometimes forbidden by selection rules, the peak can be still identified, however, with low intensity. For instance, the overtones or hot bands ( $v=0$  to  $v=2$ ,  $v=0$  to  $v=3$ ),<sup>5</sup>

### Initial distribution of Boltzmann

The probability of transition will be dependent on the population of the energy levels, which are given by Boltzmann distribution law (Eq. 22). This equation stipulates three important statements that have considerable implication in practice:<sup>5</sup>

- The greater the energy between levels, the smaller the ratio between the upper level ( $N_u$ ) with the lower level ( $N_l$ ).
- The higher the temperature, the larger the ratio.
- The higher the degeneracy ( $\frac{g_u}{g_l}$ ), the larger the ratio.

This means that if  $\Delta E$  is big, there will be more particles in  $N_l$  than in  $N_u$ , which indicate that the excitation will be difficult. However, if increasing the temperature,  $\Delta E$  will become small, promoting the transition from lower to upper level. On no account the upper level can be more populated than the upper level.<sup>5</sup>

### Eq. 22

$$\frac{N_u}{N_l} = \frac{g_u}{g_l} e^{-\left(\frac{\Delta E}{kT}\right)}$$

Where;

$N$ = is the number of species of interest in the level.

$g$ = number of levels with the same energy (degeneracy).

$k$ = Boltzmann constant,  $1.38 \times 10^{-23}$  J.

### Sample concentration

The absorption is the transition of an electron of an atom or molecule between two energy levels whose energy corresponds exactly to the energy of the incident radiation. Beer and Lambert determined that the intensity of the incident radiation when it is in contact to the atom or molecule in solution decreases exponentially with the path length and the concentration.<sup>5</sup> They established that the absorption can be related to the difference between the intensity of the incident light ( $I_0$ ) and the intensity of the transmitted light ( $I_t$ ) after it passed through a solution containing the atom or molecule whose electrons absorb the

light. They measured the transmittance of the light as the ratio between  $I_o/I_t$  and related it to the absorbance and the concentration of the sample as Eq. 23 shows.

**Eq. 23**

$$\log (I_o/I_t) = A = \epsilon l [a]$$

Where;

A= absorbance.

$I_o$ = incident light.

$I_t$ = transmitted light.

$\epsilon$ = molar absorption coefficient ( $10^5 - 1 \text{ L mol}^{-1}\text{cm}^{-1}$ ), which refers to the transition probability and the nature of the absorbing species.

$l$  = length cuvette (1 cm).

$[a]$ = concentration of analyte ( $\text{mol L}^{-1}$ ).

#### 2.4.2 Basics about ultraviolet-visible spectroscopy (UV-Vis).

UV-Vis spectroscopy is an inexpensive, simple, flexible, non-destructive analytical method that is used widely for organic and inorganic samples. It is based on electronic transitions by an electromagnetic radiation, which in this case corresponds to ultraviolet-visible region (200-800 nm). As explained in section 2.4.1, the electronic transition will occur when the energy of radiation corresponds exactly to the difference in energy between the two energy levels, ground and excited state. However, the selection rules will determine the intensity of the transition. The electron spinning around the nuclei is defined by three quantum numbers:

**n** (principal quantum number) (1,2...)

**l** (orbital angular momentum) (n-1)

**ml** (magnetic quantum number) (+l, -l)

The orbitals are sorted according to their energy and are built up by placing two electrons –with different spin multiplicity ( $-\frac{1}{2}$ ,  $\frac{1}{2}$ )- into the lowest energy orbital first, then to the next empty orbital with the lowest energy and so on. In order to the transition to take place, the electron must experience a  $\Delta l = \pm 1$ .<sup>5</sup> In molecules, the atomic orbitals combine to form molecular orbitals, which are also defined by quantum numbers and sorted according to its energy; the molecular orbital with the lowest energy is referred as sigma,  $\sigma$ , followed by  $\pi$  orbital, *non-bonding molecular orbital with un-shared pair of electrons, n*, and *anti-bonding* ( $\sigma^*$   $\pi^*$ ) that have the highest energy. The selection rules for a molecular transition to happen, requires that it should not be any change in the spin quantum number (spin multiplicity) and both molecular orbitals need to have the same symmetry (Laporte or parity). The transition between the highest occupied molecular orbital (HOMO) to the lowest unoccupied energy level (LUMO) are considered the most important.<sup>5</sup>

Figure 2.4 presents a schematic representation of a double-beam UV-Vis spectrometer that measures the electronic transitions of a molecule in solution. The sample is diluted in a

solution and placed in a cuvette made of plastic or glass. The visible light (400-800 nm) source is generally a tungsten filament lamp or tungsten halogen bulb, on the other hand, the ultraviolet source (200-400 nm) is a deuterium lamp. The radiation will pass through a monochromator, which will disperse the radiation into selectable wavelengths, usually referred to as monochromatic light. In a double-beam instrument like this one, the light is divided to reach both, the reference and the sample cuvettes respectively. The reference cuvette can be understood as the blank sample, since it contains the solvent used to dissolve the analyte into. The detector measures the intensity of the incident light at a specific wavelength ( $I_0$ ) and the transmitted light ( $I_t$ ) that passes through the cuvette, obtaining the transmittance, which is linearly related to the absorbance and the concentration of the analyte in solution according to Eq. 23.

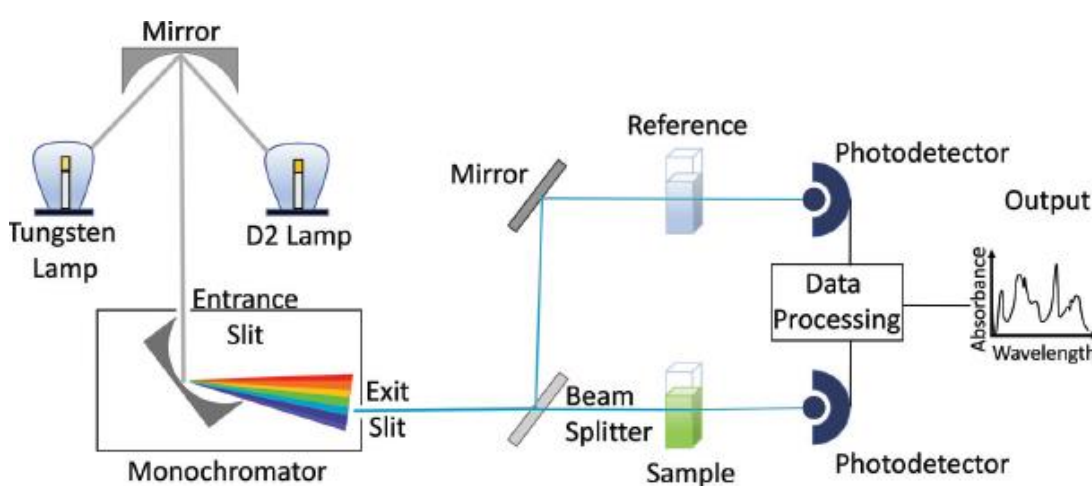


**Figure 2.4:** Schematic representation of a double beam UV-Vis spectrometer.<sup>5</sup>

One of the limitations of this technique is the analyte-solvent interactions that can decrease the resolution between peaks, especially for polar analytes and polar solvents. Ideally, there should not be any other compound in the solution that may absorb at the same wavelength as the analyte whose concentration is meant to be found, otherwise there will be interferences.<sup>6</sup> One of the most common sources of error in UV-Vis spectrometry is related to sample preparation, cell handling and cleanliness. All the experiments, including the calibration, should be used employing the same cuvette, since its composition and geometry influences the precision of the analysis. The calibration must be linear to be able to apply Beer-Lambert equation. It can happen that some analytes can decompose, aggregate or precipitate during their analysis if their concentration is too high leading to a non-linear calibration curve. In this scenario, dilutions would be required to avoid this and obtain a linear calibration curve.<sup>6</sup>

### 2.4.3 Basics about diffuse reflectance ultraviolet-visible spectroscopy (DR UV-Vis)

As mentioned above, UV-Vis measures the transmittance that can be related to the absorbance by Beer-Lambert equation, which allows the determination of analyte's concentration in a solution. However, when the sample is a solid, like a catalyst, the reflectance is measured instead of the transmittance using a DR UV-Vis. In this case, it measures the intensity of the light that is reflected from the solid sample (Figure 2.5). The absorbance is calculated from all the reflected beams of the sample using a semispherical collector. Therefore, the spectrum is shown by plotting the intensity of the absorbance versus the wavelength.<sup>6</sup> Figure 2.5 schematically represents what reflection is and compares it to other ways radiation can interact with a sample.<sup>6</sup>

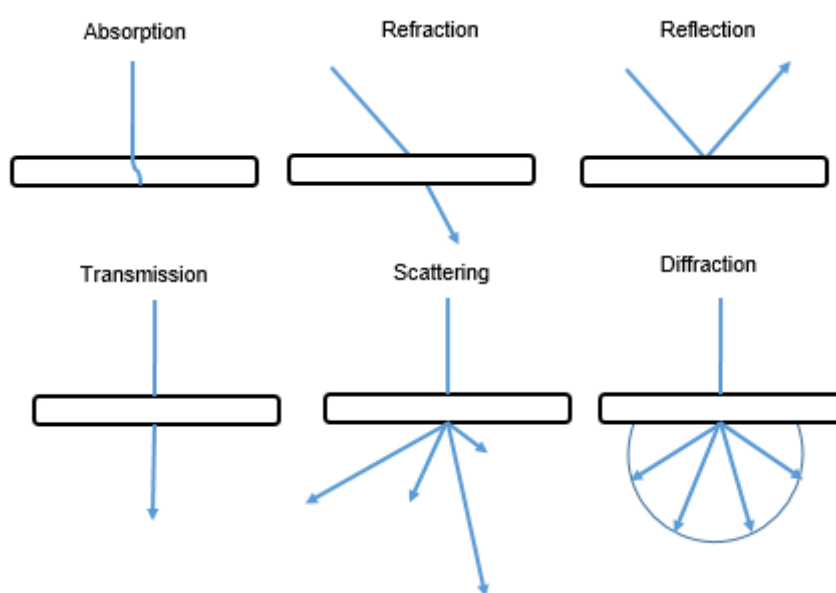


**Figure 2.5:** Schematic representation of the incident beam to the sample.

#### 2.4.3.1 Determination of the Fe species for the mono and bi-metallic 0.50 wt.% Pd/ X wt.% Fe-HZSM-5 (X:3.0-0.06) catalysts by means of DR UV-Vis.

The absorbance of mono and bi-metallic 0.5 wt.% Pd/X wt.% Fe-HZSM-5 (X:3.0-0.06) catalysts were analysed by means of a DR-UV-Vis (Cary 400 spectrometer (Varian) equipped with a diffuse reflectance accessory (Praying Mantis, Harrick)). The sample was placed in the sample holder and introduced into the instrument with the shield closed. Carey software was uploaded to scan the sample between 200-800 nm with a speed of 200 nm min<sup>-1</sup>. In this case, bare HZSM-5 was employed as blank to isolate the peaks of the Fe species from those arising from the support (HZSM-5).

### 2.4.4 Basics about fourier transform infrared (FT-IR) and raman spectroscopy.

FT-IR can provide information on the molecular structure of organic and inorganic components. It is also a versatile and non-destructive technique.<sup>7</sup> An FT-IR spectrum is

reported as transmittance or absorbance (y axis) versus wavelength (x axis). The IR region in the electromagnetic field can be divided into three regions commonly known as near (13000-4000 cm<sup>-1</sup>), mid (4000-400 cm<sup>-1</sup>) and far (400-10 cm<sup>-1</sup>) IR. For most applications, the working range is mid-IR (4000-400 cm<sup>-1</sup>). The region between 1450 to 600 cm<sup>-1</sup> is referred as fingerprint region, on the other hand, the region between 4000 to 1450 cm<sup>-1</sup> is commonly referred as group frequency region. Each functional group (e.g -OH, -COOH, -COH, -RCOR-) falls within a specific frequency region, therefore making this technique quite useful for the structural determination of an unknown molecule.<sup>8</sup>

In FT-IR, the absorption of IR radiation happens when a photon transfers to a molecule and excites it to a higher energy state that results in vibrations of molecular bonds (*i.e* stretching, bending, twisting, rocking, wagging and out of place deformation).<sup>7</sup> The vibrational frequency of a diatomic molecule can be modelled as if it was a harmonic oscillator, in which two masses (m<sub>1</sub> and m<sub>2</sub>) are held together by a spring. When the two masses are pull apart and left, the spring will vibrate to a certain frequency,  $\omega$ , given by (Eq. 24).<sup>5,9</sup>

**Eq. 24**

$$\omega = \frac{1}{2\pi} \sqrt{\frac{k}{\mu}}$$

Where;

k= force constant of the bond.

$\mu = m_1 m_2 / (m_1 + m_2)$  is the reduced mass.

The spring of a macroscopic oscillator could be ideally stretch up to any given point. However, in the microscopic world, the spring would be only able to be stretch up to certain levels or stablished points. These points or levels are usually defined by the vibrational quantum number,  $v$ , whose energy,  $E$  is defined by Eq. 25. Therefore, a molecule can absorb each time,  $h\omega$ , in order to go from one level to the subsequent one, thus, for a harmonic oscillator, the selection rule is  $\Delta v = \pm 1$ .<sup>5,9</sup>

**Eq. 25**

$$E = h \omega \left( v + \frac{1}{2} \right)$$

Where;

$h$  = plank's constant (6.62607015×10<sup>-34</sup> J·s).

$v = 0, 1, 2, \dots$  ( $v = 0$ , fundamental state).

The position of an atom can be defined by the three coordination axes (x, y, z) with respect to an origin. Thus, a molecule consisting of three atoms, can be defined by 3N coordinate positions or degrees of freedom. Apart from vibration, a 3N molecule can be also translated from (x,y,z) to (2x, 2y, 2z) or can be rotated from (x,y,z) to (-x,-y,-z). Translations and rotations are not IR active, therefore, only 3N-6 movements or modes will correspond to vibrational movements, in which the molecule stretches or bends. Only the modes in where

there is a change in the electric dipole moment can interact with the IR wavelength. For example, H<sub>2</sub>O has three modes (3\*3-6), which correspond to a symmetric, antisymmetric and bending stretching. All three are IR active because there is a change in the dipole moment (Figure 2.6).<sup>5</sup>

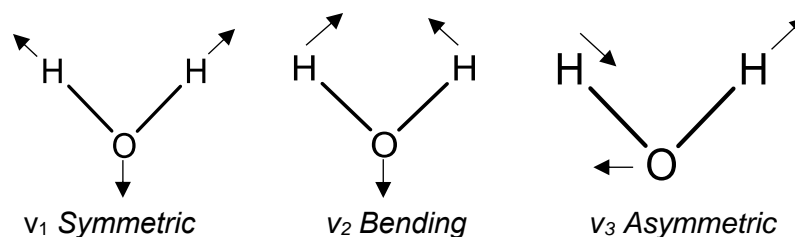


**Figure 2.6:** Schematic representation of IR active modes for H<sub>2</sub>O.

As in IR, Raman also measures the vibrational frequencies at what molecules absorbs. However, the fundamentals are different from those that apply in IR. For Raman, the incident light ( $\nu_0$ ) is absorbed to a virtual excited state and then emitted with a fraction of energy added or removed,  $\pm h\nu$ . These are referred as Stokes ( $\nu_0 - h\nu$ ) and anti-Stokes ( $\nu_0 + h\nu$ ) respectively. The Stokes are more intense than the anti-Stokes, since the Stokes come from the promotion of the fundamental state, which is the most populated.<sup>10</sup> Continuing the example of the molecule of H<sub>2</sub>O, all three modes give a change in the dipole moment, which makes them all three IR active. However, the polarizability only changes with the stretching mode since the O moves away. Therefore, only the  $\nu_1$  is Raman active. Determining the irreducible representation using the group theory is often the easiest way in order to determine which modes are active for IR and Raman, especially for big molecules.<sup>5</sup>

A schematic representation of an FT-IR instrument is shown in Figure 2.7. The radiation source consists of a silicon carbide target heated to 1200 K for a mid-IR frequency region. The beam from the source is split by the beam splitter so that half of it travels towards a mobile mirror and the other half hits a fixed mirror. Again, the beam is reflected back from both mirrors to the beam splitter, which subsequently reached the sample cell and the detector. An FT-IR replaces the monochromator for an interferometer (an instrument that superimposes two or more interfering waves to detect differences). As the mobile mirror moves, wave interferences change the intensity of each wavelength in the spectrum. The raw signals containing the spectrum of transmitted light at each mirror position is converted to frequency by a Fourier transform.<sup>8,11</sup> An FT-IR interferogram is reported as transmittance or absorbance (y axis) versus wavelength (x axis). Thus, by Lambert-Beer law, it would be able to relate the concentration with the absorbance. The detection limits of FT-IR lie in the range of 30 to 220 ppm depending on the analyte.<sup>11</sup>

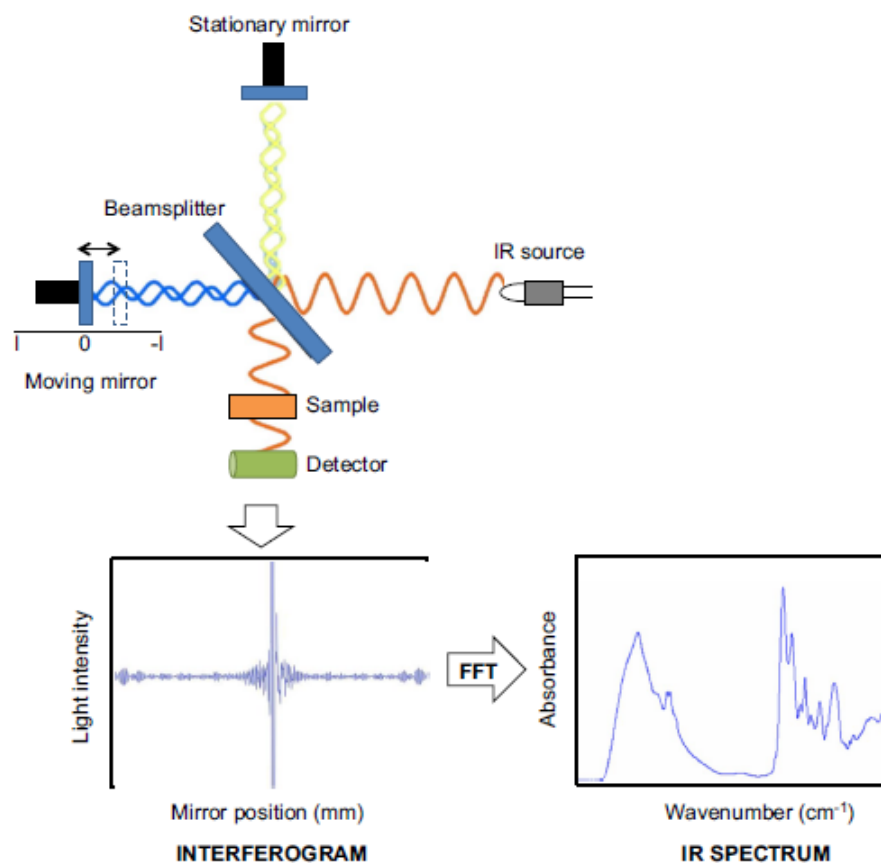


**Figure 2.7:** Schematic representation of a FT-IR spectrometer.<sup>8</sup>

IR analysis of multiple analytes can generate an interferogram with overlapping peaks that can complicate their analysis and quantification. Thus, to discern each analyte, complementary analysis would be highly recommended such as chromatography. Another important limitation of IR is that water strongly absorbs IR, which overlaps with the peak arising from the analyte. To remediate this, deuterated water (D<sub>2</sub>O) is commonly used or tetrachloromethane (CCl<sub>4</sub>) for solid samples. On the other hand, raman can work with aqueous samples because water is a weak raman scatterer.<sup>11</sup>

Figure 2.8 presents the schematic representation of a raman instrument. It consists on a sample holder, a source of radiation (UV (quadrupled, diode-pumped Nd:YAG lasers at 266 nm and NeCu hollow-cathode metal-ion lasers at 248.6 nm, visible or near IR), collection optics, a spectral analyser (monochromator or interferometer), and a detector. Raman spectrometers can also be coupled with an optical microscope to see the sample and be able to focus the beam on different regions.<sup>8</sup> The incident monochromatic light is scattered by the sample, thus producing a change in energy and light direction. The energy is gained by the analyte in the sample which involve a vibrational effect as explained above. The difference between the incident and the scattered radiation is measured and considering that the observed changes are very small (approximately only 1 in 10<sup>9</sup> photons is scattered),

the intensity of the incident beam -coming from the laser- needs to be significantly high to obtain sufficient resolution when analysing the sample.<sup>8</sup>

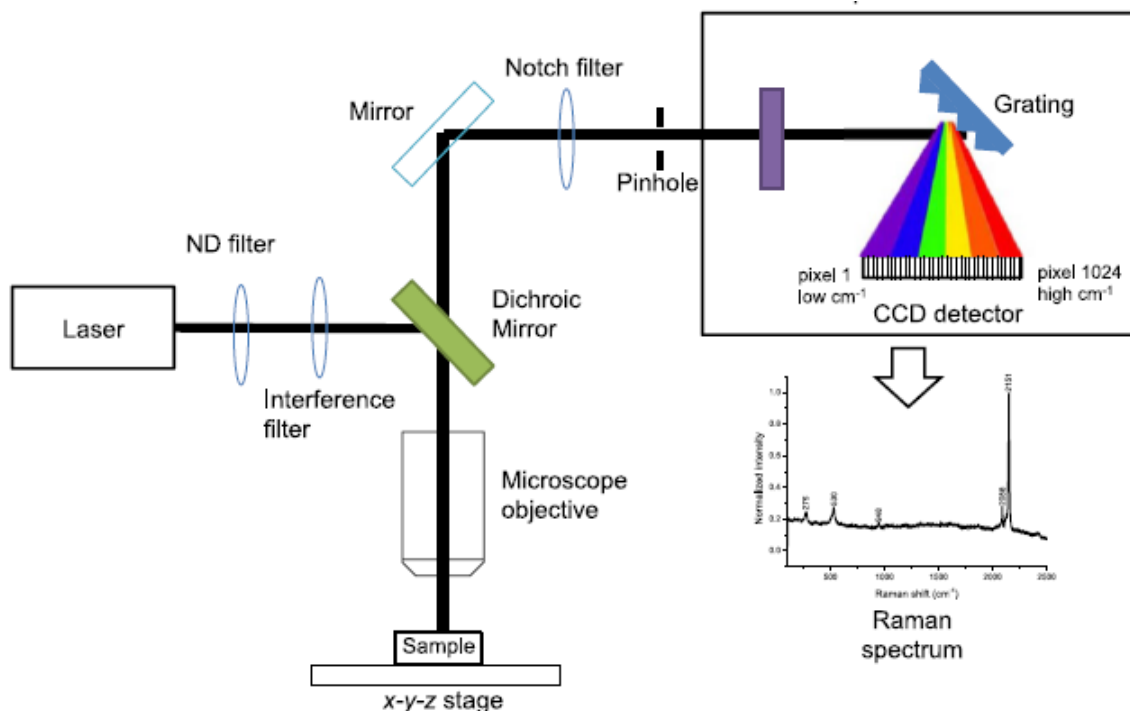


**Figure 2.8:** Schematic representation of a Raman spectrometer.<sup>8</sup>

One of the main problems when working with Raman is the interference with fluorescence. The difference between the two is that the latter involves electronic transitions, whereas Raman involves vibrations from photons that are scattered. Fluorescence can interfere with the signal in Raman, overlapping the vibrational peaks that are coming from the analyte in the sample. The best way to avoid such interference is selecting the appropriate laser in accordance with the type of sample. In fact, studying HZSM-5 samples with visible Raman is not possible due to the fluorescence interference. Therefore, UV-Raman needs to be employed instead to analyse zeolites.<sup>12</sup>

#### **2.4.4.1 Determination of the Fe species of the mono and bi-metallic 0.50 wt.% Pd/ X wt.% Fe-HZSM-5 (X:3.0-0.06) catalyst by means of FT-IR and UV-Raman.**

FT-IR spectroscopy and Raman-UV were employed to determine the nature of the Fe species formed in the mono and bi-metallic 0.5 wt.% Pd/ X wt.% Fe-HZSM-5 (X: 3.0-0.06) catalysts. These two techniques were used in a complementary manner to DR UV-Vis, which also was used for this purpose.

FT-IR analysis was conducted using Cary 630 FT-IR spectrometer (Agilent technologies) fitted with a HgCdTe (MCT) detector and operated with a Microlab software. The sample

holder needs to be wiped down with isopropanol to be able to collect a blank signal from the instrument. After, the sample is placed in the sample holder and the pellet is formed by compressing with the manual handle. At this point, the sample is already focused on the beam and ready to be analysed.

A Reinshaw inVia raman microscope, equipped with a laser excitation of 266 nm was employed to analyse the samples with WIRE software. The sample is placed on the sample holder and under the microscope lens (5x). The video camera on the computer screen allows to focus the beam on the sample, and when it is focused, the analysis is performed with 0.5 % power laser, 50 accumulations and 10 seconds per accumulation.

#### **2.4.5 Basics about CO-diffuse reflectance infrared fourier transform spectroscopy (CO-DRIFTS).**

Transmission FT-IR is perhaps the most common IR spectroscopic technique and involves incident light that traverses the sample. However, there are other configurations for IR such as attenuated total reflection (ATR), diffuse reflectance (DRIFTS), and reflection-absorption (RAIRS). As in the case of DR UV-Vis, the DRIFTS also measures the reflectance of the light from the surface of the sample.<sup>13,7</sup> Figure 2.9 presents a schematic representation of the different configurations for vibrational analysis. For the DRIFTS, the IR beam illuminates a sample in a cell and a detector collects the reflected light rather than the transmitted light.<sup>11</sup> Also, in DRIFTS, CO is employed as a probe molecule to bind with the metal nanoparticles to evaluate the dispersion and morphology of the metal nanoparticles via thermal desorption and/or vibrational spectroscopies.<sup>14</sup> However, the analysis is mostly qualitative.<sup>11</sup>

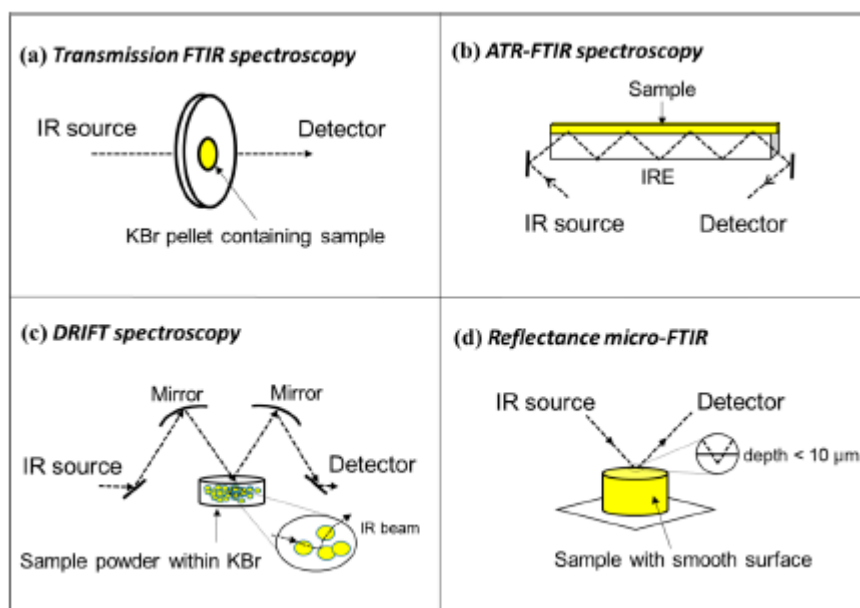


**Figure 2.9:** Schematic representation of the different configurations or modes for IR spectrometry.<sup>7</sup>

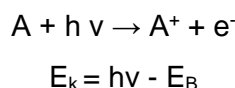
#### 2.4.5.1 Analysis of mono and bi-metallic 1 wt.% FePd/TiO<sub>2</sub> and 0.5 wt.% Pd/ X wt.% Fe-HZSM-5 (X: 3.0-0.06) catalysts by means of CO-DRIFTS.

CO-DRIFTS measurements were taken on a Bruker Tensor 27 spectrometer fitted with a mercury cadmium telluride (MCT) detector. A sample was loaded into the Praying Mantis high temperature (HVC-DRP-4) *in-situ* cell before exposure to N<sub>2</sub> and then to 1% CO/N<sub>2</sub> at a flow rate of 50 cm<sup>3</sup> min<sup>-1</sup>. A background spectrum was obtained using KBr, and measurements were recorded every 1 min at room temperature. Once the CO adsorption bands in the DRIFT spectra ceased to increase in size, the gas feed was changed back to N<sub>2</sub> and measurements were repeated until no change in subsequent spectra was observed.

#### 2.4.6 Basics about x-ray photoelectron spectroscopy (XPS).

XPS is based on the photoelectric effect. Photons coming from the incident electromagnetic ray (X-Ray or UV) can remove an electron from the sample with a certain kinetic energy (E<sub>k</sub>) generating a positive charge (Eq. 26).

**Eq. 26**



Where;

E<sub>B</sub>= binding energy (Initial energy of A, final energy of A<sup>+</sup>).

The ejected photoelectrons have a relatively slow energy (60 KeV) and are mostly scattered by adjacent electrons, losing their energy and un-able to be detected. The un-scattered electrons are the ones that are detected as photoelectron peaks (up to 10 nm of the material). The E<sub>B</sub> are tabulated in order to assign it to its corresponding metal. For example,

$\text{Pd}^0$  and  $\text{PdO}$  have the following  $E_B$ : 334.5 eV and 336.3 eV.<sup>15</sup> When an atom has lost electrons ( $\text{PdO}$ ), the remaining electrons (those in the core level) feel less repulsion and are more attracted to the nuclei, therefore the  $E_B$  will be higher than the corresponding  $\text{Pd}^0$ . These fact makes the XPS very useful when it comes to determining the oxidation state or speciation of the metal. Apart from the oxidation state, the sintering of the metal can also shift the  $E_B$  despite not changing the oxidation state.

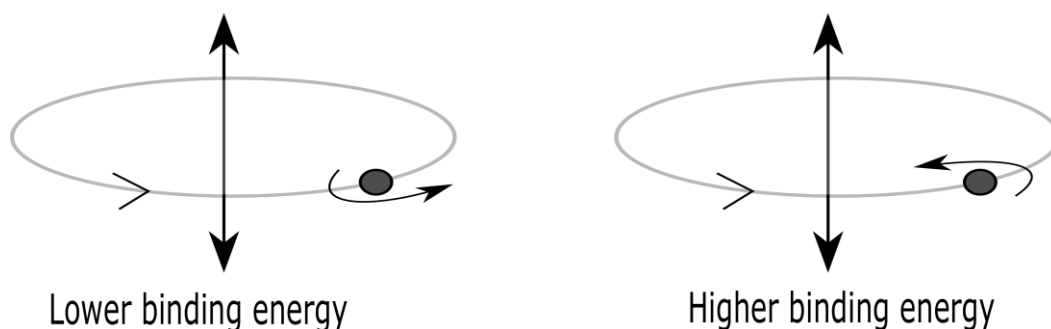


**Figure 2.10:** Parallel and anti-parallel spin moment.

The two electrons spinning around the orbital present parallel ( $1/2$ ) or anti-parallel spin ( $-1/2$ ) moment to its orbital angular momentum ( $l=0$  (s),  $l=1$  (p),  $l=2$  (d)...), giving rise to two photoelectron peaks or spin orbital peaks separated with a certain energy ( $\Delta E$ ) (Figure 2.10). For instance, the XPS of the Pd would show two photoelectron peaks at 334.5 eV and another other one at 339.9 eV separated by  $\Delta E = 5.26$  eV. The relative intensities of the two photoelectron peaks in the spectrum are proportional to the value  $2J+1$  for each state, where  $J$  is the total angular momentum vector ( $J= l+s$ ). For instance, Pd have each photoelectron peak assigned to  $3d J=3/2$  (334.5 eV) and  $3d J=1/2$  (339.9 eV). Each photoelectron peak of the Pd can now be deconvoluted into two peaks according to the oxidation state of the Pd;  $3d J=3/2$  ( $\text{Pd}^0$  335.1 eV,  $\text{PdO}$  335.6 eV) and  $3d J=1/2$  ( $\text{Pd}^0$  340.3 eV,  $\text{PdO}$  340.9 eV). The shape and the medium width (FWHM) of each deconvoluted peak are different depending on the oxidation state of the Pd. For instance,  $\text{Pd}^0$  have asymmetrical peaks with a width between 0.9-1.2 eV, whereas  $\text{PdO}$  have symmetrical shape peaks.

There are other peaks called satellite with a lower kinetic energy than the photoelectron ones. The satellite peaks rise when part of the  $E_k$  released by the ejected electron is used by another electron to be excited to a higher level of energy (Figure 2.11). The satellite peaks are also doubled and separated by fixed distance  $\Delta E$ . The intensity of both are determined by the probability of the transition. For instance,  $\text{Pd}^0$  and  $\text{PdO}$  have two satellites peaks each approximately at  $E_B$  345.8 eV and 341.3 eV for  $\text{Pd}^0$  and 335.2 eV and 340.5 eV

for PdO. These satellite peaks are also separated approximately by  $\Delta E=5.26$  eV with the same shape as their corresponding oxidation state.

The XPS of the Fe also presents two photoelectron peaks at 710 eV ( $2p J=3/2$ ) and 724 eV ( $2p J=1/2$ ). The photoelectron peaks of the Fe 2p are particularly wide due to the multiplet splitting and shake-up peaks, which makes the analysis of the Fe difficult.<sup>16</sup> Multiplet splitting arises when an atom contains un-paired electrons. When a core electron vacancy is formed by photoionization there can be coupling between the unpaired electron in the core and the unpaired electrons in the outer shell, rising a series of peaks known as multiplet splitting. Only Cr (III), Mn (II, III, IV, VI), high spin Fe (II), Fe (III), Co (II, III), high spin Ni (II) and Ni (III) present multiplet splitting.<sup>17</sup>

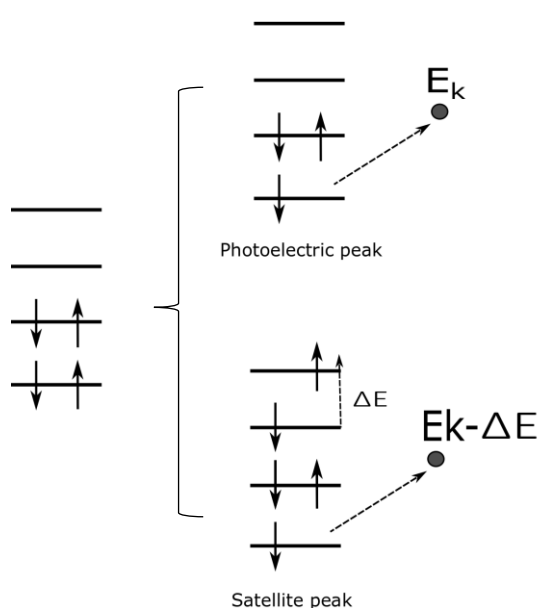


**Figure 2.11:** Schematic representation of photoelectric peak and satellite peak.

XPS is a surface technique, which experimentally means that the UV cannot penetrate more than *c.a* 10 nm into the sample. Another common problem found with XPS is during the analysis because the sample can get charged during the analysis. This can lead to have all the peaks shifted to higher binding energies. To resolve this, the XPS spectra is calibrated before its interpretation to transfer the peaks to their corresponding position or binding energy. This is usually done using the binding energy (284.6 eV) of the carbon (C 1s) which is a common ever-present contamination in all the samples. To give an example, if the XPS spectra shows the binding energy of the C at 285 eV, that will indicate that all the peaks will have also been shifted up by 0.4 eV.<sup>18</sup>

#### **2.4.6.1 Analysis of the mono and bi-metallic 1 wt.% AuPd/TiO<sub>2</sub>, 1 wt.% FePd/TiO<sub>2</sub> and 0.5 wt.% Pd/ X wt.% Fe-HZSM-5 (X: 3.0-0.06) catalysts by XPS.**

The analysis of the catalysts by XPS were carried out by Dr. Morgan, who also provided advice for the subsequent peak fitting. XPS spectra were recorded on Kratos Axis Ultra DLD spectrometer employing a monochromatic Al K $\alpha$  X-ray source (75-150 W) and analyser pass energy of 160 eV (for survey scans) or 40 eV (for detailed scans). Samples were mounted using double-sided adhesive tape, and binding energies were referenced to the C (1s) binding energy of adventitious carbon contamination which was taken to be 284.7 eV. The data was analysed by the CASA XPS where the atomic percentage and the weight percentage were calculated to quantify the metals on the surface. The photoemission peaks of the Pd and Au were fitted with the spin orbital peaks and satellites to determine their oxidation state. However, in the case of the Au, its photoemission peaks were fitted with the spin orbital peaks only since it does not present satellites peaks. In the case of the Fe, the photoemission peaks were not fitted due to its complexity, therefore the oxidation state of the Fe was estimated qualitatively by assignation of the E<sub>B</sub> to Fe<sup>0</sup>, FeO and Fe<sub>2</sub>O<sub>3</sub>.

#### **2.4.7 Basics about x-ray diffraction (XRD) spectroscopy.**

As shown in Figure 2.5, diffraction is caused when the radiation path is hindered by an "object" and its intensity consequently changes. This change in intensity is what is called diffraction pattern. However, for the diffraction to happen, the dimension of this object needs to be similar to the wavelength of the incident radiation. X-rays have wavelengths similar to the molecular bonds and the distance between atoms forming part of a crystalline structure (c.a 100 pm).<sup>19</sup> A crystal or crystal lattice is formed through the translational arrangement in the three dimensions (x, y, z) of a unit cell, which can be determined as well as its angles ( $\alpha$ ,  $\beta$ ,  $\gamma$ ).<sup>19</sup> The space between the lattice points (atoms) of the unit cell, the planes, is a quantitative characteristic that is investigated by diffraction techniques such as XRD.<sup>19</sup> Thus, in heterogeneous catalysis, XRD is widely used to identify the crystalline structure of a certain material such as TiO<sub>2</sub> as well as to obtain an indication of crystallite size. Further qualitative information can be gathered around immobilised nanoparticle size, in the case of supported metal nanoparticles. An incident x-rays (wavelength c.a 0.5–2 Å) radiation is scattered by electrons of the atoms in the sample. The x-rays can be scattered by a consecutive arrays of plains separated by a distance, d, where the angle of the diffraction ( $\theta$ ) is given by Bragg's equation (Eq. 27) (Figure 2.12).<sup>20</sup> A powder diffractometer uses a x-ray detector, which scans the diffraction angle ( $\theta$ ) of the scattered monochromatic x-rays, that are in phase (giving constructive interference), and its intensity. The rotation of the sample during the measurements enhances the number of particles that can contribute to the diffraction pattern. The number and positions of the diffracted light, which are referred as reflections, depends on the cell parameters, crystal system and lattice type. Therefore,

XRD is a very useful technique to corroborate the structure of a synthesised powder such as HZSM-5 or  $\text{TiO}_2$ .<sup>20,18</sup>

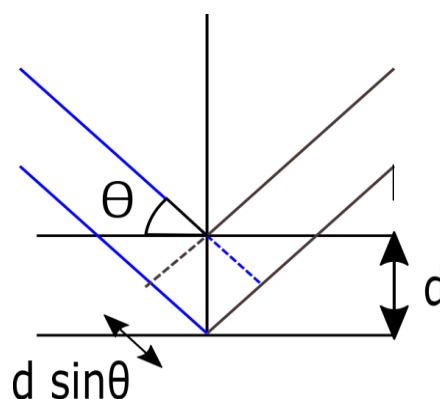


**Figure 2.12:** Schematic representation of a x-ray diffraction between two lattice planes.

**Eq. 27**

$$2d \sin \theta = n\lambda$$

Where,

$d$  = distance between two lattice planes.

$\lambda$  = wavelength of the X-rays.

$\theta$  = is the angle between the incoming x-ray and the normal to the reflecting lattice place.

$n$  = order of the reflection ( $n = 1, 2, 3 \dots$ ). If  $n=1$ , it would mean that the distance between two planes are  $d = \lambda / 2 \sin \theta$ .

The spectra, referred as a diffractogram, records the intensity of the signal versus the  $2\theta$ , which is the angle of reflection. To give an example, Figure 2.13 presents the diffractogram of mono-metallic Pd supported catalysts on  $\text{SiO}_2$  for two catalysts, 2.4 wt.% Pd/ $\text{SiO}_2$  and 1.1 wt.% Pd/ $\text{SiO}_2$ .<sup>18</sup> As the figure show, both catalysts give two reflections which each one is characteristic of a specific plane, (111 at *c.a*  $2\theta = 40^\circ$ ) and (200 at *c.a*  $2\theta = 46^\circ$ ). If the sample do not have sufficient crystallinity, that would affect the shape of the peaks and their intensity. As the figure shows, if both catalysts, 2.4 wt.% Pd/ $\text{SiO}_2$  and 1.1 wt.% Pd/ $\text{SiO}_2$ , had perfect crystals, the peaks at  $2\theta = 40^\circ$  and  $2\theta = 46^\circ$  would be narrower. For crystallite sizes below 100 nm, the peaks start bordering because the scattered x-rays are out of phase (destructive interferences).<sup>18</sup>

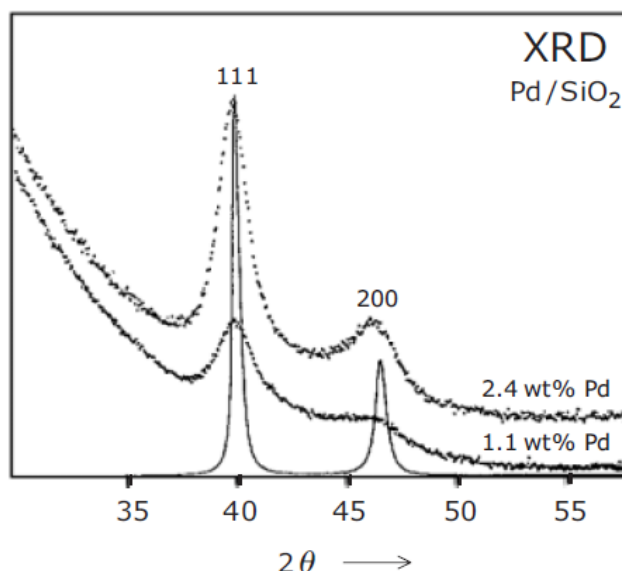


**Figure 2.13:** Diffractogram of mono-metallic Pd supported catalysts on SiO<sub>2</sub>.<sup>18</sup>

The Scherrer formula relates crystal size to line width according to the formula Eq. 28.<sup>18</sup>

**Eq. 28**

$$L = \frac{k\lambda}{\beta \cos\theta}$$

Where,

L= is a measure of the dimension of the particle in the direction perpendicular to the reflecting plane.

λ= is the X-ray wavelength.

β= is the peak width.

θ = is the angle between the beam and the normal to the reflecting plane.

k= is a constant (often taken as 1).

#### **2.4.7.1 Analysis of the mono and bi-metallic 1 wt.% AuPd/TiO<sub>2</sub>, 1 wt.% FePd/TiO<sub>2</sub> and 0.5 wt.% Pd/ X wt.% Fe-HZSM-5 (X: 3.0-0.0) catalysts by XRD.**

The bulk structure of all the catalysts was determined by XRD using a (θ–θ) PANalytical X'pert Pro powder diffractometer using a Cu Kα radiation source, operating at 40 KeV and 40 mA. The standard analysis was carried out for 40 min with a back filled sample, between 2θ values of 10–80 °. The phase identification was determined using the international centre for diffraction data (ICDD). The crystallinity of the mono and bi-metallic 0.5 wt.% Pd/ X wt.% Fe-HZSM-5 (X: 3.0-0.0) catalysts was determined comparing the intensity of the sample peaks with the one given from a commercial HZSM-5 material (Zeolyst, SiO<sub>2</sub> : Al<sub>2</sub>O<sub>3</sub> = 23), using the intensity of the of the peaks found in the region between 2θ = 22–25°.

### **2.5 Basics about microscopy techniques.**

Light microscope were first developed before the electronic ones. They employ visible (400-700 nm) light that passes through a slit, where the light is diffracted and collected by a lens that project the slit image. The smaller the slit becomes, the broader the diffraction is, projecting a blur image (Figure 2.14).<sup>21</sup>

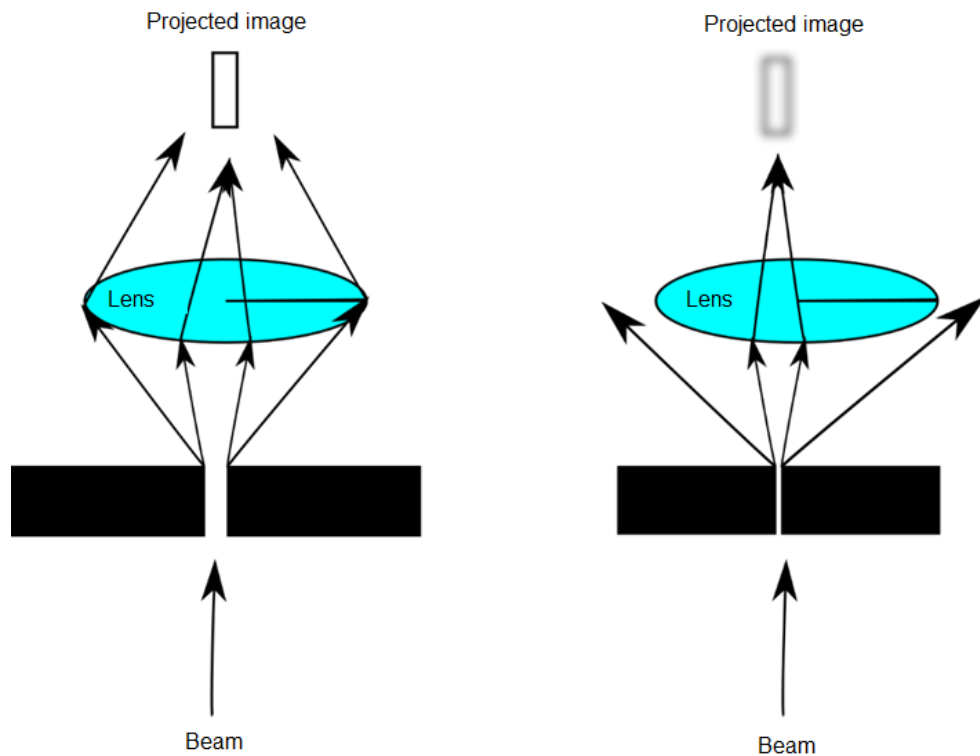


**Figure 2.14:** Representation of an optical or light microscope.

Electron microscopy were born in order to overcome this diffraction limitation and thus increase the resolution of the light microscopes. The resolution of a visible microscope can be calculated using Rayleigh equation (Eq. 29), which by simplification, it means that the resolution is half the length of the incident beam. For instance, for a 400 nm incident light, the resolution would be ca. 200 nm. Unfortunately, this is by far too big for catalysis since the nanoparticles ranges from 100-1 nm.<sup>21</sup>

**Eq. 29**

$$\delta = \frac{0.61 \lambda}{\mu \sin \beta}$$

where;  
 $\lambda$ = wavelength.  
 $\mu$ = refractive index.  
 $\beta$ = semi-angle of collection.

**2.5.1 Transmission electron microscopy (TEM).**

Based on the photoelectric effect, the beam is able to remove electrons from the atoms of the sample that leave with a  $E_k$ . The difference, compared to light microscope, is that the beam consists of ionizing radiation with high energy (100 keV) in order to enhance the resolution c.a. 0.004 nm. The incident beam triggers the scattering of many electrons which each one provides different information. The nature of scattering electrons can be grouped as forward or back scattering. Forward scattering groups; the direct beam, elastic scattering (angle, 1-10°), diffraction, refraction and inelastic scattering (angle, <1°) (Figure 2.15).

Among all, the direct beam, which are the electrons parallel to the incident beam, are the ones that can project the image of the sample in TEM. <sup>21</sup>

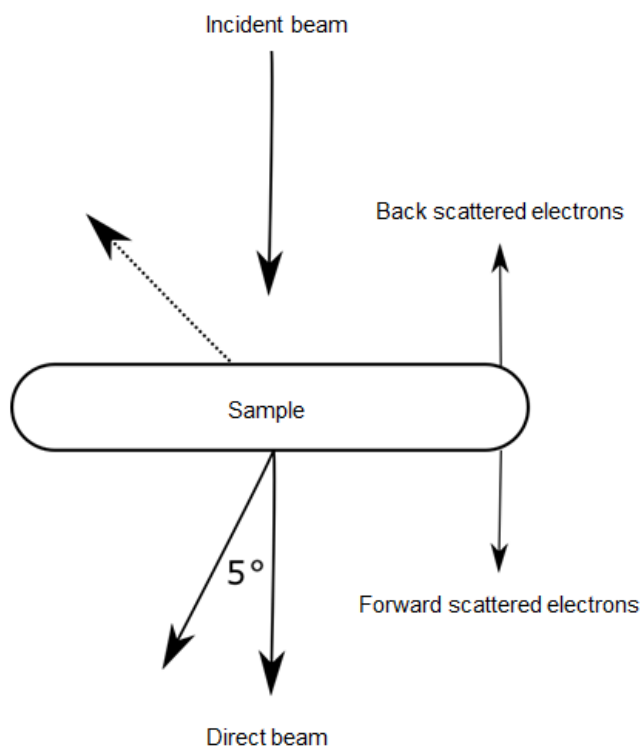


**Figure 2.15:** Schematic representation of the TEM electron scattering.

Typical operating conditions of a TEM instrument are 100–200 keV electrons,  $10^{-6}$  mbar vacuum, 0.5 nm resolution and a magnification of  $3 \times 10^5$  to  $10^6$ .<sup>18</sup> The detection of the supported nanoparticles is possible as long as there is sufficient contrast between the nanoparticles and the support, which is a limitation that may impede the use of TEM in some well dispersed supported oxides. The backscattering of the electrons when they collide with heavy metals (such as Pd) is what permits the differentiation of the metal nanoparticle from the support. The electrons that are diffracted by the metal nanoparticles allows also to obtain crystallographic information. Also, emitted x-rays are characteristic for each element and allow the determination of the chemical composition for a selected nanoparticle. This technique referred to as energy dispersive x-ray analysis is also widely employed in heterogeneous catalysis to determine the composition of metal nanoparticles. TEM can be used along with the EDX, carrying out both analysis consecutively. The determination of the particle size and their elemental distribution is therefore possible although it is assumed that the size of the imaged particle is truly proportional to the size of the actual particle and that the detection probability is the same for all the particles independently of their dimensions.<sup>18</sup>

### 2.5.1.1 Determination of the nanoparticle size and distribution for 1 wt.% AuPd/TiO<sub>2</sub>, 1 wt.% FePd/TiO<sub>2</sub> and 0.5 wt.% Pd/ X wt.% Fe-HZSM-5 (X: 3.0-0.06) catalysts by TEM.

The images and analysis of the catalysts were carried out by Dr. Tom Davies, using a JEM-2100 electron microscope. The sample was prepared by dispersing the catalysts powder onto a holey carbon film supported by a 300-mesh copper TEM grid. Bright field (BF) and high annular dark field (HAADF) images were taken using the 200 kV microscope. Mean particle size and particle size deviation was calculated by measuring approximately 300 nanoparticles, to ensure statistical relevance, using the ImageJ software.

## 2.6 Physisorption.

### 2.6.1 Brunauer-Emmett-Teller isotherm.

Brunauer-Emmett-Teller were the ones who described mathematically the phenomenon of physisorption, where the first monolayer of adsorbate can also adsorbate resulting on multiple layers of adsorbate. The mathematical formula is commonly known as BET, where multilayers of N<sub>2</sub> gas can be adsorbed on the surface of a catalyst at high pressures and at constant temperature. From a linear representation of the Eq. 30, the volume of one monolayer, V<sub>m</sub>, can be calculated. Subsequently, the surface area, S<sub>Area</sub> and the specific surface area, S<sub>BET</sub> can be obtained applying Eq. 31 and Eq. 32 respectively.<sup>19</sup>

#### Eq. 30

$$\frac{P}{V(P^*-P)} = \frac{1}{V_m c} + \frac{c-1}{V_m c} \times \frac{P}{P^*}$$

Where;

P\* = the vapour pressure of the adsorbent gas at the temperature of the experiment.

V<sub>m</sub> = the volume of one monolayer.

c = constant.

#### Eq. 31

$$S_{Area} = \frac{N_a S V_m}{V}$$

Where;

N<sub>a</sub> = Avogadro's number.

V<sub>m</sub> = the volume of one monolayer.

S = cross section area.

#### Eq. 32

$$S_{BET} = \frac{S_{tot}}{m}$$

Where;

m = mass of the catalyst.

### 2.6.1.1 Physical characterisation of mono and bi-metallic 0.5 wt.% Pd/ X wt.% Fe-HZSM-5 (X: 3.0-0.06) catalysts by physisorption analysis.

Physisorption was used to determine the specific surface area and pore volume of the mono and bi-metallic 0.5 wt.% Pd/ X wt.% Fe-HZSM-5 (X: 3.0-0.06) catalysts. The N<sub>2</sub> isotherms

were collected on a Micrometrics 3-Flex, where *c.a.* 0.07 g of sample were degassed at 350 °C for 9 h prior to start the analysis. The analysis was carried out at 77 K by measuring the quantity of N<sub>2</sub> adsorbed versus the relative pressure ( $P/P_0$ ), which allowed to obtain the specific surface area and the pore volume by applying the BET formula and the non-local density functional theory (NLDFT) by Tarazona model respectively. The relative pressure was recorded from 0 to 0.01, therefore it was not possible to assign the isotherms to one of the IUPAC classifications as shown in Figure 2.16. Each type of classification can tell the type of pores the catalysts has, for instance, a Type I (b) isotherm classification, indicates that the sample contains pore size distributions over a broader range including micropores (< 2 nm) and possibly narrow mesopores (< ~2.5 nm).<sup>22</sup>

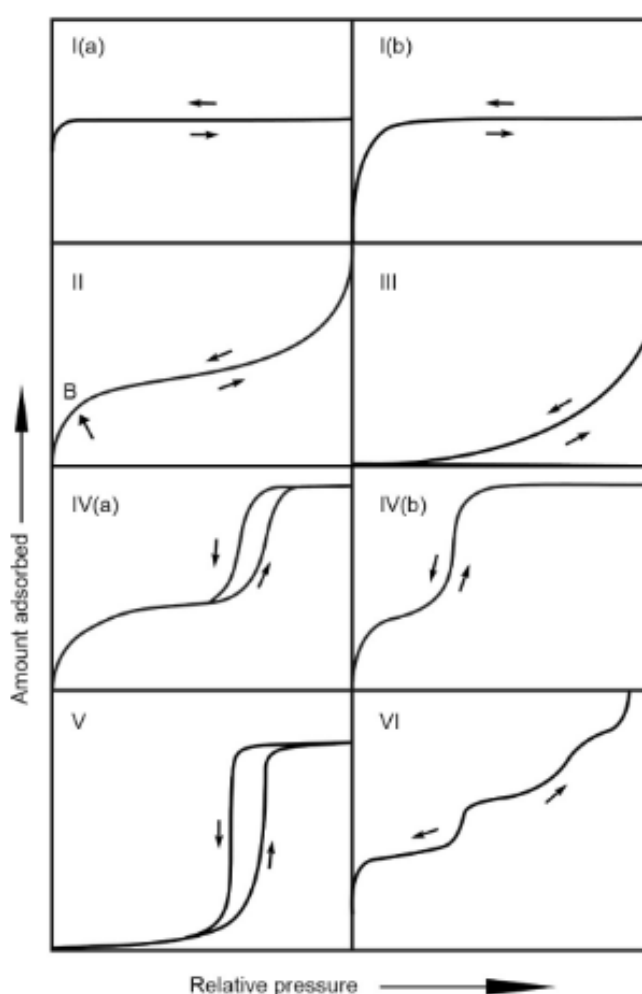


**Figure 2.16:** Classification of physisorption isotherms according from IUPAC.<sup>22</sup>

The BET equation can be applied when forming more than one mono-layer in non-porous, macroporous and mesoporous materials with a pore width > 4 nm.<sup>23</sup> However, BET cannot be strictly applicable in microporous materials (Type I isotherms). If one applies the BET equation using the classical relative pressure range ( $0.05 < P/P_0 < 0.3$ ) to the adsorption data

obtained from a microporous material, one cannot find a linear correlation and the constant, C, may be negative.<sup>23,24</sup> In order to be able to use BET surface areas from Type I isotherm materials, five criteria's need to be met according to Rouquerol *et al.*,<sup>25</sup> *i*) the pressure range selected should have values of  $v(P_o-P)$  increasing with  $P/P_o$  ( where  $v$  is the volume of  $N_2$  adsorbed per gram of material), *ii*) the y intercept of the linear region must be positive to obtain a positive C value, *iii*) the Rouquerol transform  $\eta_{ads} (1p/p^o)$  must increase with  $P/P_o$  for the data selected to calculate the BET parameters, *iv*) the monolayer capacity  $\eta$  should be within the limits of data that were used to fit the BET parameters and *v*) the value of  $1/(\sqrt{C} + 1) \approx p/p^o$  at the monolayer capacity.<sup>25,26,27</sup> Snurr and co-workers<sup>26</sup> obtained the  $N_2$  (77K) and Ar (87K) isotherms from grand canonical monte carlo (GCMC) simulations for a wide range of MOF (IR-MOFs 9, 11, 13) and zeolites (MFI, MOR, BOG, LTA, FAU). They used the simulated isotherm to determine what was the best relative pressure that one should be applying for each material in order to comply with the Rouquerol criteria.<sup>26</sup> They concluded that the relative pressure varies depending on the type of sample and adsorvative.<sup>26</sup> However, for a MFI sample, the relative pressure range should be the same regardless of the type of adsorvative ( $P/P_o$  (0.00005-0.01)).<sup>26</sup> The specific surface area ( $S_{BET}$ ) was calculated from the BET equation selecting the relative pressure range from the isotherm suggested by Snurr and co-workers for each catalyts. The BET linear regression obtained complied with Rouquerol criteria where the slope was termed as  $S_{BET}$ . The micropore volume ( $V_{micropore}$ ) was calculated using non local density functional theory (NLDFT) by Tarazona model.

## 2.7 References.

1. Meenakshisundaram, S., He, Q., Moataz, M., Pritchard, J., Freakley, S.J., Edwards, J.K., Taylor, S.H., Morgan, D.J., Carley, A.F., Knight, D.W., Kiely, C.J., Hutchings, G.J. Synthesis of stable ligand-free gold-palladium nanoparticles using a simple excess anion method. *ACS Nano*. **6**, 6600–6613 (2012).
2. Application eHandbook: Microwave Plasma Atomic Emission Spectroscopy. (Edited on January 2021 by Agilent Technologies).
3. Balaram, V. Microwave plasma atomic emission spectrometry ( MP-AES ) and its applications–A critical review. *Microchem. J.* **159**, 105483-105500 (2020).
4. Linge, K. L., Jarvis, K. E. Quadrupole ICP-MS : Introduction to Instrumentation , Measurement Techniques and Analytical Capabilities. *Geostandards and geoanalytical research.* **33**, 445–467 (2009).
5. Kealey, D., Hained, J. *Analytical chemistry*. (BIOS Scientific Publishers Ltd, 2002).
6. Volterrani, M., Minelli, A., Gaetani, M., Grossi, N., Magni, S., Caturegli, L. Reflectance, absorbance and transmittance spectra of bermudagrass and manilagrass turfgrass canopies. *PLOS ONE*. **12**, 1-13 (2017).

7. Chen, Y., Zou, C., Mastalerz, M., Hu, S., Gasaway, C., Tao, X. Applications of Micro-Fourier Transform Infrared Spectroscopy ( FTIR ) in the Geological Sciences—A Review. *Int. J. Mol. Sci.* **16**, 30223–30250 (2015).
8. Campanella, B., Palleschi, V., Legnaioli, S. Introduction to vibrational spectroscopies. *ChemTexts.* **7**, 1–21 (2021).
9. Brown, J. M. *Molecular spectroscopy.* (Oxford University Press Inc., New York, 1998).
10. Brisdon, A. K. *Inorganic spectroscopic methods.* (Oxford University Press Inc., New York, 2004).
11. Guerrero-Pérez, M.O., Patience, G.S. Experimental methods in chemical engineering: Fourier transform infrared spectroscopy—FTIR. *Can J Chem Eng.* **96**, 2512–2517 (2018).
12. Fengtao Fan, Z. F. and C. L. UV Raman spectroscopic study on the synthesis mechanism and assembly of molecular sieves. *Chem. Soc. Rev.* **39**, 4794–4801 (2010).
13. Fuller, M. P, Griffiths, P. R. Diffuse Reflectance Measurements by Infrared Fourier Transform Spectrometry. *Analytical chemistry.* **50**, 1906–1910 (1978).
14. Zeinalipour-Yazdi, C.D., Willock, D.J., Thomas, L., Wilson, K., Lee, A.F.CO adsorption over Pd nanoparticles: A general framework for IR simulations on nanoparticles. *Surface Science.* **646**, 210-220 (2016).
15. XPS Interpretation of Palladium. Available at: <https://xpssimplified.com/elements/palladium.php>. (Accessed: 6th April 2020).
16. McIntyre, N. S., Zetaruk, D. G. X-ray Photoelectron Spectroscopic Studies of Iron Oxides. *Anal. Chem.* **49**, 1521–1529 (1977).
17. Biesinger, M. C., Payne, B.P., Grosvenord, A.P., Lau, L.W.M., Gersonb, A.R., Smart, R.St.C. Resolving surface chemical states in XPS analysis of first row transition metals, oxides and hydroxides: Cr, Mn, Fe, Co and Ni. *Appl. Surf. Sci.* **257**, 2717–2730 (2011).
18. Chorkendorff, I., Niemantsverdriet, J.W. Concepts of modern catalysis and kinetics. (Wiley-VCH, 2003).
19. Atkins, Peter., de Paula, J. *Atkin's physical chemistry.* (Oxford University Press Inc., USA, 2008).
20. Atkins, P., Overton, T., Rourke, J., Weller, M., Armstrong, F. *Inorganic Chemistry.* (Shriver & Atkins, Oxford University Press, 2006).
21. William, David B., Carter, B. C. *Transmission electron microscopy.* (Springer Science Business Media, LLC, 2009).
22. Thommes, M., Kaneko, K., Neimark, A.V., Oliver, J.P., Rodriguez-Reinoso, F., Rouquerol, J., Sing, K.S.W. Physisorption of gases, with special reference to the

- evaluation of surface area and pore size distribution (IUPAC Technical Report). *Pure Appl. Chem.* **87**, 1051–1069 (2015).
23. Cychoz, K. A., Thommes, M. Progress in the Physisorption Characterization of Nanoporous Gas Storage Materials. *Engineering* **4**, 559–566 (2018).
  24. Zhang, Z., Yang, Z. Theoretical and practical discussion of measurement accuracy for physisorption with micro- and mesoporous materials. *Cuihua Xuebao/Chinese J. Catal.* **34**, 1797–1810 (2013).
  25. Rouquerol, J., Llewellyn, P., Rouquerol, F. Is the BET equation applicable to microporous adsorbents? *Stud. Surf. Sci. Catal.* **160**, 49–56 (2007).
  26. Bae, Y. S., Yazayd'n, A. Ö., Snurr, R. Q. Evaluation of the BET method for determining surface areas of MOFs and zeolites that contain Ultra-Micropores. *Langmuir.* **26**, 5475–5483 (2010).
  27. Micrometrics Instrument Corporation. Rules, A. Fitting and Optimizing BET surface Area. 1–7 (2014).
  28. Storck, S., Bretinger, H., Maier, W. F. Characterization of micro- and mesoporous solids by physisorption methods and pore-size analysis. *Appl. Catal. A Gen.* **174**, 137–146 (1998).
  29. Galarneau, A., Villemot, F., Rodriguez, J., Fajula, F., Coasne, B. Validity of the t-plot Method to Assess Microporosity in Hierarchical MicroMesoporous Materials. *Langmuir.* **30**, 13266–13274 (2014).

# Chapter 3:

## Direct synthesis of H<sub>2</sub>O<sub>2</sub> with AuPd on TiO<sub>2</sub> catalysts at ambient temperature.

### 3.1 Introduction.

The direct synthesis of H<sub>2</sub>O<sub>2</sub> from H<sub>2</sub> and O<sub>2</sub> has been widely reported and studied as one of the decentralised alternatives to the anthraquinone autoxidation process, which currently accounts for the 95 % of H<sub>2</sub>O<sub>2</sub> production. Many authors have investigated the direct synthesis using metal supported catalysts made of mono-metallic Pd or bi and tri-metallic combinations (e.g AuPd, NiPd, PtAuPd).<sup>1,2</sup> Pd is often combined with other metals to enhance its selectivity towards the production of H<sub>2</sub>O<sub>2</sub>, since Pd can also show activity to degenerate it to H<sub>2</sub>O. The activity of the mono-metallic Pd catalysts as well as any of the mentioned bi and tri-metallic combinations, are commonly studied using sub-ambient temperatures (< 10 °C) and with organic solvents such as methanol (CH<sub>3</sub>OH) or ethanol (CH<sub>3</sub>CH<sub>2</sub>OH) as well as any of these two in combination with H<sub>2</sub>O.<sup>3,4,5</sup> These conditions are often chosen as a strategy to enhance the selectivity of the catalysts to generate H<sub>2</sub>O<sub>2</sub> and avoid its subsequent degradation. Therefore, as a general statement it can be said that the standard conditions commonly used to report the activity of catalysts for the direct synthesis of H<sub>2</sub>O<sub>2</sub> involve either or both sub-ambient temperatures and organic solvents alone or in combination with H<sub>2</sub>O. Recent studies have demonstrated that supported AuPd catalysts offer excellent bactericidal activity, achieved through the release of reactive oxygen species (ROS) (O<sub>2</sub><sup>•-</sup>, HO<sup>•</sup>, RO<sub>2</sub><sup>•</sup> and HOO<sup>•</sup>) generated from *in-situ* H<sub>2</sub>O<sub>2</sub>.<sup>6</sup> However, for water remediation, the conditions typically utilised to study the direct synthesis of H<sub>2</sub>O<sub>2</sub> are clearly not appropriate. First, the organic solvents must be removed since their usage pollute the water and secondly sub-ambient temperatures are highly costly energetically. Therefore, the aim of this chapter is to investigate the effect of reaction conditions on the direct formation of H<sub>2</sub>O<sub>2</sub> over a series of mono and bi-metallic AuPd supported catalysts, transitioning the reaction conditions from sub-ambient temperatures (2 °C) and a mixture of CH<sub>3</sub>OH and H<sub>2</sub>O (67 % CH<sub>3</sub>OH in water) to ambient temperatures (25 °C) and H<sub>2</sub>O-only as a solvent. Furthermore, the role of the gaseous diluent will be also studied, which is often used to acidify the reaction medium and promote H<sub>2</sub>O<sub>2</sub> selectivity. Figure 3.1 visually represents the four reaction conditions that the AuPd catalysts activity will be reported in. Each reaction condition is labelled according to the temperature (2 °C or 25 °C), the solvent (67 % CH<sub>3</sub>OH in H<sub>2</sub>O or H<sub>2</sub>O-only solvent) and the gas diluent (CO<sub>2</sub> or N<sub>2</sub>) used. The

degradation activity will be also determined for each reaction condition as shown in Figure 3.1.

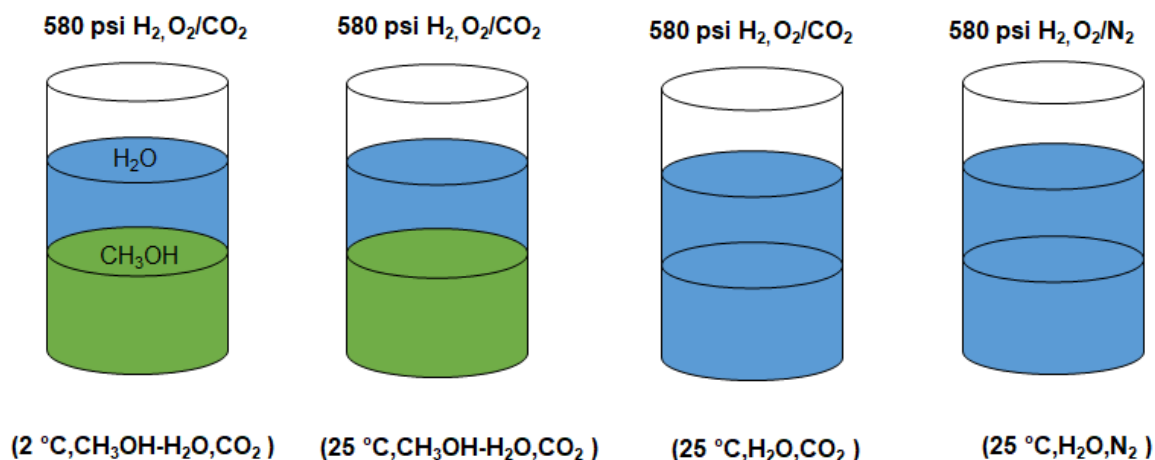


**Figure 3.1: Reaction conditions:** **(2°C,CH<sub>3</sub>OH-H<sub>2</sub>O,CO<sub>2</sub>)**: 8.5 g (5.6 g CH<sub>3</sub>OH, 2.9 g H<sub>2</sub>O), catalyst (0.01 g), 420 psi of 5 % H<sub>2</sub>/CO<sub>2</sub>, 160 psi of 25 % O<sub>2</sub>/CO<sub>2</sub>, 1200 rpm, 2 °C, 0.5 h. **(25°C,CH<sub>3</sub>OH-H<sub>2</sub>O,CO<sub>2</sub>)**: 8.5 g (5.6 g CH<sub>3</sub>OH, 2.9 g H<sub>2</sub>O), catalyst (0.01 g), 420 psi of 5 % H<sub>2</sub>/CO<sub>2</sub>, 160 psi of 25 % O<sub>2</sub>/CO<sub>2</sub>, 25 °C, 1200 rpm, 0.5 h. **(25°C,H<sub>2</sub>O,CO<sub>2</sub>)**: 8.5 g H<sub>2</sub>O, catalyst (0.01 g), 420 psi of 5 % H<sub>2</sub>/CO<sub>2</sub>, 160 psi of 25 % O<sub>2</sub>/CO<sub>2</sub>, 1200 rpm, 25 °C, 0.5 h. **(25°C,H<sub>2</sub>O,N<sub>2</sub>)**: 8.5 g H<sub>2</sub>O, catalyst (0.01 g), 420 psi of 5 % H<sub>2</sub> /N<sub>2</sub>, 160 psi of 25 % O<sub>2</sub>/N<sub>2</sub>,1200rpm, 25 °C, 0.5 h.

The supported AuPd catalysts (1.0 wt.% Au/TiO<sub>2</sub>, 0.75 wt.% Au-0.25 wt.% Pd/TiO<sub>2</sub>, 0.50 wt.% Au-0.50 wt.% Pd/TiO<sub>2</sub>, 0.25 wt.% Au-0.75 wt.% Pd/TiO<sub>2</sub> and 1.0 wt.% Pd/TiO<sub>2</sub>), synthesised by modified impregnation will be tested in an autoclave (Parr Instruments). The activity of the catalysts towards the direct synthesis of H<sub>2</sub>O<sub>2</sub> and its subsequent degradation will be presented with productivity units (mol<sub>H<sub>2</sub>O<sub>2</sub></sub> kg<sub>cat</sub><sup>-1</sup> h<sup>-1</sup>). The post reaction solution will be sampled to analyse the metal leaching after the direct synthesis of H<sub>2</sub>O<sub>2</sub> by means of microwave plasma-atomic emission spectroscopy (MP-AES). X-ray photoelectron spectroscopy (XPS) will be one of the main characterisation techniques to determine the oxidation state of the Pd for each catalysts, since Pd oxidation state can massively drive the catalyst's selectivity and activity.<sup>7</sup> X-ray diffraction (XRD) will be used to determine the reflections of the support after the impregnation of the metals and transmission electron microscopy (TEM) will be used to establish the mean nanoparticle size and distribution, since this is another relevant characteristic that can affect the activity and selectivity of the AuPd nanoparticles during the direct synthesis of H<sub>2</sub>O<sub>2</sub>.<sup>8</sup>

The activity of each catalyst throughout this Chapter 3 is given by the mean value calculated from the results obtained from three different lots of the same catalysts. The mean activity value is accompanied by the standard deviation represented by error bars in each Figure and Table of catalytic results. Chapter 2, section 2.3.3 gives a more detailed explanation of how the reproducibility was determined throughout this thesis.

### 3.2 Results and discussion.

Table 3.1 presents the catalysts whose activity will be investigated in this chapter towards the direct synthesis and degradation of H<sub>2</sub>O<sub>2</sub> at the four different reaction conditions shown in Figure 3.1. The digestion of these catalysts by aqua regia and subsequent analysis by MP-AES confirmed that the metal loading of Pd and Au were as close as the theoretical loading.

**Table 3.1:** Determination of the metal loading for the mono and bi-metallic 1.0 wt.% AuPd/TiO<sub>2</sub> catalysts by digestion with aqua regia and subsequent analysis by MP-AES.

Catalyst formulation	Actual Au loading	Actual Pd loading
	wt.% (S.D)	wt.% (S.D)
1 wt.% Au /TiO <sub>2</sub>	1.0 ± (0.01)	n.a
0.75 wt.% Au-0.25 wt.% Pd /TiO <sub>2</sub>	0.76 ± (0.08)	0.24 ± (0.02)
0.50 wt.% Au-0.50 wt.% Pd /TiO <sub>2</sub>	0.53 ± (0.06)	0.47 ± (0.06)
0.25 wt.% Au-0.75 wt.% Pd /TiO <sub>2</sub>	0.27 ± (0.04)	0.74 ± (0.04)
1 wt.% Pd /TiO <sub>2</sub>	n.a	0.93 ± (0.0)

(S.D): standard deviation. n.a: not applicable.

#### 3.2.1 Activity of the mono and bi-metallic 1.0 wt.% AuPd/TiO<sub>2</sub> catalysts at (2°C, CH<sub>3</sub>OH-H<sub>2</sub>O, CO<sub>2</sub>) conditions towards the direct synthesis and degradation of H<sub>2</sub>O<sub>2</sub>.

The activity of the mono and bi-metallic 1 wt.% AuPd/TiO<sub>2</sub> catalysts towards the direct synthesis of H<sub>2</sub>O<sub>2</sub> at (2°C, CH<sub>3</sub>OH-H<sub>2</sub>O, CO<sub>2</sub>) conditions is plotted in Figure 3.2, where the y axis show the activity in productivity units (mol<sub>H<sub>2</sub>O<sub>2</sub></sub> kg<sub>cat</sub><sup>-1</sup> h<sup>-1</sup>) and each catalysts is represented in the x axis according to their Pd loading (wt.%) (see Table 3.1).

Surprisingly, the catalytic activity was similar for all materials studied (83-97 mol<sub>H<sub>2</sub>O<sub>2</sub></sub> kg<sub>cat</sub><sup>-1</sup> h<sup>-1</sup>) except for the mono-metallic 1 wt.% Au/TiO<sub>2</sub> catalyst (4 mol<sub>H<sub>2</sub>O<sub>2</sub></sub> kg<sub>cat</sub><sup>-1</sup> h<sup>-1</sup>). This trend aligns well with previous studies that showed that, despite Au not presenting an appreciable activity, it can enhance the activity and selectivity towards the direct synthesis of H<sub>2</sub>O<sub>2</sub> when alloyed with Pd.<sup>9,2,5,10</sup> This became quite significant when comparing how similar the productivities were for 1 wt.% Pd/TiO<sub>2</sub> (83 mol<sub>H<sub>2</sub>O<sub>2</sub></sub> kg<sub>cat</sub><sup>-1</sup> h<sup>-1</sup>) and 0.75 wt.% Au-0.25 wt.% Pd/TiO<sub>2</sub> (91 mol<sub>H<sub>2</sub>O<sub>2</sub></sub> kg<sub>cat</sub><sup>-1</sup> h<sup>-1</sup>) catalysts, even though the latter presented 75 wt. % less Pd.

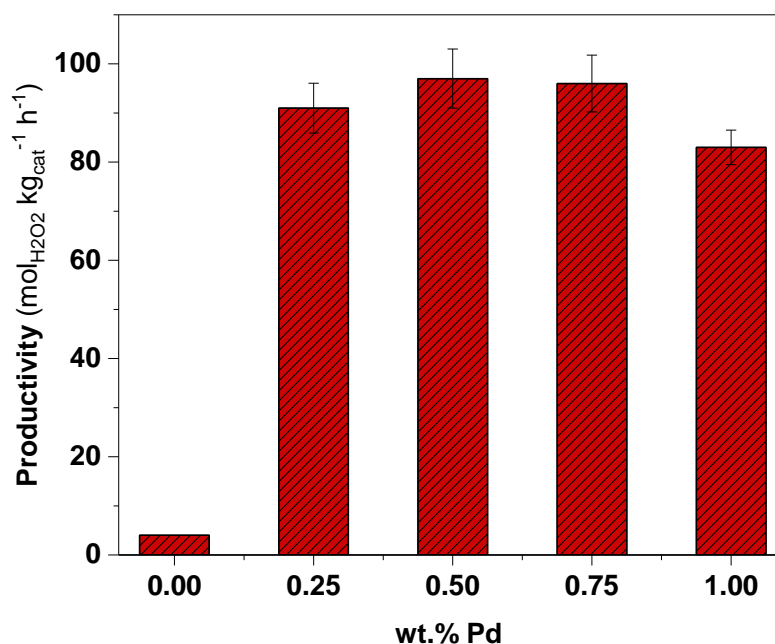


**Figure 3.2:** Activity towards the direct synthesis of H<sub>2</sub>O<sub>2</sub> for mono and bi-metallic 1.0 wt.% AuPd/TiO<sub>2</sub> catalysts. **Reaction conditions:** (2°C, CH<sub>3</sub>OH-H<sub>2</sub>O, CO<sub>2</sub>): 8.5 g (5.6 g CH<sub>3</sub>OH, 2.9 g H<sub>2</sub>O), catalyst (0.01 g), 420 psi of 5 % H<sub>2</sub>/CO<sub>2</sub>, 160 psi of 25 % O<sub>2</sub>/CO<sub>2</sub>, 1200 rpm, 2 °C, 0.5 h.

Diverse studies have shown that Au is able to promote the formation of H<sub>2</sub>O<sub>2</sub> when it is alloyed with Pd by inhibiting the Pd's activity towards the degradation of H<sub>2</sub>O<sub>2</sub>.<sup>1,11,12,7,13,14,15,16</sup> The results shown in Figure 3.3 for the degradation of H<sub>2</sub>O<sub>2</sub> are in line with what has been reported in the literature, since the degradation activity clearly correlates with Au loading. For instance, the bi-metallic 0.75 wt.% Au-0.25 wt.% Pd/TiO<sub>2</sub> catalyst presented a lower degradation activity (113 mol<sub>H<sub>2</sub>O<sub>2</sub></sub> kg<sub>cat</sub><sup>-1</sup> h<sup>-1</sup>) than the bi-metallic 0.25 wt.% Au-0.75 wt.% Pd/TiO<sub>2</sub> catalyst (332 mol<sub>H<sub>2</sub>O<sub>2</sub></sub> kg<sub>cat</sub><sup>-1</sup> h<sup>-1</sup>). However, both catalysts showed similar productivities for the formation of H<sub>2</sub>O<sub>2</sub> as depicted in Figure 3.2. This data suggests that Au improves catalytic selectivity towards H<sub>2</sub>O<sub>2</sub>, improving overall performance.

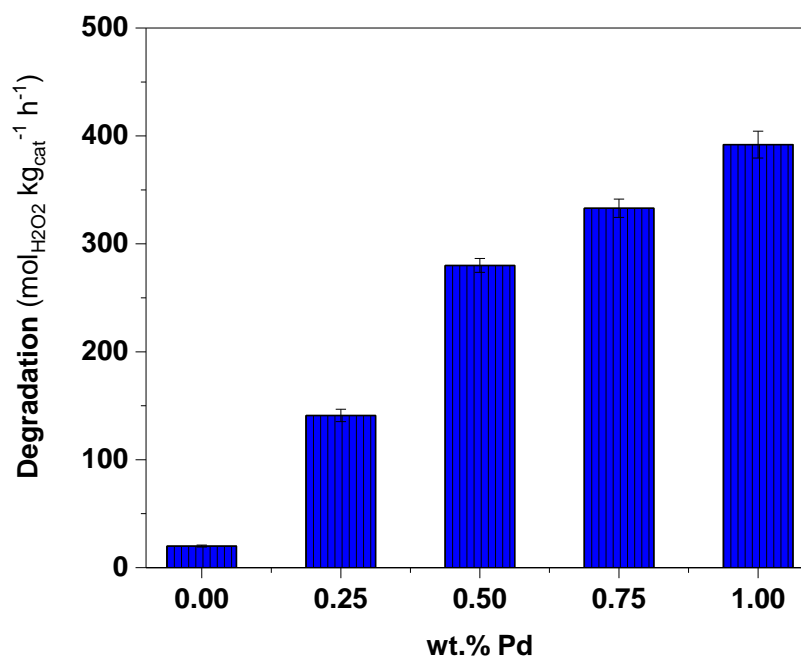


**Figure 3.3:** Activity towards the degradation of H<sub>2</sub>O<sub>2</sub> for mono and bi-metallic 1.0 wt.% AuPd/TiO<sub>2</sub> catalysts **Reaction conditions: (2 °C, CH<sub>3</sub>OH-H<sub>2</sub>O, CO<sub>2</sub>):** 8.5 g (5.6 g CH<sub>3</sub>OH, 0.68 g H<sub>2</sub>O<sub>2</sub>, 2.22 g H<sub>2</sub>O), catalyst (0.01 g), 420 psi of 5 % H<sub>2</sub>/CO<sub>2</sub>, 1200 rpm, 2 °C, 0.5 h.

### 3.2.2 Activity of mono and bi-metallic 1.0 wt.% AuPd/TiO<sub>2</sub> catalysts at (25 °C, CH<sub>3</sub>OH-H<sub>2</sub>O, CO<sub>2</sub>) conditions towards the direct synthesis and degradation of H<sub>2</sub>O<sub>2</sub>.

The activity of the mono and bi-metallic 1.0 wt.% AuPd/TiO<sub>2</sub> catalysts have been studied at 25 °C but keeping the same proportion of CH<sub>3</sub>OH and H<sub>2</sub>O (67 % CH<sub>3</sub>OH, 33 % H<sub>2</sub>O) as in (2 °C, CH<sub>3</sub>OH-H<sub>2</sub>O, CO<sub>2</sub>) conditions. As the data shows, the productivity towards the direct synthesis of H<sub>2</sub>O<sub>2</sub> has decreased accompanied with a higher degradation activity (Figure 3.4-3.5 respectively) in comparison with (2 °C, CH<sub>3</sub>OH-H<sub>2</sub>O, CO<sub>2</sub>) conditions.

High temperatures promote the decomposition of H<sub>2</sub>O<sub>2</sub> to H<sub>2</sub>O, thus affecting the stability of H<sub>2</sub>O<sub>2</sub>.<sup>17</sup> As such, it is understandable that when using temperatures of 25 °C, H<sub>2</sub>O<sub>2</sub> degradation rates were significantly higher than those that utilised sub-ambient temperatures (2 °C). Besides, the solubility of H<sub>2</sub> increases along with the temperature in CH<sub>3</sub>OH solvent, which also promoted the hydrogenation of H<sub>2</sub>O<sub>2</sub> to H<sub>2</sub>O. Thus, transitioning from 2 °C to 25 °C, made increase the degradation activity which led to lower productivities.<sup>18</sup> In addition to this, O<sub>2</sub> becomes less soluble in the reaction mixture with increasing the temperature, which also affected the formation of H<sub>2</sub>O<sub>2</sub>.<sup>18</sup> The same trend and conclusions were drawn by Salmi and co-workers<sup>19</sup> when studied the on-line formation of H<sub>2</sub>O<sub>2</sub> with Pd/C catalyst at -5 °C, 0 °C, 10 °C and 40 °C with CH<sub>3</sub>OH as a solvent. They reported that the maximum concentration of H<sub>2</sub>O<sub>2</sub> (w/w) was achieved in the first 5 minutes (min) at 40 °C, in 40 min at 10 °C and in 70 min for -5 °C. They concluded that the solubility of H<sub>2</sub> in CH<sub>3</sub>OH increased with the temperature, which promoted the formation of H<sub>2</sub>O<sub>2</sub> at shorter reaction times.<sup>19</sup>

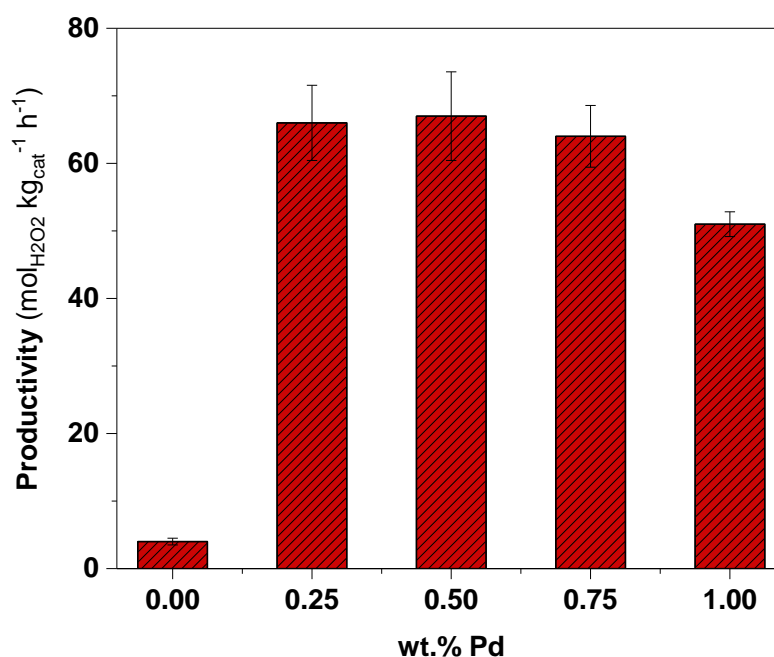


**Figure 3.4:** Activity towards the direct synthesis of H<sub>2</sub>O<sub>2</sub> for mono and bi-metallic 1.0 wt.% AuPd/TiO<sub>2</sub> catalysts. **Reaction conditions: (25°C, CH<sub>3</sub>OH-H<sub>2</sub>O, CO<sub>2</sub>):** 8.5 g (5.6 g CH<sub>3</sub>OH, 2.9 g H<sub>2</sub>O), catalyst (0.01 g), 420 psi of 5 % H<sub>2</sub>/CO<sub>2</sub>, 160 psi of 25 % O<sub>2</sub>/CO<sub>2</sub>, 25 °C, 1200 rpm, 0.5 h.

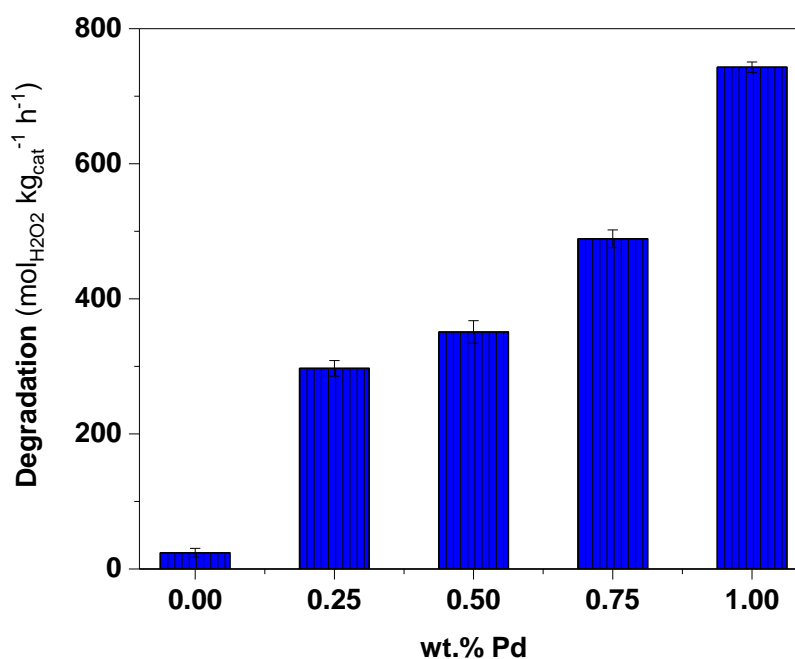


**Figure 3.5:** Activity towards the degradation of H<sub>2</sub>O<sub>2</sub> for mono and bi-metallic 1.0 wt.% AuPd/TiO<sub>2</sub> catalysts **Reaction conditions: (25°C, CH<sub>3</sub>OH-H<sub>2</sub>O, CO<sub>2</sub>):** 8.5 g (5.6 g CH<sub>3</sub>OH, 0.68 g H<sub>2</sub>O<sub>2</sub>, 2.22 g H<sub>2</sub>O), catalyst (0.01 g), 420 psi of 5 % H<sub>2</sub>/CO<sub>2</sub>, 25 °C, 1200 rpm, 0.5 h.

### 3.2.3 Activity of the mono and bi-metallic 1.0 wt.% AuPd/TiO<sub>2</sub> catalysts towards the direct synthesis and degradation of H<sub>2</sub>O<sub>2</sub> at (25 °C, H<sub>2</sub>O, CO<sub>2</sub>) and (25 °C, H<sub>2</sub>O, N<sub>2</sub>).

The effect of the organic solvents towards the direct synthesis and degradation of H<sub>2</sub>O<sub>2</sub> are reported in Figure 3.6 and Figure 3.7 respectively. Removing organic solvents from the

reaction mixture has had a significant effect on the direct synthesis and the degradation activities.

One of the main reasons why the formation of  $\text{H}_2\text{O}_2$  has decreased when removing  $\text{CH}_3\text{OH}$  from the reaction mixture is because  $\text{H}_2$  is less soluble in  $\text{H}_2\text{O}$  (1.62 mg/L at 25 °C) than in  $\text{CH}_3\text{OH}$  (7.91 mg/L at 25 °C).<sup>20</sup> Contrarily,  $\text{O}_2$ , besides being in excess during the direct synthesis reaction, is more soluble in both  $\text{H}_2\text{O}$  (40 mg/L at 25 °C) and  $\text{CH}_3\text{OH}$  (324 mg/L at 25 °C)<sup>20</sup> than  $\text{H}_2$  is. Therefore, the  $\text{H}_2$  availability during the direct synthesis of  $\text{H}_2\text{O}_2$  is lower than in the other two previous reaction conditions, which have made decrease the productivity of  $\text{H}_2\text{O}_2$ .<sup>18</sup>

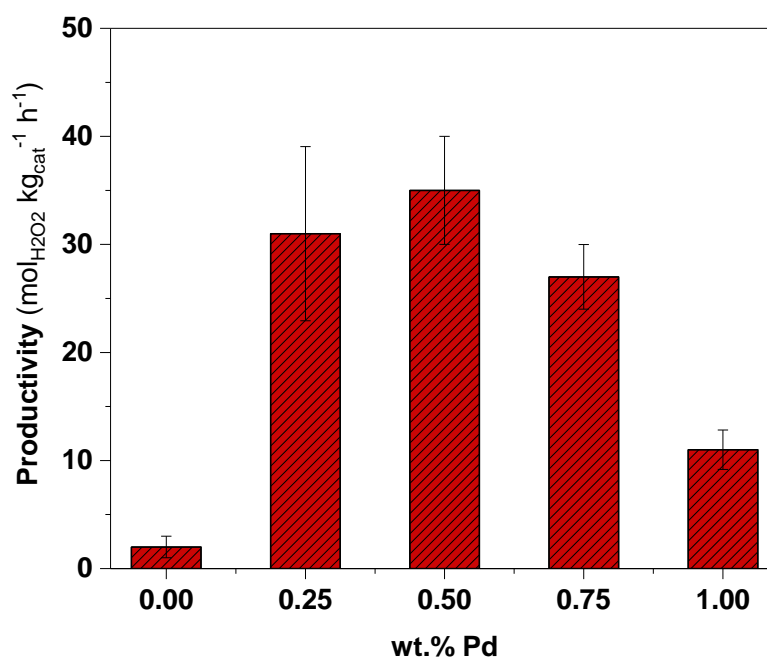


**Figure 3.6:** Activity towards the direct synthesis of  $\text{H}_2\text{O}_2$  for mono and bi-metallic 1.0 wt.% AuPd/TiO<sub>2</sub> catalysts. **Reaction conditions: (25°C, H<sub>2</sub>O, CO<sub>2</sub>):** 8.5 g H<sub>2</sub>O, catalyst (0.01 g), 420 psi of 5 % H<sub>2</sub>/CO<sub>2</sub>, 160 psi of 25 % O<sub>2</sub>/CO<sub>2</sub>, 1200 rpm, 25 °C, 0.5 h.

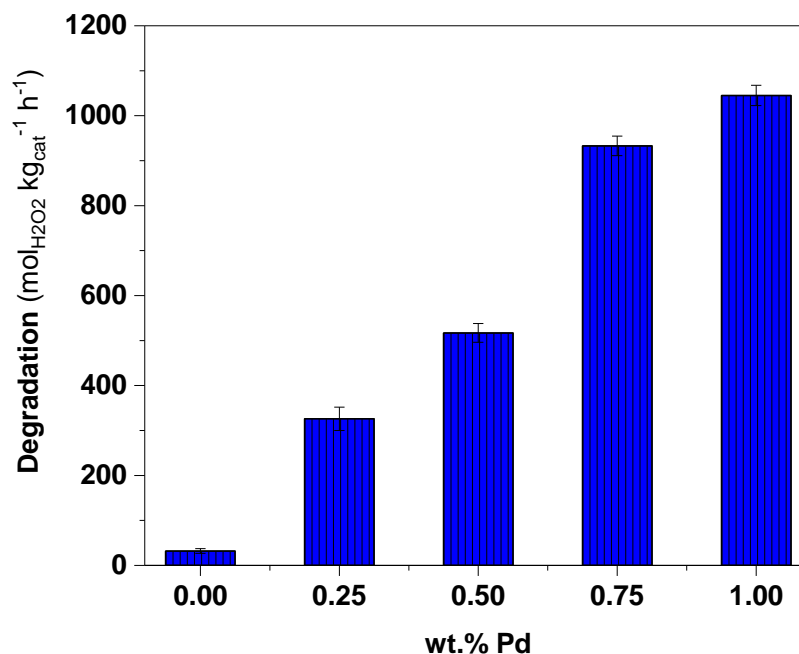
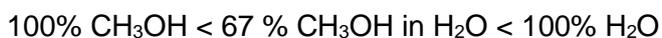


**Figure 3.7:** Activity towards the degradation of H<sub>2</sub>O<sub>2</sub> for mono and bi-metallic 1.0 wt.% AuPd/TiO<sub>2</sub> catalysts. **Reaction conditions: (25 °C, H<sub>2</sub>O, CO<sub>2</sub>):** 8.5 g (0.68 g H<sub>2</sub>O<sub>2</sub>, 7.92 g H<sub>2</sub>O), catalyst (0.01 g), 420 psi of 5 % H<sub>2</sub>/CO<sub>2</sub>, 1200 rpm, 25 °C, 0.5 h.

Hutchings and co-workers<sup>21</sup> sequenced the decomposition activity of a 2.5 wt.% Au-2.5 wt.% Pd/TiO<sub>2</sub> catalyst according to the percentage of CH<sub>3</sub>OH in H<sub>2</sub>O at 25 °C as follows:<sup>21</sup>



They found that the selectivity towards the H<sub>2</sub>O<sub>2</sub> degradation pathways was related to the solvent employed, which had a relation with the solubility of H<sub>2</sub> at the same time. For instance, there will be more hydrogenation of H<sub>2</sub>O<sub>2</sub> in a CH<sub>3</sub>OH-only solvent than in a H<sub>2</sub>O-only solvent, because the solubility of H<sub>2</sub> is higher in the former.<sup>21</sup> Therefore, it is reasonable to consider that, for reactions conditions were H<sub>2</sub>O-only is being used (25 °C, H<sub>2</sub>O, CO<sub>2</sub>), the main competitive side reaction is the decomposition rather hydrogenation. Thus, the relatively high degradation activities seen in this reaction conditions (Figure 3.7), in comparison to the two previous ones, were mainly cause by the H<sub>2</sub>O<sub>2</sub> decomposition side reaction.

Another interesting fact is that the type of organic solvent chosen also has a great influence on the selectivity towards H<sub>2</sub>O<sub>2</sub>. For instance, Ellis and co-workers<sup>22</sup> studied the performance of Pd supported catalyst towards the direct synthesis of H<sub>2</sub>O<sub>2</sub> with a wide range of solvents. They concluded that organic solvents containing alcohols were, as a general trend, the most promising since they gave a good balance between H<sub>2</sub> conversion and H<sub>2</sub>O<sub>2</sub> selectivity.<sup>22</sup> Notably another important requirement for the organic solvent chosen is that it has to be resistant against the oxidation by H<sub>2</sub>O<sub>2</sub> such as CH<sub>3</sub>OH, which is one of the least

reactive alcohols.<sup>18</sup> Ellis and co-workers<sup>22</sup> and Hutchings and co-workers<sup>18</sup> have studied the activity of Pd supported catalyst with a CH<sub>3</sub>CH<sub>2</sub>OH and CH<sub>3</sub>OH co-solvent (in addition to H<sub>2</sub>O) respectively in order to determine the best solvent composition for the formation of H<sub>2</sub>O<sub>2</sub>. They concluded that the highest activity was achieved with a solvent composition of 75% CH<sub>3</sub>CH<sub>2</sub>OH and 80% CH<sub>3</sub>OH in H<sub>2</sub>O respectively.<sup>22,18</sup> Using the appropriate ratio of organic solvents and H<sub>2</sub>O help to control the H<sub>2</sub> solubility in the reaction mixture, which subsequently helps to balance the catalyst's selectivity towards the formation and hydrogenation of H<sub>2</sub>O<sub>2</sub>.

In addition to this, Hutchings and co-workers<sup>18</sup> also evidenced that through the dissolution of CO<sub>2</sub> in H<sub>2</sub>O forming carbonic acid, leads to a reduction of the pH in the reaction solvent, which favours H<sub>2</sub>O<sub>2</sub> stability.<sup>18</sup> However, for the remediation of water streams, the use of CO<sub>2</sub> diluent is clearly unfavourable, particularly from an environmental standpoint. By replacing CO<sub>2</sub> for N<sub>2</sub> as gas diluent, the reaction conditions would become more akin to those conditions likely to be adopted in industrial scale, where air would be used as O<sub>2</sub> source (preferred on a cost basis). The H<sub>2</sub>O<sub>2</sub> formation and degradation activity shown for the mono and bi-metallic 1.0 wt.% AuPd/TiO<sub>2</sub> catalysts using (25°C, H<sub>2</sub>O, N<sub>2</sub>) conditions are depicted in Figure 3.8 and Figure 3.9 respectively.

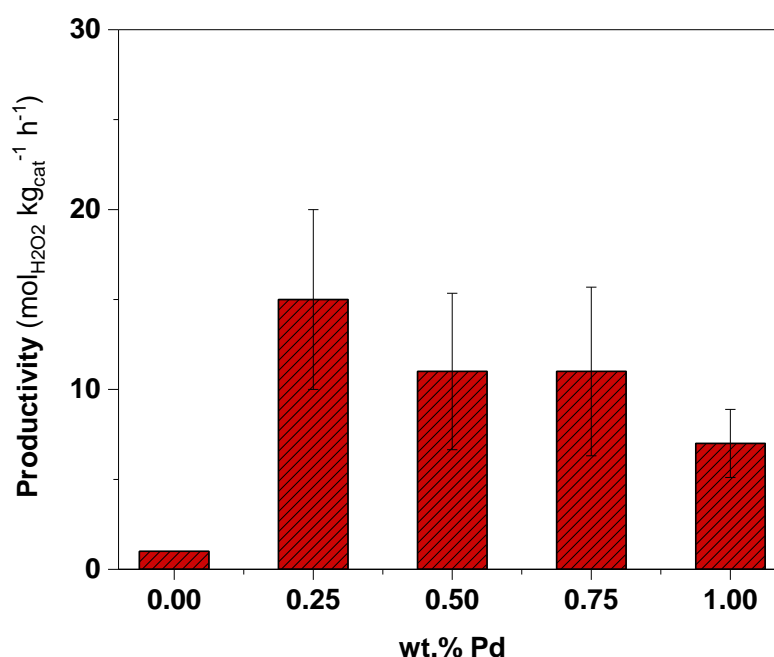


**Figure 3.8:** Activity towards the direct synthesis of H<sub>2</sub>O<sub>2</sub> for mono and bi-metallic 1.0 wt.% AuPd/TiO<sub>2</sub> catalysts. **Reaction conditions: (25°C, H<sub>2</sub>O, N<sub>2</sub>):** 8.5 g H<sub>2</sub>O, catalyst (0.01 g), 420 psi of 5 % H<sub>2</sub>/N<sub>2</sub>, 160 psi of 25 % O<sub>2</sub>/N<sub>2</sub>, 1200 rpm, 25 °C, 0.5 h.

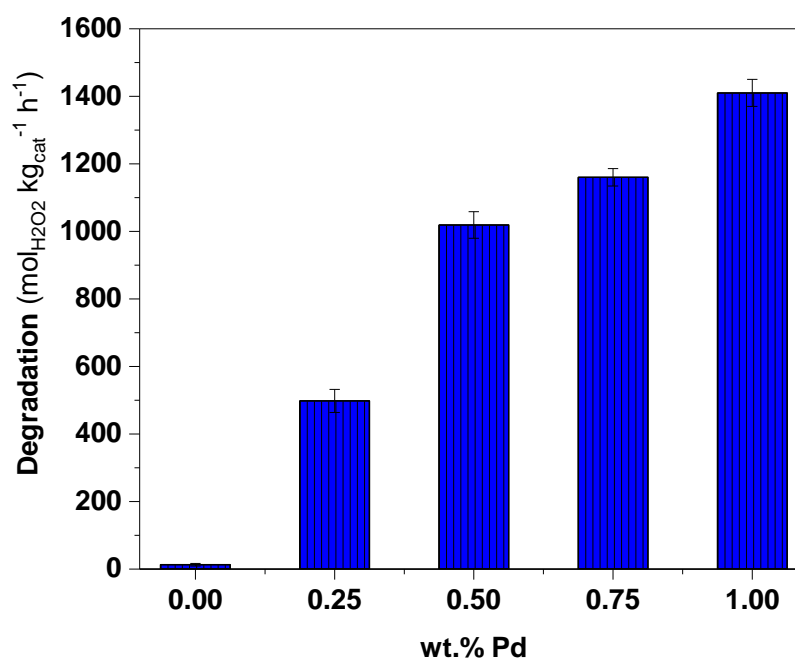


**Figure 3.9:** Activity towards the degradation of H<sub>2</sub>O<sub>2</sub> for mono and bi-metallic 1.0 wt.% AuPd/TiO<sub>2</sub> catalysts. **Reaction conditions: (25°C,H<sub>2</sub>O,N<sub>2</sub>):** 8.5 g (0.68 g H<sub>2</sub>O<sub>2</sub>, 7.92 g H<sub>2</sub>O), catalyst (0.01 g), 420 psi of 5 % H<sub>2</sub>/N<sub>2</sub>, 1200 rpm, 25 °C, 0.5 h.

These conditions showed the lowest productivities in terms of formation of H<sub>2</sub>O<sub>2</sub> because, apart from not having the carbonic acid, which stabilises H<sub>2</sub>O<sub>2</sub>, the reaction was also limited by the low solubility of H<sub>2</sub> in H<sub>2</sub>O, affecting the productivity of H<sub>2</sub>O<sub>2</sub>, besides, the ambient temperatures (25 °C), which also favoured the H<sub>2</sub>O<sub>2</sub> decomposition. Similar observations have been made by Cocero and co-workers,<sup>23</sup> who determined that the rate of decomposition ( $K_d$ ) of H<sub>2</sub>O<sub>2</sub> with N<sub>2</sub> as gas diluent ( $K_d = 0.2595 \text{ min}^{-1}$ ) was 12 times higher than when using CO<sub>2</sub> ( $K_d = 0.0218 \text{ min}^{-1}$ ), which highlighted the role of H<sub>2</sub>CO<sub>3</sub> in stabilising the *in-situ* H<sub>2</sub>O<sub>2</sub>.<sup>23</sup>

The stability of the catalysts was determined by analysing the post-reaction solution by MP-AES as shown in Table 3.2. The stability is reported by determining the amount of metal that have leached into the solution at the end of the reaction towards the direct synthesis of H<sub>2</sub>O<sub>2</sub>. These observations firstly highlighted the enhanced stability that could be achieved through alloying Pd with Au. More importantly they also demonstrate that the stability of Pd was compromised when using (25°C,H<sub>2</sub>O,N<sub>2</sub>) conditions, in comparison with the (2°C,CH<sub>3</sub>OH-H<sub>2</sub>O,CO<sub>2</sub>) ones. For example, 0.24 % of Pd was found to leach into the solution when using the bi-metallic 0.25 wt.% Au-0.75 wt.% Pd/TiO<sub>2</sub> catalyst at (25°C,H<sub>2</sub>O,N<sub>2</sub>) conditions. Contrarily, only 0.03 % of Pd leached with (2°C,CH<sub>3</sub>OH-H<sub>2</sub>O,CO<sub>2</sub>) conditions. Notably, Au did not leach under any reaction set of conditions used.

**Table 3.2:** Metal leaching determined by MP-AES for the mono and bi-metallic 1.0 wt.% AuPd/TiO<sub>2</sub> catalysts during the direct synthesis of H<sub>2</sub>O<sub>2</sub> at (2°C,CH<sub>3</sub>OH-H<sub>2</sub>O,CO<sub>2</sub>) and (25°C,H<sub>2</sub>O,N<sub>2</sub>) conditions.

Catalysts	(2°C,CH <sub>3</sub> OH-H <sub>2</sub> O,CO <sub>2</sub> )		(25°C,H <sub>2</sub> O,N <sub>2</sub> )	
	Au	Pd	Au	Pd
	%	%	%	%
1 wt.% Au/TiO <sub>2</sub>	0	-	0	-
0.75 wt.% Au-0.25 wt.% Pd/TiO <sub>2</sub>	0	0.05	0.01	0.3
0.50 wt.% Au-0.50 wt.% Pd/TiO <sub>2</sub>	0	0.02	0	0.03
0.25 wt.% Au-0.75 wt.% Pd/TiO <sub>2</sub>	0	0.03	0	0.24
1 wt.% Pd/TiO <sub>2</sub>	-	0	-	0.15

**Reaction conditions:** (2°C,CH<sub>3</sub>OH-H<sub>2</sub>O,CO<sub>2</sub>): 8.5 g (5.6 g CH<sub>3</sub>OH, 2.9 g H<sub>2</sub>O), catalyst (0.01 g), 420 psi of 5 % H<sub>2</sub>/CO<sub>2</sub>, 160 psi of 25 % O<sub>2</sub>/CO<sub>2</sub>, 1200 rpm, 2 °C, 0.5 h. (25°C,H<sub>2</sub>O,N<sub>2</sub>): 8.5 g H<sub>2</sub>O, catalyst (0.01 g), 420 psi of 5 % H<sub>2</sub>/N<sub>2</sub>, 160 psi of 25 % O<sub>2</sub>/N<sub>2</sub>,1200 rpm, 25 °C, 0.5 h.

### 3.2.4 Comparison of the H<sub>2</sub> conversion and H<sub>2</sub>O<sub>2</sub> selectivity for the bi-metallic 0.5 wt.% Au-0.5 wt.% Pd/TiO<sub>2</sub> catalyst during the direct synthesis of H<sub>2</sub>O<sub>2</sub>.

Table 3.3 presents the H<sub>2</sub> conversion and the H<sub>2</sub>O<sub>2</sub> selectivity at the four reaction conditions used within this study using bi-metallic 0.5 wt.% Au-0.5 wt.% Pd/TiO<sub>2</sub> catalyst. The H<sub>2</sub> conversion as well as the H<sub>2</sub>O<sub>2</sub> selectivity trend aligned well with the results obtained in Figure 3.2-3.9. The H<sub>2</sub> conversion decreased, as a general trend, when transitioning from (2°C,CH<sub>3</sub>OH-H<sub>2</sub>O,CO<sub>2</sub>) to (25°C,H<sub>2</sub>O,N<sub>2</sub>) conditions, with the exception of (25°C,CH<sub>3</sub>OH-H<sub>2</sub>O,CO<sub>2</sub>). When working at 25 °C with 67 % CH<sub>3</sub>OH in H<sub>2</sub>O as solvent, the conversion of H<sub>2</sub> increased from 40 % to 56 % due to the H<sub>2</sub> becoming more soluble in the reaction mixture with increasing the temperature, which subsequently led to a high degradation activity (from 288 mol<sub>H<sub>2</sub>O<sub>2</sub></sub> kg<sub>cat</sub><sup>-1</sup> h<sup>-1</sup> to 342 mol<sub>H<sub>2</sub>O<sub>2</sub></sub> kg<sub>cat</sub><sup>-1</sup> h<sup>-1</sup>) and to a lower H<sub>2</sub>O<sub>2</sub> selectivity (44 % to 14 %). There was a significant decrease in H<sub>2</sub> conversion when removing the CH<sub>3</sub>OH from the reaction mixture (from 56 % to 29 %), which was attributed to the low solubility of H<sub>2</sub> in H<sub>2</sub>O compared to CH<sub>3</sub>OH. Transitioning from (25°C,CH<sub>3</sub>OH-H<sub>2</sub>O,CO<sub>2</sub>) to (25°C,H<sub>2</sub>O,CO<sub>2</sub>) had made increase the degradation activity, which unfortunately led to a further decrease in H<sub>2</sub>O<sub>2</sub> selectivity from 14 % to 8 %. Finally, exchanging CO<sub>2</sub> for N<sub>2</sub>, decreased the selectivity towards H<sub>2</sub>O<sub>2</sub> from 8 % to 3 %, since in the absence of CO<sub>2</sub> avoided the formation of H<sub>2</sub>CO<sub>3</sub> that aided to acidify the reaction medium during the direct synthesis.

**Table 3.3:** Comparison of the activity and H<sub>2</sub>O<sub>2</sub> selectivity between the four reaction conditions evaluated for the bi-metallic 0.5 wt.% Au-0.5 wt.% Pd/TiO<sub>2</sub> catalyst.

Reaction conditions	H <sub>2</sub> conversion %	H <sub>2</sub> O <sub>2</sub> selectivity %	Productivity mol <sub>H<sub>2</sub>O<sub>2</sub></sub> kg <sub>cat</sub> <sup>-1</sup> h <sup>-1</sup>	Degradation mol <sub>H<sub>2</sub>O<sub>2</sub></sub> kg <sub>cat</sub> <sup>-1</sup> h <sup>-1</sup> (± S.D)
(2 °C, CH <sub>3</sub> OH-H <sub>2</sub> O, CO <sub>2</sub> )	40	44	93	288 ± 6
(25 °C, CH <sub>3</sub> OH-H <sub>2</sub> O, CO <sub>2</sub> )	56	14	75	342 ± 17
(25 °C, H <sub>2</sub> O, CO <sub>2</sub> )	29	8	28	522 ± 21
(25 °C, H <sub>2</sub> O, N <sub>2</sub> )	22	3	13	998 ± 39

**(S.D):** standard deviation. **Reaction conditions towards the direct synthesis: (2°C, CH<sub>3</sub>OH-H<sub>2</sub>O, CO<sub>2</sub>):** 8.5 g (5.6 g CH<sub>3</sub>OH, 2.9 g H<sub>2</sub>O), catalyst (0.01 g), 420 psi of 5 % H<sub>2</sub>/CO<sub>2</sub>, 160 psi of 25 % O<sub>2</sub>/CO<sub>2</sub>, 1200 rpm, 2 °C, 0.5 h. **(25°C, CH<sub>3</sub>OH-H<sub>2</sub>O, CO<sub>2</sub>):** 8.5 g (5.6 g CH<sub>3</sub>OH, 2.9 g H<sub>2</sub>O), catalyst (0.01 g), 420 psi of 5 % H<sub>2</sub>/CO<sub>2</sub>, 160 psi of 25 % O<sub>2</sub>/CO<sub>2</sub>, 25 °C, 1200 rpm, 0.5 h. **(25°C, H<sub>2</sub>O, CO<sub>2</sub>):** 8.5 g H<sub>2</sub>O, catalyst (0.01 g), 420 psi of 5 % H<sub>2</sub>/CO<sub>2</sub>, 160 psi of 25 % O<sub>2</sub>/CO<sub>2</sub>, 1200 rpm, 25 °C, 0.5 h. **(25°C, H<sub>2</sub>O, N<sub>2</sub>):** 8.5 g H<sub>2</sub>O, catalyst (0.01 g), 420 psi of 5 % H<sub>2</sub>/N<sub>2</sub>, 160 psi of 25 % O<sub>2</sub>/N<sub>2</sub>, 1200 rpm, 25 °C, 0.5 h. **Reaction conditions towards the degradation of H<sub>2</sub>O<sub>2</sub>: (2°C, CH<sub>3</sub>OH-H<sub>2</sub>O, CO<sub>2</sub>):** 8.5 g (5.6 g CH<sub>3</sub>OH, 0.68 g H<sub>2</sub>O<sub>2</sub>, 2.22 g H<sub>2</sub>O), catalyst (0.01 g), 420 psi of 5 % H<sub>2</sub>/CO<sub>2</sub>, 1200 rpm, 2 °C, 0.5 h. **(25°C, CH<sub>3</sub>OH-H<sub>2</sub>O, CO<sub>2</sub>):** 8.5 g (5.6 g CH<sub>3</sub>OH, 0.68 g H<sub>2</sub>O<sub>2</sub>, 2.22 g H<sub>2</sub>O), catalyst (0.01 g), 420 psi of 5 % H<sub>2</sub>/CO<sub>2</sub>, 25 °C, 1200 rpm, 0.5 h. **(25°C, H<sub>2</sub>O, CO<sub>2</sub>):** 8.5 g (0.68 g H<sub>2</sub>O<sub>2</sub>, 7.92 g H<sub>2</sub>O), catalyst (0.01 g), 420 psi of 5 % H<sub>2</sub>/CO<sub>2</sub>, 1200 rpm, 25 °C, 0.5 h. **(25°C, H<sub>2</sub>O, CO<sub>2</sub>):** 8.5 g (0.68 g H<sub>2</sub>O<sub>2</sub>, 7.92 g H<sub>2</sub>O), catalyst (0.01 g), 420 psi of 5 % H<sub>2</sub>/N<sub>2</sub>, 1200 rpm, 25 °C, 0.5 h.

### 3.2.5 Effect of the H<sub>2</sub> solubility towards the formation of H<sub>2</sub>O<sub>2</sub>.

The H<sub>2</sub>/O<sub>2</sub> ratio have been investigated (keeping constant the total pressure to 580 psi) towards the direct synthesis of H<sub>2</sub>O<sub>2</sub>, since it was seen that H<sub>2</sub> availability in the reaction mixture have shown to play a critical role (Figure 3.10). The formation of H<sub>2</sub>O<sub>2</sub> increased in a fairly linear fashion at low ratios of H<sub>2</sub>/O<sub>2</sub>; 0.12 (39 mol<sub>H<sub>2</sub>O<sub>2</sub></sub> kg<sub>cat</sub><sup>-1</sup> h<sup>-1</sup>), 0.25 (59 mol<sub>H<sub>2</sub>O<sub>2</sub></sub> kg<sub>cat</sub><sup>-1</sup> h<sup>-1</sup>) and 0.5 (97 mol<sub>H<sub>2</sub>O<sub>2</sub></sub> kg<sub>cat</sub><sup>-1</sup> h<sup>-1</sup>), which suggested that the formation towards H<sub>2</sub>O<sub>2</sub> excelled the degradation activity. However, subsequent increases of the H<sub>2</sub>/O<sub>2</sub> ratios; 0.5 (97 mol<sub>H<sub>2</sub>O<sub>2</sub></sub> kg<sub>cat</sub><sup>-1</sup> h<sup>-1</sup>), 0.69 (104 mol<sub>H<sub>2</sub>O<sub>2</sub></sub> kg<sub>cat</sub><sup>-1</sup> h<sup>-1</sup>) and 0.96 (98 mol<sub>H<sub>2</sub>O<sub>2</sub></sub> kg<sub>cat</sub><sup>-1</sup> h<sup>-1</sup>) did not affect the formation of H<sub>2</sub>O<sub>2</sub> significantly which led to conclude that the formation towards the H<sub>2</sub>O<sub>2</sub> and the degradation activity might have been similar between these ratios (0.5-0.96). Finally, higher H<sub>2</sub>/O<sub>2</sub> ratios; 2.12 (22 mol<sub>H<sub>2</sub>O<sub>2</sub></sub> kg<sub>cat</sub><sup>-1</sup> h<sup>-1</sup>) had a counterproductive effect in the formation, which suggested that the selectivity was majorly engrossed towards the degradation of H<sub>2</sub>O<sub>2</sub>. These results highlighted the requirement of controlling H<sub>2</sub>/O<sub>2</sub> ratio to regulate the H<sub>2</sub>O<sub>2</sub> formation during the direct synthesis. It was not considered that the variation of the partial pressure of the CO<sub>2</sub> played a significant role in the formation when varying the H<sub>2</sub>/O<sub>2</sub> ratios, since the solvent would have been saturated with CO<sub>2</sub> across the whole range of H<sub>2</sub>/O<sub>2</sub> ratios investigated.<sup>18</sup>

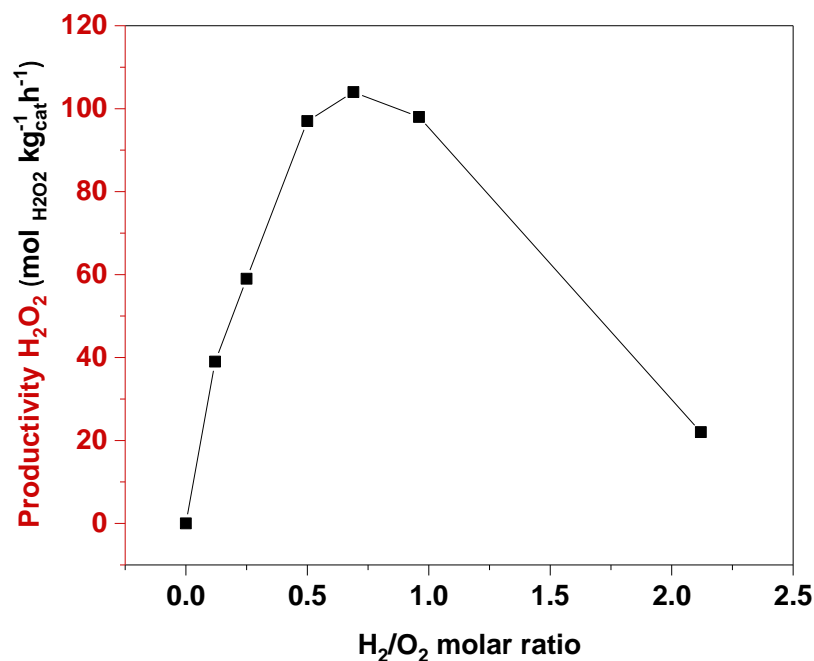


**Figure 3.10:** Effect of the H<sub>2</sub>/O<sub>2</sub> molar ratio to the direct synthesis of H<sub>2</sub>O<sub>2</sub> using bi-metallic 0.5 wt.% Au-0.5 wt.% Pd /TiO<sub>2</sub> catalyst. **Reaction conditions: (2°C,CH<sub>3</sub>OH-H<sub>2</sub>O,CO<sub>2</sub>):** 8.5 g (5.6 g CH<sub>3</sub>OH, 2.9 g H<sub>2</sub>O), catalyst (0.01 g), 580 psi (5 % H<sub>2</sub>/CO<sub>2</sub> and 25 % O<sub>2</sub>/CO<sub>2</sub>), 1200 rpm, 2 °C, 0.5 h.

### 3.2.6 Time on-line activity towards the formation of H<sub>2</sub>O<sub>2</sub> at (2°C,CH<sub>3</sub>OH-H<sub>2</sub>O,CO<sub>2</sub>) and (25°C,H<sub>2</sub>O,N<sub>2</sub>) conditions.

Figure 3.11 and Figure 3.12 presents the formation of H<sub>2</sub>O<sub>2</sub> as a function of reaction time under two sets of reaction conditions, (2°C,CH<sub>3</sub>OH-H<sub>2</sub>O,CO<sub>2</sub>) and H<sub>2</sub>O (25°C,H<sub>2</sub>O,N<sub>2</sub>). When varying reaction time, the concentration of the *in-situ* H<sub>2</sub>O<sub>2</sub> (wt. %) is a better measure of the catalytic performance than productivity (mol<sub>H<sub>2</sub>O<sub>2</sub></sub>kg<sub>cat</sub><sup>-1</sup>h<sup>-1</sup>), as the latter contains a time function which would suggest that the catalyst performance at shorter reaction times are significantly higher than those at longer times. In both sets of reaction conditions, the concentration has increased rapidly at short reaction times, reaching 0.15 wt.% H<sub>2</sub>O<sub>2</sub> over 10 min at (2 °C,CH<sub>3</sub>OH-H<sub>2</sub>O,CO<sub>2</sub>) and *c.a* 0.01 wt.% over 5 min under (25 °C,H<sub>2</sub>O,N<sub>2</sub>) conditions. However, after this time, H<sub>2</sub>O<sub>2</sub> concentration started to plateau, suggesting that the H<sub>2</sub>O<sub>2</sub> accumulated in solution started to degrade. This plateau tendency becomes more significant at (25°C,H<sub>2</sub>O,N<sub>2</sub>) conditions than at (2°C,CH<sub>3</sub>OH-H<sub>2</sub>O,CO<sub>2</sub>), which it is not surprising since the former reaction conditions have shown to be the most optimum to degrade H<sub>2</sub>O<sub>2</sub>.

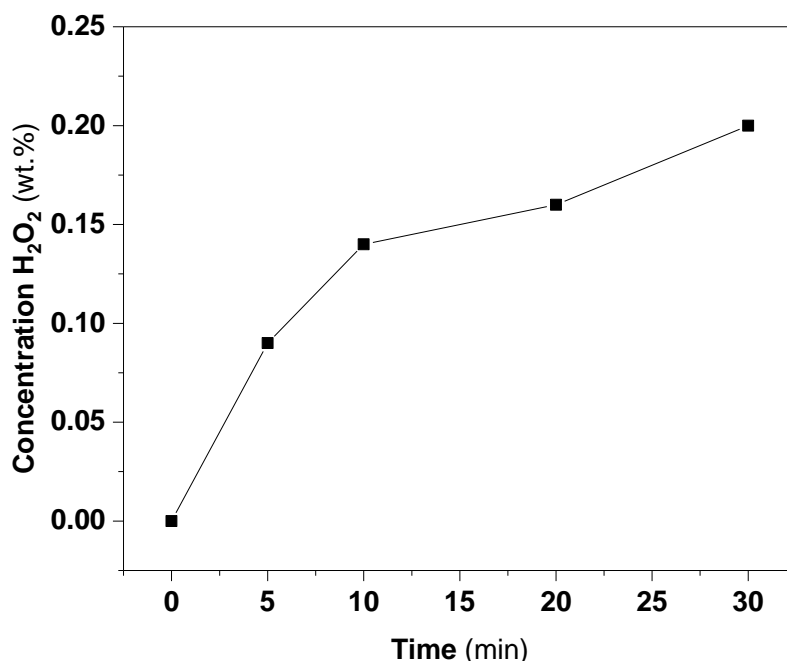


**Figure 3.11:** Time on-line activity towards the direct synthesis of H<sub>2</sub>O<sub>2</sub> using bi-metallic 0.5 wt.% Au-0.5 wt.% Pd/TiO<sub>2</sub> catalyst. **Reaction conditions: (2°C, CH<sub>3</sub>OH-H<sub>2</sub>O, CO<sub>2</sub>):** 8.5 g (5.6 g CH<sub>3</sub>OH and 2.9 g H<sub>2</sub>O), catalyst (0.01 g), 420 psi 5 % H<sub>2</sub>/CO<sub>2</sub>, 160 psi 25 % O<sub>2</sub>/CO<sub>2</sub>, 1200 rpm, 2 °C.

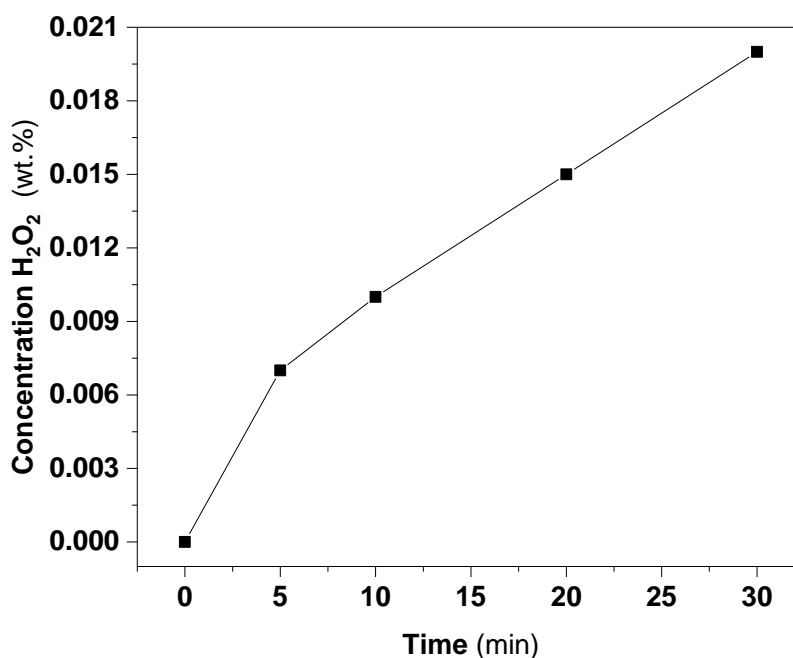


**Figure 3.12:** Time on-line activity towards the direct synthesis of H<sub>2</sub>O<sub>2</sub> using bi-metallic 0.5 wt.% Au-0.5 wt.% Pd/TiO<sub>2</sub> catalyst. **Reaction conditions: (25°C, H<sub>2</sub>O, N<sub>2</sub>):** 8.5 g (H<sub>2</sub>O), catalyst (0.01 g), 420 psi 5 % H<sub>2</sub>/N<sub>2</sub>, 160 psi 25 % O<sub>2</sub>/N<sub>2</sub>, 1200 rpm, 25 °C.

### 3.3 Characterisation of the mono and bi-metallic 1 wt.% AuPd/TiO<sub>2</sub> catalysts.

The mono and bi-metallic 1wt.%AuPd/TiO<sub>2</sub> catalysts were analysed by XRD to determine if there were any metal reflections that would give an indication of the metal dispersion and particle size. XRD analysis (Figure 3.13-3.14) revealed reflections associated with Pd for the mono-metallic 1 wt.% Pd/TiO<sub>2</sub> catalyst at 2θ= 40.1 and 46.8° respectively, which were

assigned to metallic palladium ( $\text{Pd}^0$ ).<sup>26</sup> For the rest of the mono and bi-metallic catalysts, no reflections associated with Au were observed ((111) phase ( $2\theta= 38.2^\circ$ )) or for AuPd alloys ((111)  $2\theta=38^\circ\text{-}40^\circ$  and (222)  $2\theta=44^\circ\text{-}47^\circ$ ), which was ascribed to the low metal loading of these materials.<sup>24</sup> Only reflections corresponding to the  $\text{TiO}_2$  (P25) support were observed (ICDD reference code 00-004-0477).

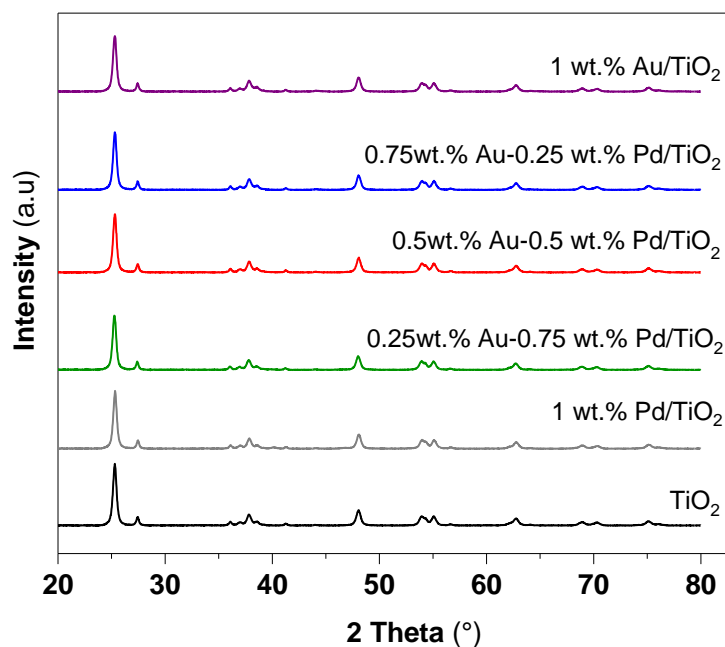


**Figure 3.13:** XRD diffractogram for mono and bi-metallic 1.0 wt.% AuPd/ $\text{TiO}_2$  catalysts.

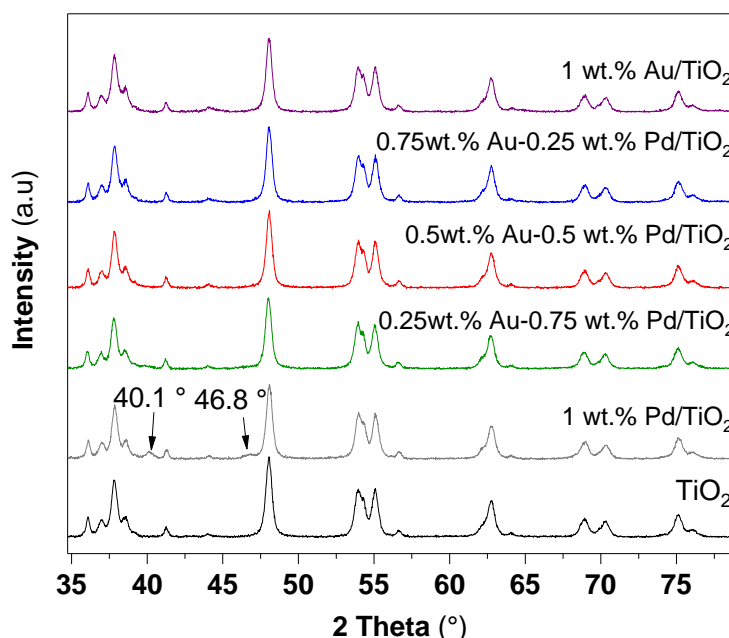


**Figure 3.14:** XRD diffractogram zoomed from  $35^\circ$  to  $80^\circ$  for mono and bi-metallic 1.0 wt.% AuPd/ $\text{TiO}_2$  catalysts.

TEM was employed to determine the mean particle size of metal nanoparticles (micrographs and histograms are shown in supplementary information section 3.6, Figure S.I. 3.1 and Figure S.I. 3.2 respectively). No nanoparticles were visible for the mono-metallic 1 wt.% Pd/TiO<sub>2</sub> catalyst by TEM analysis, which suggested that they were below the detection limit of the equipment. Energy dispersive x-ray spectroscopy (EDX) analysis corroborated that the mono-metallic 1 wt.% Pd/TiO<sub>2</sub> catalyst did have highly dispersed Pd clusters all over the surface of the TiO<sub>2</sub> (supplementary information section 3.6, Figure S.I. 3.3 and Table S.I. 3.1). The mean particle size did not seem to correlate with the loading of either Au or Pd, however, it was clear that the bi-metallic 1.0 wt.% AuPd/TiO<sub>2</sub> catalysts presented narrower particle size and distribution than the mono-metallic 1 wt.% Au/TiO<sub>2</sub>, catalyst especially the bi-metallic 0.5 wt.% Au-0.5 wt.% Pd/TiO<sub>2</sub> one (Table 3.4).

**Table 3.4:** Mean particle and size distribution for the mono and bi-metallic 1 wt.% AuPd/TiO<sub>2</sub> catalysts.

Catalysts	Mean particle size	Standard deviation
1 wt.% Au/TiO <sub>2</sub>	9.1 nm	3.0 nm
0.75 wt.% Au-0.25 wt.% Pd/TiO <sub>2</sub>	4.6 nm	1.5 nm
0.50 wt.% Au-0.50 wt.% Pd/TiO <sub>2</sub>	2.5 nm	0.8 nm
0.25 wt.% Au-0.75 wt.% Pd/TiO <sub>2</sub>	5.8 nm	2.2 nm

Sankar *et al.*,<sup>8</sup> have reported that the bi-metallic 0.5 wt.% Au-0.5 wt.% Pd/TiO<sub>2</sub> catalysts prepared by modified impregnation gave better productivity towards H<sub>2</sub>O<sub>2</sub> synthesis (99 mol H<sub>2</sub>O<sub>2</sub> kg<sub>cat</sub><sup>-1</sup> h<sup>-1</sup>) than other methodologies used such as conventional impregnation (23 mol H<sub>2</sub>O<sub>2</sub> kg<sub>cat</sub><sup>-1</sup> h<sup>-1</sup>) and sol-immobilisation (32 mol H<sub>2</sub>O<sub>2</sub> kg<sub>cat</sub><sup>-1</sup> h<sup>-1</sup>). The success of the modified impregnation over the other two methodologies relied on two critical steps: the acidification of PdCl<sub>2</sub> with hydrochloric acid (HCl) [0.58 M] and the subsequent reductive heat treatment with 5 % H<sub>2</sub>/Ar (400°C, 4h). Sankar *et al.*, reported that the concentration of the Cl<sup>-</sup> in the PdCl<sub>2</sub> precursor had an influence in the composition of AuPd nanoparticles and mean particle size; where the average mean nanoparticle size decreased with increasing the HCl concentration in the PdCl<sub>2</sub> precursor; 0 M (4.7 nm), 0.58 M (2.9 nm) and 2 M (2.6 nm).<sup>8</sup> It was concluded that the outstanding activity of the bi-metallic 0.5 wt.% Au-0.5 wt.% Pd/TiO<sub>2</sub> catalyst made by modified impregnation (99 mol<sub>H<sub>2</sub>O<sub>2</sub></sub> kg<sub>cat</sub><sup>-1</sup> h<sup>-1</sup> formation of H<sub>2</sub>O<sub>2</sub>) was due to presenting homogeneous AuPd alloys nanoparticles with similar AuPd composition and narrow particle size (2.9 nm), which was very close to what was obtained in terms of formation of H<sub>2</sub>O<sub>2</sub> and mean nanoparticle size (2.5 nm).

The variability of the mean particle size and distribution between the mono and bi-metallic 1 wt.% AuPd/TiO<sub>2</sub> catalysts might have been due to the difference in the HCl concentration

during their synthesis as Table 3.5 aims to show. For instance, 1.664 mL of PdCl<sub>2</sub> (0.58 M HCl) were added to prepare 1 wt.% Pd/TiO<sub>2</sub> catalysts, whereas 0.416 mL of PdCl<sub>2</sub> (0.58 M HCl) were only required to prepare the bi-metallic 0.75 wt.% Au-0.25 wt.% Pd/TiO<sub>2</sub> one. Thus, the concentration of HCl during the synthesis of the former and the catalysts were 0.015 M and 0.06 M respectively. As a consequence, no acidification was introduced when synthesising the mono-metallic 1 wt.% Au/TiO<sub>2</sub> catalyst since the HAuCl<sub>4</sub> precursor was not acidified. It was believed that the presence of HCl may be found responsible for the decrease in the mean particle size when comparing 1 wt.% Au/TiO<sub>2</sub> with the bi-metallic 1.0 wt.% AuPd/TiO<sub>2</sub> catalysts (Table 3.5). However, there were no direct correlation between the concentration of HCl and the mean particle size of the three bi-metallic 1 wt.% AuPd/TiO<sub>2</sub> catalysts. Since both bi-metallic 0.75 wt.% Au-0.25 wt.% Pd/TiO<sub>2</sub> and 0.25 wt.% Au-0.75 wt.% Pd/TiO<sub>2</sub> catalysts showed a higher mean particle size in comparison to the bi-metallic 0.50 wt.% Au-0.50 wt.% Pd/TiO<sub>2</sub> one, it was suggested that these two former catalysts also could have variability in terms of nanoparticle composition. The examination of the nanoparticle composition and its correlation to the nanoparticle size, as well as to examine the presence of the AuPd alloys, would have helped to assign the activity to the characterisation of the 1 wt.% AuPd/TiO<sub>2</sub> catalysts better. Unfortunately, the results from TEM and EDX analysis were not resolute enough to determine the composition or the presence of AuPd alloys, which have been widely ascribed to increase the selectivity towards the direct formation of H<sub>2</sub>O<sub>2</sub>.

**Table 3.5:** Correlation of particle size (nm) with [HCl] concentration in the PdCl<sub>2</sub> precursor solution.

<b>Catalysts</b>	<b>PdCl<sub>2</sub> (0.58 M HCl) mL</b>	<b>[HCl] M</b>	<b>Mean particle size nm</b>
<b>1 wt.% Au/TiO<sub>2</sub></b>	-	0	9.1
<b>0.75 wt.% Au-0.25 wt.% Pd/TiO<sub>2</sub></b>	0.416	0.015	5.8
<b>0.50 wt.% Au-0.50 wt.% Pd/TiO<sub>2</sub></b>	0.832	0.03	2.5
<b>0.25 wt.% Au-0.75 wt.% Pd/TiO<sub>2</sub></b>	1.248	0.05	4.6
<b>1 wt.% Pd/TiO<sub>2</sub></b>	1.664	0.06	b.d.l

**b.d.l:** below detection limit.

The oxidation state of the Pd was examined since it is a critical parameter that can influence the activity and selectivity towards the direct synthesis of H<sub>2</sub>O<sub>2</sub>. The PdO and Pd<sup>0</sup> have been reported to have different activity and selectivity, in fact, the former is acknowledged by several authors to be more selective towards the formation of H<sub>2</sub>O<sub>2</sub>.<sup>1,11,12,7</sup> By XPS analysis it was feasible to determine the Au: Pd and PdO: Pd<sup>0</sup> ratios for the fresh (Table 3.6) and used (Table 3.7) catalysts. The analysis of the fresh samples showed that the PdO: Pd<sup>0</sup>

ratio of the bi-metallic 1.0 wt.% AuPd/TiO<sub>2</sub> catalysts were comparable to the mono-metallic 1.0 wt.% Pd/TiO<sub>2</sub> analogue.

It was clear that the presence of Au in the bi-metallic 1 wt.% AuPd/TiO<sub>2</sub> ratios, had clearly improved the selectivity and activity in comparison to the mono-metallic 1 wt.% Pd/TiO<sub>2</sub> catalyst as the results from the activity towards the direct synthesis and degradation of H<sub>2</sub>O<sub>2</sub> have shown. However, the oxidation state of the Pd have had not contribution to the difference in activity shown between the three bi-metallic ratios and the mono-metallic analogue, especially towards the degradation of H<sub>2</sub>O<sub>2</sub>. Therefore, it was concluded that the difference in activity between the three bi-metallic 1 wt.% AuPd/TiO<sub>2</sub> catalysts, especially during the degradation of H<sub>2</sub>O<sub>2</sub>, could have been related to the difference in the nanoparticle's size and composition, as well as the possible formation of AuPd alloys. In addition to this, the analysis by XPS of the used catalysts revealed that the Au:Pd and PdO:Pd<sup>0</sup> ratio were not altered after one used, suggesting that the re-usability of the catalysts towards the direct formation and degradation of H<sub>2</sub>O<sub>2</sub> might have been maintained for subsequent usage.

**Table 3.6:** Determination of the Au:Pd and the PdO:Pd<sup>0</sup> ratios for the fresh mono and bi-metallic 1.0 wt.% AuPd/TiO<sub>2</sub> catalysts.

Fresh catalysts	Au:Pd	PdO:Pd <sup>0</sup>
1 wt.% Au/TiO <sub>2</sub>	n.a	n.a
0.75 wt.% Au-0.25 wt.% Pd/TiO <sub>2</sub>	0.84	0.29
0.5 wt.% Au-0.5 wt.% Pd/TiO <sub>2</sub>	0.21	0.33
0.25 wt.% Au-0.75 wt.% Pd/TiO <sub>2</sub>	0.15	0.33
1 wt.% Pd/TiO <sub>2</sub>	n.a	0.28

**n.a:** not applicable. **Heat treatment:** 5 % H<sub>2</sub>/Ar, 400 °C, 10 °C/min, 4 h. XPS spectra for each mono- and bi-metallic 1.0 wt.% AuPd/TiO<sub>2</sub> catalyst are shown in supplementary information, Figure S.I. 3.4-3.7.

**Table 3.7:** Determination of the Au:Pd and the PdO:Pd<sup>0</sup> ratios for the used mono and bi-metallic 1.0 wt.% AuPd/TiO<sub>2</sub> catalysts at (2°C, CH<sub>3</sub>OH-H<sub>2</sub>O, CO<sub>2</sub>) conditions.

Used catalysts	Au:Pd	PdO:Pd <sup>0</sup>
1 wt.% Au/TiO <sub>2</sub>	n/a	n.a
0.75 wt.% Au-0.25 wt.% Pd/TiO <sub>2</sub>	0.80	0.33
0.5 wt.% Au-0.5 wt.% Pd/TiO <sub>2</sub>	0.28	0.29
0.25 wt.% Au-0.75 wt.% Pd/TiO <sub>2</sub>	0.04	0.35
1 wt.% Pd/TiO <sub>2</sub>	n.a	0.21

**n.a:** not applicable. **Reaction conditions: (2°C, CH<sub>3</sub>OH-H<sub>2</sub>O, CO<sub>2</sub>):** 8.5 g (5.6 g CH<sub>3</sub>OH, 2.9 g H<sub>2</sub>O), catalyst (0.01 g), 420 psi 5 % H<sub>2</sub>/CO<sub>2</sub>, 160 psi 25 % O<sub>2</sub>/CO<sub>2</sub>, 1200 rpm, 2 °C, 0.5 h. XPS spectra for each mono- and bi-metallic 1.0 wt.% AuPd/TiO<sub>2</sub> catalysts are shown in supplementary information, Figure S.I. 3.8-3.11.

### 3.4 Conclusions.

A set of bi-metallic 1wt.%AuPd/TiO<sub>2</sub> catalysts were prepared by a modified impregnation procedure, previously developed by Sankar *et.al.*,<sup>8</sup> These set of mono and bi-metallic 1.0 wt.% AuPd/TiO<sub>2</sub> catalysts were investigated for their activity towards the direct synthesis and subsequent degradation of H<sub>2</sub>O<sub>2</sub>, under different reaction conditions; transitioning from sub-ambient temperatures (2 °C) and mixtures of organic solvents with H<sub>2</sub>O (67 % CH<sub>3</sub>OH in H<sub>2</sub>O) to ambient temperatures (25 °C) and H<sub>2</sub>O-only as solvent. The reaction conditions chosen are relevant if *in-situ* H<sub>2</sub>O<sub>2</sub> production is to be adopted for use on an industrial scale, particularly for large scale in water remediation. It was found that the solvent and the temperature drive the selectivity of the mono and bi-metallic 1.0 wt.% AuPd/TiO<sub>2</sub> catalysts, helping to balance the formation of H<sub>2</sub>O<sub>2</sub> and its subsequent degradation. This is because the ratio of H<sub>2</sub>/O<sub>2</sub> dissolved in the reaction mixture, depends on the solubility of H<sub>2</sub> and O<sub>2</sub> gas which varies depending on the type of solvent and the temperature used. It was seen that the activity and selectivity of the mono and bi-metallic 1 wt.% AuPd/TiO<sub>2</sub> catalysts decreased when transitioning from (2°C,67 % CH<sub>3</sub>OH in H<sub>2</sub>O) to ambient temperatures (25 °C) and H<sub>2</sub>O-only as solvent, because solubility of H<sub>2</sub> decreased significantly when doing the transition between these two sets of reaction conditions.

The H<sub>2</sub>O<sub>2</sub> synthesis rates of the 1.0 wt.% Pd/TiO<sub>2</sub> and 0.75 wt.% Au-0.25 wt.% Pd/TiO<sub>2</sub> catalysts was found to be similar regardless of the amount of Pd, while the activity of the 1.0 wt.% Au/TiO<sub>2</sub> catalyst was limited. The mono-metallic 1.0 wt.% Pd/TiO<sub>2</sub> catalyst presented the greatest activity towards the degradation of H<sub>2</sub>O<sub>2</sub>, however, with the introduction of Au, the degradation was found to be reduced significantly, leading to both catalysts 1.0 wt.% Pd/TiO<sub>2</sub> and 0.75 wt.% Au-0.25 wt.% Pd/TiO<sub>2</sub> to have similar productivities of H<sub>2</sub>O<sub>2</sub>. The oxidation state of Pd (PdO and Pd<sup>0</sup>), which is key in the catalyst performance during the direct synthesis of H<sub>2</sub>O<sub>2</sub>, was found to be the similar between the three bi-metallic 1 wt.% AuPd/TiO<sub>2</sub> ratios and the mono-metallic 1 wt.% Pd/TiO<sub>2</sub> analogue, suggesting that the oxidation state did not contribute to decrease the degradation activity of none of the bi-metallic 1 wt.% AuPd/TiO<sub>2</sub> catalysts. Instead, it was believed that the difference in catalytic activity between the three bi-metallic 1 wt.% AuPd/TiO<sub>2</sub> ratios might have been due to heterogeneity derived from the nanoparticle size and composition. Unfortunately, future work is required to corroborate this last statement.

To finalise, it was concluded that the *in-situ* formation of H<sub>2</sub>O<sub>2</sub> was possible at conditions more suitable for water remediation ((25°C, H<sub>2</sub>O-only solvent), with Au having a major standing role in stabilising the H<sub>2</sub>O<sub>2</sub> against its degradation. However, selectivity is still a major concern, and it is clear that further efforts on catalyst design are required to improve the activity and selectivity of H<sub>2</sub>O<sub>2</sub>.

### 3.5 References.

1. Choudhary, V. R., Gaikwad, A. G., Sansare, S. D. Activation of supported Pd metal catalysts for selective oxidation of hydrogen to hydrogen peroxide. *Catal. Letters*. **83**, 235–239 (2002).
2. Ouyang, L., Da, G.j., Tian, P.f., Chen, T.y., Liang, G.d., Xu, J., Han, Y.F. Insight into active sites of Pd–Au /TiO<sub>2</sub> catalysts in hydrogen peroxide synthesis directly from H<sub>2</sub> and O<sub>2</sub>. *Journal of catalysis*. **311**, 129–136 (2014).
3. Park, S., Jung, J.C., Seo, J.G., Kim, T.J., Chung, Y-M., Oh, S-H., Song, I.K. Direct Synthesis of Hydrogen Peroxide from Hydrogen and Oxygen Over Palladium Catalysts Supported on SO<sub>3</sub> H-Functionalized SiO<sub>2</sub> and TiO<sub>2</sub>. *Catalysis letters*. **130**, 604–607 (2009).
4. Ntainjua, N.E., Edwards, J.K., Carley, A.F., Lopez-Sanchez, J.A., Moulijn, J.A., Herzing, A.A., Kiely, C.J., Hutchings, G.J. The role of the support in achieving high selectivity in the direct formation of hydrogen peroxide. *Green Chem*. **10**, 1162–1169 (2008).
5. Menegazzo, F., Burti, P., Signoreto, M., Manzoli, M., Vankovab, S., Boccuzzi, F., Pinna, F., Strukul, G. Effect of the addition of Au in zirconia and ceria supported Pd catalysts for the direct synthesis of hydrogen peroxide. *Journal of catalysis*. **257**, 369–381 (2008).
6. Richards, T., Harrhy, J.H., Lewis, R., Howe, A.G.R., Suldecki, G.M., Folli, A., Morgan, D.J., Davies, T.E., Loveridge, E.J., Crole, D.A., Edwards, J.K., Gaskin, P., Kiely, C.J., He, Q., Murphy, D.M., Maillard, J-Y., Freakly, S.J., Hutchings, H.J. A residue-free approach to water disinfection using catalytic in situ generation of reactive oxygen species. *Nature catalysis*. **4**, 575-584 (2021).
7. Samanta, C., Choudhary, V. R. Direct formation of H<sub>2</sub>O<sub>2</sub> from H<sub>2</sub> and O<sub>2</sub> and decomposition / hydrogenation of H<sub>2</sub>O<sub>2</sub> in aqueous acidic reaction medium over halide-containing Pd/SiO<sub>2</sub> catalytic system. *Catalysis communications*. **8**, 2222–2228 (2007).
8. Meenakshisundaram, S., He, Q., Moataz, M., Pritchard, J., Freakley, S.J., Edwards, J.K., Taylor, S.H., Morgan, D.J., Carley, A.F., Knight, D.W., Kiely, C.J., Hutchings, G.J. Synthesis of stable ligand-free gold-palladium nanoparticles using a simple excess anion method. *ACS Nano*. **6**, 6600–6613 (2012).
9. Landon, P., Collier, P. J., Papworth, A. J., Kiely, J., Graham, J. Direct formation of hydrogen peroxide from H<sub>2</sub>/O<sub>2</sub> using a gold catalyst. *ChemComm*. **12**, 2058–2059 (2002).
10. Edwards, J. K., Solsona, B.E., Landon, P., Carley, A.F., Herzing, A., Kiely, C.J., Hutchings G.J. Direct synthesis of hydrogen peroxide from H<sub>2</sub> and O<sub>2</sub> using TiO<sub>2</sub>-supported Au-Pd catalysts. *J. Catal*. **236**, 69–79 (2005).

11. Choudhary, V. R., Samanta, C., Choudhary, T. V. Direct oxidation of H<sub>2</sub> to H<sub>2</sub>O<sub>2</sub> over Pd-based catalysts: Influence of oxidation state, support and metal additives. *Appl. Catal. A Gen.* **308**, 128–133 (2006).
12. Gemo, N., Menegazzo, F., Biasi, P., Sarkar, A., Samikannu, A., Raut, D.G., Kord, K., Rautio, A.R., Mohl, M., Bostrom, D., Shchukarevc, A., Mikkola, J.P. TiO<sub>2</sub> nanoparticles: Vs. TiO<sub>2</sub> nanowires as support in hydrogen peroxide direct synthesis: The influence of N and Au doping. *RSC Adv.* **6**, 103311–103319 (2016).
13. Tian, P., Ouyang, L., Xu, X., Ao, C., Xu, X., Si, R., Shen., X., Lin, M., Xu, J., Han, Y.F. The origin of palladium particle size effects in the direct synthesis of H<sub>2</sub>O<sub>2</sub>: Is smaller better? *J. Catal.* **349**, 30–40 (2017).
14. Ho, S., Kim, J., Soo, S., Kwan, H., Lee, Y. Direct Synthesis of Hydrogen Peroxide from Hydrogen and Oxygen Using Tailored Pd Nanocatalysts : A Review of Recent Findings. *Catal. Surv. from Asia.* **21**, 1–12 (2017).
15. Pengfei, T., Like, O., Xinchao, X. U., Jing, X. U., Fan. Density functional theory study of direct synthesis of H<sub>2</sub>O<sub>2</sub> from H<sub>2</sub> and O<sub>2</sub> on Pd (111), Pd (100), and Pd (110) surfaces. *Chinese J. Catal.* **34**, 1002–1012 (2013).
16. Tian, P., Doudou, D., Yang, S., Fuzhen, X., Xingyan, X., Jing, X., Yi-Fan, H. Theoretical study of size effects on the direct synthesis of hydrogen peroxide over palladium catalysts. *J. Catal.* **369**, 95–104 (2019).
17. Amin, V.M., Olson, N.F. Effect of Temperature on Stability of Hydrogen Peroxide in Milk. *Journal of Dairy Science.* **50**, 1336–1338 (1965).
18. Piccinini, M., Ntainjua, N.E., Edwards, J.K., Carley, A.F., Moulijn, J.A., Hutchings, G.J. Effect of the reaction conditions on the performance of Au–Pd/TiO<sub>2</sub> catalyst for the direct synthesis of hydrogen peroxide. *Phys. Chem. Chem. Phys.* **12**, 2488 (2010).
19. Gemo, N., Biasi, P., Canu, P., Salmi, T. O. Mass transfer and kinetics of H<sub>2</sub>O<sub>2</sub> direct synthesis in a batch slurry reactor. *Chem. Eng. J.* **207–208**, 539–551 (2012).
20. Samanta, C. Direct synthesis of hydrogen peroxide from hydrogen and oxygen: An overview of recent developments in the process. *Appl. Catal. A Gen.* **350**, 133–149 (2008).
21. Crole, D. A., Freakley, S. J., Edwards, J. K., Hutchings, G. J. Direct synthesis of hydrogen peroxide in water at ambient temperature. *Proc. R. Soc. A Math. Phys. Eng. Sci.* **472**, 1-9 (2016).
22. Burch, R., Ellis, P. R. An investigation of alternative catalytic approaches for the direct synthesis of hydrogen peroxide from hydrogen and oxygen. *Appl. Catal. B Environ.* **42**, 203–211 (2003).
23. Moreno, T., García-Serna, J., Cocero, M. J. Decomposition reaction of H<sub>2</sub>O<sub>2</sub> over Pd/C catalyst in an aqueous medium at high pressure: Detailed kinetic study and

modelling. *J. Supercrit. Fluids*. **57**, 227–235 (2011).

24. Pawelec, B., Venezia, A. M., Parola, V.La., Campos-Martin, J.M., Fierro, J.L.G. AuPd alloy formation in Au-Pd/Al<sub>2</sub>O<sub>3</sub> catalysts and its role on aromatics hydrogenation. *Applied Surface Science*, **242**, 380–391 (2005).

### 3.6 Supplementary information.

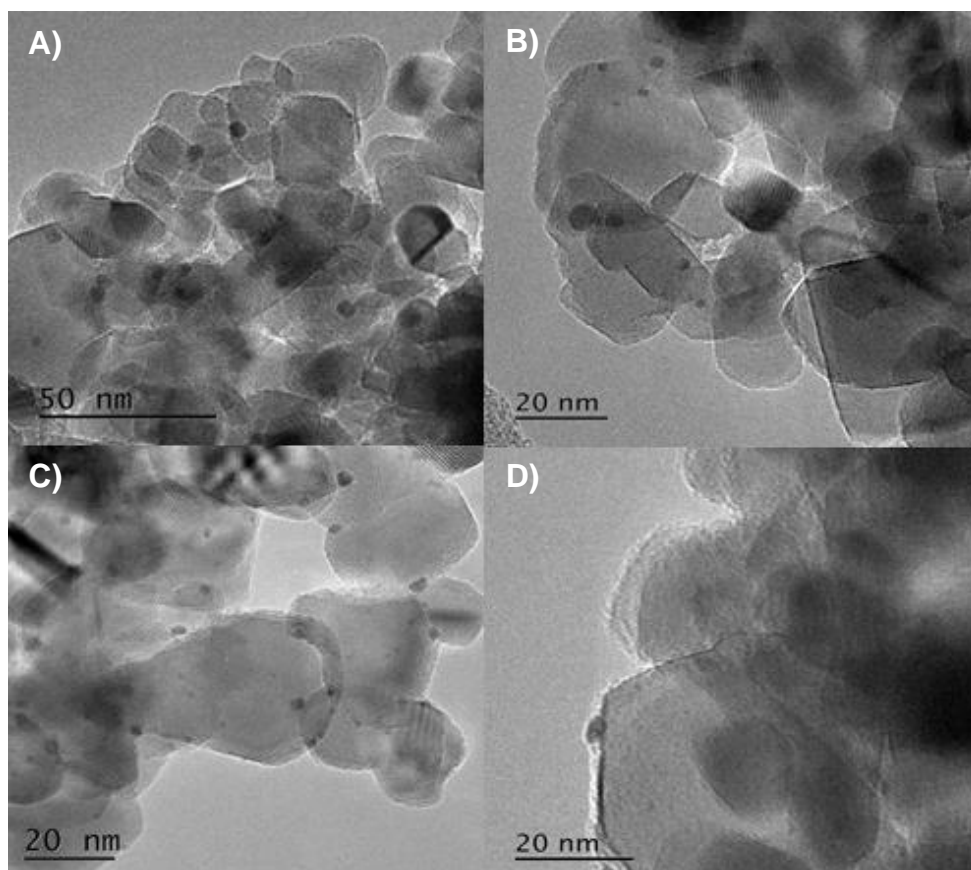


**Figure S.I. 3.1:** TEM micrographs for mono-metallic 1.0 wt.% Au/TiO<sub>2</sub> and bi-metallic 1.0 wt.% AuPd/TiO<sub>2</sub> catalysts. **Nomenclature:** A) 1 wt.% Au/TiO<sub>2</sub>, B) 0.75 wt.% Au-0.25 wt.% Pd/TiO<sub>2</sub>, C) 0.50 wt.% Au-0.50 wt.% Pd/TiO<sub>2</sub> and D) 0.25 wt.% Au-0.75 wt.% Pd/TiO<sub>2</sub>.

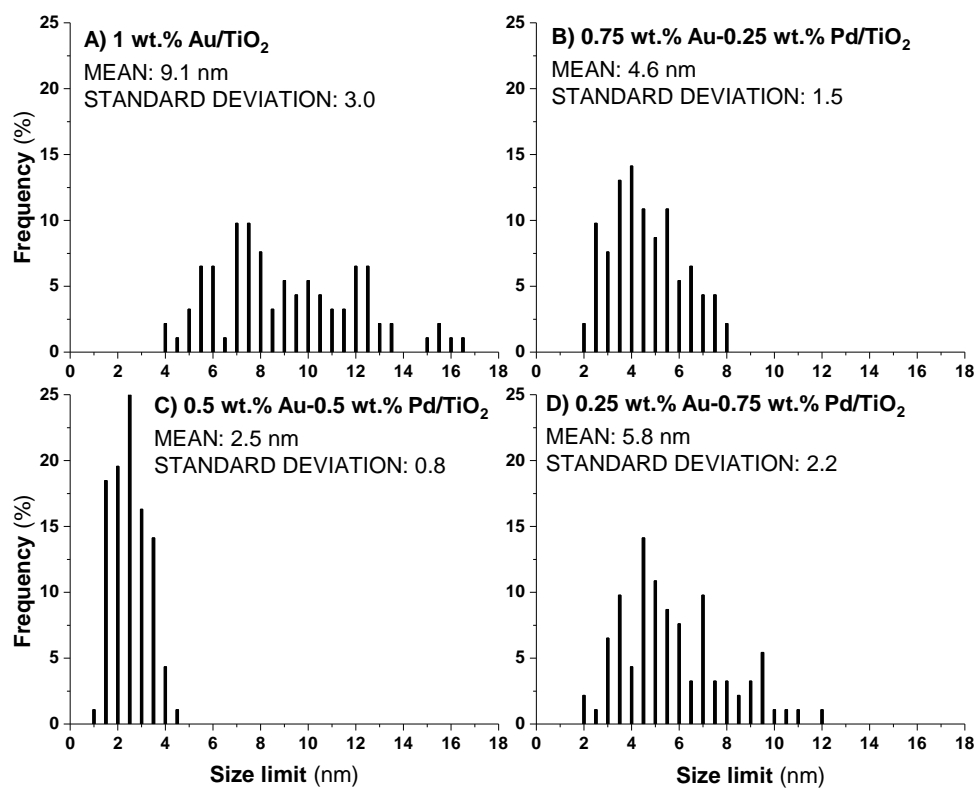


**Figure S.I. 3.2:** Mean particle size and standard deviation histograms for mono-metallic 1 wt.% Au/TiO<sub>2</sub> and bi-metallic 1.0 wt.% AuPd/TiO<sub>2</sub> catalysts.

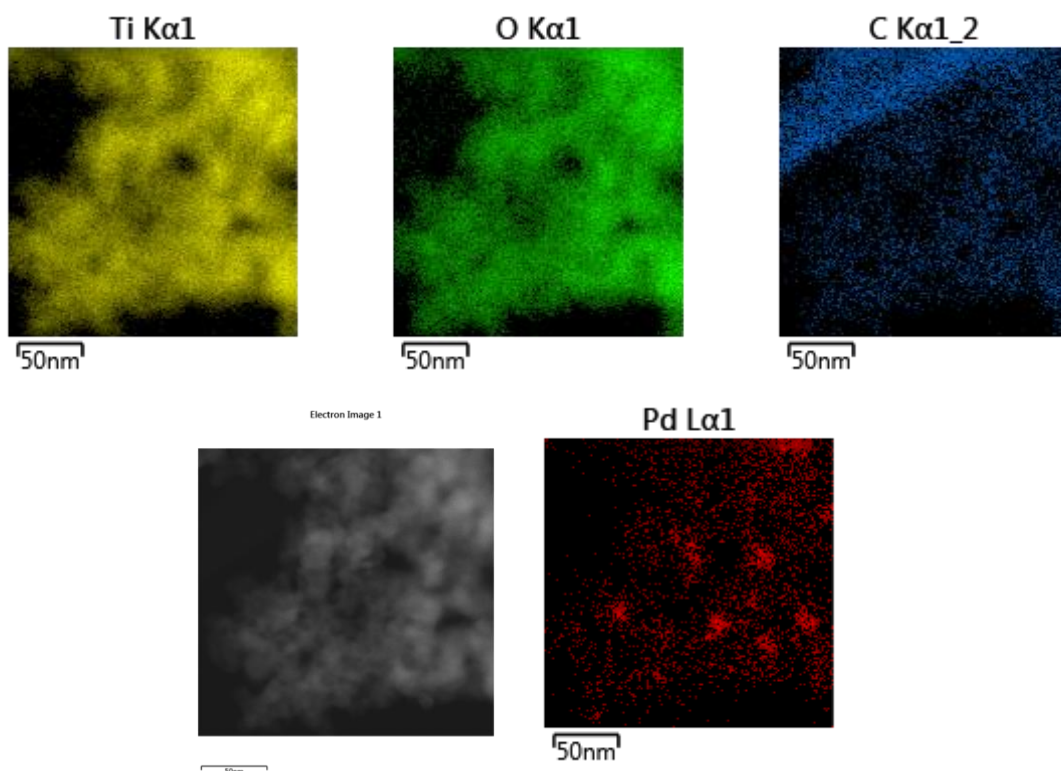


**Figure S.I. 3.3:** Elemental mapping by EDX for mono-metallic 1.0 wt.% Pd/TiO<sub>2</sub> catalyst.

**Table S.I. 3.1:** Elemental analysis by EDX for mono-metallic 1.0 wt.% Pd/TiO<sub>2</sub> catalyst.

Element	Line Type	k factor	Absorption Correction	Wt%	Wt% Sigma
<b>C</b>	K series	2.81239	1.61	5.33	0.30
<b>O</b>	K series	2.05018	2.11	54.18	0.22
<b>Ti</b>	K series	1.08940	0.90	40.10	0.18
<b>Pd</b>	L series	1.85934	0.92	0.39	0.04
<b>Total:</b>				100.00	

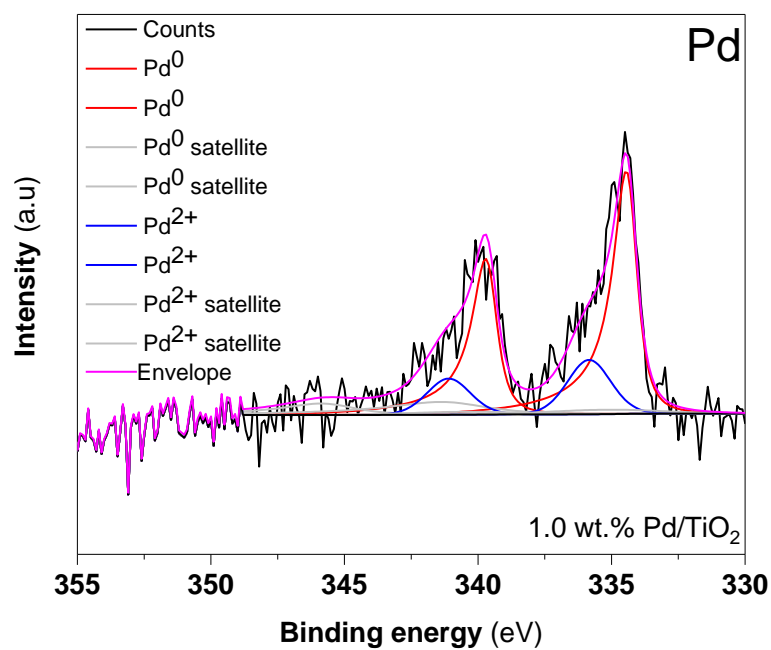


Figure S.I 3.4: XPS fitting for the fresh mono-metallic 1.0 wt.% Pd/TiO<sub>2</sub> catalyst.

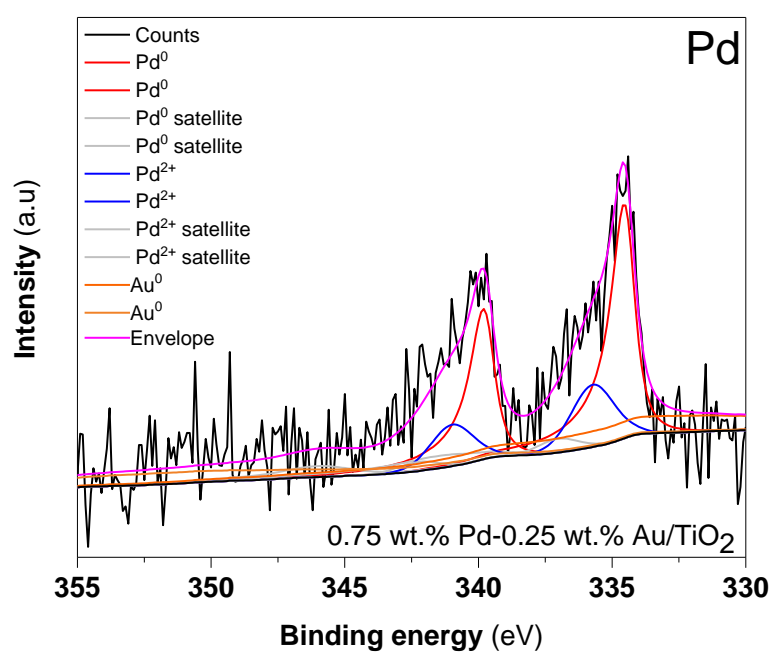


Figure S.I 3.5: XPS fitting for the fresh bi-metallic 0.75 wt.% Pd-0.25 wt.% Au/TiO<sub>2</sub> catalyst.

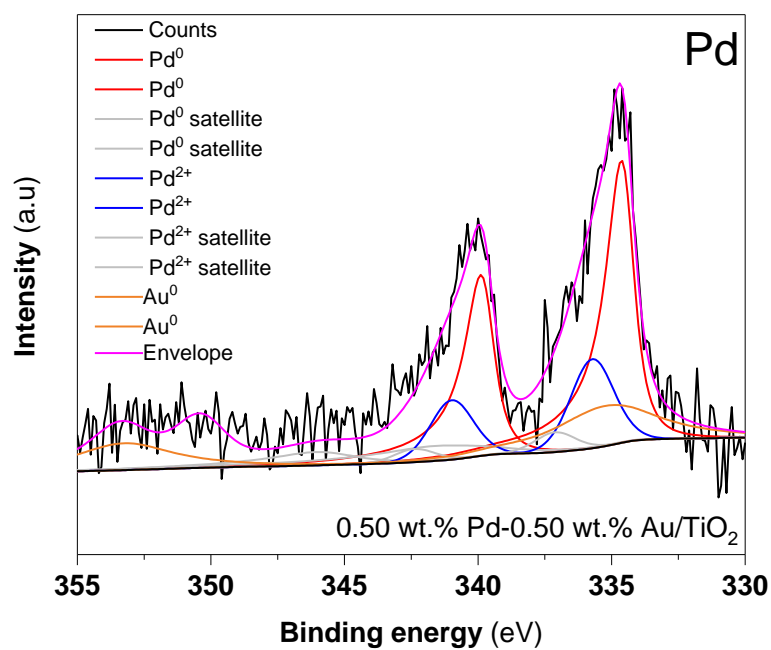


Figure S.I 3.6: XPS fitting for the fresh bi-metallic 0.50 wt.% Pd-0.50 wt.% Au/TiO<sub>2</sub> catalyst.

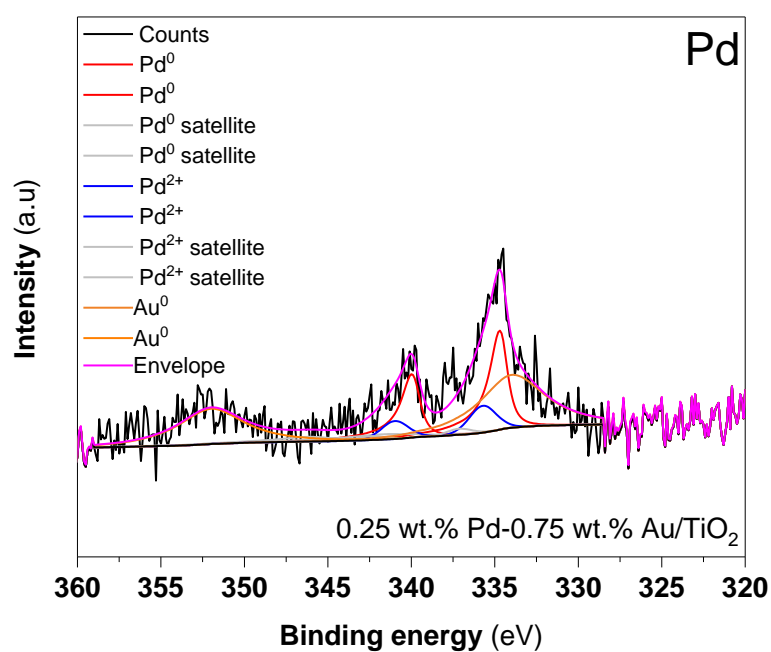


Figure S.I 3.7: XPS fitting for the fresh bi-metallic 0.25 wt.% Pd-0.75 wt.% Au/TiO<sub>2</sub> catalyst.

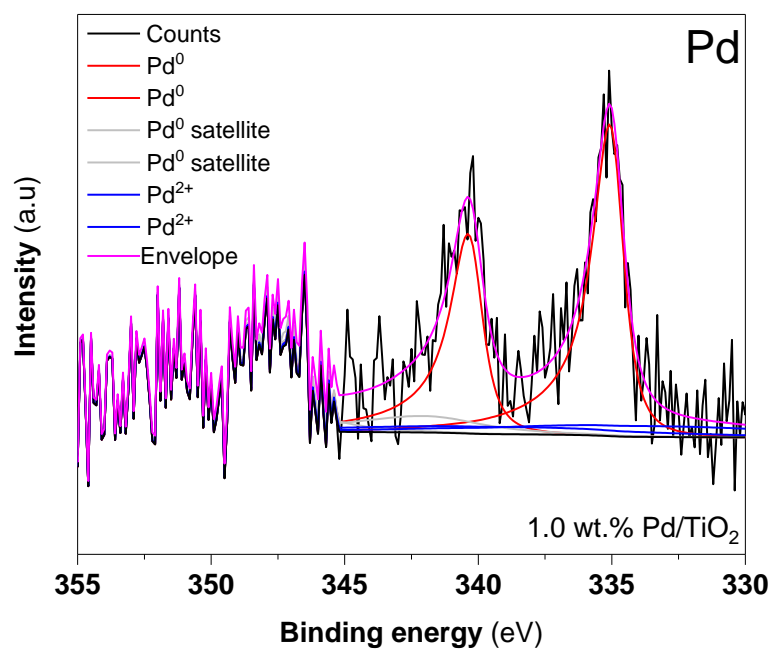


Figure S.I 3.8: XPS fitting for the used mono-metallic 1.0 wt.% Pd/TiO<sub>2</sub> catalyst.

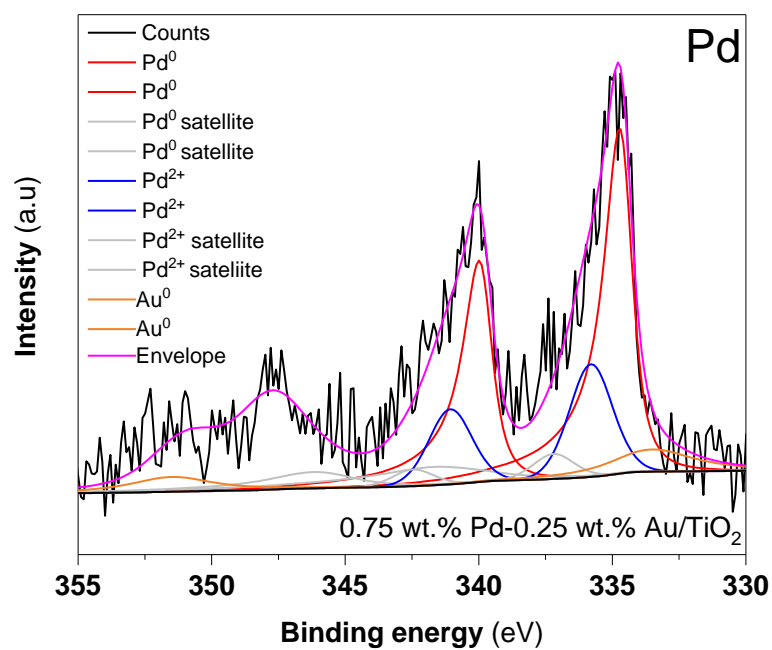


Figure S.I 3.9: XPS fitting for the used bi-metallic 0.75 wt.% Pd-0.25 wt.% Au/TiO<sub>2</sub> catalyst.

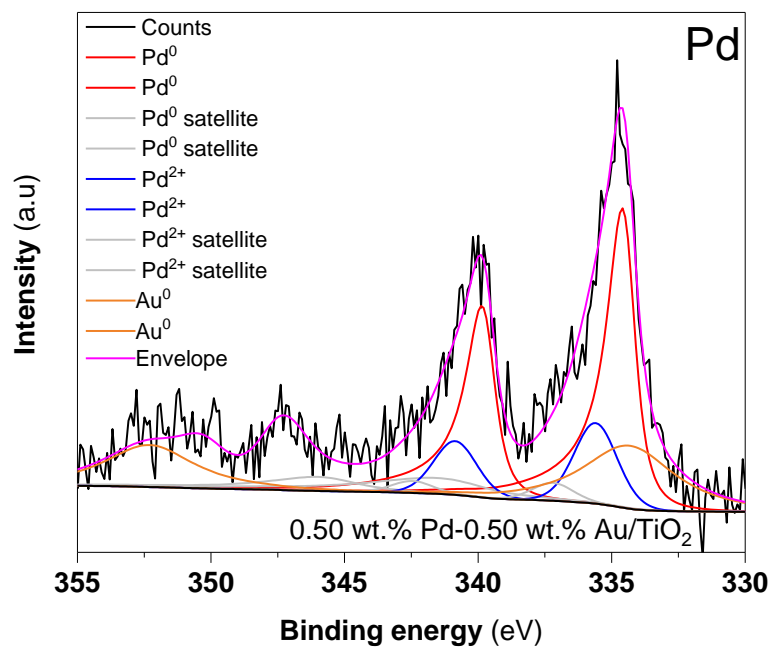


Figure S.I 3.10: XPS fitting for the used bi-metallic 0.50 wt.% Pd-0.50 wt.% Au/TiO<sub>2</sub> catalyst.

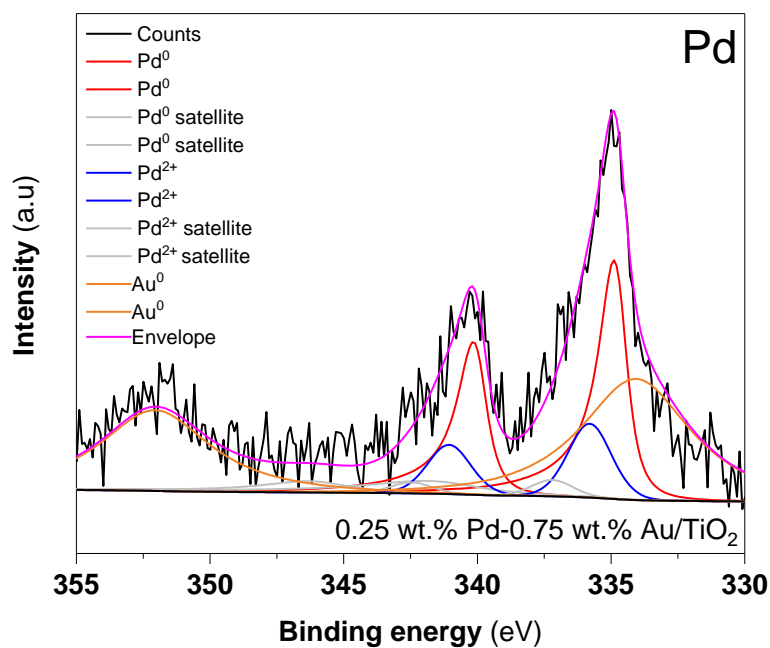


Figure fitting 3.11: XPS dfitting for the used bi-metallic 0.25 wt.% Pd-0.75 wt.% Au/TiO<sub>2</sub> catalyst.

# Chapter 4:

## Oxidation of phenol with FePd impregnated catalysts on TiO<sub>2</sub>.

### 4.1 Introduction.

The discharge of micropollutants and contaminants into the natural water cycle puts at risk the availability of potable water resources. It is estimated that around 4 billion people have no or little access to clean and sanitised water supply.<sup>1</sup> Industrial activities generate essential goods to improve human wellbeing such as electricity, medicines and clothing. However, the associated generation of waste, containing types of pollutants such as heavy metals, antibiotics and dyes endanger both human health and the environment.<sup>2,3,4,5</sup> Sodium hypochlorite (NaOCl) is globally the most widely used oxidant for water disinfection due to its low cost.<sup>6</sup> However, disinfection by-products (DBPs), known to cause detrimental effects on human health, are generated as a result of the reaction of chloride-based disinfectants with dissolved organic matter (DOM).<sup>6,7</sup> Thus, new advanced technologies for water remediation would be highly desirable to avoid the formation of DBPs.<sup>1,6,8</sup> Besides, they should be easily industrialised, affordable and accessible world-wide.

Homogeneous Fenton's oxidations, that involve pre-formed H<sub>2</sub>O<sub>2</sub> and iron salts such as iron sulphate (FeSO<sub>4</sub>), are already applied for water remediation.<sup>9</sup> At ambient temperature and pressure, Fenton's oxidations generate reactive oxygen species (ROS) (O<sub>2</sub><sup>•-</sup>, HO<sup>•</sup>, RO<sub>2</sub><sup>•</sup> and HOO<sup>•</sup>) that are more powerful oxidants than H<sub>2</sub>O<sub>2</sub> itself and chlorine or hypochlorite.<sup>10</sup> Fenton's type oxidations are a promising alternative, however, they require pH adjustments to maximise its oxidative effect and subsequent neutralisation, besides, the formation of Fe precipitates leads to the decay of the oxidation efficiency due to the Fe loss.<sup>11</sup> Thus, the immobilisation of the Fe metal would be a promising strategy in order to avoid its loss. This chapter aims to evaluate the efficiency in ROS generation from *in-situ* H<sub>2</sub>O<sub>2</sub> to degrade phenol at conditions more suitable for water remediation (30 °C and with H<sub>2</sub>O-only solvent with diluted phenol). Pd-based catalysts combined with a Fenton active metal such as Fe, Co, Cu and Au will be made by modified impregnation, to both synthesise H<sub>2</sub>O<sub>2</sub> and subsequently utilise it in water remediation via ROS formation over the Fenton metal.

A diluted phenol solution (1000 ppm) will be used as a model polluted water to test the catalysts (0.5 wt.% X-0.5 wt.% Pd/TiO<sub>2</sub> (X: Cu, Fe, Co, Au)) activity towards their efficiency in the oxidation of aromatics, which are regularly found in residual water effluents from industrial activities.<sup>8</sup> The catalysts activity, reported as phenol conversion, and the

selectivity towards the formation of phenol derivatives (catechol, resorcinol, 1,4-benzoquinone, hydroquinone) and di-acids  $\text{CO}_2$  and  $\text{H}_2\text{O}$ , will be determined by HPLC analysis (proposed phenol oxidation reaction pathway shown in Figure 4.1).<sup>12</sup> The activity of these catalysts towards the direct synthesis and degradation of  $\text{H}_2\text{O}_2$  will also be investigated to determine the correlation between both reactions; the extend of phenol conversion and formation/degradation of  $\text{H}_2\text{O}_2$ .

The post-reaction solution after the oxidation of phenol and direct synthesis of  $\text{H}_2\text{O}_2$  will be analysed by means of microwave plasma atomic emission spectroscopy (MP-AES) to determine the stability of the metals deposited on the  $\text{TiO}_2$ . X-ray diffraction (XRD) will be employed to provide an indication of nanoparticles size and the crystallinity of the  $\text{TiO}_2$  after the impregnation of the metal nanoparticles. Physisorption as well as the CO-diffuse reflectance infrared fourier transform spectroscopy (CO-DRIFTS) will be employed to determine the specific surface area and the configuration of the Pd and Fe metal species respectively. X-ray photoelectron spectroscopy (XPS) will be used to determine the oxidation state and the mean particle and size distributions by transmission electron microscopy (TEM), being the oxidation state and the mean particle size and distribution critical parameters to study in relation to the catalyst's activity towards the formation and degradation of  $\text{H}_2\text{O}_2$ .

The activity of each catalyst throughout this Chapter 4 is given by the mean value calculated from the results obtained from three different lots of the same catalysts. The mean activity value is accompanied by the standard deviation represented by error bars in each Figure and Table of catalytic results. If no error bars are shown next to the mean value given, this indicates that the catalytic activity was tested less than three times.

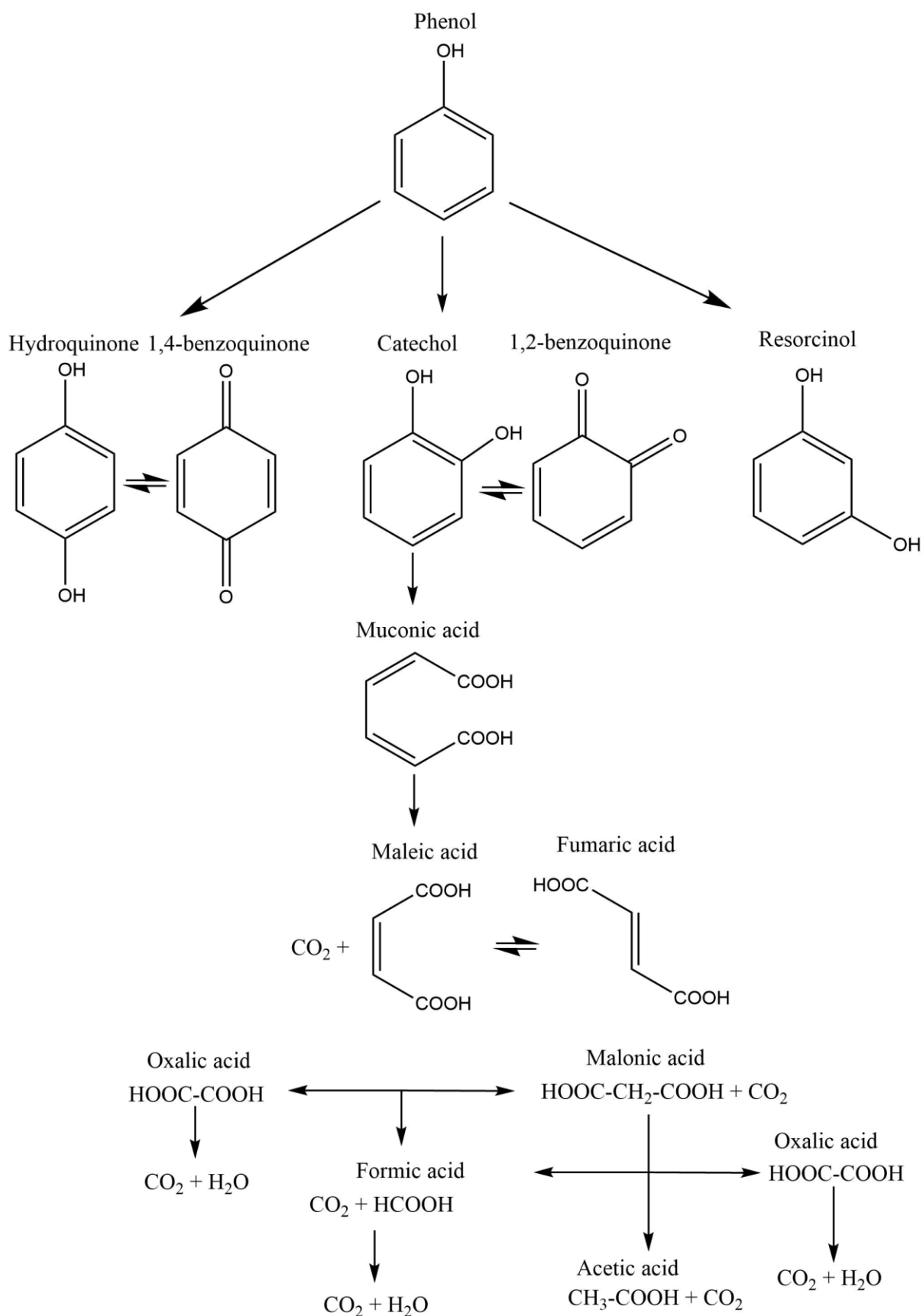


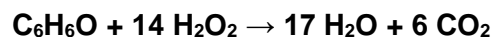
**Figure 4.1:** Schematic representation of the complete oxidation of phenol to CO<sub>2</sub> and H<sub>2</sub>O.<sup>12</sup> The products formed as a result of the oxidation of phenol were grouped in two; namely: phenol derivatives (catechol, hydroquinone, 1,4-benzoquinone and resorcinol) and others (di-acids, H<sub>2</sub>O and CO<sub>2</sub>).

## 4.2 Results and discussion.

### 4.2.1 Oxidation of phenol with pre-formed H<sub>2</sub>O<sub>2</sub>.

The oxidation of phenol with H<sub>2</sub>O<sub>2</sub> proceeds according to the chemical reaction shown in Equation 1 (Eq. 1).

#### Eq. 1



The required amount of pre-formed H<sub>2</sub>O<sub>2</sub> to oxidise 8.5 g of 1000 ppm of phenol was added to determine the oxidation effect of H<sub>2</sub>O<sub>2</sub>. (Table 4.1). The reaction was carried out under two different atmospheres, 580 psi of O<sub>2</sub>/CO<sub>2</sub> and 580 psi of N<sub>2</sub> to exclude if the CO<sub>2</sub> could be stabilising the H<sub>2</sub>O<sub>2</sub> precluding the oxidation of phenol. However, the activity (7 % and 3 %) was significantly low regardless of the atmosphere (O<sub>2</sub>/CO<sub>2</sub> or N<sub>2</sub>). These results go in line with previous reports that stated the inefficiency of H<sub>2</sub>O<sub>2</sub> to oxidise pollutants such as aromatics.<sup>13</sup>

**Table 4.1:** Oxidation of phenol with pre-formed H<sub>2</sub>O<sub>2</sub>.

Concentration of H <sub>2</sub> O <sub>2</sub>	Phenol conversion	Atmosphere
ppm	%	
182	7	O <sub>2</sub> /CO <sub>2</sub>
182	3	N <sub>2</sub>

**Reaction conditions:** 8.5 g Phenol (1000 ppm), pre-formed H<sub>2</sub>O<sub>2</sub> (182 ppm), 580 psi (25 % O<sub>2</sub>/CO<sub>2</sub> or N<sub>2</sub>), 1200 rpm, 30 °C, 2 h.

### 4.2.2 Oxidation of phenol using Fenton metals and pre-formed H<sub>2</sub>O<sub>2</sub>.

The conversion of H<sub>2</sub>O<sub>2</sub> (1.78 eV) to ROS by Fenton metals (Fe, Cu, Co) would produce species such as HO<sup>•</sup> (2.80 eV) that have a greater oxidation potential and could degrade phenol as it has been proved in previous results.<sup>14,15</sup> Thus, the oxidation of phenol was also tested with 0.005 g of 1.0 wt.% Fe/TiO<sub>2</sub> and pre-formed H<sub>2</sub>O<sub>2</sub> (Table 4.2). The activity was found to be significantly low even though the addition of Fe. However, Fe catalysts (c.a 1.5 wt.%) and pre-formed H<sub>2</sub>O<sub>2</sub> have been reported before to have high activity for the degradation of phenol (c.a 90 %).<sup>16,17,18</sup> In these instances, the amount of catalysts was higher (0.05,<sup>16</sup> 0.5,<sup>17</sup> 0.084,<sup>18</sup> g) with pre-formed H<sub>2</sub>O<sub>2</sub> concentration of 8,700,<sup>16</sup> 19,000,<sup>17</sup> 5,000,<sup>18</sup> ppm respectively in comparison to that used in this study (0.005 g, 31,353 ppm H<sub>2</sub>O<sub>2</sub>).

#### 4.2: Oxidation of phenol with pre-formed H<sub>2</sub>O<sub>2</sub> and mono-metallic 1 wt.% Fe/TiO<sub>2</sub> catalyst.

Concentration of H <sub>2</sub> O <sub>2</sub>	Phenol conversion
ppm	%
<b>647</b>	5
<b>6,4710</b>	10
<b>31,353</b>	3

**Reaction conditions:** Phenol (1000 ppm), catalyst (0.005 g), 420 psi 5 % H<sub>2</sub>/CO<sub>2</sub>, 160 psi 25 % O<sub>2</sub>/CO<sub>2</sub>, 1200 rpm, 30 °C, 2 h.

#### 4.2.3 Characterisation and activity of Pd-Fenton metals based catalysts towards the degradation of phenol, direct synthesis and degradation of H<sub>2</sub>O<sub>2</sub>.

A series of bi-metallic Fenton metal-Pd based catalysts (0.5 wt.% X-0.5 wt.% Pd/TiO<sub>2</sub>) (X: Cu, Co, Fe) were prepared following modified impregnation methodology.<sup>19</sup> Despite Au is not considered a Fenton metal, a bi-metallic 0.5 wt.% Pd-0.5 wt.% Au/TiO<sub>2</sub> catalyst was also prepared by the same synthetic procedure since it has shown to be active towards the direct synthesis of H<sub>2</sub>O<sub>2</sub> even at ambient temperatures.<sup>20</sup> All the catalysts showed the characteristic reflections arising from the TiO<sub>2</sub> (P25) (ICDD reference code 00-004-0477), indicating that the impregnation of the metals had not altered the support (Figure 4.2). No reflections associated with the others immobilised metals were observed, which could be attributed to the presence of small nanoparticles, as Sankar *et al.*, determined when studying the bi-metallic 0.5 wt.% Au-0.5 wt.% Pd/TiO<sub>2</sub> catalyst, identical to that studied in this work.<sup>19</sup> Table 4.3 shows key XRD reflections for the metallic Fe, Cu, Pd, Cu, Co and Au as well as a few of their oxide composites for reference.

**Table 4.3:** Key reflections and miller indices (h k l) for metallic Au, Pd, Fe, Cu and Co as well as a few of their oxide composites.

Metals	Reflections (Miller index (h k l))
<b>Au</b> <sup>21,22</sup>	38.2 ° (111), 45 ° (200), 65 ° (220), 78 ° (311), 82 ° (222)
<b>Pd</b> <sup>23</sup>	40 ° (111), 46 ° (200), 78 ° (220), 83 ° (311)
<b>PdO</b> <sup>24</sup>	35 ° (101), 42 ° (110), 56 ° (112), 61 ° (103), 63 ° (200)
<b>Metallic Fe (Fe<sup>0</sup>)</b> <sup>25</sup>	46 ° (110), 65 ° (200), 82 ° (211),
<b>Iron oxide (III) (FeO)</b> <sup>26</sup>	35 °(111), 42 ° (200), 62 °(220)
<b>Iron oxide (III) (Fe<sub>2</sub>O<sub>3</sub>)</b> <sup>27,28</sup>	25 °(012), 33 ° (104), 36 °(110), 41 °(113), 49 °(024), 55 °(116), 58 °(018), 63 °(214), 65 °(300)
<b>Iron oxide (IV) (Fe<sub>3</sub>O<sub>4</sub>)</b> <sup>29</sup>	32 °(220), 39 ° (222), 45 °(400), 65 °(440)
<b>Copper metallic (Cu<sup>0</sup>)</b> <sup>30</sup>	36 ° (-111), 43 ° (111), 50 ° (200), 74 ° (220)
<b>Copper oxide (CuO)</b> <sup>31,32</sup>	33 ° (110), 36 ° (002), 39 ° (111), 49 ° (-202), 54 ° (020), 62 ° (-113), 66 ° (-311), 68 ° (220)
<b>Cobalt metallic (Co<sup>0</sup>)</b> <sup>33,34</sup>	42 ° (100), 45 ° (002), 48 ° (101), 52 ° (200), 62 ° (102), 78 ° (110)
<b>Cobalt oxides (II) (CoO)</b> <sup>35,36</sup>	36 ° (111), 42 ° (200), 62 ° (220),
<b>Cobalt oxide (III) (Co<sub>2</sub>O<sub>3</sub>)</b> <sup>35,34</sup>	31 ° (220), 37 ° (311), 38 ° (222), 45 ° (400) 55 ° (422), 60 ° (511), 65 ° (440), 76 ° (533)

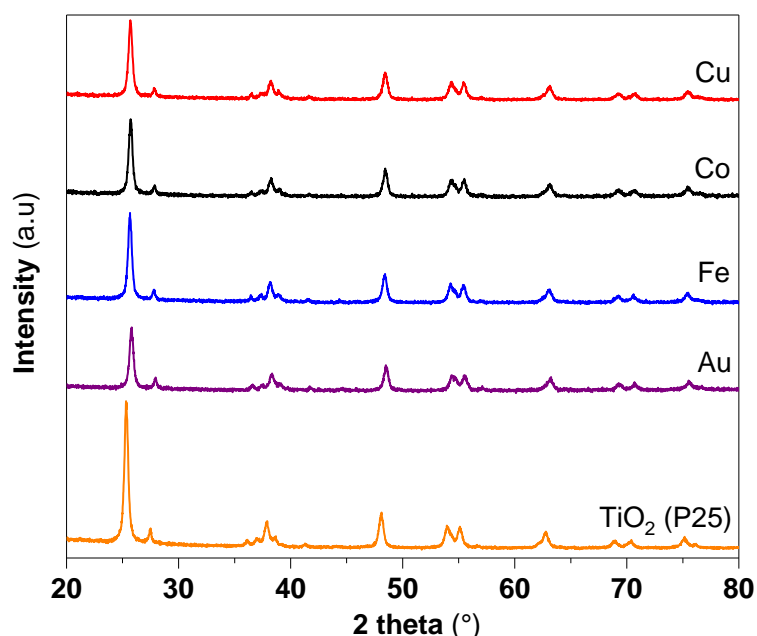


**Figure 4.2:** XRD diffractogram for the bi-metallic 0.5 wt.% X-0.5 wt.% Pd/TiO<sub>2</sub> (X: Cu, Co, Fe, Au) catalysts.

This set of bi-metallic (0.5 wt.% X-0.5 wt.% Pd/TiO<sub>2</sub>) (X: Cu, Co, Fe, Au) and mono-metallic 1 wt.% Pd/TiO<sub>2</sub> catalysts were first investigated for their efficacy towards the direct synthesis and degradation of H<sub>2</sub>O<sub>2</sub> at two sets of reaction conditions; *i*) using sub-ambient temperatures (2 °C) and with organic co-solvent with H<sub>2</sub>O (67 % CH<sub>3</sub>OH in H<sub>2</sub>O), termed sub-ambient conditions (Table 4.4) and *ii*) *c.a* ambient temperatures (25 °C) without organic solvents, termed ambient conditions (Table 4.5). The bi-metallic 0.5 wt.% Au-0.5 wt.% Pd/TiO<sub>2</sub> and mono-metallic 1 wt.% Pd/TiO<sub>2</sub> catalysts presented the most dramatic change in activity between both sets of conditions. For instance, while under sub-ambient conditions the bi-metallic 0.5 wt.% Au-0.5 wt.% Pd/TiO<sub>2</sub> catalyst had a productivity of 97 mol<sub>H<sub>2</sub>O<sub>2</sub></sub>kg<sup>-1</sup><sub>cat</sub>h<sup>-1</sup> and H<sub>2</sub>O<sub>2</sub> degradation of 279 mol<sub>H<sub>2</sub>O<sub>2</sub></sub>kg<sup>-1</sup><sub>cat</sub> h<sup>-1</sup>, under ambient conditions, the productivity decreased while the degradation raised (31 productivity mol<sub>H<sub>2</sub>O<sub>2</sub></sub>kg<sup>-1</sup><sub>cat</sub>h<sup>-1</sup>, 932 degradation mol<sub>H<sub>2</sub>O<sub>2</sub></sub>kg<sup>-1</sup><sub>cat</sub>h<sup>-1</sup>). This behaviour has been previously seen in Chapter 3, where it was shown that the activity of bi-metallic 0.5 wt.% Au-0.5 wt.% Pd/TiO<sub>2</sub> catalyst towards the direct synthesis of H<sub>2</sub>O<sub>2</sub> decayed while approaching ambient temperatures (25 °C) and using H<sub>2</sub>O-only as solvent. H<sub>2</sub> is less soluble in water than in CH<sub>3</sub>OH, thus, the productivity of H<sub>2</sub>O<sub>2</sub> for 0.5 wt.% Au-0.5 wt.% Pd/TiO<sub>2</sub> catalyst with H<sub>2</sub>O-only as solvent is expected to be lower than in organic solvents or mixtures of organic solvents with water. In additions to this, ambient temperatures enhance the H<sub>2</sub>O<sub>2</sub> decomposition. Thus, working at ambient temperatures will result in increased H<sub>2</sub>O<sub>2</sub> decomposition and in a decrease in the net H<sub>2</sub>O<sub>2</sub> synthesis rates, compared to sub-ambient temperatures.<sup>20</sup>

Another interesting fact is that the bi-metallic combinations of 0.5 wt.% X-0.50 wt.% Pd/TiO<sub>2</sub> (X: Fe, Cu, Co) had lower productivity than the mono-metallic 1 wt.% Pd/TiO<sub>2</sub> and bi-metallic 0.50 wt.% Au-0.50 wt.% Pd/TiO<sub>2</sub> catalysts regardless of the reaction temperature and the type of solvent used. The low activity during the direct synthesis of H<sub>2</sub>O<sub>2</sub> of the bi-metallic 0.5 wt.% X-0.50 wt.% Pd/TiO<sub>2</sub> (X: Fe, Cu, Co) catalysts was first thought to be associated with the ability of Fe, Cu, or Co to catalyse the degradation of H<sub>2</sub>O<sub>2</sub>. Surprisingly, their degradation activity was also relatively low in both sets of reaction conditions (Table 4.4 and Table 4.5), in comparison to the mono-metallic 1 wt.% Pd/TiO<sub>2</sub> and bi-metallic 0.50 wt.% Au-0.50 wt.% Pd/TiO<sub>2</sub> catalysts.

Crombie *et al.*, also investigated the direct synthesis and degradation of H<sub>2</sub>O<sub>2</sub> at 20 °C with CH<sub>3</sub>OH and water as a solvent using bi-metallic Fenton metal-Pd based catalysts impregnated on TiO<sub>2</sub> (0.5 wt.% X-0.5 wt.% Pd/TiO<sub>2</sub>) (X: V, Mn, Fe, Co, Ni, Cu, Au, Ce) by an analogous modified impregnation procedure.<sup>37</sup> Similar to this work, they reported that the bi-metallic 0.5 wt.% Au-0.5 wt.% Pd/TiO<sub>2</sub> had the highest H<sub>2</sub>O<sub>2</sub> synthesis and degradation activity in comparison to the other bi-metallic combinations.<sup>37</sup> They concluded that the oxidation state of the Pd upon the introduction of a secondary metal could be the

reason to explain this trend. They reported that, the introduction of the secondary metal (with the exception of Au), had formed mixed domains of palladium oxide (PdO) and palladium metallic (Pd<sup>0</sup>) which were ascribed to offer lower activity towards the degradation of H<sub>2</sub>O<sub>2</sub>.<sup>37</sup>

**Table 4.4:** Catalytic activity towards the direct synthesis and degradation of H<sub>2</sub>O<sub>2</sub> using 0.5 wt.% X-0.5 wt.% Pd/TiO<sub>2</sub> (X: Au, Fe, Cu, Co) and 1 wt.% Pd/TiO<sub>2</sub> catalysts at sub-ambient conditions.

Catalysts	Productivity	Degradation
	mol <sub>H<sub>2</sub>O<sub>2</sub></sub> kg <sub>cat</sub> <sup>-1</sup> h <sup>-1</sup> (S.D)	mol <sub>H<sub>2</sub>O<sub>2</sub></sub> kg <sub>cat</sub> <sup>-1</sup> h <sup>-1</sup> (SD)
0.5 wt.% Au-0.50 wt.% Pd/TiO <sub>2</sub>	97 ± (6)	279 ± (22)
0.5 wt.% Fe-0.50 wt.% Pd/TiO <sub>2</sub>	40 ± (2)	50 ± (4)
0.5 wt.% Cu-0.50 wt.% Pd/TiO <sub>2</sub>	12 ± (2)	83 ± (6)
0.5 wt.% Co-0.50 wt.% Pd/TiO <sub>2</sub>	39 ± (6)	114 ± (5)
1.0 wt.% Pd/TiO <sub>2</sub>	83 ± (4)	511 ± (26)

(S.D): standard deviation. **Reaction conditions: Direct synthesis towards H<sub>2</sub>O<sub>2</sub>:** 8.5 g (5.6 g CH<sub>3</sub>OH, 2.9 g HPLC grade water), catalyst (0.01 g), 420 psi 5 % H<sub>2</sub>/CO<sub>2</sub>, 160 psi 25 % O<sub>2</sub>/CO<sub>2</sub>, 1200 rpm, 2 °C, 0.5 h. **Degradation of H<sub>2</sub>O<sub>2</sub>:** 8.5 g (0.68 g H<sub>2</sub>O<sub>2</sub>, 5.6 g CH<sub>3</sub>OH 2.22 g H<sub>2</sub>O), catalyst (0.01 g), 420 psi 5 % H<sub>2</sub>/CO<sub>2</sub>, 1200 rpm, 2 °C, 0.5 h.

**Table 4.5:** Catalytic activity towards the direct synthesis and degradation of H<sub>2</sub>O<sub>2</sub> using 0.5 wt.% X-0.5 wt.% Pd/TiO<sub>2</sub> (X: Au, Fe, Cu, Co) and 1 wt.% Pd/TiO<sub>2</sub> catalysts at ambient conditions.

Catalysts	Productivity	Degradation
	mol <sub>H<sub>2</sub>O<sub>2</sub></sub> kg <sub>cat</sub> <sup>-1</sup> h <sup>-1</sup> (S.D)	mol <sub>H<sub>2</sub>O<sub>2</sub></sub> kg <sub>cat</sub> <sup>-1</sup> h <sup>-1</sup> (S.D)
0.5 wt.% Au-0.50 wt.% Pd/TiO <sub>2</sub>	31 ± (3)	932 ± (24)
0.5 wt.% Fe-0.50 wt.% Pd/TiO <sub>2</sub>	24 ± (2)	671 ± (20)
0.5 wt.% Cu-0.50 wt.% Pd/TiO <sub>2</sub>	6 ± (1)	355 ± (15)
0.5 wt.% Co-0.50 wt.% Pd/TiO <sub>2</sub>	14 ± (2)	665 ± (9)
1.0 wt.% Pd/TiO <sub>2</sub>	25 ± (3)	1545 ± (65)

(S.D): standard deviation. **Reaction conditions: Direct synthesis towards H<sub>2</sub>O<sub>2</sub>:** 8.5 g (HPLC grade water), catalyst (0.01 g), 420 psi 5 % H<sub>2</sub>/CO<sub>2</sub>, 160 psi 25 % O<sub>2</sub>/CO<sub>2</sub>, 1200 rpm, 30 °C, 0.5 h. **Degradation of H<sub>2</sub>O<sub>2</sub>:** 8.5 g (0.68 g H<sub>2</sub>O<sub>2</sub>, 7.82 g HPLC grade water), catalyst (0.01 g), 420 psi 5 % H<sub>2</sub>/CO<sub>2</sub>, 1200 rpm, 30 °C, 0.5 h.

XPS was used to determine the oxidation state of supported mono and bi-metallic catalysts shown in Table 4.4 and Table 4.5. The ratio between palladium and the secondary metal (Pd: X) was also calculated since it can give an estimation of the proportion of Pd on the surface for each catalyst (Table 4.6). The addition of a secondary metal to Pd (0.5 wt.% X-0.5 wt.% Pd/TiO<sub>2</sub> (X: Au, Fe, Cu, Co)) had influenced its oxidation state, oxidising the Pd<sup>0</sup> to PdO in comparison to the mono-metallic 1.0 wt.% Pd/TiO<sub>2</sub> catalyst. No significant difference in the oxidation state of the Pd between the bi-metallic 0.5 wt.% X-0.5 wt.%

Pd/TiO<sub>2</sub> (X: Au, Fe, Cu, Co) ones were seen as it would be expected due to the difference in activity they had during the direct synthesis and degradation of H<sub>2</sub>O<sub>2</sub> (Table 4.4 and 4.5 respectively). Therefore, this indicated that other physical characteristics such as the nanoparticle's size and composition as well as its dispersion could have played a drive role in determining the activity of these bi-metallic 0.5 wt.% X-0.5 wt.% Pd/TiO<sub>2</sub> (X: Au, Fe, Cu, Co) catalysts.

The ratio between the Pd and the secondary metal (Pd: X) determined that 0.5 wt.% Cu-0.5 wt.% Pd/TiO<sub>2</sub> and 0.5 wt.% Au-0.5 wt.% Pd/TiO<sub>2</sub> had the greater proportion of Pd on the surface in comparison to the other two bi-metallic 0.5 wt.% X-0.5 wt.% Pd/TiO<sub>2</sub> (X: Co, Fe) catalysts. Hutchings and co-workers<sup>38</sup> determined that Cu poisons the active sites of Pd since a tri-metallic 2.5 wt.% Au-2.5 wt.% Pd-1.0 wt.% Cu/TiO<sub>2</sub> (11 mol<sub>H<sub>2</sub>O<sub>2</sub></sub> kg<sub>cat</sub><sup>-1</sup> h<sup>-1</sup>) catalyst presented lower activity during the direct synthesis of H<sub>2</sub>O<sub>2</sub> in comparison to the bi-metallic 2.5 wt.% Au-2.5 wt.% Pd/TiO<sub>2</sub> (85 mol<sub>H<sub>2</sub>O<sub>2</sub></sub> kg<sub>cat</sub><sup>-1</sup> h<sup>-1</sup>) analogue.<sup>38</sup> This may be the reason why the bi-metallic 0.5 wt.% Cu-0.5 wt.% Pd/TiO<sub>2</sub> catalyst had low activity towards the direct synthesis and subsequent degradation of H<sub>2</sub>O<sub>2</sub>. It can also be pointed out that the presence of Au made excelled the activity of Pd during the direct synthesis and degradation of H<sub>2</sub>O<sub>2</sub>, despite the bi-metallic 0.5 wt.% Au-0.5 wt.% Pd/TiO<sub>2</sub> catalyst presented similar Pd: X ratio than 0.5 wt.% Fe-0.5 wt.% Pd/TiO<sub>2</sub> analogue. This is another indication of how the activity of Pd can be changed due to the addition of a second metal such as Au or Fe, or even have its activity blocked by the addition of Cu.

**Table 4.6:** XPS analysis of the bi-metallic 0.5 wt.% X-0.5 wt.% Pd/TiO<sub>2</sub> (X: Au, Fe, Cu, Co) catalysts.

Catalysts	PdO	Pd <sup>0</sup>	Pd: X
Theoretical metal loading	%	%	
<b>0.50 wt.%Au-0.50 wt.%Pd/TiO<sub>2</sub></b>	22	78	1.2
<b>0.50 wt.%Fe-0.50 wt.%Pd/TiO<sub>2</sub></b>	32	68	0.9
<b>0.50 wt.%Cu-0.50 wt.%Pd/TiO<sub>2</sub></b>	21	79	2.4
<b>0.50 wt.%Co-0.50 wt.%Pd/TiO<sub>2</sub></b>	21	79	0.4
<b>1.0 wt.% Pd/TiO<sub>2</sub></b>	10	90	n.a

**n.a:** not applicable. **Heat treatment:** 5 % H<sub>2</sub>/Ar, 400 °C, 10 °C/min, 4 h. XPS spectra for mono and bi-metallic 0.50 wt.% X-0.50 wt.% Pd/TiO<sub>2</sub> (X: Co, Cu) catalysts are shown in supplementary information, Figure S.I 4.1-4.3 and Figure S.I 4.5.

The set of bimetallic catalysts were tested for the degradation of phenol by generating *in-situ* H<sub>2</sub>O<sub>2</sub> at 30 °C and using water as an only solvent (Figure 4.3). The bi-metallic 0.5 wt.% Fe-0.5 wt.% Pd/TiO<sub>2</sub> catalyst had the most promising activity towards the degradation of phenol (37 %), followed by 0.5 wt.% Cu-0.5 wt.% Pd/TiO<sub>2</sub> (6 %), 0.5 wt.% Co-0.5 wt.% Pd/TiO<sub>2</sub> (6 %) and 0.5 wt.% Au-0.5 wt.% Pd/TiO<sub>2</sub> (5 %).

The bi-metallic 0.5 wt.% Au-0.5 wt.% Pd/TiO<sub>2</sub> catalyst gave the highest productivities of H<sub>2</sub>O<sub>2</sub> at 30 °C (Table 4.4) (31 mol<sub>H<sub>2</sub>O<sub>2</sub></sub> kg<sub>cat</sub><sup>-1</sup> h<sup>-1</sup>). However, due to the high degradation activity of H<sub>2</sub>O<sub>2</sub> (932 mol<sub>H<sub>2</sub>O<sub>2</sub></sub> kg<sub>cat</sub><sup>-1</sup> h<sup>-1</sup>) and the low activity of phenol conversion (5 %) this catalyst presented, led to conclude that most of the *in-situ* H<sub>2</sub>O<sub>2</sub> formed could have been degraded, mostly decomposed to H<sub>2</sub>O because the H<sub>2</sub> conversion shown in Figure 4.3 was relatively low (c.a 10 %). Surprisingly, the bi-metallic 0.5 wt.% Cu-0.5 wt.% Pd/TiO<sub>2</sub> (c.a 40 % H<sub>2</sub> conversion) and 0.5 wt.% Co-0.5 wt.% Pd/TiO<sub>2</sub> (c.a 50 % H<sub>2</sub> conversion) catalysts presented relatively high rates of H<sub>2</sub> conversion in comparison to the bi-metallic 0.5 wt.% Fe-0.5 wt.% Pd/TiO<sub>2</sub> (c.a 30 % H<sub>2</sub> conversion) catalyst despite the CuPd and CoPd formulations did not offer significant activity towards the oxidation of phenol (6 % both) or towards the formation or degradation of H<sub>2</sub>O<sub>2</sub> (CuPd (formation of H<sub>2</sub>O<sub>2</sub> (6 mol<sub>H<sub>2</sub>O<sub>2</sub></sub> kg<sub>cat</sub><sup>-1</sup> h<sup>-1</sup>) degradation of H<sub>2</sub>O<sub>2</sub> (355 mol<sub>H<sub>2</sub>O<sub>2</sub></sub> kg<sub>cat</sub><sup>-1</sup> h<sup>-1</sup>) and CoPd (formation of H<sub>2</sub>O<sub>2</sub> (14 mol<sub>H<sub>2</sub>O<sub>2</sub></sub> kg<sub>cat</sub><sup>-1</sup> h<sup>-1</sup>) degradation of H<sub>2</sub>O<sub>2</sub> (665 mol<sub>H<sub>2</sub>O<sub>2</sub></sub> kg<sub>cat</sub><sup>-1</sup> h<sup>-1</sup>)). What this suggested was that both bi-metallic catalysts 0.5 wt.% Cu-0.5 wt.% Pd/TiO<sub>2</sub> and 0.5 wt.% Co-0.5 wt.% Pd/TiO<sub>2</sub> could have had formed *in-situ* H<sub>2</sub>O<sub>2</sub>, but it could have been degraded to H<sub>2</sub>O rather than being converted into ROS. Therefore, what it seems this data to suggest is that the Fe is more selective to convert *in-situ* H<sub>2</sub>O<sub>2</sub> into ROS in comparison to Co, Cu or Au, and that the conversion of phenol is an indirect measurement of the efficiency of the catalyst to have had formed ROS.

The selectivity of phenol derivatives (catechol, resorcinol, hydroquinone, 1,4-benzoquinone) and di-acids, CO<sub>2</sub> and H<sub>2</sub>O (others) are shown in Figure 4.3. Bi-metallic 0.5 wt.% Fe-0.5 wt.% Pd/TiO<sub>2</sub> catalyst showed the best activity towards phenol conversion as well as selectivity towards others, indicating that phenol derivatives were successfully oxidised to di-acids, CO<sub>2</sub> and H<sub>2</sub>O. It is important that the oxidation of phenol is fully completed to CO<sub>2</sub> and H<sub>2</sub>O, oxidising any product in between, especially the phenol derivatives, which are considered as toxic as phenol itself.<sup>8</sup>

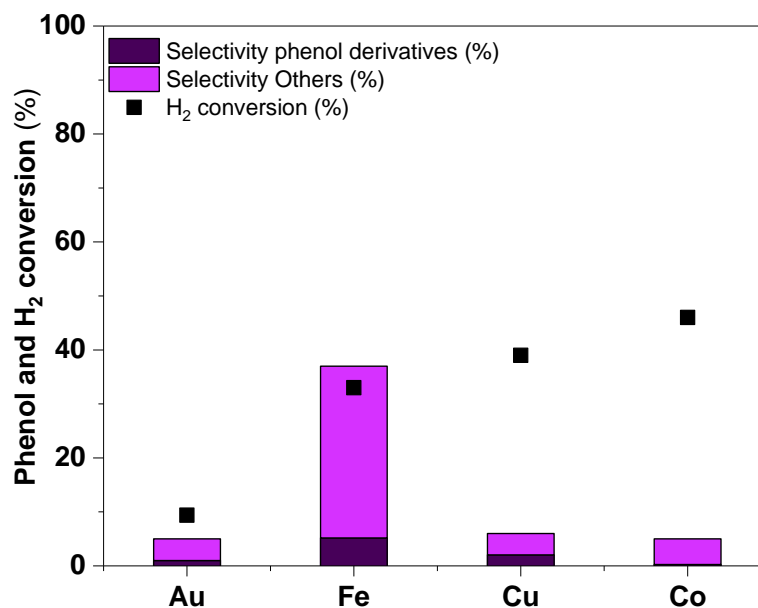


**Figure 4.3:** Degradation of phenol using bi-metallic 0.5 wt.% X-0.5 wt.% Pd/TiO<sub>2</sub> (X: Au, Fe, Cu, Co) catalysts. **Nomenclature:** Phenol derivatives (catechol, resorcinol, 1,4-benzoquinone and hydroquinone) and Others (di-acids, CO<sub>2</sub> and H<sub>2</sub>O). **Reaction conditions:** 8.5 g (1000 ppm Phenol), catalyst (0.01 g), 420 psi 5 % H<sub>2</sub>/CO<sub>2</sub>, 160 psi 25 % O<sub>2</sub>/CO<sub>2</sub>, 1200 rpm, 30 °C, 2 h.

Unfortunately, the residual H<sub>2</sub>O<sub>2</sub> could not be detected since the post-reaction solution were coloured and as such it was not possible to titrate the solution with ceria sulphate (Ce (SO<sub>4</sub>)<sub>2</sub>) and ferroin as described in Chapter 2 (section 2.3.1.1). The detection of H<sub>2</sub>O<sub>2</sub> has been previously carried out by means of ultraviolet-visible spectrscopy (UV-Vis) chelating the H<sub>2</sub>O<sub>2</sub> with potassium titanium (IV).<sup>39</sup> However, the coloration of the solution after the degradation of phenol to phenolic derivatives also precluded H<sub>2</sub>O<sub>2</sub> determination by this procedure.<sup>39</sup> However, Crombie *et al.*, had previously detected *in-situ* H<sub>2</sub>O<sub>2</sub> formation at 50 °C with mixtures of CH<sub>3</sub>OH and water as solvent employing mono-metallic 1 wt.% Pd/TiO<sub>2</sub> and bi-metallic 0.5 wt.% Au-0.5 wt.% Pd/TiO<sub>2</sub> and 0.5 wt.% Fe-0.5 wt.% Pd/TiO<sub>2</sub> catalysts (with analogues synthetic methodologies) over the course of 2 h reaction for the oxidation of benzyl alcohol.<sup>40</sup>

#### 4.2.4 Characterisation of the mono and bi-metallic 1 wt.% FePd/TiO<sub>2</sub> catalysts.

It was determined that the most promising Fenton metal to convert *in-situ* H<sub>2</sub>O<sub>2</sub> into ROS was the Fe, where the bi-metallic 0.50 wt.% Fe-0.50 wt.% Pd/TiO<sub>2</sub> offered *c.a* 40 % phenol conversion in comparison to the others Fenton metals. This observation was also evidenced by Hutchings and co-workers,<sup>15</sup> who had previously reported that bi-metallic 2.5 wt.% Fe-2.5 wt.% Pd/TiO<sub>2</sub> catalyst greatly outperformed (78 % phenol conversion) alternative combinations (2.5 wt.% Pd-2.5 wt.% X/TiO<sub>2</sub> (X; Mn, Cu, Au) with these others offering limited activity (*c.a* 5 % phenol conversion).<sup>15</sup> However, the bi-metallic 2.5 wt.% Fe-2.5 wt.% Pd/TiO<sub>2</sub> catalyst that they reported also showed to be instable, having the Fe leached at the end of the reaction. Lowering the metal loading and stablishing an optimum Fe:Pd ratio

could lead to a greater dispersion of the metals, and it may improve the activity and stability. Thus, this part of the chapter aims to find the best Fe:Pd ratio in relation to both; the *in-situ* formation of H<sub>2</sub>O<sub>2</sub> and phenol conversion as well as the best combination in relation to the stability of the Fe and Pd. Were stability is found, Au would be finally introduced to the most optimum Fe:Pd ratio to lower the degradation of H<sub>2</sub>O<sub>2</sub> into H<sub>2</sub>O.

Table 4.7 presents the set of bi-metallic 1.0 wt.% FePd/TiO<sub>2</sub> catalysts prepared by modified impregnation that will be investigated in this section of Chapter 4. The metal loading of the bi-metallic 1.0 wt.% FePd/TiO<sub>2</sub> catalysts were successfully established by aqua-regia digestion and MP-AES analysis as explained in chapter 2 section 2.2.3.1.

**Table 4.7:** Determination of the metal loading for the mono and bi-metallic 1.0 wt.% FePd/TiO<sub>2</sub> catalysts by digestion with aqua regia and subsequent analysis by MP-AES.

Catalysts formulation	Actual Fe loading	Actual Pd loading
	wt.% (S.D)	wt.% (S.D)
1.0 wt.% Fe/TiO <sub>2</sub>	0.81 ± 0.06	n.a
0.75 wt.% Fe-0.25 wt.% Pd/TiO <sub>2</sub>	0.73 ± 0.01	0.27 ± 0.01
0.5 wt.% Fe - 0.5 wt.% Pd/TiO <sub>2</sub>	0.42 ± 0.04	0.58 ± 0.04
0.25 wt.% Fe-0.75 wt.% Pd/TiO <sub>2</sub>	0.24 ± 0.01	0.76 ± 0.01
1.0 wt.% Pd/TiO <sub>2</sub>	n.a	0.91 ± 0.03

(S.D): standard deviation. n.a: not applicable.

XRD analysis of the mono and bi-metallic ratios 1.0 wt.% PdFe/TiO<sub>2</sub> catalysts were conducted to estimate the size of the particles deposited on the surface of the TiO<sub>2</sub> (Figure 4.4). The characteristic reflections of the TiO<sub>2</sub> (P25) were seen in each catalyst (ICDD reference code 00-004-0477), besides, a small reflection arose from the mono-metallic 1 wt.% Pd/TiO<sub>2</sub> and bi-metallic 0.25 wt.% Fe-0.75 wt.% Pd/TiO<sub>2</sub> catalyst at 2θ= 40.1° that could correspond to Pd<sup>0</sup>.<sup>23</sup>

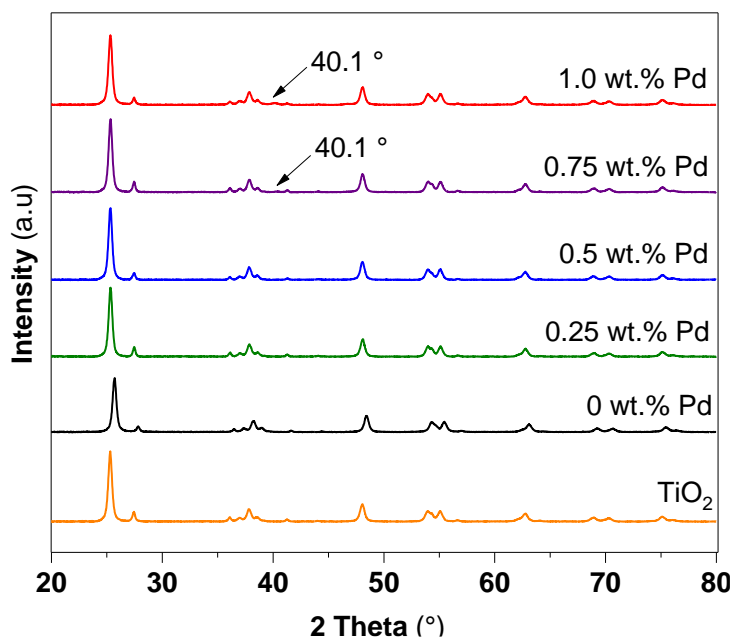


**Figure 4.4:** XRD diffractograms for mono and bi-metallic 1.0 wt.% FePd/TiO<sub>2</sub> catalysts.

The XPS of each photoelectron peak of the mono-metallic 1.0 wt.% Pd/TiO<sub>2</sub> and bi-metallic 1.0 wt.% FePd/TiO<sub>2</sub> catalysts were deconvoluted according to the oxidation state of the Pd in order to determine the percentage of Pd<sup>0</sup> and PdO as well as the Pd: Fe ratio (Table 4.8). The XPS of the Fe for the mono-metallic 1.0 wt.% Fe/TiO<sub>2</sub> catalyst and the three bi-metallic 1.0 wt.% FePd/TiO<sub>2</sub> ones determined that the Fe was present as an oxide form (Fe<sub>x</sub>O<sub>y</sub> such as FeO, Fe<sub>2</sub>O<sub>3</sub>, Fe<sub>3</sub>O<sub>4</sub>). Increasing Fe content led to an increase in PdO, which indicated that the activity towards the direct synthesis and/or degradation of H<sub>2</sub>O<sub>2</sub> may vary between these set of mono and bi-metallic 1.0 wt.% FePd/TiO<sub>2</sub> catalysts. The XPS also calculated the metal wt.% loading of Fe and Pd that was found to be very close to the experimental metal loadings shown in Table 4.7.

**Table 4.8:** XPS analysis of the mono and bi-metallic 1.0 wt.% FePd/TiO<sub>2</sub> catalysts.

Catalysts	PdO	Pd <sup>0</sup>	Pd: Fe	Pd	Fe
	%	%		wt.%	wt.%
1.0 wt.% Fe/TiO <sub>2</sub>	n.a	n.a	n.a		100
0.75 wt.% Fe-0.25 wt.% Pd/TiO <sub>2</sub>	61	39	0.3	25	75
0.5 wt.% Fe - 0.5 wt.% Pd/TiO <sub>2</sub>	32	68	0.9	46	54
0.25 wt.% Fe-0.75 wt.% Pd/TiO <sub>2</sub>	13	87	1.6	61	39
1.0 wt.% Pd/TiO <sub>2</sub>	10	90	n.a	100	

**n.a:** not applicable. **Heat treatment:** 5 % H<sub>2</sub>/Ar, 400 °C, 10 °C/min, 4 h. XPS spectra for the mono- and bi-metallic 1.0 wt.% FePd/TiO<sub>2</sub> catalysts are shown in supplementary information, Figure S.I 4.3-4.7.

TEM was used to determine the particle size and distribution of the supported metal catalysts. No particles were seen in neither of both mono-metallic 1.0 wt.% Fe/TiO<sub>2</sub> and 1.0 wt.% Pd/TiO<sub>2</sub> catalysts, indicating that the particles were smaller than the 1 nm and forming a mono layer with high metal dispersion. Likewise, the bi-metallic 1.0 wt.% FePd/TiO<sub>2</sub> catalysts did not present enough particles and thus it was concluded that most of the Fe and Pd were forming clusters smaller than 1 nm. The TEM images for the set of mono and bi-metallic 1.0 wt.% FePd/TiO<sub>2</sub> catalysts are shown in the supplementary information (Figure S.I 4.8). The energy-dispersive x-ray spectroscopy (EDX) elemental analysis corroborated the presence of the metals on the surface of the TiO<sub>2</sub> (Table S.I 4.1-4.5). However, the wt.% metal calculated by EDX for the mono and bimetallic 1.0 wt.% FePd/TiO<sub>2</sub> catalysts did not correlate entirely well with the metal loading shown in Table 4.7 and with the metal loading determined by XPS shown in Table 4.8. Thus, this result led to suggest that the EDX may not be well suited technique to determine the wt.% metal loading.

Surface area and the porosity are investigated in heterogeneous catalyst since they determine the accessibility to active sites, and thus, the surface area, pore morphology's size and distribution are related to the activity of the catalyst. Table 4.9 presents the specific surface area ( $S_{BET}$ ) calculated from the BET formula as stated in the experimental Chapter 2 section 2.6.1. The impregnation of the metals to the TiO<sub>2</sub> (P25) made decrease the  $S_{BET}$  (m<sup>2</sup>/g) in comparison to the bare support TiO<sub>2</sub> (P25). These results were to be expected since nanoparticles were deposited on the TiO<sub>2</sub>, making its surface more uniform and flatter.

**Table 4.9:** Specific surface area of mono and bi-metallic 1.0 wt.% FePd/TiO<sub>2</sub> catalysts.

<b>Catalysts</b>	<b><math>S_{BET}</math></b> m <sup>2</sup> /g	<b>C</b>
<b>1.0 wt.% Fe/TiO<sub>2</sub></b>	59.420	72.442
<b>0.75 wt.% Fe-0.25 wt.% Pd/TiO<sub>2</sub></b>	43.375	125.132
<b>0.50 wt.% Fe-0.50 wt.% Pd/TiO<sub>2</sub></b>	53.582	78.731
<b>0.25 wt.% Fe-0.75 wt.% Pd/TiO<sub>2</sub></b>	53.294	54.821
<b>1.0 wt.% Pd/TiO<sub>2</sub></b>	55.571	71.677
<b>TiO<sub>2</sub> (P25)</b>	60.690	82.843

CO-DRIFTS was used to determine the type of configuration of Pd and Fe nanoparticles in the mono and bi-metallic 1.0 wt.% FePd/TiO<sub>2</sub> catalysts. The mono-metallic 1 wt. % Fe/TiO<sub>2</sub> catalyst did not show any peak apart from the gaseous CO (giving two intensive peaks at above 2100 cm<sup>-1</sup>)<sup>41</sup> and indicating that the CO had not bonded to any of the Fe nanoparticles. Thus, Figure 4.5 only presents the peaks between 1900 cm<sup>-1</sup> and 2100 cm<sup>-1</sup>, which corresponds to frequencies were the CO had bonded to the metal nanoparticles.

There are three distinctive peaks in Figure 4.5 marked with dashed lines; *c.a* 1925  $\text{cm}^{-1}$ , *c.a* 2050  $\text{cm}^{-1}$  and *c.a* 2100  $\text{cm}^{-1}$ . The peak *c.a* 1925  $\text{cm}^{-1}$  is quite broad, which indicate that could be different types of Pd configurations, since it has been reported that ensembles sites of Pd with a bridge mode appear between 1900-2000  $\text{cm}^{-1}$ , whereas 3-fold hollow modes appear between 1800-1900  $\text{cm}^{-1}$ . Thus, this peak can be related to more than 1 atom of Pd together that formed ensembles.<sup>41</sup> The peak *c.a* 2050  $\text{cm}^{-1}$  and the peak close to 2100  $\text{cm}^{-1}$  have been reported to linear CO bonded to highly dispersed Pd<sup>0</sup>.<sup>42,41</sup> Thus, it was concluded that the mono-metallic 1 wt.% Pd/TiO<sub>2</sub> and both bi-metallic 0.25 wt.% Fe-0.75 wt.% Pd/TiO<sub>2</sub>, 0.5 wt.% Fe-0.5 wt.% Pd/TiO<sub>2</sub> catalysts contained ensembles of Pd as well as highly dispersed Pd<sup>0</sup> atoms. On the other hand, the bi-metallic catalyst that corresponds to the lowest loading of Pd, 0.75 wt.% Fe-0.25 wt.% Pd/TiO<sub>2</sub> basically consisted of highly dispersed Pd<sup>0</sup> atoms, with no ensembles.

Han and co-workers<sup>43</sup> determined that the single Pd atoms were accounted for the activity of 2.0 wt.% Pd-1.0 wt.% Au/TiO<sub>2</sub> (made by incipient wetness impregnation) towards the direct synthesis of H<sub>2</sub>O<sub>2</sub>. They determined from CO-DRIFT studies that the addition of Au induced the generation of single Pd atom sites. They concluded that the Pd atoms surrounded by Au were the cause for the high activity of the bi-metallic 2.0 wt.% Pd-1.0 wt.% Au/TiO<sub>2</sub> catalyst, compared to the monometallic Pd analogue.<sup>43</sup> Han and co-workers<sup>44</sup> concluded the same results when studying the activity towards the direct synthesis of H<sub>2</sub>O<sub>2</sub> for the mono-metallic Pd supported on TiO<sub>2</sub>.<sup>44</sup> They concluded from the study of the CO-DRIFTS that the ensembles of Pd were responsible for the dissociation of the O-O bond, leading to H<sub>2</sub>O formation.<sup>44</sup> The single Pd atoms were ascribed to be more favourable towards the direct synthesis of H<sub>2</sub>O<sub>2</sub>. They also pointed out that the ratio of Pd<sup>0</sup> and PdO was also a critical factor that influenced the high activity the mono-metallic 1.0 wt.% Pd/TiO<sub>2</sub>-H<sub>2</sub> catalyst presented, with a percentage of 71 % and 29 % of Pd<sup>0</sup> and PdO respectively, with no Pd ensembles. All four catalysts (1.0 wt.% Pd/TiO<sub>2</sub>, 1.0 wt.% Pd/TiO<sub>2</sub>-N<sub>2</sub>, 1.0 wt.% Pd/TiO<sub>2</sub>-O<sub>2</sub> and 1.0 wt.% Pd/TiO<sub>2</sub>-H<sub>2</sub>) presented between 2.2 and 2.4 nm of nanoparticles, therefore the authors concluded that the difference in activity was greatly ascribed to the oxidation state and configurations of the Pd nanoparticles.<sup>44</sup>

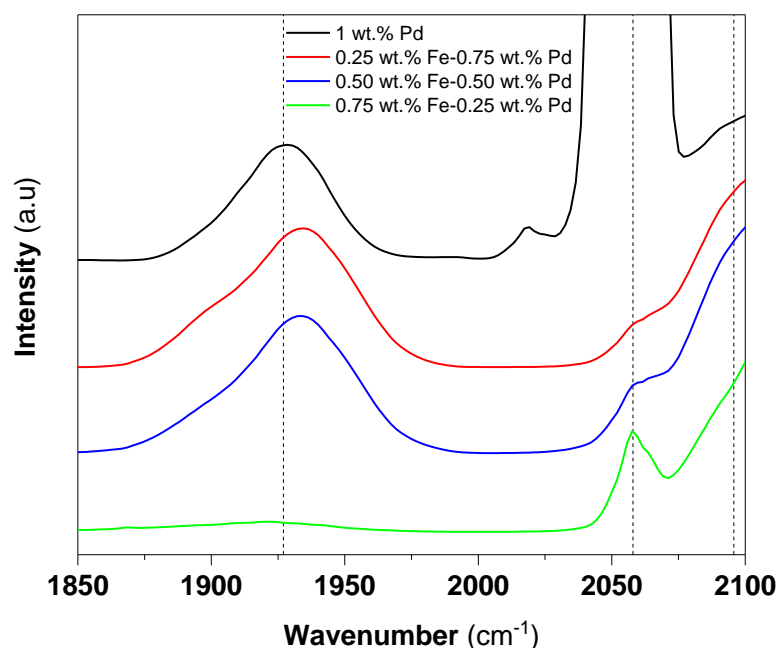


**Figure 4.5:** CO-DRIFTS for the mono and bi-metallic 1.0 wt.% FePd/TiO<sub>2</sub> catalysts.

#### 4.2.4.1 Activity of the mono and bi-metallic 1 wt.% FePd/TiO<sub>2</sub> catalysts towards the direct synthesis and degradation of H<sub>2</sub>O<sub>2</sub>.

These set of catalysts were first tested for their activity towards the direct synthesis of H<sub>2</sub>O<sub>2</sub>, at 30 °C and water-only as a solvent (Figure 4.6). Only the mono-metallic and the three bi-metallic ratios 1.0 wt.% FePd/TiO<sub>2</sub> catalysts presented activity towards the direct synthesis of H<sub>2</sub>O<sub>2</sub>. There was not a correlation between the increasing Pd loading and the amount of H<sub>2</sub>O<sub>2</sub> produced. Surprisingly, the bi-metallic 0.75 wt.% Fe-0.25 wt.% Pd/TiO<sub>2</sub> catalyst that contained 75 % less Pd than the 1.0 wt.% Pd/TiO<sub>2</sub> gave the same concentration of H<sub>2</sub>O<sub>2</sub> in an hour (c.a 0.07 wt.%). The mono-metallic 1 wt.% Fe/TiO<sub>2</sub> had minimal activity towards the synthesis of H<sub>2</sub>O<sub>2</sub> because the Fe was not able to catalyse the reaction between the O<sub>2</sub> and the H<sub>2</sub>. The concentration of H<sub>2</sub>O<sub>2</sub> did increase rapidly during short reaction times (up to c.a 30 minutes). However, after this time, the concentration of H<sub>2</sub>O<sub>2</sub> started to plateau because the H<sub>2</sub>O<sub>2</sub> accumulated started to be degraded to H<sub>2</sub>O. In fact, after 60 minutes, the concentration of H<sub>2</sub>O<sub>2</sub> decay which confirmed that the catalyst was being more active towards the hydrogenation and decomposition of H<sub>2</sub>O<sub>2</sub> than its production. Interestingly, the H<sub>2</sub> conversion was relatively similar in all the set of catalysts despite the difference in Pd loading and its oxidation state as shown by XPS analysis in Table 4.8. In addition to this, the analysis of the post-reaction solution determined that the Fe and Pd were stable, and they did not leach during the course of the reaction (Table S.I 4.6). No correlation between the activity and characterisation could be done at this point since the activity was very similar between the mono-metallic 1.0 wt.% Pd/TiO<sub>2</sub> and the three bi-metallic 1.0 wt.% FePd/TiO<sub>2</sub> catalysts.

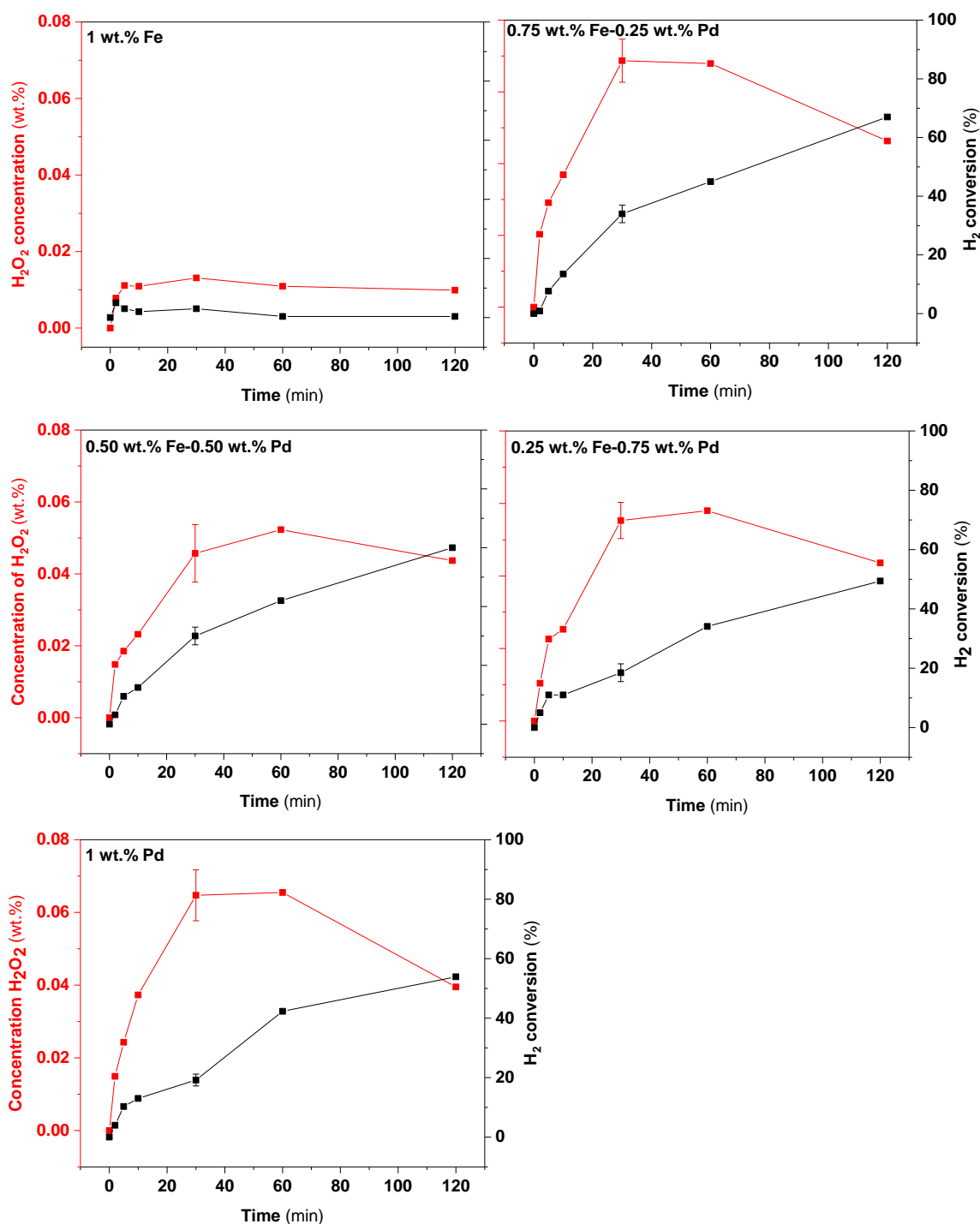


**Figure 4.6:** Time-on-line activity towards the direct synthesis of H<sub>2</sub>O<sub>2</sub> using mono and bi-metallic 1.0 wt.% FePd/TiO<sub>2</sub> catalysts. **Reaction conditions:** 8.5 g (HPLC grade water), catalyst (0.01 g), 420 psi 5 % H<sub>2</sub>/CO<sub>2</sub>, 160 psi 25 % O<sub>2</sub>/CO<sub>2</sub> 1200 rpm, 30 °C.

The H<sub>2</sub>O<sub>2</sub> degradation activity for the mono and bi-metallic 1.0 wt.% FePd/TiO<sub>2</sub> catalysts were studied to discern if the catalyst were active towards the converting the H<sub>2</sub>O<sub>2</sub> to H<sub>2</sub>O (Figure 4.7). The results indicated that there was a clear correlation between the loading of Pd and the H<sub>2</sub>O<sub>2</sub> degradation activity. The mono-metallic 1.0 wt.% Fe/TiO<sub>2</sub> did not show significant activity to degrade H<sub>2</sub>O<sub>2</sub>, as would be expected since Fe is a Fenton metal. The degradation activity decreased while decreasing the loading of Pd instead of presenting all the catalysts the similar activity as they do towards the direct synthesis of H<sub>2</sub>O<sub>2</sub> (Figure 4.6).

For instance, 96 % degradation was shown for the 1.0 wt.% Pd/TiO<sub>2</sub> and 27 % for 0.75 % Fe-0.25 wt.% Pd/TiO<sub>2</sub> in two hours of reaction. Therefore, it is possible to conclude that the low degradation activity shown by 0.75 wt.% Fe-0.25 wt.% Pd/TiO<sub>2</sub> catalyst was what made it to achieve concentrations of H<sub>2</sub>O<sub>2</sub> (0.07 wt.%, 60 min, Figure 4.6) as high as the 1.0 wt.% Pd/TiO<sub>2</sub> catalyst. The main difference between 0.75 wt.% Fe-0.25 wt.% Pd/TiO<sub>2</sub> and 1.0 wt.% Pd/TiO<sub>2</sub> catalysts arose from the oxidation state of the Pd determined by XPS (Table 4.8) and from the CO-DRIFTS (Figure 4.5). The mono-metallic 1.0 wt.% Pd/TiO<sub>2</sub> catalyst had single Pd atoms on the surface as well as ensembles according to the CO-DRIFTS. However, the bi-metallic 0.75 wt.% Pd-0.25 wt.% Pd/TiO<sub>2</sub> catalyst did present single atoms of Pd in greater extent. Thus, it is possible that both configurations (single Pd atoms and Pd ensembles) were active towards the direct synthesis. However, the bi-metallic 0.75 wt.% Pd-0.25 wt.% Pd/TiO<sub>2</sub> catalyst did not present any ensembles and gave the lowest degradation activity of H<sub>2</sub>O<sub>2</sub>. The lack of ensembles in this bi-metallic catalyst prevented the cleavage of O-O bond precluding the formation of H<sub>2</sub>O as it has been reported before.<sup>44</sup> On the other hand, 0.75 wt.% Fe-0.25 wt.% Pd/TiO<sub>2</sub> had a 61 % of PdO whereas 1.0 wt.% Pd/TiO<sub>2</sub> presented 10 % PdO. This difference in PdO percentage, between both catalysts, let to suggest that this could be one of the reasons why the bi-metallic 0.75 wt.% Fe-0.25 wt.% Pd/TiO<sub>2</sub> catalyst ended up as active as the 1.0 wt.% Pd/TiO<sub>2</sub> for the direct synthesis of H<sub>2</sub>O<sub>2</sub>.<sup>45,46,47,48</sup> It was finally concluded that the high activity towards the direct synthesis of H<sub>2</sub>O<sub>2</sub> for the 0.75 wt.% Fe-0.25 wt.% Pd/TiO<sub>2</sub> catalyst was a contribution two factors; first, presenting a beneficial ratio of Pd<sup>0</sup> and PdO on the surface (61 % PdO and 39 % Pd<sup>0</sup>) and minimal presence of Pd ensembles. Han and co-workers<sup>49</sup> draw similar conclusions when they studied the direct synthesis and degradation of H<sub>2</sub>O<sub>2</sub> with mono-metallic 1.0-5.0 wt.% Pd/TiO<sub>2</sub> and 1.0 wt.% PdO/TiO<sub>2</sub> catalyst. They stated that Pd nanoparticles were immobilised to the TiO<sub>2</sub> by forming Pd-O bonds, creating nanoparticles where PdO was on the interface and Pd<sup>0</sup> was found forming an out shell layer on the top of the nanoparticles (TiO<sub>2</sub>-PdO-Pd<sup>0</sup>). They showed that the proportion of PdO decreased with increasing the Pd loading. For instance, 1.0 wt.% Pd/TiO<sub>2</sub> (52.4 % Pd<sup>0</sup>, 47.6 % PdO), 5.0 wt.% Pd/TiO<sub>2</sub> (64.8 % Pd<sup>0</sup>, 35.2 % PdO) and 1.0 wt.% PdO/TiO<sub>2</sub> (34.3 % Pd<sup>0</sup>, 65.7 % PdO). The productivity was found to be quite different despite all the catalyst presented particle size between 2.2-2.5 nm, 1.0 wt.% Pd/TiO<sub>2</sub> (2.99 mol<sub>H<sub>2</sub>O<sub>2</sub></sub> g<sub>Pd</sub><sup>-1</sup> h<sup>-1</sup>, 10.2 % H<sub>2</sub> conversion), 5.0 wt.% Pd/TiO<sub>2</sub> (1.22 mol<sub>H<sub>2</sub>O<sub>2</sub></sub> g<sub>Pd</sub><sup>-1</sup> h<sup>-1</sup>, 31.1 % H<sub>2</sub> conversion) and 1.0 wt.% PdO/TiO<sub>2</sub> (1.07 mol<sub>H<sub>2</sub>O<sub>2</sub></sub> g<sub>Pd</sub><sup>-1</sup> h<sup>-1</sup>, 4.4 % H<sub>2</sub> conversion).<sup>49</sup> They concluded that the most promising catalyst was the mono-metallic 1.0 wt.% Pd/TiO<sub>2</sub> because there were not enough Pd<sup>0</sup> atoms on the top out shell layer of the nanoparticles (TiO<sub>2</sub>-PdO-Pd<sup>0</sup>) to have the H<sub>2</sub> dissociated. However, when the Pd<sup>0</sup> increases, it could form ensembles that dissociate the O<sub>2</sub> leading to H<sub>2</sub>O.<sup>49</sup> Thus, this data led to conclude that the ratio between Pd<sup>0</sup>: PdO as well as the formation of single Pd

atoms are two significant factors to promote the direct synthesis of  $\text{H}_2\text{O}_2$  and decrease the degradation of  $\text{H}_2\text{O}_2$ .

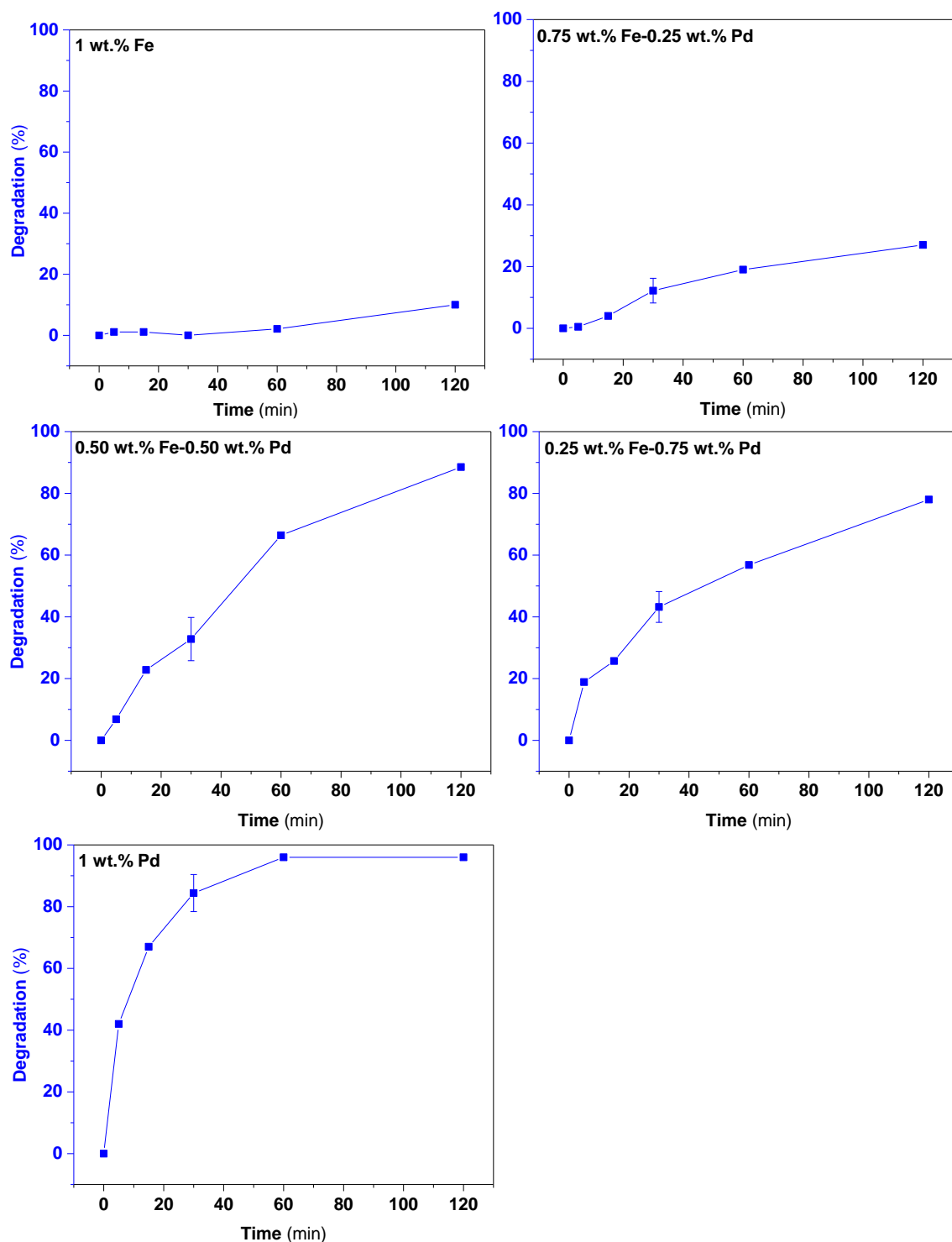


**Figure 4.7:** Time-on-line activity towards the degradation of  $\text{H}_2\text{O}_2$  using mono and bi-metallic 1.0 wt.% FePd/ $\text{TiO}_2$  catalysts. **Reaction conditions:** 8.5 g (0.68 g  $\text{H}_2\text{O}_2$ , 7.82 g HPLC grade water), catalyst (0.01 g), 420 psi 5 %  $\text{H}_2/\text{CO}_2$ , 1200 rpm, 30 °C.

The oxidation state of the Pd for the bi-metallic 0.5 wt.% Fe-0.5 wt.% Fe/ $\text{TiO}_2$  catalyst was investigated after it was used for the direct synthesis of  $\text{H}_2\text{O}_2$  for 2 and 60 min reaction

times. The proportion of Pd<sup>0</sup> increased in comparison with the fresh 0.5 wt.% Fe-0.5 wt.% Pd/TiO<sub>2</sub> catalyst with 2 min reaction time achieving 76 % Pd<sup>0</sup> and 60 min achieving 79 % Pd<sup>0</sup> (Table 4.10). Also, the ratio of Pd: Fe did decrease in comparison to the fresh catalyst, having less Pd on the surface after 2 and 60 min reaction time. The presence of H<sub>2</sub> during the direct synthesis of H<sub>2</sub>O<sub>2</sub> could have had contributed to the reduction of PdO to Pd<sup>0</sup>. This data led to conclude that the oxidation state change during the reaction which might affect the activity of the catalyst in subsequent usage.

**Table 4.10:** XPS analysis of the used bi-metallic 0.5 wt.% Fe-0.5 wt.% Pd/TiO<sub>2</sub> catalyst for the direct synthesis of H<sub>2</sub>O<sub>2</sub> at 2 and 60 min reaction.

Catalysts	PdO %	Pd <sup>0</sup> %	Pd: Fe
<b>0.5 wt.% Fe-0.5 wt.% Pd/TiO<sub>2</sub> (Fresh)</b>	32	68	0.9
<b>0.5 wt.% Fe-0.5 wt.% Pd/TiO<sub>2</sub> (Used-2 min)</b>	24	76	0.56
<b>0.5 wt.% Fe-0.5 wt.% Pd/TiO<sub>2</sub> (Used-60 min)</b>	21	79	0.39

**Reaction conditions:** 8.5 g (HPLC grade water), catalyst (0.01 g), 420 psi 5 % H<sub>2</sub>/CO<sub>2</sub>, 160 psi 25 % O<sub>2</sub>/CO<sub>2</sub>, 1200 rpm, 30 °C. XPS spectra are shown in supplementary information, Figure S.I 4.9-4.10.

#### 4.2.4.2 Activity of the mono and bi-metallic 1 wt.% FePd/TiO<sub>2</sub> catalysts towards the degradation of phenol.

The mono-metallic 1 wt.% Pd/TiO<sub>2</sub> and the three bi-metallic 1.0 wt.% FePd/TiO<sub>2</sub> catalysts were next evaluated towards the degradation of phenol (Figure 4.8). The mono-metallic 1 wt.% Pd/TiO<sub>2</sub> catalyst presented relatively low activity of phenol conversion in 2 h reaction time (10 %) despite it offered the highest performance towards H<sub>2</sub>O<sub>2</sub> synthesis (0.04 wt.%, 2h, Figure 4.6) and degradation (96 %, 2h, Figure 4.7). Since Pd did not show activity for the degradation of phenol, it is possible that most of the H<sub>2</sub>O<sub>2</sub> was mainly degraded to H<sub>2</sub>O during the course of the reaction rather than being catalysed to ROS. The mono-metallic 1 wt.% Fe/TiO<sub>2</sub> catalyst was tested for 2 h showing even lower activity towards the degradation of phenol (c.a 2 %) than the 1 wt.% Pd/TiO<sub>2</sub> catalyst which was because Fe was not able to produce H<sub>2</sub>O<sub>2</sub> as shown in Figure 4.6. On the other hand, the bi-metallic ratios 1.0 wt.% FePd/TiO<sub>2</sub> had better activity towards oxidising phenol, which may be linked to having had formed ROS from the *in-situ* H<sub>2</sub>O<sub>2</sub>. In fact, Crombie *et al.*, investigated the formation of ROS by electron paramagnetic resonance (EPR) for a 1.0 wt.% Pd/TiO<sub>2</sub>, 1.0 wt.% AuPd/TiO<sub>2</sub> and 1.0 wt.% FePd/TiO<sub>2</sub> catalysts made by an analogous modified impregnation procedure used in this work.<sup>40</sup> They studied the formation of ROS using 5,5-dimethyl-1-pyridine N-oxide (DMPO) at 50 °C with two types of solvents, CH<sub>3</sub>OH and water.<sup>40</sup> Their results showed that when water was used as a solvent, HO<sup>•</sup> and HOO<sup>•</sup> were

detected, with the bi-metallic 1.0 wt.% FePd/TiO<sub>2</sub> catalyst generating more ROS than the 1.0 wt.% AuPd/TiO<sub>2</sub> analogue.<sup>40</sup> Thus, this led to conclude that the bi-metallic 1.0 wt.% FePd/TiO<sub>2</sub> catalyst could successfully generate ROS from the *in-situ* H<sub>2</sub>O<sub>2</sub> even at 50 °C.<sup>40</sup>

The three bi-metallic 1.0 wt.% FePd/TiO<sub>2</sub> catalysts presented similar activity towards the degradation of phenol, which it was expected since the three bi-metallic ratios were also producing similar concentrations of *in-situ* H<sub>2</sub>O<sub>2</sub> as Figure 4.6 showed. Therefore, similar concentration of ROS from the *in-situ* H<sub>2</sub>O<sub>2</sub> could have been generated during the degradation of phenol for the three bi-metallic 1 wt.% FePd/TiO<sub>2</sub> catalysts irrespective of the Fe:Pd ratio. The selectivity towards the phenol derivatives and others was calculated to determine the extend of degradation according to the mechanism shown in Figure 4.1. As the results show, all catalysts where able to oxidise phenol derivatives into di-acids, H<sub>2</sub>O and CO<sub>2</sub>.

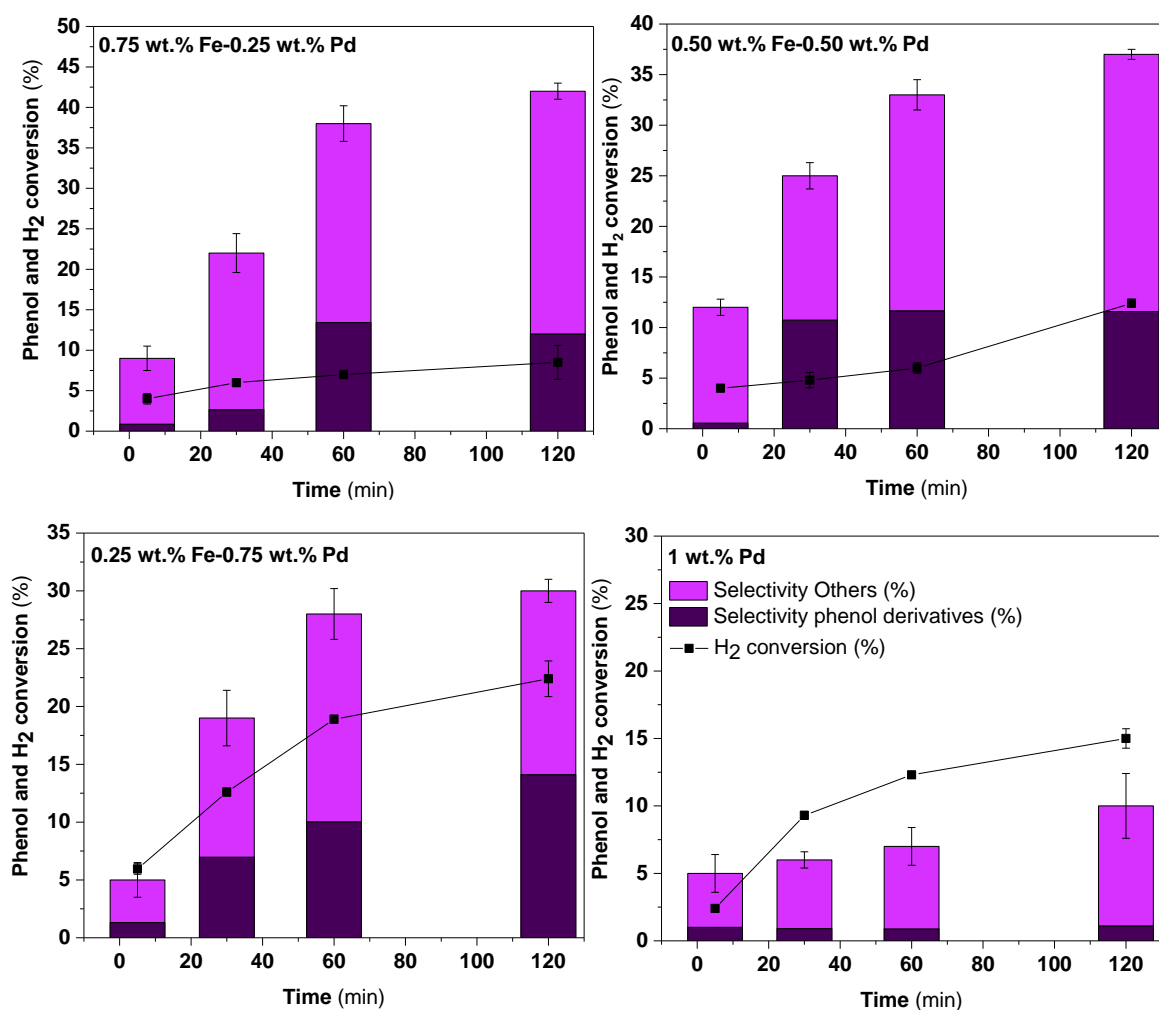


**Figure 4.8:** Time-on-line activity towards the degradation of phenol using mono and bi-metallic 1.0 wt.% FePd/TiO<sub>2</sub> catalysts. **Nomenclature:** Phenol derivatives (catechol, resorcinol, 1,4-benzoquinone and hydroquinone). Others (di-acids, CO<sub>2</sub> and H<sub>2</sub>O). **Reaction conditions:** 8.5 g (phenol (1000 ppm)), catalyst (0.01 g), 420 psi 5 % H<sub>2</sub>/CO<sub>2</sub>, 160 psi 25 % O<sub>2</sub>/CO<sub>2</sub>, 1200 rpm, 30 °C.

It was also noticed from Figure 4.8 that the H<sub>2</sub> conversion as well as the phenol conversion were reaching a plateau over the course of 2 h reaction. This led to the conclusion that the reaction could be limited by the H<sub>2</sub> availability, which would be affecting the formation of *in-situ* H<sub>2</sub>O<sub>2</sub> and subsequently the formation of ROS. Thus, to test if the H<sub>2</sub> availability was affecting the performance of the catalyst, gas replacements were conducted, replacing the used gas for fresh compositions (580 psi H<sub>2</sub>, O<sub>2</sub>/CO<sub>2</sub>) (Figure 4.9). For instance, the 4 h data point in Figure 4.9 was obtained by running a phenol oxidation reaction for 2 h at 30 °C, replacing the gas for fresh compositions of H<sub>2</sub> and O<sub>2</sub> (580 psi H<sub>2</sub>, O<sub>2</sub>/CO<sub>2</sub>) and running the reaction for an extra 2 h at 30 °C. A more detailed explanation about how to conduct the gas replacement experiments can be found in Chapter 2, section 2.3.2.2.

The results from the gas replacement experiments show that the degradation of phenol was enhanced over consecutive gas replacements reaching up to 67 % phenol conversion in 8 h and 3 gas replacements. However, the extent of phenol conversion did not increase by a

comparable amount over each reaction time, for instance, a 2 h gave c.a 40 % phenol conversion and a 4 h data point (1 gas replacement), gave c.a 50 % phenol conversion. Also, the H<sub>2</sub> conversion experimented a decay from 40 % (at 2 h data point) to c.a to 20 %, at 8 h data point. The tendency shown by the phenol conversion and the H<sub>2</sub> conversion data let to suggest that catalyst could be deactivating, for instance, due to metal leaching.

The selectivity towards phenol derivatives (catechol, resorcinol, hydroquinone and 1,4-benzoquinone) and to others (di-acids, H<sub>2</sub>O and CO<sub>2</sub>) was also found to be relatively similar; for 2 hours reaction (37 % phenol conversion, 31 % selectivity for phenol derivatives and 69 % selectivity for others) and for 8 hours reaction with three gas replacements (67 % phenol conversion, 30 % selectivity for phenol derivatives and 70 % selectivity for others).

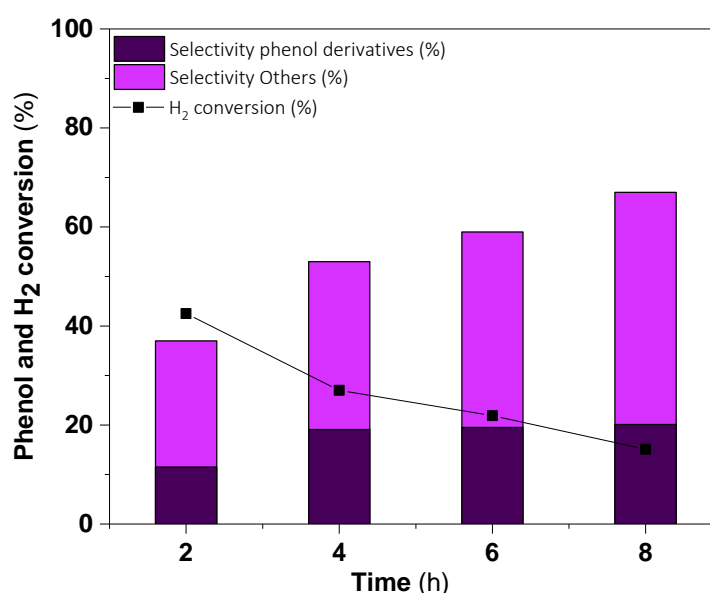


**Figure 4.9:** Conduction of gas replacement experiments during the degradation of phenol and using bi-metallic 0.50 wt.% Fe- 0.50 wt.% Pd/TiO<sub>2</sub> catalyst. **Nomenclature:** Phenol derivatives (catechol, resorcinol, 1,4-benzoquinone and hydroquinone). Others (di-acids, CO<sub>2</sub> and H<sub>2</sub>O). **Reaction conditions:** 8.5 g (phenol (1000 ppm)), catalyst (0.01 g), 420 psi 5% H<sub>2</sub>/CO<sub>2</sub>, 160 psi 25% O<sub>2</sub>/CO<sub>2</sub>, 1200 rpm, 30 °C. Fresh gas was replaced every two hours with 420 psi 5 % H<sub>2</sub>/CO<sub>2</sub> and 160 psi 25 % O<sub>2</sub>/CO<sub>2</sub>.

The formation of ROS from the *in-situ* H<sub>2</sub>O<sub>2</sub> seems to be the key in order to oxidise phenol. As seen before, the mono-metallic 1wt.% Pd/TiO<sub>2</sub> and bi-metallic 0.50 wt.% Au-0.50 wt.% Pd/TiO<sub>2</sub> catalysts gave the highest productivities towards the H<sub>2</sub>O<sub>2</sub> formation, but minimal phenol degradation. On the other hand, with the incorporation of Fe, the *in-situ* H<sub>2</sub>O<sub>2</sub> could be transformed to ROS, thus making the bi-metallic combination 0.50 wt.% Fe-0.50 wt.% Pd/TiO<sub>2</sub> a promising catalyst for water remediation. Blank experiments were conducted in order to corroborate that the *in-situ* H<sub>2</sub>O<sub>2</sub> is the main source for the formation of ROS. Table 4.11 presents the blanks performed. When O<sub>2</sub> or H<sub>2</sub> were replaced by N<sub>2</sub>, (blanks, H<sub>2</sub>,N<sub>2</sub>/CO<sub>2</sub> and O<sub>2</sub>,N<sub>2</sub>/CO<sub>2</sub> respectively), the activity of the bi-metallic 0.5 wt.% Fe-0.5 wt.%

Pd/TiO<sub>2</sub> catalyst towards phenol degradation decayed significantly, indicating that H<sub>2</sub>O<sub>2</sub> was required in order to make ROS and thus degrade phenol. Still, when replacing 160 psi 25 % O<sub>2</sub>/CO<sub>2</sub> with 160 psi of N<sub>2</sub> (H<sub>2</sub>, N<sub>2</sub>/CO<sub>2</sub>), a significant activity was achieved (5.8 % phenol conversion). However, this could have been because H<sub>2</sub>O<sub>2</sub> was formed using the reservoir of O<sub>2</sub> dissolved in the reaction solution. The direct synthesis of H<sub>2</sub>O<sub>2</sub> was carried out at the same conditions as the blank (H<sub>2</sub>, N<sub>2</sub>/CO<sub>2</sub>), in order to see if the H<sub>2</sub> could have reacted using the dissolved O<sub>2</sub>. Due to the low concentration of H<sub>2</sub>O<sub>2</sub> expected to be generated, the reaction was performed for 5 minutes and at 25 °C where degradation is lower than at long reaction times and high temperatures. It was found that 0.6 ppm of *in-situ* H<sub>2</sub>O<sub>2</sub> were formed under 420 psi 5 % H<sub>2</sub>/CO<sub>2</sub> and 160 psi N<sub>2</sub> in 5 minutes at 25 °C using bi-metallic 0.5 wt.% Fe-0.5 wt.% Pd/TiO<sub>2</sub> catalyst. The detection of H<sub>2</sub>O<sub>2</sub> was carried out by ultraviolet-visible spectroscopy (UV-Vis) chelating the H<sub>2</sub>O<sub>2</sub> with potassium titanium (IV) oxalate to give a yellowish solution that absorbs at 400 nm.<sup>39</sup> Thus, the catechol and 1,4-benzoquinone observed in the blank (H<sub>2</sub>, N<sub>2</sub>/CO<sub>2</sub>) could have been generated by ROS from the *in-situ* H<sub>2</sub>O<sub>2</sub>. No phenol degradation was detected if the catalyst was not added into the reaction mixture (blank, no catalyst) or TiO<sub>2</sub> (P25) was employed instead of the 0.5 wt.% Fe-0.5 wt.% Pd/TiO<sub>2</sub> catalyst (blank, TiO<sub>2</sub>). In addition, the physical mixture of both mono-metallic 1 wt.% Fe/TiO<sub>2</sub> and 1.0 wt.% Pd/TiO<sub>2</sub> catalysts (blank, physical mixture) had similar phenol conversion (12 %) and H<sub>2</sub> (58 %) conversion to that observed over the mono-metallic 1.0 wt.% Pd/TiO<sub>2</sub> catalyst (10 % phenol conversion, 50 % H<sub>2</sub> conversion). This result suggests that the active sites of Fe need to be in close proximity to the Pd sites (responsible for H<sub>2</sub>O<sub>2</sub> synthesis) to catalyse the formation of ROS from the H<sub>2</sub>O<sub>2</sub>, and the oxidation of pollutants is believed to happen near the Fe active sites since the ROS have a short lifespan.<sup>50</sup>

**Table 4.11:** Degradation of phenol with replacement of H<sub>2</sub> and/or O<sub>2</sub> by N<sub>2</sub>, physical mixtures of mono-metallic 1 wt.% Fe/TiO<sub>2</sub> and 1 wt.% Pd/TiO<sub>2</sub> as well as TiO<sub>2</sub> (P25).

<b>Blanks</b>	<b>Phenol conversion</b>	<b>H<sub>2</sub> conversion</b>	<b>Phenol derivatives selectivity</b>	<b>Others selectivity</b>
	%	%	%	%
<b>H<sub>2</sub>,N<sub>2</sub>/CO<sub>2</sub></b>	5.8	n.a	2	98
<b>O<sub>2</sub>,N<sub>2</sub>/CO<sub>2</sub></b>	3.5	n.a	0	0
<b>No catalyst</b>	0	n.a	0	0
<b>TiO<sub>2</sub></b>	0.5	3	0	0
<b>Physical mixture</b>	12	58	24	76

**n.a:** not applicable. **Reaction conditions:** **H<sub>2</sub>,N<sub>2</sub>/CO<sub>2</sub>:** 8.5 g (1000 ppm Phenol), 0.5 wt.% Fe-0.5 wt.% Pd/TiO<sub>2</sub> (0.01 g), 420 psi 5 % H<sub>2</sub>/CO<sub>2</sub>, 160 psi N<sub>2</sub>, 1200 rpm, 30 °C, 2 h. **O<sub>2</sub>,N<sub>2</sub>/CO<sub>2</sub>:** 8.5 g (1000 ppm Phenol), 0.5 wt.% Fe-0.5 wt.% Pd/TiO<sub>2</sub> (0.01 g), 420 psi N<sub>2</sub>, 160 psi 25 % O<sub>2</sub>/CO<sub>2</sub>, 1200 rpm, 30 °C, 2 h. **No catalyst:** 8.5 g (1000 ppm Phenol), catalyst (0.00 g), 420 psi 5 % H<sub>2</sub>/CO<sub>2</sub>, 160 psi 25 % O<sub>2</sub>/CO<sub>2</sub>, 1200 rpm, 30 °C, 2 h. **TiO<sub>2</sub>:** 8.5 g (1000 ppm Phenol), TiO<sub>2</sub> (P25) (0.01 g), 420 psi 5 % H<sub>2</sub>/CO<sub>2</sub>, 160 psi 25 % O<sub>2</sub>/CO<sub>2</sub>, 1200 rpm, 30 °C, 2 h. **Physical mixture:** 8.5 g (1000 ppm Phenol), 1.0 wt.% Pd/TiO<sub>2</sub> (0.005 g) and 1.0 wt.% Fe/TiO<sub>2</sub> (0.005 g), 420 psi 5 % H<sub>2</sub>/CO<sub>2</sub>, 160 psi 25 % O<sub>2</sub>/CO<sub>2</sub>, 1200 rpm, 30 °C, 2 h. **Nomenclature:** Selectivity towards phenol derivatives (catechol, resorcinol, 1,4-benzoquinone, hydroquinone) and selectivity towards others (di-acids, H<sub>2</sub>O and CO<sub>2</sub>).

Despite the bi-metallic ratios 1.0 wt.% FePd/TiO<sub>2</sub> offered better activity than the mono-metallic analogues for the degradation of phenol, these catalysts also leached significant amount of Fe over the course of the 2 h reaction time, irrespective of the different Fe: Pd ratios (Table 4.12). Thus, the metal leaching could be responsible for the catalyst deactivation seen in Figure 4.9 during the gas replacement experiments.

The amount of Fe leached was clearly linked to the extent of phenol conversion, since 1 wt.% Fe/TiO<sub>2</sub> did not have significant activity towards the degradation phenol and neither it had significant amount metal leached. In addition to this, it could be that the three bi-metallic 1 wt.% FePd/TiO<sub>2</sub> ratios showed similar amount of Fe leached because the three of them presented relatively similar activity towards the degradation of phenol. Rodriguez and co-workers<sup>51</sup> and Hutchings and co-workers<sup>15</sup> both assigned the formation of catechol and oxalic acid to be responsible for the Fe leaching during the degradation of phenol. Catechol and oxalic acid were ligands capable of chelate the Fe and remove it from the surface of the support.<sup>51,15</sup> Unfortunately, no relation was seen between the amount of catechol formed and percentage of Fe leached. Still, it could be that other species, apart from oxalic acid (it was not able to be determined) and catechol, were contributing the chelate both metals (Fe and Pd) and remove it from the support. What it can be concluded from this data is that the activity of the bi-metallic 1 wt.% FePd/TiO<sub>2</sub> cannot all be accounted to heterogeneous metal nanoparticles, since homogeneous Fe species are known to catalyse phenol degradation

via Fenton's pathways.<sup>51,15</sup> For instance, Rodriguez and co-workers<sup>51</sup> studied the oxidation of phenol by impregnating Fe on carbon pre-treated with HNO<sub>3</sub> (2.5 wt.% Fe/C) and using O<sub>2</sub> as oxidant. This catalyst achieved 100 % phenol conversion, however, they concluded that the Fe leached (0.3 %) had contributed to 10 % of the total conversion.<sup>51</sup>

**Table 4.12:** Leaching of the mono and bi-metallic 1.0 wt.% FePd/TiO<sub>2</sub> catalysts for the degradation of phenol in two hours' reaction.

Catalysts	Fe	Pd	Phenol conversion	Catechol
	%	%	%	ppm
1.0 wt.% Fe/TiO <sub>2</sub>	0.3	0	2	0
0.75 wt.% Fe-0.25 wt.% Pd/TiO <sub>2</sub>	37	2	40	100
0.50 wt.% Fe-0.50 wt.% Pd/TiO <sub>2</sub>	42	2	35	65
0.25 wt.% Fe-0.75 wt.% Pd/TiO <sub>2</sub>	46	2	30	44
1.0 wt.% Pd/TiO <sub>2</sub>	0	0	10	8

**Reaction conditions:** 8.5 g (phenol (1000 ppm)), catalyst (0.01 g), 420 psi 5% H<sub>2</sub>/CO<sub>2</sub>, 160 psi 25% O<sub>2</sub>/CO<sub>2</sub>, 1200 rpm, 30 °C, 2 h.

To determine the contribution of the Fe and Pd leached to the conversion of phenol, a one-hour reaction was run with the bi-metallic 0.5 wt.% Fe-0.5 wt.% Pd/TiO<sub>2</sub> catalyst towards the degradation of phenol. Afterwards, the post-reaction solution was filtered to remove the catalyst and re-run for an extra hour at 30 °C with fresh gas (420 psi 5 % H<sub>2</sub>/CO<sub>2</sub> and 160 psi 25 % O<sub>2</sub>/CO<sub>2</sub>). Analogously to the previous experiment, the post-reaction solution of the same catalyst was re-run for another hour with 10 mg of 1 wt.% Pd/TiO<sub>2</sub> catalyst to synthesise *in-situ* H<sub>2</sub>O<sub>2</sub> and react with the leached Fe. The results are shown in Table 4.13 and determined that the Fe and Pd leached after the degradation of phenol were still active, contributing to increasing the activity by 11 %. However, since there was no conversion of H<sub>2</sub>, the Fe leached could have reacted with residual H<sub>2</sub>O<sub>2</sub>. The addition of 1 wt.% Pd/TiO<sub>2</sub> to the post-reaction solution did not enhance the conversion of phenol as it would be expected since H<sub>2</sub> was being consumed during the reaction presumably making extra H<sub>2</sub>O<sub>2</sub>. Another interesting fact is that the conversion of H<sub>2</sub> (22.6 %) was halved in comparison to the one hour H<sub>2</sub> conversion of the fresh 1.0 wt.% Pd/TiO<sub>2</sub> catalyst when tested towards the degradation of phenol (6 % phenol conversion, 41 % H<sub>2</sub> conversion, Figure 4.8). This fact led to suggest there might be product inhibition affecting the activity of the Pd towards the direct synthesis of H<sub>2</sub>O<sub>2</sub>. This behaviour can also be seen when comparing the H<sub>2</sub> conversion towards the direct synthesis of H<sub>2</sub>O<sub>2</sub> in Figure 4.6 and the H<sub>2</sub> conversion towards the degradation of phenol in Figure 4.8. For instance, there was a significant difference between the H<sub>2</sub> conversion for the bi-metallic 0.5 wt.% Fe-0.5 wt.% Pd/TiO<sub>2</sub> catalyst in two hours (60 % H<sub>2</sub> conversion for the direct synthesis, 31 % H<sub>2</sub> conversion for the degradation of phenol), and 0.75 wt.% Fe-0.25 wt.% Pd/TiO<sub>2</sub> catalyst (67 % H<sub>2</sub> conversion for direct synthesis, 17 % H<sub>2</sub> conversion for the degradation of phenol). On the other hand, there was

not significant difference for the 1.0 wt.% Pd/TiO<sub>2</sub> in two hours' reaction (47 % H<sub>2</sub> conversion for the direct synthesis of H<sub>2</sub>O<sub>2</sub>, 50 % H<sub>2</sub> conversion for the degradation of phenol) and for 0.25 wt.% Fe-0.75 wt.% Pd/TiO<sub>2</sub> (50 % H<sub>2</sub> conversion for the direct synthesis of H<sub>2</sub>O<sub>2</sub>, 64 % H<sub>2</sub> conversion for the degradation of phenol). These results could suggest that Pd got inhibited by the products formed as a result of the oxidation of phenol. For instance, mono-metallic 1.0 wt.% Pd/TiO<sub>2</sub> did not seem to have been inhibited, by showing similar H<sub>2</sub> conversions for the direct synthesis of H<sub>2</sub>O<sub>2</sub> and phenol degradation, but 1.0 wt.% Pd/TiO<sub>2</sub> did not either achieve significant phenol conversion. On the other hand, the bi-metallic ratios 1.0 wt.% PdFe/TiO<sub>2</sub>, which they did present significant activity for the degradation of phenol, also had the H<sub>2</sub> conversion halved during the degradation of phenol. In addition to this, the bi-metallic ratios 0.50 wt.% Fe-0.50 wt.% Pd/TiO<sub>2</sub> and 0.75 wt.% Fe-0.25 wt.% Pd/TiO<sub>2</sub> catalysts were the ones showing less H<sub>2</sub> conversion during the degradation of phenol, and the ones having more PdO percentage.

**Table 4.13:** Hot filtration experiments activity using the 0.5 wt.% Fe-0.5 wt.% Pd/TiO<sub>2</sub> catalyst towards the degradation of phenol.

	Phenol conversion	H <sub>2</sub> conversion
	%	%
<b>0.5 wt.% Fe-0.5 wt.% Pd/TiO<sub>2</sub></b>	33	36
<b>Fresh</b>		
<b>Homogeneous</b>	40.5 ± 1.0	0
<b>Homogeneous + 1 wt.% Pd/TiO<sub>2</sub></b>	40.1 ± 4.0	23 ± 3

**Reaction conditions: Fresh:** 8.5 g (phenol (1000 ppm)), catalyst (0.01 g), 420 psi 5 % H<sub>2</sub>/CO<sub>2</sub>, 160 psi 25 % O<sub>2</sub>/CO<sub>2</sub>, 1200 rpm, 30 °C, 1 h. **Homogeneous:** 8.5 g (post-reaction filtered solution after 1 h reaction using 0.5 wt.% Fe-0.5 wt.% Pd/TiO<sub>2</sub> catalyst), 420 psi 5 % H<sub>2</sub>/CO<sub>2</sub>, 160 psi 25 % O<sub>2</sub>/CO<sub>2</sub>, 1200 rpm, 30 °C, 1 h. **Homogeneous + 1 wt.% Pd/TiO<sub>2</sub>:** 8.5 g (post-reaction filtered solution after 1 h reaction using 0.5 wt.% Fe-0.5 wt.% Pd/TiO<sub>2</sub> catalyst), 1 wt.% Pd/TiO<sub>2</sub> (0.01 g), 420 psi 5 % H<sub>2</sub>/CO<sub>2</sub>, 160 psi 25 % O<sub>2</sub>/CO<sub>2</sub>, 1200 rpm, 30 °C, 1 h.

#### 4.2.5 Re-usability of the bi-metallic 0.5 wt.% Fe-0.5 wt.% Pd/TiO<sub>2</sub> catalyst towards the degradation of phenol.

The used bi-metallic 0.5 wt.% Fe-0.5 wt.% Pd/TiO<sub>2</sub> catalyst was re-tested towards the degradation of phenol and the results can be seen in Table 4.14. The activity towards the conversion of phenol decreased after one used going from 36 % down to 20 % due to the loss of Fe, which subsequently affected the generation of ROS to degrade phenol. Surprisingly, the H<sub>2</sub> conversion was similar in both sets of reactions, however, this was not indicative that the production of H<sub>2</sub>O<sub>2</sub> had been the same. Further testing would have been required to determine if the bi-metallic 0.5 wt.% Fe-0.5 wt.% Pd/TiO<sub>2</sub> catalyst maintained the selectivity towards the direct formation of H<sub>2</sub>O<sub>2</sub> after being used towards the degradation of phenol.

**Table 4.14:** Re-usability of the 0.5 wt.% Fe-0.5 wt.% Pd/TiO<sub>2</sub> catalyst for the degradation of phenol.

Catalysts	Phenol conversion	H <sub>2</sub> conversion
	%	% (S.D)
<b>0.50 wt.% Fe-0.50 wt.%Pd/TiO<sub>2</sub></b>	36 ± 3	41 ± 5
<b>Fresh</b>		
<b>0.50 wt.% Fe-0.50 wt.% Pd/TiO<sub>2</sub></b>	20 ± 2	45 ± 2
<b>Used</b>		

**(S.D):** standard deviation. **Reaction conditions:** 8.5 g (phenol (1000 ppm)), catalyst (0.01 g), 420 psi 5 % H<sub>2</sub>/CO<sub>2</sub>, 160 psi 25 % O<sub>2</sub>/CO<sub>2</sub>, 1200 rpm, 30 °C, 2 h.

The used catalysts were analysed by XPS to determine if the oxidation state of the Pd was maintained after the bi-metallic 0.5 wt.% Fe-0.5 wt.% Pd/TiO<sub>2</sub> catalyst was used towards the degradation of phenol. Table 4.15 presents the percentage of Pd<sup>0</sup>, PdO and the Pd: Fe ratio of the fresh and used bi-metallic 0.5 wt.% Fe-0.5 wt.% Pd/TiO<sub>2</sub> catalyst for the sake of comparison. The used catalyst had higher percentage of Pd<sup>0</sup>, which suggested that the reductive atmosphere with H<sub>2</sub> could have had contributed to reduce part of the PdO to Pd<sup>0</sup>. This led to conclude that the activity and selectivity of the used bi-metallic 0.5 wt.% Fe-0.5 wt.% Pd/TiO<sub>2</sub> catalyst towards the direct synthesis of H<sub>2</sub>O<sub>2</sub> would not be expected to be the same as the fresh catalyst due to the change in the Pd oxidation state. In addition to this, the ratio between Pd and Fe had decreased when comparing the fresh and used bi-metallic 0.5 wt.% Fe-0.5 wt.% Pd/TiO<sub>2</sub> catalyst, making the Pd less exposed to the surface, which could have also influenced the activity and selectivity towards the direct synthesis of H<sub>2</sub>O<sub>2</sub> as well.

**Table 4.15:** XPS analysis of the fresh and used bi-metallic 0.5 wt.% Fe-0.5 wt.% Pd/TiO<sub>2</sub> catalyst for the degradation of phenol.

Catalysts	PdO	Pd <sup>0</sup>	Pd:X
	%	%	
<b>0.50 wt.%Fe-0.50 wt.% Pd/TiO<sub>2</sub></b>	58	42	0.9
<b>Fresh</b>			
<b>0.50 wt.%Fe-0.50 wt.% Pd/TiO<sub>2</sub></b>	19	81	0.1
<b>Used</b>			

**Reaction conditions:** 8.5 g (phenol (1000 ppm)), catalyst (0.01 g), 420 psi 5 % H<sub>2</sub>/CO<sub>2</sub>, 160 psi 25 % O<sub>2</sub>/CO<sub>2</sub>, 1200 rpm, 30 °C, 2 h. XPS spectra for the used bi-metallic 0.5 wt.% Fe-0.5 wt.% Pd/TiO<sub>2</sub> catalyst is shown in supplementary information, Figure S.I 4.11.

### 4.3 Conclusions.

The metal combination of Fe and Pd (1 wt.% FePd/TiO<sub>2</sub>) has shown to be the most promising for water treatment remediation, in concrete because it showed the best activity towards the degradation of phenol. It was seen that other bi-metallic 0.50 wt.% X-0.50 wt.% Pd/TiO<sub>2</sub> (X: Cu, Co, Au) formulations had limited activity towards the degradation of phenol for several reasons. CuPd and CoPd had significantly high H<sub>2</sub> conversion during the degradation of phenol (40 % and 50 % H<sub>2</sub> conversion respectively) suggesting that *in-situ* H<sub>2</sub>O<sub>2</sub> could have been formed, however, the limited activity shown by these formulations towards the degradation of phenol (< 10 phenol conversion, 2 h, 30 °C), indicated that most of the *in-situ* H<sub>2</sub>O<sub>2</sub> could have had been hydrogenated to H<sub>2</sub>O instead of being converted to ROS. Thus, despite Cu and Co have been reported in the literature to be highly active towards the degradation of phenol with pre-formed H<sub>2</sub>O<sub>2</sub>,<sup>52</sup> Cu and Co seemed not to be suitable Fenton metals to generate ROS from *in-situ* H<sub>2</sub>O<sub>2</sub> due to their high activity shown towards the degradation of H<sub>2</sub>O<sub>2</sub> to H<sub>2</sub>O. On the other hand, AuPd gave the lowest activity towards the degradation of phenol (<10 %) and H<sub>2</sub> conversion (10 %). This in combination to the high degradation activity shown by this catalyst (932 mol<sub>H<sub>2</sub>O<sub>2</sub></sub> kg<sub>cat</sub><sup>-1</sup> h<sup>-1</sup>, 2h, 30 °C) let to conclude that AuPd was mostly decomposing the *in-situ* H<sub>2</sub>O<sub>2</sub> instead of converting it into ROS. Thus, the bi-metallic combination of FePd was the most selective to convert the *in-situ* H<sub>2</sub>O<sub>2</sub> into ROS, rather than hydrogenate or decompose it to H<sub>2</sub>O, which resulted in the highest activity towards the degradation of phenol.

Hutchings and co-workers had previously reported the bi-metallic 2.5 wt.% Fe-2.5 wt.% Pd/TiO<sub>2</sub> catalyst to be the most promising towards the degradation of phenol in comparison to other bi-metallic analogues 2.5 wt.% X-2.5 wt.% Pd/TiO<sub>2</sub> (X: Cu, Co, Mn, Au). However, the lack of stability shown for the bi-metallic 2.5 wt.% Fe-2.5 wt.% Pd/TiO<sub>2</sub> catalyst during the degradation of phenol was reported to be caused by the oxalic acid and catechol which were able to chelate the Fe and remove it from the surface of the catalyst. In this chapter a series of mono and bi-metallic 1 wt.% FePd/TiO<sub>2</sub> catalysts with different Fe:Pd ratios were synthesised to establish if by decreasing the loading of the catalysts (1 wt.% total metal) would enhance the metal dispersion and subsequently improve the stability and activity towards the degradation of phenol. In terms of activity, both mono-metallic 1 wt.% Pd/TiO<sub>2</sub> and 1 wt.% Fe/TiO<sub>2</sub> catalysts showed minimal activity towards the degradation of phenol, whereas the bi-metallic 1 wt.% FePd/TiO<sub>2</sub> catalysts showed relatively similar activity (30-40 % phenol conversion, 2 h, 30 °C) irrespective of the Fe:Pd ratio used. It was suspected that the degradation activity for the three bi-metallic ratios was similar because similar concentration of H<sub>2</sub>O<sub>2</sub> (between 0.05-0.04 wt.%, 2 h, 30 °C) were produced, and thus, ROS generation could have been also similar during the degradation of phenol for the three bi-metallic 1 wt.% FePd/TiO<sub>2</sub> catalysts irrespective of the Fe:Pd ratio.

Despite the three bi-metallic 1 wt.% FePd/TiO<sub>2</sub> catalysts presented similar concentrations of *in-situ* H<sub>2</sub>O<sub>2</sub> (between 0.05-0.04 wt.%, 2 h, 30 °C), the H<sub>2</sub>O<sub>2</sub> degradation experiments showed that the bi-metallic 0.75 wt.% Fe-0.25 wt.% Pd/TiO<sub>2</sub> catalyst was the most selective towards the formation of H<sub>2</sub>O<sub>2</sub>. A close inspection of the mono and bi-metallic 1 wt.% FePd/TiO<sub>2</sub> ratios by TEM revealed the nanoparticle size and distribution was not a contributing factor for the bi-metallic 0.75 wt.% Fe-0.25 wt.% Pd/TiO<sub>2</sub> ratio to show the best selectivity towards the formation of *in-situ* H<sub>2</sub>O<sub>2</sub>. However, analysis by XPS and CO-DRIFTS revealed that the high selectivity shown by the bi-metallic 0.75 wt.% Fe-0.25 wt.% Pd/TiO<sub>2</sub> catalyst was a contribution of two factors; *i*) an optimum ratio of PdO:Pd<sup>0</sup> mixtures, known to be one of the main parameters that control the selectivity towards the direct synthesis of H<sub>2</sub>O<sub>2</sub> *ii*) the lack of Pd ensembles as shown by CO-DRIFTS analysis.

Unfortunately, the analysis of the post-reaction mixture after the degradation of phenol by MP-AES determined that the three bi-metallic 1 wt.% FePd/TiO<sub>2</sub> catalysts were still not stable despite having decreased the metal loading. There were no difference between the three bi-metallic ratios and the Fe and Pd metal leached (46-37 % Fe leached, 2 % Pd leached). It was seen that the metal leaching was linked to the extent of phenol conversion, since the bi-metallic 1 wt.% FePd/TiO<sub>2</sub> catalysts showed the greatest activity towards the degradation of phenol and the greatest instability. On the other hand, both mono-metallic 1 wt.% Fe/TiO<sub>2</sub> and 1 wt.% Pd/TiO<sub>2</sub> catalysts did not show relevant activity towards the degradation of phenol and neither they significantly leached. It was shown that the deactivation of the catalyst during re-usability testing towards the degradation of phenol was due to the metal leaching as the re-usability test experiments proved. Thus, since the stability of Fe and Pd were not possible to be avoided, Au was decided not to be introduced into the bi-metallic FePd system yet, because further synthetic catalytic strategies to enhance the stability of Fe had to be investigated first. Agglomerates and clusters of iron oxide particles (Fe<sub>x</sub>O<sub>y</sub>) were found to be deposited on the surface of TiO<sub>2</sub> according to XPS and they were found to be accountable for the high amount of Fe leached at the end of the reaction.

#### 4.4 References.

1. Chong, M. N., Jin, B., Chow, C. W. K., Saint, C. Recent developments in photocatalytic water treatment technology: A review. *Water Res.* **44**, 2997–3027 (2010).
2. Abu, H., Rozaimah, S., Abdullah, S., Tan, N., Jay, S. Journal of Industrial and Engineering Chemistry Interaction of environmental factors on simultaneous biosorption of lead and manganese ions by locally isolated *Bacillus cereus*. *J. Ind. Eng. Chem.* **37**, 295–305 (2016).

3. Bolisetty, S., Peydayesh, M., Mezzenga, R. Sustainable technologies for water purification from heavy metals: review and analysis. *Chem. Soc. Rev.* **48**, 463–487 (2019).
4. Väliälto, P., Kruglova, A., Mikola, A., Vahala, R. International Journal of Hygiene and Toxicological impacts of antibiotics on aquatic micro-organisms: A. *Int. J. Hyg. Environ. Health.* **220**, 558–569 (2017).
5. Cheng, D., Hao, H., Guo, W., Woong, S., Duc, D. A critical review on antibiotics and hormones in swine wastewater : Water pollution problems and control approaches. *J. Hazard. Mater.* **387**, 121682 (2020).
6. Deborde, M., Von Gunten, U. Reactions of chlorine with inorganic and organic compounds during water treatment-Kinetics and mechanisms: A critical review. *Water Res.* **42**, 13–51 (2008).
7. Von Gunten, U. Oxidation Processes in Water Treatment: Are We on Track? *Environ. Sci. Technol.* **52**, 5062–5075 (2018).
8. Ge, F., Zhu, L., Chen, H. Effects of pH on the chlorination process of phenols in drinking water. *J. Hazard. Mater.* **133**, 99–105 (2006).
9. Munoz, M., de Pedro, Z. M., Casas, J. A., Rodriguez, J. J. Preparation of magnetite-based catalysts and their application in heterogeneous Fenton oxidation - A review. *Appl. Catal. B Environ.* **176–177**, 249–265 (2015).
10. Bayir, H. Reactive oxygen species. *Crit. Care Med.* **33**, 498-501 (2005).
11. Zhu, Y., Zhua, R., Xic, Y., Zhua, J., Zhue, G., He, H. Strategies for enhancing the heterogeneous fenton catalytic reactivity: A review. *Appl. Catal. B Environ.* **255**, 117739-117750 (2019).
12. Zazo, J. A., Casas, J. A., Mohedano, A. F., Gilarranz, M. A., Rodríguez, J. J. Chemical pathway and kinetics of phenol oxidation by Fenton's reagent. *Environ. Sci. Technol.* **39**, 9295–9302 (2005).
13. Neyens, E., Baeyens, J. A review of classic Fenton's peroxidation as an advanced oxidation technique. *J. Hazard. Mater.* **98**, 33–50 (2003).
14. Sharma, S., Ruparelia, J. P., Patel, M. L. A general review on Advanced Oxidation Processes for waste water treatment. *International conference on current trends in technology.* **7**, 8–10 (2011).
15. Underhill, R., Lewis, R.J., Freakly, S.J., Douthwaite, M., Miedziak, P.J., Akdim, O., Edwards, J.K., Hutchings, G.J. Oxidative Degradation of Phenol using in situ Generated Hydrogen Peroxide Combined with Fenton's Process. *Johnson Matthey Technol. Rev.* **62**, 417–425 (2018).
16. Ghaffari, Y., Gupta, N. K., Bae, J., Kim, K. S. Heterogeneous catalytic performance and stability of iron-loaded ZSM-5, zeolite-A, and silica for phenol degradation: A microscopic and spectroscopic approach. *Catalysts.* **9**, 1-15 (2019).

17. Yan, Y., Jiang, S., Zhang, H. Catalytic wet oxidation of phenol with Fe-ZSM-5 catalysts. *RSC Adv.* **6**, 3850–3859 (2016).
18. Ovejero, G., Sotelo, J. L., Martínez, F., Melero, J. A. & Gordo, L. Wet peroxide oxidation of phenolic solutions over different iron-containing zeolitic materials. *Ind. Eng. Chem. Res.* **40**, 3921–3928 (2001).
19. Meenakshisundaram, S., He, Q., Moataz, M., Pritchard, J., Freakley, S.J., Edwards, J.K., Taylor, S.H., Morgan, D.J., Carley, A.F., Knight, D.W., Kiely, C.J., Hutchings, G.J. Synthesis of stable ligand-free gold-palladium nanoparticles using a simple excess anion method. *ACS Nano.* **6**, 6600–6613 (2012).
20. Santos, A., Lewis, R.J., Malta, G., Howe, A.G.R., Morgan, D.J., Hampton, E., Gaskin, P., Hutchings, G.J. Direct Synthesis of Hydrogen Peroxide over Au–Pd Supported Nanoparticles under Ambient Conditions. *Ind. Eng. Chem. Res.* **58**, 12623–12631 (2019).
21. Pawelec, B., Venezia, A. M., Parola, V. L., Cano-serrano, E., Campos-Martin, J.M., Fierro, J.L.G. AuPd alloy formation in Au-Pd/Al<sub>2</sub>O<sub>3</sub> catalysts and its role on aromatics hydrogenation. *Applied Surface Science.* **242**, 380–391 (2005).
22. Sun, X., Dong, S., Wang, E. Large-Scale Synthesis of Micrometer-Scale Single-Crystalline Au Plates of Nanometer Thickness by a Wet-Chemical Route. *Angew.Chem.Int.Ed.* **43**, 6360–6363 (2004).
23. Xu, L., Caiwu, X., Zhu, J.J. Green preparation and catalytic application of Pd nanoparticles. *Nanotechnologie.* **19**, 305,603-305,610 (2008).
24. Lee, S.S., Park, H.I., Park, B.K., Byeon, S.H. Influence of solvents on the formation of Pd and PdO nanoparticles in SBA-15. *Materials Science and Engineering: B.* **135**, 20-24 (2006).
25. Omar, H. D. To Investigation the Structure and Morphology of Iron Metallic by Difference Techniques. *Natural Sciences Publishing Cor.* **61**, 57–61 (2015).
26. Lak, A., Kraken, M., Ludwig, F., Kornowski, D.E., Sievers, S., Litterst, J., Weller, H., Schilling, M. Size dependent structural and magnetic properties of FeO–Fe<sub>3</sub>O<sub>4</sub> nanoparticles. *Nanoscale.* **5**, 12286–12295 (2013).
27. Krispin, M., Ullrich, A., Horn, S. Crystal structure of iron-oxide nanoparticles synthesized from ferritin. *J Nano part Res.* **14**, 669-680 (2012).
28. Qayoom, M., Shah, K. A., Pandit, A. H., Firdous, A., Dar, G. N. Dielectric and electrical studies on iron oxide ( $\alpha$ -Fe<sub>2</sub>O<sub>3</sub>) nanoparticles synthesized by modified solution combustion reaction for microwave applications. *Journal of electroceramics.* **3**, 7–14 (2020).
29. Qiang, C., Xu, J., Zhang, Z., Tian, L., Xiao, S., Liu, Y., Xu, P. Magnetic properties and microwave absorption properties of carbon fibers coated by Fe<sub>3</sub>O<sub>4</sub> nanoparticles. *J. Alloys Compd.* **506**, 93–97 (2010).

30. Nilesh V. Gandhare, N.V., Chaudhary, R.G., Meshram, V.P., Tanna, J.A., Lad, S., Gharpure, M.P., Juneja, H.D. An efficient and one-pot synthesis of 2,4,5-trisubstituted imidazole compounds catalyzed by copper nanoparticles. *Journal of the Chinese Advanced Materials Society*. **3**, 270-279 (2015).
31. Thakar, M. A., Jha, S.S., Phasinam, K., Manne, R., Qureshi, Y., Badu, H. X ray diffraction (XRD) analysis and evaluation of antioxidant activity of copper oxide nanoparticles synthesized from leaf extract of *Cissus vitiginea*. *Mater. Today Proc.* **51**, 319–324 (2022).
32. Zhu, D., Wang, L., Yu, W., Xie, H. Intriguingly high thermal conductivity increment for CuO nanowires contained nanofluids with low viscosity. *Sci. Rep.* **8**, 1–12 (2018).
33. Hui, S.R., Wu, M., Ge, S., Yan, D., Zhang, Y.D., Xiano, T.D., Yacaman, M.J., Yoshida, M., Hines, W.A., Budnick, J.I. Synthesis and Characterization of Structure Controlled Nano-cobalt Particles. *Mat. Res. Soc. Symp. Proc.* **755**, 3–8 (2003).
34. Lenzion-bielun, Z., Narkiewicz, U., Arabczyk, W. Cobalt-based Catalysts for Ammonia Decomposition. *Materials*. **6**, 2400–2409 (2013).
35. Bulavchenko, O. A., Cherepanova, S.V., Malakhov, V.V., Dovlitova, L.S., Ishchenko, A.V., Tsybulya, S.V. In Situ XRD Study of Nanocrystalline Cobalt Oxide Reduction. *50*, 205–211 (2009).
36. Barreca, D., Massignan, C. Composition and Microstructure of Cobalt Oxide Thin Films Obtained from a Novel Cobalt (II) Precursor by Chemical Vapor Deposition. *Chemical Material*. **13**, 588–593 (2001).
37. Crombie, C. M., Lewis, R.J., Kovacic, D., Slater, T.J.A., Davies, T.E., Edwards, J.K., Skov, M., Rasmussen, S., Hutchings, G.J. The Selective Oxidation of Cyclohexane via In-situ H<sub>2</sub>O<sub>2</sub> Production Over Supported Pd - based Catalysts. *Catal. Letters*. **151**, 2762–2774 (2021).
38. Ab Rahim, M. H., Armstrong, R.D., Hammond, C., Dimitratos, N., Freakley, S.J., Forde, M.M., Morgan, D.J., Lalev, G., Jenkins, R.L., Lopez-Sanchez, J.A., Taylor, S.H., Hutchings, G.J. Low temperature selective oxidation of methane to methanol using titania supported gold palladium copper catalysts. *Catal. Sci. Technol.* **6**, 3410–3418 (2016).
39. Sellers, R. M. Spectrophotometric Determination of Hydrogen Peroxide Using Potassium Titanium( IV) Oxalate. *Analyst*. **105**, 950–954 (1990).
40. Crombie, C. M., Lewis, R.J., Taylor, R.L., Morgan, D.J., Davies, T.E., Folli, A., Murphy, D.M., Edwards, J.K., Qi, J., Jiang, H., Kiely, C.J., Liu, X., Skjøth-Rasmussen, M.S., Hutchings, G.J. Enhanced Selective Oxidation of Benzyl Alcohol via In Situ H<sub>2</sub>O<sub>2</sub> Production over Supported Pd-Based Catalysts. *ACS Catal.* **11**, 2701-2714 (2021).
41. Chen, S., Liu, S., Men, Y., Li, L., Li, X., Pan, X., Sun, C., Xiong, L., Niu, X., An, W.,

- Wang, J., Wang, Y. Synergistic Catalysis of PdFe Bimetallic Nanoparticles Supported on SiO<sub>2</sub> for Hydrogenative Cleavage of C–N Bonds. *ACS Appl. Nano Mater.* **4**, 6020–6029 (2021).
42. Zhai, X., Liu, C., Chang, Q., Zhao, C., Tan, R. TiO<sub>2</sub>-nanosheet-assembled microspheres as Pd-catalyst support for highly-stable low-temperature CO oxidation. *New J. Chem.* **42**, 18066–18076 (2018).
  43. Ouyang, L., Da, G.j., Tian, P.f., Chen, T.y., Liang, G.d., Xu, J., Han, Y.F. Insight into active sites of Pd–Au/ TiO<sub>2</sub> catalysts in hydrogen peroxide synthesis directly from H<sub>2</sub> and O<sub>2</sub>. *J. Catal.* **311**, 129–136 (2014).
  44. Ao, C., Tian, P., Ouyang, L., Da, G., Xu, X., Xu, J., Han, Y.F. Dispersing Pd nanoparticles on N-doped TiO<sub>2</sub>: *Catal. Sci. Technol.* **6**, 5060–5068 (2016).
  45. Choudhary, V. R., Gaikwad, A. G., Sansare, S. D. Activation of supported Pd metal catalysts for selective oxidation of hydrogen to hydrogen peroxide. *Catal. Letters.* **83**, 235–239 (2002).
  46. Choudhary, V. R., Samanta, C., Choudhary, T. V. Direct oxidation of H<sub>2</sub> to H<sub>2</sub>O<sub>2</sub> over Pd-based catalysts: Influence of oxidation state, support and metal additives. *Appl. Catal. A Gen.* **308**, 128–133 (2006).
  47. Gemo, N., Menegazzo, F., Biasi, P., Sarkar, A., Samikannu, A., Raut, D.G., Kord, K., Rautio, A.R., Mohl, M., Bostrom, D., Shchukarevc, A., Mikkola, J.P. TiO<sub>2</sub> nanoparticles: Vs. TiO<sub>2</sub> nanowires as support in hydrogen peroxide direct synthesis: The influence of N and Au doping. *RSC Adv.* **6**, 103311–103319 (2016).
  48. Samanta, C. & Choudhary, V. R. Direct formation of H<sub>2</sub>O<sub>2</sub> from H<sub>2</sub> and O<sub>2</sub> and decomposition/hydrogenation of H<sub>2</sub>O<sub>2</sub> in aqueous acidic reaction medium over halide-containing Pd/SiO<sub>2</sub> catalytic system. *Catal. Commun.* **8**, 2222–2228 (2007).
  49. Ouyang, L., Tian, P.F., Da, G.J., Xu, X.C., Ao, C., Chen, T.Y., Si, R., Xu, J., Han, Y.F. The origin of active sites for direct synthesis of H<sub>2</sub>O<sub>2</sub> on Pd/TiO<sub>2</sub> catalysts: Interfaces of Pd and PdO domains. *J. Catal.* **321**, 70–80 (2015).
  50. Kim, J. K., Metcalfe, I. S. Investigation of the generation of hydroxyl radicals and their oxidative role in the presence of heterogeneous copper catalysts. *Chemosphere.* **69**, 689–696 (2007).
  51. Quintanilla, A., Casas, J. A. Catalytic wet air oxidation of phenol with modified activated carbons and Fe / activated carbon catalysts. *Applied Catalysis B: Environmental.* **76**, 135–145 (2007).
  52. Inchaurredo, N. S., Massa, P., Fenoglio, R., Font, J., Haure, P. Efficient catalytic wet peroxide oxidation of phenol at moderate temperature using a high-load supported copper catalyst. *Chem. Eng. J.* **198–199**, 426–434 (2012).

#### 4.5 Supplementary information.

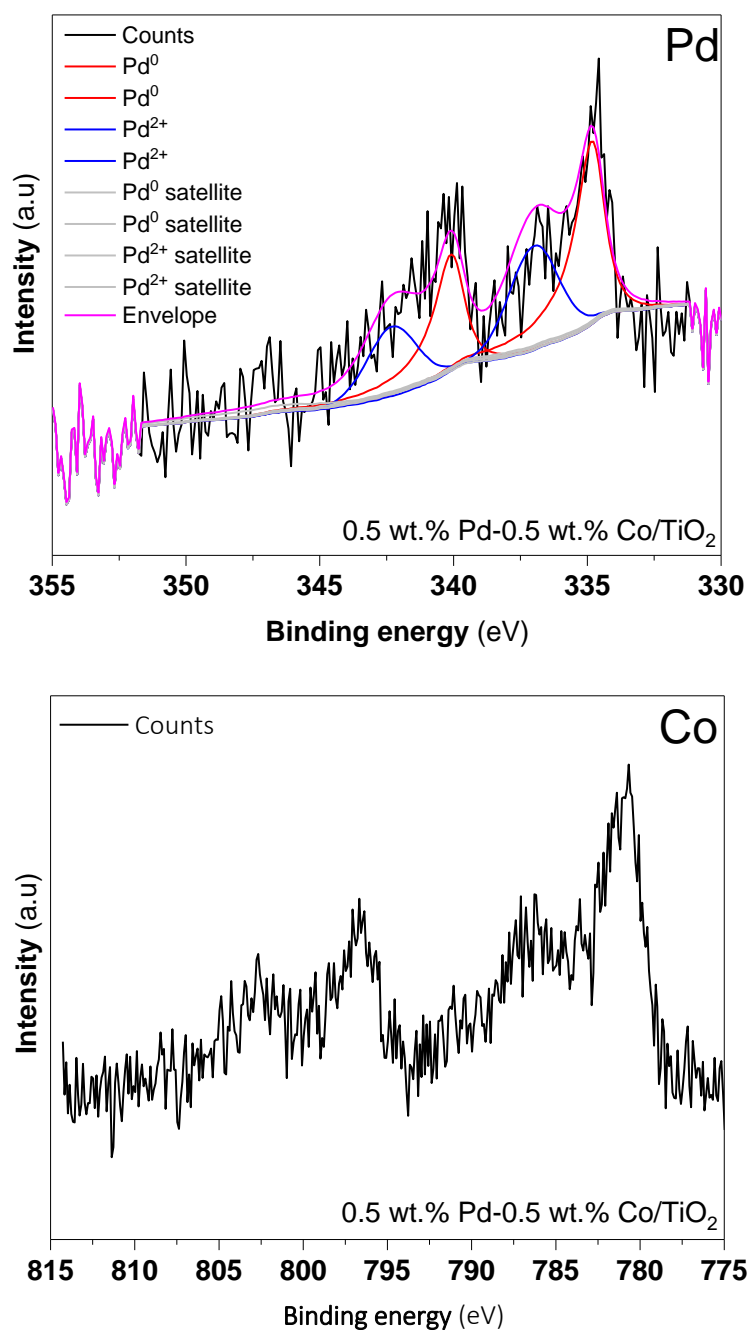
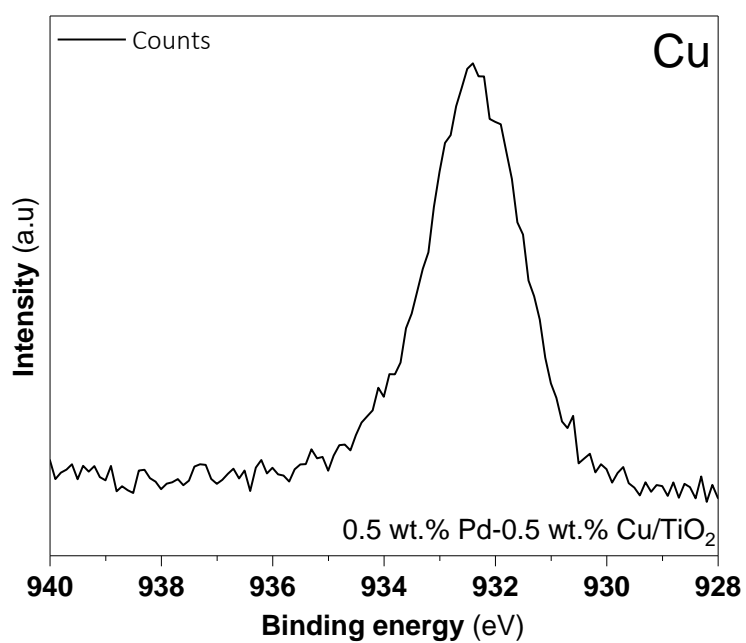
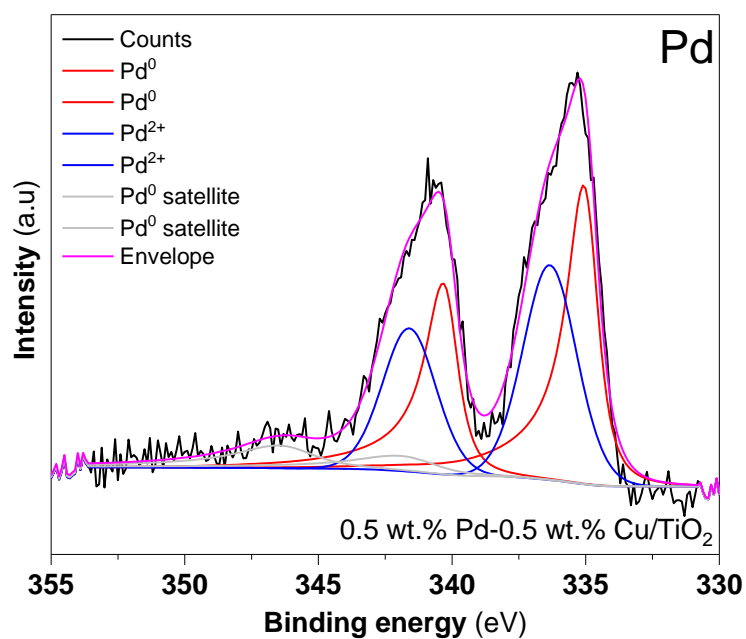


Figure S.I 4.1: XPS fitting for the bi-metallic 0.5 wt.% Pd-0.5 wt.% Co/TiO<sub>2</sub> catalyst.



**Figure S.I 4.2:** XPS fitting for the bi-metallic 0.5 wt.% Pd-0.5 wt.% Cu/TiO<sub>2</sub> catalysts.

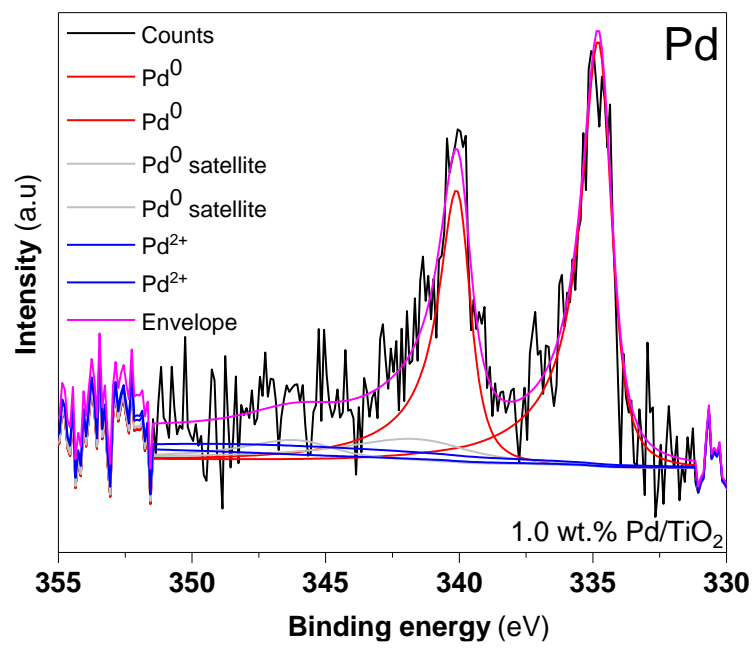


Figure S.I 4.3: XPS fitting for the mono-metallic 1 wt.% Pd/TiO<sub>2</sub> catalyst.

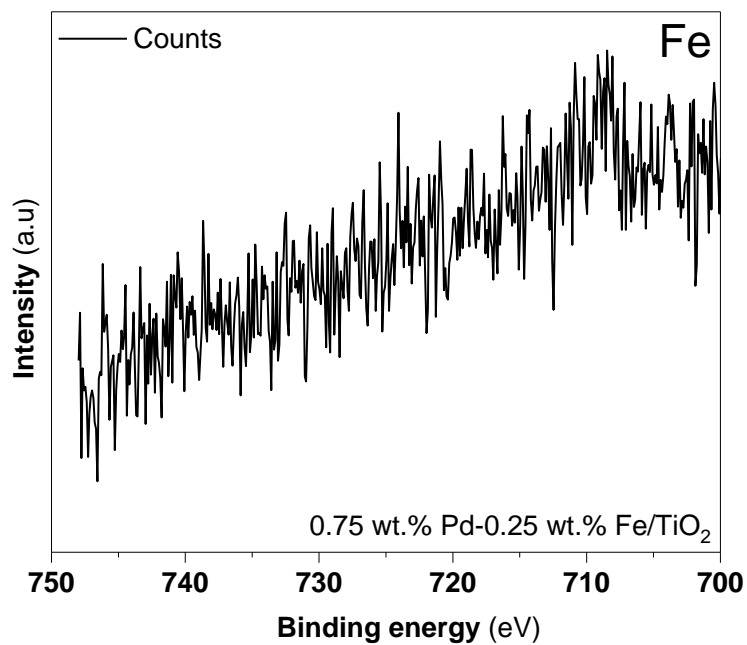
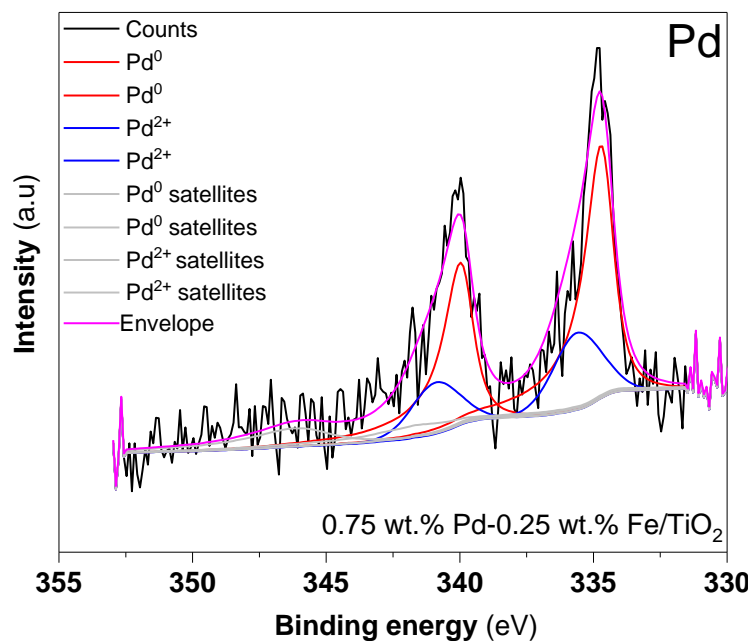


Figure S.I 4.4: XPS fitting for the bi-metallic 0.75 wt.% Pd-0.25 wt.% Fe/TiO<sub>2</sub> catalyst.

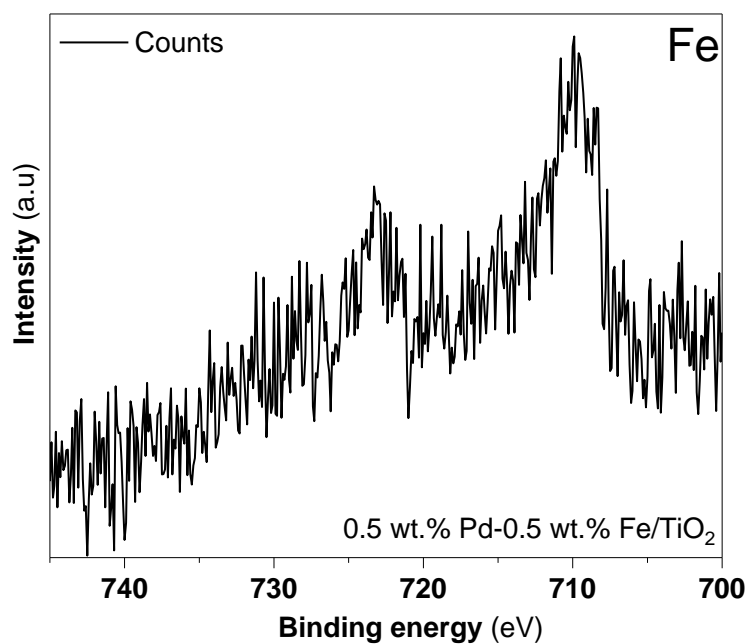
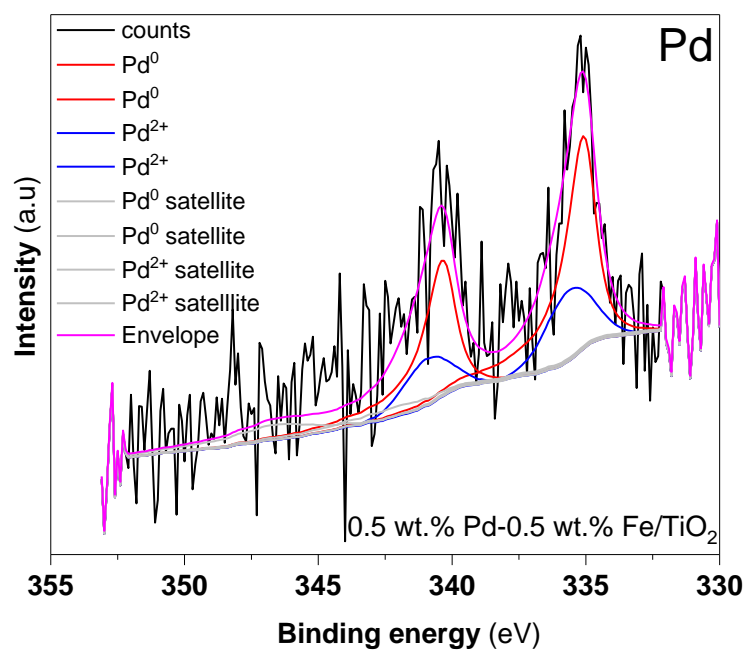
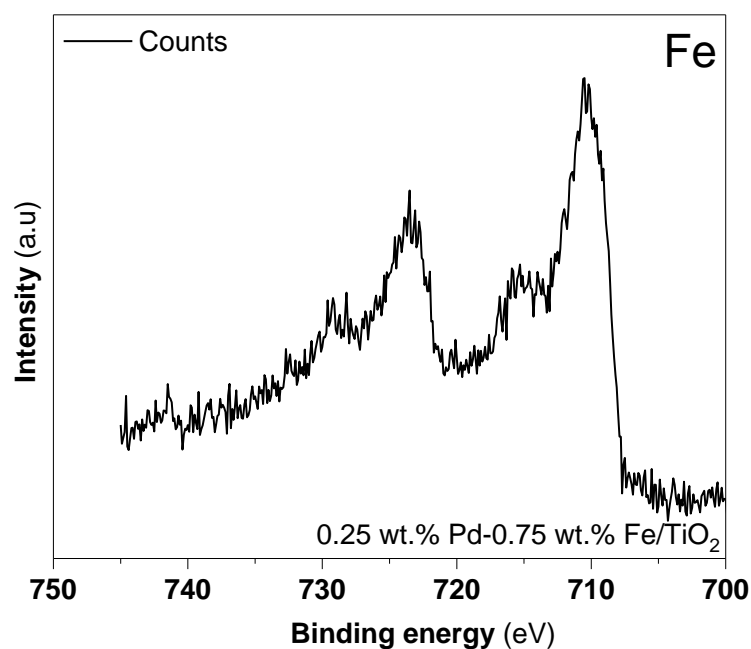
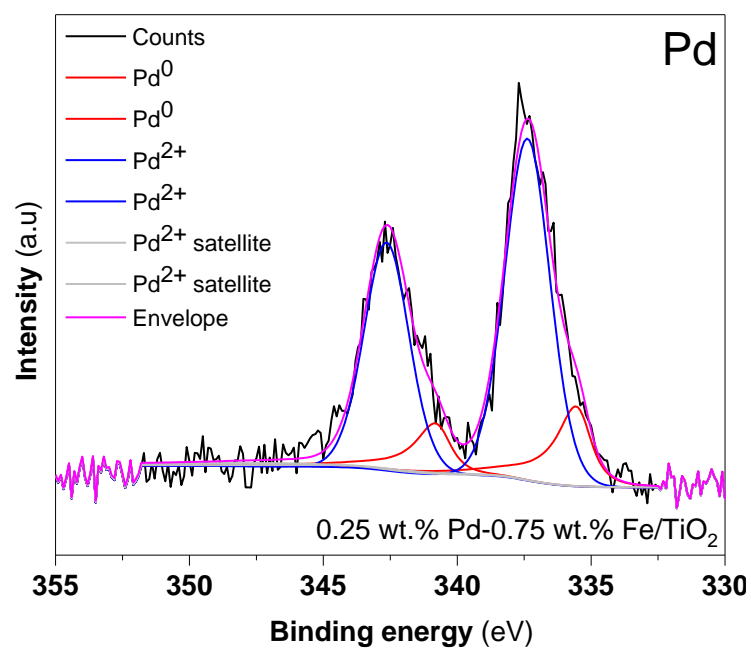
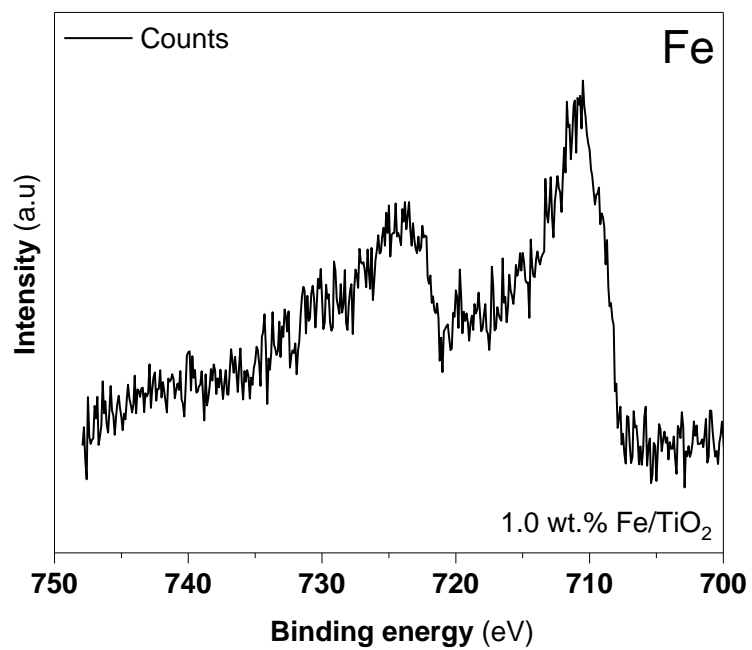


Figure S.I 4.5: XPS fitting for the bi-metallic 0.5 wt.% Pd-0.5 wt.% Fe/TiO<sub>2</sub> catalyst.



**Figure S.I 4.6:** XPS fitting for the bi-metallic 0.25 wt.% Pd-0.75 wt.% Fe/TiO<sub>2</sub> catalyst.



**Figure S.I 4.7:** XPS fitting for the mono-metallic 1.0 wt.% Fe/TiO<sub>2</sub> catalyst.

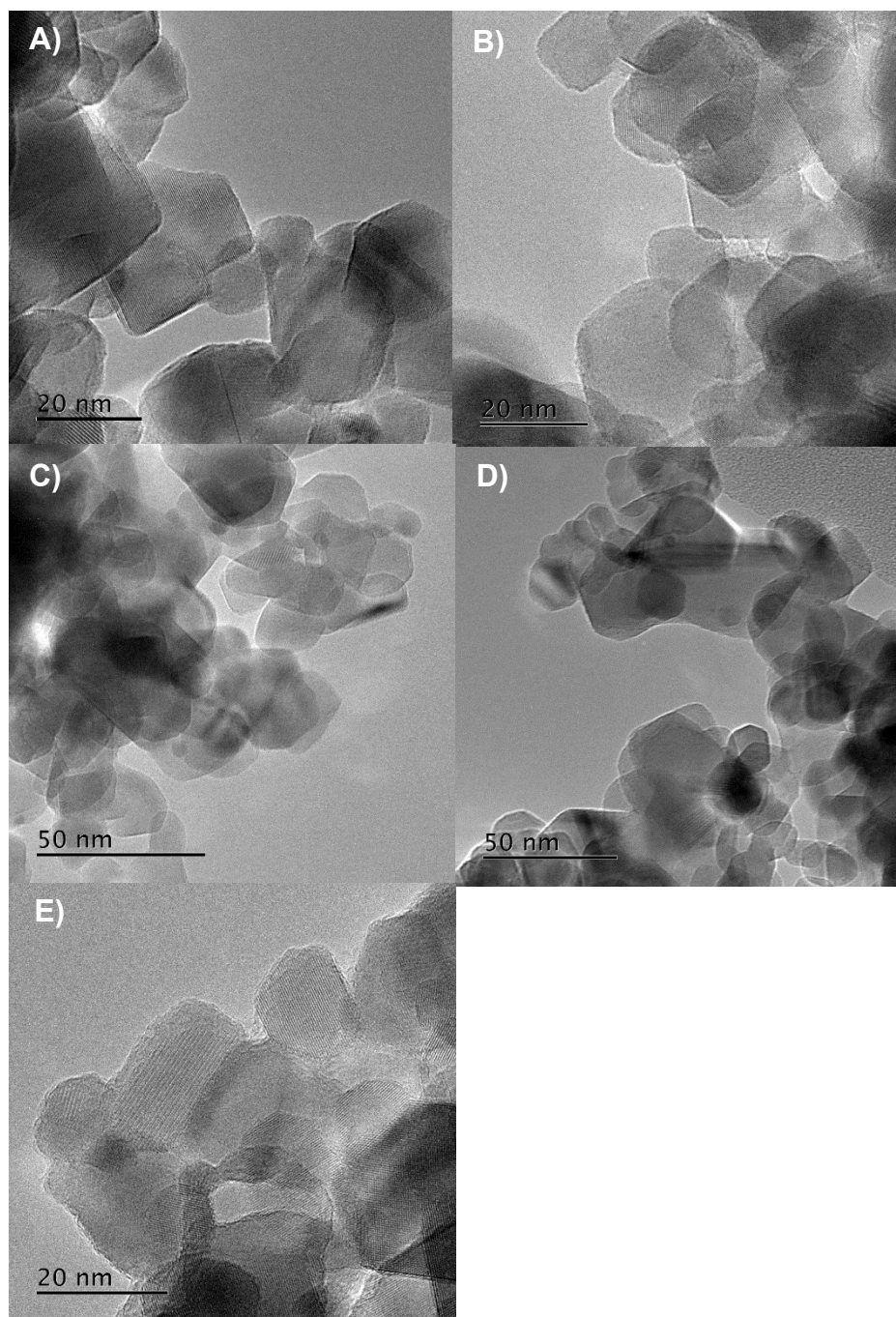


**Figure S.I 4.8:** TEM images for mono and bi-metallic fresh 1.0 wt.% FePd/TiO<sub>2</sub> catalysts.  
**Nomenclature:** **A)** 1 wt.% Pd/TiO<sub>2</sub>, **B)** 0.75 wt.% Pd-0.25 wt.% Fe/TiO<sub>2</sub>, **C)** 0.50 wt.% Pd-0.50 wt.% Fe/TiO<sub>2</sub>, **D)** 0.25 wt.% Pd-0.75 wt.% Fe/TiO<sub>2</sub> and **E)** 1 wt.% Fe/TiO<sub>2</sub>.

**Table S.I 4.1:** Elemental analysis by EDX for the mono-metallic 1 wt.% Fe/TiO<sub>2</sub> catalyst.

<b>Element</b>	<b>Line Type</b>	<b>k factor</b>	<b>Absorption Correction</b>	<b>Wt%</b>	<b>Wt% Sigma</b>
<b>O</b>	K series	2.05018	1.00	40.93	0.08
<b>Ti</b>	K series	1.08940	1.00	57.85	0.08
<b>Fe</b>	K series	1.11556	1.00	1.22	0.02
<b>Total:</b>				100.00	

**Table S.I 4.2:** Elemental analysis by EDX for the bi-metallic 0.75 wt.% Fe-0.25 wt.% Pd/ TiO<sub>2</sub> catalyst.

<b>Element</b>	<b>Line Type</b>	<b>k factor</b>	<b>Absorption Correction</b>	<b>Wt%</b>	<b>Wt% Sigma</b>
<b>O</b>	K series	2.05018	1.00	23.67	0.09
<b>Ti</b>	K series	1.08940	1.00	75.24	0.10
<b>Fe</b>	K series	1.11556	1.00	0.94	0.02
<b>Pd</b>	K series	8.24217	1.00	0.15	0.06

**Table S.I 4.3:** Elemental analysis by EDX for the bi-metallic 0.50 wt.% Fe-0.50 wt.% Pd/ TiO<sub>2</sub> catalyst.

<b>Element</b>	<b>Line Type</b>	<b>k factor</b>	<b>Absorption Correction</b>	<b>Wt%</b>	<b>Wt% Sigma</b>
<b>O</b>	K series	2.05018	1.00	40.63	0.09
<b>Ti</b>	K series	1.08940	1.00	58.26	0.10
<b>Fe</b>	K series	1.11556	1.00	0.63	0.02
<b>Pd</b>	K series	8.24217	1.00	0.48	0.08

**Table S.I 4.4:** Elemental analysis by EDX for the bi-metallic 0.25 wt.% Fe-0.75 wt.% Pd/ TiO<sub>2</sub> catalyst.

Element	Line Type	k factor	Absorption Correction	Wt%	Wt% Sigma
O	K series	2.05018	1.00	40.96	0.09
Ti	K series	1.08940	1.00	58.48	0.10
Fe	K series	1.11556	1.00	0.40	0.01
Pd	K series	8.24217	1.00	0.16	0.06

**Table S.I 4.5:** Elemental analysis by EDX for the mono-metallic 1 wt.% Pd/ TiO<sub>2</sub> catalyst.

Element	Line Type	k factor	Absorption Correction	Wt%	Wt% Sigma
C	K series	2.81239	1.61	5.33	0.30
O	K series	2.05018	2.11	54.18	0.22
Ti	K series	1.08940	0.90	40.10	0.18
Pd	L series	1.85934	0.92	0.39	0.04
<b>Total:</b>				100.00	

**Table S.I 4.6:** Leaching of the mono and bi-metallic 1.0 wt.% FePd/TiO<sub>2</sub> catalysts during the direct synthesis of H<sub>2</sub>O<sub>2</sub>.

Catalysts	Fe/ %	Pd/ %
1.0 wt.% Pd/TiO <sub>2</sub>	0	0
0.75 wt.% Pd-0.25 wt.% Fe/TiO <sub>2</sub>	0	0
0.5 wt.% Pd-0.5 wt.% Fe/TiO <sub>2</sub>	0.01	0
0.25 wt.% Pd-0.75 wt.% Fe/TiO <sub>2</sub>	0	0
1.0 wt.% Fe/TiO <sub>2</sub>	0	0

**Reaction conditions towards the direct synthesis of H<sub>2</sub>O<sub>2</sub>:** 8.5 g (5.6 g CH<sub>3</sub>OH, 2.9 g H<sub>2</sub>O), catalyst (0.01 g), 420 psi 5 % H<sub>2</sub>/CO<sub>2</sub>, 160 psi 25 % O<sub>2</sub>/CO<sub>2</sub>, 1200 rpm, 30 °C, 2 h.

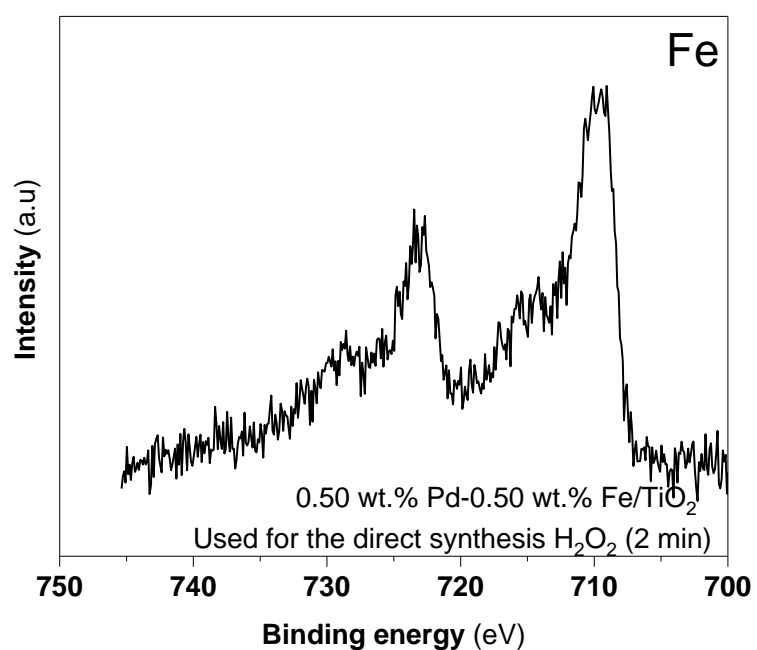
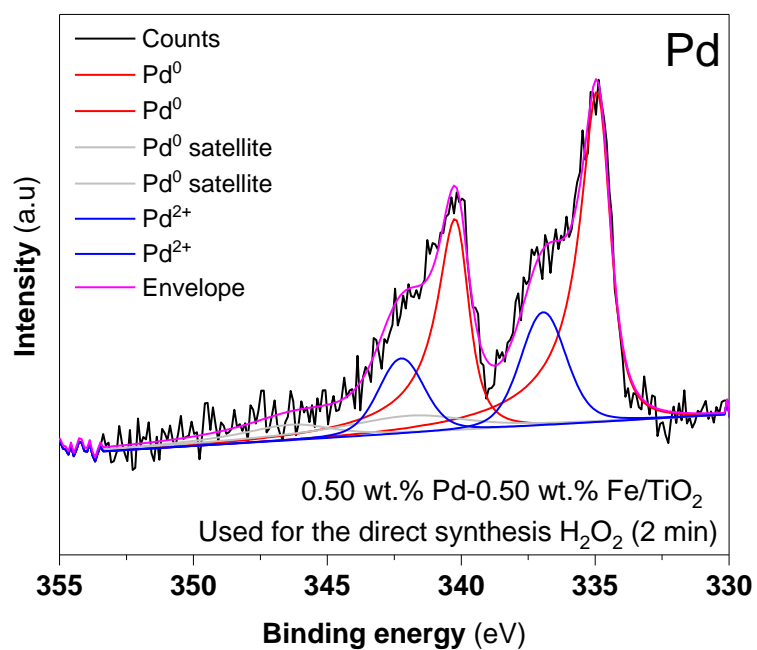


**Figure S.I 4.9:** XPS fitting for the used bi-metallic 0.5 wt.% Pd-0.5 wt.% Pd/TiO<sub>2</sub> catalysts towards the direct synthesis of H<sub>2</sub>O<sub>2</sub>. **Reaction conditions:** 8.5 g (HPLC grade water), catalyst (0.01 g), 420 psi 5 % H<sub>2</sub>/CO<sub>2</sub>, 160 psi 25 % O<sub>2</sub>/CO<sub>2</sub>, 1200 rpm, 30 °C, 2 min.

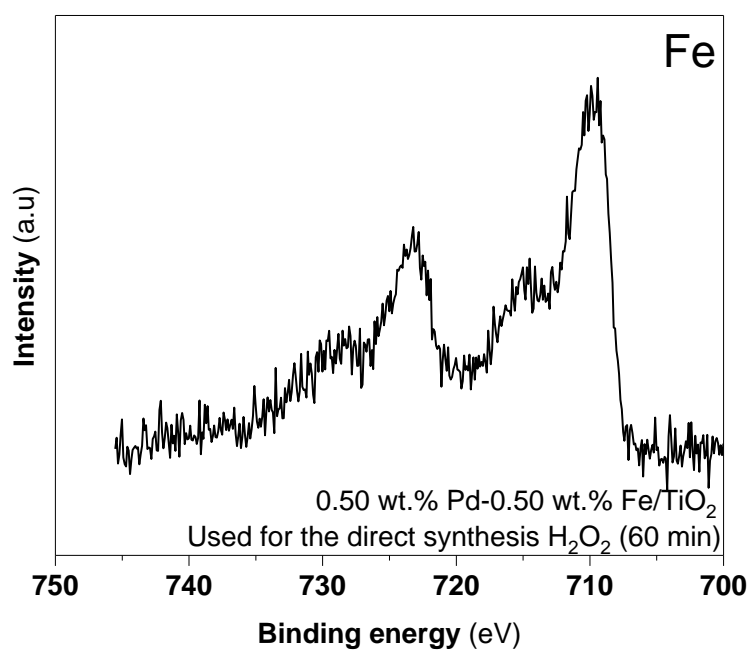
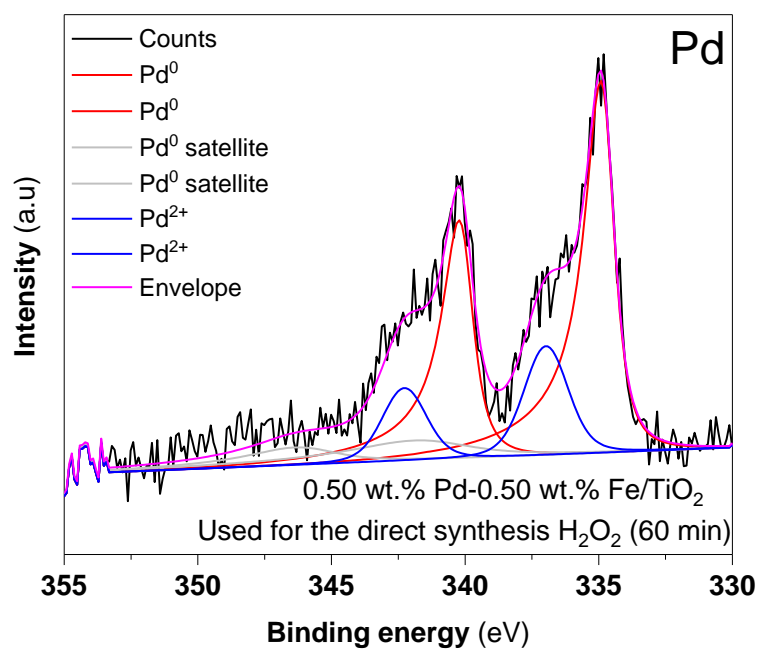


**Figure S.I 4.10:** XPS fitting for the used bi-metallic 0.5 wt.% Pd-0.5 wt.% Pd/TiO<sub>2</sub> catalyst towards the direct synthesis of H<sub>2</sub>O<sub>2</sub>. **Reaction conditions:** 8.5 g (HPLC grade water), catalyst (0.01 g), 420 psi 5 % H<sub>2</sub>/CO<sub>2</sub>, 160 psi 25 % O<sub>2</sub>/CO<sub>2</sub>, 1200 rpm, 30 °C, 1 h.

**Table S.I 4.7:** Time on-line stability measurements of the mono and bi-metallic 1.0 wt.% FePd/TiO<sub>2</sub> during the degradation of phenol.

<b>Catalysts</b>	<b>Fe/</b>	<b>Pd/</b>
	<b>%</b>	<b>%</b>
<b>1.0 wt.% Pd/TiO<sub>2</sub></b>		
min		
<b>5</b>	0	1
<b>30</b>	0	0
<b>60</b>	0.1	1
<b>120</b>	0	0
<b>0.75 wt.% Pd-0.25 wt.% Fe/TiO<sub>2</sub></b>		
min		
<b>5</b>	4	2
<b>30</b>	19	1
<b>60</b>	34	1
<b>120</b>	46	2
<b>0.5 wt.% Pd-0.5 wt.% Fe/TiO<sub>2</sub></b>		
min		
<b>5</b>	21	1
<b>30</b>	41	1
<b>60</b>	46	1
<b>120</b>	61	2
<b>0.25 wt.% Pd-0.75 wt.% Fe/TiO<sub>2</sub></b>		
min		
<b>5</b>	4	0
<b>30</b>	9	2
<b>60</b>	36	1
<b>120</b>	36	2
<b>1.0 wt.% Fe/TiO<sub>2</sub></b>		
min		
<b>5</b>	0.1	0
<b>30</b>	0.1	0
<b>60</b>	0	0
<b>120</b>	0.3	0

**Reaction conditions:** 8.5 g (phenol (1000 ppm)), catalyst (0.01 g), 420 psi 5 % H<sub>2</sub>/CO<sub>2</sub>, 160 psi 25 % O<sub>2</sub>/CO<sub>2</sub>, 1200 rpm, 30 °C.

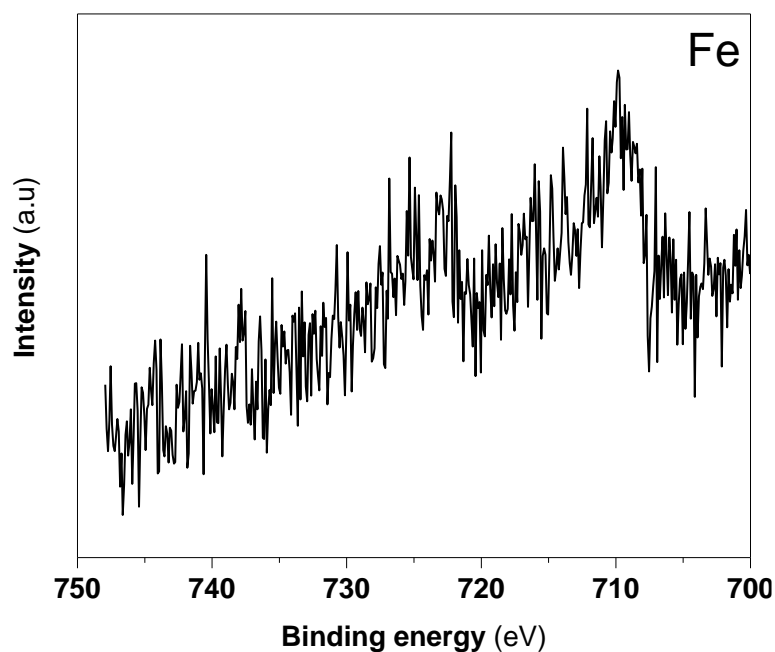
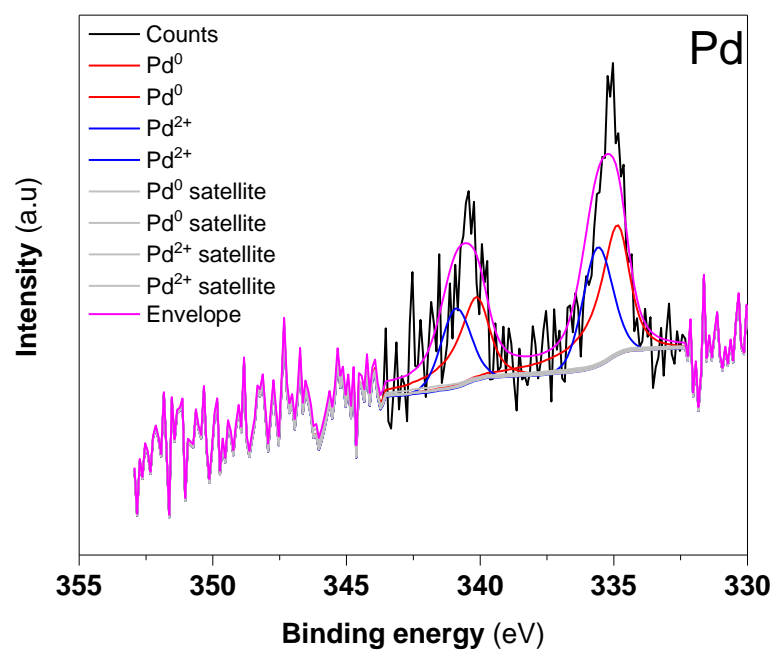


**Figure S.I 4.11:** XPS fitting for the used bi-metallic 0.5 wt.% Pd-0.5 wt.% Pd/TiO<sub>2</sub> catalyst towards the degradation of phenol. **Reaction conditions:** 8.5 g (phenol (1000 ppm)), catalyst (0.01 g), 420 psi 5 % H<sub>2</sub>/CO<sub>2</sub>, 160 psi 25 % O<sub>2</sub>/CO<sub>2</sub>, 1200 rpm, 30 °C, 2 h.

# Chapter 5: Oxidation of phenol with Pd impregnated on HZSM-5 containing Fe.

## 5.1 Introduction.

In Chapter 4 Fe has shown to be the most promising Fenton metal to convert *in-situ* H<sub>2</sub>O<sub>2</sub> into reactive oxygen species (ROS) in comparison to other Fenton metals such as Cu and Co. However, bi-metallic systems of 1 wt.% FePd/TiO<sub>2</sub> were found to be unstable, with the leaching of Fe and Pd linked to the extent of phenol conversion. This observation has also been reported in previous works highlighting the limited stability of Fe species during the degradation of phenol.<sup>1,2,3</sup> Therefore, if bi-metallic FePd supported catalysts are meant to be considered for water treatment remediation, the stability of Fe and Pd needs to be improved. Several authors have reported that the stability of the Fe during the degradation of phenol with pre-formed H<sub>2</sub>O<sub>2</sub> is dependent on the type of Fe species formed during the synthesis of the mono-metallic Fe supported catalyst.<sup>4</sup> The type of Fe species can be roughly categorise into two groups *i*) extra-framework Fe species (Fe<sub>x</sub>O<sub>y</sub> clusters and agglomerates) deposited on the surface of the support and *ii*) framework Fe species (isolated Fe species and bi-nuclear Fe species) immobilised to the framework channels of a zeolite, where the framework Fe species have been acknowledged to have better stability.<sup>1,2,3</sup>

Zeolites are hydrated aluminosilicates with the general chemical formula of Mn<sup>+</sup>(x/n) (AlO<sup>-</sup>2)<sub>x</sub> (SiO<sub>2</sub>)<sub>y</sub> (H<sub>2</sub>O)<sub>m</sub>. Fe-containing zeolites and mesoporous materials have drawn particular interest due to their catalytic properties in various reactions such as the reduction of nitrous oxides (NO, NO<sub>2</sub> and N<sub>2</sub>O) to ammonia (NH<sub>3</sub>),<sup>5</sup> oxidation of benzene to phenol <sup>6</sup> and selective oxidation of methane (CH<sub>4</sub>) to methanol (CH<sub>3</sub>OH).<sup>7,8</sup> Some zeolites have proven to have its framework hydrolysed when they are used in aqueous reactions mixtures. For instance, Sievers and co-workers <sup>9</sup> have studied the framework stability of Zeolite-Y (FAU) (SiO<sub>2</sub>:Al<sub>2</sub>O<sub>3</sub>= 5, 14, 21) and ZSM-5 (SiO<sub>2</sub>: Al<sub>2</sub>O<sub>3</sub>= 15, 25, 40) when they were in water and heat was applied (150-200 °C).<sup>9</sup> They concluded that the stability of the zeolite depends on the type of framework since ZSM-5 did not show any alterations during the study. However, the Si-O-Si bonds in Zeolite-Y were hydrolysed leading to an amorphous material, with the extent of hydrolysis being dependent on the SiO<sub>2</sub>:Al<sub>2</sub>O<sub>3</sub> ratio.<sup>9</sup> Hydrothermal synthesis is a procedure that permits the synthesis of zeolites containing Fenton metals such as Fe.<sup>1</sup> This

procedure, which is described in Chapter 2 section 2.2.2, will be employed to synthesise HZSM-5 containing Fe atomically dispersed in the zeolite lattice. Subsequent activation of the catalyst by calcination at 550 °C has been shown to promote the extraction the Fe from the lattice positions (where Fe<sup>3+</sup> is tetrahedrally co-ordinated) delivering extra-framework and/or framework Fe species depending on the Fe loading employed and the calcination heat treatment applied.<sup>10</sup>

Thus, the aim of this chapter is to investigate the activity and stability of a series of Pd/Fe-HZSM-5 catalysts that combine the efficacy of Pd to synthesise H<sub>2</sub>O<sub>2</sub> from H<sub>2</sub> and O<sub>2</sub> and the activity of Fe to convert H<sub>2</sub>O<sub>2</sub> to ROS for use in the oxidative degradation of phenol. A range of 3.0-0 wt.% Fe-HZSM-5 will be prepared by hydrothermal synthesis prior to Pd deposition (0.5 wt.%) by a modified impregnation procedure to generate bi-metallic 0.5 wt.% Pd/ X wt.% Fe-HZSM-5 (X: 3.0-0) catalysts.<sup>11</sup> The activity of the bi-metallic 0.5 wt.% Pd/ X wt.% Fe-HZSM-5 (X: 3.0-0) catalysts towards the direct synthesis and degradation of H<sub>2</sub>O<sub>2</sub> will be determined using an autoclave (Parr Instrument), in order to correlate the *in-situ* production of H<sub>2</sub>O<sub>2</sub> and its degradation to the extent of phenol conversion. The analysis of the post reaction solution after the degradation of phenol and direct synthesis of H<sub>2</sub>O<sub>2</sub> will be analysed by means of microwave plasma atomic emission spectroscopy (MP-AES) to determine the stability of the metals against leaching.

X-ray diffraction (XRD) will be used to determine the crystallinity of the bare HZSM-5, the mono-metallic X wt.% Fe-HZSM-5 (X: 3.0-0) catalysts as well as the bi-metallic 0.5 wt.% Pd/X wt.% Fe-HZSM-5 (X: 3.0-0) ones, with the inclusion of Fe into the zeolite lattice likely to disrupt the crystallinity of the zeolitic material, particularly at high Fe loadings. Also, physisorption analysis will be carried out to establish physical characteristics of the catalysts such as the surface area and pore volume after the introduction of the Fe and Pd. X-ray photoelectron spectroscopy (XPS) will be employed to determine the oxidation state of both metals, in addition CO-diffuse reflective infrared transform fourier spectroscopy (CO-DRIFTS) will be employed to determine the configuration of the metal nanoparticles. Mean nanoparticle size and distribution will be determined by means of transmission electron microscopy (TEM). Fourier transform infrared spectroscopy (FT-IR), raman-UV and diffuse reflectance ultraviolet visible spectroscopy (DR UV-Vis), will be used to discern the type of Fe species formed, which as mentioned above, can broadly consist of framework and extra-framework Fe species. Therefore, a correlation between the activity and stability of the bi-metallic 0.50 wt.% Pd/ X wt.% Fe-HZSM-5 (X: 3.0-0.06) catalysts and the type of Fe species formed is meant to be found.

The activity of each catalyst throughout this Chapter 5 is given by the mean value calculated from the results obtained from three different lots of the same catalysts. The mean activity value is accompanied by the standard deviation represented by error bars in each Figure and Table of catalytic results. If no error bars are shown next to the mean value given, this indicates that the catalytic activity was tested less than three times.

## 5.2 Results and discussion.

Table 5.1 presents the set of catalysts that will be investigated throughout this chapter. The metal loading of these set of catalysts could not be corroborated because the digestion of zeolites required high corrosive acids such as hydrofluoric, whose levels of corrosion required a special environment and safety precautions that could not be implemented lab-wise. There are known to be Fe impurities in the ammonia nitrate ( $\text{NH}_4\text{NO}_3$ ) (see Chapter 2, section 2.2.2.1) that was used during the direct synthesis of these set of mono and bi-metallic catalysts, which might have led to the Fe loading to be slightly higher than the theoretical one stated in Table 5.1.

**Table 5.1:** Mono and bi-metallic 0.5 wt.% Pd/ X wt.% Fe-HZSM-5 (X: 3.0-0) catalysts to be investigated towards the degradation of phenol.

<b>Catalyst</b>
0.5wt.%Pd/ 3.0wt.% Fe-HZSM-5
0.5wt.%Pd/ 2.0wt.% Fe-HZSM-5
0.5wt.%Pd/ 1.0wt.% Fe-HZSM-5
0.5wt.%Pd/ 0.5wt.% Fe-HZSM-5
0.5wt.%Pd/ 0.125wt.% Fe-HZSM-5
0.5wt.%Pd/ 0.06wt.% Fe-HZSM-5
0.5wt.%Pd/ 0 wt.% Fe-HZSM-5

### 5.2.1 Characterisation of the mono and bi-metallic 0.5 wt.% Pd/ X wt.% Fe-HZSM-5 (X: 3.0-0) catalysts.

The set of catalysts shown in Table 5.1 were analysed by XRD before (X wt.% Fe-HZSM-5, (X: 3.0-0) (Figure 5.1) and after the deposition of Pd (0.5 wt.% Pd/ X wt.% Fe-HZSM-5, (X: 3.0-0) (Figure 5.2). The samples presented the characteristics reflections of the HZSM-5 structure which appeared between  $\theta=7-9^\circ$  and  $\theta=23-25^\circ$  indicating that the preparation of the HZSM-5 was successfully achieved and that the incorporation of the Fe and the subsequent impregnation of the Pd had not altered the framework.<sup>12,13</sup> The crystallinity of the sample which is stated in percentage in Figure 5.1 and 5.2 for each catalyst respectively was calculated based on the comparison between the intensity of the of the peaks between

$2\theta = 22-25^\circ$  and the intensity of the same peaks for a reference commercial sample (HZSM-5 ( $\text{SiO}_2:\text{Al}_2\text{O}_3$ ) (23:1)).<sup>14,15,16</sup>

Despite the mono and bi-metallic 0.5 wt.% Pd/ X wt.% Fe-HZSM-5 (X: 3.0-0) catalysts presented reflections associated with HZSM-5 structure, the crystallinity varied among the samples; the bare zeolite (Figure 5.1, g), 0 wt.% Fe/H-ZSM-5) had the highest crystallinity (99 %). However, with the introduction of the Fe and subsequent impregnation of Pd, the crystallinity decreased along with the increasing Fe loading in the catalysts. Other authors such as Wang and co-workers<sup>17</sup> had also reported a loss in the crystallinity when Pd was deposited on HZSM-5 prepared by a similar hydrothermal synthesis procedure.<sup>17</sup> Also, Hutchings and co-workers<sup>13</sup> evidenced a decrease in crystallinity of 6 % when AuPd were deposited on HZSM-5 (0.5 wt.% Au-0.5 wt.% Pd/ HZSM-5 ( $\text{SiO}_2:\text{Al}_2\text{O}_3$ ) (30)) by co-impregnation in comparison to the bare HZSM-5 ( $\text{SiO}_2:\text{Al}_2\text{O}_3$ ) (30) zeolite.

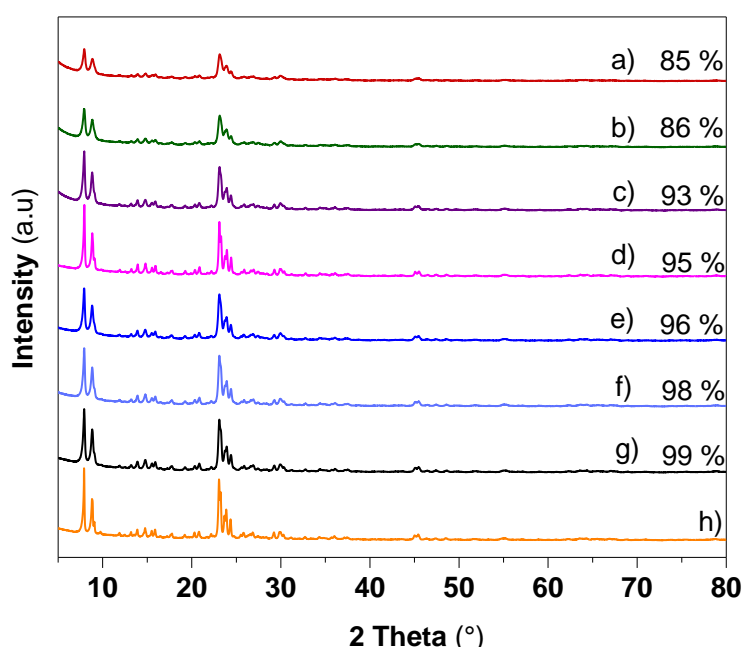


**Figure 5.1:** XRD diffractograms of mono-metallic X wt.% Fe-HZSM-5 (X: 3.0-0) catalysts prior to Pd deposition. The crystallinity is stated in percentage for each catalyst. **Nomenclature:** **a)** 3.0 wt.% Fe-HZSM-5, **b)** 2.0 wt.% Fe-HZSM-5, **c)** 1.0 wt.% Fe-HZSM-5, **d)** 0.5 wt.% Fe-HZSM-5, **e)** 0.125 wt.% Fe-HZSM-5, **f)** 0.06 wt.% Fe-HZSM-5, **g)** 0 wt.% Fe-HZSM-5, **h)** commercial sample H-ZSM-5 ( $\text{SiO}_2:\text{Al}_2\text{O}_3$ ) (23:1).

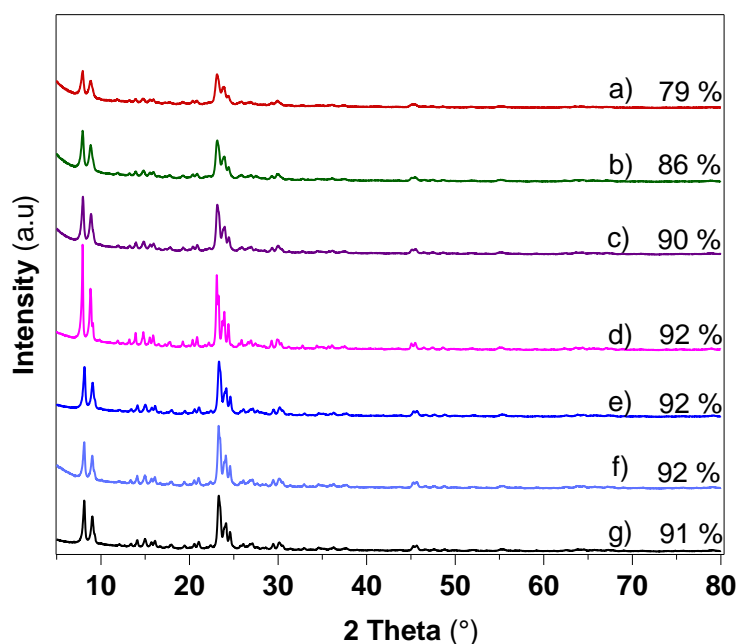


**Figure 5.2:** XRD diffractograms of bi-metallic 0.5 wt.% Pd/ X wt.% Fe-ZSM-5 (X: 3.0-0) catalysts. The crystallinity is stated in percentage for each catalyst. **Nomenclature:** **a)** 0.5 wt.% Pd/ 3.0 wt.% Fe-HZSM-5, **b)** 0.5 wt.% Pd/ 2.0 wt.% Fe-HZSM-5, **c)** 0.5 wt.% Pd/ 1.0 wt.% Fe-HZSM-5, **d)** 0.5 wt.% Pd/ 0.5 wt.% Fe-HZSM-5, **e)** 0.5 wt.% Pd/ 0.125 wt.% Fe-HZSM-5, **f)** 0.5 wt.% Pd/ 0.06 wt.% Fe-HZSM-5, **g)** 0.5 wt.% Pd/ 0 wt.% Fe-HZSM-5.

The XPS of the mono and bi-metallic 0.5 wt.% Pd/ X wt.% Fe-HZSM-5 (X: 3.0-0) catalysts presented two photoelectron peaks at 335 eV and 340 eV, which were attributed to the two oxidation states of the Pd ( $\text{Pd}^0$  and  $\text{PdO}$ ). The XPS of the Fe region also presented two photoelectron peaks at 710 eV and 724 eV, which were attributed to iron oxide species ( $\text{FeO}$ ,  $\text{Fe}_2\text{O}_3$ ,  $\text{Fe}_3\text{O}_4$ ), and no iron metallic ( $\text{Fe}^0$ ) (706.7 eV) was detected. The percentage of  $\text{Pd}^0$  and  $\text{PdO}$  were calculated, and the results are shown in Table 5.2. The oxidation state of Pd was found to be relatively similar for all the bi-metallic 0.5 wt.% Pd/X wt.% Fe-HZSM-5 catalysts, c.a 80 % of  $\text{Pd}^0$  and 20 %  $\text{PdO}$ . It is interesting to note that the mono-metallic 0.5 wt.% Pd/0 wt.% Fe-HZSM-5 presented different proportion of  $\text{Pd}^0$  and  $\text{PdO}$  in comparison to the bi-metallic 0.5 wt.% Pd/X wt.% Fe-HZSM-5 (X: 3.0-0) catalysts. This suggest that the presence of Fe may be helping to reduce the  $\text{PdO}$  to  $\text{Pd}^0$ .

**Table 5.2:** XPS analysis of the mono and bi-metallic 0.5 wt.% Pd/X wt.% Fe-HZSM-5 (X: 3.0-0) catalysts.

Catalysts	PdO	Pd <sup>0</sup>
	%	%
<b>0.5 wt.% Pd/ 3.0 wt.% Fe-HZSM-5</b>	21	79
<b>0.5 wt.% Pd/ 2.0 wt.% Fe-HZSM-5</b>	26	74
<b>0.5 wt.% Pd/ 1.0 wt.% Fe-HZSM-5</b>	33	67
<b>0.5 wt.% Pd/ 0.5 wt.% Fe-HZSM-5</b>	20	80
<b>0.5 wt.% Pd/ 0.125 wt.% Fe-HZSM-5</b>	33	67
<b>0.5 wt.% Pd/0.06 wt.% Fe-HZSM-5</b>	25	75
<b>0.5 wt.% Pd/ 0 wt.% Fe-HZSM-5</b>	51	49

**Heat treatment after the deposition of Pd:** 5 % H<sub>2</sub>/Ar, 400 °C, 10 °C/min, 4 h. XPS spectra for the bi-metallic 0.5 wt.% Pd/ X wt.% Fe-HZSM-5 (X: 3.0-0) catalysts are shown in supplementary information, Figure S.I 5.1-5.7.

TEM was employed to determine the particle size and distribution of the mono-metallic X wt.% Fe-HZSM-5 (X: 3.0, 1.0, 0.5) and bi-metallic 0.5 wt.% Pd/ X wt.% Fe-HZSM-5 (X: 3.0, 1.0, 0.5, 0) catalysts (Table 5.3). However, TEM analysis of the mono-metallic catalysts revealed that the Fe was highly dispersed forming clusters of less than 1 nm in size, which were below the limits of detection of the TEM (TEM micrographs are shown in Figure S.I 5.8). The mono-metallic 3.0 wt.% Fe-HZSM-5 catalyst presented some randomly dispersed nanoparticles (Figure S.I 5.8), unfortunately, there were not enough nanoparticles to statistically determine the mean particle size and distribution. Energy dispersive x-ray spectroscopy (EDX) was subsequently used for an elemental mapping and confirmed that the clusters of Fe were highly dispersed on the surface of the mono-metallic X wt.% Fe-HZSM-5 (X: 3.0, 1.0, 0.5) catalysts (Figure S.I 5.9-5.11 and Table S.I 5.1-5.3).

The impregnation of Pd on the mono-metallic X wt.% Fe-HZSM-5 (X: 3.0, 1.0, 0.5, 0) catalyst (TEM micrographs and histograms are shown in Figure S.I 5.12 and Figure S.I 5.13 respectively) generated nanoparticles with a significant size and wide distribution, confirming that the Pd had been deposited on the surface (Table 5.3). However, EDX would have been required in order to corroborate that the composition of these nanoparticles were Pd or/and if there were alloys of Pd and Fe. Still, it was clear that the modified impregnation methodology did not deliver the same nanoparticles, concluding that the type of support had a predominant role in controlling the size and morphology of the nanoparticles. For instance, both mono-metallic 1 wt.% Pd/TiO<sub>2</sub> (chapter 4, < 1 nm) and 0.5 wt.% Pd/ 0 wt.% Fe-HZSM-5 catalysts (20 nm) presented a massive difference in the mean nanoparticle size despite both catalysts had the Pd impregnated by modified impregnation methodology.

**Table 5.3:** Mean particle size and size distribution for mono-metallic and bi-metallic 0.5 wt.% Pd/ X wt.% Fe-HZSM-5 (X: 3.0, 1.0, 0.5 and 0 wt.%) catalysts.

Catalysts	Mean particle size	Standard deviation
	nm	nm
<b>0.5 wt.% Pd/ 3.0 wt.% Fe-HZSM-5</b>	18	11
<b>0.5 wt.% Pd/ 1.0 wt.% Fe-HZSM-5</b>	15	18
<b>0.5 wt.% Pd/ 0.5 wt.% Fe-HZSM-5</b>	26	13
<b>0.5 wt.% Pd/ 0 wt.% Fe-HZSM-5</b>	20	12

CO-DRIFTS was used to determine the configuration of Pd and Fe nanoparticles in the mono and bi-metallic 0.5 wt.% Pd/ X wt.% Fe-HZSM-5 (X: 3.0, 1.0, 0.5, 0) catalysts (Figure 5.3). Figure 5.3 overlaps the peaks of the mono-metallic X wt.% Fe-HZSM-5 (X: 3.0, 1.0, 0.5) with their respective bi-metallic 0.5 wt.% Pd/ X wt.% Fe-HZSM-5 (X: 3.0, 1.0, 0.5) analogue. Two signals centred at *c.a* 2050  $\text{cm}^{-1}$  and *c.a* 1950  $\text{cm}^{-1}$  can be attributed to CO metal bonds, whereas the two intensive peaks above 2100  $\text{cm}^{-1}$  corresponded to gaseous CO. The mono-metallic X wt.% Fe-HZSM-5 (X: 3.0, 1.0, 0.5) catalysts only presented a peak *c.a* 2050  $\text{cm}^{-1}$ , which corresponded to CO linearly bonded with highly dispersed Fe atoms. This result went in line with the TEM and EDX results that showed that the Fe was highly dispersed forming clusters *c.a* 1 nm in size in the X wt.% Fe-HZSM-5 (X: 3.0, 1.0, 0.5, 0) catalysts. On the other hand, the bi-metallic 0.5 wt.% Pd/ X wt.% Fe-HZSM-5 (X: 3.0, 1.0) catalysts have two peaks, one at 2050  $\text{cm}^{-1}$ , which indicated that there were highly dispersed metal nanoparticles that could be Fe or Pd. Also, the bi-metallic catalyst showed another peak *c.a* 1950  $\text{cm}^{-1}$ , which indicated that the Pd had different configurations, since it has been reported that ensembles sites of Pd with a bridge mode appear between 1900-2000  $\text{cm}^{-1}$ , whereas 3-fold hollow modes appear between 1800-1900  $\text{cm}^{-1}$ .<sup>18</sup> These result also went in line with the conclusions obtained from the TEM, where the impregnation of Pd had created large nanoparticles. What is interesting to note is that the 1950  $\text{cm}^{-1}$  peak decreases in intensity from 0.5 wt.% Pd/ 3.0 wt.% Fe-HZSM-5 to 0.5 wt.% Pd/ 0.5 wt.% Fe-HZSM-5 and disappears for the mono-metallic 0.5 wt.% Pd/ 0 wt.% Fe-HZSM-5 catalyst. This could indicate that despite the bi-metallic 0.5 wt.% Pd/ X wt.% Fe-HZSM-5 (X: 3.0, 1.0, 0.5, 0) catalysts contained the same amount of Pd deposited on the surface, the 0.5 wt.% Pd/ 3.0 wt.% Fe-HZSM-5 had more proportion of Pd deposited on the external surface than the 0.5 wt.% Pd/ 0 wt.% Fe-HZSM-5, therefore, making the metal nanoparticles more accessible for the CO to bind. However, it could also indicate the formation of alloys of Pd and Fe. For instance, Jones and co-workers<sup>19</sup> synthesise bi-metallic ZnPd supported catalyst on  $\text{TiO}_2$  by chemical vapour impregnation (5 % ZnPd/ $\text{TiO}_2$ ) and applied a heat treatment with 5 %  $\text{H}_2$  in Ar at 150 °C and 250 °C for 1 h. The analysis from CO-DRIFTS studies revealed that the peak *c.a* 1922  $\text{cm}^{-1}$  became narrower and less intense when

increasing the temperature from 150 °C to 250 °C due to the formation of ZnPd alloys nanoparticles.<sup>19</sup>

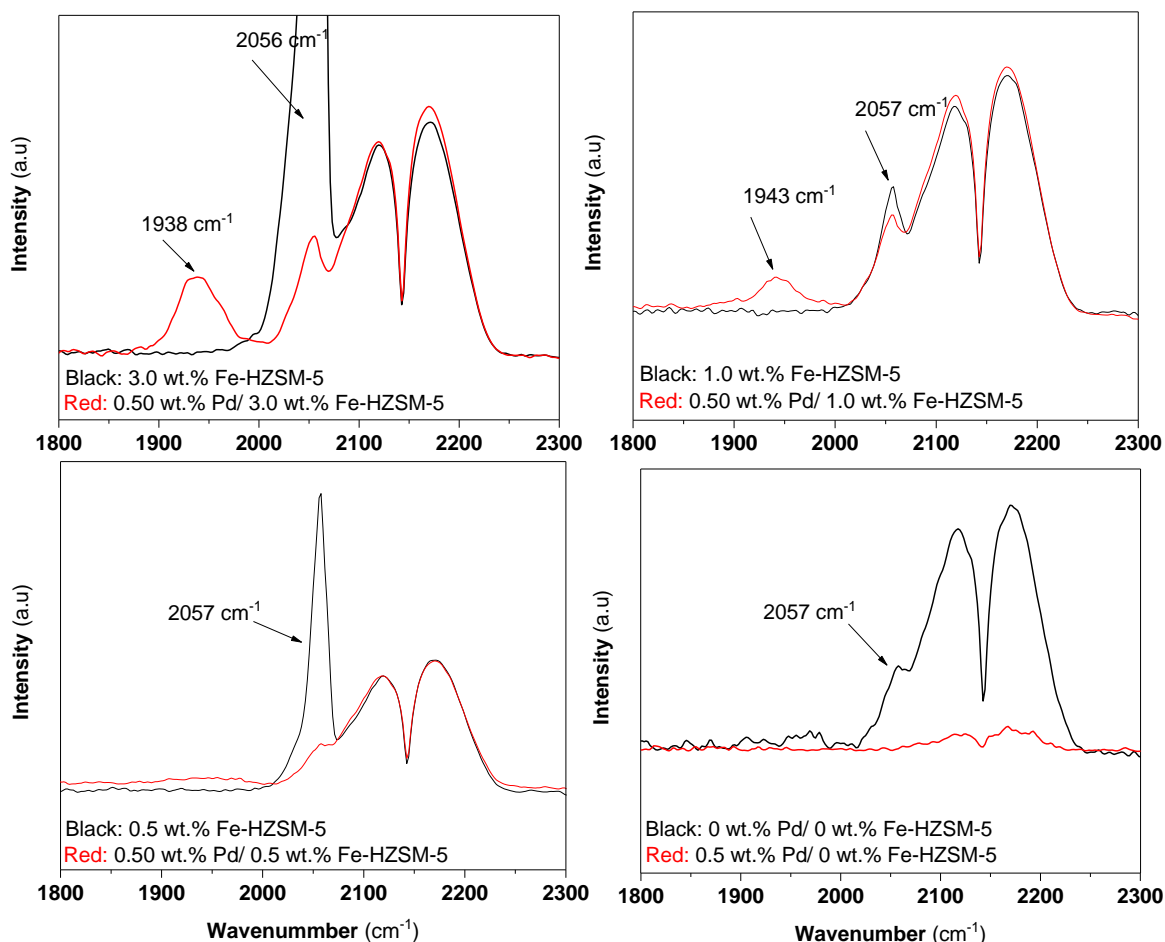


**Figure 5.3:** CO-DRIFTS for the bare zeolite (0 wt.% Pd/ 0 wt.% Fe-HZSM-5) and the mono and bi-metallic of 0.5 wt.% Pd/ X wt.% Fe-HZSM-5 (X: 3.0, 1.0, 0.5, 0) catalysts.

Gas sorption is routinely used in heterogeneous catalysis to characterise porous materials such as zeolites.<sup>20</sup> Physisorption is a general phenomenon that occurs when an absorbable gas (adsorptive, such as N<sub>2</sub> (77 K), Ar (87 K)) is in contact with the surface of a solid (adsorbent).<sup>21</sup> The surface area and the porosity characteristics of the bi-metallic 0.5 wt.% Pd/X wt.% Fe-HZSM-5 (X: 3.0-0) catalysts were calculated using N<sub>2</sub> at 77 K, where the adsorbed amount of adsorptive were recorded as a function of relative pressure at constant temperature (Figure 5.4).<sup>22</sup> In order to be able to assign the isotherm to one of the IUPAC classifications,<sup>21</sup> the relative pressure has to be recorded from 0 to 1. Therefore, no assignments can be made from the isotherm obtained to one of the IUPAC classifications.<sup>21</sup> However, Gervasini *et.al*,<sup>23</sup> and Dhar and co-workers<sup>24</sup> recorded the isotherm from P/Po=0 to for 1 HZSM-5 (SiO<sub>2</sub>:Al<sub>2</sub>O<sub>3</sub>) (33:1) and HZSM-5 (SiO<sub>2</sub>:Al<sub>2</sub>O<sub>3</sub>) (66:1) respectively concluding that both presented a Type I classification. Samples with a Type I isotherm classification indicate that contain pore size distributions over a broader range including micropores (< 2

nm) and possibly narrow mesopores ( $< \sim 2.5$  nm).<sup>21</sup> However, Gervasini *et.al*, also studied the isotherm for HZSM-5 ( $\text{SiO}_2:\text{Al}_2\text{O}_3$ ) (33:1) samples that were ion-exchanged with Co, Ni and Cu concluding that Co-ZSM-5 (0.88 mmol/g) and Ni-ZSM-5 (1.0 mmol/g) had an isotherm closer to Type II whereas the Cu-ZSM-5 (1.02 mmol/g) isotherm was closer to Type I.<sup>23</sup> This results suggested that whatever modification to the bare HZSM-5 zeolite may also chance the type isotherm. In fact, XRD had already shown how the crystallinity of the zeolite decreased along with the increasing loading of Fe. Therefore, it could be that the introduction of Fe and Pd could have modified the physical parameters of the zeolite.

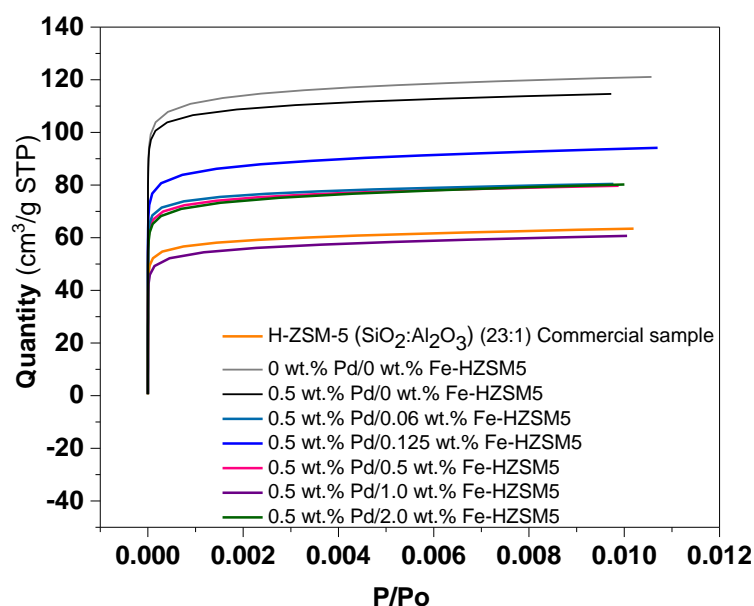


**Figure 5.4:** Isotherms of the 0.5 wt.% Pd/X wt.% Fe-HZSM-5 (X: 3.0-0) recorded at constant temperature (77 K) using  $\text{N}_2$ ,  $P/P_o$  ranging from 0 to 0.01.

The specific surface area ( $S_{\text{BET}}$ ) for the bi-metallic 0.5 wt.% Pd/X wt.% Fe-HZSM-5 (X: X: 3.0, 1.0, 0.5,0.06) catalysts were calculated by BET formula, selecting from the isotherm the relative pressure range suggested by Snurr and co-workers<sup>25</sup> to be the most appropriate for MFI zeolites to comply with Rouquerol (RQ) criteria.<sup>25</sup> Non local density functional theory (NLDFT) by Tarazona model was used to determine the pore volume ( $V^{\text{micropore}}$ ). Chapter 2, section 2.6.1.1 provides a more detailed explanation of how these parameters were estimated. Table 5.4 gathers the  $S_{\text{BET}}$  and  $V^{\text{micropore}}$  for the mono and bi-metallic 0.5 wt.% Pd/X wt.% Fe/HZSM-5 (X: 3.0, 1.0, 0.5,0.06, 0) catalysts as well as for the bare zeolite (0 wt.% Pd/0 wt.% Fe/HZSM-5).

The results indicated that the increasing loading of Fe made decrease the  $S_{\text{BET}}$  probably due to the filling of the micropores with Fe and Pd species making the surface of the zeolite smoother and even.<sup>26</sup> These results go in line with the crystallinity trend found in XRD (Figure 5.1 and 5.2), where the bare zeolite, 0 wt.% Pd/ 0 wt.% Fe-HZSM-5 presented a crystallinity of 99 % and the greatest surface area  $516 \text{ m}^2/\text{g}$ . The addition of Fe within the

crystalline structure and subsequent activation to form the framework and extra-framework Fe species led to a decrease in crystallinity which can also be reflected in Table 5.4, when comparing the total surface areas and microporous volume of the bi-metallic 0.5 wt.% Pd/ X wt.% Fe-HZSM-5 (X: 3.0-0) catalyst to the bare zeolite 0 wt.% Pd/ 0 wt.% Fe-HZSM-5. The porous got filled or maybe blocked by the formation of framework, extra-framework Fe species and metal nanoparticles, which made decrease the surface area and micropore volume.

**Table 5.4:** Physical properties of the mono and bi-metallic 0.5 wt.% Pd/ X wt.% Fe-HZSM-5 (X: 3.0-0.0) catalysts.

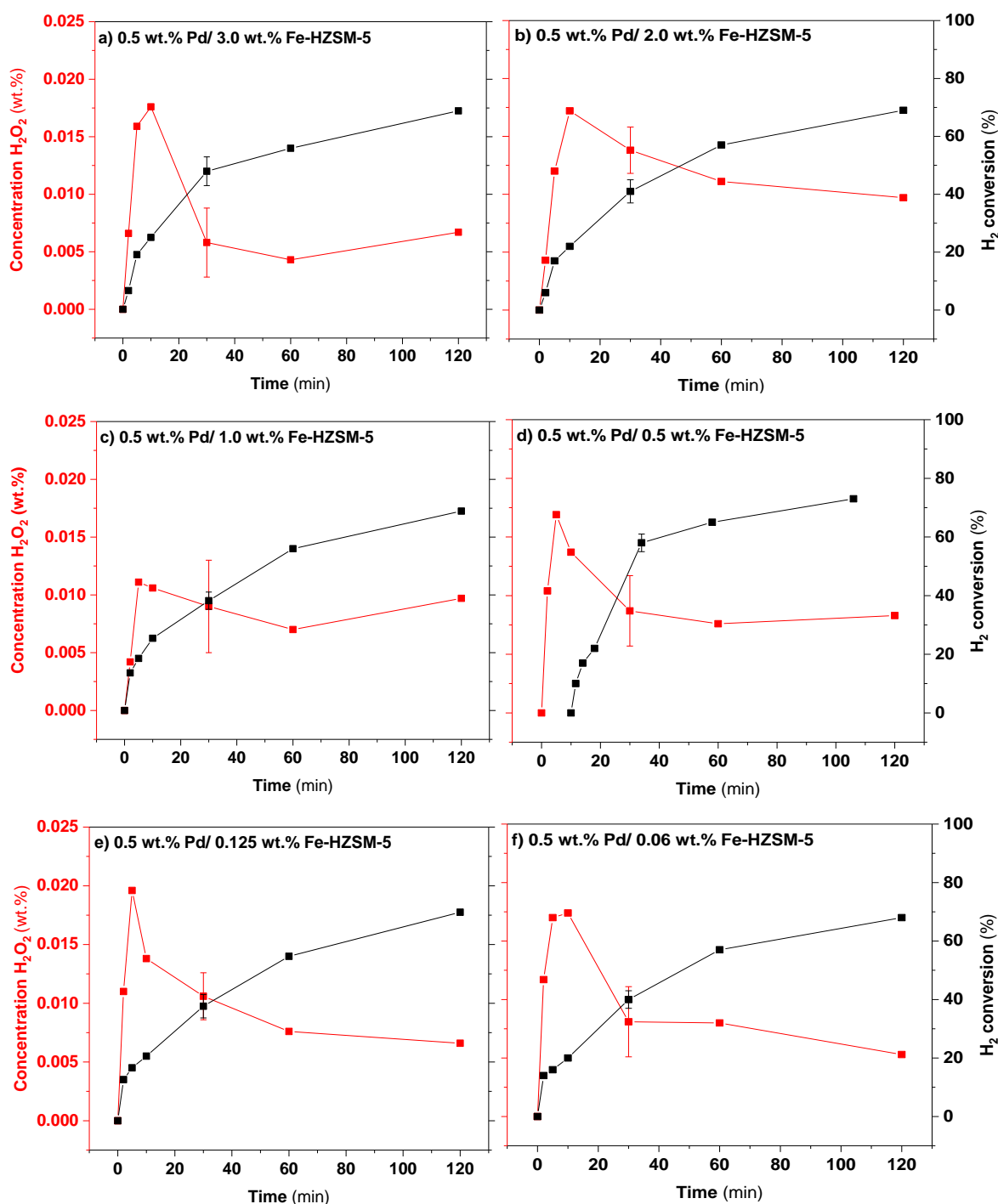
<b>Catalysts</b>	<b>S<sub>A</sub></b> m <sup>2</sup> /g	<b>V<sub>micropore</sub></b> cm <sup>3</sup> /g
<b>0.5 wt.%Pd/3.0 wt.%Fe-HZSM-5</b>	259	0.04
<b>0.5 wt.%Pd/1.0 wt.%Fe-HZSM-5</b>	281	0.05
<b>0.5 wt.%Pd/0.5 wt.%Fe-HZSM-5</b>	345	0.07
<b>0.5 wt.%Pd/0.125 wt.%Fe-HZSM-5</b>	348	0.08
<b>0.5 wt.%Pd/0.06 wt.%Fe-HZSM-5</b>	399	0.07
<b>0.5 wt.%Pd/0 wt.% Fe-HZSM-5</b>	407	0.09
<b>0 wt.%Pd/0 wt.% Fe-HZSM-5</b>	516	0.12
<b>HZSM-5 (SiO<sub>2</sub>:Al<sub>2</sub>O<sub>3</sub>) (23:1)</b>	413	0.15
<b>Commercial sample</b>		

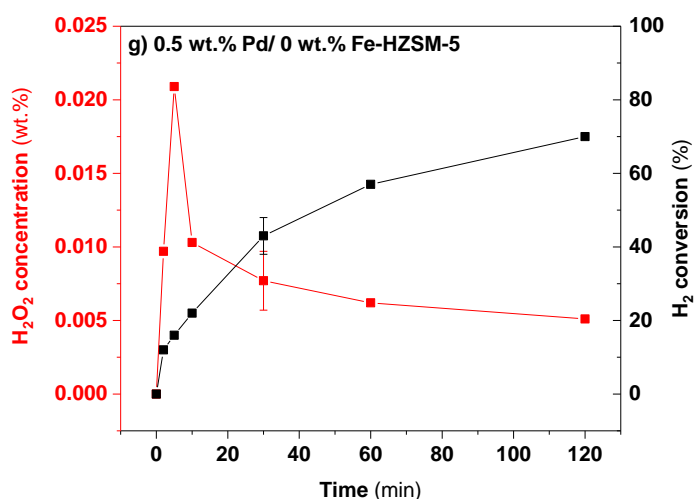
### 5.2.2 Activity of the bi-metallic 0.5 wt. % Pd/ X wt.% Fe-HZSM-5 (X: 3.0-0) catalysts towards the direct synthesis and degradation of H<sub>2</sub>O<sub>2</sub>.

The set of mono and bi-metallic 0.5 wt. % Pd/ X wt.% Fe-HZSM-5 (X: 3.0-0) catalysts were evaluated for their activity towards the direct synthesis of H<sub>2</sub>O<sub>2</sub> at 30°C with water as a solvent for two hours (Figure 5.5). The determination of the activity towards the direct synthesis and degradation of H<sub>2</sub>O<sub>2</sub> at the same reaction conditions as the degradation of phenol allow to study if there could be any correlation between the extent of phenol conversion and the *in-situ* formation and degradation of H<sub>2</sub>O<sub>2</sub>.

All mono and bi-metallic 0.5 wt. % Pd/ X wt.% Fe-HZSM-5 (X: 3.0-0) catalysts proved to be active over 2 hours with no significant difference between catalytic activity. The maximum H<sub>2</sub>O<sub>2</sub> concentration was achieved, for all catalysts, between 5 and 10 minutes of the reaction before it started to decay over time until reaching a steady state. However, the decay in H<sub>2</sub>O<sub>2</sub> concentration cannot be due to the catalyst deactivation since the H<sub>2</sub> conversion kept increasing over the course of two hours. It is possible that the catalyst selectivity changed during the course of the reaction, being more selective towards the direct synthesis of H<sub>2</sub>O<sub>2</sub> at short reaction times (5-10 min). The fact that the set of bi-metallic 0.5 wt.% Pd/ X wt.%

Fe-HZSM-5 (X: 3.0-0) catalysts gave similar activities towards the direct synthesis of  $\text{H}_2\text{O}_2$  may not be surprising since all the catalysts showed the same proportion of  $\text{Pd}^0$  (c.a 80 %) and  $\text{PdO}$  (c.a 20 %) except for the mono-metallic 0.5 wt.% Pd/ 0 wt.% Fe-HZSM-5 catalyst that showed c.a 50 %  $\text{Pd}^0$  and 50 %  $\text{PdO}$  as shown in Table 5.2 the XPS analysis. Unfortunately, the post-reaction solution analysis by MP-AES determined that the Fe and Pd were unstable and leached at the end of two hours' reaction time (Table S.I 5.4).

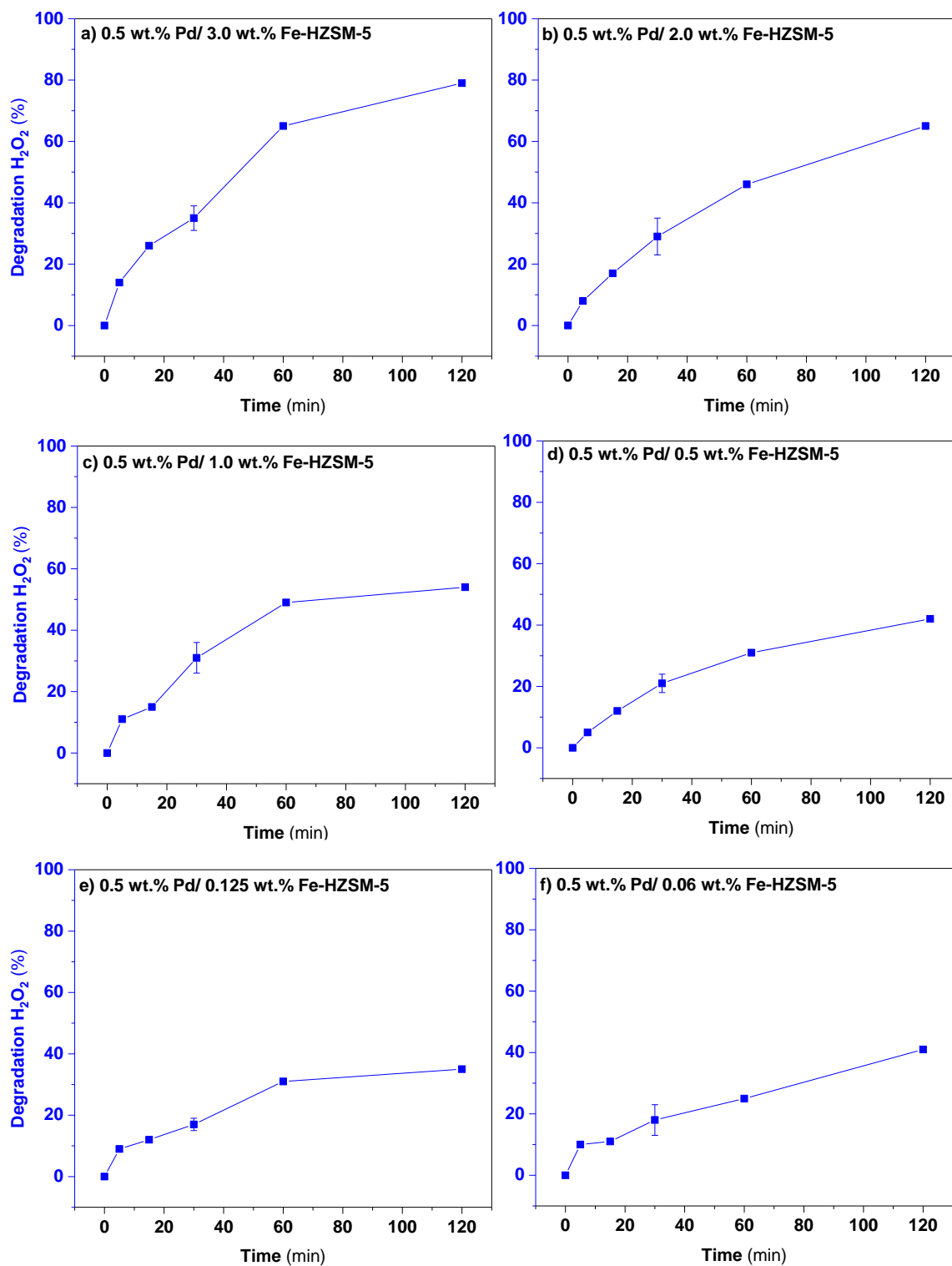




**Figure 5.5:** Time on-line activity towards the direct synthesis of H<sub>2</sub>O<sub>2</sub> using bi-metallic 0.5 wt.% Pd/ X wt.% Fe-HZSM-5 (X: 3.0-0) catalysts. **Reaction conditions:** 8.5 g (HPLC grade water), catalyst (0.01 g), 420 psi 5% H<sub>2</sub>/CO<sub>2</sub>, 160 psi 25% O<sub>2</sub>/CO<sub>2</sub>, 1200 rpm, 30 °C.

The activity of these materials towards the degradation of H<sub>2</sub>O<sub>2</sub> was next investigated (Figure 5.6). The bi-metallic 0.5 wt.% Pd/ 3.0 wt.% Fe-HZSM-5 catalyst showed the greatest activity towards the degradation of H<sub>2</sub>O<sub>2</sub> (80 %, 2 h, Figure 5.6 a)), followed by the 0.5 wt.% Pd/ 2.0 wt.% Fe-HZSM-5 (60 %, 2 h, Figure 5.6, b)) and 0.5 wt.% Pd/ 1.0 wt.% Fe-HZSM-5 (50 %, 2 h, Figure 5.6, c)). Surprisingly, the degradation was found to be similar for those catalyst which had less than 0.5 wt.% Fe, giving approximately 40 % H<sub>2</sub>O<sub>2</sub> degradation. Surprisingly, the degradation activity of the mono-metallic X wt.% Fe-HZSM-5 (X: 3.0, 1.0, 0.5, 0) catalysts was determined for 30 min at 30 °C, obtaining 9 %, 6 %, 4% and 2 % respectively. This data confirmed that the Fe and the zeolite had not relevant contribution to the degradation activity, leaving the Pd the major responsible for the degradation of H<sub>2</sub>O<sub>2</sub>. The oxidation state of the Pd, was also found to be similar for the whole set of bi-metallic 0.5 wt.% Pd/ X wt.% Fe-HZSM-5 (X:3.0-0) catalysts according to the XPS analysis (Pd<sup>0</sup> (c.a 80 %) and PdO (c.a 20 %)), leading to conclude that the difference in the activity towards the degradation of H<sub>2</sub>O<sub>2</sub> was not related to the oxidation state of the Pd. It was believed that the difference in degradation activity shown for the different bi-metallic 0.5 wt.% Pd/ X wt.% Fe-HZSM-5 (x: 3.0-0) catalysts could be reasoned based on the XRD and physisorption results. When the Pd was deposited on bare zeolite 0 wt.% Fe/HZSM-5 (99 % crystallinity) with a specific surface area (516 m<sup>2</sup>/g) and microporous volume (0.12 cm<sup>3</sup>/g), part of the Pd could have been deposited on the cavities and channels of the zeolite, making the Pd active sites less exposed to the external surface. In fact, after the deposition of the Pd, the crystallinity was reduced to 91 % and also the specific surface area (407 m<sup>2</sup>/g) and micropore volume (0.09 cm<sup>3</sup>/g). On the other hand, when Pd was deposited on 3.0 wt.% Fe-HZSM-5 with a total surface area (259 m<sup>2</sup>/g) and micropore volume (0.04 cm<sup>3</sup>/g), Pd got deposited on the external surface area of the 3.0 wt.% Fe-HZSM-5 in greater extent than in the cavities and channels. This fact could explain why the degradation activity did increase

with the bi-metallic 0.5 wt.% Pd/ (3.0-1.0) wt.% Fe-HZSM-5 catalysts, since it was likely that the Pd got deposited on the external surface area in greater extent than in the porous and channels.



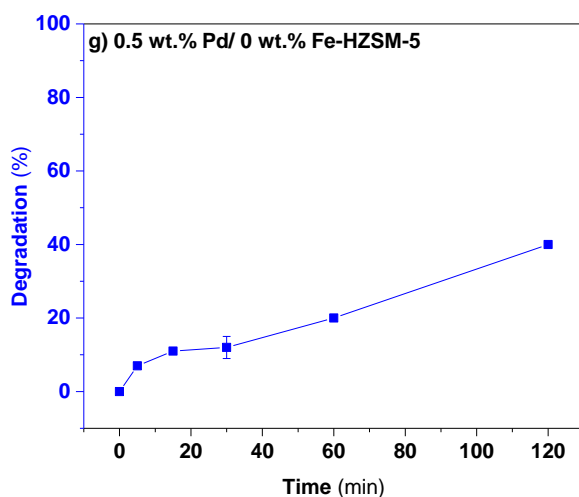


**Figure 5.6:** Time on-line activity towards the degradation of  $\text{H}_2\text{O}_2$  using bi-metallic 0.5 wt.% Pd/ X wt.% Fe-HZSM-5 (X: 3.0-0 wt.%) catalysts. **Reaction conditions:** 8.5 g (0.68 g  $\text{H}_2\text{O}_2$ , 7.82 g HPLC grade water), catalyst (0.01 g), 420 psi 5 %  $\text{H}_2/\text{CO}_2$ , 1200 rpm, 30 °C.

The particle size of the bi-metallic 0.5 wt.% Pd/ X wt.% Fe-HZSM-5 (X: 3.0-0) catalysts could have had a big influence on the activity towards the direct synthesis and degradation of  $\text{H}_2\text{O}_2$ . For instance, Han and co-workers<sup>27</sup> did a thorough study on the activity for the direct synthesis of  $\text{H}_2\text{O}_2$  with mono-metallic Pd supported catalysts on hydroxyapatite (Hap) (X wt.% Pd/Hap, X: 5, 3, 2, 1, 0.5) with nanoparticle sizes ranging from 1.4 nm to 2.9 nm. From their results, increasing the loading of Pd, also increased the  $\text{H}_2$  conversion but the productivity decayed. In fact, the best activity was shown for 0.5 wt.% Pd/HAp (1857  $\text{mmolH}_2\text{O}_2 \text{ g}_{\text{Pd}}^{-1} \text{ h}^{-1}$ , 2 %  $\text{H}_2$  conversion, 94 % selectivity  $\text{H}_2\text{O}_2$ ) and 1.0 wt.% Pd/HAp (1873  $\text{mmolH}_2\text{O}_2 \text{ g}_{\text{Pd}}^{-1} \text{ h}^{-1}$ , 6 %  $\text{H}_2$  conversion, 67 %  $\text{H}_2\text{O}_2$  selectivity) than for a 5.0 wt.% Pd/HAp (741  $\text{mmolH}_2\text{O}_2 \text{ g}_{\text{Pd}}^{-1} \text{ h}^{-1}$ , 18 %  $\text{H}_2$  conversion, 43 %  $\text{H}_2\text{O}_2$  selectivity). They showed that the catalysts performance (selectivity towards  $\text{H}_2\text{O}_2$ ) decreased while increasing the loading of Pd and the particle size, concluding that the 0.5 wt.% Pd/HAp had the best selectivity thanks to presenting particle size of 1.4 nm whereas the 5 wt.% Pd/Hap had 2.6 nm in size. They showed that increasing the particle size above 2.6 up to 30 nm, did not alter the selectivity of  $\text{H}_2\text{O}_2$  significantly. Apart from the difference in particle size, 0.5 wt.% Pd/HAp also presented greater ratio of PdO/Pd<sup>0</sup> than the 5.0 wt.% Pd/Hap, concluding that the higher percentage of PdO helped the 0.5 wt.% Pd/HAp to have the greatest selectivity.<sup>27</sup>

In Chapter 4, the bi-metallic 0.5 wt.% Pd-0.5 wt.% Fe/ $\text{TiO}_2$  catalyst showed greater productivity and degradation of  $\text{H}_2\text{O}_2$  in comparison to the bi-metallic 0.5 wt.% Pd/ 0.5 wt.% Fe-HZSM-5 analogue. The former presented 32 % PdO and 68 % of Pd<sup>0</sup> with Pd and Fe clusters smaller than 1 nm. On the other hand, the latter 20 % PdO and 80 % Pd<sup>0</sup> with a medium particle size of 26 nm. Thus, it is clear from this results that despite Pd had been incorporated by modified impregnation procedure in both catalysts, the support played a critical role in driving the formation of nanoparticle size wise.

### 5.2.3 Speciation of the Fe in the bi-metallic 0.5 wt. % Pd/ X wt.% Fe-HZSM-5 (X: 3.0-0) catalysts and their activity towards the degradation of phenol.

FTIR, DR-UV-Vis and Raman-UV are common characterisation techniques to study the speciation of Fe. The mono-metallic X wt.% Fe-HZSM-5 (X: 3.0-0 wt.%) and the bi-metallic 0.5 wt.% Pd/ X wt.% Fe-HZSM-5 (3.0-0) catalysts were first analysed by FTIR. Unfortunately, no peaks coming from the Fe were seen (Figure S.I 5.14-5.15). Three peaks were observed in both figures at  $800\text{ cm}^{-1}$ ,  $1060\text{ cm}^{-1}$  and  $1220\text{ cm}^{-1}$ , where the vibrations bands between  $1250\text{-}950\text{ cm}^{-1}$  and  $850\text{ cm}^{-1}$  and  $750\text{ cm}^{-1}$  corresponded to antisymmetric Si-O-Si stretching vibrations and symmetric vibrations respectively.<sup>28</sup>

Figure 5.7 presents the DR-UV-Vis spectra for the mono-metallic X wt.% Fe-HZSM-5 (X: 3.0-0.06) catalysts. The Fe species can be categorised according to the absorption peaks; 200-250 nm ( $\text{Fe}^{3+}$  species coordinated within the framework lattice), 250-350 nm (isolated Fe species and bi-nuclear Fe species immobilised in the framework channels), 350-450 nm (extra-framework  $\text{Fe}_x\text{O}_y$  clusters) and  $>450\text{ nm}$  (extra-framework agglomerations of  $\text{Fe}_x\text{O}_y$ ).<sup>29</sup> At low Fe loadings (0.125 wt.% and 0.06 wt.% Fe), the catalysts only showed peaks between 250-350 nm, indicating that the Fe exists as framework  $\text{Fe}^{3+}$  species consisting of isolated and bi-nuclear Fe species immobilised in the framework channels. The subsequent catalysts (1 wt.% and 0.5 wt.% Fe) showed two peaks between 200-250 nm and 250-350 nm, that corresponded to  $\text{Fe}^{3+}$  species coordinated within the lattice and isolated and bi-nuclear Fe species immobilised in the framework channels respectively. At higher Fe loadings (3 wt.% and 2 wt.% Fe), three peaks could be visualised between 200-250 nm, 250-350 nm and a shoulder at  $>450\text{ nm}$  suggesting that these two mono-metallic X wt.% Fe-HZSM-5 (X: 3.0-2.0 wt.%) catalysts presented,  $\text{Fe}^{3+}$  species coordinated within the lattice, isolated and bi-nuclear Fe species immobilised in the framework channels and extra-framework Fe species consisting of agglomerates of  $\text{Fe}_x\text{O}_y$ .

Gordo and co-workers<sup>30</sup> have studied the effect of Fe incorporation into the zeotype TS-1 (Fe/TS-1), prepared by hydrothermal synthesis.<sup>30</sup> They showed that the increasing loading of Fe from 0.64 wt.% to 4.43 wt.% decreased the crystallinity of the MFI structure, as evidenced by XRD. The loss of crystallinity provoked the formation of extra-framework  $\text{Fe}_x\text{O}_y$  species. Thus, it is likely that the signal seen at  $>450\text{ nm}$  for the materials with higher Fe loading corresponded to extra-framework  $\text{Fe}_x\text{O}_y$  species due to the loss of crystallinity shown by the mono-metallic X wt.% Fe-HZSM-5 (X: 3.0-2.0 wt.%) catalysts in Figure 5.1. In addition to this, TEM also revealed small nanoparticles in the mono-metallic 3.0 wt.% Fe-HZSM-5 catalyst that also corroborate the XRD and DR UV-Vis analysis. It was concluded that between 1.0 to 0.06 wt.% Fe, framework Fe species were formed in greater extent. Increasing the Fe loading from 1.0 wt.%, evoked to the formation of clusters and

agglomerative of  $\text{Fe}_x\text{O}_y$  which have been reported to be less stable during the degradation of phenol.

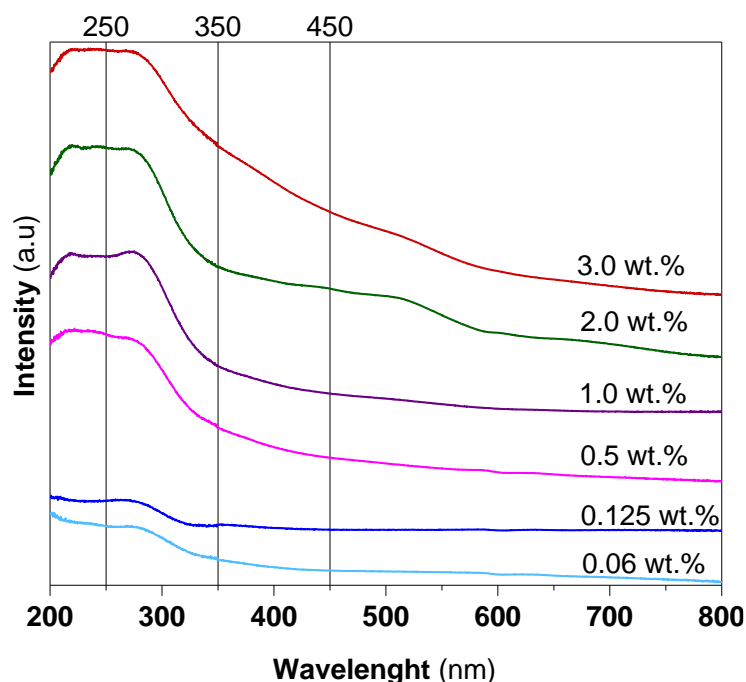


**Figure 5.7:** DR-UV-Vis spectra for the mono-metallic X wt.% Fe-HZSM-5 (X: 3.0-0.06) catalysts catalyst.

Raman-UV is shown in Figure 5.8 for the mono-metallic X wt.% Fe-HZSM-5 (X: 3.0-0.06) catalysts. The commercial sample HZSM-5 ( $\text{SiO}_2$ :  $\text{Al}_2\text{O}_3$ ) (23: 1) (Figure 5.8, h)) and the bare zeolite 0 wt.% Fe-HZSM-5 (Figure 5.8, g)) presented peaks corresponding to the HZSM-5 structure at  $290\text{ cm}^{-1}$ ,  $380\text{ cm}^{-1}$  and  $800\text{ cm}^{-1}$ .<sup>31</sup> These peaks decay in intensity with increasing Fe loading, indicating that the HZSM-5 structure was being distorted as observed via XRD (Figure 5.1) and physisorption analysis (Table 5.4). The peaks observed at  $515\text{ cm}^{-1}$ ,  $1005\text{ cm}^{-1}$ ,  $1112\text{ cm}^{-1}$  and  $1166\text{ cm}^{-1}$  are commonly assigned to  $\text{Fe}^{3+}$  in the lattice positions of the HZSM-5.<sup>32</sup> Indeed, Dimitratos *et al.*, have also hypothesised that the peak at  $515\text{ cm}^{-1}$  may be attributed to isolated and bi-nuclear Fe species immobilised within the channels of the HZSM-5.<sup>31</sup> They prepared a mono-metallic 0.5 wt.% Fe-HZSM-5 catalyst by hydrothermal synthesis and studied the speciation of Fe before and after the activation at different temperatures (550-900 °C). They reported that the catalyst exposure to elevated temperatures made progressively reduced the intensity of the peaks at  $1013\text{ cm}^{-1}$ ,  $1120\text{ cm}^{-1}$  and  $1165\text{ cm}^{-1}$ , contrarily to the intensity of the peak at  $515\text{ cm}^{-1}$ , which kept increasing with the temperature. This observation led the authors to conclude that the  $\text{Fe}^{3+}$  coordinated to the HZSM-5 lattice was being extracted to form to isolated and bi-nuclear Fe species.<sup>31</sup> Such observations correlate well with the conclusions obtained from DR-UV-Vis shown in

Figure 5.7, since it was clear that  $\text{Fe}^{3+}$  in the lattice positions as well as framework isolated and bi-nuclear Fe species immobilised to the framework were present.

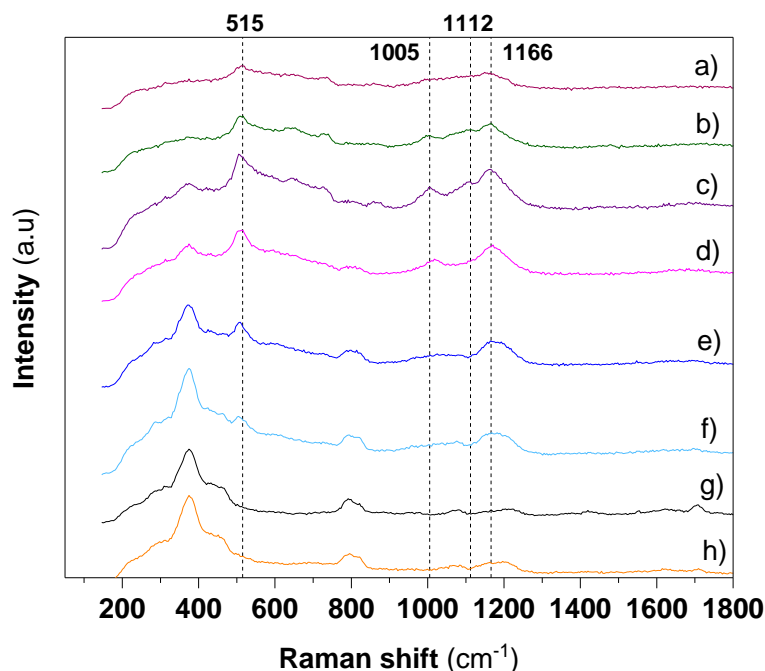


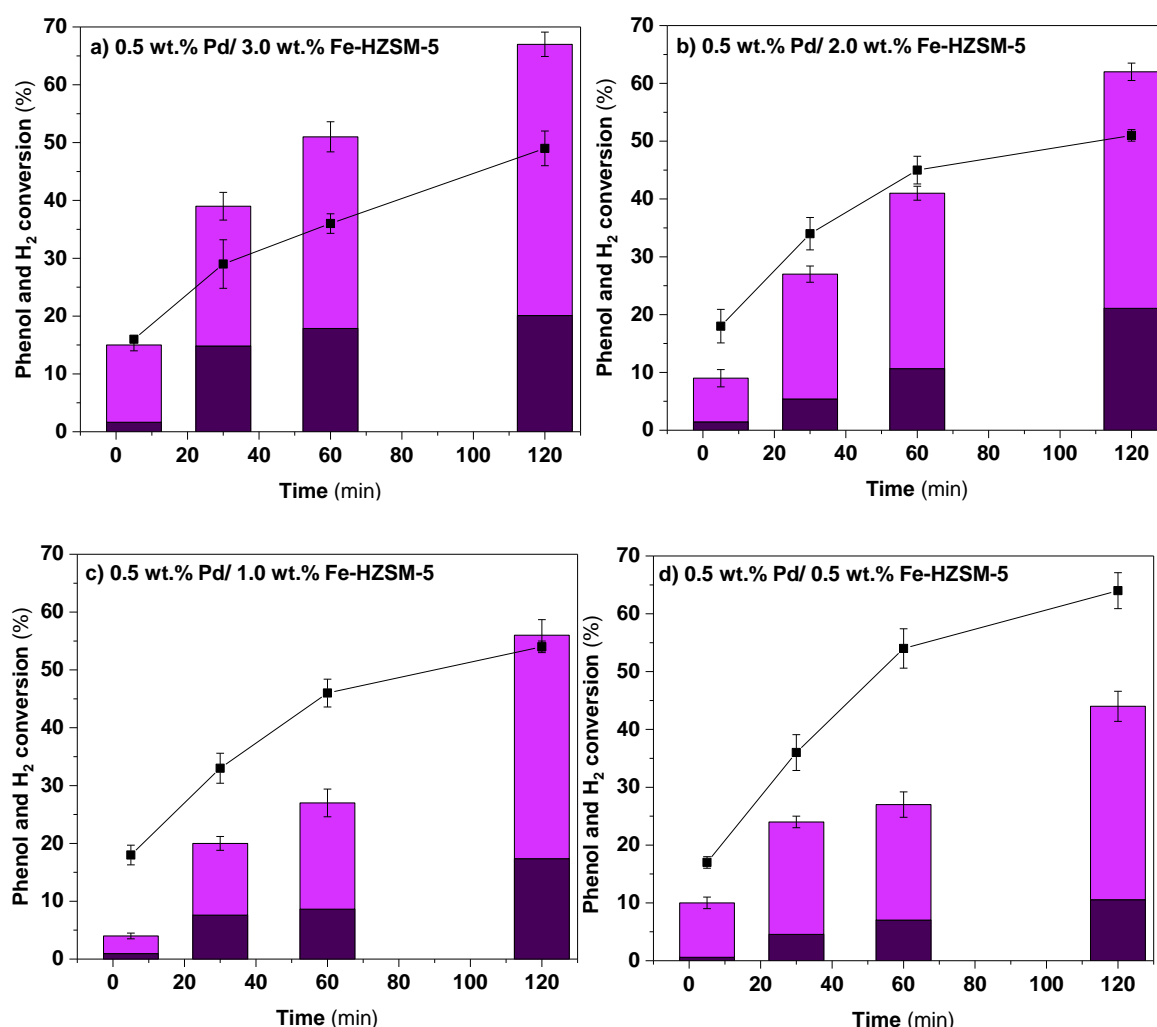
**Figure 5.8:** Raman-UV spectra of mono-metallic X wt.% Fe-HZSM-5 (X: 3.0–0) catalysts. **Nomenclature:** **a)** 3.0 wt.% Fe-HZSM-5, **b)** 2.0 wt.% Fe-HZSM-5, **c)** 1.0 wt.% Fe-HZSM-5, **d)** 0.5 wt.% Fe-HZSM-5, **e)** 0.125 wt.% Fe-HZSM-5, **f)** 0.06 wt.% Fe-HZSM-5, **g)** 0 wt.% Fe-HZSM-5, **h)** commercial sample H-ZSM-5 ( $\text{SiO}_2:\text{Al}_2\text{O}_3$ ) (23:1).

The catalytic activity towards the degradation of phenol is shown in Figure 5.9. The highest degradation was achieved by 0.5 wt.% Pd/ 3.0 wt.% Fe-HZSM-5 (67 %), followed by the 0.5 wt.% Pd/ 2.0 wt.% Fe-HZSM-5 (59 %) and 0.5 wt.% Pd/ 1.0 wt.% Fe-HZSM-5 (53 %) over 2 hours' reaction time. On the other hand, 0.5 wt.%Pd/ (0.5-0 wt.%) Fe-HZSM-5 presented similar activity (c.a 40 %). Interestingly, the mono-metallic 0.5 wt.% Pd/ 0 wt.% Fe-HZSM-5 catalyst presented activity as high as the bi-metallic 0.5 wt.%Pd/ (0.5-0.06 wt.%) Fe-HZSM-5 catalysts, which could be due to having had introduced Fe within the framework of the mono-metallic 0.5 wt.% Pd/ 0 wt.% Fe-HZSM-5 catalyst via ion-exchange with  $\text{NH}_4\text{NO}_3$ .

The activity towards the degradation of phenol could be correlated to the Fe speciation. The bi-metallic 0.5 wt.%Pd/ (0.5-0 wt.%) Fe-HZSM-5 catalysts showed a conversion c.a 40 %, whereas in subsequent catalysts, the conversion of phenol kept increasing, from 53 % for 0.5 wt.%Pd/ 1.0 wt.% Fe-HZSM-5 catalyst up to 67 % for the bi-metallic 0.5 wt.%Pd/ 3.0 wt.% Fe-HZSM-5 one. It was believed that the activity started increasing from the 0.5 wt.%Pd/ 1.0 wt.% Fe-HZSM-5 catalyst to the 0.5 wt.%Pd/ 3.0 wt.% Fe-HZSM-5 one, as the crystallinity decayed and evoked the formation of extra-framework Fe species ( $\text{Fe}_x\text{O}_y$  clusters and agglomerates). Many authors have reported that these extra-framework  $\text{Fe}_x\text{O}_y$

species are acknowledged to be more active in converting phenol than the framework ones, however, they lack stability.<sup>1</sup>

The H<sub>2</sub> conversion was similar for all the catalyst (Figure 5.9, 60-50 %) despite the difference in phenol degradation activity. This data could suggest that the amount H<sub>2</sub>O<sub>2</sub> produced could have been similar in all set of bi-metallic 0.5 wt.% Pd/ X wt.% Fe-HZSM-5 (X: 3.0-0 wt.%) catalysts. In addition, the extent of H<sub>2</sub> conversion was found to be plateauing at extended reaction times. This observation may indicate that the activity of these bi-metallic 0.5 wt.% Pd/ X wt.% Fe-HZSM-5 (X: 3.0-0) catalysts might be limited by the availability of H<sub>2</sub> or the potentially due to catalyst deactivation. All bi-metallic 0.5 wt.% Pd/ X wt.% Fe-HZSM-5 (X: 3.0-0) catalysts were efficient enough to oxidise phenol derivatives into di-acids, H<sub>2</sub>O and CO<sub>2</sub> as seen in Figure 5.9.



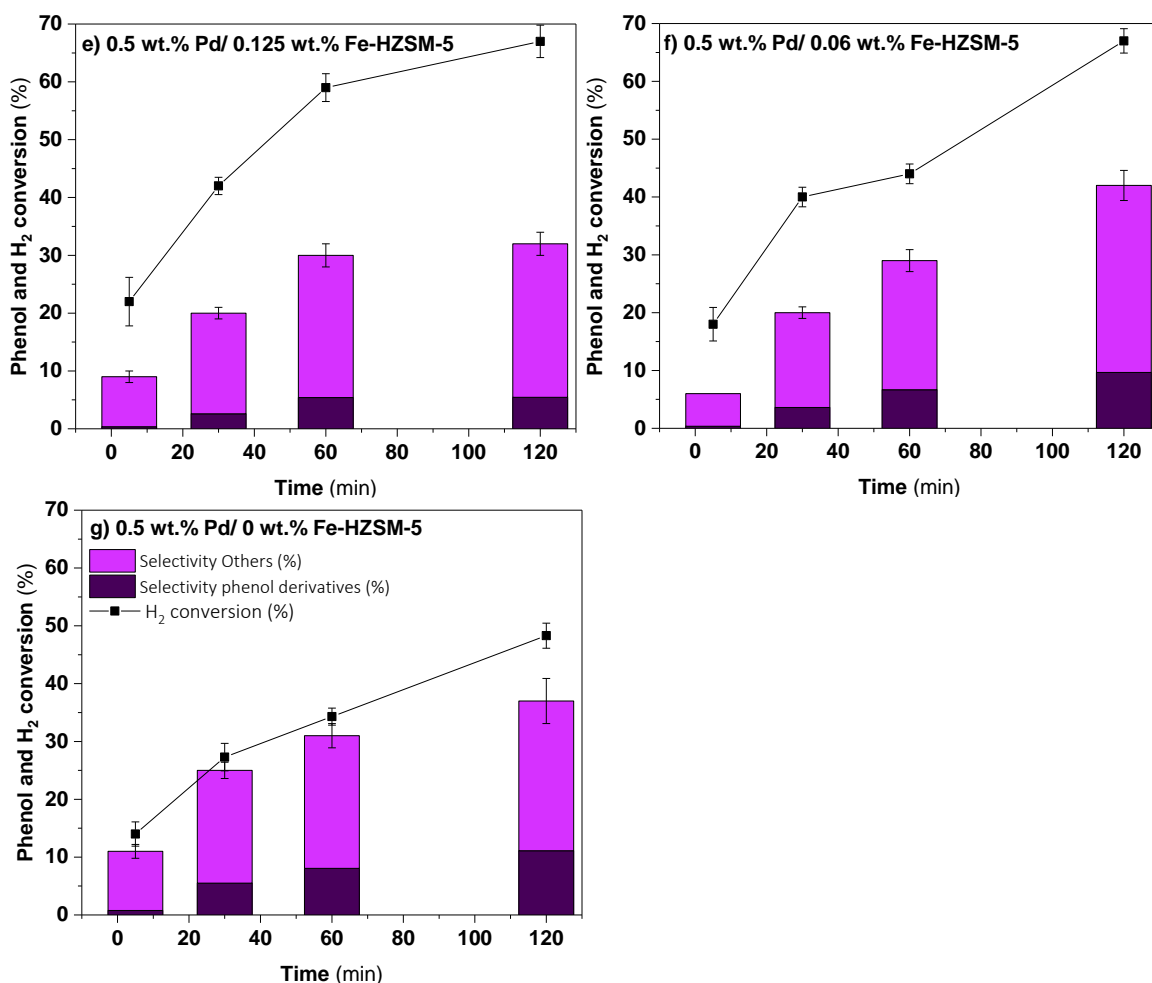


**Figure 5.9:** Time on-line activity towards the degradation of phenol using bi-metallic 0.5 wt.% Pd/ X wt.% Fe-HZSM-5 (X: 3.0-0) catalyst. **Nomenclature:** Phenol derivatives (catechol, resorcinol, 1,4-benzoquinone and hydroquinone). Others (di-acids, CO<sub>2</sub> and H<sub>2</sub>O). **Reaction conditions:** 8.5 g (phenol (1000 ppm)), catalyst (0.01 g), 420 psi 5% H<sub>2</sub>/CO<sub>2</sub>, 160 psi 25% O<sub>2</sub>/CO<sub>2</sub>, 1200 rpm, 30 °C.

Blank reactions were carried out to corroborate that the ROS formed from the *in-situ* H<sub>2</sub>O<sub>2</sub> were responsible for the activity of the bi-metallic 0.5 wt.% Pd/ X wt.% Fe-HZSM-5 (X: 3.0-0) catalysts towards the degradation of phenol (Table 5.5). When O<sub>2</sub> or H<sub>2</sub> were replaced by N<sub>2</sub>, limited phenol degradation activity was shown by the bi-metallic 0.5 wt.% Pd/ 0.5 wt.% Fe-HZSM-5 catalyst (6 and 13 % for blanks O<sub>2</sub>, N<sub>2</sub>/CO<sub>2</sub> and H<sub>2</sub>, N<sub>2</sub>/CO<sub>2</sub> respectively). However, the blank H<sub>2</sub>, N<sub>2</sub>/CO<sub>2</sub> presented relevant activity towards the conversion of phenol, which was attributed to the formation of trace concentrations of H<sub>2</sub>O<sub>2</sub> (and in-turn ROS) through the presence of dissolved O<sub>2</sub> in water. Therefore, the direct synthesis of H<sub>2</sub>O<sub>2</sub> at the same conditions as the blank H<sub>2</sub>, N<sub>2</sub>/CO<sub>2</sub> was performed to corroborate if the H<sub>2</sub>O<sub>2</sub> could actually had been formed. The reaction was carried out for 5 min at 25 °C which are conditions less favourable to degrade H<sub>2</sub>O<sub>2</sub>. Since the concentration of H<sub>2</sub>O<sub>2</sub> was expected to be low, ultraviolet-visible spectroscopy (UV-Vis) was employed, chelating the H<sub>2</sub>O<sub>2</sub> with potassium titanium (IV) oxalate to give a yellowish solution that absorbs at 400 nm.<sup>33</sup> The results determined a net concentration of 2 ppm of H<sub>2</sub>O<sub>2</sub> that could explain the enhanced

activity of the H<sub>2</sub>, N<sub>2</sub>/CO<sub>2</sub> blank. Numerous studies have reported the ability of mono-metallic Pd to catalyse the hydrogenation of phenol to cyclohexanone and cyclohexanol, although with temperatures much higher than the ones used in this work.<sup>34</sup> To exclude any hydrogenation activity leading to the formation of cyclohexanol and cyclohexanone, the post-reaction solution of the blank H<sub>2</sub>, N<sub>2</sub>/CO<sub>2</sub> (0.7 mL) was pipetted and added to an NMR glass tube containing 0.1 mL of deuterium oxide (D<sub>2</sub>O). The analysis of the post reaction solution of the the blank H<sub>2</sub>, N<sub>2</sub>/CO<sub>2</sub> was analysed qualitatively against a cyclohexanone and cyclohexanol standards (0.7 mL, both Merck) dissolved in deuterated chloroform (CDCl<sub>3</sub>, 0.1 mL Merck). The results indicated that no hydrogenation products were formed (Figure S.I 5.16).

The physical mixture of the 0.5 wt.% Pd/ 0 wt.% Fe-HZSM-5 and 0 wt.% Pd/ 0.5 wt.% Fe-HZSM-5 catalysts was found to give significant activity of phenol conversion (29 %). However, as it was mentioned, the mono-metallic 0.5 wt.% Pd/ 0 wt.% Fe-HZSM-5 catalyst contained impurities of Fe. This could explain the high activity shown by the physical mixture as it explains the high activity shown by the mono-metallic 0.5 wt.% Pd/ 0 wt.% Fe-HZSM-5 catalyst in Figure 5.9 during the degradation of phenol. Actually, the physical mixture gave very similar results to the mono-metallic 0.5 Pd/ 0 wt.% Fe-HZSM-5 catalyst towards the degradation of phenol in one hours reaction (Figure 5.9, 31 % phenol conversion, 49 % H<sub>2</sub> conversion).

Pre-formed H<sub>2</sub>O<sub>2</sub> was added accounting that all the H<sub>2</sub> moles had been converted to H<sub>2</sub>O<sub>2</sub>, in the presence of bi-metallic 0.5 wt.% Pd/ 0.5 wt.% Fe-HZSM-5 catalyst to determine if the Fe was actually active in converting H<sub>2</sub>O<sub>2</sub> into ROS. Indeed a significant amount of phenol conversion was observed (21 %), this was far greater than using H<sub>2</sub>O<sub>2</sub> alone (as seen in Chapter 4, section 4.2.1), therefore indicating that ROS was indeed generated from H<sub>2</sub>O<sub>2</sub> and they were responsible for the observed activity. Finally, the bare zeolite (0 wt.% Pd/ 0 wt.% Fe-HZSM-5) was investigated, achieving 5 % phenol conversion which is very similar to the activity shown over the bi-metallic 0.5 wt.% Pd/ 0.5 wt.% Fe-HZSM-5 catalyst using O<sub>2</sub> alone (blank, O<sub>2</sub>, N<sub>2</sub>/CO<sub>2</sub>) possibly indicating that a proportion of phenol was adsorbed during the reaction, this is particularly true given that no products were observed during analysis of post reaction solutions.

**Table 5.5:** Degradation of phenol with replacement of H<sub>2</sub> and/or O<sub>2</sub> by N<sub>2</sub>, physical mixtures of mono-metallic 0.5 wt.% Pd/ 0 wt.% Fe-HZSM-5 and 0 wt.% Pd/ 0.5 wt.% Fe-HZSM-5 as well as bare zeolite.

Blanks	Phenol conversion	H <sub>2</sub> conversion	Selectivity towards phenol derivatives	Selectivity towards others
	%	%	%	%
O <sub>2</sub> , N <sub>2</sub> /CO <sub>2</sub>	6	n/a	0	0
H <sub>2</sub> , N <sub>2</sub> /CO <sub>2</sub>	13	n.d	1	99
Physical mixture	29	57	24	76
Pre-formed H <sub>2</sub> O <sub>2</sub>	21	n/a	4	96
Bare zeolite	5	n.d	0	0

**n/a:** not applicable. **n.d:** not determined. **Reaction conditions: Blank, O<sub>2</sub>, N<sub>2</sub>/CO<sub>2</sub>:** 8.5 g (1000 ppm Phenol), 0.5 wt.% Pd/0.5 wt.% Fe/HZSM-5 (0.01 g), 420 psi N<sub>2</sub>, 160 psi 25% O<sub>2</sub>/CO<sub>2</sub>, 1200 rpm, 30 °C, 2 h. **Physical mixture. Blank, H<sub>2</sub>, N<sub>2</sub>/CO<sub>2</sub>:** 8.5 g (1000 ppm Phenol), 0.5 wt.% Pd/0.5 wt.% Fe/HZSM-5 (0.01 g), 420 psi 5% H<sub>2</sub>/CO<sub>2</sub>, 160 psi N<sub>2</sub>, 1200 rpm, 30 °C, 2 h. **Blank, physical mixture:** 8.5 g (1000 ppm Phenol), 0.5 wt.% Pd/0 wt.% Fe/HZSM-5 (0.005 g) and 0 wt.% Pd/0.5 wt.% Fe/HZSM-5 (0.005 g), 420 psi 5% H<sub>2</sub>/CO<sub>2</sub>, 160 psi O<sub>2</sub>/CO<sub>2</sub>, 1200 rpm, 30 °C, 2 h. **Blank, pre-formed H<sub>2</sub>O<sub>2</sub>:** 8.5 g (1000 ppm Phenol), H<sub>2</sub>O<sub>2</sub> (0.156 g), 0.5 wt.% Pd/0.5 wt.% Fe/HZSM-5 (0.01 g), 580 psi N<sub>2</sub>, 1200 rpm, 30 °C, 2 h. **Blank, bare zeolite:** 8.5 g (1000 ppm Phenol), 0 wt.% Pd/0 wt.% Fe/HZSM-5 (0.01 g), 420 psi 5% H<sub>2</sub>/CO<sub>2</sub>, 160 psi O<sub>2</sub>/CO<sub>2</sub>, 1200 rpm, 30 °C, 2 h. **Nomenclature:** Selectivity towards phenol derivatives (catechol, resorcinol, 1,4-benzoquinone, hydroquinone) and selectivity towards others (di-acids, H<sub>2</sub>O and CO<sub>2</sub>).

Gas replacement experiments were conducted to determine if the catalysts activity was limited by the amount of H<sub>2</sub> as it was concluded from the time on-line experiments in Figure 5.9. The experiments were carried out using the bi-metallic 0.5 wt.% Pd/3.0 wt.% Fe-HZSM-5 catalyst and consisted in replacing the gas phase with the same fresh gas composition (580 psi H<sub>2</sub>,O<sub>2</sub>/CO<sub>2</sub>) every two hours. A more detailed explanation of how this experiment was conducted can be found in Chapter 2, section 2.3.2.2. The results indicated how by providing more H<sub>2</sub> and O<sub>2</sub> the oxidation of phenol was enhanced, achieving up to 100 % conversion in 8 hours and 3 gas charges. Interestingly, as happened in the same experiments using the bi-metallic 0.5 wt. % Pd-0.5 wt.% Fe/TiO<sub>2</sub> catalyst in Chapter 4, the H<sub>2</sub> conversion decreased over time until reaching a stable value, which suggested that the Pd component was being deactivated, possibly due to metal leaching or agglomeration over the course of the reaction.

The selectivity of phenol derivatives (catechol, hydroquinone, resorcinol and 1,4-benquinone) decreased along with the reaction time, indicating that part of them had successfully being oxidised towards di-acids, CO<sub>2</sub> and H<sub>2</sub>O (termed as others).

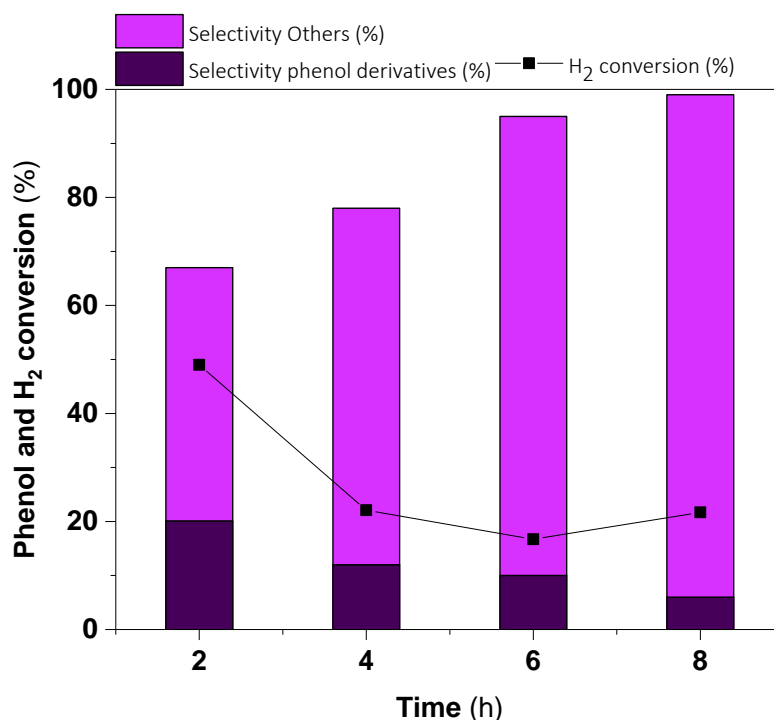


**Figure 5.10:** Conduction of gas replacement experiments during the degradation of phenol and using 0.5 wt.% Pd/3.0 wt.% Fe-HZSM-5 catalyst. **Nomenclature:** Phenol derivatives (catechol, resorcinol, 1,4-benzoquinone and hydroquinone). Others (di-acids, CO<sub>2</sub> and H<sub>2</sub>O). **Reaction conditions:** 8.5 g (phenol (1000 ppm)), catalyst (0.01 g), 420 psi 5 % H<sub>2</sub>/CO<sub>2</sub>, 160 psi 25 % O<sub>2</sub>/CO<sub>2</sub>, 1200 rpm, 30 °C. Gas was replaced by fresh by 420 psi 5 % H<sub>2</sub>/CO<sub>2</sub> and 160 psi 25 % O<sub>2</sub>/CO<sub>2</sub>.

The metal leaching was determined by analysis of post-reaction solutions by MP-AES, after a standard 2 hours' phenol degradation reaction (Table 5.6). A correlation between the extend of phenol conversion and metal leaching was observed when analysing the time on-line post reaction solution of the bi-metallic 0.5 wt.% Pd/ 3.0 wt.% Fe-HZSM-5 catalyst during the degradation of phenol (Table S.I 5.5). However, it was also observed that these catalysts were also unstable and leached during the direct synthesis of H<sub>2</sub>O<sub>2</sub> (Table S.I. 5.4), therefore it is not possible to attribute the instability of the metal species fully to exposure to phenol or its oxidation products. Regardless, the overall metal leaching of the optimal 0.5 wt.% Pd/ 3.0 wt.% Fe-HZSM-5 catalyst was found to be limited (6.0 and 3.8 % of Fe and Pd respectively), which is particularly promising given the high rate of phenol conversion obtained (67 %) in two hours' reaction time. It was possible that the Fe that had leached from the bi-metallic 0.5 wt.% Pd/ 3.0 wt.% Fe-HZSM-5 catalyst was from the clusters and agglomerative of Fe<sub>x</sub>O<sub>y</sub> species as it was evidenced by DR UV-Vis. These results also indicated that the framework (isolated and bi-nuclear Fe species) attached to the channels were more stable than the extra-framework (clusters and agglomerates Fe<sub>x</sub>O<sub>y</sub>). This could be concluded when comparing the bi-metallic 0.50 wt.% Fe-0.50 wt.% Pd/TiO<sub>2</sub> catalysts (Chapter 4, 42 % Fe leached, 2 % Pd leached and c.a 35 % phenol conversion) that contained only clusters and agglomeratives of Fe<sub>x</sub>O<sub>y</sub> species and the bi-metallic 0.5 wt.% Pd/ 0.5 wt.% Fe-HZSM-5 catalyst (4 % Fe leached, 8 % Pd leached, c.a

40 % phenol conversion) that contained framework isolated and bi-nuclear Fe species in greater extent.

Unfortunately, Pd became instable in both sets of reactions, during the direct synthesis of H<sub>2</sub>O<sub>2</sub> and during the degradation of phenol. Contrarily, in the bi-metallic 1.0 wt.% FePd/TiO<sub>2</sub> catalysts, Pd only leached during the degradation of phenol. There could be several reasons that could explain the difference in the Pd stability between these two types of bi-metallic FePd catalysts, such as *i*) the interaction between the Pd and TiO<sub>2</sub> that could have made the Pd nanoparticles more stable, *ii*) the size and composition of the nanoparticles in the bi-metallic 0.50 wt.% Pd/ X wt.% Fe-HZSM-5 (X: 3.0-0) catalysts were bigger than in the bi-metallic 1 wt.% FePd/ TiO<sub>2</sub> analogues that could have evoked the Pd to leach.

**Table 5.6:** Leaching of the mono and bi-metallic 0.5 wt.% Pd/ X wt.% Fe-HZSM-5 (X: 3.0-0) catalysts for the degradation of phenol in two hours' reaction.

Catalysts	Pd %	Fe %
0.5wt.%Pd/3.0wt.%Fe-HZSM-5	3.8	6.0
0.5wt.%Pd/2.0wt.%Fe-HZSM-5	3.7	6.1
0.5wt.%Pd/1.0wt.%Fe-HZSM-5	3.5	7.4
0.5wt.%Pd/0.5wt.%Fe-HZSM-5	4.0	8.0
0.5wt.%Pd/0.125wt.%Fe-HZSM-5	1.2	9.3
.5wt.%Pd/0.06wt.%Fe-HZSM-5	0.9	10.0
0.5wt.%Pd/0 wt.% Fe-HZSM-5	1.4	0.77

**Reaction conditions:** 8.5 g (phenol (1000 ppm)), catalyst (0.01 g), 420 psi 5% H<sub>2</sub>/CO<sub>2</sub>, 160 psi 25% O<sub>2</sub>/CO<sub>2</sub>, 1200 rpm, 30 °C, 2 h.

Hot filtration experiments were carried out with the bi-metallic 0.5 wt.% Pd/3.0 wt.% Fe-HZSM-5 catalyst to determine the contribution of leached Fe and Pd species to the observed activity (Table 5.7). After running the phenol oxidation reaction for 1 hour, the bi-metallic 0.5 wt.% Pd/ 3.0 wt.% Fe-HZSM-5 catalyst was removed via filtration and the post-reaction solution returned to the reactor for one extra hour with fresh gas mixtures (580 psi H<sub>2</sub>, O<sub>2</sub>/CO<sub>2</sub>). The activity of the leached metal species was found to be limited, with minimal additional conversion rising from 51 % to 53 % after the additional 1 h in the presence of only leached species. The H<sub>2</sub> conversion also decreased significantly from 39 % to 7 %, suggesting that the production of H<sub>2</sub>O<sub>2</sub> would have been minimal, which would have been expected given the limited amount of Pd leached. Analogously to the previous experiment, a second reaction was conducted where after the initial 1 h reaction, the post-reaction solution was filtered and re-run for an extra hour with fresh gas in the presence of mono-metallic 0.5 wt.% Pd/0 wt.% Fe-HZSM-5 catalyst, which led to an increase of phenol

conversion up to 72 % (Table 5.7, Homogeneous + 0.5 wt.% Pd/0 wt.% Fe-HZSM-5). However, given the ability of the mono-metallic 0.5 wt. %Pd/ 0 wt.% Fe-HZSM-5 catalyst to promote the degradation of phenol, this experiment was unable to confirm a contribution from homogeneous Fe species. In a final experiment, after the initial 1 h reaction utilising the bi-metallic 0.5 wt.%Pd/3.0 wt.% Fe-HZSM-5 catalyst, pre-formed H<sub>2</sub>O<sub>2</sub> was added to the post-reaction mixture at a concentration equivalent to all the moles of H<sub>2</sub> in the gas phase (580 psi H<sub>2</sub>, O<sub>2</sub>/CO<sub>2</sub>) were selectively converted to H<sub>2</sub>O<sub>2</sub>. After 1 h reaction (carried out in the presence of O<sub>2</sub>/CO<sub>2</sub> atmosphere), a small increase in phenol conversion was observed (65 %). This increase in phenol conversion from 51 % to 65 % indicated that the Fe species leached in the post-reaction solution were active and were able to react with pre-formed H<sub>2</sub>O<sub>2</sub> to give ROS. Therefore, it was concluded that the Fe leached could carry out homogeneous Fenton's oxidations and most likely they contributed to the activity.

**Table 5.7:** Hot filtration experiments using bi-metallic 0.5 wt.% Pd/ 3.0 wt.% Fe-HZSM-5 catalyst for the degradation of phenol.

Hot experiments	Phenol conversion %	H <sub>2</sub> conversion %
<b>0.5 wt.% Pd/ 3.0 wt.% Fe-HZSM-5</b>	51	39
<b>Fresh</b>		
<b>Homogeneous</b>	53	7
<b>Homogeneous + 0.5 wt.% Pd/0 wt. % Fe-HZSM-5</b>	72	38
<b>Homogeneous + pre-formed H<sub>2</sub>O<sub>2</sub></b>	64.5	n/a

**Reaction conditions: Fresh:** 8.5 g (1000 ppm Phenol), 0.5 wt.% Pd/3.0 wt.% Fe-HZSM-5 (0.01 g), 420 psi 5 % H<sub>2</sub>/CO<sub>2</sub>, 160 psi 25 % O<sub>2</sub>/CO<sub>2</sub>, 1200 rpm, 30 °C, 1 h. **Homogeneous:** 8.5 g (filtered post-reaction solution of 0.5 wt.% Pd/3.0 wt.% Fe-HZSM-5), catalyst (0.00 g), 420 psi 5 % H<sub>2</sub>/CO<sub>2</sub>, 160 psi 25 % O<sub>2</sub>/CO<sub>2</sub>, 30 °C, 1 h. **Homogeneous + 0.5 wt.% Pd/0 wt.% Fe-HZSM-5:** 8.5 g (filtered post-reaction solution of 0.5 wt.% Pd/3.0 wt.% Fe/HZSM-5), 0.5 wt.% Pd/0 wt.% Fe-HZSM-5 (0.01 g), 420 psi 5 % H<sub>2</sub>/CO<sub>2</sub>, 160 psi 25 % O<sub>2</sub>/CO<sub>2</sub>, 1200 rpm, 30 °C, 1 h. **Homogeneous + pre-formed H<sub>2</sub>O<sub>2</sub>:** 8.5 g (filtered post-reaction of 0.5 wt.% Pd/3.0 wt.% Fe-HZSM-5), H<sub>2</sub>O<sub>2</sub> (0.0551 g), 580 psi 25 %O<sub>2</sub>/CO<sub>2</sub>, 1200 rpm, 30 °C, 1 h.

Increasing the amount of catalyst was next investigated to complete the oxidation of phenol and its products. The study was carried out using the bi-metallic 0.5 wt.% Pd/ 3.0 wt.% Fe-HZSM-5 catalyst, increasing its amount from 0.01 to 0.04 g (Figure 5.11).

The conversion of phenol increased as the amount of catalyst also increased, in fact, almost all phenol was degraded with the addition of 0.02 g of 0.5 wt.% Pd/ 3.0 wt.% Fe-HZSM-5 catalyst in a standard 2 hours' reaction. The selectivity towards di-acids, CO<sub>2</sub> and H<sub>2</sub>O (others) was particularly high, indicating that phenol derivatives were being successfully oxidised as well. However, the H<sub>2</sub> conversion remained the same regardless of the amount of catalyst, which indicated that the activity of Pd could have been limited by the availability

of H<sub>2</sub> in solution. The leaching of the Fe and Pd increased significantly as it would be expected due to having had increased the oxidation of phenol (Table S.I 5.6).

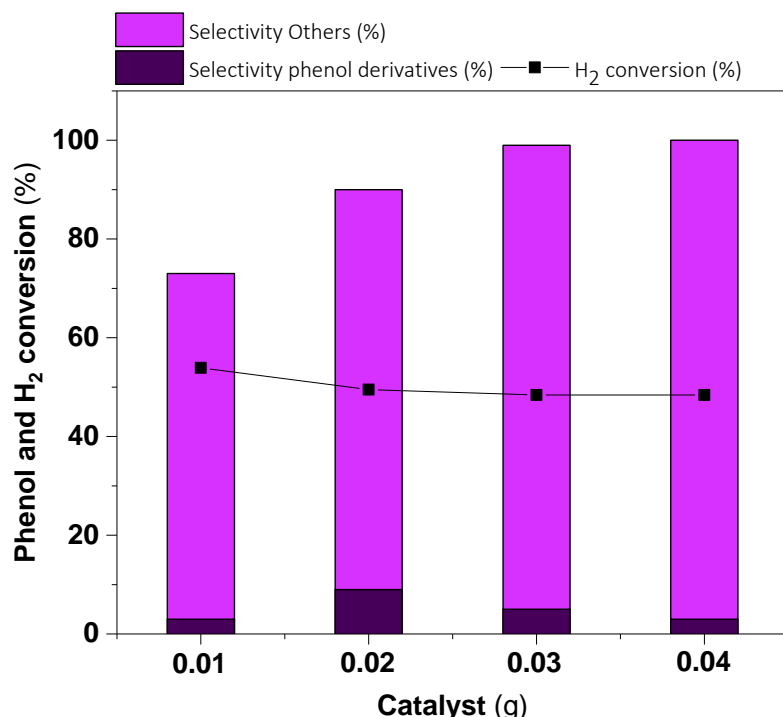


**Figure 5.11:** Increasing the amount of bi-metallic 0.5 wt.% Pd/ 3.0 wt.% Fe-HZSM-5 catalyst for the degradation of phenol. **Reaction conditions:** 8.5 g (phenol (1000 ppm)), 420 psi 5 % H<sub>2</sub>/CO<sub>2</sub>, 160 psi 25 % O<sub>2</sub>/CO<sub>2</sub>, 1200 rpm, 30 °C, 2 h.

#### 5.2.4 Characterisation and re-usability of the bi-metallic 0.5 wt.% Pd/ 0.5 wt.% Fe-HZSM-5 catalyst towards the degradation of phenol.

The analysis by XRD of the used bi-metallic 0.5 wt.% Pd/ 0.5 wt.% Fe-HZSM-5 catalyst was next conducted (Figure 5.12). The used catalyst -after the degradation of phenol- presented the characteristic reflections of the HZSM-5 structure, and the crystallinity had not significantly decreased in comparison to the fresh bi-metallic 0.5 wt.% Pd/ 0.5 wt.% Fe-HZSM-5 catalyst (Figure 5.12 b)). This data suggested that phenol, the products generated as well as the reaction conditions (30 °C, H<sub>2</sub>O-only solvents) did not significantly alter the framework.

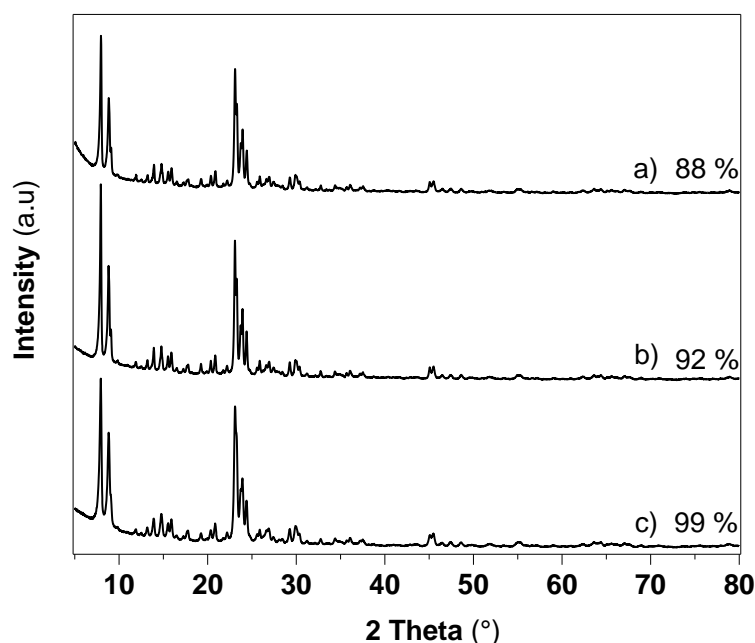


**Figure 5.12:** XRD diffractogram of the fresh and used bi-metallic 0.5 wt.% Pd/ 0.5 wt.% Fe-HZSM-5 catalyst after the degradation of phenol. **Nomenclature:** a) used, b) fresh, c) 0 wt.% Pd/ 0 wt.% Fe-HZSM-5 (fresh). **Reaction conditions for the used catalyst:** 8.5 g (phenol (1000 ppm)), catalyst (0.01 g), 420 psi 5% H<sub>2</sub>/CO<sub>2</sub>, 160 psi 25% O<sub>2</sub>/CO<sub>2</sub>, 1200 rpm, 30 °C, 2 h.

The oxidation state of Pd for the used 0.5 wt.% Pd/ 0.5 wt.% Fe-HZSM-5 catalyst was analysed by XPS and the results are shown in Table 5.8. As in the case of the bi-metallic 0.5 wt.% Pd-0.5 wt.% Fe/TiO<sub>2</sub> catalyst, the percentage of Pd<sup>0</sup> increased after use, indicating that the atmosphere of 420 psi 5 % H<sub>2</sub>/CO<sub>2</sub> had contributed to the reduction of Pd. This result led to the conclusion that the oxidation state of the Pd changes during the course of the reaction, indicating that the performance of Pd towards the direct synthesis of H<sub>2</sub>O<sub>2</sub> could be different between usages. Some authors have reported the difference in activity between the PdO and Pd<sup>0</sup>, acknowledging that the former was more active but less selective towards the direct synthesis of H<sub>2</sub>O<sub>2</sub>.<sup>35,36, 37</sup>

**Table 5.8:** XPS analysis of the fresh and used bi-metallic 0.5 wt.%Pd/ 0.5 wt.%Fe-HZSM-5 catalyst for the degradation of phenol.

Catalysts	PdO	Pd <sup>0</sup>	Pd:X
	%	%	
<b>0.5 wt.%Pd/ 0.5 wt.%Fe-HZSM-5</b>	20	80	4.2
<b>Fresh</b>			
<b>0.5 wt.%Pd/ 0.5 wt.%Fe-HZSM-5</b>	6.5	93.5	4.5
<b>Used</b>			

**Reaction conditions:** 8.5 g (phenol (1000 ppm)), catalyst (0.01 g), 420 psi 5 % H<sub>2</sub>/CO<sub>2</sub>, 160 psi 25 % O<sub>2</sub>/CO<sub>2</sub>, 1200 rpm, 30 °C, 2 h. XPS spectra for the used catalyst is shown in supplementary information, Figure S.I 5.17.

The determination of the particle size and distribution was examined to see if there could be agglomeration of particles after use the bi-metallic 0.5 wt.% Pd/ 0.5 wt.% Fe-HZSM-5 catalyst for the degradation of phenol. The mean particle size was 24 nm (standard deviation of 12 nm), which was relatively similar to the fresh catalyst (26 nm, Table 5.3). This observation led to the conclusion that the deactivation of the bi-metallic 0.5 wt.%Pd/ 0.5 wt.%Fe-HZSM-5 catalyst was not likely to be caused by particle agglomeration. The TEM micrographs and histogram are shown in supplementary information (Figure S.I 5.18 and Figure S.I 5.19 respectively).

The activity of the bi-metallic 0.5 wt% Pd/0.5 wt.% Fe-HZSM-5 catalyst was subsequently investigated towards the degradation of phenol to determine how the activity had been affected after one usage (Table 5.9). The results indicated that the activity did actually decrease from 44 % to 30 % accompanied by a decay in the H<sub>2</sub> conversion from 64 % to 28 %, clearly indicating that the formation of H<sub>2</sub>O<sub>2</sub> had been lower in comparison to the fresh catalyst, therefore indirectly affecting the formation of ROS. Two factors could have had contributed to decrease the activity of the used catalysts. On one hand, the metal leaching and on the second hand, the changed in the oxidation state of the Pd that could have had affected the formation of H<sub>2</sub>O<sub>2</sub>.

**Table 5.9:** Re-usability of the bi-metallic 0.5 wt.% Pd/ 0.5 wt.% Fe-HZSM-5 catalyst for the degradation of phenol.

Catalysts	Phenol conversion	H <sub>2</sub> conversion
	%	%
<b>0.5 wt.% Pd/ 0.5 wt.% Fe-HZSM-5</b>	44	64
<b>Fresh</b>		
<b>0.5 wt.% Pd/ 0.5 wt.% Fe-HZSM-5</b>	30	28
<b>Used</b>		

**Reaction conditions:** 8.5 g (phenol (1000 ppm)), catalyst (0.01 g), 420 psi 5 % H<sub>2</sub>/CO<sub>2</sub>, 160 psi 25 % O<sub>2</sub>/CO<sub>2</sub>, 1200 rpm, 30 °C, 2 h.

### 5.3 Conclusions.

The synthesis of HZSM-5 (SiO<sub>2</sub>: Al<sub>2</sub>O<sub>3</sub>) (28:1) was successfully achieved by hydrothermal synthesis, achieving 99 % crystallinity according to XRD analysis. However, the addition of Fe to the HZSM-5 (SiO<sub>2</sub>: Al<sub>2</sub>O<sub>3</sub>) (28:1) zeolite led to a decrease in the crystallinity of the zeolite, with the addition of Pd leading to a further reduction in crystallinity. Physisorption analysis also evidenced a decrease in the specific surface area and pore volume with the introduction of the Fe and Pd, suggesting that the surface was becoming even and smoother in comparison to the bare zeolite. XPS analysis revealed the presence of a similar

proportion of PdO (20 %) and Pd<sup>0</sup> (80 %) for the bi-metallic 0.5 wt.% Pd/ X wt.% Fe-HZSM-5 (X: 3.0-0.06) catalysts. Notably the mono-metallic 0.5 wt.% Pd/ 0 wt.% Fe-HZSM-5 catalyst had near equal proportions of Pd species (PdO (49 %), Pd<sup>0</sup> (51 %)), suggesting that the introduction of Fe could significantly alter Pd oxidation state. The specific surface area was found to decrease with the introduction of Fe and subsequent immobilisation of Pd.

The activity of these set of bi-metallic 0.5 wt.% Pd/ X wt.% Fe-HZSM-5 (X: 3.0-0.06) catalysts was promising, showing a conversion of phenol between 65-55 % for the high Fe loaded materials (3.0-1.0 wt.% of Fe), whereas the conversion achieved over the catalysts containing lower amounts of Fe (0.5-0.06 wt.%) was somewhat lower (c.a 40 %). This data suggested that the bi-metallic 0.5 wt.% Pd/ X wt.% Fe-HZSM-5 (X: 3.0-1.0) catalysts could have had generated greater proportion of ROS in comparison to the others analogues ones 0.5 wt.% Pd/ X wt.% Fe-HZSM-5 (X: 0.5-0.06), despite the whole set of bi-metallic 0.5 wt.% Pd/ X wt.% Fe-HZSM-5 (X: 3.0-0.06) catalysts had formed similar concentrations of H<sub>2</sub>O<sub>2</sub> (between 0.01–0.005 wt.% of H<sub>2</sub>O<sub>2</sub>, 2 h reaction time). Unfortunately, Fe and Pd leached during the direct synthesis of H<sub>2</sub>O<sub>2</sub> and during the degradation of phenol reaction. The formation of these extra-framework species (clusters and agglomerative of Fe<sub>x</sub>O<sub>y</sub>) on the surface of the catalysts in contact with the Pd deposited on the external surface could have had made these set of bi-metallic 0.5 wt.% Pd/ X wt.% Fe-HZSM-5 (X: 3.0-1.0) catalysts more active towards the degradation of phenol. In fact, DR UV-Vis and Raman-UV corroborated this hypothesis. For instance, DR-UV-Vis showed a shoulder at > 450 nm for the bi-metallic 0.5 wt.% Pd/ X wt.% Fe-HZSM-5 (X: 3.0-2.0) catalysts, which were assigned to extra-framework Fe<sub>x</sub>O<sub>y</sub> species.<sup>29</sup> On the other hand, the other bi-metallic 0.5 wt.% Pd/ X wt.% Fe-HZSM-5 (X: 0.5-0.06) catalysts contained isolated and bi-nuclear Fe species immobilised in the framework channels in greater extent. However, it was evidenced that the framework Fe species were more stable against leaching. This was evidenced when comparing the metal leaching and activity towards the degradation of phenol between the bi-metallic 0.5 wt.% Pd-0.5 wt.% Fe/TiO<sub>2</sub> catalyst with a conversion of 35 % of phenol and 42 % of Fe leached, whereas the same loading for the bi-metallic 0.5 wt.% Pd/ 0.5 wt.% Fe-HZSM-5 catalyst presented 40 % phenol conversion and 4 % of Fe.

The re-usage of the bi-metallic 0.5 wt.% Pd/ 0.5 wt.% Fe-HZSM-5 catalyst towards the degradation of phenol was compromised, probably due to the contribution of two main factors. On one hand, the metal leaching of Fe and Pd, and on the other hand, the oxidation state of Pd, which in the used bi-metallic 0.5 wt.% Pd/ 0.5 wt.% Fe-HZSM-5 catalyst was found to differ from the fresh one. The changed in the oxidation state, could have had contributed to generate less H<sub>2</sub>O<sub>2</sub> during the second usage of the catalyst as it was suggested from the H<sub>2</sub> conversion data. Thus, it was concluded that these bi-metallic 0.5

wt.% Pd/ X wt.% Fe-HZSM-5 (X: 0.5-0.06 wt. %) (SiO<sub>2</sub>: Al<sub>2</sub>O<sub>3</sub>) (28:1) catalysts were still not suitable for commercial use and further catalytic design technologies had to be considered.

#### 5.4 References.

1. Yan, Y., Jiang, S. & Zhang, H. Catalytic wet oxidation of phenol with Fe-ZSM-5 catalysts. *RSC Adv.* **6**, 3850–3859 (2016).
2. Nguyen Huu Phu, Kim Hoa, T. T., Nguyen Van Tan, Hoang Vinh Thang & Pham Le Ha. Characterization and activity of Fe-ZSM-5 catalysts for the total oxidation of phenol in aqueous solutions. *Appl. Catal. B Environ.* **34**, 267–275 (2001).
3. Ghaffari, Y., Gupta, N. K., Bae, J., Kim, K. S. Heterogeneous catalytic performance and stability of iron-loaded ZSM-5, zeolite-A, and silica for phenol degradation: A microscopic and spectroscopic approach. *Catalysts.* **9**, 1-15 (2019).
4. Calleja, G., Melero, J. A., Martínez, F., Molina, R. Activity and resistance of iron-containing amorphous, zeolitic and mesostructured materials for wet peroxide oxidation of phenol. *Water Res.* **39**, 1741–1750 (2005).
5. Long, R. Q., Yang, R. T. Fe-ZSM-5 for selective catalytic reduction of NO with NH<sub>3</sub>. A comparative study of different preparation techniques. *Catal. Letters* **74**, 201–205 (2001).
6. Yuranov, I., Bulushev, D. A., Renken, A., Kiwi-Minsker, L. Benzene hydroxylation over FeZSM-5 catalysts: Which Fe sites are active? *J. Catal.* **227**, 138–147 (2004).
7. Hammond, C., Forde, M.M., Ab Rahim, M.H., Thetford, A., He, Q., Jenkins, R.L., Dimitratos, N., Lopez-Sanchez, J.A., Dummer, N.F., Murphy, D.M., Carley, A.F., Taylor, S.H., Willock, D.J., Stangland, E.E., Kang, J., Hagen, H., Kiely, C.J., Hutchings, G.J. Direct catalytic conversion of methane to methanol in an aqueous medium by using copper-promoted Fe-ZSM-5. *Angew. Chemie-Int. Ed.* **51**, 5129–5133 (2012).
8. Hartmann, M., Kullmann, S., Keller, H. Wastewater treatment with heterogeneous Fenton-type catalysts based on porous materials. *J. Mater. Chem.* **20**, 9002–9017 (2010).
9. Ravenelle, R. M., Schüßler, F., D'Amico, A., Danilina, N., van, Bokhoven, J.A., Lercer, J.A., Jones, C. W., Sievers, C. Stability of Zeolites in Hot Liquid Water. *J. Phys. Chem. C.* **114**, 19582–19595 (2010).
10. Li, G., Pidko, E. A., Van Santen, R. A., Li, C., Hensen, E. J. M. Stability of extraframework iron-containing complexes in ZSM-5 zeolite. *J. Phys. Chem. C* **117**, 413–426 (2013).
11. Meenakshisundaram, S., He, Q., Moataz, M., Pritchard, J., Freakley, S.J., Edwards, J.K., Taylor, S.H., Morgan, D.J., Carley, A.F., Knight, D.W., Kiely, C.J., Hutchings, G.J. Synthesis of stable ligand-free gold-palladium nanoparticles using a simple

- excess anion method. *ACS Nano*. **6**, 6600–6613 (2012).
12. Cheng, Y., Wang, L. J., Li, J. S., Yang, Y. C., Sun, X. Y. Preparation and characterization of nanosized ZSM-5 zeolites in the absence of organic template. *Mater. Lett.* **59**, 3427–3430 (2005).
  13. Lewis, R. J., Bara-Estaun, A., Agarwal, N., Freakly, S.J., Morgan, D.J., Hutchings, G.J. The Direct Synthesis of H<sub>2</sub>O<sub>2</sub> and Selective Oxidation of Methane to Methanol Using HZSM-5 Supported AuPd Catalysts. *Catal. Letters* **149**, 3066–3075 (2019).
  14. Zhang, W., Bao, X., Guo, X., Wang, X. A high-resolution solid-state NMR study on nano-structured HZSM-5 zeolite. *Catal. Letters* **60**, 89–94 (1999).
  15. Fouad, O. A., Mohamed, R. M., Hassan, M. S., Ibrahim, I. A. Effect of template type and template/silica mole ratio on the crystallinity of synthesized nanosized ZSM-5. *Catal. Today*. **116**, 82–87 (2006).
  16. Sang, S., Chang, F., Liu, Z., He, C., He, Y., Xu, L. Difference of ZSM-5 zeolites synthesized with various templates. *Catal. Today*. **93–95**, 729–734 (2004).
  17. Liu, G., Liang, H., Tian, Y., Zhang, B., Wang, L. Chinese Journal of Chemical Engineering Direct synthesis of hydrogen peroxide over Pd nanoparticles embedded between HZSM-5 nanosheets layers. *Chinese J. Chem. Eng.* **28**, 2577–2586 (2020).
  18. Chen, S., Liu, S., Men, Y., Li, L., Li, X., Pan, X., Sun, C., Xiong, L., Niu, X., An, W., Wang, J., Wang, Y. Synergistic Catalysis of PdFe Bimetallic Nanoparticles Supported on SiO<sub>2</sub> for Hydrogenative Cleavage of C–N Bonds. *ACS Appl. Nano Mater.* **4**, 6020–6029 (2021).
  19. Bahruji, H., Ruiz Esquiús, J., Bowker, M., Hutchings, G.J., Armstrong, R.D., Jones, W. Solvent Free Synthesis of PdZn/TiO<sub>2</sub> Catalysts for the Hydrogenation of CO<sub>2</sub> to Methanol. *Top. Catal.* **61**, 144–153 (2018).
  20. Storck, S., Bretinger, H., Maier, W. F. Characterization of micro- and mesoporous solids by physisorption methods and pore-size analysis. *Appl. Catal. A Gen.* **174**, 137–146 (1998).
  21. Thommes, M., Kaneko, K., Neimark, A.V., Oliver, J.P., Rodriguez-Reinoso, F., Rouquerol, J., Sing, K.S.W. Physisorption of gases, with special reference to the evaluation of surface area and pore size distribution (IUPAC Technical Report). *Pure Appl. Chem.* **87**, 1051–1069 (2015).
  22. Sotomayor, F. J., Cychosz, K. A., Thommes, M. Characterization of Micro/Mesoporous Materials by Physisorption: Concepts and Case Studies. *Acc. Mater. Surf. Res* **3**, 34–50 (2018).
  23. Gervasini, A. Characterization of the textural properties of metal loaded ZSM-5 zeolites. *Appl. Catal. A Gen.* **180**, 71–82 (1999).
  24. Viswanadham, N., Kamble, R., Singh, M., Kumar, M., Murali Dhar, G. Catalytic

- properties of nano-sized ZSM-5 aggregates. *Catal. Today* **141**, 182–186 (2009).
25. Bae, Y. S., Yazayd'n, A. Ö., Snurr, R. Q. Evaluation of the BET method for determining surface areas of MOFs and zeolites that contain Ultra-Micropores. *Langmuir* **26**, 5475–5483 (2010).
  26. Park, M. B., Ahn, H., Mansouri, A., Ranocchiari, M. Comparative Study of Diverse Copper Zeolites for the Conversion of Methane into Methanol. *ChemCatChem*. **9**, 3705–3713 (2017).
  27. Tian, P., Ouyang, L., Xu, X., Ao, C., Xu, X., Si, R., Shen., X., Lin, M., Xu, J., Han, Y.F. The origin of palladium particle size effects in the direct synthesis of H<sub>2</sub>O<sub>2</sub>: Is smaller better? *J. Catal.* **349**, 30–40 (2017).
  28. Scarano, D., Zecchina, A., Bordiga, S., Geobaldo, F., Spoto, G. Fourier-transform Infrared and Raman Spectra of Pure and Al-, B-, Ti- and Fe-substituted Silicalites: Stretching-mode Region. *J. Chem. Soc. Faraday Trans.* **89**, 4123–4130 (1993).
  29. Xu, J., Armstrong, R.D., Shaw, G., Dummer, N.F., Freakley, S.J., Taylor, S.H., Hutchings, G.J. Continuous selective oxidation of methane to methanol over Cu- and Fe-modified ZSM-5 catalysts in a flow reactor. *Catal. Today*. **270**, 93–100 (2016).
  30. Ovejero, G., Sotelo, J. L., Martínez, F., Melero, J. A., Gordo, L. Wet peroxide oxidation of phenolic solutions over different iron-containing zeolitic materials. *Ind. Eng. Chem. Res.* **40**, 3921–3928 (2001).
  31. Hammond, C., Hermans, I., Dimitratos, N. Biomimetic oxidation with Fe-ZSM-5 and H<sub>2</sub>O<sub>2</sub>? Identification of an active, extra-framework binuclear core and an Fe<sup>III</sup>-OOH intermediate with resonance-enhanced Raman spectroscopy. *ChemCatChem*. **7**, 434–440 (2015).
  32. Sun, K., Fan, F., Xia, H., Feng, Z., Li, W.X., Can, L. Framework Fe ions in Fe-ZSM-5 zeolite studied by UV resonance raman spectroscopy and density functional theory calculations. *J. Phys. Chem. C*. **112**, 16036–16041 (2008).
  33. Sellers, R. M. Spectrophotometric Determination of Hydrogen Peroxide Using Potassium Titanium(IV) Oxalate. **105**, 950–954 (1990).
  34. Zhou, H., Han, B., Liu, T., Zhong, X., Zhuang, G., Wang, J. Selective phenol hydrogenation to cyclohexanone over alkali-metal-promoted Pd/TiO<sub>2</sub> in aqueous media. *Green chem.* **19**, 3585–3594 (2017).
  35. Choudhary, V. R., Gaikwad, A. G., Sansare, S. D. Activation of supported Pd metal catalysts for selective oxidation of hydrogen to hydrogen peroxide. *Catal. Letters*. **83**, 235–239 (2002).
  36. Choudhary, V. R., Samanta, C., Choudhary, T. V. Direct oxidation of H<sub>2</sub> to H<sub>2</sub>O<sub>2</sub> over Pd-based catalysts: Influence of oxidation state, support and metal additives. *Appl. Catal. A Gen.* **308**, 128–133 (2006).

37. Samanta, C., Choudhary, V. R. Direct formation of  $\text{H}_2\text{O}_2$  from  $\text{H}_2$  and  $\text{O}_2$  and decomposition / hydrogenation of  $\text{H}_2\text{O}_2$  in aqueous acidic reaction medium over halide-containing Pd/SiO<sub>2</sub> catalytic system. *Catalysis communications*. **8**, 2222–2228 (2007).

## 5.5 Supplementary information.

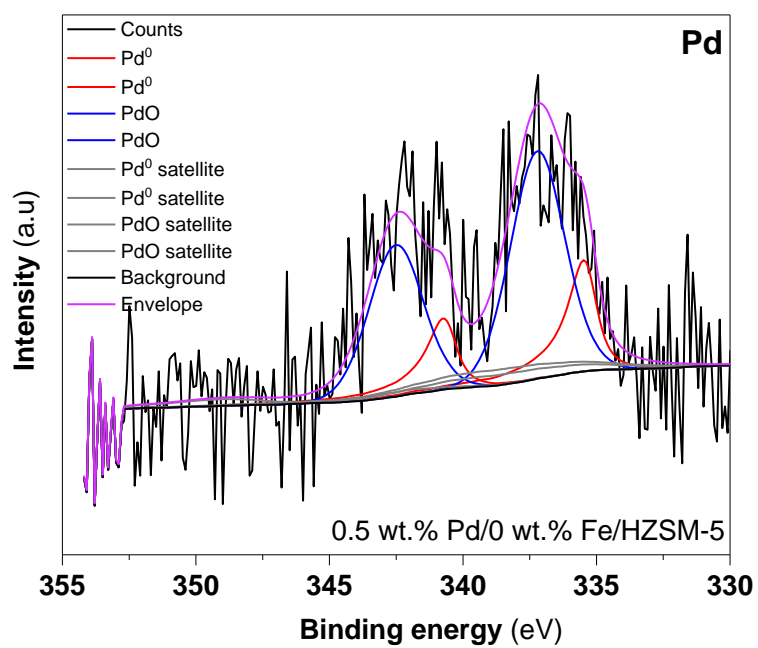


Figure S.I 5.1: XPS fitting for the bi-metallic 0.5 wt.% Pd/ 0 wt.% Fe-HZSM-5 catalyst.

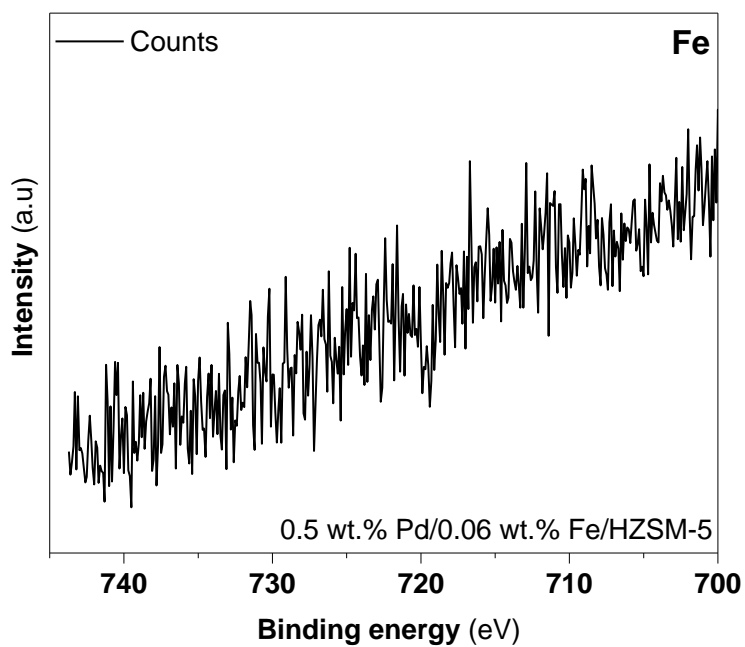
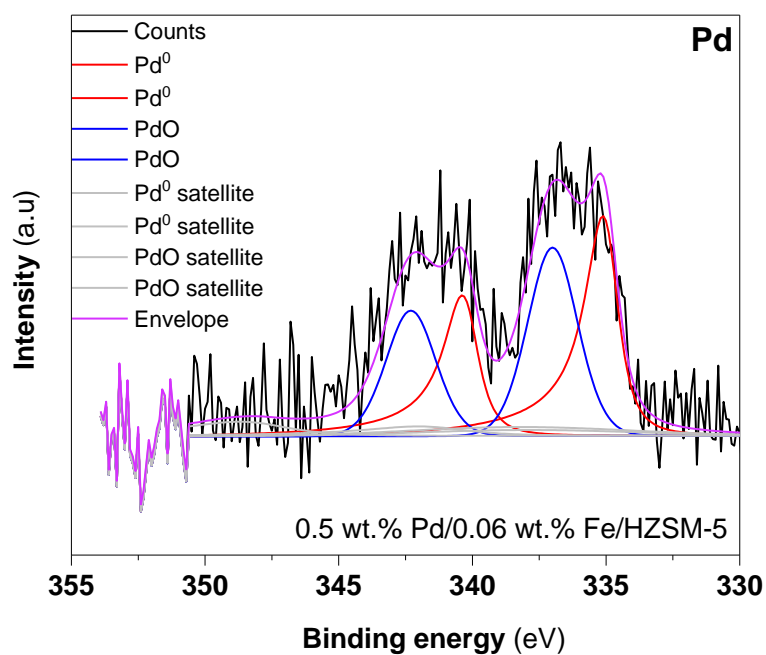
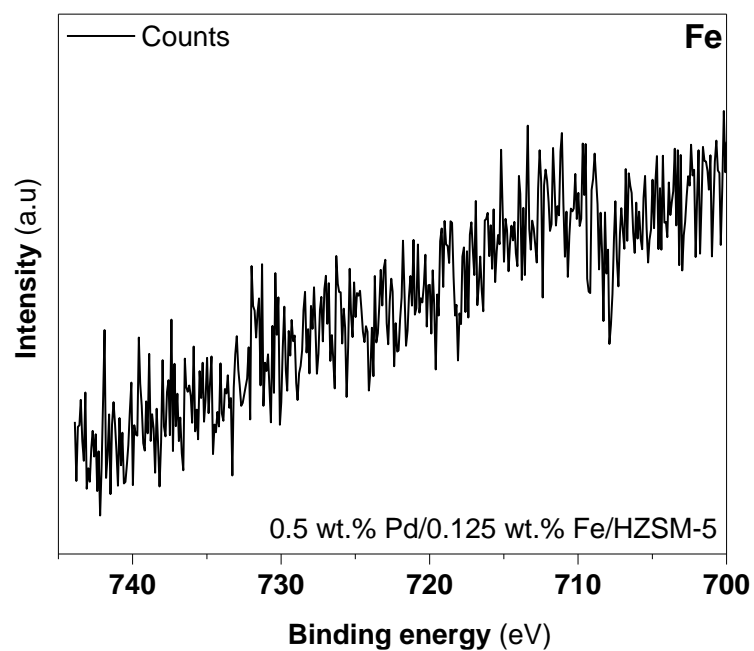
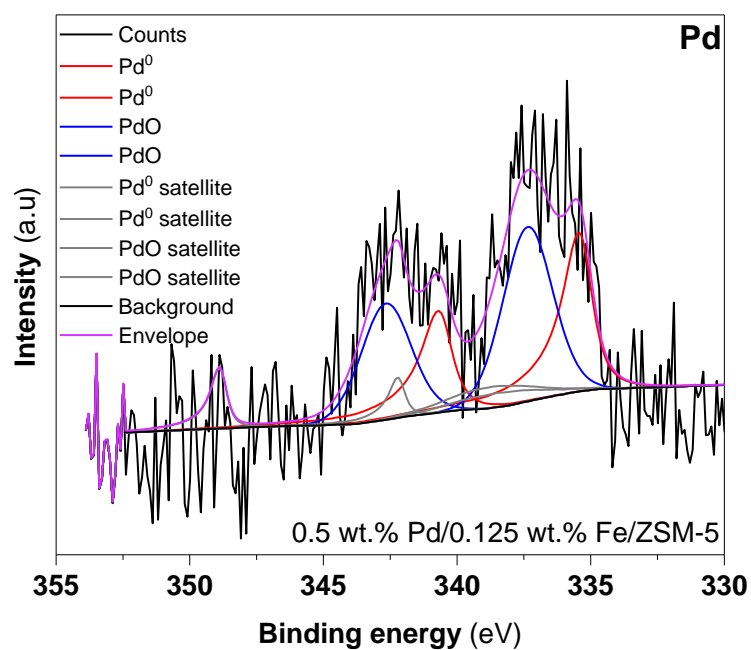
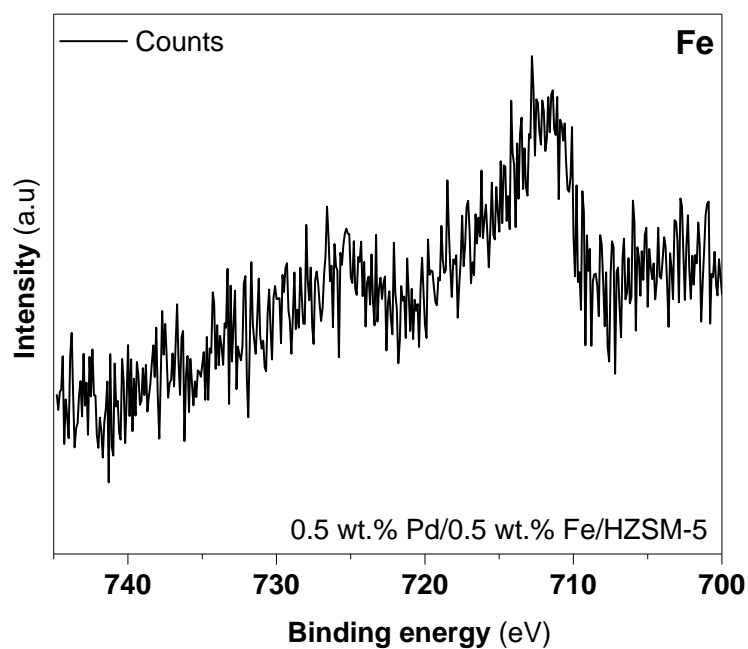
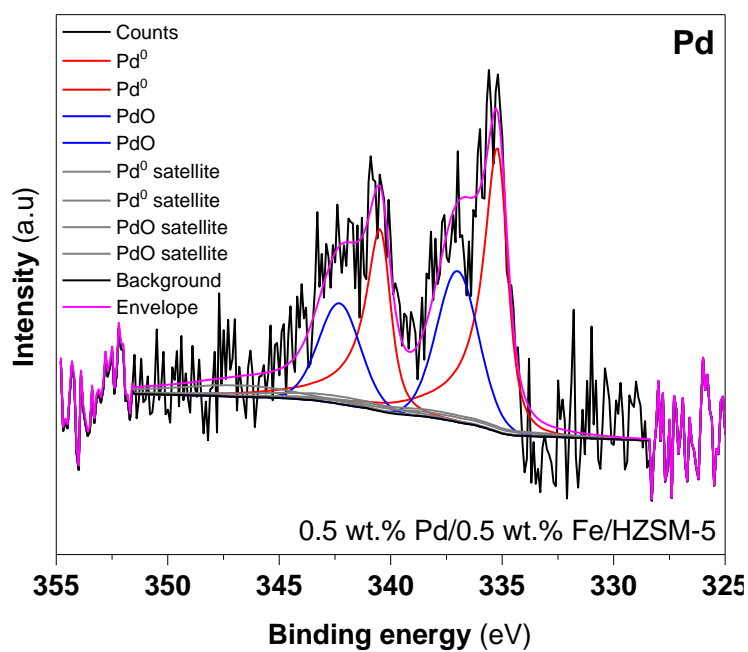


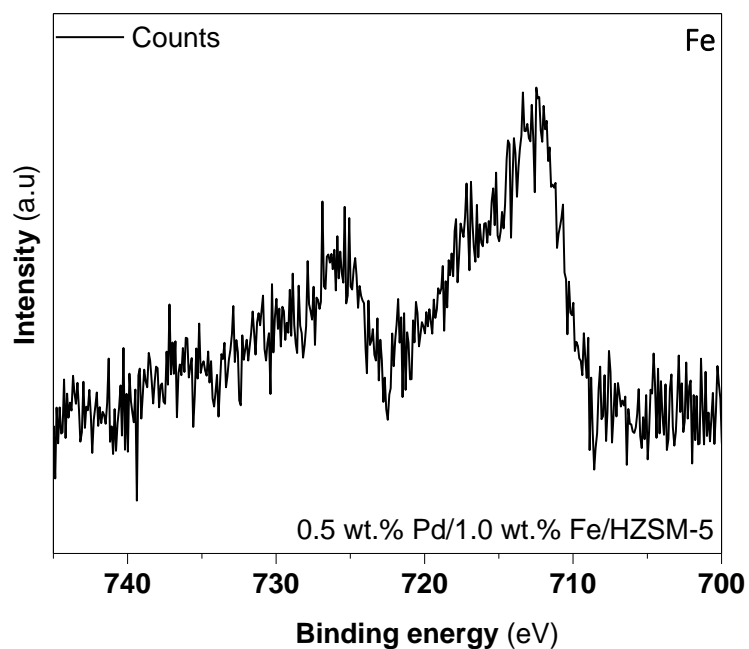
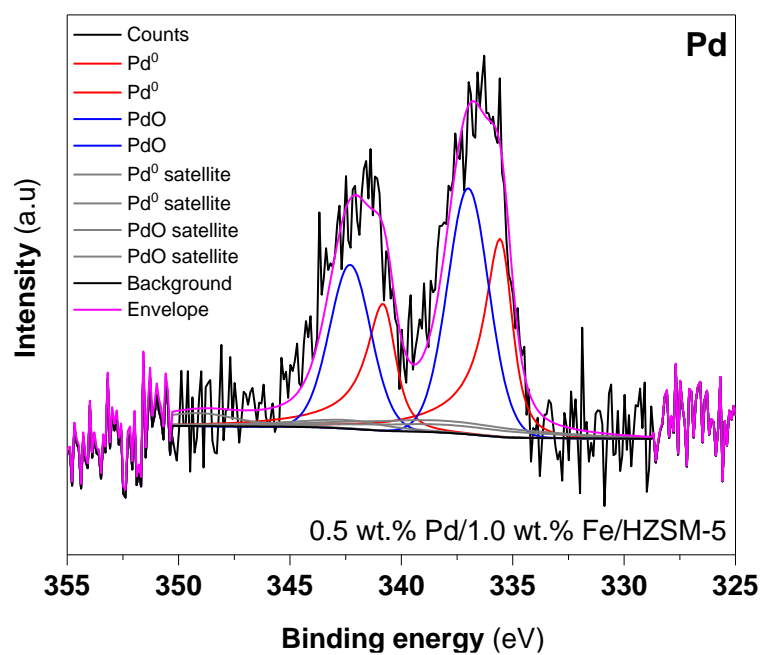
Figure S.I 5.2: XPS fitting for the bi-metallic 0.5 wt.% Pd/0.06 wt.% Fe-HZSM-5 catalyst.



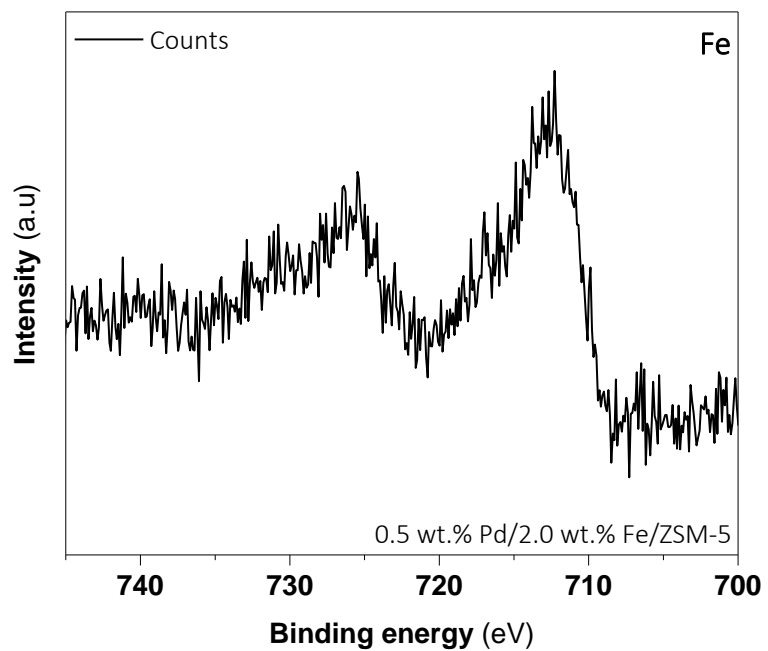
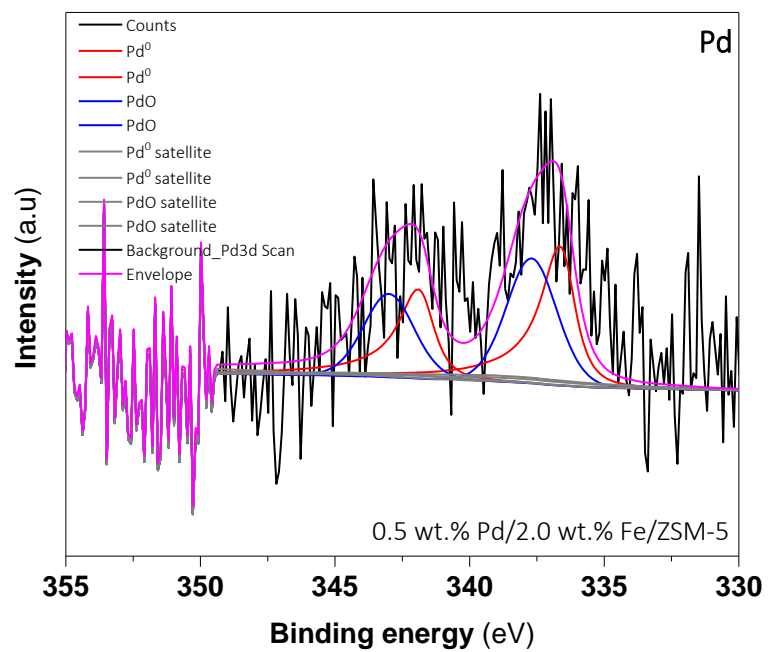
**Figure S.I 5.3:** XPS fitting for the bi-metallic 0.5 wt.% Pd/0.125 wt.% Fe-HZSM-5 catalyst.



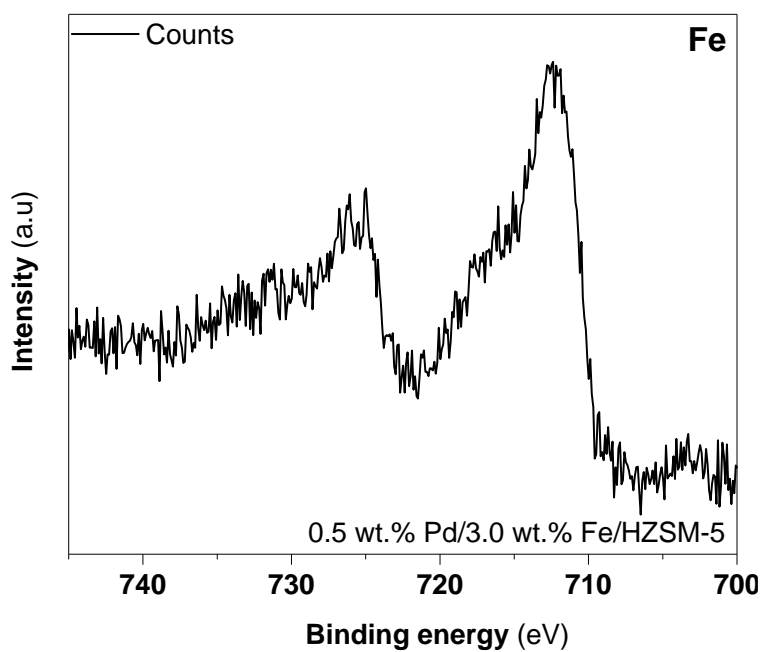
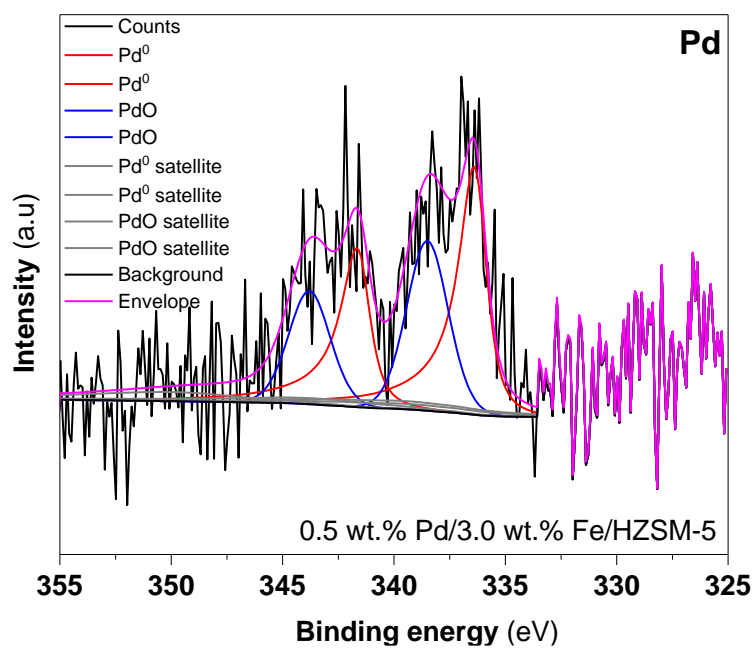
**Figure S.I 5.4:** XPS fitting for the bi-metallic 0.5 wt.% Pd/0.5 wt.% Fe-HZSM-5 catalyst.



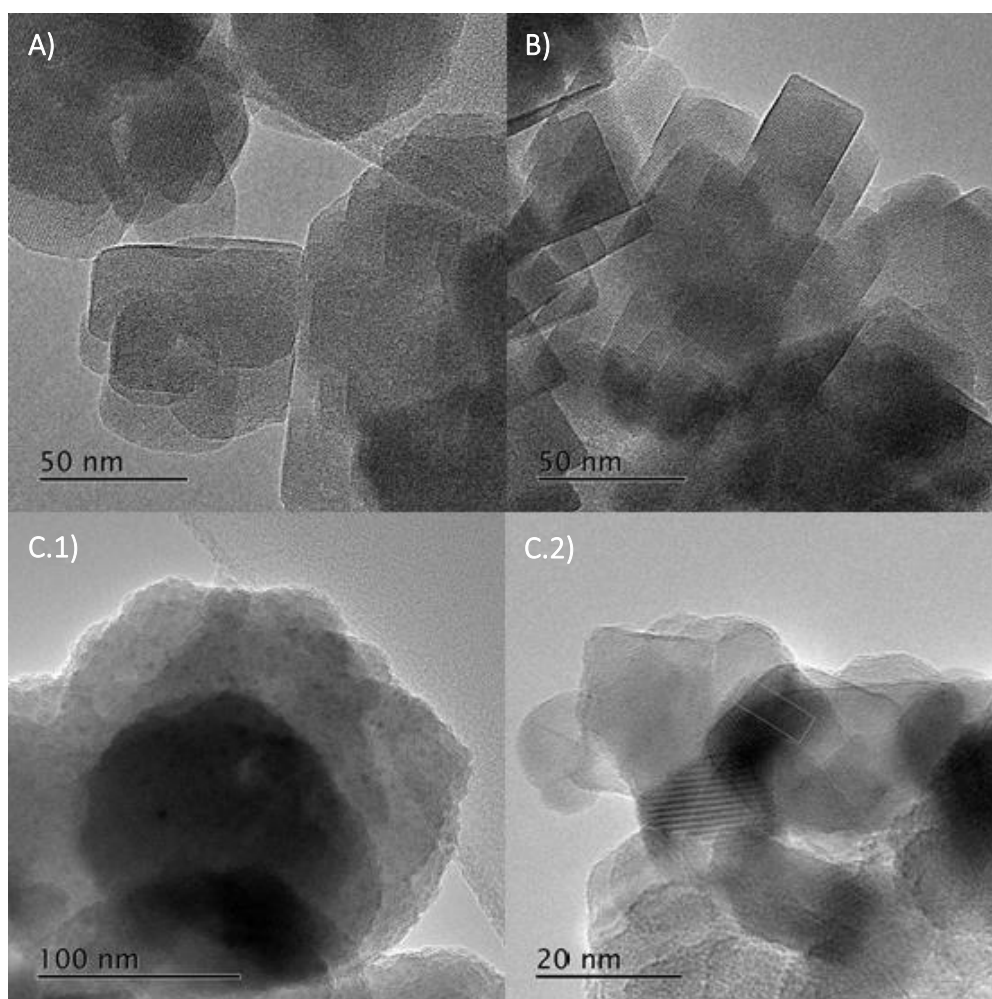
**Figure S.I 5.5:** XPS fitting for the bi-metallic 0.5 wt.% Pd/1.0 wt.% Fe-HZSM-5 catalyst.



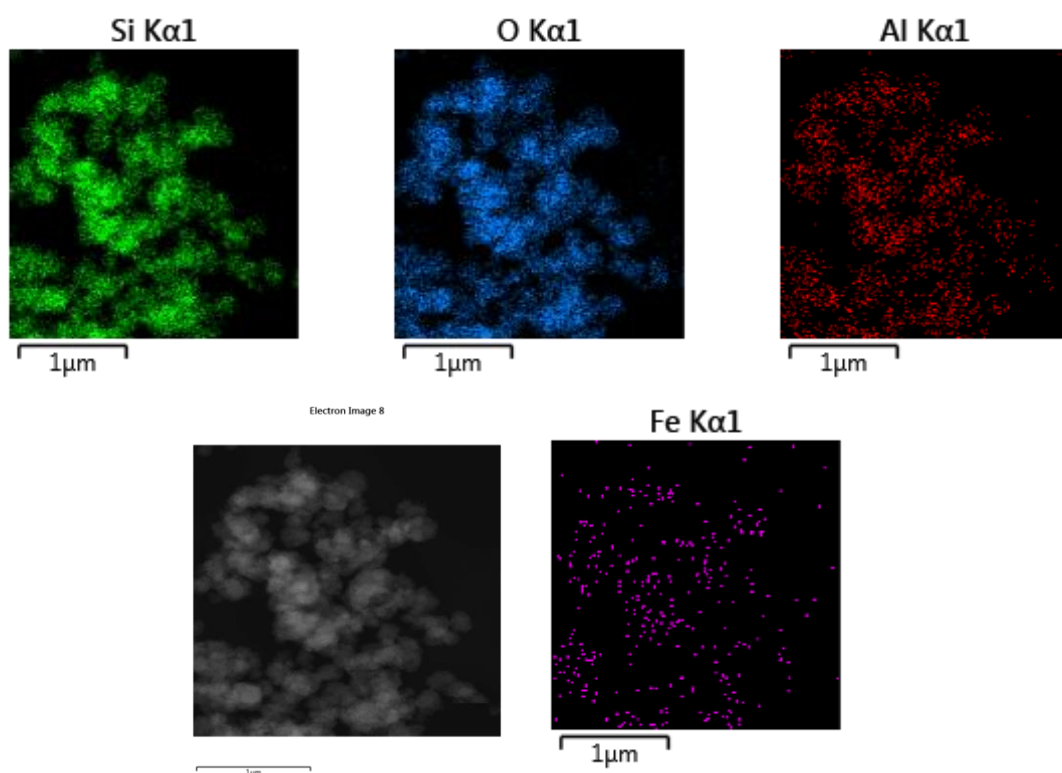
**Figure S.I 5.6:** XPS fitting for the bi-metallic 0.5 wt.% Pd/2.0 wt.% Fe-HZSM-5 catalyst.



**Figure S.I 5.7:** XPS fitting for the bi-metallic 0.5 wt.% Pd/3.0 wt.% Fe-HZSM-5 catalyst.



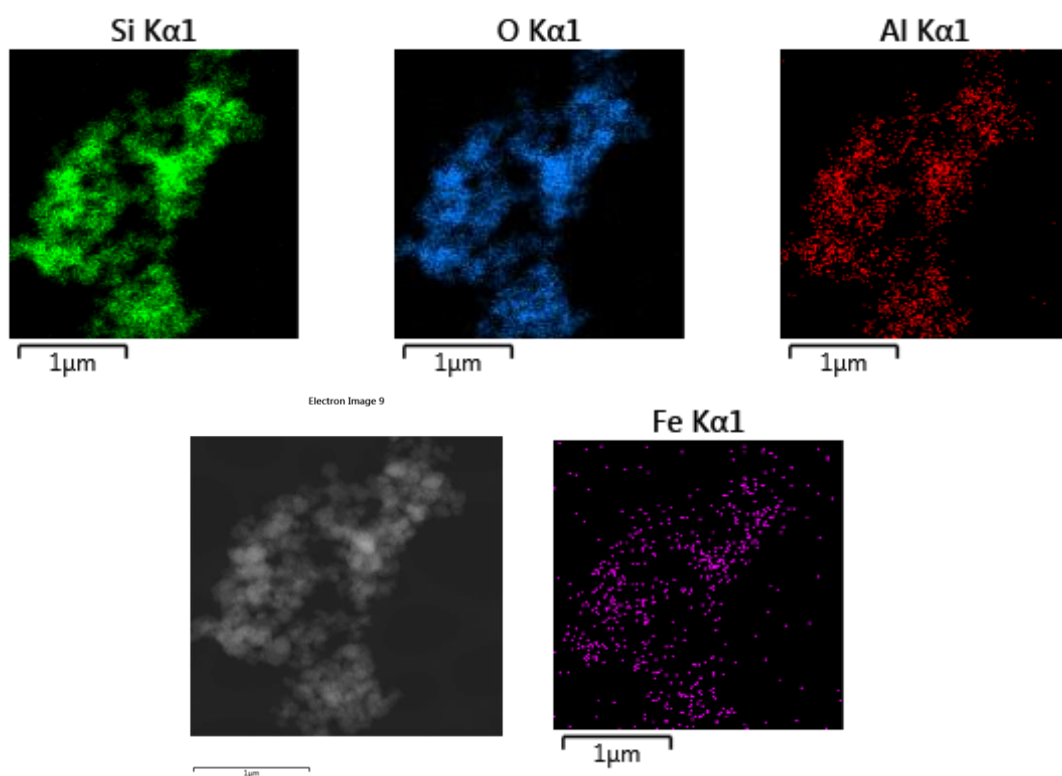
**Figure S.I.5.8:** TEM micrographs for the mono-metallic X wt.% Fe-HZSM-5 (X:3.0, 1.0, 0.5) catalysts. **Nomenclature:** **A)** 0.5 wt.% Fe-HZSM-5 (50 nm), **B)** 1.0 wt.% Fe-HZSM-5 (50 nm), **C.1)** 3.0 wt.% Fe-HZSM-5 (100 nm) and **C.2)** 3.0 wt.% Fe-HZSM-5 (20 nm).



**Figure S.I 5.9:** Elemental mapping by EDX for the mono-metallic 0.5 wt.% Fe-HZSM-5 catalysts.

**Table S.I 5.1:** Elemental analysis by EDX for the mono-metallic 0.5 wt.% Fe-HZSM-5.

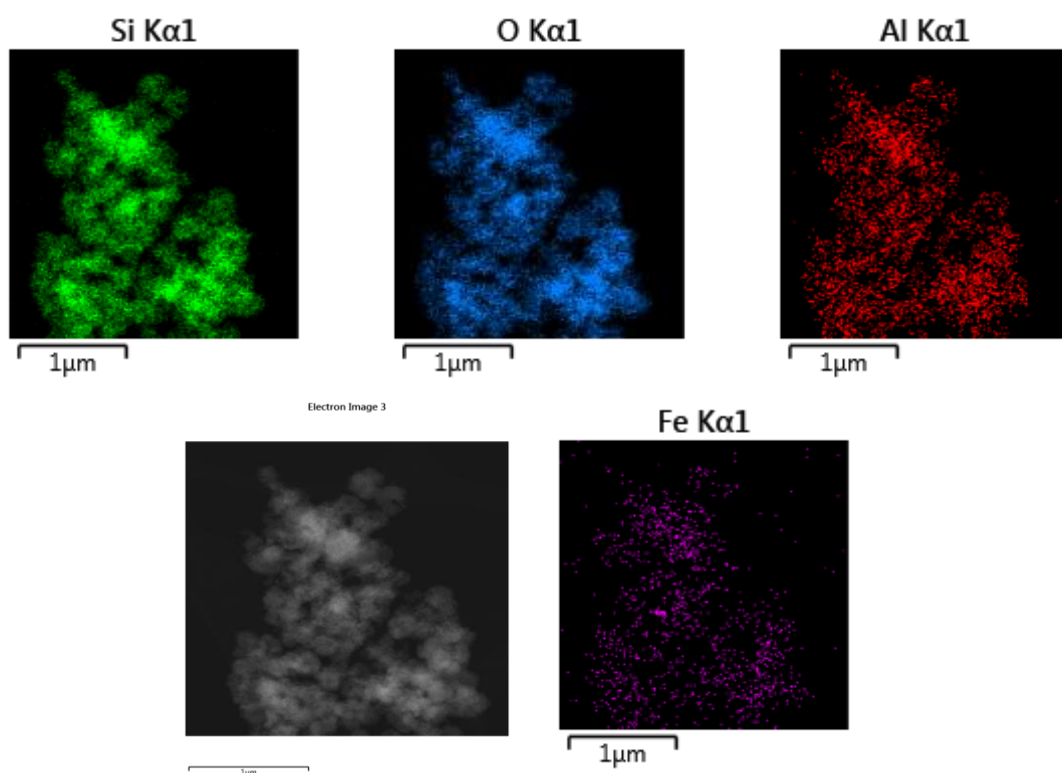
Element	Line Type	k factor	Absorption Correction	Wt%	Wt% Sigma
<b>C</b>	K series	2.81239	1.00	7.45	0.28
<b>O</b>	K series	2.05018	1.00	49.23	0.36
<b>Al</b>	K series	1.05501	1.00	2.58	0.11
<b>Si</b>	K series	1.00000	1.00	40.48	0.32
<b>Fe</b>	K series	1.11556	1.00	0.27	0.05



**Figure S.I 5.10:** Elemental mapping by EDX for the mono-metallic 1.0 wt.% Fe-HZSM-5 catalysts.

**Table S.I 5.2:** Elemental analysis by EDX for the mono-metallic 1.0 wt.% Fe-HZSM-5.

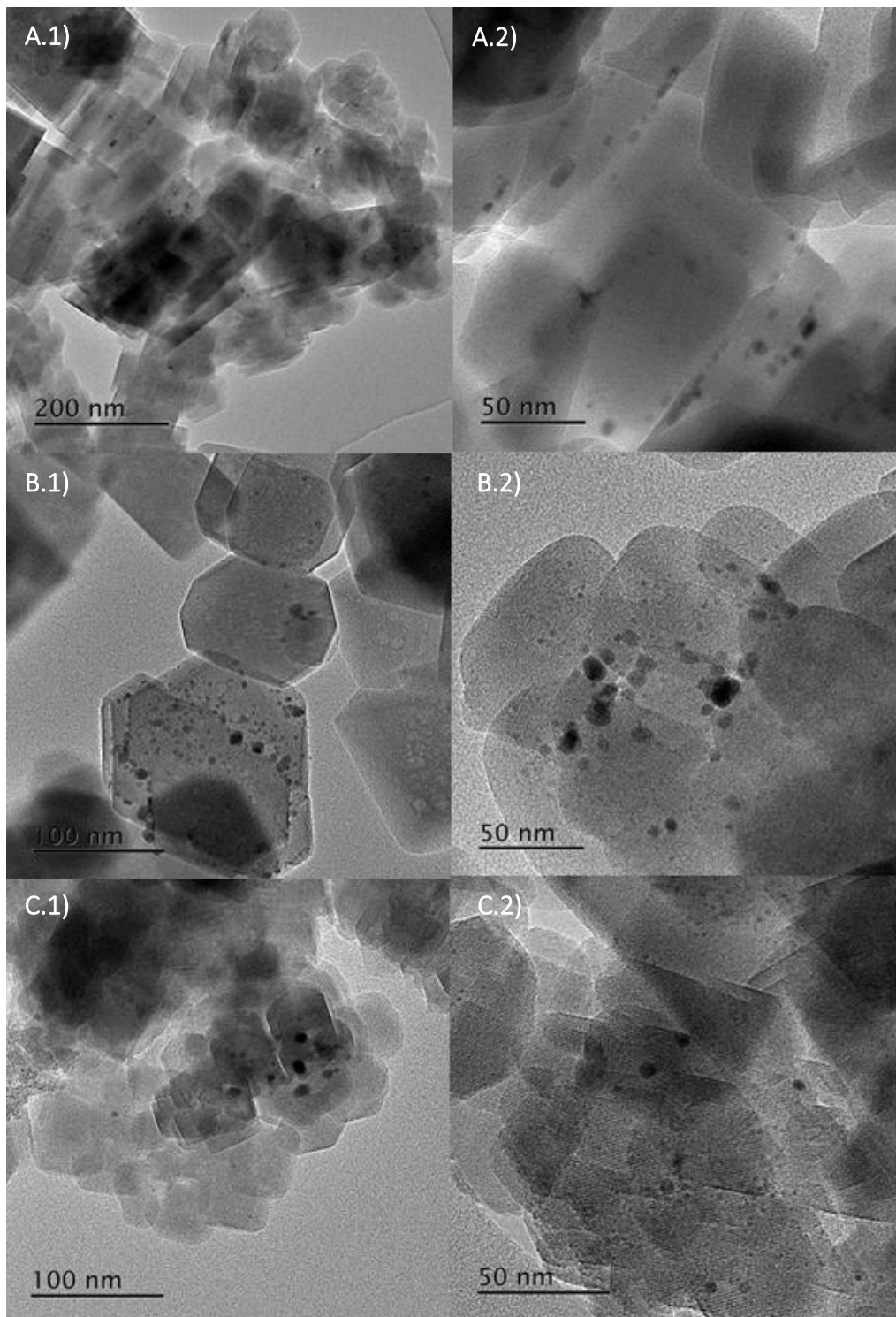
Element	Line Type	k factor	Absorption Correction	Wt%	Wt% Sigma
O	K series	2.05018	1.00	55.19	0.32
Al	K series	1.05501	1.00	2.24	0.11
Si	K series	1.00000	1.00	42.02	0.31
Fe	K series	1.11556	1.00	0.55	0.06
<b>Total:</b>				100.00	



**Figure S.I 5.11:** Elemental mapping by EDX for the mono-metallic 3.0 wt.% Fe-HZSM-5 catalysts.

**Table S.I 5.3:** Elemental analysis by EDX for the mono-metallic 3.0 wt.% Fe-HZSM-5.

Element	Line Type	k factor	Absorption Correction	Wt%	Wt% Sigma
O	K series	2.05018	1.00	53.27	0.27
Al	K series	1.05501	1.00	2.92	0.10
Si	K series	1.00000	1.00	42.78	0.26
Fe	K series	1.11556	1.00	1.02	0.06
<b>Total:</b>				100.00	



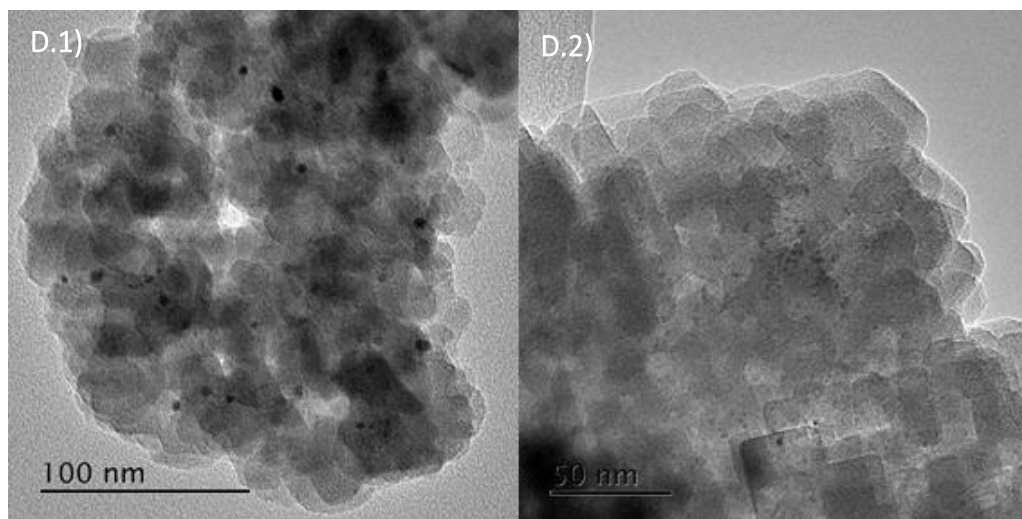


**Figure S.I 5.12:** TEM micrographs for the bi-metallic 0.5 wt.% Pd/ X wt.% Fe-HZSM-5 (X:3.0, 1.0, 0.5, 0) catalysts. **Nomenclature:** **A.1)** 0.5 wt.% Pd/ 0 wt.% Fe-HZSM-5 (100 nm) **A.2)** 0.5 wt.% Pd/ 0 wt.% Fe-HZSM-5 (50 nm), **B.1)** 0.5 wt.% Pd/ 0.5 wt.% Fe-HZSM-5 (100 nm) **B.2)** 0.5 wt.% Pd/ 0.5 wt.% Fe-HZSM-5 (50 nm), **C.1)** 0.5 wt.% Pd/ 1.0 wt.% Fe-HZSM-5 (100 nm) **C.2)** 0.5 wt.% Pd/ 1.0 wt.% Fe-HZSM-5 (50 nm), **D.1)** 0.5 wt.% Pd/ 3.0 wt.% Fe-HZSM-5 (100 nm) and **D.2)** 0.5 wt.% Pd/ 3.0 wt.% Fe-HZSM-5 (50 nm).

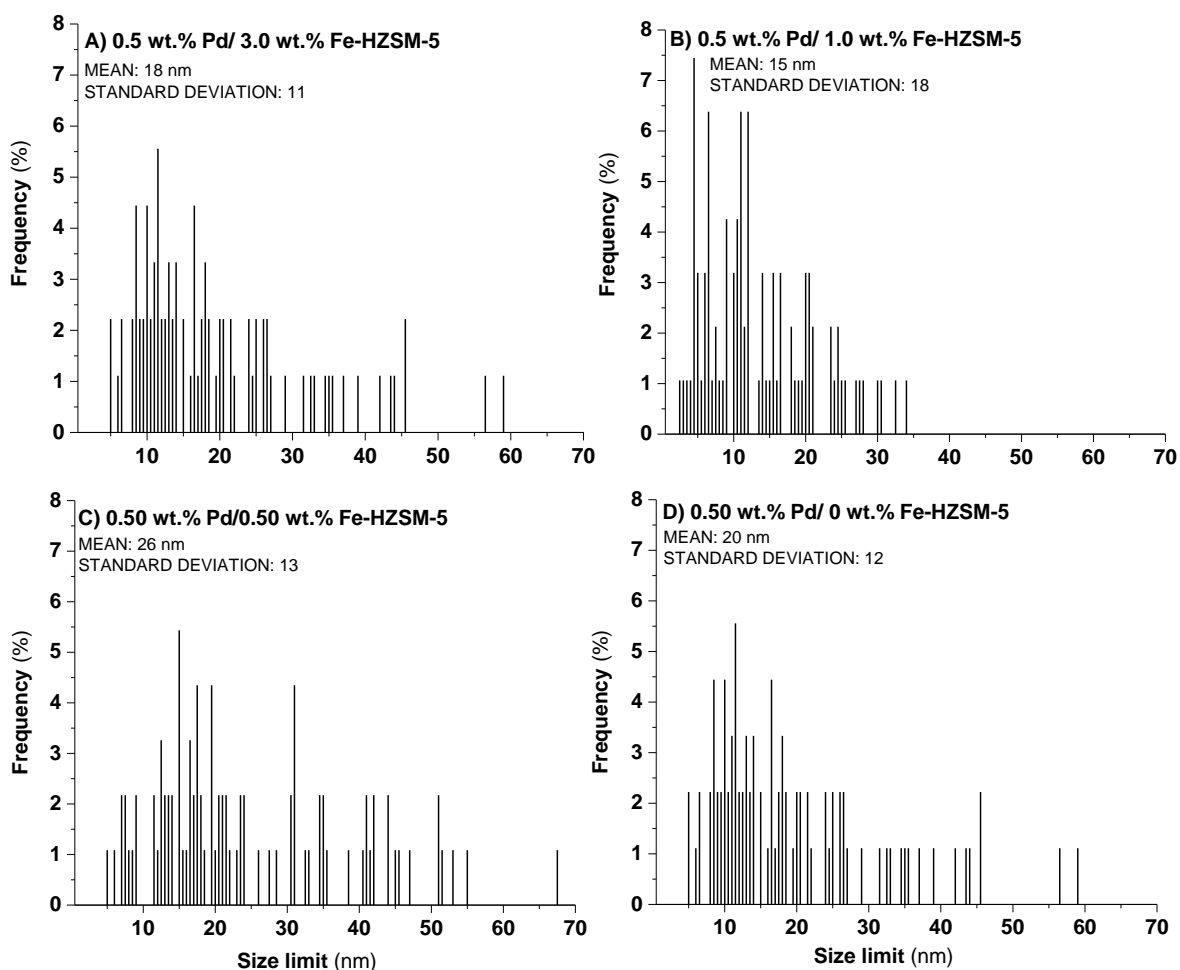


**Figure S.I 5.13:** Mean particle size and standard deviation histograms for the mono-metallic and bi-metallic 0.5 wt.% Pd/ X wt.% Fe-HZSM-5 (X: 3.0, 1.0, 0.5 and 0) catalysts.

**Table S.I 5.4:** Fe and Pd leaching during the direct synthesis of H<sub>2</sub>O<sub>2</sub> for the bi-metallic 0.5 wt.% Pd/X wt.% Fe-HZSM-5 (X:3.0-0) catalysts.

Catalysts	Fe	Pd
	%	%
<b>0.5 wt.% Pd/ 3.0 wt.% Fe-HZSM-5</b>	1.0	2.1
<b>0.5 wt.% Pd/ 2.0 wt.% Fe-HZSM-5</b>	1.3	1.8
<b>0.5 wt.% Pd/ 1.0 wt.% Fe-HZSM-5</b>	1.1	2.2
<b>0.5 wt.% Pd/ 0.5 wt.% Fe-HZSM-5</b>	4.3	2.5
<b>0.5 wt.% Pd/ 0.125 wt.% Fe-HZSM-5</b>	4.0	1.6
<b>0.5 wt.% Pd/ 0.06 wt.% Fe-HZSM-5</b>	3.0	1.8
<b>0.5 wt.% Pd/ 0 wt.% Fe-HZSM-5</b>	n/a	1.6

**n/a:** not applicable. **Reaction conditions:** 8.5 g (HPLC grade water), catalyst (0.01 g), 420 psi 5% H<sub>2</sub>/CO<sub>2</sub>, 160 psi 25% O<sub>2</sub>/CO<sub>2</sub>, 1200 rpm, 30 °C, 2 h.

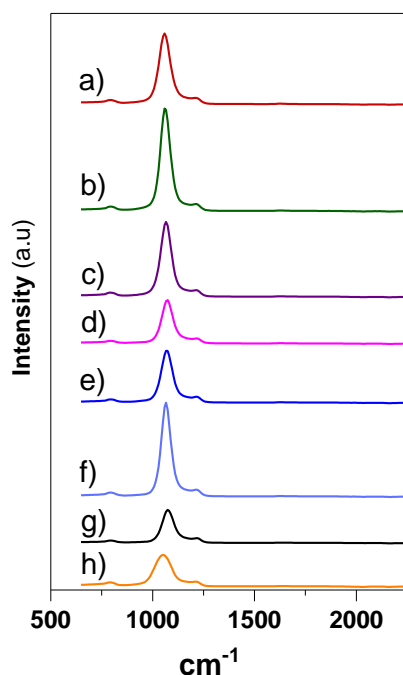


**Figure S.I 5.14:** FT-IR of the mono-metallic X wt.% Fe-HZSM-5 (X: 3.0-0.06) catalysts. **Nomenclature:** **a)** 3.0 wt.% Fe-HZSM-5, **b)** 2.0 wt.% Fe-HZSM-5, **c)** 1.0 wt.% Fe-HZSM-5, **d)** 0.5 wt.% Fe-HZSM-5, **e)** 0.125 wt.% Fe-HZSM-5, **f)** 0.06 wt.% Fe-HZSM-5, **g)** 0 wt.% Fe-HZSM-5 and **h)** HZSM-5 (SiO<sub>2</sub>:Al<sub>2</sub>O<sub>3</sub>) (23:1) Commercial sample.

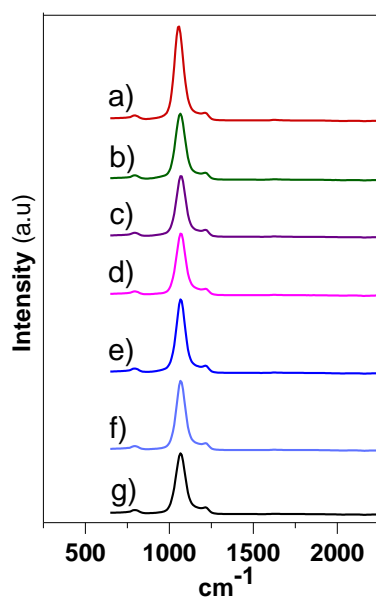


**Figure S.I 5.15:** FT-IR of the bi-metallic 0.5 wt.% Pd/X wt.% Fe-HZSM-5 (X: 3.0-0) catalysts. **Nomenclature:** **a)** 0.5 wt.% Pd/ 3.0 wt.% Fe-HZSM-5, **b)** 0.5 wt.% Pd/ 2.0 wt.% Fe-HZSM-5, **c)** 0.5 wt.% Pd/ 1.0 wt.% Fe-HZSM-5, **d)** 0.5 wt.% Pd/ 0.5 wt.% Fe-HZSM-5, **e)** 0.5 wt.% Pd/ 0.125 wt.% Fe-HZSM-5, **f)** 0.5 wt.% Pd/ 0.06 wt.% Fe-HZSM-5, **g)** 0.5 wt.% Pd/ 0 wt.% Fe-HZSM-5.

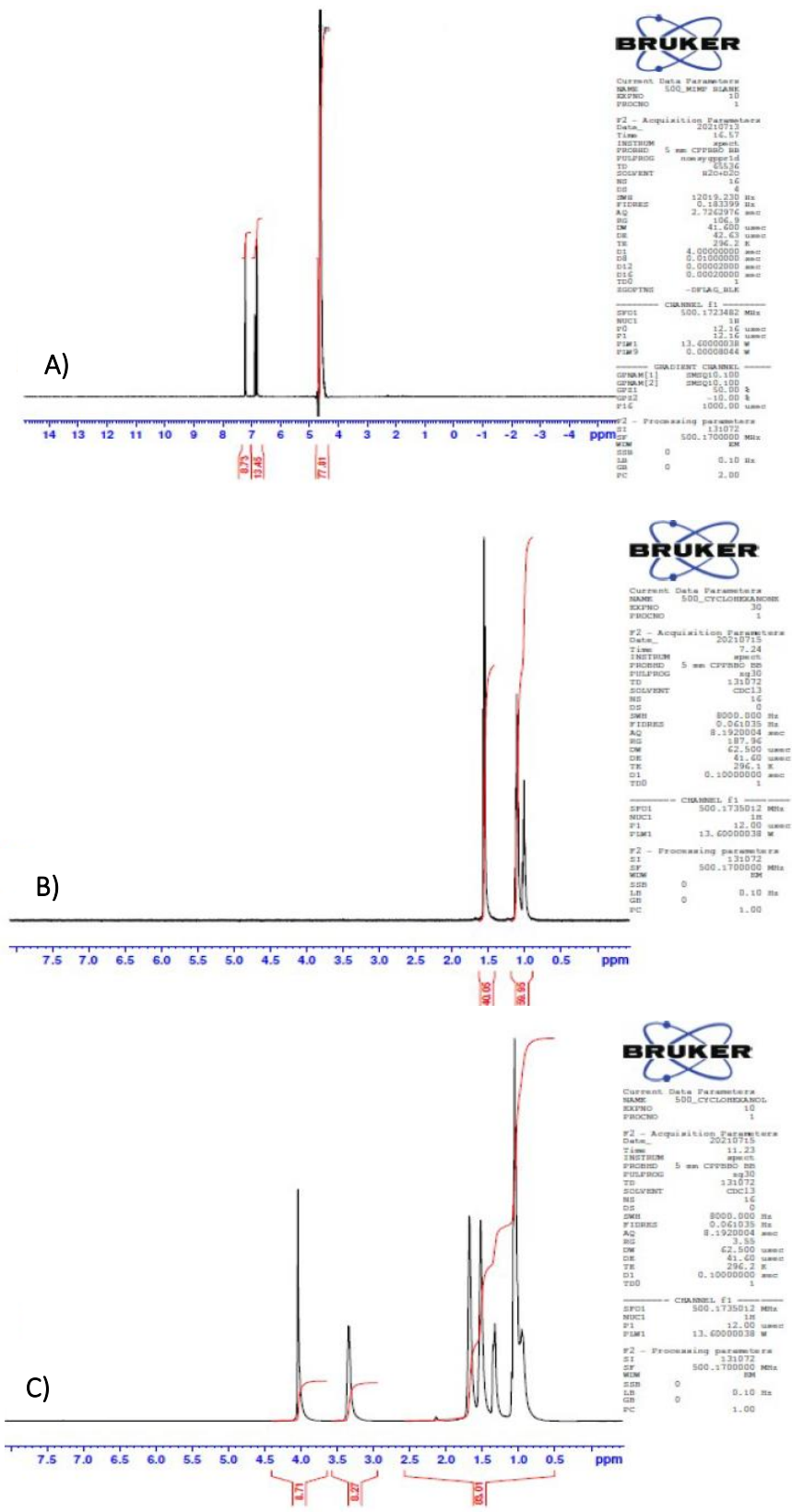


**Figure S.I.5.16:** <sup>1</sup>H NMR analysis of the post-reaction solution of the blank (H<sub>2</sub>, N<sub>2</sub>/CO<sub>2</sub>) towards the degradation of phenol. **Reaction conditions for the blank (H<sub>2</sub>, N<sub>2</sub>/CO<sub>2</sub>):** 8.5 g (1000 ppm Phenol), 0.5 wt.% Pd/ 0.5 wt.% Fe/HZSM-5 (0.01 g), 420 psi 5% H<sub>2</sub>/CO<sub>2</sub>, 160 psi N<sub>2</sub>, 1200 rpm, 30 °C, 2 h. **Nomenclature:** **A):** post-hydrogenation reaction, **B):** cyclohexanol and **C):** cyclohexanone.

**Table S.I 5.5:** Time on-line stability measurements by MP-AES for the bi-metallic 0.5 wt.% Pd/ 3.0 wt.% Fe-HZSM-5 catalyst during the degradation of phenol.

<b>min</b>	<b>Fe</b>	<b>Pd</b>
	%	%
<b>5</b>	0.2	1.1
<b>30</b>	4.4	1.8
<b>60</b>	5.5	3.0
<b>120</b>	6.0	3.8

**Reaction conditions:** 8.5 g (phenol (1000 ppm)), catalyst (0.01 g), 420 psi 5% H<sub>2</sub>/CO<sub>2</sub>, 160 psi 25% O<sub>2</sub>/CO<sub>2</sub>, 1200 rpm, 30 °C.

**Table S.I 5.6:** Fe and Pd leaching using different amounts of bi-metallic 0.5 wt.% Pd/ 3.0 wt.% Fe-HZSM-5 catalyst during the degradation of phenol.

<b>Catalyst</b>	<b>Fe</b>	<b>Pd</b>
g	%	%
<b>0.01</b>	6	4.2
<b>0.02</b>	9	7
<b>0.03</b>	10	11
<b>0.04</b>	15	23

**Reaction conditions:** 8.5 g (1000 ppm Phenol), 420 psi 5% H<sub>2</sub>/CO<sub>2</sub>, 160 psi 25% O<sub>2</sub>/CO<sub>2</sub>, 1200 rpm, 30 °C, 2h.

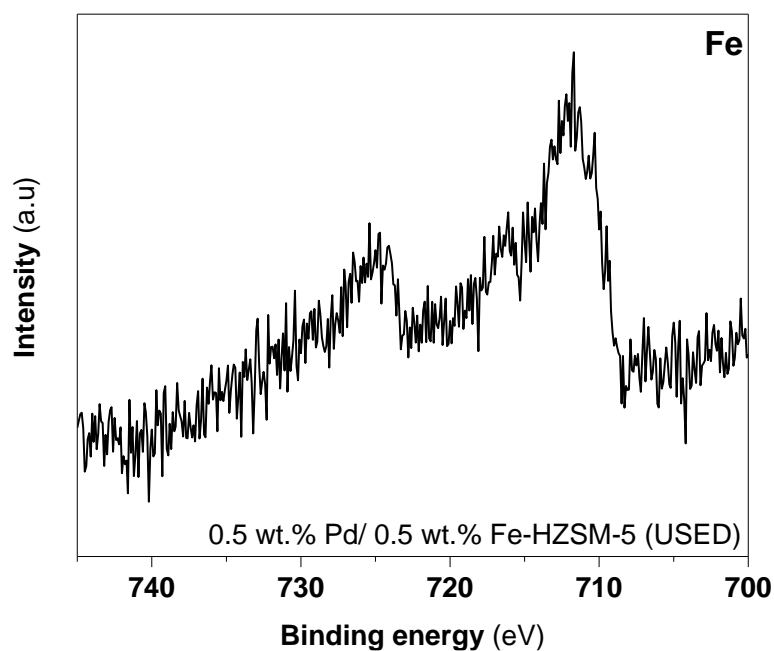
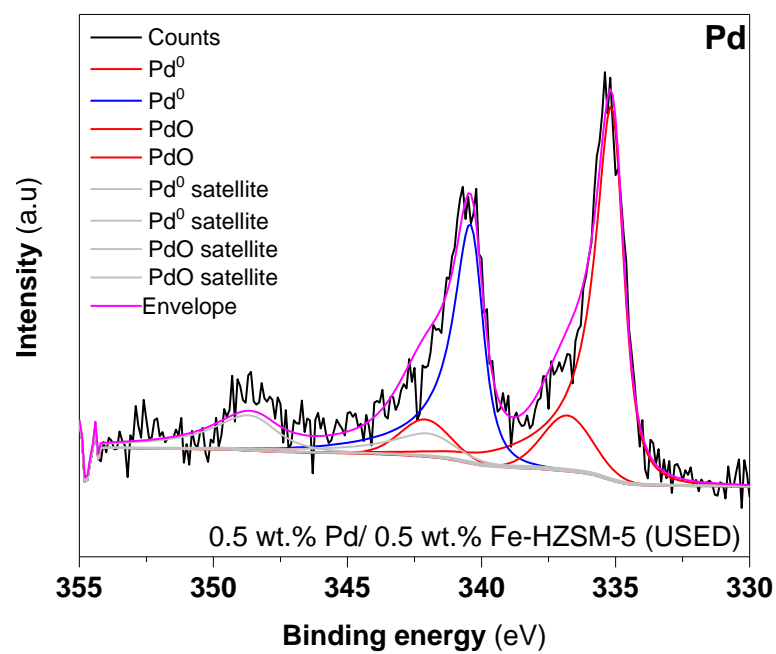


**Figure S.I 5.17:** XPS fitting for the used bi-metallic 0.5 wt.% Pd/0.5 wt.% Fe H-ZSM-5 catalyst. **Reaction conditions:** 8.5 g (1000 ppm Phenol), catalyst (0.01 g), 420 psi 5% H<sub>2</sub>/CO<sub>2</sub>, 160 psi 25% O<sub>2</sub>/CO<sub>2</sub>, 1200 rpm, 30 °C, 2h.

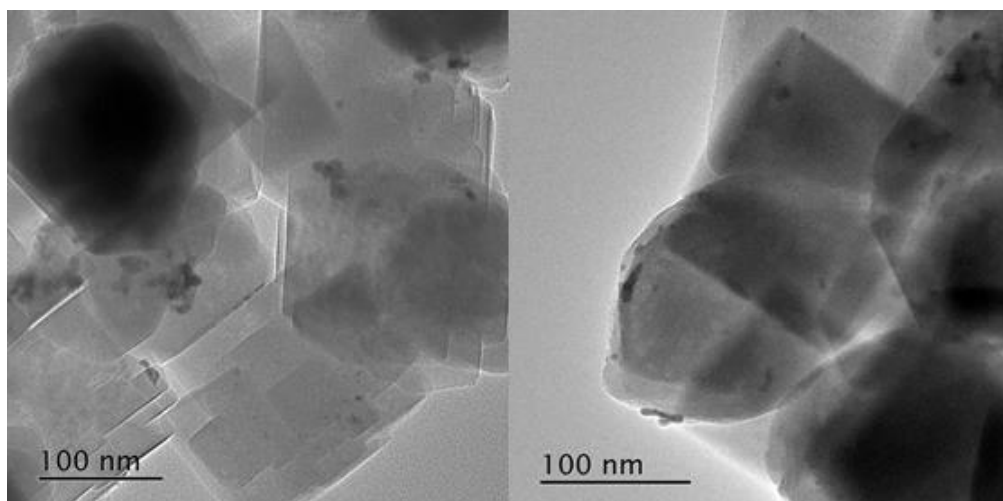


**Figure S.I 5.18:** TEM micrographs the used bi-metallic 0.5 wt.% Pd/ 0.5 wt.% Fe-HZSM-5 catalysts after the degradation of phenol. **Reaction conditions:** 8.5 g (1000 ppm Phenol), catalyst (0.01 g), 420 psi 5% H<sub>2</sub>/CO<sub>2</sub>, 160 psi 25% O<sub>2</sub>/CO<sub>2</sub>, 1200 rpm, 30 °C, 2h.

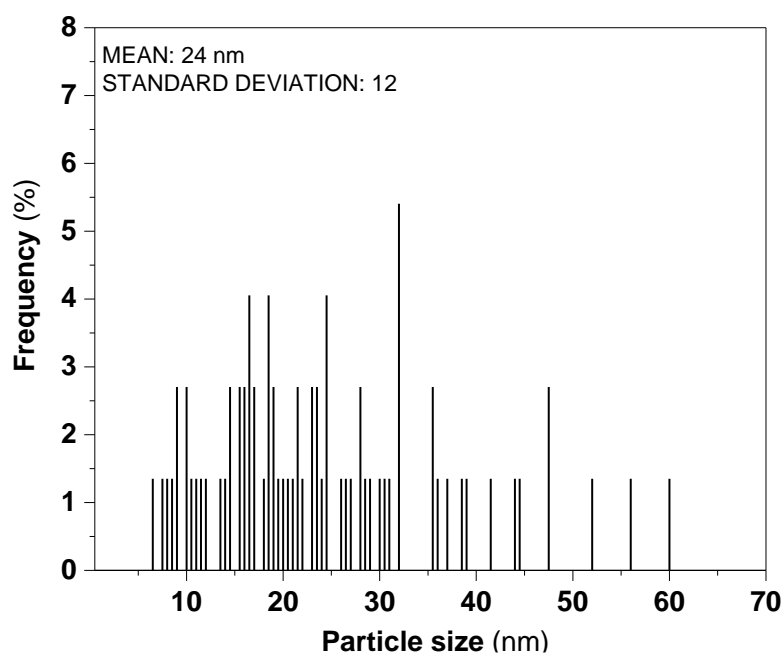


**Figure S.I 5.19:** Histogram of the mean particle size and standard deviation for the used bi-metallic 1.0 0.5 wt.% Pd/ 0.5 wt.% Fe-HZSM-5 catalyst. **Reaction conditions:** 8.5 g (phenol (1000 ppm)), catalyst (0.01 g), 420 psi 5 % H<sub>2</sub>/CO<sub>2</sub>, 160 psi 25 % O<sub>2</sub>/CO<sub>2</sub>, 1200 rpm, 30 °C, 2 h.

# Chapter 6:

## Conclusions and future work.

### 6.1 Brief thesis introduction.

$\text{H}_2\text{O}_2$  is a versatile liquid oxidant, whose annual production went over 4 million tonnes in 2021.<sup>1</sup> It has many applications ranging from bleaching of paper and textiles to the synthesis of fine chemicals such as the oxidation of propylene to propylene oxide (PO) with TS-1 as catalyst.<sup>2</sup> The anthraquinone autoxidation process governs the manufacturing of  $\text{H}_2\text{O}_2$ , accounting for the 95 % of the annual  $\text{H}_2\text{O}_2$  production.<sup>3,1</sup> This manufacture process requires the aqueous solutions of  $\text{H}_2\text{O}_2$  (c.a 70 %) to be diluted to more suitable concentrations in order to be transported to its point of use safely. Besides this, there are several drawbacks that make this manufacturing route energetically costly and environmentally unfriendly.<sup>4</sup> Anyhow, for many applications,  $\text{H}_2\text{O}_2$  is required at very low concentrations, for instance, less than 0.1 wt.% of  $\text{H}_2\text{O}_2$  is employed for water treatment remediation and less than 9 wt.% for pulp and bleaching, chemical synthesis, medical and cosmetic uses.<sup>5</sup> Thus, there has been an interest in decentralising the manufacture of  $\text{H}_2\text{O}_2$  towards on-site production. The direct synthesis of  $\text{H}_2\text{O}_2$  from  $\text{H}_2$  and  $\text{O}_2$  is one of the alternatives that has been investigated and extensively studied over supported Pd-based catalysts.<sup>1,6,7</sup> One of the main disadvantages of this alternative is control the selectivity of the catalysts towards the direct synthesis of  $\text{H}_2\text{O}_2$  and avoid its degradation (decomposition and hydrogenation) that undesirably leads to  $\text{H}_2\text{O}$ , reducing the net production of  $\text{H}_2\text{O}_2$ . Using sub-ambient temperatures ( $< 10\text{ }^\circ\text{C}$ ) and mixtures of organic solvent and water is one of the strategies that many authors employ to avoid the degradation and enhance the catalyst's selectivity towards the direct synthesis of  $\text{H}_2\text{O}_2$ .<sup>1,6,7,8,9,10</sup> However, these reaction conditions are not considered to be industrially viable, first of all, using sub-ambient temperatures ( $< 10\text{ }^\circ\text{C}$ ) is energetically costly, and second of all, the usage of organic solvents during the direct synthesis of  $\text{H}_2\text{O}_2$  is not suitable for some applications, such as for water remediation.  $\text{H}_2\text{O}_2$  would be a promising and powerful oxidant to use in water remediation. Besides to be more oxidant (1.78 eV) than others common oxidants used in water remediation such as chlorine-based chemicals (e.g  $\text{HClO}_4$  (1.49 eV)),  $\text{H}_2\text{O}_2$  only decomposes into  $\text{H}_2\text{O}$  and  $\text{O}_2$  without producing toxic residues as it undesirably happens with chlorine-based chemicals.<sup>11,12,13</sup> In fact, pre-formed  $\text{H}_2\text{O}_2$  is already applied in water remediation, for instance for the removal of sulphites or chromium.<sup>14</sup> However, some reports have shown that  $\text{H}_2\text{O}_2$  is not efficient to degrade organic pollutants such as aromatics, which are commonly found in waste water due to industrial activities.<sup>15,16</sup> The decomposition of  $\text{H}_2\text{O}_2$  to produce reactive oxygen species (ROS;  $\text{O}_2^{\cdot-}$ ,  $\text{HO}^{\cdot}$ , and  $\text{HOO}^{\cdot}$ ) can be activated via the combination of  $\text{H}_2\text{O}_2$  with

ozone ( $O_3$ ), UV light sources and iron salts ( $FeSO_4$ ) among others such as  $TiO_2$ .<sup>17,18</sup> For instance, pre-formed  $H_2O_2$  with Fe salts, referred as homogeneous Fenton's oxidations, are currently applied to treat polluted wastewater such as cosmetics, olive-mill, chemicals, pulp and paper, power plants or sawmills.<sup>19</sup> Unfortunately, in order to achieve high oxidation efficiencies, homogeneous Fenton's oxidations are pH (c.a 3) dependant, which make this reaction unsuitable to pour into the water effluents or to be consumed.<sup>20</sup> In addition to this, Fe precipitates are undesirably formed leading to its loss and subsequently increasing the cost of the process.<sup>15</sup> Heterogeneous Fenton's oxidation has been widely investigated to attach the Fe species to a given support and avoid its loss.<sup>19,21</sup> In fact, many authors have reported heterogeneous Fenton's oxidations with pre-formed  $H_2O_2$  and mono and bi-metallic FeCu supported catalysts obtaining promising activity to degrade phenol.<sup>22,23,24,25</sup> However, the stability of these mono and bi-metallic supported catalysts is reported to be dependent on the speciation of the metal species.<sup>22,23,24,25</sup>

### 6.1.1 Thesis objectives and summary.

The aim of this thesis has been the study of heterogeneous Fenton's oxidations for water remediation using mono and bi-metallic AuPd with Fenton metal-based catalysts to generate ROS from the decomposition of *in-situ*  $H_2O_2$ . This thesis consisted in three chapters of results, where Chapter 3 investigated the capability to generate *in-situ*  $H_2O_2$  at conditions more suitable for water treatment process by means of mono and bi-metallic 1 wt.% AuPd/ $TiO_2$  heterogeneous supported catalysts with different Au: Pd ratios. The variability in Au: Pd ratio in these series of bi-metallic 1 wt.% AuPd supported catalysts allowed to specify the most promising Au: Pd ratio for *in-situ* synthesise  $H_2O_2$  with minimal degradation at more suitable reaction conditions (25°C and water-only as solvent). Consecutively in Chapter 4, it was investigated the most favourable Fenton-metal to convert *in-situ*  $H_2O_2$  to ROS via measuring the activity of bi-metallic 0.5 wt.% X-0.5 wt.% Pd/ $TiO_2$  (X: Fe, Cu, Co, Au) supported catalysts towards the conversion of phenol. The combination FePd was found to be the most favourable in comparison to the other two combinations of CuPd and CoPd, or in comparison to AuPd supported catalysts. However, the lack of stability of the Fe during the degradation of phenol, led to investigate other catalytic synthetic means to anchor the Fe in the support, before investigating the incorporation of Fe to the AuPd bi-metallic based catalysts. Therefore, Chapter 5 aimed to synthesise more stable FePd supported catalysts by introducing the Fe within a zeolitic lattice, which subsequent calcination would lead to Fe species attached to the zeolitic support. As a result, a set of bi-metallic 0.5 wt.% Pd/ X wt.% Fe-HZSM-5 (X: 3.0-0.06) catalysts were synthesised to determine how the Fe speciation varies in relation to the Fe loading introduced, and therefore determine the most stable Fe specie to use during the degradation of phenol.

## 6.2 Conclusions and final remarks.

The first chapter of results (Chapter 3) investigated the direct synthesis of  $\text{H}_2\text{O}_2$  over a series of mono and bi-metallic 1 wt.%  $\text{AuPd}/\text{TiO}_2$  based catalysts made by modified impregnation (1.0 wt.%  $\text{Au}/\text{TiO}_2$ , 0.75 wt.%  $\text{Au}$ -0.25 wt.%  $\text{Pd}/\text{TiO}_2$ , 0.50 wt.%  $\text{Au}$ -0.50 wt.%  $\text{Pd}/\text{TiO}_2$ , 0.25 wt.%  $\text{Au}$ -0.75 wt.%  $\text{Pd}/\text{TiO}_2$  and 1.0 wt.%  $\text{Pd}/\text{TiO}_2$ ).<sup>26</sup> These set of mono and bi-metallic catalysts had their activity investigated at ambient temperatures (25 °C) and with water-only as solvent, which are reaction conditions more akin to those that could be suitable for industrial applications. To better understand how the reaction conditions could influence the catalytic activity and selectivity, the reaction conditions were modified stepwise, from sub-ambient temperatures and mixtures of organic solvents and water, namely (2 °C,  $\text{CH}_3\text{OH}$ - $\text{H}_2\text{O}$ ,  $\text{CO}_2$ ) to ambient temperatures and a water only solvent (25 °C,  $\text{H}_2\text{O}$ ,  $\text{CO}_2$ ). Figure 6.1 presents the four reaction conditions that the whole set of mono and bi-metallic 1 wt.%  $\text{AuPd}/\text{TiO}_2$  catalyst's activity were reported in.

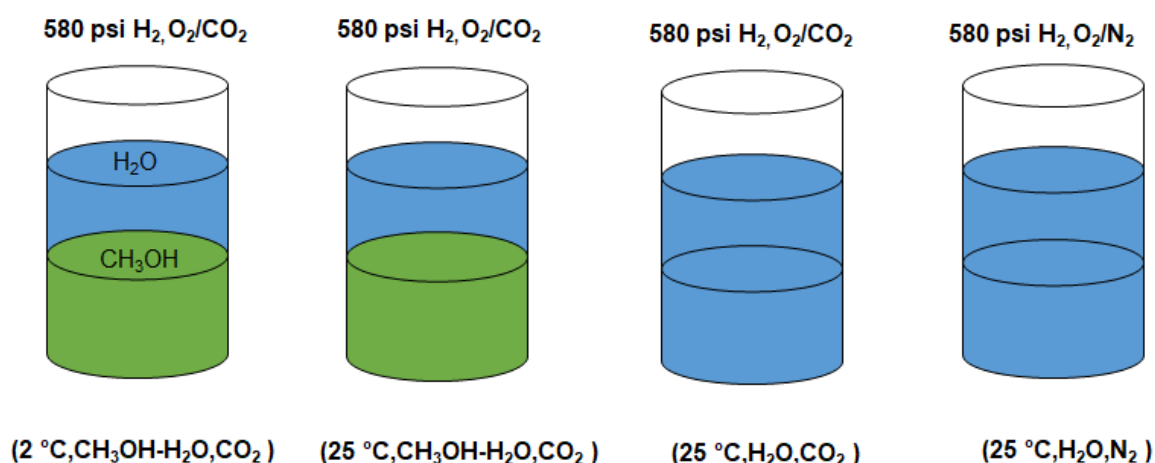


**Figure 6.1: Reaction conditions:** (2°C,  $\text{CH}_3\text{OH}$ - $\text{H}_2\text{O}$ ,  $\text{CO}_2$ ): 8.5 g (5.6 g  $\text{CH}_3\text{OH}$ , 2.9 g  $\text{H}_2\text{O}$ ), catalyst (0.01 g), 420 psi of 5 %  $\text{H}_2/\text{CO}_2$ , 160 psi of 25 %  $\text{O}_2/\text{CO}_2$ , 1200 rpm, 2 °C, 0.5 h. (25°C,  $\text{CH}_3\text{OH}$ - $\text{H}_2\text{O}$ ,  $\text{CO}_2$ ): 8.5 g (5.6 g  $\text{CH}_3\text{OH}$ , 2.9 g  $\text{H}_2\text{O}$ ), catalyst (0.01 g), 420 psi of 5 %  $\text{H}_2/\text{CO}_2$ , 160 psi of 25 %  $\text{O}_2/\text{CO}_2$ , 25 °C, 1200 rpm, 0.5 h. (25°C,  $\text{H}_2\text{O}$ ,  $\text{CO}_2$ ): 8.5 g  $\text{H}_2\text{O}$ , catalyst (0.01 g), 420 psi of 5 %  $\text{H}_2/\text{CO}_2$ , 160 psi of 25 %  $\text{O}_2/\text{CO}_2$ , 1200 rpm, 25 °C, 0.5 h. (25°C,  $\text{H}_2\text{O}$ ,  $\text{N}_2$ ): 8.5 g  $\text{H}_2\text{O}$ , catalyst (0.01 g), 420 psi of 5 %  $\text{H}_2/\text{N}_2$ , 160 psi of 25 %  $\text{O}_2/\text{N}_2$ , 1200rpm, 25 °C, 0.5 h.

The results obtained indicated that the activity and selectivity of the mono and bi-metallic 1.0 wt.%  $\text{AuPd}/\text{TiO}_2$  catalysts towards the direct synthesis of  $\text{H}_2\text{O}_2$  were influenced by the temperature and the composition of the reaction mixture (67 %  $\text{CH}_3\text{OH}$  in water or water-only) employed. This is because the extend of  $\text{H}_2$  and  $\text{O}_2$  gas dissolved in the reaction mixture, depends on its composition (67 %  $\text{CH}_3\text{OH}$  in water or water-only) and the reaction temperature (25 °C or 2 °C). When transitioning from sub-ambient temperatures (2°C,  $\text{CH}_3\text{OH}$ - $\text{H}_2\text{O}$ ,  $\text{CO}_2$ ) to ambient temperatures (25°C,  $\text{CH}_3\text{OH}$ - $\text{H}_2\text{O}$ ,  $\text{CO}_2$ ),  $\text{H}_2$  became more soluble in the reaction mixture, which caused an enhancement in the degradation activity that lead to decrease the catalyst's selectivity towards the direct synthesis of  $\text{H}_2\text{O}_2$ . Contrarily, when transitioning from (25°C,  $\text{CH}_3\text{OH}$ - $\text{H}_2\text{O}$ ,  $\text{CO}_2$ ) to (25°C,  $\text{H}_2\text{O}$ ,  $\text{CO}_2$ ) conditions,

H<sub>2</sub> became less soluble in the reaction mixture, which triggered the decomposition of H<sub>2</sub>O<sub>2</sub> and made decrease the selectivity even more in comparison to the previous reaction (25°C, CH<sub>3</sub>OH-H<sub>2</sub>O, CO<sub>2</sub>) conditions, where CH<sub>3</sub>OH was present. As evidenced by some authors, employing water-only as solvent, not only affect negatively the formation of H<sub>2</sub>O<sub>2</sub> due to the low solubility that H<sub>2</sub> has in water (1.62 mg/L at 25 °C) in comparison to CH<sub>3</sub>OH (7.91 mg/L at 25 °C), but using water-only as a solvent promote drastically the decomposition of H<sub>2</sub>O<sub>2</sub>.<sup>27,28,29</sup> Contrarily, O<sub>2</sub>, besides being in excess during the direct synthesis reaction, is more soluble in both solvents, in H<sub>2</sub>O (40 mg/L at 25 °C) and in CH<sub>3</sub>OH (324 mg/L at 25 °C)<sup>27</sup> than H<sub>2</sub> is. Therefore, the solubility of H<sub>2</sub> is one of the key parameters that needs to be controlled via the composition of the reaction mixture and the temperature, since it can drive the activity and selectivity of the catalysts towards the direct synthesis of H<sub>2</sub>O<sub>2</sub>.<sup>29</sup> To do so, many authors use mixtures of organic solvents and H<sub>2</sub>O, such as ethanol (CH<sub>3</sub>CH<sub>2</sub>OH) or CH<sub>3</sub>OH with water, to balance the formation of H<sub>2</sub>O<sub>2</sub> and the degradation activity. Employing organic solvents-only or water-only solvents is not recommended as previously reported,<sup>28,29</sup> since it would massively promote the hydrogenation and decomposition respectively, and would result in low H<sub>2</sub>O<sub>2</sub> selectivity's in both cases. On the other hand, employing mixtures of organic solvents and water, balances the formation of H<sub>2</sub>O<sub>2</sub> and its degradation, which results in better catalytic selectivity's than using water-only or organic solvents-only.<sup>28,29</sup> Finally, the formation of carbonic acid (H<sub>2</sub>CO<sub>3</sub>) via CO<sub>2</sub> dissolution in water helps to stabilise H<sub>2</sub>O<sub>2</sub> against degradation. In fact, when transitioning from (25°C, H<sub>2</sub>O, CO<sub>2</sub>) to (25°C, H<sub>2</sub>O, N<sub>2</sub>) conditions, the catalyst's degradation was enhanced, which led to a decrease in the H<sub>2</sub>O<sub>2</sub> selectivity. This has also been corroborated by other authors, that highlighted the important role of CO<sub>2</sub> in stabilising *in-situ* H<sub>2</sub>O<sub>2</sub> via H<sub>2</sub>CO<sub>3</sub> formation.<sup>30</sup>

The incorporation of Au as a secondary metal to Pd had a positive contribution towards the formation of H<sub>2</sub>O<sub>2</sub> as it was previously reported.<sup>31,32</sup> As expected, the bi-metallic 1 wt.% AuPd/TiO<sub>2</sub> catalysts outperformed both mono-metallic 1 wt.% Pd/TiO<sub>2</sub> and 1 wt.% Au/TiO<sub>2</sub> analogues with respect to the formation of H<sub>2</sub>O<sub>2</sub>. Interestingly, the activity towards the direct synthesis between the three bi-metallic 1 wt.% AuPd/TiO<sub>2</sub> ratios were similar under (2 °C, CH<sub>3</sub>OH-H<sub>2</sub>O, CO<sub>2</sub>) conditions, where catalytic productivity was found to be approximately 95 mol<sub>H<sub>2</sub>O<sub>2</sub></sub> kg<sub>cat</sub><sup>-1</sup> h<sup>-1</sup>. However, as reaction conditions became progressively swapped towards (25 °C, H<sub>2</sub>O, N<sub>2</sub>) conditions, the activity of the three bi-metallic 1 wt.% AuPd catalysts became less comparable, which was ascribed to have had increased the activity towards H<sub>2</sub>O<sub>2</sub> degradation, which was found to increase along with Pd-rich compositions. In fact, mono-metallic 1 wt.% Pd/TiO<sub>2</sub> catalyst presented a productivity of c.a 80 mol<sub>H<sub>2</sub>O<sub>2</sub></sub> kg<sub>cat</sub><sup>-1</sup> h<sup>-1</sup>, which was very similar to the productivity of the bi-metallic ratio 0.75 wt.% Au-0.25 wt.% Pd/TiO<sub>2</sub> (c.a 93 mol<sub>H<sub>2</sub>O<sub>2</sub></sub> kg<sub>cat</sub><sup>-1</sup> h<sup>-1</sup>), however, the degradation activity of the former (c.a 400

mol<sub>H<sub>2</sub>O<sub>2</sub></sub> kg<sub>cat</sub><sup>-1</sup> h<sup>-1</sup>) was much higher than the latter (c.a 150 mol<sub>H<sub>2</sub>O<sub>2</sub></sub> kg<sub>cat</sub><sup>-1</sup> h<sup>-1</sup>) catalysts. This led to suggest that the bi-metallic 0.75 wt.% Au-0.25 wt.% Pd/TiO<sub>2</sub> catalyst had reached productivities as high as the mono-metallic analogue thanks to having had less degradation activity. Therefore, this bi-metallic ratio seems to be more selective towards the direct synthesis of H<sub>2</sub>O<sub>2</sub>. However, H<sub>2</sub> conversion should be determined in future work to corroborate this last statement and prove that the bi-metallic 0.75 wt.% Au-0.25 wt.% Pd/TiO<sub>2</sub> catalyst is more selective than the two others bi-metallic ones and the mono-metallic 1 wt.% Pd/TiO<sub>2</sub> analogue as it appears to be. Table 6.1 presents the activity of the mono-metallic 1 wt.% Pd/TiO<sub>2</sub> and the bi-metallic 0.75 wt.% Au-0.25 wt.% Pd/TiO<sub>2</sub> catalysts at the four reaction conditions depicted in Figure 6.1 to evidence the promising performance of this bi-metallic AuPd catalyst.

**Table 6.1:** Comparison between the productivity towards the direct synthesis of H<sub>2</sub>O<sub>2</sub> for the mono-metallic 1 wt.% Pd/TiO<sub>2</sub> and bi-metallic 0.5 wt.% Au-0.5 wt.% Pd/TiO<sub>2</sub> catalyst.

<b>Reaction conditions</b>	<b>1 wt.% Pd/TiO<sub>2</sub></b>	<b>0.75 wt.% Au-0.25 wt.% Pd/TiO<sub>2</sub></b>
	<b>Productivity</b>	<b>Productivity</b>
	mol <sub>H<sub>2</sub>O<sub>2</sub></sub> kg <sub>cat</sub> <sup>-1</sup> h <sup>-1</sup>	mol <sub>H<sub>2</sub>O<sub>2</sub></sub> kg <sub>cat</sub> <sup>-1</sup> h <sup>-1</sup>
<b>(2 °C, CH<sub>3</sub>OH-H<sub>2</sub>O, CO<sub>2</sub>)</b>	80	89
<b>(25 °C, CH<sub>3</sub>OH-H<sub>2</sub>O, CO<sub>2</sub>)</b>	50	69
<b>(25 °C, H<sub>2</sub>O, CO<sub>2</sub>)</b>	12	26
<b>(25 °C, H<sub>2</sub>O, N<sub>2</sub>)</b>	4	16

**Reaction conditions towards the direct synthesis: (2°C, CH<sub>3</sub>OH-H<sub>2</sub>O, CO<sub>2</sub>):** 8.5 g (5.6 g CH<sub>3</sub>OH, 2.9 g H<sub>2</sub>O), catalyst (0.01 g), 420 psi of 5 % H<sub>2</sub>/CO<sub>2</sub>, 160 psi of 25 % O<sub>2</sub>/CO<sub>2</sub>, 1200 rpm, 2 °C, 0.5 h. **(25°C, CH<sub>3</sub>OH-H<sub>2</sub>O, CO<sub>2</sub>):** 8.5 g ( 5.6 g CH<sub>3</sub>OH, 2.9 g H<sub>2</sub>O), catalyst (0.01 g), 420 psi of 5 % H<sub>2</sub>/CO<sub>2</sub>, 160 psi of 25 % O<sub>2</sub>/CO<sub>2</sub>, 25 °C, 1200 rpm, 0.5 h. **(25°C, H<sub>2</sub>O, CO<sub>2</sub>):** 8.5 g H<sub>2</sub>O, catalyst (0.01 g), 420 psi of 5 % H<sub>2</sub>/CO<sub>2</sub>, 160 psi of 25 % O<sub>2</sub>/CO<sub>2</sub>, 1200 rpm, 25 °C, 0.5 h. **(25°C, H<sub>2</sub>O, N<sub>2</sub>):** 8.5 g H<sub>2</sub>O, catalyst (0.01 g), 420 psi of 5 % H<sub>2</sub>/N<sub>2</sub>, 160 psi of 25 % O<sub>2</sub>/N<sub>2</sub>, 1200 rpm, 25 °C, 0.5 h.

X-ray photoelectron spectroscopy (XPS) was employed to determine the state of the Pd, since it had been widely reported that the PdO was more selective towards the direct synthesis of H<sub>2</sub>O<sub>2</sub> than the Pd<sup>0</sup>.<sup>33,34</sup> However, no significant difference was seen between the three bi-metallic 1 wt.% AuPd/TiO<sub>2</sub> ratios and the mono-metallic analogue 1 wt.% Pd/TiO<sub>2</sub>, which led to conclude that the difference in activity between the bi-metallic catalysts 1 t.% AuPd/TiO<sub>2</sub> and the mono-metallic 1 wt.% Pd/TiO<sub>2</sub> analogue was not related to the state of the Pd. Transmission electron microscopy (TEM) was employed to determine if the difference in activity could be linked to the particle size. The nanoparticle size of the mono-metallic 1 wt.% Pd/TiO<sub>2</sub>/TiO<sub>2</sub> catalyst were found to be below the instrument detection limit. Subsequent analysis by energy dispersive x-ray spectroscopy (EDX) confirmed the presence of clusters or agglomerates with less than 1 nm in size. In addition to this, no correlation between the Au:Pd ratio and the nanoparticle and distribution size to the activity was found. In fact, the bi-metallic 0.50 wt.% Au-0.50 wt.% Pd/TiO<sub>2</sub> catalyst had

the lowest mean nanoparticle size (2.4 nm), whereas the other two ratios, 0.75 wt.% Au-0.25 wt.% Pd/TiO<sub>2</sub> and 0.25 wt.% Au-0.75 wt.% Pd/TiO<sub>2</sub> had a mean particle size of 4.6 nm and 5.8 nm respectively. The difference in the mean nanoparticle size suggested that the three bi-metallic 1 wt.% AuPd/TiO<sub>2</sub> catalysts might have also presented different nanoparticle composition (e.g. Au-rich, Pd-rich, AuPd alloys). It was believed that the difference in the activity of the bi-metallic 1 wt.% AuPd/TiO<sub>2</sub> catalysts, especially towards the degradation of H<sub>2</sub>O<sub>2</sub>, could be linked to the nanoparticle size and its composition, which unfortunately it was not able to be determined. Therefore, future work should involve the analysis of the nanoparticles for these three bi-metallic catalysts. In fact, several authors have evidenced that the formation of AuPd alloys is critical to have competitive activity and selectivity towards the direct synthesis, and Pd-rich ensembles have been widely ascribed to promote the degradation of H<sub>2</sub>O<sub>2</sub>.<sup>10,35</sup> Anyhow, this work proves that Au was key in order to decrease the degradation activity of the Pd, therefore, making the bi-metallic 0.75 wt.% Au-0.25 wt.% Pd/TiO<sub>2</sub> catalyst the most likely ratio for the *in-situ* H<sub>2</sub>O<sub>2</sub> generation at more suitable reaction conditions (25 °C, H<sub>2</sub>O, CO<sub>2</sub> and 25 °C, H<sub>2</sub>O, N<sub>2</sub>).

Diverse authors have reported that working in continuous flow reactors help to improve the catalyst's selectivity when working with a three phase (solid-liquid-gas) reaction at ambient temperature.<sup>36</sup> For instance, Han and co-workers<sup>37</sup> achieved 100 % selectivity of H<sub>2</sub>O<sub>2</sub> with 8.8 % H<sub>2</sub> conversion working with a semi-bath continuous flow reactor using PdAu/TiO<sub>2</sub> catalyst, CH<sub>3</sub>CH<sub>2</sub>OH acidified with H<sub>2</sub>SO<sub>4</sub> as a solvent at 25 °C and 0.1 MPa, Cocero and co-workers<sup>38</sup> with a semi-continuous flow reactor achieving 69 % selectivity and 55.5 % H<sub>2</sub> conversion, with a Pd/C catalyst, CH<sub>3</sub>OH acidified with H<sub>3</sub>PO<sub>4</sub> and KBr, near ambient conditions and 0.9 MPa, and Mikkola and co-workers<sup>39</sup> with a trickled bed reactor achieved 30.8 % H<sub>2</sub>O<sub>2</sub> selectivity and 79.9 % H<sub>2</sub> conversion using only H<sub>2</sub>O as a solvent and 25.5 % H<sub>2</sub>O<sub>2</sub> selectivity and 99.9 % H<sub>2</sub> conversion using CH<sub>3</sub>OH as a solvent with Pd/C catalyst, acidified with H<sub>3</sub>PO<sub>4</sub> and NaBr at 30 °C at 2.6 MPa.<sup>39</sup> Hutchings and co-workers<sup>40</sup> reported a lower H<sub>2</sub> conversion (30 %) and H<sub>2</sub>O<sub>2</sub> selectivity (10 %) when working with AuPd/TiO<sub>2</sub> catalyst in a flow continue reactor at 30 °C with H<sub>2</sub>O and CH<sub>3</sub>OH as a co-solvent at 1 MPa, however, without using acids or halides promoters.<sup>40</sup> In addition to this, Richards *et al.*, have recently published that bi-metallic AuPd/TiO<sub>2</sub> ratios are effective to remove E. coli K12 in greywaters when working in a flow reactor generating ROS from *in-situ* H<sub>2</sub>O<sub>2</sub>. Hence, transitioning from batch to flow reactors would be a promising alternative for future work activities to improve the activity and selectivity of the three bi-metallic 1 wt.% AuPd/TiO<sub>2</sub> ratios towards the direct synthesis of H<sub>2</sub>O<sub>2</sub>.

The capability of converting *in-situ* H<sub>2</sub>O<sub>2</sub> to ROS via Pd-Fenton based supported metals catalyst was next investigated in Chapter 4 by measuring the activity of bi-metallic 0.5 wt.%

X-0.5 wt.% Pd/TiO<sub>2</sub> (X: Fe, Co, Cu, Au) catalysts towards the degradation of phenol. The bi-metallic 0.5 wt.% Au-0.5 wt.% Pd/TiO<sub>2</sub> presented the highest productivities towards the direct synthesis of H<sub>2</sub>O<sub>2</sub> in comparison to the other bi-metallic FePd, CuPd and CoPd combinations, but the lowest activity towards degrading phenol (5 %). This suggested that the bi-metallic AuPd combination did not generate enough ROS to achieve significant phenol conversions, and H<sub>2</sub>O<sub>2</sub> had been degraded to H<sub>2</sub>O in greater extent. All three bi-metallic FePd, CuPd and CoPd combinations presented relatively high H<sub>2</sub> conversions (between 30-45 %), suggesting that all had produced *in-situ* H<sub>2</sub>O<sub>2</sub> during the degradation of phenol. However, only FePd system had relevant activity towards degrading phenol (c.a 40 %), indicating that the CuPd (5 %) and CoPd (5 %) combinations had the *in-situ* H<sub>2</sub>O<sub>2</sub> degraded, making the Cu and Co not suitable Fenton metals in generating ROS from *in-situ* H<sub>2</sub>O<sub>2</sub>. Crombie *et al.*, reported from electron paramagnetic resonance (EPR) analysis that FePd based catalysts, prepared by an analogous modified impregnation procedure used in this work, was producing more ROS than the bi-metallic AuPd and mono-metallic Pd combinations at 50 °C and water only solvent.<sup>41</sup> Thus, it was feasible to conclude that the Fe was the most promising metal to generate ROS from *in-situ* H<sub>2</sub>O<sub>2</sub> to degrade aromatics for water remediation.

At this point, a series of mono and bi-metallic 1 wt.% FePd/TiO<sub>2</sub> catalysts were prepared by a modified impregnation procedure, to determine the best Fe: Pd ratio in terms of activity between the degradation of phenol and the formation/degradation of H<sub>2</sub>O<sub>2</sub>. Interestingly, the mono-metallic 1 wt.% Pd/TiO<sub>2</sub> and the bi-metallic 1 wt.% FePd/TiO<sub>2</sub> catalysts presented similar concentrations of H<sub>2</sub>O<sub>2</sub> (c.a 0.05 wt.%), which was surprising despite the state the Pd was dissimilar, in fact, the PdO percentage increased with the Fe loading. Thus, the Fe was considered to contribute to the inhibition of Pd reduction during thermal heat treatment, promoting the formation of mixed Pd oxidation states, known to be more selective towards H<sub>2</sub>O<sub>2</sub>.<sup>42</sup> Interestingly, the degradation activity of H<sub>2</sub>O<sub>2</sub> of the mono and bi-metallic 1 wt.% FePd/TiO<sub>2</sub> catalysts did decrease along with increasing the PdO percentage, and thus the Fe loading. In fact, the bi-metallic 0.75 wt.% Fe-0.25 wt.% Pd/TiO<sub>2</sub> catalyst presented the lowest degradation activity in comparison to the other two bi-metallic ratios (0.50 wt.% Fe-0.50 wt.% Pd/TiO<sub>2</sub> and 0.25 wt.% Fe-0.75 wt.% Pd/TiO<sub>2</sub>) and mono-metallic 1 wt.% Fe/TiO<sub>2</sub> catalysts. CO-DRIFTS analysis also determined that the bi-metallic 0.75 wt.% Fe-0.25 wt.% Pd/TiO<sub>2</sub> catalyst did not present Pd ensembles in comparison to the other two bi-metallic ratios and mono-metallic 1 wt.% Pd/TiO<sub>2</sub> analogue. This Pd ensembles are commonly reported as being responsible for the degradation of H<sub>2</sub>O<sub>2</sub> as previously mentioned. Thus, it was suggested that the low degradation activity shown by the bi-metallic 0.75 wt.% Fe-0.25 wt.% Pd/TiO<sub>2</sub> catalyst could be a contribution of two facts, the high PdO percentage in

comparison to the other two bi-metallic catalysts and due to not having formed Pd ensembles as XPS and CO-DRIFTS suggested respectively.

Analysis by transmission electron microscopy (TEM) determined that the mono and bi-metallic 1.0 wt.% FePd/TiO<sub>2</sub> catalysts presented clusters and agglomerates c.a 1 nm, thus, it was not possible to determine if the differences in activity of the 1.0 wt.% FePd/TiO<sub>2</sub> catalysts could be aslo related to varation in the composton and particle size distribution. However, it is noteworthy that Crombie *et al.*, determined by energy-dispersive x-ray spectroscopy (XEDS) that the bi-metallic 0.50 wt.% Fe-0.50 wt.% Pd/TiO<sub>2</sub> catalyst prepared by modified impregantion consisted of both PdFe alloys and unalloyed Fe species.<sup>41</sup> Despite of this, future work should include elemental mapping and analysis by XEDS in order to investigate the nanoparticle's composition (Fe-rich, Pd-rich, FePd alloys) of these bi-metallic 1 wt.% FePd/TiO<sub>2</sub> catalysts.

The bi-metallic 1 wt.% FePd/ TiO<sub>2</sub> (c.a 40 % phenol conversion, 2 h) catalysts presented similar activity towards the degradation of phenol, followed by the mono-metallic 1 wt.% Pd/ TiO<sub>2</sub> (c.a 10 % phenol conversion, 2 h) and 1 wt.% Fe/TiO<sub>2</sub> (c.a 2 % phenol conversion, 2 h) catalysts. It was plausible to consider that the bi-metallic 1 wt.% FePd/ TiO<sub>2</sub> catalysts had shown similar activities since they also gave similar concentrations of *in-situ* H<sub>2</sub>O<sub>2</sub>. In fact, blank reactions corroborated that the formation of *in-situ* H<sub>2</sub>O<sub>2</sub> was indispensable to generate ROS and thus degrade phenol. When H<sub>2</sub> or O<sub>2</sub> were replaced by N<sub>2</sub> (inert gas), minimal activity towards the degradation of phenol was seen (between 4-6 % phenol conversion). Table 6.2 presents the activity towards the degradation of phenol for the mono and bi-metallic 1 wt.% FePd/TiO<sub>2</sub> catalysts. As it shows, the activity was relatively similar regardless of the Fe:Pd ratio.

**Table 6.2:** Activity of the mono and bi-metallic FePd/TiO<sub>2</sub> catalysts towards the degradation of phenol and direct synthesis of H<sub>2</sub>O<sub>2</sub>.

Reaction conditions	Phenol conversion	H <sub>2</sub> O <sub>2</sub>
	%	wt.%
1.0 wt.% Fe/TiO <sub>2</sub>	2	0.01
0.75 wt.% Fe-0.25 wt.% Pd/TiO <sub>2</sub>	40	0.05
0.50 wt.% Fe-0.50 wt.% Pd/TiO <sub>2</sub>	35	0.05
0.25 wt.% Fe-0.75 wt.% Pd/TiO <sub>2</sub>	30	0.05
1.0 wt.% Pd/TiO <sub>2</sub>	10	0.04

**Reaction conditions towards the conversion of phenol:** 8.5 g (phenol (1000 ppm)), catalyst (0.01 g), 420 psi 5% H<sub>2</sub>/CO<sub>2</sub>, 160 psi 25% O<sub>2</sub>/CO<sub>2</sub>, 1200 rpm, 30 °C, 2 h. **Reaction conditions towards the direct synthesis of H<sub>2</sub>O<sub>2</sub>:** 8.5 g (HPLC grade water), catalyst (0.01 g), 420 psi 5 % H<sub>2</sub>/CO<sub>2</sub>, 160 psi 25 % O<sub>2</sub>/CO<sub>2</sub> 1200 rpm, 30 °C 2 h.

The extent of metal leaching was determined by microwave plasma atomic emission spectroscopy (MP-AES) analysis from the reaction solutions after conducting the degradation of phenol reaction. It was found that the bi-metallic 1 wt.% FePd/TiO<sub>2</sub> catalysts leached between 37-46 % Fe and approximately 2 % Pd. In keeping with previous studies it was found that the amount of metal leached correlated well with the extent of phenol conversion, with all bi-metallic catalysts offering similar levels of phenol conversion and metal leaching.<sup>43,44</sup> It was proposed that the loss of Fe can be attributed with the presence of high quantities of unalloyed Fe (as Fe<sub>x</sub>O<sub>y</sub> as determined by XPS analysis), as observed by Crombie *et al.*<sup>41</sup> However, further spectroscopic analysis are required to determine the validity of this hypothesis, since it was not possible to determine the type of nanoparticle's composition. In addition, it is possible that the transition to a flow regime, where contact between catalyst and phenol degradation products is limited, may prolong catalyst lifetime and indeed, the option of a flow regime is more suitable for industrial applications.

Anyhow, Chapter 5 aimed to improve the stability of the FePd supported catalysts by anchoring the Fe species in the support of a zeolite. Many authors have reported that the introduction of the Fe or Cu within a zeolite lattice, and its subsequent extraction via calcination treatment generates a wide range of metal species, which each one may account for certain activity and stability.<sup>24,23</sup> To this end, HZSM-5 catalysts containing Fe incorporated in the framework were synthesised by hydrothermal synthesis (X wt.% Fe-HZSM-5 (X: 0-3)). Pd was subsequently impregnated on the surface of the mono-metallic X wt.% Fe-HZSM-5 (X: 3.0-0) zeolites by modified impregnation generating a set of bi-metallic (0.5 wt.% Pd/ X wt.% Fe (X: 0-3)) catalysts. The incorporation of Fe species and subsequent impregnation of Pd was found to decrease the crystallinity of the bi-metallic 0.5 wt.% Pd/ X wt.% Fe-HZSM-5 (X: 3.0-0) catalysts in comparison to the bare HZSM-5 (SiO<sub>2</sub>:Al<sub>2</sub>O<sub>3</sub>) (23:1) zeolite, as established by x-ray diffraction (XRD). This also led to a decrease in the specific surface area and micropore volume, as indicated by physisorption analysis. It has also been reported before that the crystallinity of the HZSM-5 zeolite is affected negatively by the introduction of a secondary metal.<sup>45,46</sup> The different Fe species were next investigated by means of diffuse reflectance ultraviolet-visible spectroscopy (DR UV-Vis) according to the wavelength they absorb; 200-250 nm (Fe<sup>3+</sup> species coordinated within the framework lattice), 250-350 nm (isolated Fe species and bi-nuclear Fe species immobilised in the framework channels), 350-450 nm (extra-framework Fe<sub>x</sub>O<sub>y</sub> clusters) and >450 nm (extra-framework agglomerations of Fe<sub>x</sub>O<sub>y</sub>).<sup>47</sup> It was concluded that the X wt.% Fe-HZSM-5 (X: 1.0-0.06) contained predominantly Fe<sup>3+</sup> tetrahedrally coordinated within the HZSM-5 lattice and isolated and bi-nuclear Fe species. On the other hand, the X wt.% Fe-HZSM-5 (X: 3.0-2.0) catalysts contained the same species as X wt.% Fe-HZSM-5 (X: 1.0-0.06) ones, as well as some clusters and agglomerates of Fe<sub>x</sub>O<sub>y</sub> species. Therefore, it was

evidenced that this clusters and agglomerates of  $\text{Fe}_x\text{O}_y$ , had been formed on the mono-metallic X wt.% Fe-HZSM-5 (X: 3.0-2.0) catalysts that also presented the lowest crystallinity (c.a 85 %) in comparison to the other ratios. This had been reported before by some authors, where they claimed that the loss of crystallinity evokes the formation of this type of unstable  $\text{Fe}_x\text{O}_y$  species when synthesising zeolitic materials with metals by hydrothermal synthesis procedure.<sup>24</sup> These  $\text{Fe}_x\text{O}_y$  species were suspected to have been unstable in Chapter 4 during the degradation of phenol, leading to high amounts of Fe leaching, hence, it was concluded that a loading between X wt.% Fe-HZSM-5 (X: 1.0-0.06) was the most appropriate to avoid the formation of these unstable clusters and agglomerates of  $\text{Fe}_x\text{O}_y$  species.

The activity towards the direct synthesis of  $\text{H}_2\text{O}_2$  between the different bi-metallic 0.5 wt.% Pd/ X wt.% Fe-HZSM-5 (X: 3.0-0.06) catalysts remained relatively similar, which seemed not surprising since all the catalysts showed the same proportion of  $\text{Pd}^0$  (c.a 80 %) and  $\text{PdO}$  (c.a 20 %) except the mono-metallic 0.5 wt.% Pd/ 0 wt.% Fe-HZSM-5 catalyst (c.a 50 %  $\text{Pd}^0$  and 50 %  $\text{PdO}$ ). In these catalysts, in comparison to the 1 wt.% FePd/ $\text{TiO}_2$ , Fe had not contributed to avoid the reduction of Pd during the heat treatment, which suggested that the Fe and Pd might have been segregated in greater extent in comparison to the 1 wt.% FePd/ $\text{TiO}_2$  catalysts. The degradation activity of  $\text{H}_2\text{O}_2$  decay with increasing the Fe loading, in fact, the bi-metallic 0.5 wt.% Pd/ X wt.% Fe-HZSM-5 (X: 3.0-1.0) catalysts presented between 80-60 %  $\text{H}_2\text{O}_2$  degradation, whereas the mono and bi-metallic 0.5 wt.% Pd/ X wt.% Fe-HZSM-5 (X: 0.5-0) catalysts all presented c.a 40 % of  $\text{H}_2\text{O}_2$  degradation. The degradation activity of  $\text{H}_2\text{O}_2$  was almost accounted by the Pd, since mono-metallic X wt.% Fe-HZSM-5 (X: 3.0, 1.0, 0.5, 0) catalysts had 9 %, 6 %, 4% and 2 % respectively in 30 min reaction time in comparison to the mono and bi-metallic analogues that presented 40 %, 30 %, 20 % and 10 % respectively. This result was surprising since, despite the whole set of bi-metallic catalyst had the same loading of Pd and oxidation state, the degradation activity was significantly dissimilar. It was suspected that the Pd had deposited on the external surface area in greater extent for the mono-metallic X wt.% Fe-HZSM-5 (X: 3.0-1.0) catalysts in comparison to the other mono-metallic analogues. For instance, Pd could have been deposited on the cavities and channels of the zeolite when it was impregnated on the bare zeolite 0 wt.% Fe/HZSM-5 (99 % crystallinity) with a specific surface area ( $516 \text{ m}^2/\text{g}$ ) and microporous volume ( $0.12 \text{ cm}^3/\text{g}$ ), making the Pd active sites less exposed to the external surface area. In fact, after the deposition of the Pd, the crystallinity was reduced to 91 % and the specific surface area ( $407 \text{ m}^2/\text{g}$ ) and micropore volume ( $0.09 \text{ cm}^3/\text{g}$ ) were also reduced. On the other hand, when Pd was deposited on 3.0 wt.% Fe-HZSM-5 with a total surface area ( $259 \text{ m}^2/\text{g}$ ) and micropore volume ( $0.04 \text{ cm}^3/\text{g}$ ), Pd could have been deposited on the external surface area of the 3.0 wt.% Fe-HZSM-5 in greater extent than in the cavities

and channels. However, this is a hypothesis that is needed to be corroborated, probably by more resolute microscopic techniques that the ones were available during these studies.

Interestingly, the bi-metallic 0.5 wt.% Pd/ X wt.% Fe-HZSM-5 (X: 3.0-0) catalysts were found to produce significantly less H<sub>2</sub>O<sub>2</sub> than the bi-metallic 1.0 wt.% FePd/TiO<sub>2</sub> series. The difference in activity towards the direct synthesis of H<sub>2</sub>O<sub>2</sub> between these two types of catalysts may be because of the variation shown in particle size and the oxidation state of the Pd. TEM analysis did not reveal any nanoparticles in the mono-metallic X wt.% Fe-HZSM-5 (X: 3.0, 1.0, 0.5, 0) catalysts, except for the mono-metallic 3.0 wt.% Fe-HZSM-5 one. However, they were not enough nanoparticles to statistically determine the mean particle size and distribution. On the other hand, when Pd got deposited, the bi-metallic 0.5 wt.% Pd/ X wt.% Fe-HZSM-5 (X: 3.0, 1.0, 0.5, 0) catalysts showed big nanoparticles with a wide distribution in size lying between 26-15 nm. These big nanoparticles were presumably thought to be Pd-rich, however, elemental analysis by EDX would be required to corroborate this. Anyhow, the difference in activity towards the direct synthesis of H<sub>2</sub>O<sub>2</sub> shown by the bi-metallic 0.5 wt.% Pd/ X wt.% Fe-HZSM-5 (X: 3.0-0) catalysts and the bi-metallic 1 wt.% FePd/TiO<sub>2</sub> could had been related to the nanoparticle size and composition and Pd speciation. This comparison between catalysts was needed to be highlighted to state the important role the support plays in driving the nanoparticle's size, for instance, the bi-metallic 0.50 wt.% Pd/ 0 wt.% Fe-HZSM-5 catalyst had 20 nm mean particle size with 51 % of PdO and the mono-metallic 1.0 wt.% Pd/TiO<sub>2</sub> had *c.a* 1 nm particle size with 10 % of PdO, despite both catalysts were synthesise by the same modified impregnation procedure. As such the choice of catalyst support can significantly alter the particle size and Pd speciation, with both of these factors well known to be crucial in achieving high catalytic performance to H<sub>2</sub>O<sub>2</sub> production.<sup>48</sup>

In terms of activity towards the degradation of phenol, the bi-metallic 0.5 wt.% Pd/ X wt.% Fe-HZSM-5 (X: 3.0-1.0) catalysts had a conversion of phenol between 65-55 % (Table 6.3) in two hours reaction, whereas the other ratios 0.5 wt.% Pd/ X wt.% Fe-HZSM-5 (X: 0.5-0.06) showed a conversion *c.a* 40 %. This differentiation between ratios towards the degradation of phenol activity was surprising since the whole set of bi-metallic catalysts presented relatively similar concentrations of H<sub>2</sub>O<sub>2</sub> (between 0.007-0.005 wt.%, 2 h). It was suspected that the decay in the crystallinity, that had evoked the formation of the Fe<sub>x</sub>O<sub>y</sub> agglomerative and clusters, had also made enhance the activity towards the degradation of phenol via generating more ROS.

**Table 6.3:** Phenol conversion activity and productivity towards the direct synthesis of H<sub>2</sub>O<sub>2</sub> for the mono and bi-metallic 0.5 wt.%Pd/X.0 wt.%Fe-HZSM-5 (X: 3.0-0) catalysts.

Catalysts	Phenol conversion	Yield H <sub>2</sub> O <sub>2</sub>
	%	wt.%
0.5 wt.%Pd/3.0 wt.%Fe-HZSM-5	65	0.005
0.5 wt.%Pd/1.0 wt.%Fe-HZSM-5	60	0.01
0.5 wt.%Pd/0.5 wt.%Fe-HZSM-5	55	0.01
0.5 wt.%Pd/0.125 wt.%Fe-HZSM-5	40	0.007
0.5 wt.%Pd/0.06 wt.%Fe-HZSM-5	30	0.007
0.5 wt.%Pd/0 wt.% Fe-HZSM-5	40	0.005
0 wt.%Pd/0 wt.% Fe-HZSM-5	35	0.005

**Reaction conditions towards the conversion of phenol:** 8.5 g (phenol (1000 ppm)), catalyst (0.01 g), 420 psi 5% H<sub>2</sub>/CO<sub>2</sub>, 160 psi 25% O<sub>2</sub>/CO<sub>2</sub>, 1200 rpm, 30 °C, 2 h. **Reaction conditions towards the direct synthesis of H<sub>2</sub>O<sub>2</sub>:** 8.5 g (HPLC grade water), catalyst (0.01 g), 420 psi 5 % H<sub>2</sub>/CO<sub>2</sub>, 160 psi 25 % O<sub>2</sub>/CO<sub>2</sub> 1200 rpm, 30 °C 2 h.

It was suspected that the bi-nuclear and isolated Fe species were found to offer better stability than the extra-framework Fe<sub>x</sub>O<sub>y</sub> clusters and agglomeratives. Many authors had also drawn the same conclusions previously when studying the degradation of phenol over mono and bi-metallic FeCu supported catalysts with pre-formed H<sub>2</sub>O<sub>2</sub>.<sup>49,50,51,52</sup> Comparisons between the activity and stability of the mono and bi-metallic 1 wt.% FePd/TiO<sub>2</sub> catalysts drawn in Chapter 4, revealed the improved stability of the ZSM-5 based materials. In fact, the Fe leaching was an order of magnitude greater over the 0.5 wt.% Pd-0.5 wt.% Fe/TiO<sub>2</sub> (3.57 ppm (42 %)) catalyst compared to the ZSM-5 analogue of identical metal loadings (0.5 wt.% Pd/ 0.5 wt.% Fe-HZSM-5) (0.48 ppm (4 %)). This is despite the similar rates of phenol conversion observed over the two materials (30 % over the 0.5 wt.% Pd-0.5 wt.% Fe/TiO<sub>2</sub> and 37% over the 0.5 wt.% Pd/ 0.5 wt.% Fe-HZSM-5 catalyst). However, future work should be done to narrow down the speciation of Fe in the mono and bi-metallic 0.5 wt.% Pd/ X wt.% Fe-HZSM-5 (X: 3.0-0.06) catalysts and concrete the type of Fe specie that is accountable for this enhanced stability. For instance, as it has been previously reported, via x-ray absorption near edge structure (XANES) measurements and computational calculations, it was possible to report the specific bi-nuclear Fe specie present in HZSM-5 that governed the conversion of methane (CH<sub>4</sub>) to CH<sub>3</sub>OH.<sup>53</sup>

To conclude, the activity shown by the bi-metallic 0.5wt.%Pd/ 3.0wt.% Fe-HZSM-5 catalyst was quite promising, particularly given the low amount of Fe leaching in comparison to the bi-metallic 1 wt.% FePd/TiO<sub>2</sub> ones. However, further catalyst development will be required to synthesise a totally stable catalyst, since these bi-metallic 0.5wt.%Pd/ Xwt.% Fe-HZSM-5 (X: 3.0-0) catalysts also presented leaching during the direct synthesis of H<sub>2</sub>O<sub>2</sub>. Catalyst

synthetic improvements are required to avoid the formation of such big, presumably, Pd nanoparticles that generate little  $H_2O_2$  besides are believed to be quite unstable.

In terms of catalytic design, there are several interesting approaches that could be implemented when working with zeolites as supports for metal catalysts. The big nanoparticles after the deposition of Pd determined by TEM on the mono and bi-metallic 0.5wt.%Pd/ Xwt.% Fe-HZSM-5 (X: 3.0-0) catalysts urge the necessity of finding new strategies to size-controlled nanoparticles with homogeneous compositions. In fact, Li and co-workers<sup>54</sup> reported big core-shell FePd nanoparticles (10-30 nm) when both metal were impregnated on HZSM-5. Despite of this, the bi-metallic FePd nanoparticles catalyst achieved high performance in the removal of  $Cr^{6+}$  (96 %) at pH 3, with minimal leaching of Fe and Pd.<sup>54</sup> However, when *in-situ*  $H_2O_2$  is meant to be synthesised, many authors have reported that the most optimum Pd and AuPd nanoparticles should be *c.a* 2.5 nm with homogeneous AuPd compositions. For instance, an interesting approach was reported by Xiao and co-workers,<sup>55</sup> where they synthesised H-ZSM-5 adding AuPd colloids during the synthesis of HZSM-5 by hydrothermal synthesis in order to encapsulate the AuPd nanoparticles within the HZSM-5 cavities (termed AuPd@HZSM-5). They compared the activity of the AuPd@HZSM-5 catalyst towards the direct synthesis and degradation of  $H_2O_2$  with AuPd impregnated on HZSM-5 and AuPd/TiO<sub>2</sub> analogues, finding that the AuPd@HZSM-5 had higher activity and stability than the two latter catalysts thanks to have generated homogeneous AuPd alloys nanoparticles.<sup>55</sup> Similar catalyst synthesis procedures may show promise with FePd colloids for the degradation of phenol and other pollutant molecules. However, preparing bi-metallic colloids is not a simple task, especially if both light transition metals have different redox potentials. Wang and co-workers<sup>56</sup> developed a methodology to prepare poly(N-vinyl-2-pyrrolidone) (PVP) protected Cu/Pd bi-metallic colloids for the hydration of acrylonitrile to acrylamide. The novelty of this catalytic synthetic routed lied in refluxing for 3 h at 198 °C a glycol solution of hydroxide of Cu and Pd with PVP. By this procedure, the authors claimed to obtain a homogeneous composition of Cu/Pd colloids with a particle size ranging from 1-4 nm with both metals reduced at zero oxidation state.<sup>56</sup> Hence, the formation of bi-metallic FePd colloids to form FePd alloys encapsulated within the HZSM-5 framework could be an interesting route to investigate in future work.

### **6.3 Alternative lines of research in future work.**

This section of Chapter 6 aims to give an overview of other lines that could be investigated for future work that include other type of interesting microporous structures as well as other promising technological alternatives reported for water treatment using *in-situ*  $H_2O_2$ .

One alternative, fairly similar to zeolites, and that have taken high interest in the last 30 years, is the study of metal organic frameworks (MOFs). Yaghi *et.al.*,<sup>57</sup> reported in 1995 for the first time the synthesis of MOFs. The authors defined them as microporous materials based on organic building blocks whose shape, size and functionalization can be more tunable than zeolites. Following to Yaghi *et.al.*, description of MOFs, they consist of a symmetric organic molecule as building blocks to bind metals ions and form layers of metal-organic compounds, whose functionalization is determined by the nature of the organic molecule and the metal ion. These layers create channels in which aromatic molecules may be selectively bound.<sup>57</sup> Currently, there are several methodologies to prepared MOFs that differ in simplicity and preparation time, yield and amount of organic solvents used. For instance, Ju and co-workers<sup>58</sup> and Pang and co-wokers<sup>59</sup> reviewed several routes for obtaining MOFs such as; *i*) hydrothermal synthesis, *ii*) solvothermal method, *iii*) microwave heating method, *iv*) ultrasonic synthesis method, *v*) electrochemical method, *vi*) mechanochemical method among others.<sup>58</sup> For instance, solvothermal method is usually employed if significant amount of MOFs is meant to be produced, however, this methodology requires large amounts of organic solvents and it is time consuming. On the other hand, microwave heating method is commonly used to obtain small batches of MOFs and it can take up to one hour of preparation.<sup>58</sup> On the other hand, ultrasonic synthesis methodology is low cost and take short times of preparation, however, this synthetic procedure is difficult to control and it can lead to undesired by-products.<sup>58</sup> Electrochemical methodology was first developed by BASF and it is a fast methodology where MOFs can be continually prepared without intermittent interruptions as it happens with the traditional solvothermal methodology.<sup>58</sup> Mechanochemical method is the most promising route to be implemented industrially for large-scale of MOFs manufacturing. It does not require large amount of organic solvents and MOFs are basically formed through mechanical input such as ball milling, grinding, extrusion and high pressure compression.<sup>58</sup> Finally, in regard to hydrothermal synthesis, which is the methodology that has been used in this thesis, Pang and co-workers<sup>59</sup> stated that it is an efficient route to synthesise MOFs because it permits to synthesise composites-based materials with controllable size and morphology. However, this synthetic route still presents some challenges such as low yield and long reaction time. In addition, the authors have claimed in their review in 2021 that the mechanism of formation of MOFs via hydrothermal synthesis is not fully understood.<sup>59</sup>

Since 1995, MOFs have been employed in catalysis, in concrete in electrochemistry for batteries and photocatalysis for H<sub>2</sub> production from water or conversion of CO<sub>2</sub> to CH<sub>3</sub>OH among others applications.<sup>60,59,61,62</sup> MOFs have also shown other interesting uses such as temperature regulators, where MOFs were able to show better performance than zeolites in absorbed and desorbed water as a function of pressure and temperature, which could be

applied for room acclimatization.<sup>60</sup> They have also been applied for water remediation, in fact, they have shown activity towards the degradation of organic pollutants such as pharmaceuticals or as membrane filters for desalination.<sup>58,63</sup> Au loaded on MOFs have also shown antibacterial activity against *Escherichia coli* and *Staphylococcus aureus* with pre-formed  $H_2O_2$ , where ROS were generated over the Au nanoparticles.<sup>64</sup> The authors claimed that only 10 % of the initial bacterial colonies survived after the reaction. This excellent antibacterial performance was ascribed to the release of ROS from pre-formed  $H_2O_2$  (only 100  $\mu$ l were used).<sup>64</sup> Hence, MOFs have shown to have similar applications as zeolites do, however, MOFs have been reported to be more tuneable in regard to its functionality according to the organic ligand and metal ion that are selected for its synthesis, and also in regard to its shape and size.

There are several authors that have already investigated the activity of MOFs for water treatment using *in-situ*  $H_2O_2$ . For instance, Zhao and co-workers<sup>65</sup> synthesised bifunctional MOFs(2Fe/Co) for the destruction of azo-dye rhodamine B with *in-situ*  $H_2O_2$  generation via oxygen reduction. They achieved 45 % rhodamine B removal via ROS generation with the MOF(2Fe/Co) catalysts, however, the removal of rhodamine B went up to 100 % with the introduction of solar light irradiation on the cathode with the 2:1 for MOFs(2Fe/Co) catalyst. This observation indicated to the authors that the photoinduced electrons of MOFs(2Fe/Co) could react with the *in-situ*  $H_2O_2$  and made enhance ROS generation. Unfortunately, with the introduction of the solar light irradiation, they determined that the Co and Fe had leach 0.4 and 0.15 ppm respectively.<sup>65</sup> This report from Zhao and co-workers<sup>65</sup> demonstrate that metal leaching can be difficult to eradicate in the water remediation field. Zhang and co-workers<sup>66</sup> synthesised Cu embedded in nitrogen-doped carbon composite (Cu/N-C) using *in-situ* synthesised Cu-MOFs as a precursor. The authors reported a high-efficient catalyst for *in-situ*  $H_2O_2$  and ROS production via oxygen reduction and Fenton-like reaction respectively to degrade bisphenol A. Cu was highly dispersed forming nanoparticle between 3-6 nm in size in the Cu/N-C-700 (calcined at 700 °C) catalyst. The authors have claimed that the high surface area and pore volume in the Cu/N-C-700 catalysts were favourable characteristics for this catalyst to provide with enough and highly dispersed Cu active sites. In fact, this catalyst achieved 100 % conversion of bisphenol A in one-hour reaction, however, metal leaching analysis was not reported.<sup>66</sup> Zhou and co-workers<sup>67</sup> synthesised  $ZnIn_2S_4$  nanosheets coated on defective iron-based MOFs, to obtain *in-situ*  $H_2O_2$  induced via visible light and ROS through a Fenton metal to degrade bisphenol A and ofloxacin. The catalyst achieved 99.4% and 98.5% conversion of bisphenol A and ofloxacin respectively.<sup>67</sup> However, the metal leaching, if any, was not mentioned. Some other authors<sup>68</sup> have reported Fe-MOFs catalyst with pre-formed  $H_2O_2$ . For instance, Dang and co-workers with core-shell structured  $Fe_3O_4$ -MOFs as heterogeneous photo-Fenton catalyst reported 100 %

conversion of 2,4-dichlorophenol with 3 mmol/L of H<sub>2</sub>O<sub>2</sub>, although the metal leaching was not specified.<sup>68</sup> One interesting catalyst was reported by Chen and co-workers<sup>69</sup> and consisted in ZIF-8 (MOFs) embedded with bi-metallic FePd nanoparticles for reductive dechlorination. The bi-metallic FePd-ZIF-8 catalyst is prepared by synthesising the FePd nanoparticles first. Subsequently, they were added to the *in-situ* preparation of ZIF-8.<sup>69</sup> Despite the preparation might have been time consuming, the author obtained a promising catalyst. They claimed that the ZIF-8 crystallinity was maintained after the incorporation of the FePd nanoparticles within the framework structure as evidenced by XRD. In addition, TEM images showed that the FePd nanoparticles were well distributed and exhibited uniform shapes, indicating that the existence of ZIF-8 prevented the undesirable conglomeration and agglomeration. This synthetic route is an interesting alternative that could be investigated in future work to carry out the degradation of phenol with *in-situ* H<sub>2</sub>O<sub>2</sub>. Hence, via hydrothermal synthesis, mono and bi-metallic FePd-MOFs could be synthesised to investigate their activity and stability during the degradation of phenol. Hou and co-workers<sup>70</sup> also reported AuPd-UiO-66 on ZIF-L/CC for the reduction of H<sub>2</sub>O<sub>2</sub>. They first prepared the direct synthesis of UiO-66 (MOFs) where H<sub>2</sub>PdCl<sub>4</sub> was used as a Pd precursor to obtain Pd-UiO-66 first. Subsequently, ZIF-L/CC was synthesised and had the Pd-UiO-66 deposited on to generate mono-metallic Pd supported catalyst referred as Pd-UiO-66 on ZIF-L/CC. Finally, HAuCl<sub>4</sub> was used as a precursor and introduced via electrodeposition generating bi-metallic AuPd-UiO-66 on ZIF-L/CC catalyst. The authors claimed that this methodology of *in-situ* generating MOFs-on-MOFs, despite being time consuming, allowed to have higher catalytic activity because the Pd nanoparticles were successfully encapsulated, without affecting the UiO-66 crystallinity, with a nanoparticle size ranging from 3.05 nm to 7.05 nm.<sup>70</sup>

There are several other technologies that have been reported recently for water treatment using heterogeneous Fenton catalysts and *in-situ* H<sub>2</sub>O<sub>2</sub> and have shown promising results. For instance, Romero-Cano and co-workers<sup>71</sup> reported the activity of Fe supported catalyst on C (9 wt.% Fe/C) towards the degradation of phenol, via ROS formation from *in-situ* H<sub>2</sub>O<sub>2</sub> generated electrochemically.<sup>71</sup> They concluded that this technology was promising since it could produce high concentration of ROS (100 % efficiency in ROS formation) from *in-situ* H<sub>2</sub>O<sub>2</sub> with minimal Fe leaching (0.1 ppm) and high rates of phenol degradation (100 % conversion).<sup>71</sup> Zhao and co-workers<sup>72</sup> also produced *in-situ* H<sub>2</sub>O<sub>2</sub> with FePd alloys catalysts embedded on C to degrade dichloroacetamide and dibromoacetamide electrochemically. They reported a degradation activity up to 68 % and 73 % of dichloroacetamide and dibromoacetamide respectively in four hours reaction. Interestingly, the Cl<sup>-</sup> and Br<sup>-</sup> ions released from the degradation of these two pollutants, made decrease the pH of the solution down to 2, which became beneficial for the formation or ROS. They also evidenced that the

Fe and Pd were quite stable, releasing only 0.07 and 0.02 ppm respectively.<sup>72</sup> Silva and co-workers<sup>73</sup> also reported a methodology involving photo-Fenton degradation with *in-situ* H<sub>2</sub>O<sub>2</sub> using carbon nitride doped with Fe as photocatalyst to degrade resorcinol, phenol, gallic acid, and benzoic acid –all contained in the same solution- at neutral pH. The authors managed to generate *in-situ* H<sub>2</sub>O<sub>2</sub> from metal-free carbon nitride in the presence of dissolved oxygen and visible light radiation.<sup>73</sup> They measured the activity of the photocatalyst via total organic carbon (TOC) analysis. TOC determination is commonly employed in water treatment studies, since it measures the total amount of C that the polluted water under study contains. The speciation of the products formation, for instance, after the degradation of phenol, may not be relevant in water treatment, since what is meant to achieve is a complete removal of the C to CO<sub>2</sub>, irrespective of the products that are being formed in between. Silva and co-workers<sup>73</sup> reported a 80 % TOC removal with the addition of 1 ppm of Fe in the carbon nitride photo catalyst.<sup>73</sup> What 80 % TOC removal means is that only 20 % of C remains in solution after the oxidation has taken place, and therefore, the treated water is still polluted with products that have formed from the degradation of resorcinol, phenol, gallic acid, and benzoic acid. However, in this case, the authors did not determine the type of products that were remained in solution after the reaction. Liu and co-workers<sup>74</sup> also reported an interesting approach to generate ROS from *in-situ* H<sub>2</sub>O<sub>2</sub> to degrade 4-chlorophenol with zero valent zinc doped on carbon nanotubes that contained Fe<sub>2</sub>O<sub>3</sub> (Zn<sup>0</sup>-CNT(Fe<sub>2</sub>O<sub>3</sub>)). In this case, Zn<sup>0</sup> was generating *in-situ* H<sub>2</sub>O<sub>2</sub> from O<sub>2</sub>, to have the *in-situ* H<sub>2</sub>O<sub>2</sub> consecutively converted to ROS by the Fe<sub>2</sub>O<sub>3</sub> species. Liu and co-workers<sup>74</sup> reported a 99 % 4-chlorophenol conversion and 57 % TOC removal, however, this reaction required the pH to be 1.5, which is not recommended for water remediation. All these cited authors have shown interesting approaches to treat water using *in-situ* H<sub>2</sub>O<sub>2</sub> and they are all feasible alternatives to investigate for future work.

#### 6.4 References.

1. Zhou, R., Zhang, T., Zhou, R., Wang, S., Mei, D., Mai-Prochnow, A., Weerasinghe, J., Fang, Z., Ostrikov, K., Cullen, P. Sustainable plasma-catalytic bubbles for hydrogen peroxide synthesis. *Green chem.* **23**, 2977–2985 (2021).
2. Russo, V., Tesser, R., Santacesaria, E. Serio, M. Di. Chemical and Technical Aspects of Propene Oxide Production via Hydrogen Peroxide ( HPPO Process ). *Ind. Eng. Chem. Res.* **52**, 1168-1178 (2013).
3. Yi, Y., Wang, L., Li, G., Guo, H. A review on research progress in the direct synthesis of hydrogen peroxide from hydrogen and oxygen: Noble-metal catalytic method, fuel-cell method and plasma method. *Catal. Sci. Technol.* **6**, 1593–1610 (2016).
4. Beckman, E. J. Production of H<sub>2</sub>O<sub>2</sub> in CO<sub>2</sub> and its use in the direct synthesis of propylene oxide. *Green Context.* **5**, 332–336 (2003)

5. Yang, S., Verdaguer-Casadevall, A., Arnarson, L., Silvioli, L., Čolic V., Frydendal, R., Rossmeisl, J., Chorkendorff, I., Stephens, I.E.L. Toward the Decentralized Electrochemical Production of H<sub>2</sub>O<sub>2</sub>: A Focus on the Catalysis. *ACS Catal.* **8**, 4064–4081 (2018).
6. Kim, M.C., Han, G.H., Xiano, X., Song, J., Hong, E.J., Kim, H.K., Ahn, J.P., Han, S.S., Lee, K.Y., Yu, T. Applied Surface Science Anisotropic growth of Pt on Pd nanocube promotes direct synthesis of hydrogen peroxide. *Appl. Surf. Sci.* **562**, 150031-150040 (2021).
7. Song, W., Zhao, R., Yu, L., Xie, X., Sun, M., Li, Y. Enhanced Catalytic Hydrogen Peroxide Production from Hydroxylamine Oxidation on Modified Activated Carbon Fibers : The Role of Surface Chemistry. *Catalysts.* **11**, 1515-1533 (2021).
8. Park, S., Baeck, S-H., Kim, T.J., Chung, Y-M., Oh, S-H., Song, I.K.,.Direct Synthesis of Hydrogen Peroxide from Hydrogen and Oxygen Over Palladium Catalysts Supported on SO<sub>3</sub> H-Functionalized SiO<sub>2</sub> and TiO<sub>2</sub>. *Catal Lett.* **130**, 604-607 (2009).
9. Park, S., Baeck, S-H., Kim, T.J., Chung, Y-M., Oh, S-H., Song, I.K.,.Direct Synthesis of Hydrogen Peroxide from Hydrogen and Oxygen Over Palladium Catalysts Supported on SO<sub>3</sub> H-Functionalized SiO<sub>2</sub> and TiO<sub>2</sub>. *Catal Lett.* **130**, 604-607 (2009).
10. Yook, S., Kwon, H. C., Kim, Y-G., Choi, W., Choi, M. Significant Roles of Carbon Pore and Surface Structure in AuPd/C Catalyst for Achieving High Chemoselectivity in Direct Hydrogen Peroxide Synthesis. *ACS Sustainable Chem. Eng.* **5**, 1208–1216 (2017).
11. Chong, M. N., Jin, B., Chow, C. W. K., Saint, C. Recent developments in photocatalytic water treatment technology: A review. *Water Res.* **44**, 2997–3027 (2010).
12. Deborde, M., Von Gunten, U. Reactions of chlorine with inorganic and organic compounds during water treatment-Kinetics and mechanisms: A critical review. *Water Res.* **42**, 13–51 (2008).
13. Ge, F., Zhu, L., Chen, H. Effects of pH on the chlorination process of phenols in drinking water. *J. Hazard. Mater.* **133**, 99–105 (2006).
14. Wiakowski, K.J., Marzec, M., Fiedurek, J., Ska, A.K., Gajewska, M., Wojciechowska, E., Wu, S., Dach, J., Marczuk, A., Ko, A.K.J. Application of H<sub>2</sub>O<sub>2</sub> to optimize ammonium removal from domestic wastewater. *Separation and Purification Technology.* **173**, 357–363 (2017).
15. Neyens, E., Baeyens, J. A review of classic Fenton's peroxidation as an advanced oxidation technique. *J. Hazard. Mater.* **98**, 33–50 (2003).
16. Yuan, H., Zhou, X., Zhang, Y., Environment, W. & Environment, W. Degradation of Acid Pharmaceuticals in the UV/H<sub>2</sub>O<sub>2</sub> Process : Effects of Humic Acid and Inorganic Salts. *Clean Soil Air Water.* **41**, 43–50 (2013).

17. Al-Rasheed, R.A. Water treatment by heterogeneous photocatalysis an overview. Fourth conference at Saline Water Conversion Corporation (SWCC) Symposium (Jeddah, 2005).
18. Qu, C., Liang, D. Novel electrochemical advanced oxidation processes with H<sub>2</sub>O<sub>2</sub> generation cathode for water treatment: A review. *J. Environ. Chem. Eng.* **10**, 107896-107904 (2022).
19. Munoz, M., de Pedro, Z. M., Casas, J. A., Rodriguez, J. J. Preparation of magnetite-based catalysts and their application in heterogeneous Fenton oxidation - A review. *Appl. Catal. B Environ.* **176–177**, 249–265 (2015).
20. Zhu, Y., Zhu, R., Xi, Y., Zhu, J., Zhu, G., He, H. Strategies for enhancing the heterogeneous fenton catalytic reactivity: A review. *Appl. Catal. B Environ.* **255**, 117739-117750 (2019).
21. Garrido-Ramírez, E. G., Theng, B. K. G., Mora, M. L. Clays and oxide minerals as catalysts and nanocatalysts in Fenton-like reactions - A review. *Appl. Clay Sci.* **47**, 182–192 (2010).
22. Ghaffari, Y., Gupta, N. K., Bae, J., Kim, K. S. Heterogeneous catalytic performance and stability of iron-loaded ZSM-5, zeolite-A, and silica for phenol degradation: A microscopic and spectroscopic approach. *Catalysts.* **9**, 1-17 (2019).
23. Yan, Y., Jiang, S., Zhang, H. Catalytic wet oxidation of phenol with Fe-ZSM-5 catalysts. *RSC Adv.* **6**, 3850–3859 (2016).
24. Ovejero, G., Sotelo, J. L., Martínez, F., Melero, J. A., Gordo, L. Wet peroxide oxidation of phenolic solutions over different iron-containing zeolitic materials. *Ind. Eng. Chem. Res.* **40**, 3921–3928 (2001).
25. Luca, C., Ivorra, F., Massa, P., Fenoglio, R. Iron – alumina synergy in the heterogeneous Fenton-type peroxidation of phenol solutions. *Chem. Eng. J.* **268**, 280–289 (2015).
26. Meenakshisundaram, S., He, Q., Moataz, M., Pritchard, J., Freakley, S.J., Edwards, J.K., Taylor, S.H., Morgan, D.J., Carley, A.F., Knight, D.W., Kiely, C.J., Hutchings, G.J. Synthesis of stable ligand-free gold-palladium nanoparticles using a simple excess anion method. *ACS Nano.* **6**, 6600–6613 (2012).
27. Samanta, C. Direct synthesis of hydrogen peroxide from hydrogen and oxygen: An overview of recent developments in the process. *Appl. Catal. A Gen.* **350**, 133–149 (2008).
28. Burch, R., Ellis, P. R. An investigation of alternative catalytic approaches for the direct synthesis of hydrogen peroxide from hydrogen and oxygen. *Appl. Catal. B Environ.* **42**, 203–211 (2003).
29. Piccinini, M., Ntainjua, N.E., Edwards, J.K., Carley, A.F., Moulijn, J.A., Hutchings, G.J. Effect of the reaction conditions on the performance of Au–Pd/TiO<sub>2</sub> catalyst for

- the direct synthesis of hydrogen peroxide. *Phys. Chem. Chem. Phys.* **12**, 2488 (2010).
30. Moreno, T., García-Serna, J., Cocero, M. J. Decomposition reaction of H<sub>2</sub>O<sub>2</sub> over Pd/C catalyst in an aqueous medium at high pressure: Detailed kinetic study and modelling. *J. Supercrit. Fluids.* **57**, 227–235 (2011).
  31. Landon, P., Collier, P. J., Papworth, A. J., Kiely, J., Graham, J. Direct formation of hydrogen peroxide from H<sub>2</sub>/O<sub>2</sub> using a gold catalyst. *ChemComm.* **18**, 2058–2059 (2002)
  32. Ouyang, L., Guo-jin, D., Peng-fei, T., Tian-yuan, C., Guo-da, L., Jing, X., Yi-Fan, H. Insight into active sites of Pd–Au/TiO<sub>2</sub> catalysts in hydrogen peroxide synthesis directly from H<sub>2</sub> and O<sub>2</sub>. *Journal of Catalysis.* **311**, 129–136 (2014).
  33. Choudhary, V. R., Samanta, C., Choudhary, T. V. Direct oxidation of H<sub>2</sub> to H<sub>2</sub>O<sub>2</sub> over Pd-based catalysts: Influence of oxidation state, support and metal additives. *Appl. Catal. A Gen.* **308**, 128–133 (2006).
  34. Samanta, C., Choudhary, V. R. Direct formation of H<sub>2</sub>O<sub>2</sub> from H<sub>2</sub> and O<sub>2</sub> and decomposition/hydrogenation of H<sub>2</sub>O<sub>2</sub> in aqueous acidic reaction medium over halide-containing Pd/SiO<sub>2</sub> catalytic system. *Catal. Commun.* **8**, 2222–2228 (2007).
  35. Centomo, P., Canton, P., Burato, C., Meneghini, C. Zecca, M. Resonant-XRD Characterization of Nanoalloyed Au-Pd Catalysts for the Direct Synthesis of H<sub>2</sub>O<sub>2</sub>: Quantitative Analysis of Size Dependent Composition of the Nanoparticles. *Appl. Sci.* **9**, 2959-2971 (2019).
  36. Huerta, I. Biasi, P., García-Serna, J., Cocer, M.J., Mikkola, P., Salmi, T. Continuous H<sub>2</sub>O<sub>2</sub> direct synthesis process: An analysis of the process conditions that make the difference. *Green Process. Synth.* **5**, 341–351 (2016).
  37. Tian, P., Xu, X., Ao, C., Ding, D., Li, W., Si, R., Tu, W., Xu, J., Han, Y.F. Direct and Selective Synthesis of Hydrogen Peroxide over Palladium–Tellurium Catalysts at Ambient Pressure. *ChemSusChem.* **10**, 3342–3346 (2017).
  38. Moreno, T., García-Serna, J., Plucinski, P., Sánchez-Montero, M. J. & Cocero, M. J. Direct synthesis of H<sub>2</sub>O<sub>2</sub> in methanol at low pressures over Pd/C catalyst: Semi-continuous process. *Appl. Catal. A Gen.* **386**, 28–33 (2010).
  39. Gallina, G., Biasi, P., García-Serna, J., Salmi, T. & Mikkola, J. P. Optimized H<sub>2</sub>O<sub>2</sub> production in a trickled bed reactor, using water and methanol enriched with selectivity promoters. *Chem. Eng. Sci.* **123**, 334–340 (2015).
  40. Freakley, S. J., Piccinini, M., Edwards, J.K., Ntainjua, E.N., Moulijn, J.A., Hutchings, G.J. Effect of reaction conditions on the direct synthesis of hydrogen peroxide with a AuPd/TiO<sub>2</sub> catalyst in a flow reactor. *ACS Catal.* **3**, 487–501 (2013).
  41. Crombie, C. M., Lewis, R.J., Taylor, R.L., Morgan, D.J., Davies, T.E., Folli, A.,

- Murphy, D.M., Edwards, J.K., Qi, J., Jiang, H., Kiely, C.J., Liu, X., Skjøth-Rasmussen, M.S., Hutchings, G.J. Enhanced Selective Oxidation of Benzyl Alcohol via In Situ H<sub>2</sub>O<sub>2</sub> Production over Supported Pd-Based Catalysts. *ACS Catal.* **11**, 2701-2714 (2021).
42. Melada, S., Rioda, R., Menegazzo, F., Pinna, F., Strukul, G. Direct synthesis of hydrogen peroxide on zirconia-supported catalysts under mild conditions. *Journal of catalysis.* **239**, 422–430 (2006).
  43. Quintanilla, A., Casas, J. A. Catalytic wet air oxidation of phenol with modified activated carbons and Fe / activated carbon catalysts. *Applied Catalysis B: Environmental.* **76**, 135–145 (2007).
  44. Underhill, R., Lewis, R.J., Freakly, S.J., Douthwaite, M., Miedziak, P.J., Akdim, O., Edwards, J.K., Hutchings, G.J. Oxidative Degradation of Phenol using in situ Generated Hydrogen Peroxide Combined with Fenton's Process. *Johnson Matthey Technol. Rev.* **62**, 417–425 (2018).
  45. Liu, G., Liang, H., Tian, Y., Zhang, B., Wang, L. Chinese Journal of Chemical Engineering Direct synthesis of hydrogen peroxide over Pd nanoparticles embedded between HZSM-5 nanosheets layers. *Chinese J. Chem. Eng.* **28**, 2577–2586 (2020).
  46. Lewis, R. J., Bara-Estaun, A., Agarwal, N., Freakly, S.J., Morgan, D.J., Hutchings, G.J. The Direct Synthesis of H<sub>2</sub>O<sub>2</sub> and Selective Oxidation of Methane to Methanol Using HZSM-5 Supported AuPd Catalysts. *Catal. Letters* **149**, 3066–3075 (2019).
  47. Xu, J., Armstrong, R.D., Shaw, G., Dummer, N.F., Freakley, S.J., Taylor, S.H., Hutchings, G.J. Continuous selective oxidation of methane to methanol over Cu- and Fe-modified ZSM-5 catalysts in a flow reactor. *Catal. Today.* **270**, 93–100 (2016).
  48. Ntainjua, N.E., Edwards, J.K., Carley, A.F., Lopez-Sanchez, J.A., Moulijn, J.A., Herzing, A.A., Kiely, C.J., Hutchings, G.J. The role of the support in achieving high selectivity in the direct formation of hydrogen peroxide. *Green Chem.* **10**, 1162–1169 (2008).
  49. Valkaj, K.M., Wittine, O., Margeta, K., Granato, T., Katoviæ, A., Zrnèevia, S. Phenol oxidation with hydrogen peroxide using Cu/ZSM5 and Cu/Y5 catalysts. *Polish J. Chem. Technol.* **13**, 28–36 (2011).
  50. Valkaj, K. M., Katovic, A., Zrnèeviç, S. Investigation of the catalytic wet peroxide oxidation of phenol over different types of Cu/ZSM-5 catalyst. *J. Hazard. Mater.* **144**, 663–667 (2007).
  51. Luo, L., Dai, C., Zhang, A., Wang, J., Liu, Min., Song, C., Guo, X. A facile strategy for enhancing FeCu bimetallic promotion for catalytic phenol oxidation. *Catal. Sci. Technol.* **5**, 3159–3165 (2015).
  52. Wang, Y., Zhao, H., Zhao, G. Applied Catalysis B: Environmental Iron-copper bimetallic nanoparticles embedded within ordered mesoporous carbon as effective

- and stable heterogeneous Fenton catalyst for the degradation of organic contaminants. *Applied Catal. B, Environ.* **164**, 396–406 (2015).
53. Hammond, C., Forde, M.M., Ab Rahim, M.H., Thetford, A., He, Q., Jenkins, R.L., Dimitratos, N., Lopez-Sanchez, J.A., Dummer, N.F., Murphy, D.M., Carley, A.F., Taylor, S.H., Willock, D.J., Stangland, E.E., Kang, J., Hagen, H., Kiely, C.J., Hutchings, G.J. Direct catalytic conversion of methane to methanol in an aqueous medium by using copper-promoted Fe-ZSM-5. *Angew. Chemie-Int. Ed.* **51**, 5129–5133 (2012).
  54. He, Y., Lin, H., Luo, M., Liu, J., Dong, Y., Li, B. Highly efficient remediation of groundwater co-contaminated with Cr(VI) and nitrate by using nano-Fe/Pd bimetal-loaded zeolite: Process product and interaction mechanism. *Environmental Pollution.* **263**, 114479-114490 (2020).
  55. Jin, Z., Liu, Y., Wang, L., Wang, C., Wu, Z., Zhu, Q., Wang, L., Xiao, F-S. Direct Synthesis of Pure Aqueous H<sub>2</sub>O<sub>2</sub> Solution within Aluminosilicate Zeolite Crystals. *ACS Catal.* **11**, 1946–1951 (2021).
  56. Toshima, N., Wang, Y. Novel preparation, Characterization and Catalytic Properties of Polymer-Protected Cu/Pd Bimetallic Colloid. *Chemistry Letters.* **113**, 1611-1614 (1993).
  57. Yaghi, O.M., Li, G., Li, H. Selective binding and removal of guests in a microporous metal-organic framework. *Letters to Nature.* **378**, 703-706 (1995).
  58. Xia, T., Lin, Y., Li, W., Ju, M. Photocatalytic degradation of organic pollutants by MOFs based materials : A review. *Chinese Chem. Lett.* **32**, 2975–2984 (2021).
  59. Qian, Y., Zhang, F., Pang, H. A Review of MOFs and Their Composites-Based Photocatalysts : Synthesis and Applications. *Adv. Funct. Mater.* **31**, 2104231-2104266 (2021).
  60. Shi, Y., Yang, A., Cao, C., Zhao, B. Applications of MOFs : Recent advances in photocatalytic hydrogen production from water. *Coord. Chem. Rev.* **390**, 50–75 (2019).
  61. Chen, Y., Wang, D., Deng, X., Li, Z. Metal–organic frameworks (MOFs) for photocatalytic CO<sub>2</sub> reduction. *Catal. Sci. Technol.* **7**, 4893–4904 (2017).
  62. Tajik, S., Beitollahi, H., Nejad, F.G, Kirlikovali, K.O., Le, Q.V., Jang, H.W., Varma, R.S., Farha, O.K, Shokouhimehr, M. Recent Electrochemical Applications of Metal – Organic Framework- Based Materials. *Cryst. Growth Des.* **20**, 7034–7064 (2020).
  63. Kadhom, M., Deng, B. Metal-organic frameworks ( MOFs ) in water filtration membranes for desalination and other applications. *Appl. Mater. Today* **11**, 219–230 (2018).
  64. Hu, W., Younis, M. R., Zhou, Y., Wang, C., Xia, X. In Situ Fabrication of Ultrasmall

- Gold Nanoparticles / 2D MOFs Hybrid as Nanozyme for Antibacterial Therapy. *Nano micro small*. **16**, 2000553-2000563 (2020).
65. Zhao, H., Chen, Y., Peng, Q., Wang, Q., Zhao, G. Catalytic activity of MOF(2Fe/Co)/ carbon aerogel for improving H<sub>2</sub>O<sub>2</sub>. *Applied Catalysis B: Environmental*. **203**, 127–137 (2017).
66. Wang, Y., Xue, Y., zhang, C. Copper embedded in nitrogen-doped carbon matrix derived from metal-organic frameworks for boosting peroxide production and electro-Fenton catalysis. *Electrochimica Acta*. **36**, 137643-137654 (2021).
67. Liu, M., Xing, Z., Zhao, H., Song, S., Wang, Y., Li, Z., Zhou, W. An efficient photo Fenton system for in-situ evolution of H<sub>2</sub>O<sub>2</sub> via defective iron-based metal organic framework@ZnIn<sub>2</sub>S<sub>4</sub> core-shell Z-scheme heterojunction nanoreactor. *Journal of Hazardous Materials*. **437**, 129436-129449 (2022).
68. Gong, Q., Liu, Y., Dang, Z. Core-shell structured Fe<sub>3</sub>O<sub>4</sub>@GO@MIL-100(Fe) magnetic nanoparticles as heterogeneous photo-Fenton catalyst for 2, 4-dichlorophenol degradation under visible light. *J. Hazard. Mater.* **371**, 677–686 (2019).
69. Zhou, L., Jin, X., Chen, Z. Zeolite Imidazolate Framework-8 Metal–Organic Frameworks Embedded with Bimetallic Fe/Pd Nanoparticles for Reductive Dechlorination. *ACS Appl. Nano Mater.* **3**, 8088-8095 (2020).
70. Zheng, J., Zhao, P., Zhou, S., Chen, S., Liang, Y., Tian, F., Zhou, J., Huo, D., Hou, C. Development of Au–Pd @UiO-66-on-ZIF-L/CC as a self-supported electrochemical sensor for in situ monitoring of cellular hydrogen peroxide. *J. Mater. Chem. B*. **9**, 9031–9040 (2021).
71. Godínez, L. A., Ana, I. Z., Medel-reyes, A., Carrasco-marín, F., Romero-cano, L. A. Towards understanding of heterogeneous Fenton reaction using carbon-Fe catalysts coupled to in-situ H<sub>2</sub>O<sub>2</sub> electro-generation as clean technology for wastewater treatment. *Chemosphere*. **224**, 698–706 (2019).
72. Shen, X., Xiao, F., Zhao, H., Chen, Y., Fang, C., Xiao, R., Chu, W., Zhao, G. In Situ-Formed PdFe Nanoalloy and Carbon Defects in Cathode for Synergic Reduction – Oxidation of Chlorinated Pollutants in Electro- Fenton Process. *Environ. Sci. Technol.* **54**, 4564–4572 (2020).
73. Torres-pinto, A., Sampaio, M.J., Teixeira, J., Silva, C.G., Faria, J.L, Silva, A.M.T. Photo-Fenton degradation assisted by in situ generation of hydrogen peroxide using a carbon nitride photocatalyst. *J. Water Process Eng.* **37**, 101467-101470 (2020).
74. Yang, Z., Gong, X., Peng, L., Yang, D., Liu, Y. Zn<sup>0</sup>-CNTs-Fe<sub>3</sub>O<sub>4</sub> catalytic in-situ generation of H<sub>2</sub>O<sub>2</sub> for heterogeneous Fenton degradation of 4-chlorophenol. *Chemosphere*. **208**, 665–673 (2018).

